Algebraic Statistics for Computational Biology

Edited by
Lior Pachter and Bernd Sturmfels

Contents

Preface

The title of this book reflects who we are: a computational biologist and an algebraist who share a common interest in statistics. Our collaboration sprang from the desire to find a mathematical language for discussing biological sequence analysis, with the initial impetus being provided by the Introductory Workshop on *Discrete and Computational Geometry* at the Mathematical Sciences Research Institute (MSRI) held at Berkeley in August 2003. At that workshop we began exploring the similarities between tropical matrix multiplication and the Viterbi algorithm for hidden Markov models. Our discussions ultimately led to two articles [Pachter and Sturmfels, 2004a,b] which are explained and further developed in various chapters of this book.

In the fall of 2003 we held a graduate seminar on *The Mathematics of Phylogenetic Trees.* About half of the authors in the second part of this book already participated in that seminar. It was based on topics from the books [Felsenstein, 2003, Semple and Steel, 2003] but we also discussed other projects, such as Michael Joswig's polytope propagation on graphs (now Chapter 6). That seminar got us up to speed on research topics in phylogenetics, and led us to participate in the conference on *Phylogenetic Combinatorics* which was held in July 2004 in Uppsala, Sweden. In Uppsala we were introduced to David Bryant and his statistical models for split systems (now Chapter 17).

Another milestone was the workshop on *Computational Algebraic Statistics* which was held at the American Institute for Mathematics (AIM) at Palo Alto in December 2003. That workshop was built on the algebraic statistics paradigm, which is that statistical models for discrete data can be represented as solutions to systems of polynomial equations. Our current understanding of algebraic statistical models, maximum likelihood estimation and expectation maximization was shaped by the excellent lectures and discussions at AIM.

These developments led us to offer a mathematics graduate course titled *Algebraic Statistics for Computational Biology* in the fall of 2004. The course was attended mostly by mathematics students curious about computational biology, but also by computer scientists, statisticians, and bioengineering students interested in understanding the mathematical foundations of bioinformatics. Participants ranged from senior postdocs to first year graduate students and even one undergraduate. The format consisted of lectures by us on basic principles of algebraic statistics and computational biology, as well as student participation in the form of group projects and presentations. The class was divided into four sections, reflecting the four themes of algebra, statistics, computation and biology. Each group was assigned a handful of projects to pursue, with the goal of completing a written report by the end of the semester. In some cases the groups worked on the problems we suggested, but, more often than not, original ideas by group members led to independent research plans.

Half way through the semester, it became clear that the groups were making fantastic progress, and that their written reports would contain many novel ideas and results. At that point, we thought about preparing a book. The first half of the book would be based on our own lectures, and the second half would consist of chapters based on the final term papers. A tight schedule was seen as essential for the success of such an undertaking, given that many participants would be leaving Berkeley and the momentum would be lost. It was decided that the book should be written by March 2005, or not at all.

We were fortunate to find a partner in Cambridge University Press, which agreed to work with us on our concept. We are especially grateful to our editor, David Tranah, for his strong encouragement, and his trust that our half-baked ideas could actually turn into a readable book. After all, we were proposing to write to a book with twenty-nine authors during a period of three months.

The project did become reality and the result is in your hands. It offers an accurate snapshot of what happened during our seminars at UC Berkeley in 2003 and 2004. Nothing more and nothing less. The choice of topics is certainly biased, and the presentation is undoubtedly very far from perfect. But we hope that it may serve as an invitation to biology for mathematicians, and as an invitation to algebra for biologists, statisticians and computer scientists.

We acknowledge the National Science Foundation and the National Institute of Health for their financial support, and many friends and colleagues for providing helpful comments – there are far too many to list individually. Most of all, we are grateful to our wonderful students and postdocs from whom we learned so much. Their enthusiasm and hard work have been truly amazing. You will enjoy meeting them in Part 2.

Lior Pachter and Bernd Sturmfels
Berkeley, California, March 2005

Part I

Introduction to the four themes

Part I of this book is devoted to outlining the basic principles of algebraic statistics, and their relationship to computational biology. Although some of the ideas are complex, and their relationships intricate, the underlying philosophy of our approach to biological sequence analysis is summarized in the cartoon on the cover of the book. The fictional character is DiaNA, who appears throughout the book, and who is the statistical surrogate for our biological intuition. In the cartoon, DiaNA is walking randomly on a graph and she is throwing tetrahedral dice that can land on one of the characters `A`,`C`,`G` or `T`. A key feature of the tosses is that the outcome depends on the direction she is walking. We, the observers, record the characters that appear on the successive throws, but are unable to see the path that DiaNA takes on her graph. Our goal is to guess DiaNA's path from the die roll outcomes. That is, we wish to make an inference about missing data from certain observed data.

In this book, the observed data are DNA sequences, and in Chapter 4 we explain the relevance of the example depicted on the cover to the biological problem of sequence alignment. The tetrahedral shape of the die hint at polytopes, which we see in Chapter 2 are fundamental geometric objects that play a key role in making guesses about DiaNA. Underlying the whole story is algebra, featured in Chapter 3, and which is the universal language with which to describe the underlying process at the heart of DiaNA's randomness.

Chapter 1 offers a fairly self-contained introduction to algebraic statistics. Many concepts of statistics have a natural analog in algebraic geometry, and there is an emerging dictionary which bridges the gap between these disciplines:

independence	=	Segre variety
exponential family	=	toric variety
curved exponential family	=	manifold
mixture model	=	secant variety
inference	=	tropicalization
··· ···	=	··· ··· ···

This dictionary is far from complete and finished, but it already suggests that algorithmic tools from algebraic geometry, most notably Gröbner bases, may be used for computations in statistics that may be beneficial for computational biology applications. While we are well aware of the limitations of algebraic algorithms, with Gröbner bases computations typically becoming intractable beyond toy problems, we nevertheless believe that computational biologists might benefit from adding the techniques described in Chapter 3 to their tool box. In addition, we have found the algebraic point of view to be useful in unifying and developing many computational biology algorithms. For example, the results on parametric sequence alignment in Chapter 7 do not require the language of algebra to be understood or utilized, but were motivated by concepts such as the Newton polytope of a polynomial. Chapter 2 discusses discrete algorithms which provide efficient solutions to various problems of statistical inference. Chapter 4 is an introduction to the biology, where we return to many of the examples in Chapter 1, illustrating how the statistical models we have discussed play a prominent role in computational biology.

We emphasize that Part I serves mainly as an introduction and reference for the chapters in Part II. We have therefore omitted many topics which are rightfully considered to be an integral part of computational biology. For example, we have restricted ourselves to the topic of biological sequence analysis, and within that domain have focused on eukaryotic genome analysis. Readers interested in a more complete introduction to computational biology are referred to [Durbin *et al.*, 1998], our favorite introduction to the area. Also useful may be a text on molecular biology with an emphasis on genomics, such as [Brown, 2002]. Our treatment of computational algebra in Chapter 3 is only a sliver taken from a mature and developed subject. The excellent book by [Cox *et al.*, 1997] fills in many of the details missing in our discussions.

Because Part I covers many topics, a comprehensive list of prerequisites would include a background in computer science, familiarity with molecular biology, and the benefit of having taken introductory courses in statistics and abstract algebra. Direct experience in computational biology would also be desirable. Of course, we recognize that this is asking too much. Real-life readers may be experts in one of these subjects but completely unfamiliar with others, and we have taken this into account when writing the book.

Various chapters provide natural points of entry for readers with different backgrounds. Those wishing to learn more about genomes can start with Chapter 4, biologists interested in software tools can start with Section 2.5, and statisticians who wish to brush up their algebra can start with Chapter 3.

In summary, the book is not meant to serve as the definitive text for algebraic statistics or computational biology, but rather as a first invitation to biology for mathematicians, and conversely as a mathematical primer for biologists. In other words, it is written in the spirit of interdisciplinary collaboration that is highlighted in the article *Mathematics is Biology's Next Microscope, Only Better; Biology is Mathematics' Next Physics, Only Better* [Cohen, 2004].

1
Statistics

Lior Pachter

Bernd Sturmfels

Statistics is the science of data analysis. The data to be encountered in this book are derived from *genomes*. Genomes consist of long chains of DNA which are represented by sequences in the letters `A`, `C`, `G` or `T`. These abbreviate the four nucleic acids `A`denine, `C`ytosine, `G`uanine and `T`hymine, which serve as fundamental building blocks in biology.

What do statisticians do with their data? They build models of the process that generated the data and, in what is known as *statistical inference*, draw conclusions about this process. Genome sequences are particularly interesting data to draw conclusions from: they are the blueprint for life, and yet their function, structure, and evolution are poorly understood. Statistics is fundamental for genomics, a point of view that was emphasized in [Durbin *et al.*, 1998].

The inference tools we present in this chapter look different from those found in [Durbin *et al.*, 1998], or most other texts on computational biology or mathematical statistics: they are written in the language of abstract algebra. The algebraic language for statistics clarifies many of the ideas central to analysis of discrete data, and, within the context of biological sequence analysis, unifies the main ingredients of many widely used algorithms.

Algebraic Statistics is a new field, less than a decade old, whose precise scope is still emerging. The term itself was coined by Giovanni Pistone, Eva Riccomagno and Henry Wynn, with the title of their book [Pistone *et al.*, 2001]. That book explains how polynomial algebra arises in problems from experimental design and discrete probability, and it demonstrates how computational algebra techniques can be applied to statistics.

This chapter takes some additional steps along the algebraic statistics path. It offers a self-contained introduction to algebraic statistical models, with the aim of developing inference tools necessary for studying genomes. Special emphasis will be placed on (hidden) Markov models and graphical models.

1.1 Statistical models for discrete data

Imagine a fictional character named DiaNA who produces sequences of letters over the four-letter alphabet $\{\mathtt{A}, \mathtt{C}, \mathtt{G}, \mathtt{T}\}$. An example of such a sequence is

$$\mathtt{CTCACGTGATGAGAGCATTCTCAGACCGTGACGCGTGTAGCAGCGGCTC} \qquad (1.1)$$

The sequences produced by DiaNA are called *DNA sequences*. DiaNA generates her sequences by some random process. When modeling this random process we make assumptions about part of its structure. The resulting *statistical model* is a family of probability distributions, one of which we believe governs the process by which DiaNA generates her sequences. In this book we consider parametric statistical models, which are families of probability distributions that can be parameterized by a finite-dimensional parameter. One important task is to estimate DiaNA's parameters from the sequences she generates. Estimation is also called *learning* in the computer science literature.

DiaNA uses *tetrahedral dice* to generate DNA sequences. Each tetrahedral die has the shape of a tetrahedron, and its four faces are labeled with the letters `A`, `C`, `G` and `T`. If DiaNA rolls a fair die then each of the four letters will appear with the same probability 1/4. If she uses a loaded tetrahedral die then the four probabilities can be any four non-negative numbers that sum to one.

Example 1.1 Suppose that DiaNA uses three tetrahedral dice. Two of her dice are loaded and one die is fair. The probabilities of rolling the four letters are known to us. They are the numbers in the rows of the following table:

	A	C	G	T
first die	0.15	0.33	0.36	0.16
second die	0.27	0.24	0.23	0.26
third die	0.25	0.25	0.25	0.25

(1.2)

DiaNA generates each letter in her DNA sequence independently using the following process. She first picks one of her three dice at random, where her first die is picked with probability θ_1, her second die is picked with probability θ_2, and her third die is picked with probability $1 - \theta_1 - \theta_2$. The probabilities θ_1 and θ_2 are unknown to us, but we do know that DiaNA makes one roll with the selected die, and then she records the resulting letter, `A`, `C`, `G` or `T`.

In the setting of biology, the first die corresponds to DNA which is `G` + `C` rich. the second die corresponds to DNA which is `G` + `C` poor, and the third is a fair die. We got the specific numbers in the first two rows of (1.2) by averaging the rows of the two tables in [Durbin *et al.*, 1998, page 50] (for more on this example and its connection to `CpG` island identification see Chapter 4).

Suppose we are given the DNA sequence of length $N = 49$ shown in (1.1).

One question that may be asked is whether the sequence was generated by DiaNA using this process, and, if so, which parameters θ_1 and θ_2 did she use?

Let $p_{\mathtt{A}}$, $p_{\mathtt{C}}$, $p_{\mathtt{G}}$ and $p_{\mathtt{T}}$ denote the probabilities that DiaNA will generate any of her four letters. The statistical model we have discussed is written in algebraic notation as

$$\begin{aligned} p_{\mathtt{A}} &= -0.10 \cdot \theta_1 + 0.02 \cdot \theta_2 + 0.25, \\ p_{\mathtt{C}} &= 0.08 \cdot \theta_1 - 0.01 \cdot \theta_2 + 0.25, \\ p_{\mathtt{G}} &= 0.11 \cdot \theta_1 - 0.02 \cdot \theta_2 + 0.25, \\ p_{\mathtt{T}} &= -0.09 \cdot \theta_1 + 0.01 \cdot \theta_2 + 0.25. \end{aligned}$$

Note that $p_{\mathtt{A}} + p_{\mathtt{C}} + p_{\mathtt{G}} + p_{\mathtt{T}} = 1$, and we get the three distributions in the rows of (1.2) by specializing (θ_1, θ_2) to $(1, 0)$, $(0, 1)$ and $(0, 0)$ respectively.

To answer our questions, we consider the *likelihood* of observing the particular data (1.1). Since each of the 49 characters was generated independently, that likelihood is the product of the probabilities of the individual letters:

$$L \quad = \quad p_{\mathtt{C}} p_{\mathtt{T}} p_{\mathtt{A}} p_{\mathtt{C}} p_{\mathtt{C}} p_{\mathtt{G}} \cdots p_{\mathtt{A}} \quad = \quad p_{\mathtt{A}}^{10} \cdot p_{\mathtt{C}}^{14} \cdot p_{\mathtt{G}}^{15} \cdot p_{\mathtt{T}}^{10}.$$

This expression is the *likelihood function* of DiaNA's model for the data (1.1). To stress the fact that the parameters θ_1 and θ_2 are unknowns we write

$$L(\theta_1, \theta_2) \quad = \quad p_{\mathtt{A}}(\theta_1, \theta_2)^{10} \cdot p_{\mathtt{C}}(\theta_1, \theta_2)^{14} \cdot p_{\mathtt{G}}(\theta_1, \theta_2)^{15} \cdot p_{\mathtt{T}}(\theta_1, \theta_2)^{10}.$$

This likelihood function is a real-valued function on the triangle

$$\Theta \quad = \quad \bigl\{ (\theta_1, \theta_2) \in \mathbb{R}^2 \; : \; \theta_1 > 0 \text{ and } \theta_2 > 0 \text{ and } \theta_1 + \theta_2 < 1 \bigr\}.$$

In the paradigm of *maximum likelihood* we estimate the parameter values that DiaNA used by those values which make the likelihood of observing her data as large as possible. Thus our task is to maximize $L(\theta_1, \theta_2)$ over the triangle Θ. It is equivalent but more convenient to maximize the *log-likelihood function*

$$\begin{aligned} \ell(\theta_1, \theta_2) \quad &= \quad \log\bigl(L(\theta_1, \theta_2)\bigr) \\ &= \quad 10 \cdot \log(p_{\mathtt{A}}(\theta_1, \theta_2)) + 14 \cdot \log(p_{\mathtt{C}}(\theta_1, \theta_2)) \\ &\qquad + 15 \cdot \log(p_{\mathtt{G}}(\theta_1, \theta_2)) + 10 \cdot \log(p_{\mathtt{T}}(\theta_1, \theta_2)). \end{aligned}$$

The solution to this optimization problem can be computed in closed form, by equating the two partial derivatives of the log-likelihood function to zero:

$$\begin{aligned} \frac{\partial \ell}{\partial \theta_1} \quad &= \quad \frac{10}{p_{\mathtt{A}}} \cdot \frac{\partial p_{\mathtt{A}}}{\partial \theta_1} + \frac{14}{p_{\mathtt{C}}} \cdot \frac{\partial p_{\mathtt{C}}}{\partial \theta_1} + \frac{15}{p_{\mathtt{G}}} \cdot \frac{\partial p_{\mathtt{G}}}{\partial \theta_1} + \frac{10}{p_{\mathtt{T}}} \cdot \frac{\partial p_{\mathtt{T}}}{\partial \theta_1} \quad = \quad 0, \\ \frac{\partial \ell}{\partial \theta_2} \quad &= \quad \frac{10}{p_{\mathtt{A}}} \cdot \frac{\partial p_{\mathtt{A}}}{\partial \theta_2} + \frac{14}{p_{\mathtt{C}}} \cdot \frac{\partial p_{\mathtt{C}}}{\partial \theta_2} + \frac{15}{p_{\mathtt{G}}} \cdot \frac{\partial p_{\mathtt{G}}}{\partial \theta_2} + \frac{10}{p_{\mathtt{T}}} \cdot \frac{\partial p_{\mathtt{T}}}{\partial \theta_2} \quad = \quad 0. \end{aligned}$$

Each of the two expressions is a rational function in (θ_1, θ_2). By clearing denominators and by applying the algebraic technique of *Gröbner bases* (Section

3.1), we can transform the two equations above into the equivalent equations

$$\begin{array}{rcl} 13003050 \cdot \theta_1 + 2744 \cdot \theta_2^2 - 2116125 \cdot \theta_2 - 6290625 & = & 0, \\ 134456 \cdot \theta_2^3 - 10852275 \cdot \theta_2^2 - 4304728125 \cdot \theta_2 + 935718750 & = & 0. \end{array} \tag{1.3}$$

The second equation has a unique solution $\hat{\theta}_2$ between 0 and 1. The corresponding value of $\hat{\theta}_1$ is obtained by solving the first equation. Approximately,

$$(\hat{\theta}_1, \hat{\theta}_2) \quad = \quad \big(0.5191263945, 0.2172513326\big).$$

The log-likelihood function attains its maximum value at this point:

$$\ell(\hat{\theta}_1, \hat{\theta}_2) \quad = \quad -67.08253037.$$

The corresponding probability distribution

$$(\hat{p}_{\mathtt{A}}, \hat{p}_{\mathtt{C}}, \hat{p}_{\mathtt{G}}, \hat{p}_{\mathtt{T}}) \quad = \quad \big(0.202432, 0.289358, 0.302759, 0.205451\big) \tag{1.4}$$

is very close (in a statistical sense [Bickel, 1971]) to the empirical distribution

$$\frac{1}{49}(10, 14, 15, 10) \quad = \quad \big(0.204082, 0.285714, 0.306122, 0.204082\big). \tag{1.5}$$

We conclude that the proposed model is a good fit for the data (1.1) and guess that DiaNA used the probabilities $\hat{\theta}_1$ and $\hat{\theta}_2$ for choosing among her dice.

We now turn to our general discussion of statistical models for discrete data. A *statistical model* is a family of probability distributions on some state space. In this book we assume that the state space is finite, but possibly quite large. We often identify the state space with the set of the first m positive integers,

$$[m] \quad := \quad \{1, 2, \ldots, m\}. \tag{1.6}$$

A probability distribution on the set $[m]$ is a point in the *probability simplex*

$$\Delta_{m-1} \quad := \quad \Big\{ (p_1, \ldots, p_m) \in \mathbb{R}^m \, : \, \sum_{i=1}^{m} p_i = 1 \text{ and } \; p_j \geq 0 \; \text{ for all } j \Big\}. \tag{1.7}$$

The index $m - 1$ indicates the dimension of the simplex Δ_{m-1}. We write Δ for the simplex Δ_{m-1} when the underlying state space $[m]$ is understood.

Example 1.2 The state space for DiaNA's dice is the set $\{\mathtt{A}, \mathtt{C}, \mathtt{G}, \mathtt{T}\}$ which we identify with the set $[4] = \{1, 2, 3, 4\}$. The simplex Δ is a tetrahedron. The probability distribution associated with a fair die is the point $(\frac{1}{4}, \frac{1}{4}, \frac{1}{4}, \frac{1}{4})$, which is the centroid of the tetrahedron Δ. Equivalently, we may think about our model via the concept of a *random variable*, that is a function X taking values in the state space $\{\mathtt{A}, \mathtt{C}, \mathtt{G}, \mathtt{T}\}$. Then the point corresponding to a fair die gives the probability distribution of X as $\mathrm{Prob}(X = \mathtt{A}) = \frac{1}{4}$, $\mathrm{Prob}(X = \mathtt{C}) =$

$\frac{1}{4}$, Prob$(X = \mathtt{G}) = \frac{1}{4}$, Prob$(X = \mathtt{T}) = \frac{1}{4}$. All other points in the tetrahedron Δ correspond to loaded dice.

A statistical model for discrete data is a family of probability distributions on $[m]$. Equivalently, a statistical model is simply a subset of the simplex Δ. The i-th coordinate p_i represents the probability of observing the state i, and in that capacity p_i must be a non-negative real number. However, when discussing algebraic computations (as in Chapter 3), we sometimes relax this requirement and allow p_i to be negative or even a complex number.

An *algebraic statistical model* arises as the image of a polynomial map

$$\mathbf{f} \;:\; \mathbb{R}^d \to \mathbb{R}^m \;, \quad \theta = (\theta_1, \ldots, \theta_d) \mapsto \big(f_1(\theta), f_2(\theta), \ldots, f_m(\theta)\big). \tag{1.8}$$

The unknowns $\theta_1, \ldots, \theta_d$ represent the model parameters. In most cases of interest, d is much smaller than m. Each coordinate function f_i is a polynomial in the d unknowns, which means it has the form

$$f_i(\theta) \quad = \quad \sum_{a \in \mathbb{N}^d} c_a \cdot \theta_1^{a_1} \theta_2^{a_2} \cdots \theta_d^{a_d}, \tag{1.9}$$

where all but finitely many of the coefficients $c_a \in \mathbb{R}$ are zero. We use $\mathbb{N}$ to denote the non-negative integers, that is, $\mathbb{N} = \{0, 1, 2, 3, \ldots\}$.

The parameter vector $(\theta_1, \ldots, \theta_d)$ ranges over a suitable non-empty open subset Θ of $\mathbb{R}^d$ which is called the *parameter space* of the model $\mathbf{f}$. We assume that the parameter space Θ satisfies the condition

$$f_i(\theta) \; > \; 0 \qquad \text{for all } \; i \in [m] \; \text{ and } \; \theta \in \Theta \tag{1.10}$$

Under these hypotheses, the following two conditions are equivalent:

$$\mathbf{f}(\Theta) \; \subseteq \; \Delta \qquad \Longleftrightarrow \qquad f_1(\theta) + f_2(\theta) + \cdots + f_m(\theta) \; = \; 1 \tag{1.11}$$

This is an identity of polynomial functions, which means that all non-constant terms of the polynomials f_i cancel, and the constant terms add up to 1. If (1.11) holds, then our model is simply the set $\mathbf{f}(\Theta)$.

Example 1.3 DiaNA's model in Example 1.1 is a *mixture model* which mixes three distributions on $\{\mathtt{A}, \mathtt{C}, \mathtt{G}, \mathtt{T}\}$. Geometrically, the image of DiaNA's map

$$\mathbf{f} : \mathbb{R}^2 \to \mathbb{R}^4 \,, \;\; (\theta_1, \theta_2) \mapsto (p_{\mathtt{A}}, p_{\mathtt{C}}, p_{\mathtt{G}}, p_{\mathtt{T}})$$

is the plane in $\mathbb{R}^4$ which is cut out by the two linear equations

$$p_{\mathtt{A}} + p_{\mathtt{C}} + p_{\mathtt{G}} + p_{\mathtt{T}} \; = \; 1 \qquad \text{and} \qquad 11\, p_{\mathtt{A}} + 15\, p_{\mathtt{G}} \; = \; 17\, p_{\mathtt{C}} + 9\, p_{\mathtt{T}}. \tag{1.12}$$

This plane intersects the tetrahedron Δ in the quadrangle whose vertices are

$$\big(0, 0, \frac{3}{8}, \frac{5}{8}\big) \,, \;\; \big(0, \frac{15}{32}, \frac{17}{32}, 0\big) \,, \;\; \big(\frac{9}{20}, 0, 0, \frac{11}{20}\big) \quad \text{and} \quad \big(\frac{17}{28}, \frac{11}{28}, 0, 0\big). \tag{1.13}$$

Inside this quadrangle is the triangle $\mathbf{f}(\Theta)$ whose vertices are the three rows of the table in (1.2). The point (1.4) lies in that triangle and is near (1.5).

Some statistical models are naturally given by a polynomial map $\mathbf{f}$ for which (1.11) does not hold. If this is the case then we scale each vector in $\mathbf{f}(\Theta)$ by the positive quantity $\sum_{i=1}^m f_i(\theta)$. Regardless of whether (1.11) holds or not, our model is the family of all probability distributions on $[m]$ of the form

$$\frac{1}{\sum_{i=1}^m f_i(\theta)} \cdot \bigl(f_1(\theta), f_2(\theta), \ldots, f_m(\theta)\bigr) \qquad \text{where} \quad \theta \in \Theta. \tag{1.14}$$

We generally try to keep things simple and assume that (1.11) holds. However, there are some cases, such as the general toric model in the next section, when the formulation in (1.14) is more natural. It poses no great difficulty to extend our theorems and algorithms from polynomials to rational functions.

Our *data* are typically given in the form of a sequence of observations

$$i_1, i_2, i_3, i_4, \ldots, i_N. \tag{1.15}$$

Each data point i_j is an element from our state space $[m]$. The integer N, which is the length of the sequence, is called the *sample size*. We summarize the data (1.15) in the *data vector* $u = (u_1, u_2, \ldots, u_m)$ where u_k is the number of indices $j \in [N]$ such that $i_j = k$. Hence u is a vector in $\mathbb{N}^m$ with $u_1+u_2+\cdots+u_m = N$. The *empirical distribution* corresponding to the data (1.15) is the scaled vector $\frac{1}{N}u$ which is a point in the probability simplex Δ. The coordinates u_i/N of the vector $\frac{1}{N}u$ are the *observed frequencies* of the various possible outcomes.

We consider the model $\mathbf{f}$ to be a "good fit" for the data u if there exists a parameter vector $\theta \in \Theta$ such that the probability distribution $\mathbf{f}(\theta)$ is very close, in a statistically meaningful sense [Bickel, 1971], to the empirical distribution $\frac{1}{N}u$. Suppose we independently draw N times at random from the set $[m]$ with respect to the probability distribution $\mathbf{f}(\theta)$. Then the probability of observing the sequence (1.15) equals

$$L(\theta) \quad = \quad f_{i_1}(\theta) f_{i_2}(\theta) \cdots f_{i_N}(\theta) \quad = \quad f_1(\theta)^{u_1} \cdots f_m(\theta)^{u_m}. \tag{1.16}$$

This expression depends on the parameter vector θ as well as the data vector u. However, we think of u as being fixed and then L is a function from Θ to the positive real numbers. It is called the *likelihood function* to emphasize that it is a function that depends on θ, and to distinguish it from an expression for a probability. Note that any reordering of the sequence (1.15) leads to the same data vector u. Hence the probability of observing the data vector u is equal to

$$\frac{(u_1 + u_2 + \cdots + u_m)!}{u_1! u_2! \cdots u_m!} \cdot L(\theta). \tag{1.17}$$

The vector u plays the role of a *sufficient statistic* for the model $\mathbf{f}$. This means that the likelihood function $L(\theta)$ depends on the data (1.15) only through u. In practice one often replaces the likelihood function by its logarithm

$$\ell(\theta) \;=\; \log L(\theta) \;=\; u_1 \cdot \log(f_1(\theta)) + u_2 \cdot \log(f_2(\theta)) + \cdots + u_m \cdot \log(f_m(\theta)). \quad (1.18)$$

This is the *log-likelihood function*. Note that $\ell(\theta)$ is a function from the parameter space $\Theta \subset \mathbb{R}^d$ to the negative real numbers $\mathbb{R}_{<0}$.

The problem of *maximum likelihood estimation* is to maximize the likelihood function $L(\theta)$ in (1.16), or, equivalently, the scaled likelihood function (1.17), or, equivalently, the log-likelihood function $\ell(\theta)$ in (1.18). Here θ ranges over the parameter space $\Theta \subset \mathbb{R}^d$. Formally, we consider the optimization problem:

$$\text{Maximize } \ell(\theta) \quad \text{subject to } \theta \in \Theta. \quad (1.19)$$

A solution to this optimization problem is denoted $\hat{\theta}$ and is called a *maximum likelihood estimate* of θ with respect to the model $\mathbf{f}$ and the data u. Sometimes, if the model satisfies certain properties, it may be that the maximum likelihood estimate $\hat{\theta}$ is always unique. This happens for *linear models* and *toric models*, due to the concavity of their log-likelihood function, as we shall see in Section 1.2. For most statistical models, however, the situation is not as simple. There can be more than one global maximum, in fact, there can be infinitely many of them. And it may be difficult to find any one of these global maxima. In that case, one may content oneself with a local maximum of the likelihood function. In Section 1.3 we shall discuss the *EM algorithm* which is a numerical method for finding solutions to the maximum likelihood estimation problem (1.19).

1.2 Linear models and toric models

In this section we introduce two classes of models which have the property that maximum likelihood estimation (1.19) is a convex optimization problem. Assuming that the parameter domain Θ is bounded, it follows that the likelihood function has exactly one local maximum $\hat{\theta} \in \Theta$, and it is easy to numerically compute the *maximum likelihood estimate* $\hat{\theta}$ using any of the hill-climbing methods of convex optimization, such as the gradient ascent algorithm.

1.2.1 Linear models

An algebraic statistical model $\mathbf{f} : \mathbb{R}^d \to \mathbb{R}^m$ is called a *linear model* if each of its coordinate polynomials $f_i(\theta)$ is a linear function. Being a linear function means there exist real numbers $a_{i1}, \ldots, a_{1d}$ and b_i such that

$$f_i(\theta) \quad = \quad \sum_{j=1}^{d} a_{ij}\theta_j + b_i. \quad (1.20)$$

The m linear functions $f_1(\theta), \ldots, f_m(\theta)$ have the property that their sum is the constant function 1. DiaNA's model studied in Example 1.1 is a linear model. For the data discussed in that example, the log-likelihood function $\ell(\theta)$ had a unique local maximum on the parameter triangle Θ. The following proposition states that this desirable property holds for every linear model.

Proposition 1.4 *For any linear model* $\mathbf{f}$ *and data* $u \in \mathbb{N}^m$, *the log-likelihood function* $\ell(\theta) = \sum_{i=1}^m u_i \log(f_i(\theta))$ *is concave. If the linear map* $\mathbf{f}$ *is one-to-one and all* u_i *are positive then the log-likelihood function is strictly concave.*

Proof Our assertion that the log-likelihood function $\ell(\theta)$ is concave states that the *Hessian matrix* $\left(\frac{\partial^2 \ell}{\partial\theta_j \partial\theta_k}\right)$ is negative semi-definite. In other words, we need to show that every eigenvalue of this symmetric matrix is non-positive.

The partial derivative of the linear function $f_i(\theta)$ in (1.20) with respect to the unknown θ_j is the constant a_{ij}. Hence the partial derivative of the log-likelihood function $\ell(\theta)$ equals

$$\frac{\partial \ell}{\partial \theta_j} \quad = \quad \sum_{i=1}^m \frac{u_i a_{ij}}{f_i(\theta)}. \tag{1.21}$$

Taking the derivative again, we get the following formula for the Hessian matrix

$$\left(\frac{\partial^2 \ell}{\partial\theta_j \,\partial\theta_k}\right) \quad = \quad -A^T \cdot \operatorname{diag}\left(\frac{u_1}{f_1(\theta)^2}, \frac{u_2}{f_2(\theta)^2}, \ldots, \frac{u_m}{f_m(\theta)^2}\right) \cdot A. \tag{1.22}$$

Here A is the $m \times d$ matrix whose entry in row i and column j equals a_{ij}. This shows that the Hessian (1.22) is a symmetric $d \times d$ matrix each of whose eigenvalues is non-positive.

The argument above shows that $\ell(\theta)$ is a concave function. Moreover, if the linear map $\mathbf{f}$ is one-to-one then the matrix A has rank d. In that case, provided all u_i are strictly positive, all eigenvalues of the Hessian are strictly negative, and we conclude that $\ell(\theta)$ is strictly concave for all $\theta \in \Theta$. □

The critical points of the likelihood function $\ell(\theta)$ of the linear model $\mathbf{f}$ are the solutions to the following system of d equations in d unknowns which are obtained by equating (1.21) to zero. What we get are the *likelihood equations*

$$\sum_{i=1}^m \frac{u_i a_{i1}}{f_i(\theta)} \;=\; \sum_{i=1}^m \frac{u_i a_{i2}}{f_i(\theta)} \;=\; \cdots \;=\; \sum_{i=1}^m \frac{u_i a_{id}}{f_i(\theta)} \;=\; 0. \tag{1.23}$$

The study of these equations involves the combinatorial theory of hyperplane arrangements. Indeed, consider the m hyperplanes in d-space $\mathbb{R}^d$ which are defined by the equations $f_i(\theta) = 0$ for $i = 1, 2, \ldots, m$. The complement of this arrangement of hyperplanes in $\mathbb{R}^d$ is the following set of parameter values

$$\mathcal{C} \quad = \quad \left\{ \theta \in \mathbb{R}^d \,:\, f_1(\theta) f_2(\theta) f_3(\theta) \cdots f_m(\theta) \;\neq\; 0 \right\}.$$

This set is the disjoint union of finitely many open convex polyhedra defined by inequalities $f_i(\theta) > 0$ or $f_i(\theta) < 0$. These polyhedra are called the *regions* of the arrangement. Some of these regions are bounded, and others are unbounded. Let μ denote the number of bounded regions of the arrangement.

Theorem 1.5 (Varchenko's Formula) *If the u_i are positive, then the likelihood equations (1.23) of the linear model $\mathbf{f}$ have precisely μ distinct real solutions, one in each bounded region of the hyperplane arrangement $\{f_i = 0\}_{i\in[m]}$. All solutions have multiplicity one and there are no other complex solutions.*

This result first appeared in [Varchenko, 1995]. The connection to maximum likelihood estimation was explored by [Catanese *et al.*, 2004].

We already saw one instance of Varchenko's Formula in Example 1.1. The four lines defined by the vanishing of DiaNA's probabilities $p_{\mathtt{A}}$, $p_{\mathtt{C}}$, $p_{\mathtt{G}}$ or $p_{\mathtt{T}}$ partition the (θ_1, θ_2)-plane into eleven regions. Three of these eleven regions are bounded: one is the quadrangle (1.13) in Δ and two are triangles outside Δ. Thus DiaNA's linear model has $\mu = 3$ bounded regions. Each region contains one of the three solutions of the transformed likelihood equations (1.3).

Example 1.6 Consider a one-dimensional ($d = 1$) linear model $\mathbf{f} : \mathbb{R}^1 \to \mathbb{R}^m$. Here θ is a scalar parameter, each $f_i = a_i\theta + b_i$ is a linear function in one unknown θ. We have $a_1+a_2+\cdots+a_m = 0$ and $b_1+b_2+\cdots+b_m = 1$. Assuming the m quantities $-b_i/a_i$ are all distinct, they divide the real line into $m-1$ bounded segments and two unbounded half-rays. One of the bounded segments is $\Theta = \mathrm{f}^{-1}(\Delta)$. The derivative of the log-likelihood function equals

$$\frac{d\ell}{d\theta} \quad = \quad \sum_{i=1}^{m} \frac{u_i a_i}{a_i\theta + b_i}.$$

For positive u_i, this rational function has precisely $m-1$ zeros, one in each of the bounded segments. The maximum likelihood estimate $\widehat{\theta}$ is the unique zero of $d\ell/d\theta$ in the statistically meaningful segment $\Theta = \mathbf{f}^{-1}(\Delta)$.

Example 1.7 Many statistical models used in biology have the property that the polynomials $f_i(\theta)$ are multilinear. The concavity result of Proposition 1.4 is a useful tool for varying the parameters one at a time. Here is such a model with $d = 3$ and $m = 5$. Consider the trilinear map $\mathbf{f} : \mathbb{R}^3 \to \mathbb{R}^5$ given by

$$\begin{aligned}
f_1(\theta) &= -24\theta_1\theta_2\theta_3 + 9\theta_1\theta_2 + 9\theta_1\theta_3 + 9\theta_2\theta_3 - 3\theta_1 - 3\theta_2 - 3\theta_3 + 1 \\
f_2(\theta) &= -48\theta_1\theta_2\theta_3 + 6\theta_1\theta_2 + 6\theta_1\theta_3 + 6\theta_2\theta_3 \\
f_3(\theta) &= 24\theta_1\theta_2\theta_3 + 3\theta_1\theta_2 - 9\theta_1\theta_3 - 9\theta_2\theta_3 + 3\theta_3 \\
f_4(\theta) &= 24\theta_1\theta_2\theta_3 - 9\theta_1\theta_2 + 3\theta_1\theta_3 - 9\theta_2\theta_3 + 3\theta_2 \\
f_5(\theta) &= 24\theta_1\theta_2\theta_3 - 9\theta_1\theta_2 - 9\theta_1\theta_3 + 3\theta_2\theta_3 + 3\theta_1.
\end{aligned}$$

This is a small instance of the *Jukes-Cantor model* of phylogenetics. Its derivation and its relevance for computational biology will be discussed in detail in Chapter 18. Let us fix two of the parameters, say θ_1 and θ_2, and vary only the third parameter θ_3. The result is a linear model as in Example 1.6, with $\theta = \theta_3$. We compute the maximum likelihood estimate $\widehat{\theta}_3$ for this linear model, and then we replace θ_3 by $\widehat{\theta}_3$. Next fix the two parameters θ_2 and θ_3, and vary the third parameter θ_1. Thereafter, fix (θ_3, θ_1) and vary θ_2, etc. Iterating this procedure, we may compute a local maximum of the likelihood function.

1.2.2 Toric Models

Our second class of models with well-behaved likelihood functions are the *toric models*, also known as *exponential families*. Let $A = (a_{ij})$ be a non-negative integer $d \times m$ matrix with the property that all column sums are equal:

$$\sum_{i=1}^{d} a_{i1} \quad = \quad \sum_{i=1}^{d} a_{i2} \quad = \quad \cdots \quad = \quad \sum_{i=1}^{d} a_{im}. \qquad (1.24)$$

The j-th column vector a_j of the matrix A represents the monomial

$$\theta^{a_j} \quad = \quad \prod_{i=1}^{d} \theta_i^{a_{ij}} \qquad \text{for } j = 1, 2, \ldots, n.$$

Our assumption (1.24) says that these monomials all have the same degree. The toric model of A is the image of the orthant $\Theta = \mathbb{R}^d_{>0}$ under the map

$$\mathbf{f} : \mathbb{R}^d \to \mathbb{R}^m, \ \theta \mapsto \frac{1}{\sum_{j=1}^{m} \theta^{a_j}} \cdot \big(\theta^{a_1}, \theta^{a_2}, \ldots, \theta^{a_m}\big). \qquad (1.25)$$

Note that we can scale the parameter vector without changing the image: $\mathbf{f}(\theta) = \mathbf{f}(\lambda \cdot \theta)$. Hence the dimension of the toric model $\mathbf{f}(\mathbb{R}^d_{>0})$ is at most $d - 1$. In fact, the dimension of $\mathbf{f}(\mathbb{R}^d_{>0})$ is one less than the rank of A. The denominator polynomial $\sum_{j=1}^{m} \theta^{a_j}$ is known as the *partition function*.

Sometimes we are also given positive constants $c_1, \ldots, c_m > 0$ and the map $\mathbf{f}$ is modified as follows:

$$\mathbf{f} : \mathbb{R}^d \to \mathbb{R}^m, \quad \theta \mapsto \frac{1}{\sum_{j=1}^{m} c_j \theta^{a_j}} \cdot \big(c_1\theta^{a_1}, c_2\theta^{a_2}, \ldots, c_m\theta^{a_m}\big). \qquad (1.26)$$

In a toric model, the logarithms of the probabilities are linear functions in the logarithms of the parameters θ_i. For that reason, statisticians refer to some toric models as *log-linear models* . For simplicity we stick with the formulation (1.25) but the discussion would be analogous for (1.26).

Maximum likelihood estimation for the toric model (1.25) means solving the following optimization problem

$$\text{Maximize } p_1^{u_1} \cdots p_m^{u_m} \text{ subject to } (p_1, \ldots, p_m) \in \mathbf{f}(\mathbb{R}^d_{>0}). \tag{1.27}$$

This optimization problem is equivalent to

$$\text{Maximize } \theta^{Au} \text{ subject to } \theta \in \mathbb{R}^d_{>0} \text{ and } \sum_{j=1}^{m} \theta^{a_j} \;=\; 1. \tag{1.28}$$

Here we are using multi-index notation for monomials in $\theta = (\theta_1, \ldots, \theta_d)$:

$$\theta^{Au} \;=\; \prod_{i=1}^{d} \prod_{j=1}^{m} \theta_i^{a_{ij}u_j} \;=\; \prod_{i=1}^{d} \theta_i^{a_{i1}u_1 + a_{i2}u_2 + \cdots + a_{im}u_m} \qquad \text{and} \qquad \theta^{a_j} \;=\; \prod_{i=1}^{d} \theta_i^{a_{ij}}.$$

Writing $b = Au$ for the *sufficient statistic*, our optimization problem (1.28) is

$$\text{Maximize } \theta^{b} \text{ subject to } \theta \in \mathbb{R}^d_{>0} \text{ and } \sum_{j=1}^{m} \theta^{a_j} \;=\; 1. \tag{1.29}$$

Example 1.8 Let $d = 2$, $m = 3$, $A = \begin{pmatrix} 2 & 1 & 0 \\ 0 & 1 & 2 \end{pmatrix}$ and $u = (11, 17, 23)$. The sample size is $N = 51$. Our problem is to maximize the likelihood function $\theta_1^{39}\theta_2^{63}$ over all positive real vectors (θ_1, θ_2) that satisfy $\theta_1^2 + \theta_1\theta_2 + \theta_2^2 = 1$. The unique solution $(\hat\theta_1, \hat\theta_2)$ to this problem has coordinates

$$\begin{aligned} \hat\theta_1 &= \frac{1}{51}\sqrt{1428 - 51\sqrt{277}} \;=\; 0.4718898805 \quad \text{and} \\ \hat\theta_2 &= \frac{1}{51}\sqrt{2040 - 51\sqrt{277}} \;=\; 0.6767378938. \end{aligned}$$

The probability distribution corresponding to these parameter values is

$$\hat p \;=\; (\hat p_1, \hat p_2, \hat p_3) \;=\; \big(\hat\theta_1^2, \hat\theta_1\hat\theta_2, \hat\theta_2^2\big) \;=\; \big(0.2227, 0.3193, 0.4580\big).$$

Proposition 1.9 *Fix a toric model A and data $u \in \mathbb{N}^m$ with sample size $N = u_1 + \cdots + u_m$ and sufficient statistic $b = Au$. Let $\widehat{p} = \mathbf{f}(\widehat{\theta})$ be any local maximum for the equivalent optimization problems (1.27),(1.28),(1.29). Then*

$$A \cdot \widehat{p} \quad = \quad \frac{1}{N} \cdot b. \tag{1.30}$$

Writing $\hat p$ as a column vector, we check that (1.30) holds in Example 1.8:

$$A \cdot \hat p \quad = \quad \begin{pmatrix} 2\hat\theta_1^2 + \hat\theta_1\hat\theta_2 \\ \hat\theta_1\hat\theta_2 + 2\hat\theta_2^2 \end{pmatrix} \quad = \quad \frac{1}{51} \cdot \begin{pmatrix} 39 \\ 63 \end{pmatrix} \;=\; \frac{1}{N} \cdot Au.$$

Proof We introduce a *Lagrange multiplier* λ. Every local optimum of (1.29) is a critical point of the following function in $d+1$ unknowns $\theta_1, \ldots, \theta_d, \lambda$:

$$\theta^b \; + \; \lambda \cdot \big(1 - \sum_{j=1}^{m} \theta^{a_j}\big).$$

We apply the scaled gradient operator

$$\theta \cdot \nabla_\theta \quad = \quad \big(\theta_1 \frac{\partial}{\partial \theta_1}, \, \theta_2 \frac{\partial}{\partial \theta_2}, \, \ldots, \, \theta_d \frac{\partial}{\partial \theta_d}\big)$$

to the function above. The resulting critical equations for $\widehat{\theta}$ and $\widehat{p}$ state that

$$(\widehat{\theta})^b \cdot b \quad = \quad \lambda \cdot \sum_{j=1}^{m} (\widehat{\theta})^{a_j} \cdot a_j \quad = \quad \lambda \cdot A \cdot \widehat{p}.$$

This says that the vector $A \cdot \widehat{p}$ is a scalar multiple of the vector $b = Au$. Since the matrix A has the vector $(1, 1, \ldots, 1)$ in its row space, and since $\sum_{j=1}^m \widehat{p}_j = 1$, it follows that the scalar factor which relates the sufficient statistic $b = A \cdot u$ to $A \cdot \widehat{p}$ must be the sample size $\sum_{j=1}^m u_j = N$. $\square$

Given the matrix $A \in \mathbb{N}^{d \times m}$ and any vector $b \in \mathbb{R}^d$, we consider the set

$$P_A(b) \quad = \quad \big\{ p \in \mathbb{R}^m \; : \; A \cdot p = \frac{1}{N} \cdot b \;\text{ and }\; p_j > 0 \;\text{ for all } j \; \big\}.$$

This is a relatively open *polytope*. (See Section 2.3 for an introduction to polytopes). We shall prove that $P_A(b)$ is either empty or meets the toric model in precisely one point. This result was discovered and re-discovered many times by different people from various communities. In toric geometry, it goes under the keyword "moment map". In the statistical setting of exponential families, it appears in the work of Birch in the 1960's. See [Agresti, 1990, page 168].

Theorem 1.10 (Birch's Theorem) *Fix a toric model A and let $u \in \mathbb{N}^m_{>0}$ be a strictly positive data vector with sufficient statistic $b = Au$. The intersection of the polytope $P_A(b)$ with the toric model $\mathbf{f}(\mathbb{R}^d_{>0})$ consists of precisely one point. That point is the maximum likelihood estimate $\widehat{p}$ for the data u.*

Proof Consider the *entropy function*

$$H \; : \; \mathbb{R}^m_{\geq 0} \to \mathbb{R}_{\geq 0} \; , \quad (p_1, \ldots, p_m) \mapsto -\sum_{i=1}^{m} p_i \cdot \log(p_i).$$

This function is well-defined for nonnegative vectors because $p_i \cdot \log(p_i)$ is 0 for $p_i = 0$. The entropy function H is strictly concave in $\mathbb{R}^m_{>0}$, i.e.,

$$H\big(\lambda \cdot p + (1-\lambda) \cdot q\big) \;\; > \;\; \lambda \cdot H(p) \, + \, (1-\lambda) \cdot H(q) \quad \text{for } p \neq q \text{ and } 0 < \lambda < 1,$$

because the Hessian matrix $\big(\partial^2 H / \partial p_i \partial p_j\big)$ is a diagonal matrix, with diagonal entries $-1/p_1, -1/p_2, \ldots, -1/p_m$. The restriction of the entropy function H to the relatively open polytope $P_A\big(\frac{1}{N} \cdot b\big)$ is strictly concave as well, so it attains its maximum at a unique point $p^* = p^*(b)$ in the polytope $P_A\big(\frac{1}{N} \cdot b\big)$.

For any vector $u \in \mathbb{R}^m$ which lies in the kernel of A, the directional derivative of the entropy function H vanishes at the point $p^* = (p_1^*, \ldots, p_m^*)$:

$$u_1 \cdot \frac{\partial H}{\partial p_1}(p^*) \,+\, u_2 \cdot \frac{\partial H}{\partial p_2}(p^*) \,+\, \cdots \,+\, u_m \cdot \frac{\partial H}{\partial p_m}(p^*) \quad = \quad 0. \tag{1.31}$$

Since the derivative of $x \cdot \log(x)$ is $\log(x) + 1$, and since $(1, 1, \ldots, 1)$ is in the row span of the matrix A, the equation (1.31) implies

$$0 \;=\; \sum_{j=1}^{m} u_j \cdot \log(p_j^*) + \sum_{j=1}^{m} u_j \;=\; \sum_{j=1}^{m} u_j \cdot \log(p_j^*) \quad \text{for all } u \in \text{kernel}(A). \tag{1.32}$$

This implies that $\big(\log(p_1^*), \log(p_2^*), \ldots, \log(p_m^*)\big)$ lies in the row span of A. Pick a vector $\eta^* = (\eta_1^*, \ldots, \eta_d^*)$ such that $\sum_{i=1}^{d} \eta_i^* a_{ij} \;=\; \log(p_j^*)$ for all j. If we set $\theta_i^* = \exp(\eta_i^*)$ for $i = 1, \ldots, d$ then

$$p_j^* \;=\; \prod_{i=1}^{d} \exp(\eta_i^* a_{ij}) \;=\; \prod_{i=1}^{d} (\theta_i^*)^{a_{ij}} \;=\; \theta^* a_j \qquad \text{for } j = 1, 2, \ldots, m.$$

This shows that $p^* = \mathbf{f}(\theta^*)$ for some $\theta^* \in \mathbb{R}^d_{>0}$, so p^* lies in the toric model. Moreover, if A has rank d then θ^* is uniquely determined (up to scaling) by $p^* = \mathbf{f}(\theta)$. We have shown that p^* is a point in the intersection $P_A\big(\frac{1}{N} b\big) \cap \mathbf{f}(\mathbb{R}^d_{>0})$.

It remains to be seen that there is no other point. Suppose that q lies in $P_A\big(\frac{1}{N} b\big) \cap \mathbf{f}(\mathbb{R}^d_{>0})$. Then (1.32) holds, so that q is a critical point of the entropy function H. Since the Hessian matrix is negative definite at q, this point is a maximum of the strictly concave function H, and therefore $q = p^*$.

Let $\widehat{\theta}$ be a maximum likelihood estimate for the data u and let $\widehat{p} = \mathbf{f}(\widehat{\theta})$ be the corresponding probability distribution. Proposition 1.9 tells us that $\widehat{p}$ lies in $P_A(b)$. The uniqueness property in the previous paragraph implies $\widehat{p} \,=\, p^*$ and, assuming A has rank d, we can further conclude $\widehat{\theta} \,=\, \theta^*$. $\square$

Example 1.11 (Example 1.8 continued) Let $d \,=\, 2$, $m \,=\, 3$ and $A \,=\, \begin{pmatrix} 2 & 1 & 0 \\ 0 & 1 & 2 \end{pmatrix}$. If b_1 and b_2 are positive reals then the polytope $P_A(b_1, b_2)$ is a line segment. The maximum likelihood point $\widehat{p}$ is characterized by the equations

$$2\widehat{p}_1 + \widehat{p}_2 \;=\; \frac{1}{N} \cdot b_1 \;\text{ and }\; \widehat{p}_2 + 2\widehat{p}_3 \;=\; \frac{1}{N} \cdot b_2 \;\text{ and }\; \widehat{p}_1 \cdot \widehat{p}_3 \;=\; \widehat{p}_2 \cdot \widehat{p}_2.$$

The unique positive solution to these equations equals

$$\begin{aligned}
\widehat{p}_1 &= \tfrac{1}{N} \cdot \bigl(\tfrac{7}{12} b_1 + \tfrac{1}{12} b_2 - \tfrac{1}{12}\sqrt{{b_1}^2 + 14\, b_1 b_2 + {b_2}^2}\bigr),\\
\widehat{p}_2 &= \tfrac{1}{N} \cdot \bigl(-\tfrac{1}{6} b_1 - \tfrac{1}{6} b_2 + \tfrac{1}{6}\sqrt{{b_1}^2 + 14\, b_1 b_2 + {b_2}^2}\bigr),\\
\widehat{p}_3 &= \tfrac{1}{N} \cdot \bigl(\tfrac{1}{12} b_1 + \tfrac{1}{12} b_2 - \tfrac{1}{12}\sqrt{{b_1}^2 + 14\, b_1 b_2 + {b_2}^2}\bigr).
\end{aligned}$$

The most classical example of a toric model in statistics is the *independence model* for two random variables. Let X_1 be a random variable on $[m_1]$ and X_2 a random variable on $[m_2]$. The two random variables are *independent* if

$$\mathrm{Prob}(X_1 = i, X_2 = j) \quad = \quad \mathrm{Prob}(X_1 = i) \cdot \mathrm{Prob}(X_2 = j).$$

Using the abbreviation $p_{ij} = \mathrm{Prob}(X_1 = i, X_2 = j)$, we rewrite this as

$$p_{ij} \quad = \quad \Bigl(\sum_{\nu=1}^{m_2} p_{i\nu}\Bigr) \cdot \Bigl(\sum_{\mu=1}^{m_1} p_{\mu j}\Bigr) \qquad \text{for all } i \in [m_1], j \in [m_2].$$

The independence model is a toric model with $m = m_1 \cdot m_2$ and $d = m_1 + m_2$. Let Δ be the $(m-1)$-dimensional simplex (with coordinates p_{ij}) consisting of all joint probability distributions. A point $p \in \Delta$ lies in the image of the map

$$\mathbf{f} \,:\, \mathbb{R}^d \to \mathbb{R}^m, \ (\theta_1, \ldots, \theta_d) \mapsto \frac{1}{\sum_{ij} \theta_i \theta_{j+m_1}} \cdot \bigl(\theta_i \theta_{j+m_1}\bigr)_{i \in [m_1], j \in [m_2]}$$

if and only if X_1 and X_2 are independent if and only if the $m_1 \times m_2$ matrix (p_{ij}) has rank one. The map $\mathbf{f}$ can be represented by a $d \times m$ matrix A whose entries are in $\{0, 1\}$, with precisely two ones per column. Here is an example.

Example 1.12 As an illustration consider the independence model for a binary random variable and a ternary random variable $(m_1 = 2, m_2 = 3)$. Here

$$A \quad = \quad \begin{array}{c} \\ \theta_1 \\ \theta_2 \\ \theta_3 \\ \theta_4 \\ \theta_5 \end{array} \!\!\begin{array}{c} \begin{array}{cccccc} p_{11} & p_{12} & p_{13} & p_{21} & p_{22} & p_{23} \end{array} \\ \begin{pmatrix} 1 & 1 & 1 & 0 & 0 & 0 \\ 0 & 0 & 0 & 1 & 1 & 1 \\ 1 & 0 & 0 & 1 & 0 & 0 \\ 0 & 1 & 0 & 0 & 1 & 0 \\ 0 & 0 & 1 & 0 & 0 & 1 \end{pmatrix} \end{array}$$

This matrix A encodes the rational map $\mathbf{f} : \mathbb{R}^5 \to \mathbb{R}^{2\times 3}$ given by

$$(\theta_1, \theta_2; \theta_3, \theta_4, \theta_5) \quad \mapsto \quad \frac{1}{(\theta_1 + \theta_2)(\theta_3 + \theta_4 + \theta_5)} \cdot \begin{pmatrix} \theta_1\theta_3 & \theta_1\theta_4 & \theta_1\theta_5 \\ \theta_2\theta_3 & \theta_2\theta_4 & \theta_2\theta_5 \end{pmatrix}.$$

Note that $\mathbf{f}(\mathbb{R}^5_{>0})$ consists of all positive 2×3 matrices of rank 1 whose entries sum to 1. The effective dimension of this model is three, which is one less than the rank of A. We can represent this model with only three parameters $(\theta_1, \theta_3, \theta_4)$, ranging over $\Theta = (0, 1)^3$, by setting $\theta_2 = 1 - \theta_1$ and $\theta_5 = 1 - \theta_3 - \theta_4$.

Maximum likelihood estimation for the independence model is easy: the optimal parameters are the normalized row and column sums of the data matrix.

Proposition 1.13 *Let $u = (u_{ij})$ be an $m_1 \times m_2$ matrix of positive integers. Then the maximum likelihood parameters $\widehat{\theta}$ for these data in the independence model are given by the normalized row and column sums of the matrix:*

$$\widehat{\theta}_\mu = \frac{1}{N} \cdot \sum_{\nu \in [m_2]} u_{\mu\nu} \quad \textit{and} \quad \widehat{\theta}_{\nu+m_1} = \frac{1}{N} \cdot \sum_{\mu \in [m_1]} u_{\mu\nu} \qquad \textit{for } \mu \in [m_1],\ \nu \in [m_2].$$

Proof We present the proof for the case $m_1 = 2, m_2 = 3$ in Example 1.12. The general case is completely analogous. Consider the reduced parameterization

$$\mathbf{f}(\theta) \quad = \quad \begin{pmatrix} \theta_1\theta_3 & \theta_1\theta_4 & \theta_1(1-\theta_3-\theta_4) \\ (1-\theta_1)\theta_3 & (1-\theta_1)\theta_4 & (1-\theta_1)(1-\theta_3-\theta_4) \end{pmatrix}.$$

The log-likelihood function equals

$$\ell(\theta) \quad = \quad (u_{11}+u_{12}+u_{13}) \cdot \log(\theta_1) \;+\; (u_{21}+u_{22}+u_{23}) \cdot \log(1-\theta_1)$$
$$+(u_{11}+u_{21}) \cdot \log(\theta_3) + (u_{12}+u_{22}) \cdot \log(\theta_4) + (u_{13}+u_{23}) \cdot \log(1-\theta_3-\theta_4).$$

Taking the derivative of $\ell(\theta)$ with respect to θ_1 gives

$$\frac{\partial \ell}{\partial \theta_1} \quad = \quad \frac{u_{11}+u_{12}+u_{13}}{\theta_1} - \frac{u_{21}+u_{22}+u_{23}}{1-\theta_1}.$$

Setting this expression to zero, we find that

$$\widehat{\theta}_1 \quad = \quad \frac{u_{11}+u_{12}+u_{13}}{u_{11}+u_{12}+u_{13}+u_{21}+u_{22}+u_{23}} \quad = \quad \frac{1}{N} \cdot (u_{11}+u_{12}+u_{13}).$$

Similarly, by setting $\partial\ell/\partial\theta_3$ and $\partial\ell/\partial\theta_4$ to zero, we get

$$\widehat{\theta}_3 \quad = \quad \frac{1}{N} \cdot (u_{11}+u_{21}) \qquad \text{and} \qquad \widehat{\theta}_4 \quad = \quad \frac{1}{N} \cdot (u_{12}+u_{22}). \qquad \square$$

1.3 Expectation maximization

In the last section we saw that linear models and toric models enjoy the property that the likelihood function has at most one local maximum. Unfortunately, this property fails for most other algebraic statistical models, including the ones that are actually used in computational biology. A simple example of a model whose likelihood function has multiple local maxima will be featured in this section. For many models that are neither linear nor toric, statisticians use a numerical optimization technique called *Expectation-Maximization* (or *EM* for short) for maximizing the likelihood function. This technique is known to perform well on many problems of practical interest. However, it must be emphasized that EM is not guaranteed to reach a global maximum.

Under some conditions, it will converge to a local maximum of the likelihood function, but sometimes even this fails, as we shall see in our little example.

We introduce Expectation-Maximization for the following class of algebraic statistical models. Let $F = \big(f_{ij}(\theta)\big)$ be an $m \times n$ matrix of polynomials (or rational functions, as in the toric case) in the unknown parameters $\theta = (\theta_1, \ldots, \theta_d)$. We assume that the sum of all the $f_{ij}(\theta)$ equals the constant 1, and there exists an open subset $\Theta \subset \mathbb{R}^d$ of admissible parameters such that $f_{ij}(\theta) > 0$ for all $\theta \in \Theta$. We identify the matrix F with the polynomial map $F : \mathbb{R}^d \to \mathbb{R}^{m\times n}$ whose coordinates are the $f_{ij}(\theta)$. Here $\mathbb{R}^{m\times n}$ denotes the mn-dimensional real vector space consisting of all $m \times n$ matrices. We shall refer to F as the *hidden model* or the *complete data model.*

The key assumption we make about the hidden model F is that it has an easy and reliable algorithm for solving the maximum likelihood problem (1.19). For instance, F could be a linear model or a toric model, so that the likelihood function has at most one local maximum in Θ, and that this global maximum can be found efficiently and reliably using the techniques of convex optimization. For special toric models, such as the independence model and certain Markov models, there are simple explicit formulas for the maximum likelihood estimates. See Propositions 1.13, 1.17 and 1.18 for such formulas.

Consider the linear map which takes an $m\times n$ matrix to its vector of row sums

$$\rho \,:\, \mathbb{R}^{m\times n} \to \mathbb{R}^m\,, \quad G = (g_{ij}) \;\mapsto\; \Big(\sum_{j=1}^n g_{1j}, \sum_{j=1}^n g_{2j}, \ldots, \sum_{j=1}^n g_{mj}\Big).$$

The *observed model* is the composition $\mathbf{f} = \rho\circ F$ of the hidden model F and the *marginalization map* ρ. The observed model is the one we really care about:

$$\mathbf{f} \,:\, \mathbb{R}^d \to \mathbb{R}^m\,, \quad \theta \;\mapsto\; \Big(\sum_{j=1}^n f_{1j}(\theta), \sum_{j=1}^n f_{2j}(\theta), \ldots, \sum_{j=1}^n f_{mj}(\theta)\Big). \tag{1.33}$$

Hence $f_i(\theta) = \sum_{j=1}^m f_{ij}(\theta)$. The model $\mathbf{f}$ is also known as *partial data model.*

Suppose we are given a vector $u = (u_1, u_2, \ldots, u_m) \in \mathbb{N}^m$ of data for the observed model $\mathbf{f}$. Our problem is to maximize the likelihood function for these data with respect to the observed model:

$$\text{maximize} \;\; L_{obs}(\theta) \;=\; f_1(\theta)^{u_1} f_2(\theta)^{u_2} \cdots f_m(\theta)^{u_m} \quad \text{subject to } \theta \in \Theta. \tag{1.34}$$

This is a hard problem, for instance, because of multiple local solutions. Suppose we have no idea how to solve (1.34). It would be much easier to solve the corresponding problem for the hidden model F instead:

$$\text{maximize} \;\; L_{hid}(\theta) \;=\; f_{11}(\theta)^{u_{11}} \cdots f_{mn}(\theta)^{u_{mn}} \quad \text{subject to} \;\; \theta \in \Theta. \tag{1.35}$$

The trouble is, however, that we do not know the *hidden data*, that is, we do not know the matrix $U = (u_{ij}) \in \mathbb{N}^{m \times n}$. All we know about the matrix U is that its row sums are equal to the data we do know, in symbols, $\rho(U) = u$.

The idea of the EM algorithm is as follows. We start with some initial guess what the parameter vector θ might be. Then we make an estimate, given θ, of what we expect the hidden data U should be. This latter step is called the *expectation step* (or *E-step* for short). Note that the expected values for the hidden data vector to not have to be integers. Next we solve the problem (1.35) to optimality, using the easy and reliable subroutine which we assumed is available for the hidden model F. This step is called the *maximization step* (or *M-step* for short). Let θ^* be the optimal solution found in the M-step. We then replace the old parameter guess θ by the new and improved parameter guess θ^*, and we iterate the process $\mathrm{E} \rightarrow \mathrm{M} \rightarrow \mathrm{E} \rightarrow \mathrm{M} \rightarrow \mathrm{E} \rightarrow \mathrm{M} \rightarrow \cdots$ until we are satisfied. Of course, what needs to be shown is that the likelihood function increases during this process and that the sequence of parameter guesses θ converges to a local maximum of $L_{obs}(\theta)$. We present the formal statement of EM algorithm in Algorithm 1.14. As before, it is more convenient to work with log-likelihood functions instead of the likelihood functions, and we abbreviate

$$\ell_{obs}(\theta) \;:=\; \log\bigl(L_{obs}(\theta)\bigr) \qquad \text{and} \qquad \ell_{hid}(\theta) \;:=\; \log\bigl(L_{hid}(\theta)\bigr).$$

Algorithm 1.14 (EM Algorithm)
Input: An $m \times n$ matrix of polynomials $f_{ij}(\theta)$ representing the hidden model F and observed data $u \in \mathbb{N}^m$.
Output: A proposed maximum $\widehat{\theta} \in \Theta \subset \mathbb{R}^d$ of the log-likelihood function $\ell_{obs}(\theta)$ for the observed model $\mathbf{f}$.

Step 0: Select a threshold $\epsilon > 0$ and select starting parameters $\theta \in \Theta$ satisfying $f_{ij}(\theta) > 0$ for all i, j.
E-Step: Define the *expected hidden data matrix* $U = (u_{ij}) \in \mathbb{R}^{m \times n}$ by

$$u_{ij} \quad := \quad u_i \cdot \frac{f_{ij}(\theta)}{\sum_{j=1}^{m} f_{ij}(\theta)} \quad = \quad \frac{u_i}{f_i(\theta)} \cdot f_{ij}(\theta).$$

M-Step: Compute the solution $\theta^* \in \Theta$ to the maximum likelihood problem (1.35) for the hidden model $F = (f_{ij})$.
Step 3: If $\ell_{obs}(\theta^*) - \ell_{obs}(\theta) > \epsilon$ then set $\theta := \theta^*$ and go back to the E-Step.
Step 4: Output the parameter vector $\widehat{\theta} := \theta^*$ and the corresponding probability distribution $\widehat{p} = f(\widehat{\theta})$ on the set $[m]$.

The justification for this algorithm is given by the following theorem.

Theorem 1.15 *The value of the likelihood function increases during each iteration of the EM algorithm, namely, if θ is chosen in the open set Θ prior to* *the E-step and θ^* is computed by one E-step and one M-step then $L_{obs}(\theta) \leq L_{obs}(\theta^*)$. Equality holds if θ is a local maximum of the likelihood function.*

Proof We use the following fact about the logarithm of a positive number x:

$$\log(x) \leq x - 1 \quad \text{with equality if and only if} \quad x = 1. \tag{1.36}$$

Let $u \in \mathbb{N}^n$ and $\theta \in \Theta$ be given prior to the E-step, let $U = (u_{ij})$ be the matrix computed in the E-step, and let $\theta^* \in \Theta$ be the vector computed in the subsequent M-step. We consider the difference between the values at θ^* and θ of the log-likelihood function of the observed model:

$$\begin{aligned}\ell_{obs}(\theta^*) - \ell_{obs}(\theta) &= \sum_{i=1}^{m} u_i \cdot \big[\log(f_i(\theta^*)) - \log(f_i(\theta))\big] \\ &= \sum_{i=1}^{m}\sum_{j=1}^{n} u_{ij} \cdot \big[\log(f_{ij}(\theta^*)) - \log(f_{ij}(\theta))\big] \\ &\quad + \sum_{i=1}^{m} u_i \cdot \left(\log\big(\frac{f_i(\theta^*)}{f_i(\theta)}\big) - \sum_{j=1}^{n} \frac{u_{ij}}{u_i} \cdot \log\big(\frac{f_{ij}(\theta^*)}{f_{ij}(\theta)}\big)\right).\end{aligned}$$

The double-sum in the middle equals $\ell_{hid}(\theta^*) - \ell_{hid}(\theta)$. This difference is non-negative because the parameter vector θ^* was chosen so as to maximize the log-likelihood function for the hidden model with data (u_{ij}). We next show that the last sum is non-negative as well. The parenthesized expression equals

$$\log\big(\frac{f_i(\theta^*)}{f_i(\theta)}\big) - \sum_{j=1}^{n} \frac{u_{ij}}{u_i} \log\big(\frac{f_{ij}(\theta^*)}{f_{ij}(\theta)}\big) = \log\big(\frac{f_i(\theta^*)}{f_i(\theta)}\big) + \sum_{j=1}^{n} \frac{f_{ij}(\theta)}{f_i(\theta)} \log\big(\frac{f_{ij}(\theta)}{f_{ij}(\theta^*)}\big).$$

We rewrite this expression as follows

$$\begin{aligned} &\textstyle\sum_{j=1}^{n} \frac{f_{ij}(\theta)}{f_i(\theta)} \cdot \log\big(\frac{f_i(\theta^*)}{f_i(\theta)}\big) + \sum_{j=1}^{n} \frac{f_{ij}(\theta)}{f_i(\theta)} \cdot \log\big(\frac{f_{ij}(\theta)}{f_{ij}(\theta^*)}\big) \\ = \quad &\textstyle\sum_{j=1}^{n} \frac{f_{ij}(\theta)}{f_i(\theta)} \cdot \log\big(\frac{f_i(\theta^*)}{f_{ij}(\theta^*)} \cdot \frac{f_{ij}(\theta)}{f_i(\theta)}\big). \end{aligned} \tag{1.37}$$

This last expression is non-negative. This can be seen as follows. Consider the non-negative quantities

$$\pi_j = \frac{f_{ij}(\theta)}{f_i(\theta)} \quad \text{and} \quad \sigma_j = \frac{f_{ij}(\theta^*)}{f_i(\theta^*)} \qquad \text{for } j = 1, 2, \ldots, n.$$

We have $\pi_1 + \cdots + \pi_n = \sigma_1 + \cdots + i_n = 1$, so the vectors π and σ can be regarded as probability distributions on the set $[n]$. The expression (1.37) equals the *Kullback-Leibler distance* between these two probability distributions:

$$H(\pi||\sigma) = \sum_{j=1}^{n} (-\pi_j) \cdot \log\big(\frac{\sigma_j}{\pi_j}\big) \geq \sum_{j=1}^{n} (-\pi_j) \cdot (1 - \frac{\sigma_j}{\pi_j}) = 0. \tag{1.38}$$

The inequality follows from (1.36). Equality holds in (1.38) if and only if $\pi = \sigma$.

By applying a Taylor expansion argument to the difference $\ell_{obs}(\theta^*) - \ell_{obs}(\theta)$, one sees that every local maximum of the log-likelihood function is a stationary point of the EM algorithm, and, moreover, every stationary point of the EM algorithm must be a critical point of the log-likelihood function [Wu and Jeff, 1983]. □

The remainder of this section is devoted to a simple example which will illustrate the EM algorithm and the issue of multiple local maxima for $\ell(\theta)$.

Example 1.16 Our data are two DNA sequences of length 40:

$$\begin{array}{c}\texttt{ATCACCAAACATTGGGATGCCTGTGCATTTGCAAGCGGCT}\\ \texttt{ATGAGTCTTAAACGCTGGCCATGTGCCATCTTAGACAGCG}\end{array} \qquad (1.39)$$

We wish to test the hypothesis that these two sequences were generated by DiaNA using one biased coin and four tetrahedral dice, each with four faces labeled by the letters `A`, `C`, `G` and `T`. Two of her dice are in her left pocket, and the other two dice are in her right pocket. Our model states that DiaNA generated each column of this alignment independently by the following process. She first tosses her coin. If the coin comes up heads, she rolls the two dice in her left pocket, and if the coin comes up tails she rolls the two dice in her right pocket. In either case DiaNA reads off the column of the alignment from the two dice she rolled. All dice have a different color, so she knows which of the dice correspond to the first and second sequences.

To represent this model algebraically, we introduce the vector of parameters

$$\theta \quad = \quad \big(\pi,\, \lambda^1_{\texttt{A}}, \lambda^1_{\texttt{C}}, \lambda^1_{\texttt{G}}, \lambda^1_{\texttt{T}},\, \lambda^2_{\texttt{A}}, \lambda^2_{\texttt{C}}, \lambda^2_{\texttt{G}}, \lambda^2_{\texttt{T}},\, \rho^1_{\texttt{A}}, \rho^1_{\texttt{C}}, \rho^1_{\texttt{G}}, \rho^1_{\texttt{T}},\, \rho^2_{\texttt{A}}, \rho^2_{\texttt{C}}, \rho^2_{\texttt{G}}, \rho^2_{\texttt{T}}\big).$$

The parameter π represents the probability that DiaNA's coin comes up heads. The parameter λ^i_j represents the probability that the i-th dice in her left pocket comes up with nucleotide j. The parameter ρ^i_j represents the probability that the i-th dice in her right pocket comes up with nucleotide j. In total there are $d = 13$ free parameters because

$$\lambda^i_{\texttt{A}} + \lambda^i_{\texttt{C}} + \lambda^i_{\texttt{G}} + \lambda^i_{\texttt{T}} \quad = \quad \rho^i_{\texttt{A}} + \rho^i_{\texttt{C}} + \rho^i_{\texttt{G}} + \rho^i_{\texttt{T}} \quad = \quad 1 \qquad \text{for } i = 1, 2.$$

More precisely, the parameter space in this example is a product of simplices

$$\Theta \quad = \quad \Delta_1 \,\times\, \Delta_3 \times \Delta_3 \,\times\, \Delta_3 \times \Delta_3.$$

The model is given by the polynomial map

$$\mathbf{f} \;:\; \mathbb{R}^{13} \to \mathbb{R}^{4\times 4},\; \theta \mapsto (f_{ij}) \quad \text{where} \quad f_{ij} \;=\; \pi\cdot\lambda^1_i\cdot\lambda^2_j + (1{-}\pi)\cdot\rho^1_i\cdot\rho^2_j. \quad (1.40)$$

The image of $\mathbf{f}$ is an 11-dimensional algebraic variety in the 15-dimensional probability simplex Δ, namely, $\mathbf{f}(\Theta)$ consists of all non-negative 4×4 matrices of rank at most two having coordinate sum 1. The difference in dimensions (11 versus 13) means that this model is *non-identifiable*: the preimage $\mathbf{f}^{-1}(v)$ of a rank 2 matrix $v \in \mathbf{f}(\Theta)$ is a surface in the parameters space Θ.

Now consider the given alignment (1.39). Each pair of distinct nucleotides occurs in precisely two columns. For instance, the pair `CG` occurs in the third and fifth columns of (1.39). Each of the four identical pairs of nucleotides (namely `AA`, `CC`, `GG` and `TT`) occurs in precisely four columns of the alignment. We summarize our data in the following 4×4 matrix of counts:

$$u \quad = \quad \begin{array}{c|cccc} & \mathtt{A} & \mathtt{C} & \mathtt{G} & \mathtt{T} \\ \hline \mathtt{A} & 4 & 2 & 2 & 2 \\ \mathtt{C} & 2 & 4 & 2 & 2 \\ \mathtt{G} & 2 & 2 & 4 & 2 \\ \mathtt{T} & 2 & 2 & 2 & 4 \end{array}. \qquad (1.41)$$

Our goal is to find parameters θ which maximize the log-likelihood function

$$\ell_{obs}(\theta) \quad = \quad 4 \cdot \sum_i \log(f_{ii}(\theta)) \, + \, 2 \cdot \sum_{i \neq j} \log(f_{ij}(\theta)),$$

Here the summation indices i, j range over $\{\mathtt{A}, \mathtt{C}, \mathtt{G}, \mathtt{T}\}$. Maximizing $\ell_{obs}(\theta)$ means finding a 4×4 matrix $\mathbf{f}(\theta)$ of rank 2 that is close (in the statistical sense of maximum likelihood) to the empirical distribution $(1/40) \cdot u$.

We apply the EM algorithm to this problem. The hidden data is the decomposition of the given alignment into two subalignments according to the contributions made by dice from DiaNA's left and right pocket respectively:

$$u_{ij} \quad = \quad u^l_{ij} + u^r_{ij} \qquad \text{for all} \quad i, j \in \{\mathtt{A}, \mathtt{C}, \mathtt{G}, \mathtt{T}\}.$$

The hidden model equals

$$F : \mathbb{R}^{13} \rightarrow \mathbb{R}^{2 \times 4 \times 4}, \;\; \theta \mapsto (f^l_{ij}, f^r_{ij})$$
$$\text{where} \quad f^l_{ij} \; = \; \pi \cdot \lambda^1_i \cdot \lambda^2_j \quad \text{and} \quad f^r_{ij} \; = \; (1 - \pi) \cdot \rho^1_i \cdot \rho^2_i.$$

The hidden model consists of two copies of the independence model for two random variables on $\{\mathtt{A}, \mathtt{C}, \mathtt{G}, \mathtt{T}\}$, one copy for left and the other copy for right. In light of Proposition 1.13, it is easy to maximize the hidden likelihood function $L_{hid}(\theta)$: we just need to divide the row and column sums of the hidden data matrices by the grand total. This is the M-step in our algorithm.

The EM algorithm starts in Step 0 by selecting a vector of initial parameters

$$\theta \, = \, \big(\pi, (\lambda^1_{\mathtt{A}}, \lambda^1_{\mathtt{C}}, \lambda^1_{\mathtt{G}}, \lambda^1_{\mathtt{T}}), (\lambda^2_{\mathtt{A}}, \lambda^2_{\mathtt{C}}, \lambda^2_{\mathtt{G}}, \lambda^2_{\mathtt{T}}), (\rho^1_{\mathtt{A}}, \rho^1_{\mathtt{C}}, \rho^1_{\mathtt{G}}, \rho^1_{\mathtt{T}}), (\rho^2_{\mathtt{A}}, \rho^2_{\mathtt{C}}, \rho^2_{\mathtt{G}}, \rho^2_{\mathtt{T}})\big). \quad (1.42)$$

Then the current value of the log-likelihood function equals

$$\ell_{obs}(\theta) \quad = \quad \sum_{ij} u_{ij} \cdot \log\big(\pi \cdot \lambda^1_i \cdot \lambda^2_j + (1 - \pi) \cdot \rho^1_i \cdot \rho^2_j\big). \qquad (1.43)$$

In the E-step we compute the expected hidden data by the following formulas:

$$u^l_{ij} \quad := \quad u_{ij} \cdot \frac{\pi \cdot \lambda^1_i \cdot \lambda^2_j}{\pi \cdot \lambda^1_i \cdot \lambda^2_j + (1-\pi) \cdot \rho^1_i \cdot \rho^2_j} \qquad \text{for } i,j \in \{\mathtt{A},\mathtt{C},\mathtt{G},\mathtt{T}\},$$

$$u^r_{ij} \quad := \quad u_{ij} \cdot \frac{(1-\pi) \cdot \rho^1_i \cdot \rho^2_j}{\pi \cdot \lambda^1_i \cdot \lambda^2_j + (1-\pi) \cdot \rho^1_i \cdot \rho^2_j} \qquad \text{for } i,j \in \{\mathtt{A},\mathtt{C},\mathtt{G},\mathtt{T}\}.$$

In the subsequent M-step we now compute the maximum likelihood parameters $\theta^* = \big(\pi^*, \lambda^{1*}_{\mathtt{A}}, \lambda^{1*}_{\mathtt{C}}, \ldots, \rho^{2*}_{\mathtt{T}}\big)$ for the hidden model F. This is done by taking row sums and column sums of the matrix (u^l_{ij}) and the matrix (u^r_{ij}), and by defining the next parameters π to be the relative total counts of these two matrices. In symbols, in the M-step we perform the following computations:

$$\begin{array}{rl} \pi^* = \frac{1}{N} \cdot \sum_{ij} u^l_{ij}, & \\ \lambda^{1*}_i = \frac{1}{N} \cdot \sum_j u^l_{ij} \quad \text{and} \quad \rho^{1*}_i = \frac{1}{N} \cdot \sum_j u^r_{ij} & \text{for} \quad i \in \{\mathtt{A},\mathtt{C},\mathtt{G},\mathtt{T}\}, \\ \lambda^{2*}_j = \frac{1}{N} \cdot \sum_i u^l_{ij} \quad \text{and} \quad \rho^{2*}_j = \frac{1}{N} \cdot \sum_i u^r_{ij} & \text{for} \quad j \in \{\mathtt{A},\mathtt{C},\mathtt{G},\mathtt{T}\}. \end{array}$$

Here $N = \sum_{ij} u_{ij} = \sum_{ij} u^l_{ij} + \sum_{ij} u^r_{ij}$ is the sample size of the data.

After we are done with the M-step, the new value $\ell_{obs}(\theta^*)$ of the likelihood function is computed, using the formula (1.43). If $\ell_{obs}(\theta^*) - \ell_{obs}(\theta)$ is small enough then we stop and output the vector $\widehat{\theta} = \theta^*$ and the corresponding 4×4 matrix $\mathbf{f}(\widehat{\theta})$. Otherwise we set $\theta = \theta^*$ and return to the E-step.

Here are four numerical examples for the data (1.41) with sample size $N = 40$. In each of our experiments, the starting vector θ is indexed as in (1.42).

Experiment 1: We pick uniform starting parameters

$$\begin{array}{rcl} \theta & = & \big(0.5, \quad (0.25, 0.25, 0.25, 0.25), (0.25, 0.25, 0.25, 0.25), \\ & & \qquad (0.25, 0.25, 0.25, 0.25), (0.25, 0.25, 0.25, 0.25)\big). \end{array}$$

The parameter vector θ is a stationary point of the EM algorithm, so after one step we output $\widehat{\theta} = \theta$. The resulting estimated probability distribution on pairs of nucleotides is the uniform distribution

$$\mathbf{f}(\widehat{\theta}) \quad = \quad \frac{1}{16} \begin{pmatrix} 1 & 1 & 1 & 1 \\ 1 & 1 & 1 & 1 \\ 1 & 1 & 1 & 1 \\ 1 & 1 & 1 & 1 \end{pmatrix}, \qquad \ell_{obs}(\widehat{\theta}) \quad = \quad -110.903548889592\ldots$$

Here $\widehat{\theta}$ is a critical point of the log-likelihood function $\ell_{obs}(\theta)$ but it is not a local maximum. The Hessian matrix of $\ell_{obs}(\theta)$ evaluated at $\widehat{\theta}$ has both positive and negative eigenvalues. The characteristic polynomial of the Hessian equals

$$z(z-64)(z-16)^2(z+16)^2(z+64)(z+80)^4(z+320)^2.$$

Experiment 2: We decrease the starting parameter $\lambda^1_{\mathtt{A}}$ and we increase $\lambda^1_{\mathtt{C}}$:

$$\begin{aligned}\theta \quad = \quad \big(0.5, \quad &(0.2, 0.3, 0.25, 0.25), (0.25, 0.25, 0.25, 0.25),\\ &(0.25, 0.25, 0.25, 0.25), (0.25, 0.25, 0.25, 0.25)\big).\end{aligned}$$

Now the EM algorithm converges to a distribution which is a local maximum:

$$\mathbf{f}(\widehat{\theta}) \quad = \quad \frac{1}{54}\cdot\begin{pmatrix}6&3&3&3\\3&4&4&4\\3&4&4&4\\3&4&4&4\end{pmatrix}, \qquad \ell_{obs}(\widehat{\theta}) \quad = \quad -110.152332481077...$$

The Hessian of $\ell_{obs}(\theta)$ at $\widehat{\theta}$ has rank 11, and all eleven non-zero eigenvalues are distinct and negative.

Experiment 3: We next increase the starting parameter $\rho^1_{\mathtt{A}}$ and we decrease $\rho^1_{\mathtt{C}}$:

$$\begin{aligned}\theta \quad = \quad \big(0.5, \quad &(0.2, 0.3, 0.25, 0.25), (0.25, 0.25, 0.25, 0.25),\\ &(0.3, 0.2, 0.25, 0.25), (0.25, 0.25, 0.25, 0.25)\big).\end{aligned}$$

The EM algorithm converges to a distribution which is a saddle point of ℓ_{obs}:

$$\mathbf{f}(\widehat{\theta}) \quad = \quad \frac{1}{48}\cdot\begin{pmatrix}4&2&3&3\\2&4&3&3\\3&3&3&3\\3&3&3&3\end{pmatrix}, \qquad \ell_{obs}(\widehat{\theta}) \quad = \quad -110.223952742410...$$

The Hessian of $\ell_{obs}(\theta)$ at $\widehat{\theta}$ has rank 11, with nine eigenvalues negative.

Experiment 4: Let us now try the following starting parameters:

$$\begin{aligned}\theta \quad = \quad \big(0.5, \quad &(0.2, 0.3, 0.25, 0.25), (0.25, 0.2, 0.3, 0.25),\\ &(0.25, 0.25, 0.25, 0.25), (0.25, 0.25, 0.25, 0.25)\big).\end{aligned}$$

The EM algorithm converges to a probability distribution which is a local maximum of the likelihood function, which is better than the local maximum found previously in Experiment 2. The new winner is

$$\mathbf{f}(\widehat{\theta}) \quad = \quad \frac{1}{40}\cdot\begin{pmatrix}3&3&2&2\\3&3&2&2\\2&2&3&3\\2&2&3&3\end{pmatrix}, \qquad \ell_{obs}(\widehat{\theta}) \quad = \quad -110.098128348563...$$

All 11 nonzero eigenvalues of the Hessian of $\ell_{obs}(\theta)$ are distinct and negative.

We repeated this experiment many more times with random starting values, and we never found a parameter vector that was better than the one found in

Experiment 4. Based on this, we would like to conclude that the maximum value of the observed likelihood function is attained by our best solution:

$$\max\left\{ L_{obs}(\theta) \ : \ \theta \in \Theta \right\} \quad = \quad \frac{2^{16} \cdot 3^{24}}{40^{40}} \ = \ e^{-110.0981283}. \tag{1.44}$$

Assuming that this conclusion is correct, let us discuss the set of all optimal solutions. Since the data matrix u is invariant under the action of the symmetric group on $\{\mathtt{A}, \mathtt{C}, \mathtt{G}, \mathtt{T}\}$, that group also acts on the set of optimal solutions. There are three matrices like the one found in Experiment 4:

$$\frac{1}{40} \cdot \begin{pmatrix} 3 & 3 & 2 & 2 \\ 3 & 3 & 2 & 2 \\ 2 & 2 & 3 & 3 \\ 2 & 2 & 3 & 3 \end{pmatrix}, \quad \frac{1}{40} \cdot \begin{pmatrix} 3 & 2 & 3 & 2 \\ 2 & 3 & 2 & 3 \\ 3 & 2 & 3 & 2 \\ 2 & 3 & 2 & 3 \end{pmatrix} \quad \text{and} \quad \frac{1}{40} \cdot \begin{pmatrix} 3 & 2 & 2 & 3 \\ 2 & 3 & 3 & 2 \\ 2 & 3 & 3 & 2 \\ 3 & 2 & 2 & 3 \end{pmatrix}. \tag{1.45}$$

The preimage of each of these matrices under the polynomial map $\mathbf{f}$ is a surface in the space of parameters θ, namely, it consists of all representations of a rank 2 matrix as a convex combination of two rank 1 matrices. The topology of such "spaces of explanations" were studied in [Mond *et al.*, 2003]. The finding (1.44) indicates that the set of optimal solutions to the maximum likelihood problem is the disjoint union of three "surfaces of explanations".

But how do we know that (1.44) is actually true? Does running the EM algorithm $100,000$ times without converging to a parameter vector whose likelihood is larger constitute a mathematical proof? Can it be turned into a mathematical proof? Algebraic techniques for addressing such questions will be introduced in Section 3.3. For a numerical approach see Chapter 20.

1.4 Markov models

We now introduce Markov chains, hidden Markov models and Markov models on trees, using the algebraic notation of the previous sections. While our presentation is self-contained, readers may find it useful to compare with the (more standard) description of these models in [Durbin *et al.*, 1998] or other text books. A natural point of departure is the following toric model.

1.4.1 Toric Markov chains

We fix an alphabet Σ with l letters, and we fix a positive integer n. We shall define a toric model whose state space is the set Σ^n of all words of length n. The model is parameterized by the set Θ of non-negative $l \times l$ matrices. Thus the number of parameters is $d = l^2$ and the number of states is $m = l^n$.

Every toric model with d parameters and m states is represented by a $d \times m$ matrix A with integer entries as in Section 1.2. The $d \times m$ matrix which represents the toric Markov model will be denoted by $A_{l,n}$. Its rows are indexed by Σ^2 and its columns indexed by Σ^n. The entry of the matrix $A_{l,n}$ in the row indexed by the pair $\sigma_1\sigma_2 \in \Sigma^2$ and the column indexed by the word $\pi_1\pi_2\cdots\pi_n \in \Sigma^n$ is the number of occurrences of the pair inside the word, i.e., the number of indices $i \in \{1,\ldots,n-1\}$ such that $\sigma_1\sigma_2 = \pi_i\pi_{i+1}$. We define the *toric Markov chain model* to be the toric model specified by the matrix $A_{l,n}$.

For a concrete example let us consider words of length $n = 4$ over the binary alphabet $\Sigma = \{0, 1\}$, so that $l = 2$, $d = 4$ and $m = 16$. The matrix $A_{2,4}$ which was defined in the previous paragraph is the following 4×16 matrix:

$$\begin{array}{c|cccccccccccccccc|}
 & 0000 & 0001 & 0010 & 0011 & 0100 & 0101 & 0110 & 0111 & 1000 & 1001 & 1010 & 1011 & 1100 & 1101 & 1110 & 1111 \\
00 & 3 & 2 & 1 & 1 & 1 & 0 & 0 & 0 & 2 & 1 & 0 & 0 & 1 & 0 & 0 & 0 \\
01 & 0 & 1 & 1 & 1 & 1 & 2 & 1 & 1 & 0 & 1 & 1 & 1 & 0 & 1 & 0 & 0 \\
10 & 0 & 0 & 1 & 0 & 1 & 1 & 1 & 0 & 1 & 1 & 2 & 1 & 1 & 1 & 1 & 0 \\
11 & 0 & 0 & 0 & 1 & 0 & 0 & 1 & 2 & 0 & 0 & 0 & 1 & 1 & 1 & 2 & 3
\end{array}.$$

We write $\mathbb{R}^{2\times 2}$ for the space of 2×2 matrices

$$\theta \quad = \quad \begin{pmatrix} \theta_{00} & \theta_{01} \\ \theta_{10} & \theta_{11} \end{pmatrix}.$$

The parameter space $\Theta \subset \mathbb{R}^{2\times 2}$ consists of all matrices θ whose four entries θ_{ij} are positive. The toric Markov chain model of length $n = 4$ for the binary alphabet ($l = 2$) is the image of $\Theta = \mathbb{R}^{2\times 2}_{>0}$ under the monomial map

$$\mathbf{f}_{2,4} \,:\, \mathbb{R}^{2\times 2} \to \mathbb{R}^{16}\,, \quad \theta \;\mapsto\; \frac{1}{\sum_{ijkl} p_{ijkl}} \cdot (p_{0000}, p_{0001}, \ldots, p_{1111}),$$

$$\text{where} \qquad p_{i_1 i_2 i_3 i_4} \;=\; \theta_{i_1 i_2} \cdot \theta_{i_2 i_3} \cdot \theta_{i_3 i_4} \qquad \text{for all} \;\; i_1 i_2 i_3 i_4 \in \{0,1\}^4.$$

The map $\mathbf{f}_{l,n}$ is defined analogously for larger alphabets and longer sequences.

The toric Markov chain model $\mathbf{f}_{2,4}(\Theta)$ is a three-dimensional object inside the 15-dimensional simplex Δ which consists of all probability distributions on the state space $\{0,1\}^4$. Algebraically, the simplex is specified by the equation

$$p_{0000} + p_{0001} + p_{0010} + p_{0011} + \cdots + p_{1110} + p_{1111} \;=\; 1. \tag{1.46}$$

where the p_{ijkl} are unknowns which represent the probabilities of the 16 states. To understand the geometry of the toric Markov chain model, we examine the matrix $A_{2,4}$. The 16 columns of $A_{2,4}$ represent twelve distinct points in

$$\bigl\{\, (u_{00}, u_{01}, u_{10}, u_{11}) \in \mathbb{R}^{2\times 2} \;:\; u_{00} + u_{01} + u_{10} + u_{11} \;=\; 3 \,\bigr\} \quad \simeq \quad \mathbb{R}^3.$$

The convex hull of these twelve points is the three-dimensional polytope depicted in Figure 1.1. We refer to Section 2.3 for a general introduction to polytopes. Only eight of the twelve points are vertices of the polytope.

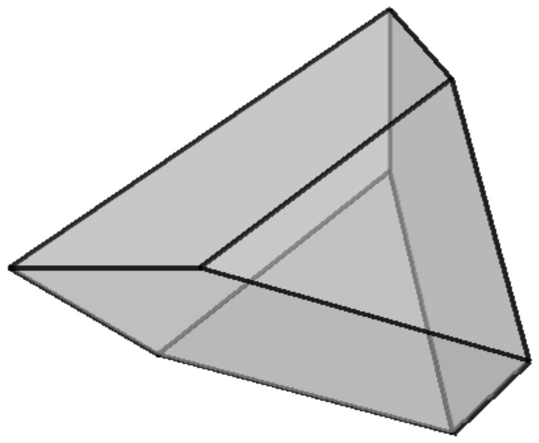

Fig. 1.1. The polytope of the toric Markov chain model $\mathbf{f}_{2,4}(\Theta)$.

Polytopes like the one in Figure 1.1 are important for parametric inference in computational biology. In particular, we shall see in Chapter 10 that *Viterbi sequences* of Markov chains correspond to vertices of the polytope of $\mathbf{f}_{l,n}(\Theta)$.

The adjective "toric" is used for the toric Markov chain model $\mathbf{f}_{2,4}(\Theta)$ because $\mathbf{f}_{2,4}$ is a monomial map, and so its image is a *toric variety.* (An introduction to varieties is given in Section 3.1). Every variety is characterized by a finite list of polynomials that vanish on that variety. In the context of statistics, these polynomials are called *model invariants.* A model invariant is an algebraic relation that holds for all probability distributions in the model. For a toric model these invariants can be derived from the geometry of its polytope. We explain this derivation for the toric Markov chain model $\mathbf{f}_{2,4}(\Theta)$.

The simplest model invariant is the equation (1.46). The other linear invariants come from the fact that the matrix $A_{2,4}$ has some repeated columns:

$$p_{0110} = p_{1011} = p_{1101} \quad \text{and} \quad p_{0010} = p_{0100} = p_{1001}. \tag{1.47}$$

These relations state that $A_{2,4}$ is a configuration of only 12 distinct points. Next there are four relations which specify the location of the four non-vertices. Each of them is the midpoint on the segment between two of the eight vertices:

$$\begin{array}{ll} p_{0011}^2 = p_{0001}p_{0111} & p_{1001}^2 = p_{0001}p_{1010}, \\ p_{1100}^2 = p_{1000}p_{1110} & p_{1101}^2 = p_{0101}p_{1110}. \end{array} \tag{1.48}$$

For instance, the first equation $p_{0011}^2 = p_{0001}p_{0111}$ corresponds to the following additive relation among the fourth, second and eighth column of $A_{2,4}$:

$$2 \cdot (1,1,0,1) \quad = \quad (2,1,0,0) + (0,1,0,2).$$

The remaining eight columns of $A_{2,4}$ are vertices of the polytope depicted above. The corresponding probabilities satisfy the following relations:

$$\begin{array}{lll} p_{0111}p_{1010} = p_{0101}p_{1110} & p_{0111}p_{1000} = p_{0001}p_{1110} & p_{0101}p_{1000} = p_{0001}p_{1010}, \\ p_{0111}p_{1110}^2 = p_{1010}p_{1111}^2 & p_{0111}^2 p_{1110} = p_{0101}p_{1111}^2 & p_{0001}p_{1000}^2 = p_{0000}^2 p_{1010}, \\ p_{0000}^2 p_{0101} = p_{0001}^2 p_{1000} & p_{0000}^2 p_{1110}^3 = p_{1000}^3 p_{1111}^2 & p_{0000}^2 p_{0111}^3 = p_{0001}^3 p_{1111}^2. \end{array}$$

These nine equations together with (1.46), (1.47) and (1.48) characterize the set of distributions $p \in \Delta$ that lie in the toric Markov chain model $\mathbf{f}_{2,4}(\Theta)$. Tools for computing such lists of model invariants will be presented in Chapter 3.

1.4.2 Markov Chains

The Markov chain model is a submodel of the toric Markov chain model. Let Θ_1 denote the subset of all matrices $\theta \in \mathbb{R}_{>0}^{l \times l}$ whose rows sum to one. The *Markov chain model* is the image of Θ_1 under the map $\mathbf{f}_{l,n}$. By a *Markov chain* we mean any point p in the model $\mathbf{f}_{l,n}(\Theta_1)$. This definition agrees with the familiar description of Markov chains in [Durbin *et al.*, 1998, Chapter 3], except that we require the initial distribution at the first state to be uniform.

For instance, if $l = 2$ then the parameter space Θ_1 is a square. Namely, Θ_1 is the set of all pairs $(\theta_0, \theta_1) \in \mathbb{R}^2$ such that the following matrix is positive:

$$\theta \quad = \quad \begin{pmatrix} \theta_0 & 1-\theta_0 \\ 1-\theta_1 & \theta_1 \end{pmatrix}$$

The Markov chain model is the image of the square under the map $\mathbf{f}_{2,n}$. A Markov chain of length $n = 4$ is any probability distribution of the form

$$p_{0000} = \frac{1}{2}\theta_0^3, \;\; p_{0001} = \frac{1}{2}\theta_0^2(1-\theta_0), \;\; p_{0010} = p_{1001} = p_{0100} = \frac{1}{2}\theta_0(1-\theta_0)(1-\theta_1),$$

$$p_{0011} = \frac{1}{2}\theta_0(1-\theta_0)\theta_1\,, \quad p_{0101} = \frac{1}{2}(1-\theta_0)^2(1-\theta_1)\,, \quad p_{0111} = \frac{1}{2}(1-\theta_0)\theta_1^2,$$

$$p_{0110} = p_{1011} = p_{1101} = \frac{1}{2}(1-\theta_0)\theta_1(1-\theta_1)\,, \qquad p_{1010} = \frac{1}{2}(1-\theta_1)^2(1-\theta_0),$$

$$p_{1000} = \frac{1}{2}(1-\theta_1)\theta_0^2, \;\; p_{1100} = \frac{1}{2}\theta_1(1-\theta_1)\theta_0, \;\; p_{1110} = \frac{1}{2}\theta_1^2(1-\theta_1), \;\; p_{1111} = \frac{1}{2}\theta_1^3.$$

Thus the Markov chain model is the surface in the 15-dimensional simplex Δ given by this parameterization. It satisfies all the model invariants of the toric Markov chain (a threefold in Δ) plus some extra model invariants due to the fact that probabilities must sum to 1, and the initial distribution is uniform. For example,

$$p_{0000} + p_{0001} + p_{0010} + p_{0011} + p_{0100} + p_{0101} + p_{0110} + p_{0111} \quad = \quad \frac{1}{2}.$$

We next discuss maximum likelihood estimation for Markov chains. Fix a data vector $u \in \mathbb{N}^{l^n}$ representing N observed sequences in Σ^n. The sufficient statistic $v = A_{l,n} \cdot u \in \mathbb{N}^{l^2}$ is regarded as an $l \times l$ matrix. The entry $v_{\sigma_1 i_2}$ in row σ_1 and column i_2 of the matrix v equals the number of occurrences of $\sigma_1 i_2 \in \Sigma^2$ as a consecutive pair in any of the N observed sequences.

Proposition 1.17 *The maximum likelihood estimate of the data $u \in \mathbb{N}^{l^n}$ in the Markov chain model is the $l \times l$ matrix $\widehat{\theta} = \big(\widehat{\theta}_{ij}\big)$ in Θ_1 with coordinates*

$$\widehat{\theta}_{ij} \quad = \quad \frac{v_{ij}}{\sum_{s \in \Sigma} v_{is}} \qquad\qquad \textit{where} \quad v \, = \, A_{l,n} \cdot u.$$

Proof The likelihood function for the toric Markov chain model equals

$$L(\theta) \quad = \quad \theta^{A_{l,n} \cdot u} \quad = \quad \theta^{v} \quad = \quad \prod_{ij \in \Sigma^2} \theta_{ij}^{v_{ij}}.$$

The log-likelihood function can be written as follows:

$$\ell(\theta) \quad = \quad \sum_{i \in \Sigma} \big(v_{i1} \cdot \log(\theta_{i1}) + v_{i2} \cdot \log(\theta_{i2}) + \cdots + v_{i,l-1} \cdot \log(\theta_{i,l-1}) + v_{il} \cdot \log(\theta_{il}) \big).$$

The log-likelihood function for the Markov chain model is obtained by restricting this function to the set Θ_1 of $l \times l$ matrices whose row sums are all equal to one. Therefore, $\ell(\theta)$ is the sum over all $i \in \Sigma$ of the expressions

$$v_{i1} \cdot \log(\theta_{i1}) + v_{i2} \cdot \log(\theta_{i2}) + \cdots + v_{i,l-1} \cdot \log(\theta_{i,l-1}) + v_{il} \cdot \log(1 - \sum_{s=1}^{l-1} \theta_{is}). \quad (1.49)$$

These expressions have disjoint sets of unknowns for different values of the index $i \in \Sigma$. To maximize $\ell(\theta)$ over Θ_1, it hence suffices to maximize the concave function (1.49) over the $(l-1)$-dimensional simplex consisting of all non-negative vectors $(\theta_{i1}, \theta_{i2}, \ldots, \theta_{i,l-1})$ of coordinate sum at most one. By equating the partial derivatives of (1.49) to zero, we see that the unique critical point has coordinates $\theta_{ij} = v_{ij}/(v_{i1} + v_{i2} + \cdots + v_{il})$ as desired. □

We next introduce the *fully observed Markov model* that underlies the hidden Markov model considered in Subsection 1.4.3. We fix the sequence length n and we consider a first alphabet Σ with l letters and a second alphabet Σ' with l' letters. The observable states in this model are pairs $(\sigma, \tau) \in \Sigma^n \times (\Sigma')^n$ of words of length n. A sequence of N observations in this model is summarized in a matrix $u \in \mathbb{N}^{l^n \times (l')^n}$ where $u_{(\sigma,\tau)}$ is the number of times the pair (σ, τ) was observed. Hence, in this model, $m = (l \cdot l')^n$.

The fully observed Markov model is parameterized by a pair of matrices (θ, θ') where θ is an $l \times l$ matrix and θ' is an $l \times l'$ matrix. The matrix θ encodes a Markov chain as before: the entry θ_{ij} represents the probability of transitioning from state $i \in \Sigma$ to $j \in \Sigma$. The matrix θ' encodes the interplay between the two alphabets: the entry θ'_{ij} represents the probability of outputting symbol $j \in \Sigma'$ when the Markov chain is in state $i \in \Sigma$. As before in the Markov chain model, we restrict ourselves to non-negative matrices whose rows sum to one. To be precise, Θ_1 now denotes the set of pairs of matrices $(\theta, \theta') \in \mathbb{R}^{l \times l}_{>0} \times \mathbb{R}^{l \times l'}_{>0}$ whose row sums are equal to one. Hence $d = l(l + l' + 2)$.

The fully observed Markov model is the restriction to Θ_1 of the toric model

$$F : \mathbb{R}^d \to \mathbb{R}^m, \quad (\theta, \theta') \mapsto p = \big(p_{\sigma,\tau}\big)$$

$$\text{where} \qquad p_{\sigma,\tau} \;=\; \frac{1}{l}\theta'_{\sigma_1\tau_1}\theta_{\sigma_1\sigma_2}\theta'_{\sigma_2\tau_2}\theta_{\sigma_2\sigma_3}\theta'_{\sigma_3\tau_3}\theta_{\sigma_3\sigma_4}\cdots\theta_{\sigma_{n-1}\sigma_n}\theta'_{\sigma_n\tau_n}. \tag{1.50}$$

The computation of maximum likelihood estimates for this model is an easy extension of the method for Markov chains in Proposition 1.17. The role of the matrix $A_{l,n}$ for Markov chains is now played by the following linear map

$$A : \mathbb{N}^{l^n \times (l')^n} \to \mathbb{N}^{l \times l} \oplus \mathbb{N}^{l \times l'}.$$

The image of the basis vector $e_{\sigma,\tau}$ corresponding to a single observation (σ, τ) under A is the pair of matrices (w, w'), where w_{rs} is the number of indices i such that $\sigma_i\sigma_{i+1} = rs$, and w'_{rt} is the number of indices i such that $\sigma_i\tau_i = rt$.

Let $u \in \mathbb{N}^{l^n \times (l')^n}$ be a matrix of data. The sufficient statistic is the pair of matrices $A \cdot u = (v, v')$. Here $v \in \mathbb{N}^{l \times l}$ and $v' \in \mathbb{N}^{l \times l'}$. The likelihood function $L_{hid} : \Theta_1 \to \mathbb{R}$ of the fully observed Markov model is the monomial

$$L_{hid}(\theta) \quad = \quad \theta^v \cdot (\theta')^{v'}.$$

Proposition 1.18 *The maximum likelihood estimate for the data* $u \in \mathbb{N}^{l^n \times (l')^n}$ *in the fully observed Markov model is the matrix pair* $(\widehat{\theta}, \widehat{\theta'}) \in \Theta_1$ *with*

$$\widehat{\theta}_{ij} \;=\; \frac{v_{ij}}{\sum_{s \in \Sigma} v_{is}} \qquad \text{and} \qquad \widehat{\theta'}_{ij} \;=\; \frac{v'_{ij}}{\sum_{t \in \Sigma'} v'_{it}} \tag{1.51}$$

Proof This is entirely analogous to the proof of Proposition 1.17, the point being that the log-likelihood function $\ell_{hid}(\theta)$ decouples as a sum of expressions like (1.49), each of which is easy to maximize over the relevant simplex. $\square$

1.4.3 Hidden Markov Models

The hidden Markov model $\mathbf{f}$ is derived from the fully observed Markov model F by summing out the first indices $\sigma \in \Sigma^n$. More precisely, consider the map

$$\rho \,:\, \mathbb{R}^{l^n \times (l')^n} \longrightarrow \mathbb{R}^{(l')^n}$$

obtained by taking the column sums of a matrix with l^n rows and $(l')^n$ columns. The *hidden Markov model* is the algebraic statistical model defined by composing the fully observed Markov model F with the marginalization map ρ:

$$\mathbf{f} \;=\; \rho \circ F \;:\; \Theta_1 \subset \mathbb{R}^d \longrightarrow \mathbb{R}^{(l')^n}. \tag{1.52}$$

Here, $d = l(l + l' - 2)$ and it is natural to write $\mathbb{R}^d = \mathbb{R}^{l(l-1)} \times \mathbb{R}^{l(l'-1)}$ since the parameters are pairs of matrices (θ, θ'). We summarize:

Remark 1.19 The hidden Markov model is a polynomial map $\mathbf{f}$ from the parameter space $\mathbb{R}^{l(l-1)} \times \mathbb{R}^{l(l'-1)}$ to the probability space $\mathbb{R}^{(l')^n}$. The degree of $\mathbf{f}$ in the entries of θ is $n-1$, and the degree of $\mathbf{f}$ in the entries of θ' is n.

The notation in the definition in (1.52) is consistent with our discussion of the Expectation Maximization (EM) algorithm in Section 1.3. Thus we can find maximum likelihood estimates for the hidden Markov model by applying the EM algorithm to $\mathbf{f} = \rho \circ F$.

Remark 1.20 The *Baum-Welch algorithm* is the special case of the EM algorithm obtained by applying EM to the hidden Markov model $\mathbf{f} = \rho \circ F$.

The Baum-Welch algorithm in general, and Remark 1.20 in particular, are discussed in Section 11.6 of [Durbin *et al.*, 1998].

Example 1.21 Consider the *occasionally dishonest casino* which is featured as running example in [Durbin *et al.*, 1998]. In that casino they use a fair die most of the time, but occasionally they switch to a loaded die. Our two alphabets are $\Sigma = \{\text{fair}, \text{loaded}\}$ and $\Sigma' = \{1,2,3,4,5,6\}$ for the six possible outcomes of rolling a die. Suppose a particular game involves rolling the dice $n = 4$ times. This hidden Markov model has $d = 12$ parameters, appearing in

$$\theta \quad = \quad \begin{array}{c} \\ \text{fair} \\ \text{loaded} \end{array} \begin{array}{c} \begin{array}{cc} \text{fair} & \text{loaded} \end{array} \\ \begin{pmatrix} x & 1-x \\ 1-y & y \end{pmatrix} \end{array} \qquad\qquad \text{and}$$

$$\theta' \quad = \quad \begin{array}{c} \\ \text{fair} \\ \text{loaded} \end{array} \begin{array}{c} \begin{array}{cccccc} 1 & 2 & 3 & 4 & 5 & 6 \end{array} \\ \begin{pmatrix} f_1 & f_2 & f_3 & f_4 & f_5 & 1-\sum_{i=1}^5 f_i \\ l_1 & l_2 & l_3 & l_4 & l_5 & 1-\sum_{j=1}^5 l_j \end{pmatrix} \end{array}.$$

Presumably, the fair die is really fair, so that $f_1 = f_2 = f_3 = f_4 = f_5 = 1/6$, but, to be on the safe side, let us here keep the f_i as unknown parameters

This hidden Markov model (HMM) has $m = 6^4 = 1,296$ possible outcomes, namely, all the words $\tau = \tau_1\tau_2\tau_3\tau_4$ in $(\Sigma')^4$. The coordinates of the map $\mathbf{f} : \mathbb{R}^{12} \to \mathbb{R}^{1296}$ in (1.52) are polynomials of degree $7 = 3 + 4$:

$$p_{\tau_1\tau_2\tau_3\tau_4} \quad = \quad \frac{1}{2} \cdot \sum_{\sigma_1\in\Sigma}\sum_{\sigma_2\in\Sigma}\sum_{\sigma_3\in\Sigma}\sum_{\sigma_4\in\Sigma} \theta'_{\sigma_1\tau_1}\theta_{\sigma_1\sigma_2}\theta'_{\sigma_2\tau_2}\theta_{\sigma_2\sigma_3}\theta'_{\sigma_3\tau_3}\theta_{\sigma_3\sigma_4}\theta'_{\sigma_4\tau_4}.$$

Thus our HMM is specified by a list of $1,296$ polynomials p_τ in the twelve unknowns. The sum of all polynomials is 1. Each polynomial has degree three in the two unknowns x, y and degree four in the ten unknowns $f_1, f_2, \ldots, l_5$.

Suppose we observe the game N times. These observations are our data. The sufficient statistic is the vector $(u_\tau) \in \mathbb{N}^{1296}$, where $u_\tau = u_{\tau_1\tau_2\tau_3\tau_4}$ counts the number of times the output sequence $\tau = \tau_1\tau_2\tau_3\tau_4$ was observed. Hence $\sum_{\tau\in(\Sigma')^4} u_\tau = N$. The goal of EM is to maximize the log-likelihood function

$$\ell\big(x, y, f_1, \ldots, f_5, l_1, \ldots, l_5\big) \quad = \quad \sum_{\tau\in\Sigma'^4} u_{\tau_1\tau_2\tau_3\tau_4} \cdot \log(p_{\tau_1\tau_2\tau_3\tau_4}),$$

where (x, y) ranges over a square, $(f_1, \ldots, f_5)$ runs over a 5-simplex, and so does $(l_1, \ldots, l_5)$. Our parameter space $\Theta_1 \subset \mathbb{R}^{12}$ is the product of the square and the two 5-simplices. The Baum-Welch algorithm (i.e., the EM algorithm for the HMM) aims to maximize ℓ over the 12-dimensional polytope Θ_1.

1.4.4 Tree Models

Markov chains and hidden Markov models are special instances of *tree models*, a class of models which we discuss next. We begin by defining the *fully observed tree model*, from which we then derive the *hidden tree model*. These models relate to each other in the same way that the hidden Markov model is the composition of the fully observed Markov model with a marginalization map.

Let T be a rooted tree with n leaves. We write $N(T)$ for the set of all nodes of T. This set includes the root, which is denoted $\mathbf{r}$, and the leaves, which are indexed by $[n] = \{1, 2, \ldots, n\}$. The set $E(T)$ of edges of T is a subset of $N(T) \times N(T)$. Every edge is directed away from the root $\mathbf{r}$. We use the abbreviation kl for edges $(k, l) \in E(T)$. Every node $i \in N(T)$ represents a random variable which takes values in a finite alphabet Σ_i. Our tree models are parameterized by a collection of matrices θ^{kl}, one for each edge $kl \in E(T)$. The rows of the matrix θ^{kl} are indexed by Σ_k, and the columns are indexed by Σ_l. As before, we restrict ourselves to non-negative matrices whose rows sum to one. Let Θ_1 denote the collection of tuples $\big(\theta^{kl}\big)_{kl\in E(T)}$ of such matrices. The dimension of the parameter space Θ_1 is therefore $d = \sum_{kl\in E(T)} |\Sigma_k|(|\Sigma_l| - 1)$.

The *fully observed tree model* is the restriction to Θ_1 of the monomial map

$$F_T : \mathbb{R}^d \to \mathbb{R}^m , \ \theta = \left(\theta^{kl}\right)_{kl\in E(T)} \mapsto p = (p_\sigma)$$

$$p_\sigma \ = \ \frac{1}{|\Sigma_{\mathbf{r}}|} \cdot \prod_{kl\in E(T)} \theta^{kl}_{\sigma_k \sigma_l}. \tag{1.53}$$

Here $m = \prod_{i\in N(T)} |\Sigma_i|$. The state space of this model is the Cartesian product of the sets Σ_i. A state is a vector $\sigma = \left(\sigma_i\right)_{i\in N(T)}$ where $\sigma_i \in \Sigma_i$. The factor $1/|\Sigma_{\mathbf{r}}|$ means that we are assuming the root distribution to be uniform.

The fully observed tree model F_T is (the restriction to Θ_1 of) a toric model. There is an easy formula for computing maximum likelihood parameters in this model. The formula and its derivation is similar to that in Proposition 1.18.

The *hidden tree model* $\mathbf{f}_T$ is obtained from the fully observed tree model F_T by summing out the internal nodes of the tree. Hidden tree models are therefore defined on a restricted state space corresponding only to leaves of the tree. The state space of the hidden tree model is $\Sigma_1 \times \Sigma_2 \times \cdots \times \Sigma_n$, the product of the alphabets associated with the leaves of T. The cardinality of the state space is $m' = |\Sigma_1|\cdot|\Sigma_2|\cdots|\Sigma_n|$. There is a natural linear *marginalization map* $\rho_T : \mathbb{R}^m \to \mathbb{R}^{m'}$ which takes real-valued functions on $\prod_{i\in N(T)} \Sigma_i$ to real-valued functions on $\prod_{i=1}^n \Sigma_i$. We have $\mathbf{f}_T = \rho_T \circ F_T$.

Proposition 1.22 *The hidden tree model $\mathbf{f}_T : \mathbb{R}^d \to \mathbb{R}^{m'}$ is a multilinear polynomial map. Each of its coordinates has total degree $|E(T)|$, but is linear when regarded as a function of the entries of each matrix θ^{kl} separately.*

The model $\mathbf{f}_T$ described here is also known as the *general Markov model* on the tree T, relative to the given alphabets Σ_i. The adjective "general" refers to the fact that the matrices θ^{kl} are distinct and their entries obey no constraints beyond non-negativity and rows summing to one. In most applications of tree models, the parameters $(\theta^{kl})_{kl\in E(T)}$ are specialized in some manner, either by requiring that some matrices are identical or by specializing each individual matrix θ^{kl} to have fewer than $|\Sigma_k| \cdot (|\Sigma_l| - 1)$ free parameters.

Example 1.23 The hidden Markov model is a (specialization of the) hidden tree model, where the tree T is the *caterpillar tree* depicted in Figure 1.2.

In the HMM there are only two distinct alphabets: $\Sigma_i = \Sigma$ for $i \in N(T)\backslash[n]$ and $\Sigma_i = \Sigma'$ for $i \in [n]$. The matrices θ^{kl} are all square and identical along the non-terminal edges of the tree. A second matrix is used for all terminal edges.

Maximum likelihood estimation for the hidden tree model can be done with the EM algorithm, as described in Section 1.3. Indeed, the hidden tree model

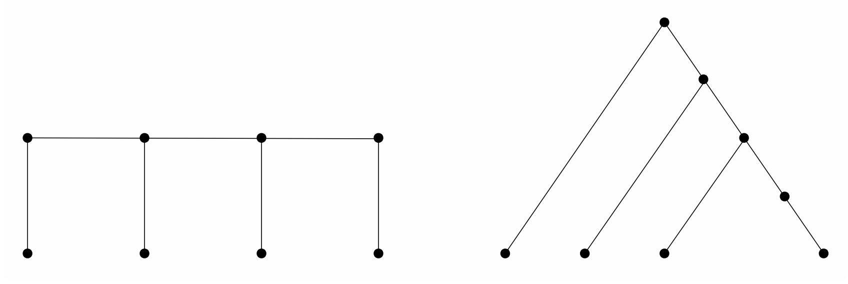

Fig. 1.2. Two views of the caterpillar tree.

is the composition $\mathbf{f}_T = \rho_T \circ F_T$ of an easy toric model F_T and the marginalization map ρ_T, so Algorithm 1.14 is directly applicable to this situation.

Tree models used in phylogenetics have the same alphabet Σ on each edge, but the transition matrices remain distinct and independent. The two alphabets most commonly used are $\Sigma = \{0, 1\}$ and $\Sigma = \{\mathtt{A}, \mathtt{C}, \mathtt{G}, \mathtt{T}\}$. We present one example for each alphabet. In both cases, the tree T is the *claw tree*, which has no internal nodes other than the root: $N(T) = \{1, 2, \ldots, n, \mathbf{r}\}$.

Example 1.24 Let $\Sigma = \{0, 1\}$ and T the claw tree with $n = 6$ leaves. The hidden tree model $\mathbf{f}_T$ has $d = 12$ parameters. It has $m = 64$ states which are indexed by binary strings $i_1 i_2 i_3 i_4 i_5 i_6 \in \Sigma^6$. The model $\mathbf{f}_T(\Theta_1)$ is the 12-dimensional variety in the 63-simplex given by the parameterization

$$p_{i_1 i_2 i_3 i_4 i_5 i_6} \;=\; \frac{1}{2}\theta^{\mathbf{r}1}_{0i_1}\theta^{\mathbf{r}2}_{0i_2}\theta^{\mathbf{r}3}_{0i_3}\theta^{\mathbf{r}4}_{0i_4}\theta^{\mathbf{r}5}_{0i_5}\theta^{\mathbf{r}6}_{0i_6} \;+\; \frac{1}{2}\theta^{\mathbf{r}1}_{1i_1}\theta^{\mathbf{r}2}_{1i_2}\theta^{\mathbf{r}3}_{1i_3}\theta^{\mathbf{r}4}_{1i_4}\theta^{\mathbf{r}5}_{1i_5}\theta^{\mathbf{r}6}_{1i_6}.$$

If the root distribution is unspecified then $d = 13$ and the parameterization is

$$p_{i_1 i_2 i_3 i_4 i_5 i_6} \;=\; \lambda\theta^{\mathbf{r}1}_{0i_1}\theta^{\mathbf{r}2}_{0i_2}\theta^{\mathbf{r}3}_{0i_3}\theta^{\mathbf{r}4}_{0i_4}\theta^{\mathbf{r}5}_{0i_5}\theta^{\mathbf{r}6}_{0i_6} \;+\; (1-\lambda)\theta^{\mathbf{r}1}_{1i_1}\theta^{\mathbf{r}2}_{1i_2}\theta^{\mathbf{r}3}_{1i_3}\theta^{\mathbf{r}4}_{1i_4}\theta^{\mathbf{r}5}_{1i_5}\theta^{\mathbf{r}6}_{1i_6}. \quad (1.54)$$

The algebraic geometry of Examples 1.24 and 1.25 is discussed in Section 3.2.

Example 1.25 Let $\Sigma = \{\mathtt{A}, \mathtt{C}, \mathtt{G}, \mathtt{T}\}$ and let T be the claw tree with $n = 3$ leaves. The hidden tree model $\mathbf{f}_T$ has $m = 64$ states which are the triples $ijk \in \Sigma^3$. Writing $\lambda = (\lambda_{\mathbf{A}}, \lambda_{\mathbf{C}}, \lambda_{\mathbf{G}}, \lambda_{\mathbf{T}})$ for the root distribution, we have

$$p_{ijk} \;=\; \lambda_{\mathtt{A}}\theta^{\mathbf{r}1}_{\mathtt{A}i}\theta^{\mathbf{r}2}_{\mathtt{A}j}\theta^{\mathbf{r}3}_{\mathtt{A}k} + \lambda_{\mathtt{C}}\theta^{\mathbf{r}1}_{\mathtt{C}i}\theta^{\mathbf{r}2}_{\mathtt{C}j}\theta^{\mathbf{r}3}_{\mathtt{C}k} + \lambda_{\mathtt{G}}\theta^{\mathbf{r}1}_{\mathtt{G}i}\theta^{\mathbf{r}2}_{\mathtt{G}j}\theta^{\mathbf{r}3}_{\mathtt{G}k} + \lambda_{\mathtt{T}}\theta^{\mathbf{r}1}_{\mathtt{T}i}\theta^{\mathbf{r}2}_{\mathtt{T}j}\theta^{\mathbf{r}3}_{\mathtt{T}k}. \quad (1.55)$$

If λ is unspecified then this model has $d = 12 + 12 + 12 + 3 = 39$ parameters. If the root distribution is uniform, i.e., $\lambda = (\frac{1}{4}, \frac{1}{4}, \frac{1}{4}, \frac{1}{4})$, then $d = 36 = 12 + 12 + 12$. We note that the small Jukes-Cantor model in Example 1.7 is the three-dimensional submodel of this 36-dimensional model obtained by setting

$$\theta^{\mathbf{r}\nu} \quad = \quad \begin{array}{c} \\ \mathtt{A} \\ \mathtt{C} \\ \mathtt{G} \\ \mathtt{T} \end{array} \!\!\begin{array}{c} \begin{array}{cccc} \quad\mathtt{A}\quad & \quad\mathtt{C}\quad & \quad\mathtt{G}\quad & \quad\mathtt{T}\quad \end{array} \\ \begin{pmatrix} 1-3\theta_\nu & \theta_\nu & \theta_\nu & \theta_\nu \\ \theta_\nu & 1-3\theta_\nu & \theta_\nu & \theta_\nu \\ \theta_\nu & \theta_\nu & 1-3\theta_\nu & \theta_\nu \\ \theta_\nu & \theta_\nu & \theta_\nu & 1-3\theta_\nu \end{pmatrix} \end{array} \qquad \text{for } \nu \in \{1,2,3\}.$$

The number of states drops from $m = 64$ in Example 1.25 to $m = 5$ in Example 1.7 since many of the probabilities p_{ijk} become equal under this specialization.

A key statistical problem associated with hidden tree models is *model selection*. The general model selection problem is as follows: suppose we have a data vector $u = (u_1, \ldots, u_m)$, a collection of models $\mathbf{f^1}, \ldots, \mathbf{f^k}$ where $\mathbf{f^i} : \mathbb{R}^{d_i} \to \mathbb{R}^m$, and we would like to select a "good" model for the data. In the case where $d_1 = \cdots = d_m$, we may select the model $\mathbf{f^i}$ whose likelihood function attains the largest value of all. This problem arises for hidden tree models where there the leaf set $[n]$ and data are fixed, but we would like to select from among all phylogenetic trees on $[n]$ that tree which maximizes the likelihood of the data. Since the number of trees grows exponentially when n increases, this approach leads to combinatorial explosion. In applications to biology, this explosion is commonly dealt with by using the distance-based techniques in Section 2.4. Hidden tree models are studied in detail in Chapters 15 through 20.

1.5 Graphical models

Almost all the statistical models we have discussed in the previous four sections are instances of *graphical models*. Discrete graphical models are certain algebraic statistical models for joint probability distributions of n random variables $X_1, X_2, \ldots, X_n$ which can be specified in two possible ways:

- by a parameterization $\mathbf{f} : \mathbb{R}^d \to \mathbb{R}^m$ (with polynomial coordinates as before),
- by a collection of conditional independence statements.

Our focus in this section is the latter representation, and its connection to the former via a result of statistics known as the *Hammersley-Clifford Theorem*, which concerns conditional independence statements derived from graphs. The graphs that underlie graphical models are key to developing efficient inference algorithms, an important notion which is the final topic of this section and is the basis for applications of graphical models to problems in biology.

We assume that each random variable X_i takes its values in a finite alphabet Σ_i. The common state space of all models to be discussed in this section is therefore the Cartesian product of the alphabets:

$$\prod_{i=1}^{n} \Sigma_i \quad = \quad \Sigma_1 \times \Sigma_2 \times \cdots \times \Sigma_n \tag{1.56}$$

and the number of states is $m = \prod_{i=1}^{n} |\Sigma_i|$. This number is fixed throughout this section. A probability distribution on the state space (1.56) corresponds to an n-dimensional table $(p_{i_1 i_2 \cdots i_n})$. We think of $p_{i_1 i_2 \cdots i_n}$ as an unknown which represents the probability of the event $X_1 = i_1, X_2 = i_2, \ldots, X_n = i_n$.

A *conditional independence statement* about $X_1, X_2, \ldots, X_n$ has the form

$$A \text{ is independent of } B \text{ given } C \qquad \text{(in symbols: } A \perp\!\!\!\perp B \,|\, C\text{)}, \tag{1.57}$$

where A, B, C are pairwise disjoint subsets of $\{X_1, X_2, \ldots, X_n\}$. If C is the empty set then (1.57) reads "A is independent of B" and is denoted by $A \perp\!\!\!\perp B$.

Remark 1.26 The independence statement (1.57) translates into a set of quadratic equations in the unknowns $p_{i_1 \cdots i_n}$. The equations are indexed by

$$\binom{\prod_{X_i \in A} \Sigma_i}{2} \times \binom{\prod_{X_j \in B} \Sigma_j}{2} \times \prod_{X_k \in C} \Sigma_k. \tag{1.58}$$

An element of the set (1.58) is a triple consisting of two distinct elements a and a' in $\prod_{X_i \in A} \Sigma_i$, two distinct elements b and b' in $\prod_{X_j \in B} \Sigma_j$, and an element c in $\prod_{X_k \in C} \Sigma_k$. The independence condition $A \perp\!\!\!\perp B \,|\, C$ is equivalent to the statement that, for all triples $\{a, a'\}, \{b, b'\}$ and $\{c\}$,

$$\begin{aligned} &\text{Prob}(A = a, B = b, C = c) \cdot \text{Prob}(A = a', B = b', C = c) \\ -&\text{Prob}(A = a', B = b, C = c) \cdot \text{Prob}(A = a, B = b', C = c) \quad = \quad 0. \end{aligned}$$

To get our quadrics indexed by (1.58), we translate each of the probabilities above into a linear form in the unknowns $p_{i_1 i_2 \cdots i_n}$. Namely, $\text{Prob}(A = a, B = b, C = c)$ is replaced by a marginalization which is the sum of all $p_{i_1 i_2 \cdots i_n}$ which satisfy

- for all $X_\alpha \in A$, the X_α-coordinate of a equals i_α,
- for all $X_\beta \in B$, the X_β-coordinate of b equals i_β, and
- for all $X_\gamma \in C$, the X_γ-coordinate of c equals i_γ.

We define $\mathcal{Q}_{A \perp\!\!\!\perp B \,|\, C}$ to be the set of quadratic forms in the unknowns $p_{i_1 i_2 \cdots i_n}$ which result from this substitution. Thus $\mathcal{Q}_{A \perp\!\!\!\perp B \,|\, C}$ is indexed by (1.58).

We illustrate the definition of the set of quadrics $\mathcal{Q}_{A \perp\!\!\!\perp B \,|\, C}$ with an example:

Example 1.27 Let $n = 3$ and $i_1 = i_2 = i_3 = \{0, 1\}$, so that $\big(p_{i_1 i_2 i_3}\big)$ is a

$2 \times 2 \times 2$ table whose eight entries are unknowns. The independence statement $\{X_2\}$ *is independent of* $\{X_3\}$ *given* $\{X_1\}$ describes the pair of quadrics

$$\mathcal{Q}_{X_2 \perp\!\!\!\perp X_3 \,|\, X_1} \quad = \quad \big\{\, p_{000}p_{011} - p_{001}p_{010},\, p_{100}p_{111} - p_{101}p_{110} \,\big\}. \qquad (1.59)$$

The statement $\{X_2\}$ *is independent of* $\{X_3\}$ corresponds to a single quadric

$$\mathcal{Q}_{X_2 \perp\!\!\!\perp X_3} \quad = \quad \big\{\, (p_{000}+p_{100})(p_{011}+p_{111}) \,-\, (p_{001}+p_{101})(p_{010}+p_{110}) \,\big\}. \quad (1.60)$$

The set $\mathcal{Q}_{X_1 \perp\!\!\!\perp \{X_2, X_3\}}$ representing the statement $\{X_1\}$ *is independent of* $\{X_2, X_3\}$ consists of the six 2×2 subdeterminants of the 2×4 matrix

$$\begin{pmatrix} p_{000} & p_{001} & p_{010} & p_{011} \\ p_{100} & p_{101} & p_{110} & p_{111} \end{pmatrix}. \qquad (1.61)$$

Each of these three statements specifies a model, which is a subset of the 7-simplex Δ with coordinates $p_{i_1 i_2 i_3}$. The model (1.59) has dimension five, the model (1.60) has dimension six, and the model (1.61) has dimension four.

In general, we write $V_\Delta(A \perp\!\!\!\perp B \,|\, C)$ for the family of all joint probability distributions that satisfy the quadratic equations in $\mathcal{Q}_{A \perp\!\!\!\perp B \,|\, C}$. The model $V_\Delta(A \perp\!\!\!\perp B \,|\, C)$ is a subset of the $(m-1)$-dimensional probability simplex Δ.

Consider any finite collection of conditional independence statements (1.57):

$$\mathcal{M} \quad = \quad \big\{A^{(1)} \perp\!\!\!\perp B^{(1)} \,|\, C^{(1)},\, A^{(2)} \perp\!\!\!\perp B^{(2)} \,|\, C^{(2)},\, \ldots,\, A^{(m)} \perp\!\!\!\perp B^{(m)} \,|\, C^{(m)}\big\}.$$

We write $\mathcal{Q}_\mathcal{M}$ for the set of quadratic forms representing these statements:

$$\mathcal{Q}_\mathcal{M} \quad = \quad \mathcal{Q}_{A^{(1)} \perp\!\!\!\perp B^{(1)} \,|\, C^{(1)}} \,\cup\, \mathcal{Q}_{A^{(2)} \perp\!\!\!\perp B^{(2)} \,|\, C^{(2)}} \,\cup\, \cdots \,\cup\, \mathcal{Q}_{A^{(m)} \perp\!\!\!\perp B^{(m)} \,|\, C^{(m)}}.$$

The common zero set of these quadratic forms in the simplex Δ equals

$$V_\Delta(\mathcal{M}) \quad = \quad V_\Delta(A^{(1)} \perp\!\!\!\perp B^{(1)} \,|\, C^{(1)}) \,\cap\, \cdots \,\cap\, V_\Delta(A^{(m)} \perp\!\!\!\perp B^{(m)} \,|\, C^{(m)}).$$

We call $V_\Delta(\mathcal{M})$ the *conditional independence model* of $\mathcal{M}$. This model is the family of joint probability distributions which satisfy all the statements in $\mathcal{M}$.

Example 1.28 Let $n = 3$ and $i_1 = i_2 = i_3 = \{0, 1\}$. Consider the model

$$\mathcal{M} \quad = \quad \big\{\, X_1 \perp\!\!\!\perp X_2 \,|\, X_3 \,,\; X_1 \perp\!\!\!\perp X_3 \,|\, X_2 \,\big\}.$$

These two independence statements translate into four quadratic forms:

$$\begin{aligned} \mathcal{Q}_\mathcal{M} \quad = \quad \big\{\, & p_{000}p_{110} - p_{010}p_{100} \,,\; p_{001}p_{111} - p_{011}p_{101} \,, \\ & p_{000}p_{101} - p_{001}p_{100} \,,\; p_{010}p_{111} - p_{011}p_{110} \,\big\}. \end{aligned}$$

The model $V_\Delta(\mathcal{M})$ consists of three components. Two of them are tetrahedra which are faces of the 7-dimensional simplex Δ. These two tetrahedra are

$$\begin{aligned} X_2 = X_3 : &\qquad \{\, p \in \Delta \;:\; p_{001} = p_{010} = p_{101} = p_{110} = 0 \,\} \\ X_2 \neq X_3 : &\qquad \{\, p \in \Delta \;:\; p_{000} = p_{011} = p_{100} = p_{111} = 0 \,\}. \end{aligned}$$

Only the third component meets the interior of the simplex. That component is the four-dimensional variety $V_\Delta(X_1 \perp\!\!\!\perp \{X_2, X_3\})$ which consists of all distributions $p \in \Delta$ for which the 2×4 matrix in (1.61) has rank one. This analysis shows that for strictly positive probability distributions we have

$$X_1 \perp\!\!\!\perp X_2 \,|\, X_3 \quad \text{and} \quad X_1 \perp\!\!\!\perp X_3 \,|\, X_2 \quad \text{implies} \quad X_1 \perp\!\!\!\perp \{X_2, X_3\}, \tag{1.62}$$

but there exist distributions under which some probabilities are zero such that (1.62) is wrong.

We are now prepared to define graphical models, starting with the undirected case. Let G be an undirected graph with vertices $X_1, X_2, \ldots, X_n$. Let $\mathcal{M}_G$ denote the set of all conditional independence statements

$$X_i \perp\!\!\!\perp X_j \,|\, \{X_1, \ldots, X_n\} \backslash \{X_i, X_j\} \tag{1.63}$$

where (X_i, X_j) runs over all pairs of nodes that are **not** connected by an edge in G. In what follows we let Δ^0 denote the **open** probability simplex of dimension $m-1$. The *Markov random field* (or *undirected graphical model* or *Markov network*) defined by the graph G is the model $V_{\Delta^0}(\mathcal{M}_G)$. This is the set of all strictly positive distributions which satisfy the statements in $\mathcal{M}_G$.

In the literature on graphical models, the set $\mathcal{M}_G$ is known as the *pairwise Markov property* on the graph G. There are also two larger sets of conditional independence statements that can be derived from the graph, called the *local Markov property* and the *global Markov property* [Lauritzen, 1996], which specify the same variety $V_{\Delta^0}(\mathcal{M}_G)$ in the open simplex Δ^0. For simplicity, we restrict our presentation to the pairwise Markov property (1.63).

Example 1.29 Let $n = 4$ and G the 4-chain graph (Figure 1.3). The graph G is drawn with the random variables labeling the nodes, and shaded nodes indicating that all random variables are observed.

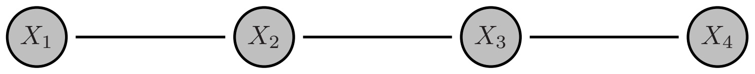

Fig. 1.3. Graph of the 4-chain Markov random field.

There are 3 pairs of nodes not connected by an edge, so that

$$\mathcal{M}_G \quad = \quad \big\{X_1 \perp\!\!\!\perp X_3 \,|\, \{X_2, X_4\}\,,\; X_1 \perp\!\!\!\perp X_4 \,|\, \{X_2, X_3\}\,,\; X_2 \perp\!\!\!\perp X_4 \,|\, \{X_1, X_3\}\big\}.$$

For binary alphabets Σ_i the set $\mathcal{Q}_{\mathcal{M}_G}$ consists of the twelve quadratic forms

$$\begin{gathered}
p_{0010}p_{1000} - p_{0000}p_{1010}\,,\; p_{0001}p_{1000} - p_{0000}p_{1001}\,,\; p_{0001}p_{0100} - p_{0000}p_{0101}\,,\\
p_{0011}p_{1001} - p_{0001}p_{1011}\,,\; p_{0011}p_{1010} - p_{0010}p_{1011}\,,\; p_{0011}p_{0110} - p_{0010}p_{0111}\,,\\
p_{0110}p_{1100} - p_{0100}p_{1110}\,,\; p_{0101}p_{1100} - p_{0100}p_{1101}\,,\; p_{1001}p_{1100} - p_{1000}p_{1101}\,,\\
p_{0111}p_{1101} - p_{0101}p_{1111}\,,\; p_{0111}p_{1110} - p_{0110}p_{1111}\,,\; p_{1011}p_{1110} - p_{1010}p_{1111}.
\end{gathered}$$

Every Markov random field $V_{\Delta^0}(\mathcal{M}_G)$ is, in fact, a toric model specified parametrically by a matrix A_G with entries in $\{0,1\}$. The columns of the matrix A_G are indexed by $\prod_{i=1}^{n} \Sigma_i$. The rows are indexed by all the possible assignments to the maximal cliques in G. A *clique* in G is a collection of nodes any of two of which are connected by an edge. If the graph G contains no triangles (as in Example 1.29 then the maximal cliques are just the edges.

An entry in the matrix A_G is 1 if the states corresponding to the column agree with the assignments specified by the row and is 0 otherwise. Returning to Example 1.29, the matrix A_G has 16 columns, and 12 rows. The rows are indexed by tuples (i,j,σ_i,σ_j) where $\{X_i, X_j\}$ is an edge of the graph G and $\sigma_i \in \Sigma_i$ and $\sigma_j \in \Sigma_j$. The nonzero entries of A_G are therefore given by rows (i,j,σ_i,σ_j) and columns $\pi_1\pi_2\cdots\pi_n$ where $\sigma_i = \pi_i$ and $\sigma_j = \pi_j$:

$$\begin{array}{c|cccccccccccccccc|}
 & 0000 & 0001 & 0010 & 0011 & 0100 & 0101 & 0110 & 0111 & 1000 & 1001 & 1010 & 1011 & 1100 & 1101 & 1110 & 1111 \\
00\cdot\cdot & 1&1&1&1&0&0&0&0&0&0&0&0&0&0&0&0\\
01\cdot\cdot & 0&0&0&0&1&1&1&1&0&0&0&0&0&0&0&0\\
10\cdot\cdot & 0&0&0&0&0&0&0&0&1&1&1&1&0&0&0&0\\
11\cdot\cdot & 0&0&0&0&0&0&0&0&0&0&0&0&1&1&1&1\\
\cdot 00\cdot & 1&1&0&0&0&0&0&0&1&1&0&0&0&0&0&0\\
\cdot 01\cdot & 0&0&1&1&0&0&0&0&0&0&1&1&0&0&0&0\\
\cdot 10\cdot & 0&0&0&0&1&1&0&0&0&0&0&0&1&1&0&0\\
\cdot 11\cdot & 0&0&0&0&0&0&1&1&0&0&0&0&0&0&1&1\\
\cdot\cdot 00 & 1&0&0&0&1&0&0&0&1&0&0&0&1&0&0&0\\
\cdot\cdot 01 & 0&1&0&0&0&1&0&0&0&1&0&0&0&1&0&0\\
\cdot\cdot 10 & 0&0&1&0&0&0&1&0&0&0&1&0&0&0&1&0\\
\cdot\cdot 11 & 0&0&0&1&0&0&0&1&0&0&0&1&0&0&0&1
\end{array}$$

Each of the 12 rows corresponds to pairs in $i_1 \times i_2$ or $i_2 \times i_3$ or $i_3 \times i_4$. For instance, the label $\cdot 12 \cdot$ of the sixth row represents $(i,j,\sigma_i,\sigma_j) = (2,3,1,2)$. We note that each of the twelve quadrics in Example 1.29 corresponds to a vector in the kernel of the matrix A_G. For instance, the quadric $p_{0010}p_{1000} - p_{0000}p_{1010}$ corresponds to the following vector in the kernel of A_G:

$$\begin{array}{cccccccccccccccc}
0000 & 0001 & 0010 & 0011 & 0100 & 0101 & 0110 & 0111 & 1000 & 1001 & 1010 & 1011 & 1100 & 1101 & 1110 & 1111 \\
-1 & 0 & 1 & 0 & 0 & 0 & 0 & 0 & 1 & 0 & -1 & 0 & 0 & 0 & 0 & 0
\end{array}$$

The relationship between $\mathcal{M}_G$ and the matrix A_G generalizes as follows:

Theorem 1.30 (Undirected Hammersley-Clifford) *The Markov random field $V_{\Delta^0}(\mathcal{M}_G)$ coincides with the toric model specified by the matrix A_G.*

Proof See [Lauritzen, 1996] and [Geiger *et al.*, 2005]. □

Markov random fields are toric because their defining conditional independence statements $A \perp\!\!\!\perp B \,|\, C$ have the property that

$$A \cup B \cup C = \{X_1, X_2, \ldots, X_n\}. \tag{1.64}$$

This property ensures that all the quadrics in $\mathcal{Q}_{A \perp\!\!\!\perp B \,|\, C}$ are differences of two monomials of the form $p_{\cdots}p_{\cdots} - p_{\cdots}p_{\cdots}$. If the property (1.64) does not hold, then the quadrics have more terms and the models are generally not toric.

Remark 1.31 It is important to note that the conditional independence statements for a Markov random field are based on pairs of random variables not joined by an edge in the graph. This should be contrasted with the parameters in the toric model, where there are sets of parameters for each maximal clique in the graph. The toric model parameters do not, in general, have an interpretation as conditional probabilities. They are sometimes called *potentials.*

We now define directed graphical models which are generally not toric. We also return to the closed simplex Δ. Let D be an acyclic directed graph with nodes $X_1, X_2, \ldots, X_n$. For any nodes X_i, let $\mathrm{pa}(X_i)$ denote the set of *parents* of X_i in D and let $\mathrm{nd}(X_i)$ denote the set of *non-descendants* of X_i in D which are not parents of X_i. The *directed graphical model* of D is described by the following set of independence statements:

$$\mathcal{M}_D \quad = \quad \big\{ X_i \perp\!\!\!\perp \mathrm{nd}(X_i) \,|\, \mathrm{pa}(X_i) \;\; : \;\; i = 1, 2, \ldots, n \big\}.$$

The directed graphical model $V_\Delta(\mathcal{M}_D)$ admits a polynomial parameterization, which amounts to a directed version of the Hammersley-Clifford theorem. Before stating this parameterization in general, we first discuss a small example.

Example 1.32 Let D be the directed graph with nodes $1, 2, 3, 4$ and four edges $(1,2), (1,3), (2,4), (3,4)$. Then $\mathcal{M}_D \; = \; \big\{ \, X_2 \perp\!\!\!\perp X_3 \,|\, X_1 \, , \;\, X_4 \perp\!\!\!\perp X_1 \,|\, \{X_2, X_3\} \, \big\}$. The quadrics associated with this directed graphical model are

$$\begin{aligned} \mathcal{Q}_{\mathcal{M}_D} \quad = \quad \big\{ \, & (p_{0000} + p_{0001})(p_{0110} + p_{0111}) - (p_{0010} + p_{0011})(p_{0100} + p_{0101}), \\ & (p_{1000} + p_{1001})(p_{1110} + p_{1111}) - (p_{1010} + p_{1011})(p_{1100} + p_{1101}), \\ & p_{0000}p_{1001} - p_{0001}p_{1000} \, , \;\, p_{0010}p_{1011} - p_{0011}p_{1010}, \\ & p_{0100}p_{1101} - p_{0101}p_{1100} \, , \;\, p_{0110}p_{1111} - p_{0111}p_{1110} \big\}. \end{aligned}$$

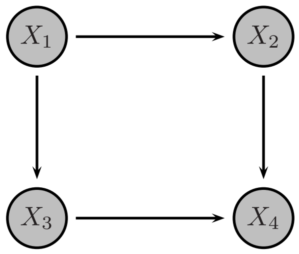

Fig. 1.4. The directed graphical model in Example 1.32

The model $V_\Delta(\mathcal{M}_D)$ is nine-dimensional inside the 15-dimensional simplex Δ.

We present this model as the image of a polynomial map $F_D : \mathbb{R}^9 \to \mathbb{R}^{16}$. The vector of $9 = 2^0 + 2^1 + 2^1 + 2^2$ parameters for this model is written

$$\theta \quad = \quad \big(a,\, b_1, b_2,\, c_1, c_2,\, d_{11}, d_{12}, d_{21}, d_{22}\big).$$

The letters a, b, c, d correspond to the random variables X_1, X_2, X_3, X_4 in this order. The parameters represent the probabilities of each node given its parents. For instance, the parameter d_{21} is the probability of the event "$X_4 = 1$ given $X_2 = 2$ and $X_3 = 1$". The coordinates of the map $\mathbf{f} : \theta \mapsto p$ are

$$\begin{aligned}
p_{0000} &= a \cdot b_1 \cdot c_1 \cdot d_{11} \\
p_{0001} &= a \cdot b_1 \cdot c_1 \cdot (1 - d_{11}) \\
p_{0010} &= a \cdot b_1 \cdot (1 - c_1) \cdot d_{12} \\
p_{0011} &= a \cdot b_1 \cdot (1 - c_1) \cdot (1 - d_{12}) \\
p_{0100} &= a \cdot (1 - b_1) \cdot c_1 \cdot d_{21} \\
p_{0101} &= a \cdot (1 - b_1) \cdot c_1 \cdot (1 - d_{21}) \\
p_{0110} &= a \cdot (1 - b_1) \cdot (1 - c_1) \cdot d_{22} \\
p_{0111} &= a \cdot (1 - b_1) \cdot (1 - c_1) \cdot (1 - d_{22}) \\
p_{1000} &= (1 - a) \cdot b_2 \cdot c_2 \cdot d_{11} \\
p_{1001} &= (1 - a) \cdot b_2 \cdot c_2 \cdot (1 - d_{11}) \\
p_{1010} &= (1 - a) \cdot b_2 \cdot (1 - c_2) \cdot d_{12} \\
p_{1011} &= (1 - a) \cdot b_2 \cdot (1 - c_2) \cdot (1 - d_{12}) \\
p_{1100} &= (1 - a) \cdot (1 - b_2) \cdot c_2 \cdot d_{21} \\
p_{1101} &= (1 - a) \cdot (1 - b_2) \cdot c_2 \cdot (1 - d_{21}) \\
p_{1110} &= (1 - a) \cdot (1 - b_2) \cdot (1 - c_2) \cdot d_{22} \\
p_{1111} &= (1 - a) \cdot (1 - b_2) \cdot (1 - c_2) \cdot (1 - d_{22}).
\end{aligned}$$

Note that the six quadrics in $\mathcal{Q}_{\mathcal{M}_D}$ are zero for these expressions, and also

$$\sum_{i=1}^{2}\sum_{j=1}^{2}\sum_{k=1}^{2}\sum_{l=1}^{2} p_{ijkl} \quad = \quad 1.$$

Let us return to our general discussion, where D is an acyclic directed graph on n nodes, each associated with a finite alphabet Σ_i. It is known that the dimension of the directed graphical model $V_\Delta(\mathcal{M}_D)$ equals

$$d \quad = \quad \sum_{i=1}^{n} (|\Sigma_i| - 1) \cdot \prod_{j \in \mathrm{pa}(X_i)} |\Sigma_j|. \tag{1.65}$$

We introduce a parameter $\theta_{(\nu,\pi)}$ for each element $(\nu,\sigma) \in \Sigma_i \times \prod_{j\in \mathrm{pa}(i)} \Sigma_j$, where i ranges over all nodes. Thus the total number of parameters is d. These parameters are supposed to satisfy the linear equations

$$\sum_{\nu \in \Sigma_i} \theta_{(\nu,\pi)} \quad = \quad 1 \qquad \text{for all} \quad \sigma \in \prod_{j \in \mathrm{pa}(X_i)} \Sigma_j. \tag{1.66}$$

Thus the number of free parameters is equal to the right hand side of (1.65). With the directed acyclic graph D we associate the following monomial map:

$$\begin{aligned} &F_D \,:\, \mathbb{R}^d \,\rightarrow\, \mathbb{R}^m\,,\ \theta \,\mapsto\, p \\ &\text{where} \quad p_\sigma \ = \ \textstyle\prod_{i=1}^{n} \theta_{(\sigma_i, \sigma|_{\mathrm{pa}(X_i)})} \quad \text{for all} \quad \sigma \in \prod_{i=1}^{n} \Sigma_i \end{aligned}$$

Here $\sigma|_{\mathrm{pa}(X_i)}$ denotes the restriction of the vector σ to $\prod_{j\in \mathrm{pa}(X_i)} \Sigma_j$. Let Θ_1 be the set of non-negative parameter vectors $\theta \in \mathbb{R}^d$ which satisfy (1.66). The following theorem generalizes the result derived for the graph in Example 1.32.

Theorem 1.33 (Directed Hammersley-Clifford) *The directed graphical model $V_\Delta(\mathcal{M}_D)$ equals the image of the parameter space Θ_1 under the map F_D.*

Proof See Theorem 3.27 in [Lauritzen, 1996] and Theorem 3 in [Garcia *et al.*, 2004]. □

Remark 1.34 Suppose that $D = T$ is a rooted tree with all edges directed away from the root $\mathbf{r}$. The directed graphical model $V_\Delta(\mathcal{M}_D)$ is precisely the fully observed tree model, and the parameterization F_D specializes to the parameterization given in (1.53). It is known that the model $V_\Delta(\mathcal{M}_T)$ does not depend on the location of the root $\mathbf{r}$, and, in fact, the model coincides with the Markov random field $V_\Delta(\mathcal{M}_G)$, where G denotes the undirected tree.

The *inference* problem for graphical models is to compute

$$\sum_{\sigma \in S} p_\sigma, \tag{1.67}$$

where S ranges over certain subsets of $\prod_{i=1}^{n} \Sigma_i$.

The evaluation of the sum in (1.67) may be performed using ordinary arithmetic, or with the *tropical semiring*, using *min* instead of $+$, and $+$ instead of $\times$, and replacing p_σ with the negative of its logarithm (see Section 2.1). In the case where $S = \prod_{i=1}^{n} \Sigma_i$, (1.67) is equivalent to computing the partition function. If S is not equal to the entire product of the alphabets, then it often fixes some of the coordinates. Here the inference problem involves a marginalization, which we think of as evaluating one coordinate polynomial of the model. Both of these problems are important statistically and very relevant for biological applications. For example, if some of the variables X_i of a Markov random field or directed graphical model D are hidden, then this gives rise to a marginalization map ρ_D and to a hidden model $\mathbf{f}_D = \rho_D \circ F_D$. Evaluating one coordinate of the polynomial map $\mathbf{f}_D$, also known as *maximum a posteriori (MAP) inference* , is therefore exactly the evaluation of a subsum of the partition function. The case of trees (discussed in Remark 1.34) is of particular interest in computational biology. More examples are discussed in Chapter 2, and connections to biology are developed in Chapter 4.

Remark 1.35 If inference with a graphical model involves computing the partition function tropically, then the model is referred to as *discriminative*. In the case where a specific coordinate(s) are selected before summing (1.67), then the model is *generative*. These terms are used in statistical learning theory.

Inference can be computationally nontrivial for two reasons. In order to compute the partition function, the number of terms in the sum is equal to m which can be very large since many applications of graphical models require that the models have large numbers of random variables. One may easily encounter $n = 200$ binary random variables, in which case

$$m = 1606938044258990275541962092341162602522202993782792835301376.$$

The success of graphical models has been due to the possibility of efficient inference for many models of interest. The organizing principle is the generalized distributive law which gives a recursive decomposition of (1.67) according to the graph underlying the model.

Rather than explaining the details of the generalized distributive law in general, we illustrate its origins and application with the hidden Markov model:

Example 1.36 Recall that the hidden Markov model is a polynomial map $\mathbf{f}$ from the parameter space $\mathbb{R}^{l(l-1)} \times \mathbb{R}^{l(l'-1)}$ to the probability space $\mathbb{R}^{(l')^n}$. Consider the case $n = 4$. If we treat the hidden Markov model as a special case of the tree model (compare Figure 1.5 with Figure 1.2), allowing for different parameters on each edge, then a coordinate polynomial is

$$p_{j_1j_2j_3j_4} \;=\; \sum_{i_1\in\Sigma}\sum_{i_2\in\Sigma}\sum_{i_3\in\Sigma}\sum_{i_4\in\Sigma} \theta^{X_1Y_1}_{i_1j_1}\theta^{X_1X_2}_{i_1i_2}\theta^{X_2Y_2}_{i_2j_2}\theta^{X_2X_3}_{i_2i_3}\theta^{X_3Y_3}_{\sigma_3j_3}\theta^{X_3X_4}_{\sigma_3i_4}\theta^{X_4Y_4}_{i_4j_4}.$$

This sum $p_{j_1j_2j_3j_4}$ can be rewritten as follows:

$$\sum_{i_1\in\Sigma}\theta^{X_1Y_1}_{i_1j_1}\left(\sum_{i_2\in\Sigma}\theta^{X_1X_2}_{i_1i_2}\theta^{X_2Y_2}_{i_2j_2}\left(\sum_{i_3\in\Sigma}\theta^{X_2X_3}_{i_2i_3}\theta^{X_3Y_3}_{i_3j_3}\left(\sum_{i_4\in\Sigma}\theta^{X_3X_4}_{i_3i_4}\theta^{X_4Y_4}_{i_4j_4}\right)\right)\right).$$

The graph for the hidden Markov model is shown in Figure 1.5. Note that the unshaded nodes correspond to random variables which are summed in the marginalization map, thus resulting in one sum for each unshaded node.

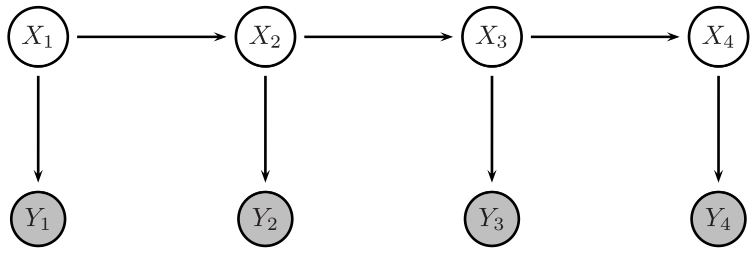

Fig. 1.5. Graph of the hidden Markov model.

This connection between graphs and recursive decompositions is exactly what is made precise by the *junction tree algorithm* (or *sum-product algorithm* or *generalized distributive law* [Aji and McEliece, 2000]). Note that in terms of algorithmic complexity, the latter formulation, while equivalent to the first, requires only $O(n)$ additions and multiplications for an HMM of length n in order to compute $p_{j_1j_2\cdots j_n}$. The naive formulation requires $O(l^n)$ additions.

The inference problem for graphical models can be formulated as an instance of a more general *marginalization of a product function* (MPF) problem. Formally, suppose that we have n indeterminates $x_1,\ldots,x_n$ taking on values in finite sets $A_1,\ldots,A_n$. Let R be a commutative semiring and α_i : $A_1\times A_2\cdots\times A_n\to R$ $(i=1,\ldots,m)$ be functions with values in R. The MPF problem is to evaluate, for a set $S=\{j_1,\ldots,j_r\}\subset[n]$,

$$\beta(S) \quad = \bigoplus_{x_{j_1}\in A_{j_1},\ldots,x_{j_r}\in A_{j_r}} \bigodot_{i=1}^{M}\alpha_i(x_1,\ldots,x_n).$$

Two important semirings R which make their appearance in the next chapter are the *tropical semiring* (or *min-plus algebra*, in Section 2.1) and the *polytope algebra* (in Section 2.3).

2
Computation

Lior Pachter

Bernd Sturmfels

Many of the algorithms used for biological sequence analysis are *discrete algorithms*, i.e., the key feature of the problems being solved is that some optimization needs to be performed on a finite set. Discrete algorithms are complementary to *numerical algorithms*, such as Expectation Maximization, Singular Value Decomposition and Interval Arithmetic, which make their appearance in later chapters. They are also distinct from *algebraic algorithms*, such as the Buchberger Algorithm, which is discussed in Section 3.1. In what follows we introduce discrete algorithms and mathematical concepts which are relevant for biological sequence analysis. The final section of this chapter offers an annotated list of the computer programs which are used throughout the book. The list ranges over all three themes (discrete, algebraic, numerical) and includes software tools which are useful for research in computational biology.

Some discrete algorithms arise naturally from algebraic statistical models, which are characterized by finitely many polynomials, each with finitely many terms. Inference methods for drawing conclusions about missing or hidden data depend on the combinatorial structure of the polynomials in the algebraic representation of the models. In fact, many widely used dynamic programming methods, such as the *Needleman-Wunsch algorithm* for sequence alignment, can be interpreted as evaluating polynomials, albeit with *tropical arithmetic*.

The combinatorial structure of a polynomial, or polynomial map, is encoded in its *Newton polytope*. Thus every algebraic statistical model has a Newton polytope, and it is the structure of this polytope which governs dynamic programming related to that model. Computing the entire polytope is what we call *parametric inference*. This computation can be done efficiently in the *polytope algebra* which is a natural generalization of tropical arithmetic. In Section 2.4 we study the combinatorics of one of the central objects in genome analysis, phylogenetic trees, with an emphasis on the *neighbor joining algorithm*.

2.1 Tropical arithmetic and dynamic programming

Dynamic programming was introduced by Bellman in the 1950s to solve sequential decision problems with a compositional cost structure. Dynamic programming offers efficient methods for progressively building a set of scores or probabilities in order to solve a problem, and many discrete algorithms for biological sequence analysis are based on the principles of dynamic programming.

A convenient algebraic structure for stating various dynamic programming algorithms is the *tropical semiring* $(\mathbb{R} \cup \{\infty\}, \oplus, \odot)$. The tropical semiring consists of the real numbers $\mathbb{R}$, together with an extra element ∞, and with the arithmetic operations of addition and multiplication redefined as follows:

$$x \oplus y \;:=\; \min(x, y) \qquad \text{and} \qquad x \odot y \;:=\; x + y.$$

In other words, the *tropical sum* of two real numbers is their minimum, and the *tropical product* of two numbers is their sum. Here are some examples of how to do arithmetic in this strange number system. The tropical sum of 3 and 7 is 3. The tropical product of 3 and 7 equals 10. We write this as follows:

$$3 \oplus 7 \;=\; 3 \qquad \text{and} \qquad 3 \odot 7 \;=\; 10.$$

Many of the familiar axioms of arithmetic remain valid in the tropical semiring. For instance, both addition and multiplication are *commutative*:

$$x \oplus y \;=\; y \oplus x \qquad \text{and} \qquad x \odot y \;=\; y \odot x.$$

The *distributive law* holds for tropical addition and tropical multiplication:

$$x \odot (y \oplus z) \quad = \quad x \odot y \;\oplus\; x \odot z.$$

Both arithmetic operations have a *neutral element*. Infinity is the neutral element for addition and zero is the neutral element for multiplication:

$$x \;\oplus\; \infty \;=\; x \qquad \text{and} \qquad x \;\odot\; 0 \;=\; x.$$

The tropical *addition table* and the tropical *multiplication table* look like this:

$\oplus$	**1**	**2**	**3**	**4**	**5**	**6**	**7**
1	1	1	1	1	1	1	1
2	1	2	2	2	2	2	2
3	1	2	3	3	3	3	3
4	1	2	3	4	4	4	4
5	1	2	3	4	5	5	5
6	1	2	3	4	5	6	6
7	1	2	3	4	5	6	7

$\odot$	**1**	**2**	**3**	**4**	**5**	**6**	**7**
1	2	3	4	5	6	7	8
2	3	4	5	6	7	8	9
3	4	5	6	7	8	9	10
4	5	6	7	8	9	10	11
5	6	7	8	9	10	11	12
6	7	8	9	10	11	12	13
7	8	9	10	11	12	13	14

Although tropical addition and multiplication are straightforward, subtraction is tricky. There is no tropical "10 minus 3" because the equation $3 \oplus x = 10$ has no solution x. In this book we use addition $\oplus$ and multiplication $\odot$ only.

Example 2.1 It is important to keep in mind that 0 is the multiplicatively neutral element. For instance, the *tropical binomial coefficients* are all 0, as in

$$\begin{aligned}(x \oplus y)^3 &= (x \oplus y) \odot (x \oplus y) \odot (x \oplus y) \\ &= 0 \odot x^3 \oplus 0 \odot x^2 y \oplus 0 \odot xy^2 \oplus 0 \odot y^3.\end{aligned}$$

The zero coefficients can be dropped in this identity, and we conclude

$$(x \oplus y)^3 \quad = \quad x^3 \oplus x^2 y \oplus xy^2 \oplus y^3 \quad = \quad x^3 \oplus y^3.$$

This identity is known as *Freshman's dream* and is verified by noting that

$$3 \cdot \min\{x, y\} \quad = \quad \min\{\, 3x,\, 2x+y,\, x+2y,\, 3y \,\} \quad = \quad \min\{\, 3x,\, 3y \,\}$$

holds for all real numbers x and y.

The familiar linear algebra operations of adding and multiplying vectors and matrices make perfect sense over the tropical semiring. For instance, the tropical scalar product in $\mathbb{R}^3$ of a row vector with a column vector is the scalar

$$\begin{aligned}(u_1, u_2, u_3) \odot (v_1, v_2, v_3)^T &= u_1 \odot v_1 \oplus u_2 \odot v_2 \oplus u_3 \odot v_3 \\ &= \min\bigl\{u_1 + v_1,\, u_2 + v_2,\, u_3 + v_3\bigr\}.\end{aligned}$$

Here is the product of a column vector and a row vector of length three:

$$\begin{aligned}&(u_1, u_2, u_3)^T \odot (v_1, v_2, v_3) \\ &= \begin{pmatrix} u_1 \odot v_1 & u_1 \odot v_2 & u_1 \odot v_3 \\ u_2 \odot v_1 & u_2 \odot v_2 & u_2 \odot v_3 \\ u_3 \odot v_1 & u_3 \odot v_2 & u_3 \odot v_3 \end{pmatrix} = \begin{pmatrix} u_1 + v_1 & u_1 + v_2 & u_1 + v_3 \\ u_2 + v_1 & u_2 + v_2 & u_2 + v_3 \\ u_3 + v_1 & u_3 + v_2 & u_3 + v_3 \end{pmatrix}.\end{aligned}$$

This 3×3 matrix is said to have *tropical rank one.*

To see why tropical arithmetic is relevant for discrete algorithms we consider the problem of finding shortest paths in a weighted directed graph. This is a standard problem of dynamic programming. Let G be a directed graph with n nodes which are labeled by $1, 2, \ldots, n$. Every directed edge (i, j) in G has an associated length d_{ij} which is a non-negative real number. If (i, j) is not an edge of G then we set $d_{ij} = +\infty$. We represent the weighted directed graph G by its $n \times n$ adjacency matrix $D_G = \bigl(d_{ij}\bigr)$ whose off-diagonal entries are the edge lengths d_{ij}. The diagonal entries of D_G are zero, i.e., $d_{ii} = 0$ for all i.

If G is an undirected graph with edge lengths, then we can represent G as a directed graph with two directed edges (i, j) and (j, i) for each undirected edge $\{i, j\}$. In that special case, D_G is a symmetric matrix, and we can think of $d_{ij} = d_{ji}$ as the distance between node i and node j. For a general directed graph G, the adjacency matrix D_G will not be symmetric. Consider the result of tropically multiplying the $n \times n$ matrix D_G with itself $n-1$ times:

$$D_G^{\odot n-1} \quad = \quad D_G \odot D_G \odot \cdots \odot D_G. \tag{2.1}$$

This is an $n \times n$ matrix with entries in $\mathbb{R}_{\geq 0} \cup \{+\infty\}$.

Proposition 2.2 *Let G be a weighted directed graph on n nodes with $n \times n$ adjacency matrix D_G. Then the entry of the matrix $D_G^{\odot n-1}$ in row i and column j equals the length of a shortest path from node i to node j in G.*

Proof Let $d_{ij}^{(r)}$ denote the minimum length of any path from node i to node j which uses at most r edges in G. Thus $d_{ij}^{(1)} = d_{ij}$ for any two nodes i and j. Since the edge weights d_{ij} were assumed to be non-negative, a shortest path from node i to node j visits each node of G at most once. In particular, any such shortest path in the directed graph G uses at most $n-1$ directed edges. Hence the length of a shortest path from i to j equals $d_{ij}^{(n-1)}$.

For $r \geq 2$ we have the following recursive formula for these shortest paths:

$$d_{ij}^{(r)} \quad = \quad \min\bigl\{d_{ik}^{(r-1)} + d_{kj} \,:\, k = 1, 2, \ldots, n\bigr\}. \tag{2.2}$$

Using tropical arithmetic, this formula can be rewritten as follows

$$\begin{aligned} d_{ij}^{(r)} \quad &= \quad d_{i1}^{(r-1)} \odot d_{1j} \;\oplus\; d_{i2}^{(r-1)} \odot d_{2j} \;\oplus\; \cdots \;\oplus\; d_{in}^{(r-1)} \odot d_{nj}. \\ &= \quad (d_{i1}^{(r-1)}, d_{i2}^{(r-1)}, \ldots, d_{in}^{(r-1)}) \odot (d_{1j}, d_{2j}, \ldots, d_{nj})^T. \end{aligned}$$

From this it follows, by induction on r, that $d_{ij}^{(r)}$ coincides with the entry in row i and column j of the $n \times n$ matrix $D_G^{\odot r}$. Indeed, the right hand side of the recursive formula is the tropical product of row i of $D_G^{\odot r-1}$ and column j of D_G, which is the (i,j) entry of $D_G^{\odot r}$. In particular, $d_{ij}^{(n-1)}$ coincides with the entry in row i and column j of $D_G^{\odot n-1}$. This proves the claim. □

The iterative evaluation of the formula (2.2) is known as the *Floyd-Warshall Algorithm* [Floyd, 1962, Warshall, 1962] for finding shortest paths in a weighted digraph. Floyd-Warshall simply means performing the matrix multiplication

$$D_G^{\odot r} \quad = \quad D_G^{\odot r-1} \odot D_G \qquad \text{for } r = 2, \ldots, n-1.$$

Example 2.3 Let G be the complete bi-directed graph on $n = 4$ nodes with

$$D_G \quad = \quad \begin{pmatrix} 0 & 1 & 3 & 7 \\ 2 & 0 & 1 & 3 \\ 4 & 5 & 0 & 1 \\ 6 & 3 & 1 & 0 \end{pmatrix}.$$

The first and second tropical power of this matrix are found to be

$$D_G^{\odot 2} \;=\; \begin{pmatrix} 0 & 1 & 2 & 4 \\ 2 & 0 & 1 & 2 \\ 4 & 4 & 0 & 1 \\ 5 & 3 & 1 & 0 \end{pmatrix} \qquad \text{and} \qquad D_G^{\odot 3} \;=\; \begin{pmatrix} 0 & 1 & 2 & 3 \\ 2 & 0 & 1 & 2 \\ 4 & 4 & 0 & 1 \\ 5 & 3 & 1 & 0 \end{pmatrix}.$$

The entries in $D_G^{\odot 3}$ are the lengths of the shortest paths in the graph G.

The tropical computation above can be related to the following matrix computation in ordinary arithmetic. Let ϵ denote an indeterminate, and let $A_G(\epsilon)$ be the $n \times n$ matrix whose entries are the monomials $\epsilon^{d_{ij}}$. In our example,

$$A_G(\epsilon) \;=\; \begin{pmatrix} 1 & \epsilon^1 & \epsilon^3 & \epsilon^7 \\ \epsilon^2 & 1 & \epsilon^1 & \epsilon^3 \\ \epsilon^4 & \epsilon^5 & 1 & \epsilon^1 \\ \epsilon^6 & \epsilon^3 & \epsilon^1 & 1 \end{pmatrix}.$$

Now compute the third power of this matrix in ordinary arithmetic

$$A_G(\epsilon)^3 \;=\; \begin{pmatrix} 1+3\epsilon^3+\cdots & 3\epsilon+\epsilon^4+\cdots & 3\epsilon^2+3\epsilon^3+\cdots & \epsilon^3+6\epsilon^4+\cdots \\ 3\epsilon^2+4\epsilon^5+\cdots & 1+3\epsilon^3+\cdots & 3\epsilon+\epsilon^3+\cdots & 3\epsilon^2+3\epsilon^3+\cdots \\ 3\epsilon^4+2\epsilon^6+\cdots & 3\epsilon^4+6\epsilon^5+\cdots & 1+3\epsilon^2+\cdots & 3\epsilon+\epsilon^3+\cdots \\ 6\epsilon^5+3\epsilon^6+\cdots & 3\epsilon^3+\epsilon^5+\cdots & 3\epsilon+\epsilon^3+\cdots & 1+3\epsilon^2+\cdots \end{pmatrix}.$$

The entry of $A_G(\epsilon)^3$ in row i and column j is a polynomial in ϵ which represents the lengths of all paths from node i to node j using at most three edges. The lowest exponent appearing in this polynomial is the (i,j)-entry in the matrix $D_G^{\odot 3}$. This is a general phenomenon, summarized informally as follows:

$$\text{tropical} \;=\; \lim_{\epsilon\to 0} \log\bigl(\text{classical}(\epsilon)\bigr) \tag{2.3}$$

This process of passing from classical arithmetic to tropical arithmetic is referred to as *tropicalization*. In the later sections of Chapter 3, we shall discuss the tropicalization of algebraic-geometric objects such as curves and surfaces.

We shall give two more examples on how tropical arithmetic ties in naturally with familiar algorithms in discrete mathematics. The first concerns the dynamic programming approach to *integer linear programming*. The general integer linear programming problem can be stated as follows. Let $A = (a_{ij})$ be a $d \times n$ matrix of non-negative integers, let $w = (w_1, \ldots, w_n)$ be a row vector with real entries, and let $b = (b_1, \ldots, b_d)^T$ be a column vector with non-negative integer entries. Our task is to find a non-negative integer column vector $u = (u_1, \ldots, u_n)$ which solves the following optimization problem:

$$\text{Maximize } w \cdot u \text{ subject to } u \in \mathbb{N}^n \text{ and } A \cdot u \;=\; b. \tag{2.4}$$

Let us further assume that all columns of the matrix A sum to the same number

α and that $b_1 + \cdots + b_d = m \cdot \alpha$. This assumption is convenient because it ensures that all feasible solutions $u \in \mathbb{N}^n$ of (2.4) satisfy $u_1 + \cdots + u_n = m$.

We can solve the integer programming problem (2.4) using tropical arithmetic as follows. Let $q_1, \ldots, q_d$ be indeterminates and consider the expression

$$w_1 \odot q_1^{a_{11}} \odot q_2^{a_{21}} \odot \cdots \odot q_d^{a_{d1}} \;\oplus\; \cdots \;\oplus\; w_n \odot q_1^{a_{1n}} \odot q_2^{a_{2n}} \odot \cdots \odot q_d^{a_{dn}}. \qquad (2.5)$$

Proposition 2.4 *The optimal value of (2.4) is the coefficient of the monomial $q_1^{b_1} q_2^{b_2} \cdots q_d^{b_n}$ in the m-th power, evaluated tropically, of the expression (2.5).*

The proof of this proposition is not difficult and is similar to that of Proposition 2.2. The process of taking the m-th power of the tropical polynomial (2.5) can be regarded as solving the shortest path problem in a certain graph. This is precisely the dynamic programming approach to integer linear programming, as described in [Schrijver, 1986]. Prior to the result by [Lenstra, 1983] that integer linear programming can be solved in polynomial time for fixed dimensions, the dynamic programming method provided a polynomial-time algorithm under the assumption that the integers in A are bounded.

Example 2.5 Let $d = 2$, $n = 5$ and consider the instance of (2.4) given by

$$A \;=\; \begin{pmatrix} 4 & 3 & 2 & 1 & 0 \\ 0 & 1 & 2 & 3 & 4 \end{pmatrix}, \quad b \;=\; \begin{pmatrix} 5 \\ 7 \end{pmatrix} \quad \text{and} \quad w \;=\; (2, 5, 11, 7, 3).$$

Here we have $\alpha = 4$ and $m = 3$. The matrix A and the cost vector w are encoded by a tropical polynomial as in (2.5):

$$f \quad = \quad 2q_1^4 + 5q_1^3 q_2 + 11 q_1^2 q_2^2 + 7 q_1 q_2^3 + 3 q_2^4.$$

The third power of this polynomial, evaluated tropically, is equal to

$$\begin{aligned} f \odot f \odot f \quad = \quad & 6q_1^{12} + 9q_1^{11}q_2 + 12q_1^{10}q_2^2 + 11q_1^9q_2^3 + 7q_1^8q_2^4 + 10q_1^7q_2^5 + 13q_1^6q_2^6 \\ & +12q_1^5q_2^7 + 8q_1^4q_2^8 + 11q_1^3q_2^9 + 17q_1^2q_2^{10} + 13q_1q_2^{11} + 9q_2^{12}. \end{aligned}$$

The coefficient 12 of $q_1^5 q_2^7$ in this tropical polynomial is the optimal value. An optimal solution to this integer programming problem is $u = (1, 1, 0, 0, 1)^T$.

Our final example concerns the notion of the determinant of an $n \times n$ matrix $Q = (q_{ij})$. Since there is no negation in tropical arithmetic, the *tropical determinant* is the same as the *tropical permanent*, namely, it is the sum over the diagonal products obtained by taking all $n!$ permutations π of $\{1, 2, \ldots, n\}$:

$$\operatorname{tropdet}(Q) \quad := \quad \bigoplus_{\pi \in S_n} q_{1\pi(1)} \odot q_{2\pi(2)} \odot \cdots \odot q_{n\pi(n)}. \qquad (2.6)$$

Here S_n denotes the *symmetric group* of permutations of $\{1, 2, \ldots, n\}$. The evaluation of the tropical determinant is the classical *assignment problem* of combinatorial optimization. Consider a company which has n jobs and n workers, and each job needs to be assigned to exactly one of the workers. Let q_{ij} be the cost of assigning job i to worker j. The company wishes to find the cheapest assignment $\pi \in S_n$. The optimal total cost is the following minimum:

$$\min\bigl\{ q_{1\pi(1)} + q_{2\pi(2)} + \cdots + q_{n\pi(n)} \;:\; \pi \in S_n \bigr\}.$$

This number is precisely the tropical determinant of the matrix $Q = (q_{ij})$.

Remark 2.6 The tropical determinant solves the assignment problem.

In the assignment problem we need to find the minimum over $n!$ quantities, which appears to require exponentially many operations. However, there is a well-known polynomial-time algorithm for solving this problem. The method was introduced in [Kuhn, 1955] and is known as the *Hungarian Assignment Method*. It maintains a price for each job and an (incomplete) assignment of workers and jobs. At each iteration, the method chooses an unassigned worker and computes a shortest augmenting path from this person to the set of jobs. The total number of arithmetic operations is $O(n^3)$.

In classical arithmetic, the evaluation of determinants and the evaluation of permanents are in different complexity classes. The determinant of an $n \times n$ matrix can be computed in $O(n^3)$ steps, namely by *Gaussian elimination*, while computing the permanent of an $n \times n$ matrix is a fundamentally harder problem (it is #P-complete [Valiant, 1979]). It would be interesting to explore whether the Hungarian Method can be derived from some version of Gaussian Elimination by the principle of tropicalization (2.3).

To see what we mean, consider a 3×3 matrix $A(\epsilon)$ whose entries are polynomials in the indeterminate ϵ. For each entry we list the term of lowest order:

$$A(\epsilon) \quad = \quad \begin{pmatrix} a_{11}\epsilon^{q_{11}} + \cdots & a_{12}\epsilon^{q_{12}} + \cdots & a_{13}\epsilon^{q_{13}} + \cdots \\ a_{21}\epsilon^{q_{21}} + \cdots & a_{22}\epsilon^{q_{22}} + \cdots & a_{23}\epsilon^{q_{23}} + \cdots \\ a_{31}\epsilon^{q_{31}} + \cdots & a_{32}\epsilon^{q_{32}} + \cdots & a_{33}\epsilon^{q_{33}} + \cdots \end{pmatrix}.$$

Suppose that the a_{ij} are sufficiently general non-zero real numbers, so that no cancellation occurs in the lowest-order coefficient when we expand the determinant of $A(\epsilon)$. Writing Q for the 3×3 matrix with entries q_{ij}, we have

$$\det(A(\epsilon)) \quad = \quad \alpha \cdot \epsilon^{\mathrm{tropdet}(Q)} + \cdots \qquad \text{for some } \alpha \in \mathbb{R}\backslash\{0\}.$$

Thus the tropical determinant of Q can be extracted from this expression by taking the logarithm and letting ϵ tend to zero, as suggested by (2.3).

The reader may have wondered where the adjective "tropical" comes from. The algebraic structure $(\mathbb{R} \cup \{\infty\}, \oplus, \odot)$, which is also known as the *min-plus algebra*, has been invented (or re-invented) many times by many people. One of its early developers, in the 1960s, was the Brazilian mathematician Imre

Simon. Simon's work was followed up on by French scholars [Pin, 1998], who coined the term "tropical semiring" for the min-plus algebra, in the honor of their Brazilian colleague. Hence "tropical" stands for the French view of Brazil. Currently, many mathematicians are working on tropical mathematics and they are exploring a wide range of applications [Litvinov, 2005].

2.2 Sequence alignment

A fundamental task in computational biology is the alignment of DNA or protein sequences. Since biological sequences arising in practice are usually fairly long, researchers have developed highly efficient algorithms for finding optimal alignments. Although in some cases heuristics are used to reduce the combinatorial complexity, most of the algorithms are based on, or incorporate the dynamic programming principle. An excellent introduction to the computer science aspects of this subject is [Gusfield, 1997]. What we hope to accomplish in this section is to explain what algebraic statistics and tropical arithmetic have to do with discrete algorithms used for sequence alignment.

First, we give a self-contained explanation of the Needleman-Wunsch algorithm for aligning biological sequences. Second, we explain a algebraic statistical model for pairs of sequences, namely the *pair hidden Markov model*, and we use Needleman-Wunsch to illustrate how dynamic programming algorithms arise naturally from the tropicalization of this model.

We begin by specifying the sequence alignment problem in precise terms. Fix a finite alphabet Σ with l letters, for instance, $\Sigma = \{0, 1, \ldots, l-1\}$. If $l = 4$ then the alphabet of choice is $\Sigma = \{\mathtt{A}, \mathtt{C}, \mathtt{G}, \mathtt{T}\}$. Suppose we are given two sequences $\sigma^1 = \sigma^1_1 \sigma^1_2 \cdots \sigma^1_n$ and $\sigma^2 = \sigma^2_1 \sigma^2_2 \cdots \sigma^2_m$ over the alphabet Σ. The sequence lengths n and m may be different. Our aim is to measure the complexity of transforming the sequence σ^1 into the sequence σ^2 by changes to individual characters, insertion of new characters, or deletion of existing characters. Such changes are called *edits*. The *sequence alignment problem* is to find the shortest sequence of edits that relates the two sequences σ^1 and σ^2.

Such sequences of edits are called *alignments*. The shortest sequence of edits between σ_1 and σ_2 consists of at most $n + m$ edits, and therefore it is a finite problem to identify the best alignment: one can exhaustively enumerate all edit sequences and then pick the shortest one. However, the exhaustive solution can be improved on considerably. We shall present a dynamic programming algorithm for solving the alignment problem which requires only $O(nm)$ steps.

Each alignment of the pair (σ^1, σ^2) is represented by a string h over the *edit alphabet* $\{H, I, D\}$. These letters stand for **h**omology, **i**nsertion and **d**eletion; this terminology is explained in more detail in Chapter 4. We call the string h the *edit string* of the alignment. An I in the edit string represents an insertion in the first sequence σ^1, a D in the edit string is a deletion in the first sequence σ^1, and an H is either a character change, or lack thereof. Writing $\#H$, $\#I$ and $\#D$ for the number of characters H, I and D in an edit string for an alignment of the pair (σ^1, σ^2), we find that

$$\#H + \#D = n \quad \text{and} \quad \#H + \#I = m. \tag{2.7}$$

Example 2.7 Let $n = 7$ and $m = 9$ and consider the sequences $\sigma^1 = \texttt{ACGTAGC}$ and $\sigma^2 = \texttt{ACCGAGACC}$. Then the following table shows an alignment of σ^1 and σ^2 with $\#H = 6$, $\#I = 3$ and $\#D = 1$. The first row is the edit string:

$$\begin{array}{cccccccccc} H & H & I & H & I & H & H & I & D & H \\ \texttt{A} & \texttt{C} & - & \texttt{G} & - & \texttt{T} & \texttt{A} & - & \texttt{G} & \texttt{C} \\ \texttt{A} & \texttt{C} & \texttt{C} & \texttt{G} & \texttt{A} & \texttt{G} & \texttt{A} & \texttt{C} & - & \texttt{C} \end{array} \tag{2.8}$$

Although the alignment has length ten, it represents the transformation of σ^1 into σ^2 by five edit steps which are performed from the left to the right. This transformation is uniquely encoded by the edit string $HHIHIHHIDH$.

Proposition 2.8 *A string over the edit alphabet $\{H, I, D\}$ represents an alignment of an n-letter sequence σ^1 and an m-letter sequence σ^2 if and only if (2.7) holds.*

Proof As we perform the edits from the left to the right, every letter in σ^1 either corresponds to a letter in σ^2, in which case we record an H in the edit string, or it gets deleted, in which case we record a D. This shows the first identity in (2.7). The second identity holds because every letter σ^2 either corresponds to a letter in σ^1, in which case there is an H in the edit string, or it has been inserted, in which case we record an I in the edit string. Any string over $\{H, I, D\}$ with (2.7), when read from left to right, produces a valid sequence of edits that transforms σ^1 into σ^2. □

We write $\mathcal{A}_{n,m}$ for the set of all strings over $\{H, I, D\}$ which satisfy (2.7). We call $\mathcal{A}_{n,m}$ as the *set of all alignments* of the sequences σ^1 and σ^2, in spite of the fact that it only depends on n and m rather than the specific sequences σ^1 and σ^2. Each element h in $\mathcal{A}_{n,m}$ corresponds to a pair of sequences (μ^1, μ^2) over the alphabet $\Sigma \cup \{-\}$ such that μ^1 consists of a copy of σ^1 together with inserted "$-$" characters, and similarly μ^2 is a copy of σ^2 with inserted "$-$" characters. The cardinalities of the sets $\mathcal{A}_{n,m}$ are the *Delannoy numbers* [Stanley, 1999, §6.3]. They can be computed by a generating function.

Proposition 2.9 *The cardinality of the set $\mathcal{A}_{n,m}$ of all alignments can be computed as the coefficient of $x^m y^n$ in the generating function $1/(1-x-y-xy)$.*

Proof Consider the expansion of the given generating function

$$\frac{1}{1-x-y-xy} \quad = \quad \sum_{m=0}^{\infty}\sum_{n=0}^{\infty} a_{m,n}x^m y^n.$$

The coefficients are characterized by the linear recurrence

$$a_{m,n} \; = \; a_{m-1,n}+a_{m,n-1}+a_{m-1,n-1} \;\text{ with }\; a_{0,0}=1,\; a_{m,-1}=a_{-1,n}=0. \quad (2.9)$$

The same recurrence is valid for the cardinality of $\mathcal{A}_{n,m}$. Indeed, for $m+n \geq 1$, every string in $\mathcal{A}_{n,m}$ is either a string in $\mathcal{A}_{n-1,m-1}$ followed by an H, or a string in $\mathcal{A}_{n-1,m}$ followed by an I, or it is a string in $\mathcal{A}_{n,m-1}$ followed by a D. Also, $\mathcal{A}_{0,0}$ has only one element, namely the empty string, and $\mathcal{A}_{n,m}$ is the empty set if $m<0$ or $n<0$. Hence the numbers $a_{m,n}$ and $\#\mathcal{A}_{n,m}$ satisfy the same initial conditions and the same recurrence (2.9), so they must be equal. □

In light of the recurrence (2.9), it is natural to introduce the following graph.

Definition 2.10 The *alignment graph* $\mathcal{G}_{n,m}$ is the directed graph on the set of nodes $\{0,1,\ldots,n\} \times \{0,1,\ldots,m\}$ and three classes of directed edges as follows: there are edges labeled by I between pairs of nodes $(i,j) \to (i,j+1)$, there are edges labeled by D between pairs of nodes $(i,j) \to (i+1,j)$, and there are edges labeled by H between pairs of nodes $(i,j) \to (i+1,j+1)$.

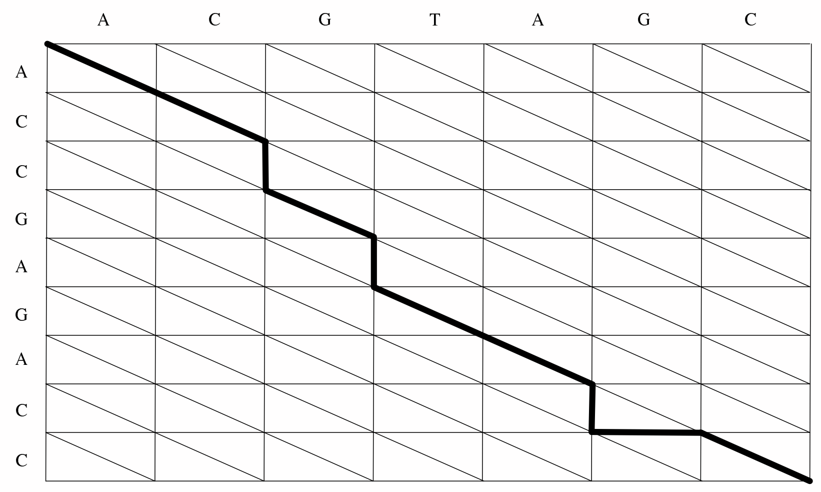

Fig. 2.1. The alignment (2.8) shown as a path in the alignment graph $\mathcal{G}_{7,9}$.

Remark 2.11 The set $\mathcal{A}_{n,m}$ of all alignments is in bijection with the set of paths from the node $(0,0)$ to the node (n,m) in the alignment graph $\mathcal{G}_{n,m}$.

We have introduced three equivalent combinatorial objects: strings over $\{H, I, D\}$ satisfying (2.7), sequence pairs (μ^1, μ^2) that are equivalent to σ^1, σ^2 with the possible insertion of "$-$" characters, and paths in the alignment graph $\mathcal{G}_{n,m}$. All three represent alignments, and they are useful in designing algorithms for finding good alignments. In order to formalize what "good" means, we need to give scores to alignments. A *scoring scheme* is a pair of maps

$$\begin{aligned} w &: \Sigma \cup \{-\} \times \Sigma \cup \{-\} \rightarrow \mathbb{R}, \\ w' &: \{H, I, D\} \times \{H, I, D\} \rightarrow \mathbb{R}. \end{aligned}$$

Scoring schemes induce weights on alignments of sequences as follows. Fix the two given sequences σ^1 and σ^2 over the alphabet $\Sigma = \{\mathtt{A}, \mathtt{C}, \mathtt{G}, \mathtt{T}\}$. Each alignment is given by an edit string h over $\{H, I, D\}$. We write $|h|$ for the length of h. The edit string h determines the two sequences μ^1 and μ^2 of length $|h|$ over $\Sigma \cup \{-\}$. The weight of the alignment h is defined to be

$$W(h) \quad := \quad \sum_{i=1}^{|h|} w(\mu_i^1, \mu_i^2) + \sum_{i=2}^{|h|} w'(h_{i-1}, h_i). \tag{2.10}$$

We represent a scoring scheme (w, w') by a pair of matrices. The first one is

$$w \quad = \quad \begin{pmatrix} w_{\mathtt{A},\mathtt{A}} & w_{\mathtt{A},\mathtt{C}} & w_{\mathtt{A},\mathtt{G}} & w_{\mathtt{A},\mathtt{T}} & w_{\mathtt{A},-} \\ w_{\mathtt{C},\mathtt{A}} & w_{\mathtt{C},\mathtt{C}} & w_{\mathtt{C},\mathtt{G}} & w_{\mathtt{C},\mathtt{T}} & w_{\mathtt{C},-} \\ w_{\mathtt{G},\mathtt{A}} & w_{\mathtt{G},\mathtt{C}} & w_{\mathtt{G},\mathtt{G}} & w_{\mathtt{G},\mathtt{T}} & w_{\mathtt{G},-} \\ w_{\mathtt{T},\mathtt{A}} & w_{\mathtt{T},\mathtt{C}} & w_{\mathtt{T},\mathtt{G}} & w_{\mathtt{T},\mathtt{T}} & w_{\mathtt{T},-} \\ w_{-,\mathtt{A}} & w_{-,\mathtt{C}} & w_{-,\mathtt{G}} & w_{-,\mathtt{T}} & \end{pmatrix}. \tag{2.11}$$

Here the lower right entry $w_{-,-}$ is left blank because it is never used in computing the weight of an alignment. The second matrix is a 3×3 matrix:

$$w' \quad = \quad \begin{pmatrix} w'_{H,H} & w'_{H,I} & w'_{H,D} \\ w'_{I,H} & w'_{I,I} & w'_{I,D} \\ w'_{D,H} & w'_{D,I} & w'_{D,D} \end{pmatrix} \tag{2.12}$$

Thus the total number of parameters in the alignment problem is $24 + 9 = 33$. We identify the space of parameters with $\mathbb{R}^{33}$. Each alignment $h \in \mathcal{A}_{n,m}$ of a pair of sequences (σ^1, σ^2) gives rise to a linear functional $W(h)$ on $\mathbb{R}^{33}$.

For instance, the weight of the alignment $h = HHIHIHHIDH$ of our sequences $\sigma^1 = \mathtt{ACGTAGC}$ and $\sigma^2 = \mathtt{ACCGAGACC}$ is the linear functional

$$\begin{aligned} W(h) \quad = \quad & 2 \cdot w_{\mathtt{A},\mathtt{A}} + 2 \cdot w_{\mathtt{C},\mathtt{C}} + w_{\mathtt{G},\mathtt{G}} + w_{\mathtt{T},\mathtt{G}} + 2 \cdot w_{-,\mathtt{C}} + w_{-,\mathtt{A}} + w_{\mathtt{G},-} \\ & + 2 \cdot w'_{H,H} + 3 \cdot w'_{H,I} + 2 \cdot w'_{I,H} + w'_{I,D} + w'_{D,H}. \end{aligned}$$

Suppose we are given two input sequences σ^1 and σ^2 of lengths n and m over the alphabet Σ. Suppose further that we are given a fixed scoring scheme

(w, w'). The *global alignment problem* is to compute an alignment $h \in \mathcal{A}_{n,m}$ whose weight $W(h)$ is minimal among all alignments in $\mathcal{A}_{n,m}$. In the computational biology literature, it is more common to use "maximal" instead of "minimal", but, of course, that is equivalent if we replace (w, w') by $(-w, -w')$.

In the following discussion let us simplify the problem and assume that $w' = 0$, so the weight of an alignment is the linear functional $W(h) = \sum_{i=1}^{|h|} w(\mu_i^1, \mu_i^2)$ on $\mathbb{R}^{24}$. The problem instance (σ^1, σ^2, w) induces weights on the edges of the alignment graph $\mathcal{G}_{n,m}$ as follows. The weight of the edge $(i,j) \to (i+1, j)$ is $w(\sigma_{i+1}^1, -)$, the weight of the edge $(i,j) \to (i, j+1)$ is $w(-, \sigma_{j+1}^2)$, and the weight of the edge $(i,j) \to (i+1, j+1)$ is $w(\sigma_{i+1}^1, \sigma_{j+1}^2)$. This gives a graph-theoretic reformulation of the global alignment problem.

Remark 2.12 The global alignment problem is equivalent to finding the minimum weight path from $(0,0)$ to (n,m) in the alignment graph $\mathcal{G}_{n,m}$.

Thus the global alignment problem is equivalent to finding shortest paths in a weighted graph. Proposition 2.2 gave general dynamic programming algorithm for the shortest path problem, the Floyd-Warshall algorithm, which amounts to multiplying matrices in tropical arithmetic. For the specific graph and weights arising in the global alignment problem, this translates into an $O(nm)$ dynamic programming algorithm, called the *Needleman-Wunsch algorithm*.

Algorithm 2.13 (Needleman-Wunsch)
Input: Two sequences $\sigma^1 \in \Sigma^n$, $\sigma^2 \in \Sigma^m$ and a scoring scheme $w \in \mathbb{R}^{24}$.
Output: An alignment $h \in \mathcal{A}_{n,m}$ whose weight $W(h)$ is minimal.

Initialization: Create an $(n+1) \times (m+1)$ matrix M whose rows are indexed by $\{0, 1, \ldots, n\}$ and whose columns indexed by $\{0, 1, \ldots, m\}$. Set $M[0,0] = 0$.

$$\begin{array}{lrcll} \text{Set} & M[i,0] & := & M[i-1,0] + w(\sigma_i^1, -) & \text{for} \quad i = 1, \ldots, n \\ \text{and} & M[0,j] & := & M[0,j-1] + w(-, \sigma_j^2) & \text{for} \quad j = 1, \ldots, m. \end{array}$$

Loop: For $i = 1, \ldots, n$ and $j = 1, \ldots, m$ set

$$M[i,j] \quad := \quad \min \begin{cases} M[i-1, j-1] + w(\sigma_i^1, \sigma_j^2) \\ M[i-1, j] + w(-, \sigma_j^2) \\ M[i, j-1] + w(\sigma_i^1, -) \end{cases}$$

Color one or more of the three edges which are adjacent to and directed towards (i,j), and which attain the minimum.

Backtrack: Trace an optimal path from in backwards direction from (n,m) to $(0,0)$. This is done by following an arbitrary sequence of colored edges.

Output: The edge labels in $\{H, I, D\}$ of an optimal path in forward direction.

The more general case when the 3×3 matrix w' is not zero can be modeled by replacing each interior node in $\mathcal{G}_{n,m}$ by a complete bipartite graph $K_{3,3}$ whose edge weights are $w'_{HH}, w'_{H,I}, \ldots, w'_{DD}$. These $9(m-1)(n-1)$ new edges represent transitions between the different states in $\{H, I, D\}$. The resulting graph is denoted $\mathcal{G}'_{n,m}$ and called the *extended alignment graph*. Figure 2.2 illustrates what happens to a node of $\mathcal{G}_{n,m}$ when passing to $\mathcal{G}'_{n,m}$.

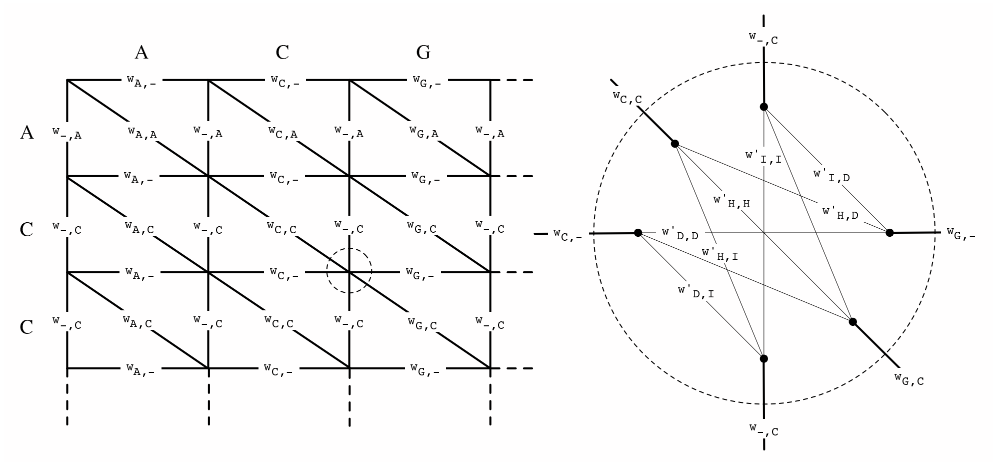

Fig. 2.2. Creating the extended alignment graph by inserting $K_{3,3}$'s

The minimum weight path in $\mathcal{G}'_{n,m}$ is found by a variant of the Needleman-Wunsch algorithm. In the following example we stick to the case $w' = 0$.

Example 2.14 Consider the sequences $\sigma^1 =$ `ACGTAGC` and $\sigma^2 =$ `ACCGAGACC` from Example 2.7. According to Proposition 2.9, the number of alignments is

$$\#\mathcal{A}_{7,9} \quad = \quad 224,143.$$

We assume $w' = 0$. The alignment graph $\mathcal{G}_{7,9}$ is depicted in Figure 2.1.

For any particular choice of a scoring scheme $w \in \mathbb{R}^{24}$, the Needleman-Wunsch algorithm easily finds an optimal alignment. Consider the example

$$w \quad = \quad \begin{pmatrix} -91 & 114 & 31 & 123 & x \\ 114 & -100 & 125 & 31 & x \\ 31 & 125 & -100 & 114 & x \\ 123 & 31 & 114 & -91 & x \\ x & x & x & x & \end{pmatrix},$$

where the *gap penalty* x is an unknown number between 150 and 200. The 16 specified parameter values in the matrix w are the ones used in the `blastz` alignment program scoring matrix [Schwartz *et al.*, 2003]. For $x \geq 169.5$ an optimal alignment is

$$\begin{pmatrix} h \\ \mu^1 \\ \mu^2 \end{pmatrix} = \begin{pmatrix} H & D & H & H & D & H & H & H & H \\ \mathtt{A} & - & \mathtt{C} & \mathtt{G} & - & \mathtt{T} & \mathtt{A} & \mathtt{G} & \mathtt{C} \\ \mathtt{A} & \mathtt{C} & \mathtt{C} & \mathtt{G} & \mathtt{A} & \mathtt{G} & \mathtt{A} & \mathtt{C} & \mathtt{C} \end{pmatrix} \text{ with } W(h) = 2x - 243.$$

If the gap penalty x is below 169.5 then an optimal alignment is

$$\begin{pmatrix} h \\ \mu^1 \\ \mu^2 \end{pmatrix} = \begin{pmatrix} H & D & H & H & I & H & H & D & D & H \\ \mathtt{A} & - & \mathtt{C} & \mathtt{G} & \mathtt{T} & \mathtt{A} & \mathtt{G} & - & - & \mathtt{C} \\ \mathtt{A} & \mathtt{C} & \mathtt{C} & \mathtt{G} & - & \mathtt{A} & \mathtt{G} & \mathtt{A} & \mathtt{C} & \mathtt{C} \end{pmatrix} \text{ with } W(h) = 4x - 582.$$

After verifying this computation, the reader may now wish to vary all 24 parameters in the matrix w and run the Needleman-Wunsch algorithm many times. How does the resulting optimal alignment change? How many of the 224, 143 alignments occur for some choice of scoring scheme w? Is there a scoring scheme $w \in \mathbb{R}^{24}$ which makes the alignment (2.8) optimal? Such questions form the subject of *parametric alignment* [Gusfield *et al.*, 1994, Gusfield, 1997] which is the topic of Chapter 7.

We now shift gears and present the *pair hidden Markov model* for alignments. This is an algebraic statistical model which depends on two integers n and m:

$$\mathbf{f} \; : \; \mathbb{R}^{33} \; \rightarrow \; \mathbb{R}^{4^{n+m}}. \qquad (2.13)$$

The 4^{n+m} states are the pairs (σ^1, σ^2) of sequences of length n and m. The $33 = 24 + 9$ parameters are written as a pair of matrices (θ, θ') where

$$\theta = \begin{pmatrix} \theta_{\mathtt{A},\mathtt{A}} & \theta_{\mathtt{A},\mathtt{C}} & \theta_{\mathtt{A},\mathtt{G}} & \theta_{\mathtt{A},\mathtt{T}} & \theta_{\mathtt{A},-} \\ \theta_{\mathtt{C},\mathtt{A}} & \theta_{\mathtt{C},\mathtt{C}} & \theta_{\mathtt{C},\mathtt{G}} & \theta_{\mathtt{C},\mathtt{T}} & \theta_{\mathtt{C},-} \\ \theta_{\mathtt{G},\mathtt{A}} & \theta_{\mathtt{G},\mathtt{C}} & \theta_{\mathtt{G},\mathtt{G}} & \theta_{\mathtt{G},\mathtt{T}} & \theta_{\mathtt{G},-} \\ \theta_{\mathtt{T},\mathtt{A}} & \theta_{\mathtt{T},\mathtt{C}} & \theta_{\mathtt{T},\mathtt{G}} & \theta_{\mathtt{T},\mathtt{T}} & \theta_{\mathtt{T},-} \\ \theta_{-,\mathtt{A}} & \theta_{-,\mathtt{C}} & \theta_{-,\mathtt{G}} & \theta_{-,\mathtt{T}} & \end{pmatrix}, \quad \theta' = \begin{pmatrix} \theta'_{H,H} & \theta'_{H,I} & \theta'_{H,D} \\ \theta'_{I,H} & \theta'_{I,I} & \theta'_{I,D} \\ \theta'_{D,H} & \theta'_{D,I} & \theta'_{D,D} \end{pmatrix} \qquad (2.14)$$

In order to be statistically meaningful these parameters have to be non-negative and satisfy six independent linear equations. Namely, they must lie in

$$\Theta \; = \; \Delta_{15} \times \Delta_3 \times \Delta_3 \times \Delta_2 \times \Delta_2 \times \Delta_2 \quad \subset \quad \mathbb{R}^{33}.$$

The parameter space Θ is the product of six simplices of dimensions $15, 3, 3, 2, 2$ and 2. The big simplex Δ_{15} consists of all non-negative 4×4 matrices $(\theta_{ij})_{i,j \in \Sigma}$ whose entries sum to 1. The two tetrahedra Δ_3 come from requiring that

$$\theta_{-,\mathtt{A}} + \theta_{-,\mathtt{C}} + \theta_{-,\mathtt{G}} + \theta_{-,\mathtt{T}} \; = \; \theta_{\mathtt{A},-} + \theta_{\mathtt{C},-} + \theta_{\mathtt{G},-} + \theta_{\mathtt{T},-} \; = \; 1.$$

The three triangles Δ_2 come from requiring that

$$\theta'_{H,H} + \theta'_{H,I} + \theta'_{H,D} \; = \; \theta'_{I,H} + \theta'_{I,I} + \theta'_{I,D} \; = \; \theta'_{D,H} + \theta'_{D,I} + \theta'_{D,D} \; = \; 1.$$

The coordinate f_{σ^1,σ^2} of the pair hidden Markov model $\mathbf{f}$ represents the probability of observing the pair of sequences (σ^1, σ^2). This is the polynomial

$$f_{\sigma^1,\sigma^2} \quad = \quad \sum_{h \in \mathcal{A}_{n,m}} \prod_{i=1}^{|h|} \theta_{\mu_i^1,\mu_i^2} \cdot \prod_{i=2}^{|h|} \theta'_{h_{i-1},h_i}. \tag{2.15}$$

Here (μ^1, μ^2) is the pair of sequences over $\Sigma \cup \{-\}$ which corresponds to h. The following observation is crucial for understanding parametric alignment.

Proposition 2.15 *The objective function of the sequence alignment problem is the tropicalization of a coordinate polynomial f_{σ^1,σ^2} of the pair HMM.*

Proof The tropicalization of the polynomial (2.15) is gotten by replacing the outer sum by a tropical sum $\oplus$ and the inner products by tropical products $\odot$. We replace each unknown $\theta_{\dots}$ by the corresponding unknown $w_{\dots}$, which we think of as the negated logarithm of $\theta_{\dots}$. The result is the tropical polynomial

$$\mathrm{trop}(f_{\sigma^1,\sigma^2}) \quad = \quad \bigoplus_{h \in \mathcal{A}_{n,m}} \bigodot_{i=1}^{|h|} w_{\mu_i^1,\mu_i^2} \cdot \bigodot_{i=2}^{|h|} w'_{h_{i-1},h_i}. \tag{2.16}$$

The tropical product inside the tropical sum is precisely the weight $W(h)$ of the alignment h or (μ^1, μ^2) as defined in (2.10). Hence (2.16) is equivalent to

$$\mathrm{trop}(f_{\sigma^1,\sigma^2}) \quad = \quad \min_{h \in \mathcal{A}_{n,m}} W(h).$$

Evaluating the right hand side of this expression is therefore equivalent to finding an optimal alignment of the two sequences σ^1 and σ^2. □

Remark 2.16 Since the logarithm of a probability is always negative, the correspondence in Proposition 2.15 only accounts for scoring schemes in which the weights have the same sign. Scoring schemes in which the weights have mixed signs, as in Example 2.14, result from associating $w_{\dots}$ with the *log-odds ratio* $\log(\theta_{\dots}/\tilde{\theta}_{\dots})$ where the $\tilde{\theta}_{\dots}$ are additional new parameters.

It is an instructive exercise to show that the sum of the polynomials f_{σ^1,σ^2} over all 4^{n+m} pairs of sequences (σ^1, σ^2) simplifies to 1 when (θ, θ') lies in Θ. The key idea is to derive a recursive decomposition of the polynomial f_{σ^1,σ^2} by grouping together all summands with fixed last factor pair $\theta'_{h_{|h|-1},h_{|h|}} \theta_{\mu^1_{|h|},\mu^2_{|h|}}$. This recursive decomposition is equivalent to performing dynamic programming along the extended alignment graph $\mathcal{G}'_{n,m}$. The variant of the Needleman-Wunsch algorithm on the graph $\mathcal{G}'_{n,m}$ is precisely the efficient evaluation of the tropical polynomial $\mathrm{trop}(f_{\sigma^1,\sigma^2})$ using the same recursive decomposition.

We explain this circle of ideas for the simpler case of Algorithm 2.13 where

$$w' \quad = \quad \begin{pmatrix} 0 & 0 & 0 \\ 0 & 0 & 0 \\ 0 & 0 & 0 \end{pmatrix}$$

To be precise, we shall implement dynamic programming on the alignment graph $\mathcal{G}_{n,m}$ as the efficient computation of a (tropical) polynomial. In term of the pair HMM, this means that we are fixing all entries of the 3×3 matrix θ' to be identical. Let us consider the following two possible specializations:

$$\theta' = \begin{pmatrix} 1/3 & 1/3 & 1/3 \\ 1/3 & 1/3 & 1/3 \\ 1/3 & 1/3 & 1/3 \end{pmatrix} \qquad \text{and} \qquad \theta' = \begin{pmatrix} 1 & 1 & 1 \\ 1 & 1 & 1 \\ 1 & 1 & 1 \end{pmatrix}$$

The first specialization is the statistically meaningful one, but it leads to more complicated formulas in the coefficients. For that reason we use the second specialization in our implementation. We write g_{σ^1,σ^2} for the polynomial in the 24 unknowns $\theta_{\cdot\cdot}$ gotten from f_{σ^1,σ^2} by setting each of the 9 unknowns $\theta_{\cdot\cdot}$ to 1. The following short `Maple` code computes the polynomial $g_{\texttt{s1},\texttt{s2}}$ for

```
s1 := [A,C,G]: s2 := [A,C,C]:

T := array([ [ tAA, tAC, tAG, tAT, t_A ],
             [ tCA, tCC, tCG, tCT, t_C ],
             [ tGA, tGC, tGG, tGT, t_G ],
             [ tTA, tTC, tTG, tTT, t_T ],
             [ tA_, tC_, tG_, tT_, 0 ]]):
```

This represents the matrix θ with $\texttt{tAA} = \theta_{\texttt{AA}}$, $\texttt{tAC} = \theta_{\texttt{AC}}, \ldots$ etc. We initialize

```
n := nops(s1): m := nops(s2):
u1 := subs({A=1,C=2,G=3,T=4},s1):
u2 := subs({A=1,C=2,G=3,T=4},s2):
M := array([],0..n,0..m): M[0,0] := 1:
for i from 1 to n do
M[i,0] := M[i-1,0] * T[u1[i],5]:
od:
for j from 1 to m do
M[0,j] := M[0,j-1] * T[5,u2[j]]:
od:
```

We then perform a loop precisely as in Algorithm 2.13, with tropical arithmetic on real numbers replaced by ordinary arithmetic on polynomials.

```
for i from 1 to n do
```

```
 for j from 1 to m do
     M[i,j] := M[i-1,j-1] * T[u1[i],u2[j]] + M[i-1, j ] *
                T[u1[i], 5 ] + M[ i ,j-1] * T[ 5 ,u2[j]]:
 od:
od:
lprint(M[n,m]);
```

Our `Maple` code produces a recursive decomposition of the polynomial $g_{\texttt{ACG,ACC}}$:

```
((tAA+2*tA_*t_A)*tCC+(tA_*tAC+tA_*tC_*t_A+(tAA+2*tA_*t_A)*tC_)
*t_C+(t_A*tCA+(tAA+2*tA_*t_A)*t_C+t_A*t_C*tA_)*tC_)*tGC+((tA_*
tAC+tA_*tC_*t_A+(tAA+2*tA_*t_A)*tC_)*tCC+(tA_*tC_*tAC+tA_*tC_^2
*t_A+(tA_*tAC+tA_*tC_*t_A+(tAA+2*tA_*t_A)*tC_)*tC_)*t_C+((tAA+
2*tA_*t_A)*tCC+(tA_*tAC+tA_*tC_*t_A+(tAA+2*tA_*t_A)*tC_)*t_C+
(t_A*tCA+(tAA+2*tA_*t_A)*t_C+t_A*t_C*tA_)*tC_)*tC_)*t_G+((t_A*
tCA+(tAA+2*tA_*t_A)*t_C+t_A*t_C*tA_)*tGC+((tAA+2*tA_*t_A)*tCC+
(tA_*tAC+tA_*tC_*t_A+(tAA+2*tA_*t_A)*tC_)*t_C+(t_A*tCA+(tAA+2*
tA_*t_A)*t_C+t_A*t_C*tA_)*tC_)*t_G+(t_A*t_C*tGA+(t_A*tCA+(tAA+
2*tA_*t_A)*t_C+t_A*t_C*tA_)*t_G+t_A*t_C*t_G*tA_)*tC_)*tC_
```

The expansion of this polynomial has 14 monomials. The sum of its coefficients is $\#\mathcal{A}_{3,3} = 63$. Next we run same code for the sequences of Example 2.7:

```
s1 := [A,C,G,T,A,G,C]: s2 := [A,C,C,G,A,G,A,C,C]:
```

The expansion of the resulting polynomial $g_{\texttt{s1,s2}}$ has $1,615$ monomials, and the sum of its coefficients equals $\#\mathcal{A}_{7,9} = 224,143$. Each monomial in $g_{\texttt{s1,s2}}$ represents a family of alignments h all of which have the same $W(h)$. We have chosen a simple example to illustrate the main points, but the method shown can be used for computing the polynomials associated to much longer sequence pairs. We summarize our discussion of sequence alignment as follows:

Remark 2.17 The Needleman-Wunsch algorithm is the tropicalization of the pair hidden Markov model for sequence alignment.

In order to answer parametric questions, such as the ones raised at the end of Example 2.14, we need to better understand the combinatorial structure encoded in the polynomials f_{σ^1,σ^2} and g_{σ^1,σ^2}. The key to unraveling this combinatorial structure lies in the study of polytopes, which is the our next topic.

2.3 Polytopes

In this section we review basic facts about convex polytopes and algorithms for computing them, and we explain how they relate to algebraic statistical models. Every polynomial and every polynomial map has an associated polytope, called its *Newton polytope*. This allows us to replace tropical arithmetic by the *polytope algebra*, which is useful for solving parametric inference problems.

As a motivation for the mathematics in this section, let us give a sneak preview of Newton polytopes arising from the pair HMM for sequence alignment.

Example 2.18 Consider the following 14 points v_i in 11-dimensional space:

$$\begin{array}{rc}
v_1 = (0,0,1,0,0,2,0,0,1,1,1) & 20\,\theta_{\mathtt{A-}}\,\theta_{\mathtt{-A}}\,\theta_{\mathtt{C-}}^2\,\theta_{\mathtt{-C}}\,\theta_{\mathtt{-G}} \\
v_2 = (1,0,0,0,0,2,0,0,0,1,1) & 6\,\theta_{\mathtt{AA}}\,\theta_{\mathtt{C-}}^2\,\theta_{\mathtt{-C}}\,\theta_{\mathtt{-G}} \\
v_3 = (0,0,1,0,1,1,0,0,1,0,1) & 7\,\theta_{\mathtt{A-}}\,\theta_{\mathtt{-A}}\,\theta_{\mathtt{CC}}\,\theta_{\mathtt{C-}}\,\theta_{\mathtt{-G}} \\
v_4 = (0,0,1,0,0,1,0,1,1,1,0) & 9\,\theta_{\mathtt{A-}}\,\theta_{\mathtt{-A}}\,\theta_{\mathtt{C-}}\,\theta_{\mathtt{-C}}\,\theta_{\mathtt{GC}} \\
v_5 = (0,1,1,0,0,1,0,0,0,1,1) & 4\,\theta_{\mathtt{A-}}\,\theta_{\mathtt{AC}}\,\theta_{\mathtt{C-}}\,\theta_{\mathtt{-C}}\,\theta_{\mathtt{-G}} \\
v_6 = (0,0,0,0,0,2,1,0,1,1,0) & \theta_{\mathtt{-A}}\,\theta_{\mathtt{C-}}^2\,\theta_{\mathtt{-C}}\,\theta_{\mathtt{GA}} \\
v_7 = (0,0,0,1,0,2,0,0,1,0,1) & 3\,\theta_{\mathtt{-A}}\,\theta_{\mathtt{C-}}^2\,\theta_{\mathtt{CA}}\,\theta_{\mathtt{-G}} \\
v_8 = (1,0,0,0,1,1,0,0,0,0,1) & 3\,\theta_{\mathtt{AA}}\,\theta_{\mathtt{CC}}\,\theta_{\mathtt{C-}}\,\theta_{\mathtt{-G}} \\
v_9 = (1,0,0,0,0,1,0,1,0,1,0) & 3\,\theta_{\mathtt{AA}}\,\theta_{\mathtt{C-}}\,\theta_{\mathtt{-C}}\,\theta_{\mathtt{GC}} \\
v_{10} = (0,0,1,0,1,0,0,1,1,0,0) & 2\,\theta_{\mathtt{A-}}\,\theta_{\mathtt{-A}}\,\theta_{\mathtt{CC}}\,\theta_{\mathtt{GC}} \\
v_{11} = (0,1,1,0,1,0,0,0,0,0,1) & \theta_{\mathtt{A-}}\,\theta_{\mathtt{CC}}\,\theta_{\mathtt{AC}}\,\theta_{\mathtt{-G}} \\
v_{12} = (0,1,1,0,0,0,0,1,0,1,0) & \theta_{\mathtt{A-}}\,\theta_{\mathtt{AC}}\,\theta_{\mathtt{-C}}\,\theta_{\mathtt{GC}} \\
v_{13} = (0,0,0,1,0,1,0,1,1,0,0) & 2\,\theta_{\mathtt{-A}}\,\theta_{\mathtt{C-}}\,\theta_{\mathtt{CA}}\,\theta_{\mathtt{GC}} \\
v_{14} = (1,0,0,0,1,0,0,1,0,0,0) & \theta_{\mathtt{AA}}\,\theta_{\mathtt{CC}}\,\theta_{\mathtt{GC}}
\end{array}$$

To the right of each point v_i is the corresponding monomial in the unknowns $(\theta_{\mathtt{AA}}, \theta_{\mathtt{AC}}, \theta_{\mathtt{A-}}, \theta_{\mathtt{CA}}, \theta_{\mathtt{CC}}, \theta_{\mathtt{C-}}, \theta_{\mathtt{GA}}, \theta_{\mathtt{GC}}, \theta_{\mathtt{-A}}, \theta_{\mathtt{-C}}, \theta_{\mathtt{-G}})$. The j-th coordinate in v_i equals the exponent of the j-th unknown. The sum of these 14 monomials is the polynomial $g_{\mathtt{ACG,ACC}}$ computed by the `Maple` code at the end of Section 2.2.

The 14 points v_i span a six-dimensional linear space in $\mathbb{R}^{11}$, and it is their location inside that space which determines which alignment is optimal. For instance, the gapless alignment (H, H, H) which is corresponds to the last monomial $\theta_{\mathtt{AA}}\,\theta_{\mathtt{CC}}\,\theta_{\mathtt{GC}}$ is optimal if and only if the scoring scheme w satisfies

$$\begin{array}{ll}
w_{\mathtt{C-}} + w_{\mathtt{-G}} \geq w_{\mathtt{GC}}\,, & w_{\mathtt{A-}} + w_{\mathtt{AC}} + w_{\mathtt{-G}} \geq w_{\mathtt{AA}} + w_{\mathtt{GC}}\,, \\
w_{\mathtt{C-}} + w_{\mathtt{-C}} \geq w_{\mathtt{CC}}\,, & w_{\mathtt{A-}} + w_{\mathtt{AC}} + w_{\mathtt{-C}} \geq w_{\mathtt{AA}} + w_{\mathtt{CC}}\,, \\
w_{\mathtt{A-}} + w_{\mathtt{-A}} \geq w_{\mathtt{AA}}\,, & w_{\mathtt{-A}} + w_{\mathtt{C-}} + w_{\mathtt{CA}} \geq w_{\mathtt{AA}} + w_{\mathtt{CC}}\,, \\
\text{and} \quad w_{\mathtt{-A}} + 2w_{\mathtt{C-}} + w_{\mathtt{-C}} + w_{\mathtt{GA}} \ \geq \ w_{\mathtt{AA}} + w_{\mathtt{CC}} + w_{\mathtt{GC}}. &
\end{array}$$

The aim of this section is to introduce the geometry behind such derivations.

Given any points $v_1, \ldots, v_n$ in $\mathbb{R}^d$, their *convex hull* is the set

$$P \quad = \quad \Big\{ \sum_{i=1}^{n} \lambda_i v_i \in \mathbb{R}^d \ : \ \lambda_1, \ldots, \lambda_n \geq 0 \text{ and } \sum_{i=1}^{n} \lambda_i = 1 \Big\}. \qquad (2.17)$$

Any subset of $\mathbb{R}^d$ of this form is called a *convex polytope* or just a *polytope*, for short. The *dimension* of the polytope P is the dimension of its affine span $\{\sum_{i=1}^{b} \lambda_i v_i \in \mathbb{R}^d \;:\; \sum_{i=1}^{n} \lambda_i = 1\}$. We can also represent a polytope as a finite intersection of closed half-spaces. Let A be a real $d \times m$ matrix and let $b \in \mathbb{R}^m$. Each row of A and corresponding entry of b defines a half-space in $\mathbb{R}^d$. Their intersection is the following set which may be bounded or unbounded:

$$P \quad = \quad \{\, x \in \mathbb{R}^d \;:\; A \cdot x \,\geq\, b \,\}. \tag{2.18}$$

Any subset of $\mathbb{R}^d$ of this form is called a *convex polyhedron*.

Theorem 2.19 *Convex polytopes are precisely the bounded convex polyhedra.*

Proof A proof (and lots of information on polytopes) can be found in the books [Grünbaum, 2003] and [Ziegler, 1995]. This theorem is known as the *Weyl-Minkowski Theorem.* □

Thus every polytope can be represented either in the form (2.17) or in the form (2.18). These representations are known as *V-polytopes* and *H-polytopes*. Transforming one into the other is a fundamental algorithmic task in geometry.

Example 2.20 Let P be the standard cube of dimension $d = 3$. As an H-polytope the cube is the solution to $m = 6$ linear inequalities

$$P \quad = \quad \{\, (x, y, z) \in \mathbb{R}^3 \;:\; 0 \leq x \leq 1 \,,\; 0 \leq y \leq 1 \,,\; 0 \leq z \leq 1 \,\},$$

and as a V-polytope the cube is the convex hull of $n = 8$ points

$$P = \mathrm{conv}\{(0,0,0), (0,0,1), (0,1,0), (0,1,1), (1,0,0), (1,0,1), (1,1,0), (1,1,1)\}.$$

Closely related computational tasks are to make the V-representation (2.17) irredundant by removing points v_i, and to make the H-representation (2.18) irredundant by removing halfspaces, each while leaving the set P unchanged. To understand the underlying geometry, we need to define faces of polytopes. Given a polytope $P \subset \mathbb{R}^d$ and a vector $w \in \mathbb{R}^d$, consider the set of all points in P at which the linear functional $x \mapsto x \cdot w$ attains its minimum. It is denoted

$$\mathrm{face}_w(P) \quad = \quad \{\, x \in P \;:\; x \cdot w \leq y \cdot w \;\text{ for all } y \in P \,\}. \tag{2.19}$$

Let $w^* = \min\{x \cdot w \,:\, x \in P\}$. Then we can write (2.19) equivalently as

$$\mathrm{face}_w(P) \quad = \quad \{\, x \in P \;:\; x \cdot w \leq w^* \,\}.$$

This shows that $\mathrm{face}_w(P)$ is a bounded polyhedron, and hence it is a polytope by Theorem 2.19. Every polytope of this form is called a *face* of P. In particular P is a face of itself, gotten by taking $w = 0$. A face of dimension zero consists of a single point and is called a *vertex* of P. A face of dimension one is called an *edge*, a face of dimension $\dim(P) - 1$ is called a *facet*, and a face of dimension

$\dim(P) - 2$ is called a *ridge*. The cube in Example 2.20 has 27 faces. Of these, there are 8 vertices, 12 edges (= ridges), 6 facets, and the cube itself.

We write $f_i(P)$ for the number of i-dimensional faces of a polytope P. The vector $f(P) = \big(f_0(P), f_1(P), f_2(P), \ldots, f_{d-1}(P)\big)$ is called the *f-vector* of P. So, the three-dimensional cube P has the f-vector $f(P) = (8, 12, 6)$. Its dual polytope P^*, which is the octahedron, has the f-vector $f(P^*) = (6, 12, 8)$.

Let P be a polytope and F a face of P. The *normal cone* of P at F is

$$N_P(F) \quad = \quad \big\{ w \in \mathbb{R}^d \,:\, \mathrm{face}_w(P) = F \,\big\}.$$

This is a relatively open convex polyhedral cone in $\mathbb{R}^d$. Its dimension satisfies

$$\dim N_P(F) \quad = \quad d - \dim(F).$$

In particular, if $F = \{v\}$ is a vertex of P then its normal cone $N_P(v)$ is d-dimensional and consists of all linear functionals w that are minimized at v.

Example 2.21 Let P be the convex hull of the points $v_1, \ldots, v_{14}$ in Example 2.18. The normal cone $N_P(v_{14})$ consists of all weights for which the gapless alignment (H, H, H) is optimal. It is characterized by the seven inequalities.

The collection of all cones $N_P(F)$ as F runs over all faces of P is denoted $\mathcal{N}(P)$ and is called the *normal fan* of P. Thus the normal fan $\mathcal{N}(P)$ is a partition of $\mathbb{R}^d$ into cones. The cones in $\mathcal{N}(P)$ are in bijection with the faces of P. For instance, if P is the 3-cube then $\mathcal{N}(P)$ is the partition of $\mathbb{R}^3$ into cones with constant sign vectors. Hence $\mathcal{N}(P)$ is combinatorially isomorphic to the octahedron P^*. Figure 2.3 shows a two-dimensional example.

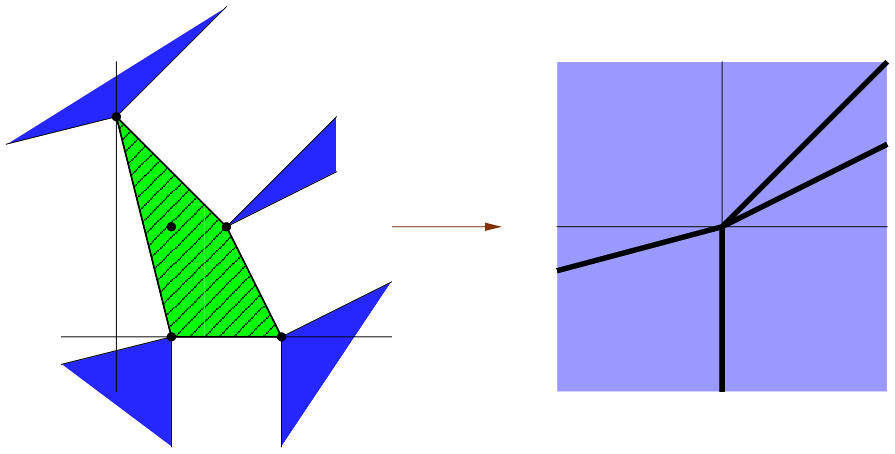

Fig. 2.3. The (negated) normal fan of a quadrangle in the plane.

Our next result ties in the faces of a polytope P with its irredundant representations. Let a_i be one of the row vectors of the matrix A in (2.18) and let b_i be the corresponding entry in the vector b. This defines the face

$$\mathrm{face}_{a_i}(P) \quad = \quad \{\, x \in P \,:\, a_i \cdot x \,=\, b_i \,\}.$$

Proposition 2.22 *The V-representation (2.17) of the polytope P is irredundant if and only if v_i is a vertex of P for $i = 1, \dots, n$. The H-representation (2.18) is irredundant if and only if $\mathrm{face}_{a_i}(P)$ is a facet of P for $i = 1, \dots, m$.*

A comprehensive software system for computing with polytopes is the program `POLYMAKE`. We show the use of `POLYMAKE` by computing the polytope of the toric Markov chain model $\mathbf{f}_{2,4}(\Theta)$. This model has $m = 16$ states and $d = 4$ parameters. We create an input file named `foo` which looks like this:

```
POINTS
1 3 0 0 0
1 2 1 0 0
1 1 1 1 0
1 1 1 0 1
1 1 1 1 0
1 0 2 1 0
1 0 1 1 1
1 0 1 0 2
1 2 0 1 0
1 1 1 1 0
1 0 1 2 0
1 0 1 1 1
1 1 0 1 1
1 0 1 1 1
1 0 0 1 2
1 0 0 0 3
```

These 16 points are the columns of the 4×16-matrix in Subsection 1.4.1. The extra character `1` is prepended for technical reasons. We run the command

```
polymake foo VERTICES
```

Then the system responds by listing the eight vertices of this polytope

```
VERTICES
1 3 0 0 0
1 2 1 0 0
1 0 2 1 0
1 0 1 0 2
1 2 0 1 0
```

```
1 0 1 2 0
1 0 0 1 2
1 0 0 0 3
```

Furthermore, on the file `foo` itself we find the irredundant H-representation

```
FACETS
1 0 -1 1 0
0 1 0 0 0
1 0 1 -1 0
0 0 1 0 0
0 0 0 1 0
3 -1 -1 -1 0

AFFINE_HULL
-3 1 1 1 1
```

This output tells us that our polytope is defined by the one linear equation $x_1 + x_2 + x_3 + x_4 = 3$ and the six linear inequalities

$$x_2 - x_3 \leq 1,\ x_1 \geq 0,\ x_3 - x_2 \leq 1,\ x_2 \geq 0,\ x_3 \geq 0,\ x_1 + x_2 + x_3 \leq 3.$$

Indeed, the command `DIM` confirms that the polytope is three-dimensional:

```
polymake foo DIM
DIM
3
```

The f-vector of our polytope coincides with that of the three-dimensional cube

```
polymake foo F_VECTOR
F_VECTOR
8 12 6
```

But our polytope is not a cube at all. Inspecting the updated file `foo` reveals that its facets are two triangles, two quadrangles and two pentagons:

```
VERTICES_IN_FACETS
{1 2 3}
{2 3 5 6 7}
{4 5 6}
{0 4 6 7}
{0 1 3 7}
{0 1 2 4 5}
```

This is the polytope depicted in Figure 1.1. We return to our general discussion.

Let $\mathcal{P}_d$ denote the set of all polytopes in $\mathbb{R}^d$. There are two natural operations, namely addition $\oplus$ and multiplication $\odot$, defined on the set $\mathcal{P}_d$. The resulting structure is the *polytope algebra* $\big(\mathcal{P}_d, \oplus, \odot\big)$. Namely, if $P, Q \in \mathcal{P}_d$ are polytopes then their sum $P \oplus Q$ is the convex hull of the union of P and Q:

$$\begin{aligned} P \oplus Q \quad &:= \quad \mathrm{conv}(P \cup Q) \\ &= \quad \big\{ \lambda p + (1-\lambda) q \in \mathbb{R}^d \,:\, p \in P,\, q \in Q,\, 0 \le \lambda \le 1 \big\}. \end{aligned}$$

The product in the polytope algebra is defined to be the *Minkowski sum*:

$$\begin{aligned} P \odot Q \quad &:= \quad P + Q \\ &= \quad \big\{ p + q \in \mathbb{R}^d \,:\, p \in P,\, q \in Q \big\}. \end{aligned}$$

It follows from the Weyl-Minkowski Theorem that both $P \oplus Q$ and $P \odot Q$ are polytopes in $\mathbb{R}^d$. The polytope algebra $\big(\mathcal{P}_d, \oplus, \odot\big)$ satisfies many of the familiar axioms of arithmetic. Clearly, addition and multiplication are commutative. But it is also the case that the distributive law holds for polytopes:

Proposition 2.23 *If P, Q, R are polytopes in $\mathbb{R}^d$ then*

$$(P \oplus Q) \odot R \quad = \quad (P \odot R) \oplus (Q \odot R). \tag{2.20}$$

Proof Consider points $p \in P$, $q \in Q$ and $r \in R$. For $0 \le \lambda \le 1$ note that

$$(\lambda p + (1-\lambda) q) + r \quad = \quad \lambda(p + r) + (1-\lambda)(q + r).$$

The left hand side represents an arbitrary point in the left hand side of (2.20), and the right hand side represents a point in the right hand side of (2.20). □

Example 2.24 *(The tropical semiring revisited)* Let us consider the algebra $(\mathcal{P}_1, \oplus, \odot)$ of all polytopes on the real line ($d = 1$). Each element of $\mathcal{P}_1$ is a segment $[a, b]$ where $a < b$ are real numbers. The arithmetic operations are

$$\begin{aligned} [a, b] \oplus [c, d] \quad &= \quad [\,\min(a, c), \max(b, d)\,], \\ [a, b] \odot [c, d] \quad &= \quad [\,a + c,\, b + d\,]. \end{aligned}$$

Thus the one-dimensional polytope algebra is essentially the same as the tropical semiring $(\mathbb{R}, \oplus, \odot)$. Or, stated differently, the polytope algebra $(\mathcal{P}_d, \oplus, \odot)$ is a natural higher-dimensional generalization of the tropical semiring.

One of the main connections between polytopes and algebraic statistics is via the Newton polytopes of the polynomials which parameterize a model. Consider the polynomial

$$f \quad = \quad \sum_{i=1}^{n} c_i \cdot \theta_1^{v_{i1}} \theta_2^{v_{i2}} \cdots \theta_d^{v_{id}}, \tag{2.21}$$

where c_i is a non-zero real number and $v_i = (v_{i1}, v_{i2}, \ldots, v_{id}) \in \mathbb{N}^d$ for $i = 1, 2, \ldots, n$. We define the *Newton polytope* of the polynomial f as the convex hull of all exponent vectors that appear in the expansion (2.21) of f:

$$\mathrm{NP}(f) \quad := \quad \mathrm{conv}\{v_1, v_2, \ldots, v_n\} \quad \subset \quad \mathbb{R}^d. \tag{2.22}$$

Hence the Newton polytope $\mathrm{NP}(f)$ is precisely the V-polytope in (2.17). The operation of taking Newton polytopes respects the arithmetic operations:

Theorem 2.25 *Let f and g be polynomials in $\mathbb{R}[\theta_1, \ldots, \theta_d]$. Then*

$$\mathrm{NP}(f \cdot g) = \mathrm{NP}(f) \odot \mathrm{NP}(g) \quad \textit{and} \quad \mathrm{NP}(f+g) \subseteq \mathrm{NP}(f) \oplus \mathrm{NP}(g).$$

If all coefficients of f and g are positive then $\mathrm{NP}(f+g) \;=\; \mathrm{NP}(f) \oplus \mathrm{NP}(g)$.

Proof Let $f = \sum_{i=1}^{n} c_i \cdot \theta^{v_i}$ be as in (2.21) and let $g = \sum_{j=1}^{n'} c'_j \cdot \theta^{v'_j}$. For any $w \in \mathbb{R}^d$ let $\mathrm{in}_w(f)$ denote the *initial form* of f. This is the subsum of all terms $c_i\theta^{v_i}$ such that $v_i \cdot w$ is minimal. Then the following identity holds:

$$\mathrm{NP}\big(\mathrm{in}_w(f)\big) \quad = \quad \mathrm{face}_w\big(\mathrm{NP}(f)\big). \tag{2.23}$$

The initial form of a product is the product of the initial forms:

$$\mathrm{in}_w(f \cdot g) \quad = \quad \mathrm{in}_w(f) \cdot \mathrm{in}_w(g). \tag{2.24}$$

For generic $w \in \mathbb{R}^d$, the initial form (2.24) is a monomial $\theta^{v_i + v'_j}$, and its coefficient in $f \cdot g$ is the product of the corresponding coefficients in f and g. Finally, the face operator $\mathrm{face}_w(\,\cdot\,)$ is a linear map on the polytope algebra:

$$\mathrm{face}_w\big(\mathrm{NP}(f) \odot \mathrm{NP}(g)\big) \quad = \quad \mathrm{face}_w\big(\mathrm{NP}(f)\big) \odot \mathrm{face}_w\big(\mathrm{NP}(g)\big). \tag{2.25}$$

Combining the three identities (2.23), (2.24) and (2.25), for w generic, shows that the polytopes $\mathrm{NP}(f \cdot g)$ and $\mathrm{NP}(f) \odot \mathrm{NP}(g)$ have the same set of vertices.

For the second identity, note that $\mathrm{NP}(f) \oplus \mathrm{NP}(g)$ is the convex hull of $\{v_1, \ldots, v_n, v'_1, \ldots, v'_{n'}\}$. Every term of $f+g$ has its exponent in this set, so this convex hull contains $\mathrm{NP}(f+g)$. If all coefficients are positive then equality holds because there is no cancellation when forming the sum $f+g$. □

Example 2.26 Consider the polynomials $f = (x+1)(y+1)(z+1)$ and $g = (x+y+z)^2$. Then $\mathrm{NP}(f)$ is a cube and $\mathrm{NP}(g)$ is a triangle. The Newton polytope $\mathrm{NP}(f+g)$ of their sum is the *bipyramid* with vertices $(0,0,0)$, $(2,0,0)$, $(0,2,0)$, $(0,0,2)$, $(1,1,1)$. The Newton polytope $\mathrm{NP}(f \cdot g)$ of their product is the Minkowski sum of the cube with the triangle. It has 15 vertices.

Newton polytopes allow us to transfer constructions from the algebraic setting of polynomials to the geometric setting of polytopes. To illustrate consider the following example. Suppose we are given a 4×4 matrix of polynomials,

$$A(x,y,z) \quad = \quad \begin{pmatrix} a_{11}(x,y,z) & a_{12}(x,y,z) & a_{13}(x,y,z) & a_{14}(x,y,z) \\ a_{21}(x,y,z) & a_{22}(x,y,z) & a_{23}(x,y,z) & a_{24}(x,y,z) \\ a_{31}(x,y,z) & a_{32}(x,y,z) & a_{33}(x,y,z) & a_{34}(x,y,z) \\ a_{41}(x,y,z) & a_{42}(x,y,z) & a_{43}(x,y,z) & a_{44}(x,y,z) \end{pmatrix},$$

and suppose we are interested in the Newton polytope of its determinant $\det\bigl(A(x,y,z)\bigr)$. One possible way to compute this Newton polytope is to evaluate the determinant, list all terms that occur in that polynomial, and then compute the convex hull. However, assuming that the coefficients of the $a_{ij}(x,y,z)$ are such that no cancellations occur, it is more efficient to do the arithmetic directly at the level of Newton polytopes. Namely, we replace each matrix entry by its Newton polytope $P_{ij} = \mathrm{NP}(a_{ij})$, consider the 4×4 matrix of polytopes (P_{ij}), and compute its determinant in the polytope algebra. Just like in the tropical semiring (2.6), here the determinant equals the permanent:

$$\det \begin{pmatrix} P_{11} & P_{12} & P_{13} & P_{14} \\ P_{21} & P_{22} & P_{23} & P_{24} \\ P_{31} & P_{32} & P_{33} & P_{34} \\ P_{41} & P_{42} & P_{43} & P_{44} \end{pmatrix} \quad = \quad \bigoplus_{\sigma \in S_4} P_{1\sigma(1)} \odot P_{2\sigma(2)} \odot P_{3\sigma(3)} \odot P_{4\sigma(4)}.$$

This determinant of polytopes represents a parameterized family of assignment problems. Indeed, suppose the cost q_{ij} of assigning job i to worker j depends piecewise-linearly on a vector of three parameters $w = (w_x, w_y, w_z)$, namely

$$q_{ij} \quad = \quad \min\{w \cdot p \, : \, p \in P_{ij}\}.$$

Thus the cost q_{ij} is determined by solving the linear programming problem with polytope P_{ij}. The *parametric assignment problem* would be to solve the assignment problem simultaneously for all vectors $w \in \mathbb{R}^3$. In other words, we wish to preprocess the problem specification so that the cost of an optimal assignment can be computed rapidly. This preprocessing amounts to computing the irredundant V-representation of the polytope gotten from the determinant. Then the cost of an optimal assignment can be computed as follows:

$$\min\{w \cdot p \; : \; p \in \det\bigl((P_{ij})_{1 \leq i,j \leq 4}\bigr)\}.$$

Our discussion furnishes a higher-dimensional generalization of Remark 2.6:

Remark 2.27 The parametric assignment problem is solved by computing the determinant of the matrix of polytopes (P_{ij}) in the polytope algebra.

We can similarly define the *parametric shortest path problem* on a directed graph. The weight of each edge is now a polytope P_{ij} in $\mathbb{R}^d$, and for a specific parameter vector $w \in \mathbb{R}^d$ we recover the scalar edge weights by linear programming on that polytope: $d_{ij} = \min\{w \cdot p \,:\, p \in P_{ij}\}$. Then the shortest path from i to j is given by $d_{ij}^{(n-1)} = \min\{w \cdot p \,:\, p \in P_{ij}^{(n-1)}\}$, where $P_{ij}^{(n-1)}$ is the (i,j)-entry in the $(n-1)$-st power of the matrix (P_{ij}). Here matrix multiplication is carried out in the polytope algebra $\big(\mathcal{P}_d, \oplus, \odot\big)$.

The Hungarian algorithm for assignments and the Floyd-Warshall algorithm for shortest paths can be extended to the parametric setting. Provided the number d of parameters is fixed, these algorithms still run in polynomial time. The efficient computation of such polytopes by dynamical programming using polytope algebra arithmetic along a graph is referred to as *polytope propagation* (see Chapters 5–8). We close this section by revisiting the case of alignments.

Remark 2.28 The problem of parametric alignment of two DNA sequences σ^1 and σ^2 is to compute the Newton polytopes $\mathrm{NP}(f_{\sigma^1,\sigma^2})$ of the corresponding coordinate polynomial f_{σ^1,σ^2} of the pair hidden Markov model (2.13).

If some of the scores have been specialized then we compute Newton polytopes of polynomials in fewer unknowns. For instance, if $w' = 0$ then our task is to compute the Newton polytope $\mathrm{NP}(g_{\sigma^1,\sigma^2})$ of the specialized polynomial g_{σ^1,σ^2}. This can be done efficiently by running the Needleman-Wunsch Algorithm 2.13 in the polytope algebra and is the topic of Chapters 5–7.

Example 2.29 Returning to Example 2.18, we observe that the 14 points $v_1, \ldots, v_{14}$ are the vertices of the Newton polytope $P = \mathrm{NP}(g_{\texttt{ACG},\texttt{ACC}})$. It is important to note that all of the 14 points corresponding to monomials in $g_{\texttt{ACG},\texttt{ACC}}$ are in fact vertices of P, which means that every possible alignment of `ACG` and `ACC` is an optimal alignment for some choice of parameters.

The polytope P is easily computed in `POLYMAKE`, which confirms that the polytope is six-dimensional. The f-vector is $f(P) = (14, 51, 86, 78, 39, 10)$. These numbers have an interpretation in terms of alignments. For example, there is an edge between two vertices in the polytope if for two different optimal alignments (containing different numbers of matches, mismatches, and gaps) the parameter regions which yield the optimal alignments share a boundary. In other words, the fact that the polytope has 51 edges tells us that there are precisely 51 "parameter boundaries", where an infinitesimal change in parameters can result in a different optimal alignment. The normal cones and their defining inequalities (like the seven in Example 2.18) characterize these boundaries, thus offering a solution to the parametric alignment problem.

2.4 Trees and metrics

One of the important mathematical structures that arises in biology is the phylogenetic tree [Darwin, 1859, Felsenstein, 2003, Semple and Steel, 2003]. A *phylogenetic tree* is a tree T together with a labeling of its leaves. The number of combinatorial types of phylogenetic trees with the same leaves grows exponentially (Lemma 2.32). In phylogenetics a typical problem is to select a tree, based on data, from the large number of possible choices.

This section introduces some basic concepts in combinatorics of trees that are important for phylogeny. The notion of *tree space* is related to the tropicalization principle introduced in Section 2.1 and will be revisited in Section 3.5. A widely used algorithm in phylogenetics, the neighbor joining algorithm, is a method for projecting a metric onto tree space. This algorithm draws on a number of ideas in phylogenetics and serves as the focus of our presentation in this section. We begin by discussing a number of different, yet combinatorially equivalent, characterizations of trees.

A *dissimilarity map* on $[n] = \{1, 2, \ldots, n\}$ is a function $d : [n] \times [n] \to \mathbb{R}$ such that $d(i,i) = 0$ and $d(i,j) = d(j,i) \geq 0$. The set of all dissimilarity maps on $[n]$ is a real vector space of dimension $\binom{n}{2}$, which we identify with $\mathbb{R}^{\binom{n}{2}}$. A dissimilarity map d is called a *metric on* $[n]$ if the triangle inequality holds:

$$d(i,j) \;\leq\; d(i,k) + d(k,j) \qquad \text{for } i,j,k \in [n]. \tag{2.26}$$

A dissimilarity map d can be written as a non-negative symmetric $n \times n$ matrix $D = (d_{ij})$ where $d_{ij} = d(i,j)$ and $d_{ii} = 0$. The triangle inequality (2.26) can be expressed by matrix multiplication where the arithmetic is tropical.

Remark 2.30 The matrix D represents a metric if and only if $D \odot D = D$.

Proof The entry of the matrix $D \odot D$ in row i and column j equals

$$d_{i1} \odot d_{1j} \;\oplus\; \cdots \;\oplus\; d_{in} \odot d_{nj} \quad = \quad \min\big\{\, d_{ik} + d_{kj} \;:\; 1 \leq k \leq n \,\big\}. \tag{2.27}$$

This quantity is less than or equal to $d_{ij} \;=\; d_{ii} \odot d_{ij} \;=\; d_{ij} \odot d_{jj}$, and it equals d_{ij} if and only if the triangle inequality $d_{ij} \leq d_{ik} + d_{kj}$ holds for all k. □

The set of all metrics on $[n]$ is a full-dimensional convex polyhedral cone in $\mathbb{R}^{\binom{n}{2}}$, called the *metric cone*. The metric cone has a distinguished subcone, known as the *cut cone*, which is the $\mathbb{R}_{\geq 0}$-linear span of all metrics $d_{\{A,B\}}$ arising as follows from all splits $\{A, B\}$ of $[n]$ into two non-empty subsets A and B:

$$\begin{aligned} d_{\{A,B\}}(i,j) \;&=\; 1 \qquad\qquad \text{if } i,j \in A \;\text{ or }\; i,j \in B \\ d_{\{A,B\}}(i,j) \;&=\; 0 \qquad\qquad \text{if } \;\; i \in A, j \in B \text{ or } i \in B, j \in A. \end{aligned} \tag{2.28}$$

The cut cone is strictly contained in the metric cone if $n \geq 6$. This and many other results on metrics can be found in [Deza and Laurent, 1997].

A metric d is a *tree metric* if there exists a tree T with n leaves, labeled by $[n] = \{1, 2, \ldots, n\}$, and a non-negative length for each edge of T, such that the length of the unique path from leaf x to leaf y equals $d(x, y)$ for all $x, y \in [n]$. We sometimes write d_T for the tree metric d which is derived from the tree T.

Example 2.31 Let $n = 4$ and consider the metric d given by the matrix

$$D \quad = \quad \begin{pmatrix} 0 & 1.1 & 1.0 & 1.4 \\ 1.1 & 0 & 0.3 & 1.3 \\ 1.0 & 0.3 & 0 & 1.2 \\ 1.4 & 1.3 & 1.2 & 0 \end{pmatrix}$$

The metric d is a tree metric, as can be verified by examining the tree

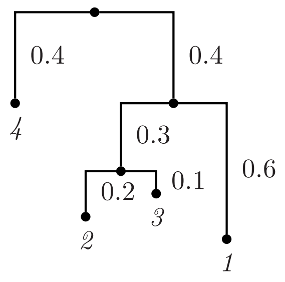

Fig. 2.4. The metric in Example 2.31 is a tree metric.

The *space of trees* is the following subset of the metric cone:

$$\mathcal{T}_n \quad = \quad \{\, d_T \;:\; d_T \text{ is a tree metric} \,\} \quad \subset \quad \mathbb{R}^{\binom{n}{2}}. \tag{2.29}$$

The structure of $\mathcal{T}_n$ is best understood by separating the combinatorial types of trees from the lengths of the edges. A tree T is *trivalent* if every interior node is adjacent to three edges. A trivalent tree T has $n-2$ interior nodes and $2n-3$ edges. We can create any tree on $n+1$ leaves by attaching the new leaf to any of the $2n-3$ edges of T. By induction on n, we derive:

Lemma 2.32 *The number of combinatorial types of unrooted trivalent trees on a fixed set of n leaves is the* Schröder number

$$(2n-5)!! \quad = \quad 1 \cdot 3 \cdot 5 \cdot \;\cdots\; \cdot (2n-7) \cdot (2n-5). \tag{2.30}$$

Each edge of a tree T corresponds to a split $\{A, B\}$ of the leaf set $[n]$ into two disjoint subsets A and B. Two splits $\{A_1, B_1\}$ and $\{A_2, B_2\}$ are *compatible* if at least one of the four intersections $A_1 \cap A_2$, $A_1 \cap B_2$, $B_1 \cap A_2$, and $B_1 \cap B_2$ is empty. We have the following easy combinatorial lemma:

Lemma 2.33 *If $\{A_1, B_1\}$ and $\{A_2, B_2\}$ are splits corresponding to two edges on a tree T with leaf set $[n]$ then $\{A_1, B_1\}$ and $\{A_2, B_2\}$ are compatible.*

Let $\{A_1, B_1\}$ and $\{A_2, B_2\}$ be two distinct compatible splits. We say that A_1 is *mixed* with respect to $\{A_2, B_2\}$ if $A_1 \cap A_2$ and $A_1 \cap B_2$ are both nonempty. Otherwise A_1 is *pure* with respect to $\{A_2, B_2\}$. Of the two components A_1 and B_1 exactly one is pure and the other is mixed with respect to the other split $\{A_2, B_2\}$. Let $\mathrm{Splits}(T)$ denote the collection of all $2n-3$ splits (A, B) arising from T. For instance, if $n = 4$ and T is the tree in Figure 2.4 then

$$\mathrm{Splits}(T) \;=\; \big\{\{1, 234\}, \{14, 23\}, \{123, 4\}, \{134, 2\}, \{124, 3\}\big\}. \qquad (2.31)$$

Theorem 2.34 (Splits Equivalence Theorem) *A collection S of splits is pairwise compatible if and only if there exists a tree T such that $S = \mathrm{Splits}(T)$. Moreover, if such a tree T exists then it is unique.*

Proof If there are no splits then the tree is a single node. Otherwise, we proceed by induction. Consider the set of splits $S' = S \backslash \{\{A, B\}\}$ where $\{A, B\}$ is a split in S. There is a unique tree T' corresponding to the set of splits S'. Any split in S' has one pure and one mixed component with respect to $\{A, B\}$. We orient the corresponding edge e of T' so that it is directed from the pure component to the mixed component. We claim that no node in T' can have out-degree ≥ 2. If this was the case there would be a split with a component that is both pure and mixed with respect to (A, B). Thus every node of T' has out-degree either 0 or 1. Since the number of nodes is one more than the number of edges, we conclude that the directed tree T' has a unique sink v'. Replace v' with two new nodes v_A and v_B and add a new edge between them as indicated in Figure 2.5. The result is the unique tree T with $S = \mathrm{Splits}(T)$. □

We next establish the classical *four point condition* which characterizes membership in tree space $\mathcal{T}_n$. The proof is based on the notion of a *quartet*, which for any phylogenetic tree T is a subtree spanned by four taxa i, j, k, l. If $\big\{\{i, j\}, \{k, l\}\big\}$ is a split of that subtree then we denote the quartet by $(ij; kl)$.

Theorem 2.35 (The four point condition) *A metric d is a tree metric if and only if, for any four leaves u, v, x, y, the maximum of the three numbers $d(u, v) + d(x, y)$, $d(u, x) + d(v, y)$ and $d(u, y) + d(v, x)$ is attained at least twice.*

Proof If $d = d_T$ for some tree then for any quartet $(uv; xy)$ of T it is clear that

$$d(u, v) + d(x, y) \;\leq\; d(u, x) + d(v, y) \;=\; d(u, y) + d(v, x).$$

Hence the "only if" direction holds.

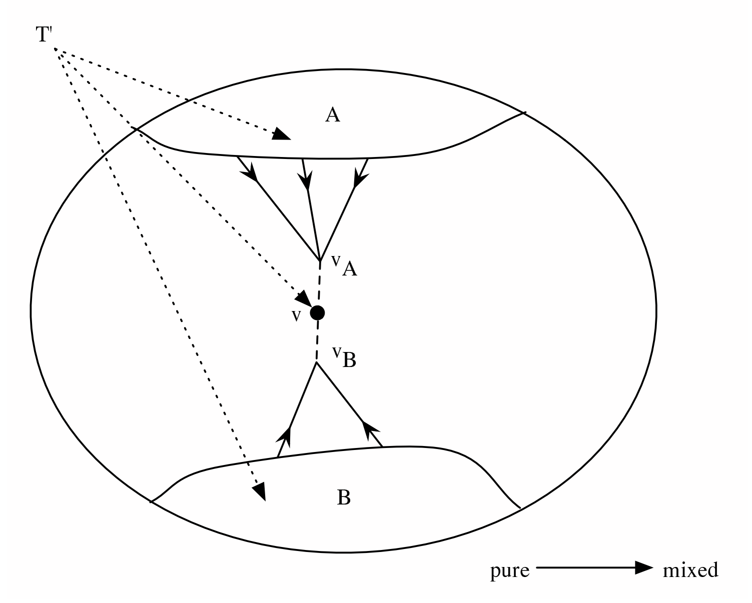

Fig. 2.5. Proof of the Splits Equivalence Theorem

For the converse, let d be any metric which satisfies the four point condition. Let S denote the set whose elements are all splits $\{A, B\}$ with the property

$$d(i,j)+d(k,l) < d(i,k)+d(j,l) = d(i,l)+d(j,k) \text{ for all } i,j \in A \text{ and } k,l \in B.$$

We claim that S is pairwise compatible. If not then there exist two splits $\{A_1, B_1\}$ and $\{A_2, B_2\}$ in S and elements i, j, k, l with $i \in A_1 \cap A_2$, $j \in A_1 \cap B_2$, $k \in B_1 \cap A_2$, and $l \in B_1 \cap B_2$. Then $i, j \in A_1$ and $k, l \in B_1$ implies $d(i,j)+d(k,l) < d(i,k)+d(j,l)$ while $i, k \in A_2$ and $j, l \in B_2$ implies $d(i,j)+d(k,l) > d(i,k)+d(j,l)$, a contradiction.

By Theorem 2.34, there exists a unique tree T such that $S = \text{splits}(T)$. It remains to assign lengths $l(e)$ to the edges e of T so that the resulting tree metric d_T is equal to d. We show that this can be done by induction. Let i, j be two leaves adjacent to the same vertex x in T. Such a pair is called a cherry and at least one can be found in every tree. Let T' be the tree with i, j pruned and replaced by x. Consider the metric d' defined on the leaves of T' where $d'(x,k) = \frac{1}{2}(d(i,k)+d(j,k)-d(i,j))$. By induction, there exists a tree metric $d'_T = d'$. We extend d'_T to a tree metric d_T defined on T. If e is the edge adjacent to the leaf i, then we set $l(e) = \frac{1}{2}(d(i,j)+d(i,k)-d(j,k))$. This assignment is well defined because, for any quartet $(ij;kl)$, we have

$$d(i,l)+d(i,j)-d(j,l) \;\;=\;\; d(i,j)+d(i,k)-d(j,k).$$

Similarly, if f is the edge adjacent to the leaf j, we set $l(f) = \frac{1}{2}(d(i,j)+$

$d(j,k) - d(i,k))$. Since $d_T(i,j) = l(e) + l(f)$ it follows that $d_T(i,j) = d(i,j)$. Similarly, for any $k \neq i,j$, $d_T(i,k) = d(i,k)$ and $d_T(j,k) = d(j,k)$. $\square$

The previous argument shows that the set of split metrics

$$\big\{ d_{\{A,B\}} \,:\, (A,B) \in \mathrm{Splits}(T) \,\big\} \tag{2.32}$$

is linearly independent in $\mathbb{R}^{\binom{n}{2}}$. We wrote the tree metric d_T uniquely as a linear combination of this set of split metrics. Let $\mathcal{C}_T$ denote the non-negative span of the set (2.32). The cone $\mathcal{C}_T$ is isomorphic to the orthant $\mathbb{R}^{2n-3}_{\geq 0}$.

Proposition 2.36 *The space of trees $\mathcal{T}_n$ is the union of the $(2n-5)!!$ orthants $\mathcal{C}_T$. More precisely, $\mathcal{T}_n$ is a simplicial fan of pure dimension $2n-3$ in $\mathbb{R}^{\binom{n}{2}}$.*

We return to tree space (and its relatives) in Section 3.5, where we show that $\mathcal{T}_n$ can be interpreted as a Grassmannian in tropical algebraic geometry.

The relevance of tree space to efficient statistical computation is this: suppose that our data consists of measuring the frequency of occurrence of the different words in $\{\mathtt{A},\mathtt{C},\mathtt{G},\mathtt{C}\}^n$ as columns of an alignment on n DNA sequences. As discussed in Section 1.4, we would like to select a tree model. In principle, we could compute the MLE for each of the $(2n-5)!!$ trees, however, this approach has a number of difficulties. First, even for a single tree the MLE computation is very difficult, even if we are satisfied with a reasonable local maximum of the likelihood function. Even if the MLE computation were feasible, a naive approach to model selection requires examining all exponentially many (in n) trees. One popular way to avoid these problems is the "distance based approach" which is to collapse the data to a dissimilarity map and then to obtain a tree via a projection onto tree space (see 4.21). The projection of choice for most biologists is the *neighbor joining algorithm* which provides an easy-to-compute map from the metric cone onto $\mathcal{T}_n$. The algorithm is based on Theorem 2.35 and the Cherry Picking Theorem [Saitou and Nei, 1987, Studier and Keppler, 1988].

Fix a dissimilarity map d on the set $[n]$. For any $a_1, a_2, b_1, b_2 \in [n]$ we set

$$\begin{aligned} w(a_1a_2;b_1b_2) \;:=&\\ &\tfrac{1}{4}[d(a_1,b_1) + d(a_1,b_2) + d(a_2,b_1) + d(a_2,b_2) - 2[d(a_1,a_2) + d(b_1,b_2)]]. \end{aligned}$$

The function w provides a natural "weight" for quartets when d is a tree metric. The following result on quartets is proved by inspecting a tree with four leaves.

Lemma 2.37 *If d is a tree metric with $(a_1a_2;b_1b_2)$ a quartet in the tree, then $w(a_1a_2;b_1b_2) = -2\cdot w(a_1b_1;a_2b_2)$, and this number is the length of the path which connects the path between a_1 and a_2 with the path between b_1 and b_2.*

A *cherry* of a tree is a pair of leaves which are both adjacent to the same node. The following theorem gives a criterion for identifying cherries.

Theorem 2.38 (Cherry picking theorem) *If d is a tree metric on $[n]$ and*

$$Z_d(i,j) \quad = \sum_{k,l \in [n]\setminus\{i,j\}} w(ij;kl) \tag{2.33}$$

then any pair of leaves that maximizes $Z_d(i,j)$ is a cherry in the tree.

Proof Suppose that i,j is not a cherry in the tree. Without loss of generality, we may assume that either there is a leaf k forming a cherry with i, or neither i nor j form a cherry with any leaf. In the first case, observe that

$$\begin{aligned} Z_d(i,k) - Z_d(i,j) \quad &= \sum_{x,y\neq i,j,k} (w(ik;xy) - w(ij;xy)) \\ &\quad + \sum_{x\neq i,j,k} (w(ik;xj) - w(ij;xk)) \quad > \quad 0. \end{aligned}$$

Here we are using Lemma 2.37. In the latter case, there must be cherries (k,l) and (p,q) arranged as in Figure 2.6. Without loss of generality, we assume that the cherry (k,l) has the property that the number of leaves in $T\setminus e$ in the same component as k is less than or equal to the number of leaves in $T\setminus e'$ in the same component as p. We now compare $Z_d(k,l)$ to $Z_d(i,j)$:

$$\begin{aligned} Z_d(k,l) - Z_d(i,j) \quad &= \sum_{x,y\neq i,j,k,l} (w(kl;xy) - w(ij;xy)) \\ &\quad + \sum_{x\neq i,j,k,l} (w(kl;xj) + w(kl;ix) - w(ij;xl) - w(ij;kx)). \end{aligned}$$

The two sums are each greater than 0. In the first sum, we need to evaluate all possible positions for x and y within the tree. If, for example, x and y lie in the component of $T\backslash\{x,y\}$ that contains i and j then it is clear that $w(kl;xy) - w(ij;xy) > 0$. If x and y lie in the same component of $T\setminus e$ as leaf k, then it may be that $w(kl;xy) - w(ij;xy) < 0$, however for each such pair x,y there will be another pair that lies in the same component of $T\setminus e'$ as leaf p. The deficit for the former pair will be less than the surplus provided by the second. The remaining cases follow directly from Lemma 2.37. □

Theorem 2.38 is conceptually simple and useful, and we will see that it is useful for understanding the neighbor joining algorithm. It is however not computationally efficient because $O(n^2)$ additions are necessary just to find one cherry. An equivalent, but computationally superior, formulation is:

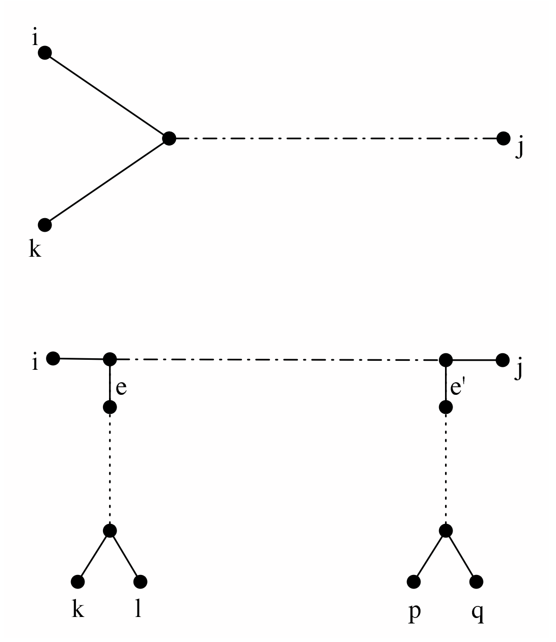

Fig. 2.6. Cases in the proof of the Cherry Picking Theorem.

Corollary 2.39 *Let d be a tree metric on $[n]$. For every pair $i, j \in [n]$ set*

$$Q_d(i,j) \quad = \quad (n-2) \cdot d(i,j) - \sum_{k \neq i} d(i,k) - \sum_{k \neq j} d(j,k). \qquad (2.34)$$

Then the pair $x, y \in [n]$ that minimizes $Q_d(x,y)$ is a cherry in the tree.

Proof Let $\tau = \sum_{x,y \in [n]} d(x,y)$. A direct calculation reveals the identity

$$Z_d(i,j) \quad = \quad -\frac{1}{2} \cdot \tau \; - \; \frac{n-2}{2} \cdot Q_d(i,j).$$

Thus maximizing $Z_d(x,y)$ is equivalent to minimizing $Q_d(x,y)$. □

The neighbor joining algorithm makes use of the cherry picking theorem by peeling off cherries to recursively build a tree:

Algorithm 2.40 (Neighbor joining algorithm)
Input: A dissimilarity map d on the set $[n]$.
Output: A phylogenetic tree T whose tree metric d_T is "close" to d.
Step 1: Construct the $n \times n$ matrix Q_d whose (i,j)-entry is given by the formula (2.34), and identify the minimum off-diagonal entry $Q_d(x,y)$.
Step 2: Remove x, y from the tree and replace them with a new leaf z. For

each leaf k among the the remaining $n-2$ leaves, set

$$d(z,k) \quad = \quad \frac{1}{2}\big(d(x,k)+d(y,k)-d(x,y)\big). \tag{2.35}$$

This replaces the $n \times n$ matrix Q_d by an $(n-1)\times(n-1)$ matrix. Return to Step 1 until there are no more leaves to collapse.
Step 3*:* Output the tree T. The edge lengths of T are determined recursively: If (x,y) is a cherry connected to node z as in Step 2, then the edge from x to z has length $d(x,k)-d_T(z,k)$ and the edge from y to z has length $d(y,k)-d_T(z,k)$.

This neighbor joining algorithm recursively constructs a tree T whose metric d_T is hopefully close to the given metric d. If d is a tree metric to begin with then the method is guaranteed to reconstruct the correct tree. More generally, instead of estimating pairwise distances, one can attempt to (more accurately) estimate the sum of the branch lengths of subtrees of size $m \geq 3$.

For any positive integer $d \geq 2$, we define a *d-dissimilarity map* on $[n]$ to be a function $D : [n]^d \to \mathbb{R}$ such that $D(i_1,i_2,\ldots,i_d) = D(i_{\pi(1)},i_{\pi(2)},\ldots,i_{\pi(d)})$ for all permutations π on $\{1,\ldots,d\}$ and $D(i_1,i_2,\ldots,i_d) = 0$ if the taxa $i_1,i_2,\ldots,i_d$ are not distinct. The set of all d-dissimilarity maps on $[n]$ is a real vector space of dimension $\binom{n}{d}$ which we identify with $\mathbb{R}^{\binom{n}{d}}$. Every tree T gives rise to an d-dissimilarity map D_T as follows. We define $D_T(i_1,\ldots,i_d)$ to be the sum of all branch lengths in the subtree of T spanned by $i_1,\ldots,i_d \in [n]$.

The following theorem is a generalization of Corollary 2.39. It leads to a generalized neighbor joining algorithm which provides a better approximation of the maximum likelihood tree and parameters. A proof is given in Chapter 18 together with an explanation of the relevance of algebraic techniques for maximum likelihood estimation.

Theorem 2.41 *Let T be a tree on $[n]$ and $d<n$. For any $i,j \in [n]$ set*

$$Q_T(i,j) \;=\; \binom{n-2}{d-1}\sum_{Y\in\binom{[n]\backslash\{i,j\}}{d-2}} D_T(i,j,Y) \;-\; \sum_{Y\in\binom{[n]\backslash\{i\}}{d-1}} D_T(i,Y) \;-\; \sum_{Y\in\binom{[n]\backslash\{j\}}{d-1}} D_T(j,Y).$$

Then the pair $x,y \in [n]$ that minimizes $Q_T(x,y)$ is a cherry in the tree T.

The subset of $\mathbb{R}^{\binom{n}{d}}$ consisting of all d-dissimilarity maps D_T arising from trees T is a polyhedral space which is the image of the tree space $\mathcal{T}_n$ under a linear map $\mathbb{R}^{\binom{n}{2}} \to \mathbb{R}^{\binom{n}{d}}$. This polyhedral space is related to the tropicalization of the Grassmannian $G_{d,n}$, which is discussed in Section 3.5, but the details of this relationship are still not fully understood and deserve further study.

2.5 Software

In this section we introduce the software packages which were used by the authors of this book. These programs were discussed in our seminar in the Fall of 2004 and they played a key role for the studies which are presented in part 2 of this book. The subsection on *Mathematical Software* describes packages traditionally used by mathematicians but which may actually be very useful for statisticians and biologists. The section on *Computational Biology Software* summarizes programs more traditionally used for biological sequence analysis. In each subsection the software packages are listed in alphabetic order by name. Short examples or pointers to such examples are included for each package. These illustrate how the software was used in our computations.

2.5.1 Mathematical Software

We describe ten packages for mathematical calculations relevant for this book.

4TI2

Summary: A package for linear algebra over the non-negative integers (e.g. integer programming). Very useful for studying toric models (Section 2.2).
Example: To solve the linear equation $2x + 5y = 3u + 4v$ for non-negative integers x, y, u, v we create a file named `foo` with the following two lines

```
1 4 2 5 -3 -4
```

Running the command `hilbert foo` creates a 10×4 matrix on a file `foo.hil`:

```
10 4
2 0 0 1
3 0 2 0
1 1 1 1
2 1 3 0
1 2 0 3
0 2 2 1
1 2 4 0
0 3 1 3
0 3 5 0
0 4 0 5
```

Every solution to the equation is an $\mathbb{N}$-linear combination of these ten rows.
Availability: Executable only.
Website: `www.4ti2.de/`

LINPACK

Summary: A Fortran library for linear algebra, originally from the 1970s but still widely used for scientific computation. It contains fast implementations of certain linear algebra algorithms, such as singular value decomposition.
Example: The singular value decomposition subroutine in `LINPACK` is used in Chapter 19 to construct phylogenetic trees from alignments of DNA sequences.
Availability: Open source.
Website: `www.netlib.org/linpack/`

MACAULAY2

Summary: A software system supporting research in algebraic geometry and commutative algebra [Grayson and Stillman, 2002].
Example: We illustrate the computation of toric models in `MACAULAY2`. Consider the toric Markov chain of length $n = 4$ with alphabet $\Sigma = \{0, 1\}$ that appears in Subsection 1.4.2. The model is specified with the commands:

```
i1 : R = QQ[p0000,p0001,p0010,p0011, p0100,p0101,p0110,p0111,
              p1000,p1001,p1010,p1011, p1100,p1101,p1110,p1111];

i2 : S = QQ[a00,a01,a10,a11];

i3 : f = map(S,R,{ a00*a00*a00, a00*a00*a01, a00*a01*a10,
     a00*a01*a11, a01*a10*a00, a01*a10*a01, a01*a11*a10,
     a01*a11*a11, a10*a00*a00, a10*a00*a01, a10*a01*a10,
     a10*a01*a11, a11*a10*a00, a11*a10*a01, a11*a11*a10,
     a11*a11*a11});

o3 : RingMap S <--- R
```

We have used the indeterminates `a00,a01,a10,a11` for the parameters

$$\theta \quad = \quad \begin{pmatrix} \theta_{00} & \theta_{01} \\ \theta_{10} & \theta_{11} \end{pmatrix}.$$

The labels `i1,i2,i3` indicate input to the program, `o3` is output generated by `MACAULAY2`. We compute a Gröbner basis for the ideal $I_{\mathbf{f}}$ (see Section 3.2):

```
i4 : time If = kernel(f); -- Used 0.88 seconds

o4 : Ideal of R

i5 : gb If

o5 = | p1011-p1101 p0110-p1101 p0100-p1001 p0010-p1001
```

```
        p1101p1110-p1010p1111 p0111p1110-p1101p1111
        p0011p1110-p1001p1111 p1101^2-p0101p1110
        p1100p1101-p1001p1110 p0111p1101-p0101p1111
        p1100^2-p1000p1110 p1001p1100-p1000p1101
        p0111p1100-p1001p1111 p0101p1100-p1001p1101
        p0011p1100-p0001p1110 p0001p1100-p0000p1101
        p0111p1010-p0101p1110 p0011p1010-p1001p1101
        p1001^2-p0001p1010 p1000p1001-p0000p1010
        p0111p1001-p0011p1101 p0011p1001-p0001p1101
        p0111p1000-p0001p1110 p0101p1000-p0001p1010
        p0011p1000-p0000p1101 p0001p1000-p0000p1001
        p0000p0101-p0001p1001 p0011^2-p0001p0111
        p0101p1110^2-p1010p1101p1111 p1001p1110^2-p1010p1100p1111
        p0001p1110^2-p1000p1101p1111 p0000p1010p1100-p1000^2p1101
        p0000p0011p1101-p0001^2p1110 p0000p1110^2-p1000p1100p1111
        p0000p1100p1110-p1000^2p1111 p0000p0111^2-p0001p0011p1111
        p0000p0011p0111-p0001^2p1111 |
```

These are the constraints on probabilities listed at the end of Subsection 1.4.1.
Availability: Open source.
Website: `www.math.uiuc.edu/Macaulay2/`

MAGMA

Summary: A software package for computation with algebraic, geometric and combinatorial structures such as graphs, groups, rings and fields. Includes a new fast implementation of the Faugère F4 algorithm for computing Gröbner bases [Bosma *et al.*, 1997].
Example: We compute a Gröbner basis for the example in Section 3.1.

```
Q := RationalField();
P<p1,p2,p3> := PolynomialRing(Q, 3);
I := ideal<P | p1^4+p2^4-p3^4,p1^4+p2^4+p3^4-2*p1*p2*p3,p1+p2+p3-1>;
G := GroebnerBasis(I);
G;
[ p1 + p2 + p3 - 1,
  p2^4 - 2*p2^3 + 3*p2^2 - 2*p2*p3^4 + p2*p3^3 - p2*p3^2 + 2*p2*p3
  - 2*p2 - p3^5 + 4*p3^4 - 2*p3^3 + 3*p3^2 - 2*p3 + 1/2,
  p2^2*p3 + p2*p3^2 - p2*p3 + p3^4,
  p3^7 - 2*p3^6 + 4*p3^5 - 4*p3^4 + 3*p3^3 - 2*p3^2 + 1/2*p3 ]
```

Availability: Commercial software.
Website: `magma.maths.usyd.edu.au/magma/`

MAPLE

Summary:General purpose platform for symbolic and numerical computation
Example: `MAPLE` is an extremely versatile and powerful system, which includes many toolboxes and routines for standard symbolic and numerical computations. It is also an intuitive high-level interpreted language, which is convenient for quick computations. In Section 2.2, a specific example is provided showing how to compute sequence alignment polynomials using `MAPLE`.
Availability: Commercial software.
Website: `www.maplesoft.com/`

MATHEMATICA

Summary:General purpose platform for symbolic and numerical computation
Example: In Chapter 12 `MATHEMATICA` is used to plot the likelihood surface for various hidden Markov models.
Availability: Commercial software.
Website: `www.wolfram.com/products/mathematica/index.html`

MATLAB

Summary: A general purpose high level mathematics package, particularly suited towards numerical linear algebra computations. MATLAB is supported by numerous specialized toolboxes: the statistics toolbox and bioinformatics toolbox are useful for computational biology.
Example: The following example illustrates the use of the statistics toolbox for experimenting with hidden Markov models. The example shows how to set up a simple model with $l = 2$ and $l' = 4$, generate data from the model, and how to run basic inference routines.

```
S=[0.8 0.2; 0.1 0.9]

S = 0.8 0.2
    0.1 0.9

T=[0.25 0.25 0.25 0.25; 0.125 0.375 0.375 0.125]

T =

  0.250 0.250 0.250 0.250
  0.125 0.375 0.375 0.125
```

These commands set up the matrices θ and θ'. In other words, we have fixed a point on the model. The command `hmmgenerate` generates data from the model, and also specifies the alphabets Σ and Σ' to be used:

```
DNAseq=hmmgenerate(100,S,T,'Statenames',{'exon','intron'},
       'Symbols',{'A','C','G','T'})

DNAseq =

 Columns 1 through 14

 'G' 'C' 'C' 'C' 'G' 'A' 'C' 'G' 'T' 'C' 'T' 'A' 'C' 'C'

 ...
```

The probability of `DNAseq` given the model, i.e. the evaluation of the `DNAseq` coordinate polynomial, is done with

```
[PSTATES,logpseq]=hmmdecode[DNAseq,S,T,'Symbols',
                           {'A','C','G','T'}]
```

The matrix `PSTATES` returns the forward variables (see Chapter 12) . The logarithm of the probability of the sequence is also returned:

```
logpseq =

   -1.341061974974420e+02
```

The tropicalization of the coordinate polynomial is evaluated as follows:

```
STATES=hmmviterbi(DNAseq,S,T,'Statenames',{'exon','intron'},
                 'Symbols',{'A','C','G','T'}}

STATES =

 Columns 1 through 7

 'intron' 'intron' 'intron' 'intron' 'intron' 'intron' 'intron'

 ...

 Columns 99 through 100

 'exon' 'exon'
```

The `MATLAB` statistics toolbox also has an implementation of the EM algorithm for hidden Markov models, using the command `hmmtrain`.
Availability: Commercial software.
Website: `www.mathworks.com/`

POLYMAKE

Summary: A collection of programs for building, manipulating, analyzing and otherwise computing with polytopes and related polyhedral objects [Gawrilow and Joswig, 2000, Gawrilow and Joswig, 2001].
Example: Several computations with polytopes are shown in Section 2.3.
Availability: Open source.
Website: `www.math.tu-berlin.de/polymake/`

SINGULAR

Summary: A system for polynomial computations, commutative algebra, and computational algebraic geometry. Very useful for algebraic statistics.
Example: See Sections 2.1, 2.2 and 2.3 for various examples. For a reference on `SINGULAR` with many worked out examples see [Greuel and Pfister, 2002].
Availability: Free under the GNU (**G**NU's **N**ot **U**nix) Public License.
Website: `www.singular.uni-kl.de/`

R

Summary: A statistical computing language and environment, similar in syntax and focus to the `S` language [Ihaka and Gentleman, 1996]. Mathematicians find `R` comparable to `MATLAB`. The `BIOCONDUCTOR` package for R [Gentleman *et al.*, 2004] provides support for bioinformatics. related problems.
Example: The following R code was used to produce Figure 3.1:

```
# Hardy-Weinberg curve
p <- c(seq(0, 1, 0.001), seq(1, 100, 0.01))
z0 <- p^2/(1+p)^2
z1 <- 2*p/(1+p)^2
z2 <- 1/(1+p)^2
x.rec <- cbind((2*z0+z1)/sqrt(3), z1)

## plot the Hardy-Weinberg curve
plot(x.rec[,1], x.rec[,2], type='l', xlim=c(0, 2/sqrt(3)), ylim=c(0, 1), xlab='', ylab

# plot simplex
lines(x=c(0, 2/sqrt(3)), y=c(0, 0))
lines(x=c(0, 1/sqrt(3)), y=c(0, 1))
lines(x=c(1/sqrt(3), 2/sqrt(3)), y=c(1, 0))
```

Availability: Open source.
Website: `www.r-project.org/`

2.5.2 Computational Biology Software

The five software programs highlighted here were all used during the preparation of the book, and are mostly accessible through web servers.

BLAST

Summary: A tool for searching through large biological sequence databases for matches to a query [Altschul *et al.*, 1990].
Example: There are many different "flavors" of `BLAST`, which allow for querying databases of DNA or protein, automatic translation of the input sequence, and other similar modifications. In what follows we illustrate the use of the `BLASTN` tool. We begin by submitting the sequence

```
ATGGCGGAGTCTGTGGAGCGCCTGCAGCAGCGGGTCCAGGAGCTGGAGCGGGAACTT
```

taken from an example in Section 7.4, to the `BLASTN` website. There are a number of important variables that can be set for the search, for example: the low complexity filter removes repeated subsequences, such as `TTTT...TTT` from the search. The word size is the minimum size of an exact match necessary for `BLAST` to return a "hit". The `Expect` parameter sets the threshold at which to report "significant" hits. It is based on the Karlin-Altschul model used to calculate statistical significance [Karlin and Altschul, 1990]. The remaining choices during submission are which database to search against (the default is `nr` which consists of all non-redundant nucleotide sequences in `GENBANK`), and various options for formatting the output. We selected the default for all settings, with the exception of `Alignments` which was set to 100, i.e. we opted to receive up to 100 reported alignments rather than the default 50.

Upon submitting the query, `BLAST` takes a few seconds (or minutes), and returns a page with a graphic showing which parts of the submitted sequence matched sequences in the database, and a text part containing links to the database hits, as well as the alignments. In our example, the text output is

```
                                            Score   E
Sequences producing significant alignments: (bits) Value

Homo sapiens ubiquitin-activat...           113    3e-23
Homo sapiens ubiquitin-activat...           113    3e-23
Homo sapiens ThiFP1 mRNA,comple..           113    3e-23
Homo sapiens cDNA FLJ31676 fis,..           113    3e-23
Homo sapiens cDNA: FLJ23251 fis..           113    3e-23
Homo sapiens ubiquitin-activatin.           113    3e-23
Homo sapiens 3 BAC RP11-333H9(...           113    3e-23
full-length cDNA clone CS0DI066...          113    3e-23
```

```
Homosapiens Uba5 mRNA for Ubiq...          113    3e-23
Homo sapiens mRNA;cDN...                   113    3e-23
PREDICTED: Pan troglodytes sim...          105    8e-21
Pongo pygmaeus mRNA; cDNA DKFZp...         98     2e-18
Sus scrofa cloneClu_21888.scr.m...         72     1e-10
...  ...
```

The entries are preceded with a GENBANK identifier (and a link to the original sequence in the database). Below this are the actual alignments, for example:

```
gi|33942036|emb|AL928824.13|   Zebrafish DNA sequence from clone
                               CH211-105D18 in linkage group 6,
                               complete sequence
          Length = 189742

 Score = 38.2 bits (19), Expect = 1.6
 Identities = 19/19 (100%)
 Strand = Plus / Minus

Query: 37     caggagctggagcgggaac 55
              |||||||||||||||||||
Sbjct: 155640 caggagctggagcgggaac 155622
```

A handy reference on how to use BLAST is [Korf *et al.*, 2003]. There are many variants of BLAST that have been designed for specialized tasks, including BLASTZ [Schwartz *et al.*, 2003] for rapid local alignment or large genomic regions and BLAT [Kent, 2002] for fast mRNA/DNA alignments.
Availability: Open source.
Website: www.ncbi.nlm.nih.gov/blast/

MAVID

Summary: A multiple alignment program designed for large genomic sequences [Bray and Pachter, 2004].
Example: Sequences can be submitted in multi-fasta format through the website or the program can be downloaded for standalone use. A sequence in FASTA format begins with a single-line description, followed by lines of sequence data. The description line is distinguished from the sequence data by a greater-than (">") symbol in the first column. Sequences are expected to be represented in the standard IUB/IUPAC nucleic acid code, with these exceptions: lower-case letters are accepted and are mapped into upper-case; any characters other than A,C,G,T are converted into 'N' (unknown). The nucleic acid codes supported are:

```
  A --> Adenine
  C --> Cytosine
  G --> Guanine
  T --> Thymine
  N --> A G C T (any)
```

Multi-Fasta format consists of alternating description lines followed by sequence data. It is important that each ">" symbol appear on a new line. For example:

```
human
AGTGAGACACGACGAGCCTACTATCAGGACGAGAGCAGGAGAGTGATGATGAGTAGCG
CACAGCGACGATCATCACGAGAGAGTAAGAAGCAGTGATGATGTAGAGCGACGAGAGC
ACAGCGGCGACTACTACTAGG
mouse
AGTGTGTCTCGTCGTGCCTACTTTCAGGACGAGAGCAGGTGAGTGTTGATGAGTTGCG
CTCTGCGACGTTCATCTCGAGTGAGTTAGAAAGTGAAGGTATAACACAAGGTGTGAAG
GCAGTGATGATGTAGAGCGACGAGAGCACAGCGGCGGGATGATATATCTAGGAGGATG
CCCAATTTTTTTTT
platypus
CTCTGCGGCGTTCGTCTCGGGTGGGTTGGGGGGTGGGGGTGTGGCGCAAGGTGTGAAG
CACGACGACGATCTACGACGAGCGAGTGATGAGAGTGATGAGCGACGACGAGCACTAG
AAGCGACGACTACTATCGACGAGCAGCCGAGATGATGATGAAAGAGAGAGA
```

The `MAVID` program can align sequences much longer than the ones above (including alignments of sequences up to megabases long). Once the multi-FASTA file has been prepared it is uploaded to the website. Consider for example, 13 sequences from the Cystic Fibrosis gene region (CFTR): human chimp, baboon, cow, pig, cat, dog, mouse, rat, chicken, zebra fish, fugu fish and tetraodon fish. This region is one of the ENCODE regions (see Chapter 21). The result of the `MAVID` run, including the original sequences is too large to include here, but is stored on a website, in this case:
`baboon.math.berkeley.edu/mavid/examples/zoo.target1/`.

The website contains the alignment in multifasta format (`MAVID.mfa`), as well as in `PHYLIP` format (`MAVID.phy`). A phylogenetic tree inferred from the alignment using neighbor joining is also included:

The trees agrees well with the known phylogeny of the species, with the exception of the rodent placement, this issue is discussed in Section 21.4
Availability: Open source.
Website: `baboon.math.berkeley.edu/mavid/`

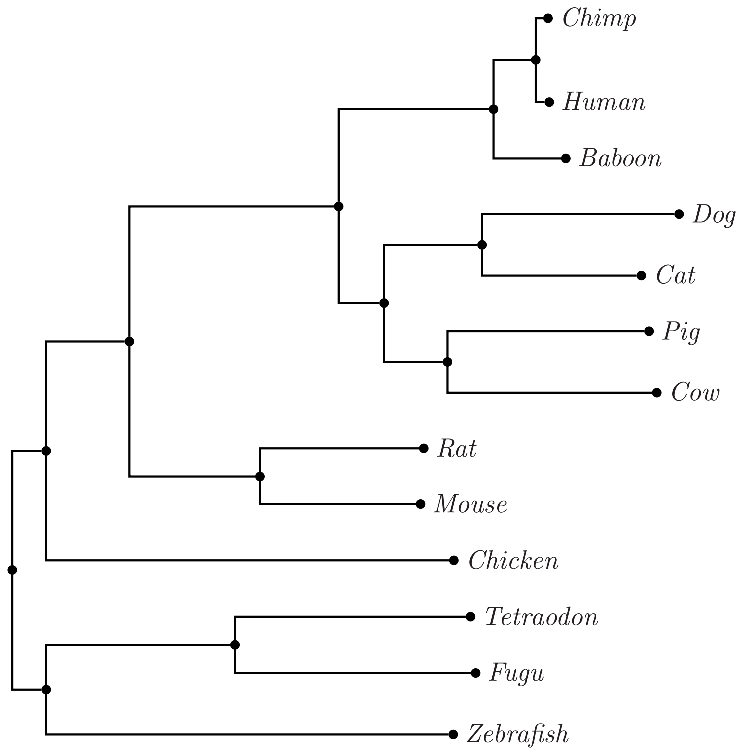

Fig. 2.7. Neighbor joining tree from `MAVID` alignment of the CFTR region (branch lengths omitted).

PAML

Summary: Software for **P**hylogenetic **A**nalysis by **M**aximum **L**ikelihood. Consists of a collection of programs for estimating rate matrices and branch lengths for different tree models.
Example: Chapter 21 contains examples showing how to use `PAML` with different model assumptions (e.g. Jukes-Cantor, HKY).
Availability: Open source.
Website: `abacus.gene.ucl.ac.uk/software/paml.html`

PHYLIP

Summary: A collection of programs for inferring phylogenies. This software has been continuously developed since 1981, and includes many routines utilities for manipulating and working with trees [Felsenstein, 2004].
Availability: Open source.
Example: `PHYLIP` reads alignments in a format which looks like this:

```
5 10
```

```
human   AAGTGA
mouse   CAA--A
rat     AGCA-G
dog     G-AGCT
chicken T-ACCA
```

The first number in the first row is the number of sequences, and the second number if the number of columns in the alignment. Any of a number of routines can then be called, for example `dnaml` which constructs a tree.
Website: `evolution.genetics.washington.edu/phylip.html`

SPLITSTREE

Summary: Implementation of the neighbor-net algorithm, as well as split decomposition, neighbor joining and other related methods. Includes a versatile visualization tool for splits graphs.
Availability: Open source.
Example: See Chapter 17.
Website: `www-ab.informatik.uni-tuebingen.de/software/jsplits/`

3
Algebra

Lior Pachter

Bernd Sturmfels

The philosophy of algebraic statistics is that *statistical models are algebraic varieties*. We encountered many such models in Chapter 1. The purpose of this chapter is to give an elementary introduction to the relevant algebraic concepts, with examples drawn from statistics and computational biology.

Algebraic varieties are zero sets of systems of polynomial equations in several unknowns. These geometric objects appear in many contexts. For example, in genetics, the familiar *Hardy-Weinberg curve* is an algebraic variety (see Figure 3.1). In statistics, the distributions corresponding to independent random variables form algebraic varieties, called *Segre varieties*, that are well known to mathematicians. There are many questions one can ask about a system of polynomial equations, for example whether the solution set is empty, nonempty but finite, or infinite. Gröbner bases are used to answer these questions.

Algebraic varieties can be described in two different ways, either by equations or parametrically. Each of these representations is useful. We encountered this dichotomy in the *Hammersley-Clifford Theorem* which says that a graphical model can be described by conditional independence statements or by a polynomial parameterization. Clearly, efficient methods for switching between these two representations are desirable. We discuss such methods in Section 3.2.

The study of systems of polynomial equations is the main focus of a central area in mathematics called *algebraic geometry*. This is a rich, beautiful, and well-developed subject, at whose heart lies a deep connection between algebra and geometry. In algebraic geometry, it is customary to study varieties over the field $\mathbb{C}$ of complex numbers even if the given polynomials have their coefficients in a subfield of $\mathbb{C}$ such as the real numbers $\mathbb{R}$ or the rational numbers $\mathbb{Q}$. This perspective leads to an algebraic approach to maximum likelihood estimation which may be unfamiliar to statisticians and is explained in Section 3.3.

Algebraic geometry makes sense also over the tropical semiring $(\mathbb{R}, \oplus, \odot)$. In that setting, algebraic varieties are piecewise-linear spaces. An important example for biology is the *space of trees* which will be discussed in Section 3.5.

3.1 Varieties and Gröbner bases

We write $\mathbb{Q}[p] = \mathbb{Q}[p_1, p_2, \ldots, p_m]$ for the set of all polynomials in m unknowns $p_1, p_2, \ldots, p_m$ with coefficients in the field $\mathbb{Q}$ of rational numbers. The set $\mathbb{Q}[p]$ has the structure of a $\mathbb{Q}$-vector space and also that of a ring. We call $\mathbb{Q}[p]$ the *polynomial ring*. A distinguished $\mathbb{Q}$-linear basis of $\mathbb{Q}[p]$ is the set of *monomials*

$$\{\, p_1^{i_1} p_2^{i_2} \cdots p_m^{i_m} \quad : \quad i_1, i_2, \ldots, i_m \in \mathbb{N} \,\}. \tag{3.1}$$

To write down polynomials in a systematic way, we need to order the monomials. A *monomial order* is a total order $\prec$ on the set (3.1) which satisfies:

- the monomial $1 = p_1^0 p_2^0 \cdots p_m^0$ is smaller than all other monomials, and
- if $p_1^{i_1} \cdots p_m^{i_m} \prec p_1^{j_1} \cdots p_m^{j_m}$ then $p_1^{i_1+k_1} \cdots p_m^{i_m+k_m} \prec p_1^{j_1+k_1} \cdots p_m^{j_m+k_m}$.

For polynomials in one unknown ($m = 1$) there is only one monomial order,

$$1 \prec p_1 \prec p_1^2 \prec p_1^3 \prec p_1^4 \prec \cdots,$$

but in several unknowns ($m \geq 2$) there are infinitely many monomial orders. One example is the *lexicographic monomial order* $\prec_{\text{lex}}$ which is defined as follows: $p_1^{i_1} \cdots p_m^{i_m} \prec_{\text{lex}} p_1^{j_1} \cdots p_m^{j_m}$ if the leftmost non-zero entry in the vector $(j_1 - i_1, j_2 - i_2, \ldots, j_m - i_m)$ is positive. In this section, all polynomials are written with their monomials in decreasing $\prec_{\text{lex}}$ order. The first monomial, or *initial monomial*, is often underlined: it is the $\prec_{\text{lex}}$ largest monomial appearing with non-zero coefficients in that polynomial. Here are three examples of polynomials in $\mathbb{Q}[p_1, p_2, p_3]$, each with its terms sorted in lexicographic order:

$$\begin{aligned}
f_1 &= \underline{p_1 p_3} - 4p_2^2 \\
f_2 &= \underline{p_1^2} - 2p_1 + p_2^2 - 4p_2 - p_3^2 + 6p_3 - 8 \\
f_3 &= \underline{p_1 p_2^2} + p_1 p_3^3 + p_1 + p_2^3 + p_2^2 + p_2 p_3^3 + p_2 + p_3^3 + 1
\end{aligned}$$

What we are interested in is the geometry of these polynomials. The zero set of each of them is a surface in three-dimensional space $\mathbb{R}^3$. For instance, $\{f_2 = 0\}$ is the sphere of radius 4 around the point with coordinates $(1, 2, 3)$, and $\{f_3 = 0\}$ is the union of a plane with a parabolic surface. The surface $\{f_1 = 0\}$ is a quadratic cone: its intersection with the probability triangle is known as the *Hardy-Weinberg curve* in statistical genetics (Figure 3.1).

In our applications, the unknown p_i represents the probability of the i-th event among m possible ones. But for now think of p_i just as a formal symbol.

Every polynomial $f \in \mathbb{Q}[p_1, \ldots, p_m]$ in m unknowns defines a *hypersurface*

$$V(f) \quad = \quad \{\, (z_1, \ldots, z_m) \in \mathbb{C}^m \,:\, f(z_1, \ldots, z_m) = 0 \,\}.$$

Note that $V(f)$ is defined over the complex numbers $\mathbb{C}$. If S is any subset of $\mathbb{C}^m$ then we write $V_S(f) := V(f) \cap S$ for the part of the hypersurface that

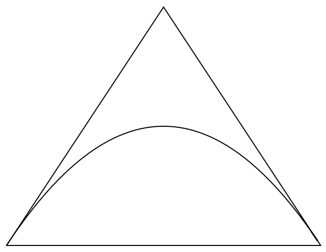

Fig. 3.1. The Hardy Weinberg curve

lies in S. For instance, $V_{\mathbb{R}^m}(f)$ is the set of solutions to $f = 0$ over the real numbers, and $V_\Delta(f)$ is the set of solutions to $f = 0$ in the probability simplex

$$\Delta \quad = \quad \Big\{ (z_1, \ldots, z_m) \in \mathbb{R}^m \, : \, \sum_{i=1}^{m} z_i = 1 \text{ and } z_1, z_2, \ldots, z_m \geq 0 \Big\}.$$

A polynomial is *homogeneous* if all of its monomials $p_1^{i_1} p_2^{i_2} \cdots p_m^{i_m}$ have the same *total degree* $i_1 + i_2 + \cdots + i_m$. The following three polynomials in $\mathbb{Q}[p_1, p_2, p_3]$ have total degree four. The first two are homogeneous but the third is not:

$$\begin{aligned} g_1 \quad &= \quad p_1^4 + p_2^4 - p_3^4 \\ g_2 \quad &= \quad p_1^4 + p_2^4 + p_3^4 \\ g_3 \quad &= \quad p_1^4 + p_2^4 + p_3^4 - 2p_1p_2p_3 \end{aligned}$$

All three of $V(g_1), V(g_2)$ and $V(g_3)$ are complex surfaces in $\mathbb{C}^3$, and $V_{\mathbb{R}^3}(g_1)$ and $V_{\mathbb{R}^3}(g_3)$ are real surfaces in $\mathbb{R}^3$, but $V_{\mathbb{R}^3}(g_2)$ is just the point $(0, 0, 0)$. (Note that $V_{\mathbb{N}^3}(g_1) = \{(0, 0, 0)\}$ by Fermat's Last Theorem). Restricting to the probability triangle Δ, we see that $V_\Delta(g_2) = \emptyset$, while $V_\Delta(g_1)$ and $V_\Delta(g_3)$ are curves in the triangle Δ.

To understand why algebraic geometers prefer to work over the complex numbers $\mathbb{C}$ rather than over the real numbers $\mathbb{R}$, let us consider polynomials in one unknown p. For $a_0, a_1, \ldots, a_s \in \mathbb{Q}$ with $a_s \neq 0$ consider

$$f(p) \quad = \quad a_s \cdot p^s + a_{s-1} \cdot p^{s-1} + \cdots + a_2 \cdot p^2 + a_1 \cdot p + a_0.$$

Recall that the following basic result holds over the complex numbers:

Theorem 3.1 (Fundamental Theorem of Algebra) *If f is a polynomial of degree s then $V(f)$ consists of s complex numbers, counting multiplicities.*

By contrast, the number of real roots of $f(p)$, i.e. the cardinality of $V_{\mathbb{R}}(f)$, does depend on the particular coefficients a_i. It can range anywhere between 0 and s, and the dependence is very complicated. So, the reason we use $\mathbb{C}$ is quite simple: *It is easier to do algebraic geometry over the complex numbers $\mathbb{C}$*

than over the real numbers $\mathbb{R}$. In algebraic statistics, we postpone issues of real numbers and inequalities as long as we can get away with it. But of course, at the end of the day, we are dealing with parameters and probabilities, and those are real numbers which are constrained by inequalities.

Let $\mathcal{F}$ be an arbitrary subset of the polynomial ring $\mathbb{Q}[p_1, \ldots, p_m]$. We define its *variety* $V(\mathcal{F})$ as the intersection of the hypersurfaces $V(f)$ where f ranges over $\mathcal{F}$. Similarly, $V_S(\mathcal{F}) = \cap_{f \in \mathcal{F}} V_S(f)$ for any subset $S \subset \mathbb{C}^m$. Using the example above, the variety $V(\{g_1, g_3\})$ is a curve in three-dimensional space $\mathbb{C}^3$. That curve meets the probability triangle Δ in precisely two points:

$$V_\Delta(\{g_1, g_3\}) = \{(0.41167, 0.17346, 0.41487), (0.17346, 0.41167, 0.41487)\} \quad (3.2)$$

These two points are found by first computing the variety $V\big(\{\, g_1,\, g_3,\, p_1 + p_2 + p_3 - 1\,\}\big)$. We did this by running the following sequence of six commands in the computer algebra package `Singular`. See Section 2.5 for software references.

```
ring R = 0, (p1,p2,p3), lp;
ideal I = (p1^4+p2^4-p3^4,p1^4+p2^4+p3^4-2*p1*p2*p3,p1+p2+p3-1);
ideal G = groebner(I); G; LIB ‘‘solve.lib’’; solve(G,10);
```

For an explanation of these commands, and a discussion of how to solve polynomial systems in general, see Section 2.5 of [Sturmfels, 2002]. Running this `Singular` code shows that $V\big(\{\, g_1,\, g_3,\, p_1 + p_2 + p_3 - 1\,\}\big)$ consists of 16 distinct points (which is consistent with *Bézout's Theorem* [Cox *et al.*, 1997]). Only two of the 16 points have all their coordinates real. They lie in the triangle Δ.

Algebraists feel notoriously uneasy about floating point numbers. For a specific numerical example consider the common third coordinate of the two points in $V_\Delta(\{g_1, g_3\})$. When an algebraist sees the floating point number

$$\widehat{p}_3 \;=\; 0.4148730882..., \quad (3.3)$$

(s)he will want to know whether $\widehat{p}_3$ can be expressed in terms of radicals.

Indeed, the floating point coordinates produced by the algorithms in this book are usually *algebraic numbers*. An algebraic number has a *degree* which is the degree of its minimal polynomial over $\mathbb{Q}$. For instance, our floating point number $\widehat{p}_3$ is an algebraic number of degree six. Its minimal polynomial equals

$$f(p_3) \quad = \quad 2 \cdot p_3^6 \,-\, 4 \cdot p_3^5 \,+\, 8 \cdot p_3^4 \,-\, 8 \cdot p_3^3 \,+\, 6 \cdot p_3^2 \,-\, 4 \cdot p_3 \,+\, 1.$$

This polynomial appears in the output of the command line `G;` in our `Singular` program. Most algebraists would probably prefer the following description (3.4) of our number over the description given earlier in (3.3):

$$\widehat{p}_3 \;=\; \text{the smaller of the two real roots of the polynomial } f(p_3). \quad (3.4)$$

The other real root is 0.7845389895 but this does not appear in $V_\Delta(\{g_1, g_3\})$. Our number $\widehat{p}_3$ cannot be written in terms of radicals over $\mathbb{Q}$. This is because the *Galois group* of the polynomial $f(p_3)$ is the symmetric group on six letters, which is not a solvable group. To see this, run the following in `Maple`:

```
galois( 2*p3^6-4*p3^5+8*p3^4-8*p3^3+6*p3^2-4*p3+1, p3);
```

In summary, algorithms used in algebraic statistics produce floating numbers, and these numbers are often algebraic numbers, which means they have a well-defined *algebraic degree over* $\mathbb{Q}$. In algebraic statistics, we are sensitive to this intrinsic measure of complexity of the real numbers we are dealing with.

The command `ideal G = groebner(I);` in our `Singular` code computes the lexicographic *Gröbner basis* for the *ideal* generated by the three given polynomials. In what follows, we give a very brief introduction to these notions. For further details, the reader is referred to any of the numerous textbooks on computational algebraic geometry which have appeared in the last decade.

Let $\mathcal{F} \subset \mathbb{Q}[p] = \mathbb{Q}[p_1, \ldots, p_m]$. The *ideal generated* by $\mathcal{F}$ is the set $\langle \mathcal{F} \rangle$ consisting of all polynomial linear combinations of the elements in $\mathcal{F}$. In symbols,

$$\langle \mathcal{F} \rangle \quad = \quad \big\{\, h_1 f_1 + \cdots + h_r f_r \; : \; f_1, \ldots, f_r \in \mathcal{F} \text{ and } h_1, \ldots, h_r \in \mathbb{Q}[p] \,\big\}.$$

An ideal I in $\mathbb{Q}[p]$ is any set of the form $I = \langle \mathcal{F} \rangle$. It is quite possible for two different subsets $\mathcal{F}$ and $\mathcal{F}'$ of $\mathbb{Q}[p]$ to generate the same ideal I, i.e.,

$$\langle\, \mathcal{F} \,\rangle \quad = \quad \langle\, \mathcal{F}' \,\rangle.$$

This equation means that every polynomial in $\mathcal{F}$ is a $\mathbb{Q}[p]$-linear combination of elements in $\mathcal{F}'$, and vice versa. If this holds then the two varieties coincide:

$$V(\mathcal{F}) \quad = \quad V(\mathcal{F}').$$

Hilbert's basis theorem implies that every variety is the intersection of finitely many hypersurfaces:

Theorem 3.2 (Hilbert's basis theorem) *Every infinite set $\mathcal{F}$ of polynomials in $\mathbb{Q}[p]$ has a finite subset $\mathcal{F}' \subset \mathcal{F}$ such that $\langle\, \mathcal{F} \,\rangle = \langle\, \mathcal{F}' \,\rangle$.*

The theorem is often stated in the following form:

Every ideal in a polynomial ring is finitely generated.

Let us now fix a term order $\prec$. Every polynomial $f \in \mathbb{Q}[p]$ has a unique *initial monomial* denoted $\mathrm{in}_\prec(f)$. The initial monomial of f is the $\prec$-largest monomial $p^a = p_1^{a_1} p_2^{a_2} \cdots p_m^{a_m}$ which appears with non-zero coefficient in the expansion of f. Let I be an ideal in $\mathbb{Q}[p]$. Then its *initial ideal* $\mathrm{in}_\prec(I)$ is the ideal generated by the initial monomials of all the polynomials in I:

$$\mathrm{in}_\prec(I) \quad := \quad \langle\, \mathrm{in}_\prec(f) \; : \; f \in I \,\rangle.$$

A finite subset $\mathcal{G}$ of an ideal I is a *Gröbner basis* with respect to the monomial order $\prec$ if the initial monomials of elements in $\mathcal{G}$ generate the initial ideal:

$$\text{in}_\prec(I) \quad = \quad \langle\, \text{in}_\prec(g) \,:\, g \in \mathcal{G} \,\rangle. \tag{3.5}$$

As we have defined it in (3.5), there is no minimality requirement for being a Gröbner basis. If $\mathcal{G}$ is a Gröbner basis for I then we can augment $\mathcal{G}$ by any additional elements from I and the resulting set is still a Gröbner basis. To remedy this non-minimality, we make one more definition. We say that $\mathcal{G}$ is a *reduced Gröbner basis* if the following three additional conditions hold:

(i) For each $g \in \mathcal{G}$, the coefficient of $\text{in}_\prec(g)$ in g is 1.
(ii) The set $\{\, \text{in}_\prec(g) \,:\, g \in \mathcal{G} \,\}$ minimally generates $\text{in}_\prec(I)$.
(iii) No trailing term of any $g \in \mathcal{G}$ lies in $\text{in}_\prec(I)$.

For a fixed term order $\prec$, every ideal I in $\mathbb{Q}[p_1, \ldots, p_m]$ has a unique reduced Gröbner basis $\mathcal{G}$. This reduced Gröbner basis is finite, and it can be computed from an arbitrary generating set $\mathcal{F}$ of I by the so-called *Buchberger algorithm*. Any Gröbner basis generates the ideal for which it is a Gröbner basis, so in particular, the reduced Gröbner basis satisfies $\langle \mathcal{G} \rangle = \langle \mathcal{F} \rangle = I$.

We will discuss the Buchberger algorithm towards the end of this section. First, we concentrate on some applications to the study of algebraic varieties. Recall that varieties are the solution sets of polynomial equations in several unknowns. Here we take polynomials with rational coefficients, and we consider a finite set of them $\mathcal{F} \subset \mathbb{Q}[p_1, \ldots, p_m]$. The *variety* of $\mathcal{F}$ is the set of all common zeros of $\mathcal{F}$ over the field of complex numbers. As above it is denoted

$$\mathcal{V}(\mathcal{F}) \quad = \quad \big\{\, (z_1, \ldots, z_m) \in \mathbb{C}^m \,:\, f(z_1, \ldots, z_m) = 0 \ \text{ for all } f \in \mathcal{F} \,\big\}.$$

The variety does not change if we replace $\mathcal{F}$ by another set of polynomials that generates the same ideal in $\mathbb{Q}[p_1, \ldots, p_m]$. In particular, the reduced Gröbner basis $\mathcal{G}$ for the ideal $\langle \mathcal{F} \rangle$ specifies the same variety:

$$\mathcal{V}(\mathcal{F}) \ = \ \mathcal{V}(\langle \mathcal{F} \rangle) \ = \ \mathcal{V}(\langle \mathcal{G} \rangle) \ = \ \mathcal{V}(\mathcal{G}).$$

The advantage of $\mathcal{G}$ is that it reveals geometric properties of the variety which are not visible from the given polynomials $\mathcal{F}$. A most basic question which one might ask about the variety $V(\mathcal{F})$ is whether it is non-empty: does the given system of equations $\mathcal{F}$ have any solution over the complex numbers?

Theorem 3.3 (Hilbert's Nullstellensatz) *The variety $V(\mathcal{F})$ is empty if and only if the reduced Gröbner basis $\mathcal{G}$ of the ideal $\langle \mathcal{F} \rangle$ equals $\{1\}$.*

Example 3.4 Consider a set of three polynomials in two unknowns:

$$\mathcal{F} \quad = \quad \{\, \theta_1^2 + \theta_1\theta_2 - 10,\ \theta_1^3 + \theta_1\theta_2^2 - 25,\ \theta_1^4 + \theta_1\theta_2^3 - 70 \,\}.$$

Running the Buchberger algorithm on the input $\mathcal{F}$, we find that $\mathcal{G} = \{1\}$, so the three given polynomials have no common zero (θ_1, θ_2) in $\mathbb{C}^2$. We now change the constant term of the middle polynomial as follows:

$$\mathcal{F} \quad = \quad \{\, \theta_1^2 + \theta_1\theta_2 - 10,\ \theta_1^3 + \theta_1\theta_2^2 - \underline{26},\ \theta_1^4 + \theta_1\theta_2^3 - 70 \,\}.$$

The reduced Gröbner basis of $\langle \mathcal{F} \rangle$ is $\mathcal{G} = \{\, \theta_1 - 2,\ \theta_2 - 3 \,\}$. This shows that the variety of $\mathcal{F}$ consists of a single point in $\mathbb{C}^2$, namely, $\mathcal{V}(\mathcal{F}) \,=\, \mathcal{V}(\mathcal{G}) \,=\, \{\, (2,3) \,\}$.

Our next question is *how many zeros* does a given system of equations have ? To answer this we need one more definition. Given a fixed ideal I in $\mathbb{Q}[p_1, \ldots, p_m]$ and a fixed term order $\prec$, a monomial $p^a = p_1^{a_1} \cdots p_m^{a_m}$ is called *standard* if it is not in the initial ideal $\mathrm{in}_\prec(I)$. The number of standard monomials is finite if and only if every unknown p_i appears to some power among the generators of the initial ideal. For example, if $\mathrm{in}_\prec(I) = \langle\, p_1^3, p_2^4, p_3^5 \,\rangle$ then there are 60 standard monomials, but if $\mathrm{in}_\prec(I) = \langle\, p_1^3, p_2^4, p_1 p_3^4 \,\rangle$ then the set of standard monomials is infinite (because every power of p_3 is standard).

Theorem 3.5 *The variety $\mathcal{V}(I)$ is finite if and only if the set of standard monomials is finite. In this case, the number of standard monomials equals the cardinality of $\mathcal{V}(I)$, when zeros are counted with multiplicity.*

In the case of one unknown p, this result is the Fundamental Theorem of Algebra (Theorem 3.1), which states that the variety $\mathcal{V}(f)$ of a polynomial $f \in \mathbb{Q}[p]$ of degree s consists of s complex numbers. Indeed, in this case $\{f\}$ is a Gröbner basis for its ideal $I = \langle f \rangle$, we have $\mathrm{in}_\prec(I) = \langle p^s \rangle$, and there are precisely s standard monomials: $1, p, p^2, \ldots, p^{s-1}$. Thus we can regard Theorem 3.5 as the *Multidimensional Fundamental Theorem of Algebra*.

Example 3.6 Consider the system of three polynomials in three unknowns

$$\mathcal{F} \quad = \quad \{\, p_1^4 + p_2^4 - p_3^4\,,\ p_1^4 + p_2^4 + p_3^4 - 2p_1p_2p_3\,,\ p_1 + p_2 + p_3 - 1 \,\}$$

Its Gröbner basis for the purely lexicographic order $p_1 > p_2 > p_3$ equals

$$\mathcal{G} \ = \ \{\, \underline{p_1} + p_2 + p_3 - 1\,,\ \underline{p_2^2 p_3} + p_2 p_3^2 - p_2 p_3 + p_3^4,\ \underline{2p_3^7} - 4p_3^6 + 8p_3^5 + \cdots, \\ \underline{2p_2^4} + 4p_2^3 p_3 - 4p_2^3 + 6p_2^2 p_3^2 - 10p_2^2 p_3 + 6p_2^2 + 4p_2 p_3^3 - 10 p_2 p_3^2 + \cdots \,\}.$$

The underlined initial monomials show that there are 16 standard monomials:

$$1,\ p_2,\ p_2^2,\ p_2^3,\ p_3,\ p_3^2,\ p_3^3,\ p_3^4,\ p_3^5,\ p_3^6,\ p_2p_3,\ p_2p_3^2,\ p_2p_3^3,\ p_2p_3^4,\ p_2p_3^5,\ p_2p_3^6.$$

Theorem 3.5 says $V(\mathcal{F})$ consists of 16 points. Two of them appear in (3.2).

Our criterion in Theorem 3.5 for deciding whether a variety is finite generalizes to the following formula for the dimension of a variety. A subset S of the set of unknowns $\{p_1, p_2, \ldots, p_m\}$ is a *standard set* if every monomial $\prod_{p_j \in S} p_j^{a_j}$ in those unknowns is standard. Equivalently, $\text{in}_\prec(I) \cap \mathbb{C}[\, p_j \,:\, j \in S\,] = \{0\}$.

Theorem 3.7 (Dimension Formula) *The dimension of an algebraic variety $\mathcal{V}(I) \subset \mathbb{C}^m$ is the maximal cardinality of any standard set for the ideal I.*

For a proof of this combinatorial dimension formula, and many other basic results on Gröbner basis, we refer to [Cox *et al.*, 1997].

Example 3.8 Let $I \subset \mathbb{Q}[p_1, p_2, p_3]$ be the ideal generated by the Hardy-Weinberg polynomial $f_1 = \underline{p_1 p_3} - 4p_2^2$. The maximal standard sets for I in the lexicographic monomial order are $\{p_1, p_2\}$ and $\{p_2, p_3\}$. Both have cardinality two. Hence the variety $V(f_1)$ has dimension two: it is a surface in $\mathbb{C}^3$.

Another basic result states that the set of standard monomials is a $\mathbb{Q}$-vector space basis for the *residue ring* $\mathbb{Q}[p_1, \ldots, p_m]/I$. The image of any polynomial h in this residue ring can be expressed uniquely as a $\mathbb{Q}$-linear combination of standard monomials. This expression is the *normal form* of h modulo the Gröbner basis $\mathcal{G}$. The process of computing the normal form is the *division algorithm.* In the case of one unknown p, where $I = \langle f \rangle$ and f has degree s, the division algorithm writes any polynomial $h \in \mathbb{Q}[p]$ as a unique $\mathbb{Q}$-linear combination of the standard monomials $1, p, p^2, \ldots, p^{s-1}$. The division algorithm works relative to a Gröbner basis in any number m of unknowns.

Example 3.9 Let $\mathbb{Q}[p]$ be the polynomial ring in 16 unknowns, denoted

$$p \quad = \quad \begin{pmatrix} p_{\mathtt{AA}} & p_{\mathtt{AC}} & p_{\mathtt{AG}} & p_{\mathtt{AT}} \\ p_{\mathtt{CA}} & p_{\mathtt{CC}} & p_{\mathtt{CG}} & p_{\mathtt{CT}} \\ p_{\mathtt{GA}} & p_{\mathtt{GC}} & p_{\mathtt{GG}} & p_{\mathtt{GT}} \\ p_{\mathtt{TA}} & p_{\mathtt{TC}} & p_{\mathtt{TG}} & p_{\mathtt{TT}} \end{pmatrix}$$

DiaNA's model in Example 1.16 for generating two DNA sequences is

$$p_{ij} \;=\; \pi \cdot \lambda_i^1 \cdot \lambda_j^2 \;+\; (1-\pi) \cdot \rho_i^1 \cdot \rho_j^2 \qquad \text{where} \;\; i, j \in \{\mathtt{A}, \mathtt{C}, \mathtt{G}, \mathtt{T}\}. \tag{3.6}$$

Since *"statistical models are algebraic varieties"*, this model can be represented as a variety $V(I)$ in $\mathbb{C}^{4\times 4}$. The homogeneous ideal $I \subset \mathbb{Q}[p]$ corresponding to the model (3.6) is generated by the sixteen 3×3-minors of the 4×4-matrix p. These sixteen determinants form a reduced Gröbner basis for I:

$$\begin{aligned} \mathcal{G} = \big\{ \, & \underline{p_{\mathtt{AA}}p_{\mathtt{CC}}p_{\mathtt{GG}}} - p_{\mathtt{AA}}p_{\mathtt{CG}}p_{\mathtt{GC}} - p_{\mathtt{AC}}p_{\mathtt{CA}}p_{\mathtt{GG}} + p_{\mathtt{AC}}p_{\mathtt{CG}}p_{\mathtt{GA}} + p_{\mathtt{AG}}p_{\mathtt{CA}}p_{\mathtt{GC}} - p_{\mathtt{AG}}p_{\mathtt{CC}}p_{\mathtt{GA}}, \\ & \underline{p_{\mathtt{AA}}p_{\mathtt{CC}}p_{\mathtt{GT}}} - p_{\mathtt{AA}}p_{\mathtt{CT}}p_{\mathtt{GC}} - p_{\mathtt{AC}}p_{\mathtt{CA}}p_{\mathtt{GT}} + p_{\mathtt{AC}}p_{\mathtt{CT}}p_{\mathtt{GA}} + p_{\mathtt{AT}}p_{\mathtt{CA}}p_{\mathtt{GC}} - p_{\mathtt{AT}}p_{\mathtt{CC}}p_{\mathtt{GA}}, \\ & \qquad\qquad \cdots\cdots\cdots \qquad \cdots\cdots\cdots \qquad \cdots\cdots\cdots \\ & \underline{p_{\mathtt{CC}}p_{\mathtt{GG}}p_{\mathtt{TT}}} - p_{\mathtt{CC}}p_{\mathtt{GT}}p_{\mathtt{TG}} - p_{\mathtt{CG}}p_{\mathtt{GC}}p_{\mathtt{TT}} + p_{\mathtt{CG}}p_{\mathtt{GT}}p_{\mathtt{TC}} + p_{\mathtt{CT}}p_{\mathtt{GC}}p_{\mathtt{TG}} - p_{\mathtt{CT}}p_{\mathtt{GG}}p_{\mathtt{TC}} \big\}. \end{aligned}$$

Indeed, it is known [Sturmfels, 1990] that, for any $a, b, c \in \mathbb{N}$, the $a \times a$-minors of a $b \times c$-matrix of unknowns form a reduced Gröbner basis with respect to a term order that makes the main diagonal terms of any determinant highest. We are looking at the case $a = 3, b = c = 4$. The variety $V(\mathcal{G}) = V(I)$ consists of all complex 4×4-matrices of rank ≤ 2. We can compute the dimension of this variety using Theorem 3.7. There are twenty maximal standard sets for I. They all have cardinality 12. One such standard set is

$$S \quad = \quad \big\{\, p_{\mathtt{AA}}, p_{\mathtt{AC}}, p_{\mathtt{AG}}, p_{\mathtt{AT}}\,,\; p_{\mathtt{CA}}, p_{\mathtt{CC}}, p_{\mathtt{CG}}, p_{\mathtt{CT}}\,,\; p_{\mathtt{GA}}, p_{\mathtt{GC}}\,,\; p_{\mathtt{TA}}, p_{\mathtt{TC}} \,\big\}.$$

Indeed, none of the monomials in these twelve unknowns lie in the initial ideal

$$\mathrm{in}_{\prec}(I) \quad = \quad \big\langle\, p_{\mathtt{AA}}p_{\mathtt{CC}}p_{\mathtt{GG}}\,,\; p_{\mathtt{AA}}p_{\mathtt{CC}}p_{\mathtt{GT}}\,,\; p_{\mathtt{AA}}p_{\mathtt{CG}}p_{\mathtt{GT}}\,,\; \ldots,\; p_{\mathtt{CC}}p_{\mathtt{GG}}p_{\mathtt{TT}} \,\big\rangle.$$

Theorem 3.7 implies that the variety $V(I)$ has dimension $|S| = 12$, and its intersection with the probability simplex, $V_\Delta(I)$, has dimension 11.

To illustrate the division algorithm, we consider the non-standard monomial

$$h \quad = \quad p_{\mathtt{AA}} \cdot p_{\mathtt{CC}} \cdot p_{\mathtt{GG}} \cdot p_{\mathtt{TT}}$$

The normal form of h modulo $\mathcal{G}$ is the following sum of 12 standard monomials:

$$\begin{aligned}\mathrm{nf}_{\mathcal{G}}(h) \quad = \quad & p_{\mathtt{AA}}p_{\mathtt{CT}}p_{\mathtt{GG}}p_{\mathtt{TC}} + p_{\mathtt{AC}}p_{\mathtt{CA}}p_{\mathtt{GT}}p_{\mathtt{TG}} - p_{\mathtt{AC}}p_{\mathtt{CT}}p_{\mathtt{GG}}p_{\mathtt{TA}} + p_{\mathtt{AG}}p_{\mathtt{CC}}p_{\mathtt{GA}}p_{\mathtt{TT}} \\ & - p_{\mathtt{AG}}p_{\mathtt{CC}}p_{\mathtt{GT}}p_{\mathtt{TA}} - p_{\mathtt{AG}}p_{\mathtt{CT}}p_{\mathtt{GA}}p_{\mathtt{TC}} + p_{\mathtt{AG}}p_{\mathtt{CT}}p_{\mathtt{GC}}p_{\mathtt{TA}} - p_{\mathtt{AT}}p_{\mathtt{CA}}p_{\mathtt{GG}}p_{\mathtt{TC}} \\ & - p_{\mathtt{AT}}p_{\mathtt{CC}}p_{\mathtt{GA}}p_{\mathtt{TG}} + p_{\mathtt{AT}}p_{\mathtt{CG}}p_{\mathtt{GA}}p_{\mathtt{TC}} - p_{\mathtt{AT}}p_{\mathtt{CG}}p_{\mathtt{GC}}p_{\mathtt{TA}} + 2 \cdot p_{\mathtt{AT}}p_{\mathtt{CC}}p_{\mathtt{GG}}p_{\mathtt{TA}}\end{aligned}$$

We have $h \equiv \mathrm{nf}_{\mathcal{G}}(h)$ for all probability distributions as in (3.6).

Our assertion in Example 3.9 that the 3×3-minors form a Gröbner basis raises the following question. Given a fixed term order $\prec$, how can one test whether a given set of polynomials $\mathcal{G}$ is a Gröbner basis or not? The answer is given by the following criterion [Buchberger, 1965]. Consider any two polynomials g and g' in $\mathcal{G}$ and form their *S-polynomial* $m'g - mg'$. Here m and m' are monomials of smallest possible degree such that $m' \cdot \mathrm{in}_{\prec}(g) = m \cdot \mathrm{in}_{\prec}(g')$. The S-polynomial $m'g - mg'$ lies in the ideal $\langle \mathcal{G} \rangle$. We apply the division algorithm modulo the tentative Gröbner basis $\mathcal{G}$ to the input $m'g - mg'$. The resulting normal form $\mathrm{nf}_{\mathcal{G}}(m'g - mg')$ is a $\mathbb{Q}$-linear combination of monomials none of which is divisible by an initial monomial from $\mathcal{G}$. A necessary condition for $\mathcal{G}$ to be a Gröbner basis is that this result be zero:

$$\mathrm{nf}_{\mathcal{G}}(m'g - mg') \quad = \quad 0 \qquad \text{for all } g, g' \in \mathcal{G}. \tag{3.7}$$

Theorem 3.10 (Buchberger's Criterion) *A finite set of polynomials $\mathcal{G} \subset \mathbb{Q}[p_1, \ldots, p_m]$ is a Gröbner basis for its ideal $\langle \mathcal{G} \rangle$ if and only if (3.7) holds, that is, if and only if all S-polynomials have normal form zero.*

So, to check that the set $\mathcal{G}$ of the sixteen 3×3-determinants in Example 3.9 is indeed a Gröbner basis, it suffices to compute the normal forms of all $\binom{16}{2}$ pairwise S-polynomials, such as

$$\begin{aligned} & p_{\texttt{TG}} \cdot (\underline{p_{\texttt{AA}} p_{\texttt{CC}} p_{\texttt{GG}}} - p_{\texttt{AA}} p_{\texttt{CG}} p_{\texttt{GC}} - \cdots) - p_{\texttt{GG}} \cdot (\underline{p_{\texttt{AA}} p_{\texttt{CC}} p_{\texttt{TG}}} - p_{\texttt{AA}} p_{\texttt{CG}} p_{\texttt{TC}} - \cdots) \\ = \quad & -p_{\texttt{AA}} p_{\texttt{CG}} p_{\texttt{GC}} p_{\texttt{TG}} + p_{\texttt{AA}} p_{\texttt{CG}} p_{\texttt{GG}} p_{\texttt{TC}} + p_{\texttt{AC}} p_{\texttt{CG}} p_{\texttt{GA}} p_{\texttt{TG}} - p_{\texttt{AC}} p_{\texttt{CG}} p_{\texttt{GG}} p_{\texttt{TA}} \\ & +p_{\texttt{AG}} p_{\texttt{CA}} p_{\texttt{GC}} p_{\texttt{TG}} - p_{\texttt{AG}} p_{\texttt{CA}} p_{\texttt{GG}} p_{\texttt{TC}} - p_{\texttt{AG}} p_{\texttt{CC}} p_{\texttt{GA}} p_{\texttt{TG}} + p_{\texttt{AG}} p_{\texttt{CC}} p_{\texttt{GG}} p_{\texttt{TA}} \end{aligned}$$

The normal form of this expression modulo $\mathcal{G}$ is zero, as promised.

We are now prepared to state the algorithm for computing Gröbner bases.

Algorithm 3.11 (Buchberger's Algorithm)
Input: A finite set $\mathcal{F}$ of polynomials in $\mathbb{Q}[p_1, p_2, \ldots, p_m]$ and a term order $\prec$.
Output: The reduced Gröbner basis $\mathcal{G}$ of the ideal $\langle \mathcal{F} \rangle$ with respect to $\prec$.
Step 1: Apply Buchberger's Criterion to see whether $\mathcal{F}$ is already a Gröbner basis. If yes go to Step 3.
Step 2: If no, we found a non-zero polynomial $\mathrm{nf}_{\mathcal{G}}(m'g - mg')$. Enlarge the set $\mathcal{F}$ by adding this non-zero polynomial and go back to Step 1.
Step 3: Transform the Gröbner basis $\mathcal{F}$ to a reduced Gröbner basis $\mathcal{G}$.

This loop between Steps 1 and 2 will terminate after finitely many iterations because at each stage the ideal generated by the current initial monomials get strictly bigger. However, in light of Hilbert's Basis Theorem, every strictly increasing sequence of ideals $\mathbb{Q}[p_1, \ldots, p_m]$ must stabilize eventually.

The Gröbner basis $\mathcal{F}$ produced in Steps 1 & 2 is usually not reduced, so in Step 3 we perform *auto-reduction* to make $\mathcal{F}$ reduced. To achieve the three conditions in the definition of reduced Gröbner basis, here is what Step 3 does. First, each polynomial in $\mathcal{F}$ is divided by its leading coefficient to achieve condition 1. Next, one removes redundant polynomials to achieve condition 2. Finally, each polynomial is replaced by its normal form with respect to $\mathcal{F}$ to achieve condition 3. The resulting set $\mathcal{G}$ satisfies all three conditions.

We illustrate Buchberger's algorithm for a very simple example with $m = 1$:

$$\mathcal{F} = \{ \underline{p^2} + 3p - 4, \, \underline{p^3} - 5p + 4 \}.$$

This set is not a Gröbner basis because the S-polynomial

$$p \cdot (p^2 + 3p - 4) - 1 \cdot (p^3 - 5p + 4) \quad = \quad 3p^2 + p - 4$$

has the non-zero normal form

$$3p^2 + p - 4 \, - \, 3 \cdot (p^2 + 3p - 4) \quad = \quad -8p + 8.$$

The new set $\mathcal{F} \cup \{-8p + 8\}$ now passes the test imposed by Buchberger's Criterion: it is a Gröbner basis. The resulting reduced Gröbner basis equals $\mathcal{G} = \{ p - 1 \}$. In particular, we conclude $V(\mathcal{F}) = \{1\} \subset \mathbb{C}$.

Remark 3.12 If $\mathcal{F} \subset \mathbb{Q}[p]$ is a set of polynomials in one unknown p then the reduced Gröbner basis $\mathcal{G}$ of the ideal $\langle \mathcal{F} \rangle$ consists of only one polynomial g. The polynomial g is the greatest common divisor of $\mathcal{F}$.

Buchberger's algorithm is therefore a generalization of the Euclidean algorithm for polynomials in one unknown. Likewise, the Buchberger Algorithm simulates Gaussian elimination if we apply it to a set $\mathcal{F}$ of linear polynomials. We can thus think of Gröbner bases as a *Euclidean algorithm for multivariate polynomials* or a *Gaussian elimination for non-linear equations*.

In summary, Gröbner bases and the Buchberger Algorithm for finding them are fundamental notions in computational algebra. They also furnish the engine for more advanced algorithms for algebraic varieties. Polynomial models are ubiquitous across the sciences, and play a role in numerous biological contexts, including settings quite different from those described in this book. For example, they are used in computational systems biology [Laubenbacher, 2003] and for finding equilibria in reaction networks [Craciun and Feinberg, 2004, Gatermann and Wolfrum, 2005]. Computer programs for algebraic geometry include `CoCoA`, `Macaulay 2` and `Singular`. All three are free and easy to use. Within minutes you will be able to test whether a variety $\mathcal{V}(\mathcal{F})$ is empty, and, if not, compute its dimension.

3.2 Implicitization

Consider the polynomial map which represents an algebraic statistical model:

$$\mathbf{f} \; : \; \mathbb{C}^d \rightarrow \mathbb{C}^m. \tag{3.8}$$

Here the ambient spaces are taken over the complex numbers, but the coordinates $f_1, \ldots, f_m$ of the map $\mathbf{f}$ are polynomials with rational coefficients, i.e., $f_1, \ldots, f_m \in \mathbb{Q}[\theta_1, \ldots, \theta_d]$. These assumptions are consistent with our discussion in the previous section. We start out by investigating the following basic question: is the image of a polynomial map $\mathbf{f}$ really an algebraic variety?

Example 3.13 Consider the following map from the plane into three-space:

$$\mathbf{f} \, : \, \mathbb{C}^2 \rightarrow \mathbb{C}^3 \, , \;\; (\theta_1, \theta_2) \;\mapsto\; \big(\theta_1^2, \, \theta_1 \cdot \theta_2, \, \theta_1 \cdot \theta_2 \,\big)$$

The image of $\mathbf{f}$ is a dense subset of a plane in three-space, namely, it is

$$\begin{aligned} \mathbf{f}(\mathbb{C}^2) \quad &= \quad \big\{ \, (p_1, p_2, p_3) \in \mathbb{C}^3 \;:\; p_2 = p_3 \text{ and } \big(\, p_1 = 0 \text{ implies } p_2 = 0 \, \big) \big\} \\ &= \qquad \big(V(p_2 - p_3) \setminus V(p_1, p_2 - p_3) \big) \;\cup\; V(p_1, p_2, p_3). \end{aligned}$$

Thus the image of $\mathbf{f}$ is not an algebraic variety, but its closure is: $\overline{\mathbf{f}(\mathbb{C}^2)} = V(p_2 - p_3)$. The set $\mathbf{f}(\mathbb{C}^2)$ is a Boolean combination of algebraic varieties.

The following general theorem holds in algebraic geometry. It can be derived from the *Closure Theorem* in Section 3.2 of [Cox *et al.*, 1997].

Theorem 3.14 *The image of a polynomial map* $\mathbf{f} : \mathbb{C}^d \to \mathbb{C}^m$ *is a Boolean combination of algebraic varieties in* $\mathbb{C}^m$*. The topological closure* $\overline{\mathbf{f}(\mathbb{C}^d)}$ *of the image* $\mathbf{f}(\mathbb{C}^d)$ *in* $\mathbb{C}^m$ *is an algebraic variety.*

The statements in this theorem are not true if we replace the complex numbers $\mathbb{C}$ by the real numbers $\mathbb{R}$. This can already be seen for the map $\mathbf{f}$ in Example 3.13. The image of this map over the reals equals

$$\mathbf{f}(\mathbb{R}^2) \quad = \quad \big\{ (p_1, p_2, p_3) \in \mathbb{R}^3 \ : \ p_2 = p_3 \text{ and } (\, p_1 > 0 \text{ or } p_1 = p_2 = p_3 = 0 \,) \big\}.$$

The closure of the image is a half-plane in $\mathbb{R}^3$, which is not an algebraic variety:

$$\overline{\mathbf{f}(\mathbb{R}^2)} \quad = \quad \big\{ (p_1, p_2, p_3) \in \mathbb{R}^3 \ : \ p_2 = p_3 \text{ and } p_1 \geq 0 \,\big\}.$$

It is instructive to carry this example a little further and compute the images of various subsets Θ of $\mathbb{R}^2$. For instance, what is the image $\mathbf{f}(\Theta)$ of the square $\Theta = \{0 \leq \theta_1, \theta_2 \leq 1\}$? For answering such questions in general, we need algorithms for solving *polynomial inequalities over the real numbers.* Such algorithms exists in *real algebraic geometry*, which is an active area of research. However, real algebraic geometry lies beyond what we are hoping to explain in this book. In this chapter, we restrict ourselves to the much simpler setting of *polynomial equations over the complex numbers.* For an introduction to algorithms in real algebraic geometry see [Basu *et al.*, 2003].

We shall adopt the following convention: By *the image of the polynomial map* $\mathbf{f}$ in (3.8) we shall mean the algebraic variety $\overline{\mathbf{f}(\mathbb{C}^d)}$ in $\mathbb{C}^m$. Thus we disregard potential points p in $\overline{\mathbf{f}(\mathbb{C}^d)} \backslash \mathbf{f}(\mathbb{C}^d)$. This is not to say they are not important. In fact, in a statistical model for a biological problem, such boundary points p might represent probability distributions we really care about. If so, we need to refine our techniques. For the discussion in this chapter, however, we keep the algebra as simple as possible and refer to $\overline{\mathbf{f}(\mathbb{C}^d)}$ as the image of $\mathbf{f}$.

Let $I_{\mathbf{f}}$ denote the set of all polynomials in $\mathbb{Q}[p_1, \ldots, p_m]$ that vanish on the set $\mathbf{f}(\mathbb{C}^d)$. Thus $I_{\mathbf{f}}$ is the ideal which represents the variety $\overline{\mathbf{f}(\mathbb{C}^d)}$. A polynomial $h \in \mathbb{Q}[p_1, \ldots, p_m]$ lies in the ideal $I_{\mathbf{f}}$ if and only if

$$h\big(f_1(t), f_2(t), \ldots f_m(t)\big) \quad = \quad 0 \qquad \text{for all } t = (t_1, t_2, \ldots, t_d) \in \mathbb{R}^d. \tag{3.9}$$

The ideal $I_{\mathbf{f}}$ is a *prime ideal.* This means that if a factorizable polynomial $h = h' \cdot h''$ satisfies (3.9) then one of its factors h' or h'' will also satisfy (3.9). In the condition (3.9) we can replace $\mathbb{R}^d$ by any open subset $\Theta \subset \mathbb{R}^d$ and we get an equivalent condition. Thus $I_{\mathbf{f}}$ equals the set of all polynomials that vanish on the points $\mathbf{f}(t)$ where t runs over the parameter space Θ. The polynomials in the prime ideal $I_{\mathbf{f}}$ are known as *model invariants* in algebraic statistics. For instance, for DiaNA's model in Example 3.9, the model invariants include the 3×3-minors of the 4×4-matrix of probabilities.

The computational task resulting from our discussion is called *implicitization*: Given m polynomials $f_1, \ldots, f_m$ in $\mathbb{Q}[\theta_1, \ldots, \theta_d]$ which represent a polynomial map $\mathbf{f} : \mathbb{C}^d \to \mathbb{C}^m$, implicitization seeks to compute a finite set $\mathcal{F}$ of polynomials in $\mathbb{Q}[p_1, p_2, \ldots, p_m]$ such that $\langle \mathcal{F} \rangle = I_{\mathbf{f}}$. Actually, it would be preferable to have a Gröbner basis $\mathcal{G}$ of the ideal $I_{\mathbf{f}}$. Our point of view is this:

"compute the image of a polynomial map $\mathbf{f}$

means "compute generators of the prime ideal $I_{\mathbf{f}}$"

Example 3.15 We compute the images of five different maps $\mathbf{f} : \mathbb{C}^2 \to \mathbb{C}^3$:

(a) If $\mathbf{f} = (\,\theta_1^2,\, \theta_1\theta_2,\, \theta_1\theta_2\,)$ then $I_{\mathbf{f}} = \langle\, p_2 - p_3 \,\rangle$. This is Example 3.13.
(b) If $\mathbf{f} = (\,\theta_1^2,\, 2\theta_1\theta_2,\, \theta_2^2\,)$ then $I_{\mathbf{f}} = \langle\, p_1p_3 - 4p_2^2 \,\rangle$ = Hardy-Weinberg.
(c) If $\mathbf{f} = (\,\theta_1^5,\, \theta_1\theta_2,\, \theta_2^4\,)$ then $I_{\mathbf{f}} = \langle\, p_1^4 p_3^5 - p_2^{20} \,\rangle$.
(d) If $\mathbf{f} = (\,\theta_1^5 + \theta_1\theta_2,\, \theta_1^5 + \theta_2^4,\, \theta_1\theta_2 + \theta_2^4\,)$ then we get the same ideal in new coordinates: $I_{\mathbf{f}} = \langle\, 2^{11}(p_1 + p_2 - p_3)^4 (p_2 + p_3 - p_1)^5 - (p_1 + p_3 - p_2)^{20} \,\rangle$.
(e) If $\mathbf{f} = (\,\theta_1^2 + \theta_2^2,\, \theta_1^3 + \theta_2^3,\, \theta_1^4 + \theta_2^4\,)$ then we actually have to do a computation to find $I_{\mathbf{f}} = \langle\, p_1^6 - 4p_1^3p_2^2 - 4p_2^4 + 12p_1p_2^2p_3 - 3p_1^2p_3^2 - 2p_3^3 \,\rangle$.

The last ideal $I_{\mathbf{f}}$ was computed in `Singular` using the following six commands:

```
ring s=0, (p1,p2,p3),lp;
ring r=0, (t1,t2), lp;
map f = s, t1^2+t2^2, t1^3+t2^3, t1^4+t2^4;
ideal i0 = 0;
setring s;
preimage(r,f,i0);
```

It should be tried and then redone with the third line replaced as follows:

```
map f = s, t1^5+t1*t2, t1^5+t2^4, t1*t2+t2^4;
```

This produces the surface of degree 20 in Example 3.15 (d). The output is very large, and underlines the importance of identifying a coordinate change that will simplify a computation. This will be crucial for the applications to phylogenetics discussed in Chapter 15 and 16.

In order to understand the way Gröbner basis software (such as `Singular`) computes images of polynomial maps, we need to think about the ideal $I_{\mathbf{f}}$ in the following algebraic manner. Our polynomial map $\mathbf{f} : \mathbb{C}^d \to \mathbb{C}^m$ induces the map between polynomial rings in the opposite direction:

$$\begin{aligned} \mathbf{f}^* \,:\, \mathbb{Q}[p_1, p_2, \ldots, p_m] &\to \mathbb{Q}[\theta_1, \ldots, \theta_d] \\ h(p_1, p_2, \ldots, p_m) &\mapsto h(f_1(\theta), f_2(\theta), \ldots, f_m(\theta)) \end{aligned}$$

The map $\mathbf{f}^*$ is a *ring homomorphism*, which means that $\mathbf{f}^*(h'+h'') = \mathbf{f}^*(h') + \mathbf{f}^*(h'')$ and $\mathbf{f}^*(h' \cdot h'') = \mathbf{f}^*(h') \cdot \mathbf{f}^*(h'')$. Thus the ring homomorphism is uniquely specified by saying that $\mathbf{f}^*(p_i) = f_i(\theta)$ for all i. The *kernel* of $\mathbf{f}^*$ is the set $(\mathbf{f}^*)^{-1}(0)$ of all polynomials $h \in \mathbb{Q}[p_1, \ldots, p_m]$ that get mapped to zero by $\mathbf{f}^*$.

Proposition 3.16 *The kernel of* $\mathbf{f}^*$ *equals the prime ideal* $I_{\mathbf{f}} \subset \mathbb{Q}[p_1, \ldots, p_m]$.

Proof A polynomial h satisfies $\mathbf{f}^*(h) = 0$ if and only if the condition (3.9) holds. Thus h lies in $\mathrm{kernel}(\mathbf{f}^*) = (\mathbf{f}^*)^{-1}(0)$ if and only if h lies in $I_{\mathbf{f}}$. □

If I is any ideal in $\mathbb{Q}[\theta_1, \ldots, \theta_d]$ then its preimage $(\mathbf{f}^*)^{-1}(I)$ is an ideal in $\mathbb{Q}[p_1, \ldots, p_m]$. The next theorem characterizes the variety in $\mathbb{C}^m$ of this ideal.

Theorem 3.17 *The variety of* $(\mathbf{f}^*)^{-1}(I)$ *is the closure in* $\mathbb{C}^m$ *of the image of the variety* $V(I) \subset \mathbb{C}^d$ *under the map* $\mathbf{f}$*; in symbols,*

$$V\big((\mathbf{f}^*)^{-1}(I)\big) \quad = \quad \overline{\mathbf{f}\big(V(I)\big)} \quad \subset \quad \mathbb{C}^m. \tag{3.10}$$

Proof We identify the ideal I with its image in the enlarged polynomial ring $\mathbb{Q}[\theta_1, \ldots \theta_d, p_1, p_2, \ldots, p_m]$. Inside this big polynomial ring we consider the ideal

$$J \quad = \quad I \; + \; \langle\, p_1 - f_1(\theta),\, p_2 - f_2(\theta),\, \ldots,\, p_m - f_m(\theta) \,\rangle. \tag{3.11}$$

The ideal J represents the graph of the restricted map $\mathbf{f} : V(I) \to \mathbb{C}^m$. Indeed, that graph is precisely the variety $V(J) \subset \mathbb{C}^{d+m}$. The desired image $\mathbf{f}(V(I))$ is obtained by projecting the graph $V(J)$ onto the space $\mathbb{C}^m$ with coordinates $p_1, \ldots, p_m$. Algebraically, this corresponds to computing the *elimination ideal*

$$(\mathbf{f}^*)^{-1}(I) \quad = \quad J \,\cap\, \mathbb{Q}[p_1, \ldots, p_m]. \tag{3.12}$$

Now use the Closure Theorem in [Cox *et al.*, 1997, Sect. 3.2]. □

The `Singular` code displayed earlier is designed for the setup in (3.10). The `map` command specifies a homomorphism `f` from the second polynomial ring `s` to the first polynomial ring `r`, and the `preimage` command computes the preimage of an ideal `i0` in `r` under the homomorphism `f`. The computation inside `Singular` is done by cleverly executing the two steps (3.11) and (3.12).

Example 3.18 We compute the image of the hyperbola $V(\theta_1\theta_2 - 1)$ under the map $\mathbf{f}$ in Example 3.15 (e) by replacing the line `ideal i0 = 0 ;` by the new line `ideal i0 = t1*t2-1 ;` in our code. The image of the hyperbola in three-space is a curve which is the intersection of two quadratic surfaces:

$$(\mathbf{f}^*)^{-1}\big(\langle\theta_1\theta_2 - 1\rangle\big) \quad = \quad \langle\, p_1p_3 - p_1 - p_2^2 + 2\,,\; p_1^2 - p_3 - 2 \,\rangle \qquad \subset \quad \mathbb{Q}[p_1, p_2, p_3]$$

Example 3.19 Consider the *hidden Markov model* of Subsection 1.4.3 where $n = 3$ and both the hidden and observed states are binary ($l = l' = 2$). The parameterization (1.52) is a map $\mathbf{f} : \mathbb{R}^4 \to \mathbb{R}^8$ which we enter into `Singular`:

```
ring s = 0, (p000, p001, p010, p011, p100, p101, p110, p111),lp;
ring r = 0, ( x,y, u,v ), lp;
map f = s, x^2*u^3 + x*(1-x)*u^2*(1-v) +
 (1-x)*(1-y)*u^2*(1-v) + (1-x)*y*u*(1-v)^2 + (1-y)*x*(1-v)*u^2 +
 (1-y)*(1-x)*(1-v)^2*u + y*(1-y)*(1-v)^2*u + y^2*(1-v)^3,
x^2*u^2*(1-u) + x*(1-x)*u^2*v + (1-x)*(1-y)*u*(1-v)*(1-u) +
 (1-x)*y*u*(1-v)*v + (1-y)*x*(1-v)*u*(1-u) +
 (1-y)*(1-x)*(1-v)*u*v + y*(1-y)*(1-v)^2*(1-u) + y^2*(1-v)^2*v,
x^2*u^2*(1-u) + x*(1-x)*u*(1-u)*(1-v) + (1-x)*(1-y)*u^2*v +
 (1-x)*y*u*(1-v)*v + (1-y)*x*(1-v)*u*(1-u) +
 (1-y)*(1-x)*(1-v)^2*(1-u) + y*(1-y)*(1-v)*v*u +y^2*(1-v)^2*v,
x^2*u*(1-u)^2 + x*(1-x)*u*(1-u)*v + (1-x)*(1-y)*u*v*(1-u) +
 (1-x)*y*u*v^2 + (1-y)*x*(1-v)*(1-u)^2 + y^2*(1-v)*v^2 +
 (1-y)*(1-x)*(1-v)*(1-u)*v + y*(1-y)*(1-v)*v*(1-u),
x^2*u^2*(1-u) + x*(1-x)*u*(1-u)*(1-v) +
 (1-x)*(1-y)*u*(1-v)*(1-u) + (1-x)*y*(1-u)*(1-v)^2 +
 (1-y)*x*v*u^2 + (1-y)*(1-x)*(1-v)*u*v + y*(1-y)*(1-v)*v*u +
y^2*(1-v)^2*v, x^2*u*(1-u)^2 + x*(1-x)*u*(1-u)*v +
 (1-x)*(1-y)*(1-u)^2*(1-v) + (1-x)*y*(1-u)*(1-v)*v +
 (1-y)*x*v*u*(1-u) + (1-y)*(1-x)*v^2*u + y*(1-y)*(1-v)*v*(1-u) +
y^2*(1-v)*v^2, x^2*u*(1-u)^2 + x*(1-x)*(1-u)^2*(1-v) +
 (1-x)*(1-y)*u*v*(1-u) + (1-x)*y*(1-u)*(1-v)*v +
 (1-y)*x*v*u*(1-u) + (1-y)*(1-x)*(1-v)*(1-u)*v + y*(1-y)*v^2*u +
y^2*(1-v)*v^2, x^2*(1-u)^3 + x*(1-x)*(1-u)^2*v +
 (1-x)*(1-y)*(1-u)^2*v + (1-x)*y*(1-u)*v^2 + (1-y)*x*v*(1-u)^2 +
 (1-y)*(1-x)*v^2*(1-u) + y*(1-y)*v^2*(1-u) + y^2*v^3;
```

Here the eight probabilities have been scaled by a factor of two (the initial distribution is uniform), and the model parameters are abbreviated

$$\theta_{00} = \mathtt{x}, \quad \theta_{01} = 1-\mathtt{x}, \quad \theta_{10} = 1-\mathtt{y}, \quad \theta_{11} = \mathtt{y}$$
$$\theta'_{00} = \mathtt{u}, \quad \theta'_{01} = 1-\mathtt{u}, \quad \theta'_{10} = 1-\mathtt{v}, \quad \theta'_{11} = \mathtt{v}.$$

The model invariants of the hidden Markov model can now be computed using

```
ideal i0 = 0; setring s; preimage(r,f,i0);
```

This computation will be discussed in Chapter 11. Suppose we are interested (for some strange reason) in the submodel obtained by equating the transition matrix θ with the inverse of the output matrix θ'. The invariants of this two-dimensional submodel are found by the method of Theorem 3.17, using

```
ideal i = x*u + x*v - x - v, y*u + y*v - y - u ; setring s;
preimage(r,f,i);
```

The extension of these computations to longer chains ($n \geq 4$) becomes prohibitive. Off-the-shelf implementations in any Gröbner basis package will always run out of steam quickly when the instances get bigger. More specialized linear algebra techniques need to be employed in order to compute invariants of larger statistical model. Chapter 11 is devoted to these important issues.

We next discuss an implicitization problem which concerns an algebraic variety known as the *Grassmannian*. In our discussion of the *space of phylogenetic trees* in Section 3.5, we shall argue that the Grassmannian is a valuable geometric tool for understanding and designing algorithms for biology. Let $\mathbb{Q}[\,\theta\,]$ be the polynomial ring in the unknown entries of the $2 \times n$ matrix

$$\theta \quad = \quad \begin{pmatrix} \theta_{11} & \theta_{12} & \theta_{13} & \dots & \theta_{1n} \\ \theta_{21} & \theta_{22} & \theta_{23} & \dots & \theta_{2n} \end{pmatrix}.$$

Let $\mathbb{Q}[\,p\,] = \big[\,p_{ij} \,:\, 1 \leq i < j \leq n\,\big]$ be the polynomial ring in the unknowns

$$\big\{\, p_{12},\, p_{13},\, p_{23},\, p_{14},\, p_{24},\, p_{34},\, p_{15},\, \dots,\, p_{n-1,n} \,\big\}. \qquad (3.13)$$

Consider the ring homomorphism $\mathbf{f}^* \,:\, \mathbb{Q}[\,p\,] \rightarrow \mathbb{Q}[\,\theta\,]\,,\; p_{ij} \mapsto \theta_{1i}\theta_{2j} - \theta_{1j}\theta_{2i}$. The corresponding polynomial map $\mathbf{f} \,:\, \mathbb{C}^{2\times n} \mapsto \mathbb{C}^{\binom{n}{2}}$ takes a $2 \times n$-matrix to the vector of 2×2-subdeterminants of θ. The image of this map is the *Grassmannian*, denoted $G_{2,n} \;=\; \overline{\mathbf{f}(\mathbb{C}^{2n})}$. The Grassmannian is an algebraic variety, i.e., it is closed: $\mathbf{f}(\mathbb{C}^{2n}) \;=\; \overline{\mathbf{f}(\mathbb{C}^{2n})}$. The prime ideal of the Grassmannian is denoted $I_{2,n} = \text{kernel}(\mathbf{f}^*)$. This ideal has a nice Gröbner basis:

Theorem 3.20 *The ideal $I_{2,n}$ is generated by the quadratic polynomials*

$$\underline{p_{ik}p_{jl}} - p_{ij}p_{kl} - p_{il}p_{jk} \qquad\qquad (1 \leq i < j < k < l \leq n). \qquad (3.14)$$

These form the reduced Gröbner basis when the underlined terms are leading.

Proof See Theorem 3.1.7 and Proposition 3.7.4 in [Sturmfels, 1993]. □

The dimension of the Grassmannian $G_{2,n}$ is computed using Theorem 3.7. The initial ideal $\text{in}_\prec(I_{2,n}) \;=\; \langle\, p_{ik} \cdot p_{jl} \;:\; 1 \leq i < j < k < l \leq n \,\rangle$ can be visualized as follows. Draw a convex n-gon with vertices labeled $1, 2, 3, \dots, n$. We identify the unknown p_{ij} with the line segment connecting the vertex i

and the vertex j. The generators of $\mathrm{in}_\prec(I_{2,n})$ are the pairs of line segments that cross each other. Consider an arbitrary monomial in $\mathbb{Q}[p]$:

$$m \quad = \quad \prod_{(i,j)\in S} p_{ij}^{a_{ij}} \qquad\qquad (\text{where } a_{ij} > 0 \text{ for all } (i,j) \in S).$$

This monomial m is standard if and only if m does not lie in $\mathrm{in}_\prec(I_{2,n})$ if and only if the set S contains no crossing diagonals if and only if the line segments in S form a subdivision of the n-gon. Hence a subset S of (3.13) is a maximal standard set if and only if the edges in S form a triangulation of the n-gon.

The number of triangulations S of the n-gon is the *Catalan number* $\frac{1}{n+1}\binom{2n}{n}$. The number of edges in each triangulation S equals $|S| = 2n-3$.

Corollary 3.21 *The Grassmannian $G_{2,n} = V(I_{2,n})$ has dimension $2n-3$.*

The ideal $I_{2,n}$ is known as the *Plücker ideal*, and the quadratic polynomials in (3.14) are known as the *Plücker relations*. The Plücker ideal $I_{2,n}$ has two natural generalizations. First, we can replace θ by a $d \times n$-matrix of unknowns (for any $d < n$) and we can define the Plücker ideal $I_{d,n}$ by taking the algebraic relations among the $d \times d$-minors of θ. Thus $I_{d,n}$ is a prime ideal in the polynomial ring in $\binom{n}{d}$ unknowns $\mathbb{Q}[p] = \mathbb{Q}\big[p_{i_1 i_2 \cdots i_d} : 1 \le i_1 < i_2 < \cdots < i_d \le n\big]$. The corresponding variety in $\mathbb{C}^{\binom{n}{d}}$ is the Grassmannian $G_{d,n} = V(I_{d,n})$. Regarding $G_{d,n}$ as projective variety, the points in $G_{d,n}$ are in a natural bijection with the d-dimensional linear subspaces of the n-dimensional vector space $\mathbb{C}^n$. Here $p = \mathbf{f}(\theta) \in \mathbb{C}^{\binom{n}{d}}$ corresponds to the row space of the matrix θ. Theorem 3.20 generalizes to this situation: the ideal $I_{d,n}$ is generated by quadratic polynomials known as the Plücker relations. Among these are the *three-term Plücker relations* which are derived from (3.14):

$$p_{\nu_1\cdots\nu_{d-2}ik}\cdot p_{\nu_1\cdots\nu_{d-2}jl} - p_{\nu_1\cdots\nu_{d-2}ij}\cdot p_{\nu_1\cdots\nu_{d-2}kl} - p_{\nu_1\cdots\nu_{d-2}il}\cdot p_{\nu_1\cdots\nu_{d-2}jk}. \quad (3.15)$$

The three-term Plücker relations are not quite enough to not generate $I_{d,n}$.

The second natural generalization of the ideal $I_{2,n}$ is based on the identity

$$\big(p_{ik}p_{jl} - p_{ij}p_{kl} - p_{il}p_{jk}\big)^2 \quad = \quad \det\begin{pmatrix} 0 & p_{ij} & p_{ik} & p_{il} \\ -p_{ij} & 0 & p_{jk} & p_{jl} \\ -p_{ik} & -p_{jk} & 0 & p_{kl} \\ -p_{il} & -p_{jl} & -p_{kl} & 0 \end{pmatrix}. \quad (3.16)$$

This is a skew-symmetric 4×4-matrix with unknown entries p_{ij}. The square root of the determinant of a skew-symmetric $2k\times 2k$-matrix is a polynomial of degree k known as its *pfaffian*. Hence the Plücker relation (3.14) is the pfaffian of the matrix in (3.16). Skew-symmetric matrices of odd size are singular, so the determinant of a skew-symmetric $(2k+1)\times(2k+1)$-matrix is zero.

Remark 3.22 By Theorem 3.20 and (3.16), the Plücker ideal $I_{2,n}$ is generated by the 4×4-subpfaffians of an indeterminate skew-symmetric $n\times n$-matrix (p_{ij}).

Let $I_{2,n,k}$ be the ideal generated by the $2k \times 2k$-subpfaffians of a skew-symmetric $n \times n$-matrix p_{ij}. Thus $I_{2,n,2} = I_{2,n}$, and $I_{2,6,3}$ is generated by

$$\begin{aligned} &\underline{p_{14}p_{25}p_{36}} - p_{15}p_{24}p_{36}p_{14}p_{26}p_{35} + p_{15}p_{26}p_{34} - +p_{16}p_{24}p_{35} \\ &p_{16}p_{25}p_{34} + p_{13}p_{26}p_{45} - p_{12}p_{36}p_{45}p_{16}p_{23}p_{45}p_{13}p_{25}p_{46} \\ &- + p_{12}p_{35}p_{46} + p_{15}p_{23}p_{46} + p_{13}p_{24}p_{56} - p_{12}p_{34}p_{56}p_{14}p_{23}p_{56} \\ = \quad &\det{}^{1/2}\begin{pmatrix} 0 & p_{12} & p_{13} & p_{14} & p_{15} & p_{16} \\ -p_{12} & 0 & p_{23} & p_{24} & p_{25} & p_{26} \\ -p_{13} & -p_{23} & 0 & p_{34} & p_{35} & p_{36} \\ -p_{14} & -p_{24} & -p_{34} & 0 & p_{45} & p_{46} \\ -p_{15} & -p_{25} & -p_{35} & -p_{45} & 0 & p_{56} \\ -p_{16} & -p_{26} & -p_{36} & -p_{46} & -p_{56} & 0 \end{pmatrix} . \end{aligned} \tag{3.17}$$

It turns out that $I_{2,n,k}$ is always a prime ideal. We introduce $k-1$ matrices

$$\theta^{(s)} \quad = \quad \begin{pmatrix} \theta^{(s)}_{11} & \theta^{(s)}_{12} & \theta^{(s)}_{13} & \cdots & \theta^{(s)}_{1n} \\ \theta^{(s)}_{21} & \theta^{(s)}_{22} & \theta^{(s)}_{23} & \cdots & \theta^{(s)}_{2n} \end{pmatrix} \qquad (s = 1, 2, \ldots, k-1).$$

The $2(k-1)n$ entries of these $k-1$ matrices are the parameters for the map

$$\mathbf{g} : (\mathbb{C}^{2\times n})^{k-1} \to \mathbb{C}^{\binom{n}{2}}, \ (\theta^{(1)}, \ldots, \theta^{(k-1)}) \mapsto \mathbf{f}(\theta^{(1)}) + \cdots + \mathbf{f}(\theta^{(k-1)}). \tag{3.18}$$

Theorem 3.23 *The image of the map* $\mathbf{g}$ *is the variety defined by the* $2k\times 2k$-*subpfaffians. We have* $I_{\mathbf{g}} = I_{2,n,k}$ *and* $\text{image}(\mathbf{g}) = V(I_{2,n,k})$.

The variety $V(I_{2,n,k})$ consists of all skew-symmetric $n \times n$-matrices of rank less than $2k$. Geometrically, $V(I_{2,n,k})$ is the $(k-1)$st *secant variety of the Grassmannian*. Indeed, the passage from the polynomial map $\mathbf{f}$ to the polynomial map $\mathbf{g}$ in (3.18) corresponds to the geometric construction of passing from a projective variety to its $(k-1)$st *secant variety*. For a proof of Theorem 3.23 see [De Concini *et al.*, 1982]. The Gröbner basis in Theorem 3.20 generalizes from $I_{2,n}$ to $I_{2,n,k}$, and so does its convex n-gon interpretation. The initial ideal $\text{in}_{\prec}(I_{2,n,k})$ for a suitable term order $\prec$ is generated by the k-element sets of pairwise crossing diagonals (see [Dress *et al.*, 2002]). As an example consider the 15 monomials in the cubic pfaffian given above (this is the case $k = 3, n = 6$). The underline initial monomial is the only one that represents three pairwise crossing diagonals.

There are many biologically important models for which a complete description of the prime ideal has not yet been established. For instance, consider the two hidden tree models in Examples 1.24 and 1.25. When taken with unspecified root distributions, these models are specified by polynomial maps

$$\mathbf{f} : \mathbb{C}^{13} \to \mathbb{C}^{64} \qquad \text{and} \qquad \mathbf{f}' : \mathbb{C}^{39} \to \mathbb{C}^{64}$$

The corresponding prime ideals $I_{\mathbf{f}}$ and $I_{\mathbf{f}'}$ have a conjectural description which we summarize as follows. Here we disregard the linear form $\sum p_{\cdot\cdot} - 1$ and consider the ideals of all homogeneous polynomials vanishing on the models.

Conjecture 3.24 *The ideal $I_{\mathbf{f}}$ is generated by homogeneous polynomials of degree* 3*, and $I_{\mathbf{f}'}$ is generated by homogeneous polynomials of degree* 5 *and* 9*.*

This conjecture represents the borderline of our knowledge on what is known as the *naive Bayes model* in statistics and as *secant varieties of Segre varieties* in Geometry. For known results and further background see Chapters 15 and 16, [Allman and Rhodes, 2004b, Section 6], and [Garcia *et al.*, 2004, Section 7].

Example 3.25 Here we make the first part of Conjecture 3.24 precise by describing an explicit set of cubics which are believed to generate the kernel of

$$\begin{aligned} \mathbf{f}^* : \mathbb{Q}[p] &\to \mathbb{Q}[\theta, \lambda] \\ p_{i_1 i_2 i_3 i_4 i_5 i_6} &\mapsto \lambda \theta^{\mathbf{r}1}_{0 i_1} \theta^{\mathbf{r}2}_{0 i_2} \theta^{\mathbf{r}3}_{0 i_3} \theta^{\mathbf{r}4}_{0 i_4} \theta^{\mathbf{r}5}_{0 i_5} \theta^{\mathbf{r}6}_{0 i_6} + (1-\lambda) \theta^{\mathbf{r}1}_{1 i_1} \theta^{\mathbf{r}2}_{1 i_2} \theta^{\mathbf{r}3}_{1 i_3} \theta^{\mathbf{r}4}_{1 i_4} \theta^{\mathbf{r}5}_{1 i_5} \theta^{\mathbf{r}6}_{1 i_6}. \end{aligned}$$

Consider any split of $\{1,2,3,4,5,6\}$ into two subsets A and B of size at least two. We can write the $2 \times 2 \times 2 \times 2 \times 2 \times 2$-table $(p_{i_1 i_2 i_3 i_4 i_5 i_6})$ as an ordinary two-dimensional matrix where the rows are indexed by functions $A \to \{1,2\}$ and the columns are indexed by functions $B \to \{1,2\}$. These matrices have rank at most two for all distributions in the model, hence their 3×3-subdeterminants lie in the ideal $I_{\mathbf{f}}$. It is conjectured that $I_{\mathbf{f}}$ is generated by these 3×3-determinants. For example, the 8×8-matrix for $A = \{1,2,3\}$ and $B = \{4,5,6\}$ equals

$$\begin{pmatrix}
p_{000000} & p_{000001} & p_{000010} & p_{000011} & p_{000100} & p_{000101} & p_{000110} & p_{000111} \\
p_{001000} & p_{001001} & p_{001010} & p_{001011} & p_{001100} & p_{001101} & p_{001110} & p_{001111} \\
p_{010000} & p_{010001} & p_{010010} & p_{010011} & p_{010100} & p_{010101} & p_{010110} & p_{010111} \\
p_{011000} & p_{011001} & p_{011010} & p_{011011} & p_{011100} & p_{011101} & p_{011110} & p_{011111} \\
p_{100000} & p_{100001} & p_{100010} & p_{100011} & p_{100100} & p_{100101} & p_{100110} & p_{100111} \\
p_{101000} & p_{101001} & p_{101010} & p_{101011} & p_{101100} & p_{101101} & p_{101110} & p_{101111} \\
p_{110000} & p_{110001} & p_{110010} & p_{110011} & p_{110100} & p_{110101} & p_{110110} & p_{110111} \\
p_{111000} & p_{111001} & p_{111010} & p_{111011} & p_{111100} & p_{111101} & p_{111110} & p_{111111}
\end{pmatrix}$$

Chapter 19 presents a new algorithm for phylogenetic reconstruction based on the fact that such matrices have low rank for all splits (A, B) in the tree. That algorithm is an algebraic variant of Neighbor Joining (Section 2.4), where the decision about which cherries to pick rests on singular value decompositions.

3.3 Maximum likelihood estimation

An algebraic statistical model is a map $\mathbf{f} : \mathbb{C}^d \to \mathbb{C}^m$ whose coordinate functions $f_1, \ldots, f_m$ are polynomials with rational coefficients in the parameters $\theta = (\theta_1, \ldots, \theta_d)$. The parameter space Θ is an open subset of $\mathbb{R}^d$ such that $\mathbf{f}(\Theta) \subseteq \mathbb{R}^m_{>0}$. If we make the extra assumption that $f_1 + \cdots + f_m - 1$ is the zero polynomial then $\mathbf{f}(\Theta)$ is a family of probability distributions on the state space $[m] = \{1, \ldots, m\}$. A given data set is summarized in a vector $u = (u_1, \ldots, u_m)$ of positive integers. The problem of *maximum likelihood estimation* is to find a parameter vector $\widehat{\theta}$ in Θ which best explains the data u. This leads to the problem of maximizing the log-likelihood function

$$\ell_u(\theta) \;=\; \sum_{i=1}^{m} u_i \cdot \log(f_i(\theta)). \tag{3.19}$$

Every local and global maximum $\widehat{\theta}$ in Θ is a solution of the *critical equations*

$$\frac{\partial \ell_u}{\partial \theta_1} \;=\; \frac{\partial \ell_u}{\partial \theta_2} \;=\; \cdots \;=\; \frac{\partial \ell_u}{\partial \theta_d} \;=\; 0. \tag{3.20}$$

The derivative of $\ell_u(\theta)$ with respect to the unknown θ_i is the rational function

$$\frac{\partial \ell_u}{\partial \theta_i} \quad = \quad \frac{u_1}{f_1(\theta)}\frac{\partial f_1}{\partial \theta_i} + \frac{u_2}{f_2(\theta)}\frac{\partial f_2}{\partial \theta_i} + \cdots + \frac{u_m}{f_m(\theta)}\frac{\partial f_m}{\partial \theta_i}. \tag{3.21}$$

The problem to be studied in this section is computing all solutions $\theta \in \mathbb{C}^d$ to the critical equations (3.20). Since (3.21) is a rational function, this set is an algebraic variety outside the locus where the denominators of these rational functions are zero. Hence the closure of this set is an algebraic variety in $\mathbb{C}^d$, called the *likelihood variety* of the model $\mathbf{f}$ with respect to the data u.

In order to compute the likelihood variety we proceed as follows. We introduce m new unknowns $z_1, \ldots, z_m$ where z_i represents the inverse of $f_i(\theta)$. The polynomial ring $\mathbb{Q}[\theta, z] \;=\; \mathbb{Q}[\theta_1, \ldots, \theta_d, z_1, \ldots, z_m]$ is our "big ring", as opposed to the "small ring" $\mathbb{Q}[\theta] \;=\; \mathbb{Q}[\theta_1, \ldots, \theta_d]$ which is a subring of $\mathbb{Q}[\theta, z]$. We introduce an ideal generated by $m + d$ polynomials in the big ring $\mathbb{Q}[\theta, z]$:

$$J_u \quad := \quad \Big\langle\, z_1 f_1(\theta) - 1, \, \ldots, \, z_m f_m(\theta) - 1, \; \sum_{j=1}^{m} u_j z_j \frac{\partial f_j}{\partial \theta_1}, \; \ldots \;, \; \sum_{j=1}^{m} u_j z_j \frac{\partial f_j}{\partial \theta_d} \,\Big\rangle.$$

A point $(\theta, z) \in \mathbb{C}^{d+m}$ lies in the variety $V(J_u)$ of this ideal if and only if θ is a critical point of the log-likelihood function with $f_j(\theta) \neq 0$ and $z_j = 1/f_j(\theta)$ for all j. We next compute the elimination ideal in the small ring:

$$I_u \quad = \quad J_u \,\cap\, \mathbb{Q}[\theta_1, \ldots, \theta_d]. \tag{3.22}$$

We call I_u the *likelihood ideal* of the model $\mathbf{f}$ with respect to the data u. A point $\theta \in \mathbb{C}^d$ with all $f_j(\theta)$ nonzero lies in $V(I_u)$ if and only if θ is a critical point of the log-likelihood function $\ell_u(\theta)$. Thus $V(I_u)$ is the likelihood variety.

The algebraic approach to solving our optimization problem is this: Compute the variety $V(I_u) \subset \mathbb{C}^d$, intersect it with the preimage $\mathbf{f}^{-1}(\Delta)$ of the $(m-1)$-dimensional probability simplex Δ, and identify all local maxima among the points in $V(I_u) \cap \mathbf{f}^{-1}(\Delta)$. We demonstrate this for an example.

Example 3.26 Let $d = 2$ and $m = 5$ and consider the following model:

```
ring bigring = 0, (t1,t2,z1,z2,z3,z4,z5), dp;
poly f1 = 2/5 - 6/5*t2 -6/5*t1 + 21/5*t1*t2;
poly f2 = 6/5*t2 - 18/5*t1*t2 + 6/5*t1;
poly f3 = 3/5 - 9/5*t2 - 9/5*t1 + 39/5*t1*t2;
poly f4 = 6/5*t2 - 21/5*t1*t2 + 3/5*t1;
poly f5 = 6/5*t1 - 21/5*t1*t2 + 3/5*t2;
```

We use `Singular` notation with $\theta_1 = $ `t1` and $\theta_2 = $ `t2`. This map $\mathbf{f} : \mathbb{C}^2 \to \mathbb{C}^5$ is the submodel of the Jukes-Cantor model in Examples 1.7 and 4.21 obtained by fixing the third parameter θ_3 to be 1/5. Suppose the given data are

```
int u1 = 31; int u2 = 5; int u3 = 7; int u4 = 11; int u5 = 13;
```

We specify the ideal J_u in the big ring $\mathbb{Q}[\theta_1, \theta_2, z_1, z_2, z_3, z_4, z_5]$:

```
ideal Ju = z1*f1-1, z2*f2-1, z3*f3-1, z4*f4-1, z5*f5-1,
u1*z1*diff(f1,t1)+u2*z2*diff(f2,t1)+u3*z3*diff(f3,t1)
+u4*z4*diff(f4,t1)+u5*z5*diff(f5,t1),
u1*z1*diff(f1,t2)+u2*z2*diff(f2,t2)+u3*z3*diff(f3,t2)
+u4*z4*diff(f4,t2)+u5*z5*diff(f5,t2);
```

Next we carry out the elimination step in (3.22) to get the likelihood ideal I_u:

```
ideal Iu = eliminate( Ju, z1*z2*z3*z4*z5 );
ring smallring = 0, (t1,t2), dp;
ideal Iu = fetch(bigring,Iu); Iu;
```

The likelihood ideal I_u is generated by six polynomials in (θ_1, θ_2) with large integer coefficients. Its variety $V(I_u) \subset \mathbb{C}^2$ is a finite set (it has dimension zero) consisting of 16 points. This is seen with the commands

```
ideal G = groebner(Iu); dim(G); vdim(G);
```

The numerical solver in `Singular` computes the 16 points in $V(I_u)$:

```
ideal G = groebner(Iu); LIB "solve.lib"; solve(G,20);
```

Precisely ten of the 16 points in $V(I_u)$ have real coordinates, and of these precisely three correspond to probability distributions in our model. They are:

$$\theta^{(1)} = (0.1476, -0.0060),\ \theta^{(2)} = (0.3652, 0.3553) \text{ and } \theta^{(3)} = (0.3038, 0.3000).$$

The corresponding probability distributions in $\Delta \subset \mathbb{R}^5$ are

$$\begin{aligned} \mathbf{f}(\theta^{(1)}) &= \big(0.22638,\ 0.17309,\ 0.33823,\ 0.08507,\ 0.17723\big), \\ \mathbf{f}(\theta^{(2)}) &= \big(0.08037,\ 0.39748,\ 0.31518,\ 0.10053,\ 0.10644\big), \\ \mathbf{f}(\theta^{(3)}) &= \big(0.05823,\ 0.39646,\ 0.22405,\ 0.15950,\ 0.16177\big), \end{aligned}$$

and the values of the log-likelihood function at these distributions are

$$\ell_u(\theta^{(1)}) = -112.0113\,,\ \ell_u(\theta^{(2)}) = -145.2426 \text{ and } \ell_u(\theta^{(3)}) = -147.1159.$$

To determine the nature of the critical points we examine the Hessian matrix

$$\begin{pmatrix} \partial^2\ell_u/\partial\theta_1^2 & \partial^2\ell_u/\partial\theta_1\theta_2 \\ \partial^2\ell_u/\partial\theta_1\theta_2 & \partial^2\ell_u/\partial\theta_2^2 \end{pmatrix}$$

At $\theta^{(1)}$ and $\theta^{(2)}$ both eigenvalues of the Hessian matrix are negative, so these are local maxima, while at $\theta^{(3)}$ there is one positive eigenvalue and one negative eigenvalue, so $\theta^{(3)}$ is a saddle point. We conclude that $\widehat{\theta} = \theta^{(1)}$ is the maximum likelihood estimate for the data $u = (31, 5, 7, 11, 13)$ in the Jukes-Cantor model specialized at $\theta_3 = 0.2$. The local maximum $\theta^{(2)}$ shows that the likelihood function for this specialized model is multimodal.

An important question for computational statistics is this: What happens to the maximum likelihood estimate $\widehat{\theta}$ when the model $\mathbf{f}$ is fixed but the data u vary? This variation is continuous in u because the log-likelihood function $\ell_u(\theta)$ is well-defined for all real vectors $u \in \mathbb{R}^m$. While the u_i are positive integers when dealing with data, there is really no mathematical reason for assuming that the u_i are integers. The problem (3.19) and the algebraic approach explained in Example 3.26 make sense for any real vector $u \in \mathbb{R}^m$.

If the model is algebraic (i.e. the f_i are polynomials or rational functions) then the maximum likelihood estimate $\widehat{\theta}$ is an algebraic function of the data u. Being an *algebraic function* means that each coordinate $\widehat{\theta}_i$ of the vector $\widehat{\theta}$ is one of the zeroes of a polynomial of the following form in one unknown θ_i:

$$a_r(u)\cdot\theta_i^r + a_{r-1}(u)\cdot\theta_i^{r-1} + \cdots + a_2(u)\cdot\theta_i^2 + a_1(u)\cdot\theta_i + a_0(u). \qquad (3.23)$$

Here each coefficient $a_i(u)$ is a polynomial in $\mathbb{Q}[u_1, \ldots, u_m]$, and the leading coefficient $a_r(u)$ is non-zero. We can further assume that the polynomial (3.23) irreducible as an element of $\mathbb{Q}[u_1, \ldots, u_m, \theta_i]$. This means that the *discriminant* of (3.23) with respect to θ_i is a non-zero polynomial in $\mathbb{Q}[u_1, \ldots, u_m]$.

We say that a vector $u \in \mathbb{R}^m$ is *generic* if u is not a zero of that discriminant polynomial for all $i \in \{1, \ldots, m\}$. The generic vectors u are dense in $\mathbb{R}^m$.

Definition 3.27 The *maximum likelihood degree* (or *ML degree*) of an algebraic statistical model is the number of complex critical points of the log-likelihood function $\ell_u(\theta)$ for a generic vector $u \in \mathbb{R}^m$.

For most models $\mathbf{f}$ and most data u, the following three things will happen:

- The variety $V(I_u)$ is finite, so the ML degree is a well-defined positive integer.
- The ideal $\mathbb{Q}[\theta_i] \cap I_u$ is prime and is generated by the polynomial (3.23).
- The ML degree equals the degree r of the polynomial (3.23).

The ML degree is an invariant of the statistical model $\mathbf{f}$. It measures the algebraic complexity of the process of maximum likelihood estimation for that model. In particular, the ML degree of $\mathbf{f}$ is an upper bound for the number of critical points in Θ of the likelihood function, and hence an upper bound for the number of local maxima. For instance, for the specialized Jukes-Cantor model in Example 3.26, the ML degree is 16, and the maximum likelihood estimate $\widehat{\theta} = (\widehat{\theta}_1, \widehat{\theta}_2)$ is an algebraic function of degree 16 of the data $(u_1, \ldots, u_5)$. Hence, for any specific $u \in \mathbb{N}^5$, the number of local maxima is bounded above by 16. In general, the following upper bound for the ML degree is available.

Theorem 3.28 *Let $\mathbf{f} : \mathbb{C}^d \to \mathbb{C}^m$ be an algebraic statistical model whose coordinates are polynomials $f_1, \ldots, f_m$ of degrees $b_1, \ldots, b_m$ in the d unknowns $\theta_1, \ldots, \theta_d$. If the maximum likelihood degree of the model $\mathbf{f}$ is finite then it is less than or equal to the coefficient of z^d in the rational generating function*

$$\frac{(1-z)^d}{(1-zb_1)(1-zb_2)\cdots(1-zb_m)}. \tag{3.24}$$

Equality holds if the coefficients of the polynomials $f_1, f_2, \ldots, f_m$ are generic.

Proof See [Catanese *et al.*, 2004]. □

Example 3.29 Consider any statistical model which is parameterized by $m = 5$ quadratic polynomials f_i in $d = 2$ parameters θ_1 and θ_2. The formula in Theorem 3.28 says that the maximum likelihood degree of the model $\mathbf{f} = (f_1, f_2, f_3, f_4, f_5)$ is at most the coefficient of z^2 in the generating function

$$\frac{(1-z)^2}{(1-2z)^5} \quad = \quad 1 + 8z + \underline{41}z^2 + 170z^3 + 620z^4 + \cdots.$$

Hence the ML degree is 41 if the f_i are generic, and ≤ 41 for special quadrics f_i. An instance is Example 3.26, where the model was given by five special quadrics in two unknowns, and the ML degree was $16 < 41$.

We derive the number 41 from first principles. The critical equations are

$$\frac{u_1}{f_1}\frac{\partial f_1}{\partial \theta_1} + \frac{u_2}{f_2}\frac{\partial f_2}{\partial \theta_1} + \cdots + \frac{u_5}{f_5}\frac{\partial f_5}{\partial \theta_1} \;=\; \frac{u_1}{f_1}\frac{\partial f_1}{\partial \theta_2} + \frac{u_2}{f_2}\frac{\partial f_2}{\partial \theta_2} + \cdots + \frac{u_5}{f_5}\frac{\partial f_5}{\partial \theta_2} \;=\; 0.$$

We claim that these equations have 41 solutions. Clearing denominators gives

$$u_1\frac{\partial f_1}{\partial \theta_i} f_2 f_3 f_4 f_5 \,+\, u_2\frac{\partial f_2}{\partial \theta_i} f_1 f_3 f_4 f_5 \,+\, \cdots + u_5\frac{\partial f_5}{\partial \theta_i} f_1 f_2 f_3 f_4 \;=\; 0. \qquad (3.25)$$

for $i = 1, 2$. Each of these two equations specifies a curve of degree 9 in the plane $\mathbb{C}^2$. By Bézout's Theorem, these two curves intersect in $81 = 9 \cdot 9$ points. However, of these 81 points, precisely $40 = \binom{5}{2} \cdot 2 \cdot 2$ points are accounted for by pairwise intersecting the given quadratic curves:

$$f_i(\theta_1, \theta_2) \quad = \quad f_j(\theta_1, \theta_2) \quad = \quad 0 \qquad\qquad (1 \le i < j \le 5).$$

Each of the four solutions to this system will also be a solution to (3.25). After removing these extraneous solutions, we are left with $41 = 81 - 40$ solutions to the two critical equations. Theorem 3.28 says that a similar argument works not just for plane curves but for algebraic varieties in any dimension.

For some applications it is advantageous to replace the unconstrained optimization problem (3.19) by the *constrained optimization problem*

$$\text{Maximize} \quad u_1 \cdot \log(p_1) \,+\, \cdots \,+\, u_m \cdot \log(p_m) \quad \text{subject to} \quad p \in \mathbf{f}(\Theta). \quad (3.26)$$

The image of $\mathbf{f}$ can be computed, in the sense discussed in the previous section, using the algebraic techniques of implicitization. Let $I_{\mathbf{f}} \subset \mathbb{Q}[p_1, p_2, \ldots, p_m]$ denote the prime ideal consisting of all polynomials that vanish on the image of the map $\mathbf{f} : \mathbb{C}^d \to \mathbb{C}^m$. Then we can replace $\mathbf{f}(\Theta)$ by $V_\Delta(I_{\mathbf{f}})$ in (3.26).

Algebraic geometers prefer to work with homogeneous polynomials and projective spaces rather than non-homogeneous polynomials and affine spaces. For that reason we introduce the ideal $P_{\mathbf{f}}$ generated by all *homogeneous* polynomials. The homogeneous ideal $P_{\mathbf{f}}$ represents the model $\mathbf{f}$ just as well because

$$I_{\mathbf{f}} \quad = \quad P_{\mathbf{f}} \,+\, \langle\, p_1 + p_2 + \cdots + p_m - 1 \,\rangle \qquad \text{and} \qquad V_\Delta(I_{\mathbf{f}}) \;=\; V_\Delta(P_{\mathbf{f}}).$$

For instance, Conjecture 3.24 is all about the homogeneous ideals $P_{\mathbf{f}}$ and $P_{\mathbf{f}'}$.

Example 3.30 The homogeneous ideal for the model in Example 3.26 equals

$$P_{\mathbf{f}} \quad = \quad \big\langle\, 4p_2^2 - 3p_2p_3 - 6p_2p_4 - 6p_2p_5 + 2p_3p_4 + 2p_3p_5 + 10p_4p_5\,, \\ 6p_1 + 3p_2 - 4p_3 - 2p_4 - 2p_5 \,\big\rangle.$$

Thus $V(P_{\mathbf{f}})$ is a quadratic surface which lies in a (three-dimensional) hyperplane. Our computation in Example 3.26 was aimed at finding the critical points of the function $p_1^{u_1} p_2^{u_2} p_3^{u_3} p_4^{u_4} p_5^{u_5}$ in the surface $V_\Delta(P_{\mathbf{f}})$. This constrained optimization problem has 16 complex critical points for generic $u_1, \ldots, u_5$. Thus the maximum likelihood degree of this quadratic surface is equal to 16.

Once we are working with statistical models in their implicitized form, there is no longer a need for the map $\mathbf{f}$. Thus we may suppose that $P \subset \mathbb{Q}[p_1, \ldots, p_m]$ be an arbitrary homogeneous ideal. The *MLE problem* for P is

$$\text{Maximize } u_1 \cdot \log(p_1) + \cdots + u_m \cdot \log(p_m) \quad \text{subject to} \quad p \in V_\Delta(P). \tag{3.27}$$

Since P is homogeneous, we can regard $V(P)$ as a variety in complex projective $(m-1)$-space $\mathbb{P}^{m-1}$. Let $\mathrm{Sing}(P)$ denote the singular locus of the projective variety $V(P)$, and let $V_{\mathbb{C}^*}(P)$ be the set of points in $V(P)$ all of whose coordinates are non-zero. We define the *likelihood locus* of P for the data u to be the set of all points in $V_{\mathbb{C}^*}(P)\backslash\mathrm{Sing}(P)$ that are critical points of the function $\sum_{j=1}^m u_j \cdot \log(p_j)$. The *maximum likelihood degree* (or *ML degree*) of the ideal P is the cardinality of the likelihood locus when u is a generic vector in $\mathbb{R}^m$.

To characterize the likelihood locus algebraically, we use the technique of *Lagrange multipliers*. Suppose that $P = \langle g_1, g_2, \ldots, g_r \rangle$ where the g_i are homogeneous polynomials in $\mathbb{Q}[p_1, p_2, \ldots, p_m]$. We consider

$$u_1 \cdot \log(p_1) + \cdots + u_m \cdot \log(p_m) + \lambda_0(1 - \sum_{i=1}^m p_i) + \lambda_1 g_1 + \cdots + \lambda_r g_r. \tag{3.28}$$

This is a function of the $m+r+1$ unknowns $p_1, \ldots, p_m, \lambda_0, \lambda_1, \ldots, \lambda_r$. A point $p \in V_{\mathbb{C}^*}(P)\backslash\mathrm{Sing}(P)$ lies in the likelihood locus if there exists $\lambda \in \mathbb{C}^{r+1}$ such that (p, λ) is a critical point of (3.28). Thus we can compute the likelihood locus (and hence the ML degree) from the ideal P using Gröbner basis elimination techniques. Details are described in [Hoşten *et al.*, 2004].

If the generators $g_1, \ldots, g_r$ of the homogeneous ideal P are chosen at random relative to their degrees $d_1, \ldots, d_r$ then the projective variety $V(P)$ is smooth of codimension r (by Bertini's Theorem), and we call $V(P)$ a *generic complete intersection*. The following formula for the ML degree is valid in this case.

Theorem 3.31 *Let $P = \langle g_1, \ldots, g_r \rangle$ be an ideal in $\mathbb{Q}[p_1, \ldots, p_m]$ where g_i is a homogeneous polynomial of degree d_i for $i = 1, \ldots, r$. Then the maximum likelihood degree of P is finite and is bounded above by*

$$\sum_{\substack{i_1+i_2+\cdots+i_r \leq m-1 \\ i_1>0,\ldots,i_r 0}} d_1^{i_1} d_2^{i_2} \cdots d_r^{i_r}.$$

Equality holds when $V(P)$ is a generic complete intersection, that is, when the coefficients of the defining polynomials $g_1, g_2, \ldots, g_r$ are chosen at random.

Proof See [Hoşten *et al.*, 2004]. $\square$

Example 3.32 Let $m = 5, r = 2$ and $P = \langle g_1, g_2 \rangle$ where g_1 and g_2 are random homogeneous polynomials of degrees d_1 and d_2 in $\mathbb{Q}[p_1, p_2, p_3, p_4, p_5]$. Then $V(P)$ is a surface in $\mathbb{P}^4$, and $V_\Delta(P)$ is either empty or is a surface in the 4-simplex Δ. The maximum likelihood degree of such a random surface equals

$$d_1 d_2 \,+\, d_1^2 d_2 + d_1 d_2^2 \,+\, d_1^3 d_2 + d_1^2 d_2^2 + d_1 d_2^3.$$

In particular, if $d_1 = 1$ and $d_2 = 2$, so $V(P)$ is a quadratic surface in a hyperplane, then the ML degree is $2 + 2 + 4 + 2 + 4 + 8 = 22$. This is to be compared with the ML degree 16 of the surface in Example 3.30. Indeed, $P_{\mathbf{f}}$ has codimension 2 and is generated by two polynomials with $d_1 = 1$ and $d_2 = 2$. But the coefficients of the two generators of $P_{\mathbf{f}}$ are not generic enough, so the ML degree drops from 22 to 16 for the specific surface $V(P_{\mathbf{f}})$.

3.4 Tropical geometry

In the first three sections of this chapter we introduced algebraic varieties and we showed how computations in algebraic geometry might be useful for statistical analysis. In this section we give an introduction to algebraic geometry in the piecewise-linear setting of the *tropical semiring* $(\mathbb{R} \cup \{\infty\}, \oplus, \odot)$.

We had our first encounter with the tropical universe in Chapter 2. While the emphasis there was on tropical *arithmetic* and its computational significance, here we aim to develop the elements of tropical *algebraic geometry*. We shall see that every algebraic variety can be tropicalized, and, since statistical models are algebraic varieties, statistical models can be tropicalized.

Let $q_1, \ldots, q_m$ be unknowns which represent elements in the tropical semiring $(\mathbb{R} \cup \{\infty\}, \oplus, \odot)$. A *monomial* is any product of these unknowns, where repetition is allowed. By commutativity, we can sort the product and write monomials in the usual notation, with the unknowns raised to exponent, e.g.,

$$q_2 \odot q_1 \odot q_3 \odot q_1 \odot q_4 \odot q_2 \odot q_3 \odot q_2 \quad = \quad q_1^2 q_2^3 q_3^2 q_4. \qquad (3.29)$$

When evaluating a tropical monomial in classical arithmetic we get a linear function in the unknowns. For instance, the monomial in (3.29) represents

$$q_2 + q_1 + q_3 + q_1 + q_4 + q_2 + q_3 + q_2 \quad = \quad 2q_1 + 3q_2 + 2q_3 + q_4.$$

Every linear function with integer coefficients arises in this manner. A *tropical polynomial* is a finite tropical linear combination of tropical monomials:

$$p(q_1, \ldots, q_m) \quad = \quad a \odot q_1^{i_1} q_2^{i_2} \cdots q_m^{i_m} \,\oplus\, b \odot q_1^{j_1} q_2^{j_2} \cdots q_m^{j_m} \,\oplus\, \cdots$$

Here the coefficients $a, b, \ldots,$ are real numbers and the exponents $i_1, j_1, \ldots$ are nonnegative integers. Every tropical polynomial represents a function g :

$\mathbb{R}^m \to \mathbb{R}$. When evaluating this function in classical arithmetic, what we get is the minimum of a finite collection of linear functions, namely,

$$g(q_1, \ldots, q_m) \quad = \quad \min\bigl(a + i_1 q_1 + \cdots + i_m q_m \,,\, b + j_1 q_1 + \cdots + j_m q_m \,,\, \ldots\bigr)$$

This function $g : \mathbb{R}^m \to \mathbb{R}$ has the following three characteristic properties:

- g is continuous,
- g is piecewise-linear, where the number of pieces is finite, and
- g is concave, i.e., $g\bigl((q+q')/2)\bigr) \geq \frac{1}{2}(g(q) + g(q'))$ for all $q, q' \in \mathbb{R}^m$.

Every function $g : \mathbb{R}^m \to \mathbb{R}$ which satisfies these three properties can be represented as the minimum of a finite collection of linear functions. We conclude:

Proposition 3.33 *The tropical polynomials in n unknowns $q_1, \ldots, q_m$ are the piecewise-linear concave functions on $\mathbb{R}^m$ with non-negative integer coefficients.*

Example 3.34 Let $m = 1$, so we are considering tropical polynomials in one variable q. A general cubic polynomial has the form

$$g(q) \quad = \quad a \odot q^3 \;\oplus\; b \odot q^2 \;\oplus\; c \odot q \;\oplus\; d \qquad \text{where } a, b, c, d \in \mathbb{R}. \tag{3.30}$$

To graph this function we draw four lines in the (q, q') plane: $q' = 3q + a$, $q' = 2q + b$, $q' = q + c$ and the horizontal line $q' = d$. The value of $g(q)$ is the smallest q-value such that (q, q') is on of these four lines, i.e., the graph of $g(q)$ is the lower envelope of the lines. All four lines actually contribute if

$$b - a \;\leq\; c - b \;\leq d - c. \tag{3.31}$$

These three values of q are the breakpoints where $g(q)$ fails to be linear, and the cubic has a corresponding factorization into three linear factors:

$$g(q) \quad = \quad a \odot (q \,\oplus\, (b-a)) \odot (q \,\oplus\, (c-b)) \odot (q \,\oplus\, (d-c)). \tag{3.32}$$

Generalizing this example, we can see that every tropical polynomial function in one unknown q can be written as a tropical product of tropical linear functions. This representation is essentially unique. In other words, the *Fundamental Theorem of Algebra* (Theorem 3.1) holds for tropical polynomials.

Example 3.35 The factorization of tropical polynomials in $m \geq 2$ unknowns into irreducible tropical polynomials is not unique. Here is a simple example:

$$\begin{aligned} &(0 \odot q_1 \,\oplus\, 0) \;\odot\; (0 \odot q_2 \,\oplus\, 0) \;\odot\; (0 \odot q_1 \odot q_2 \,\oplus\, 0) \\ =\;\; &(0 \odot q_1 \odot q_2 \,\oplus\, 0 \odot q_1 \,\oplus\, 0) \odot (0 \odot q_1 \odot q_2 \,\oplus\, 0 \odot q_2 \,\oplus\, 0). \end{aligned}$$

Do not be alarmed by the zeros. Zero is the multiplicatively neutral element! This identity is equivalent to an identity in the *polytope algebra* (Section 2.3): a regular hexagon factors either into two triangles or into three line segments.

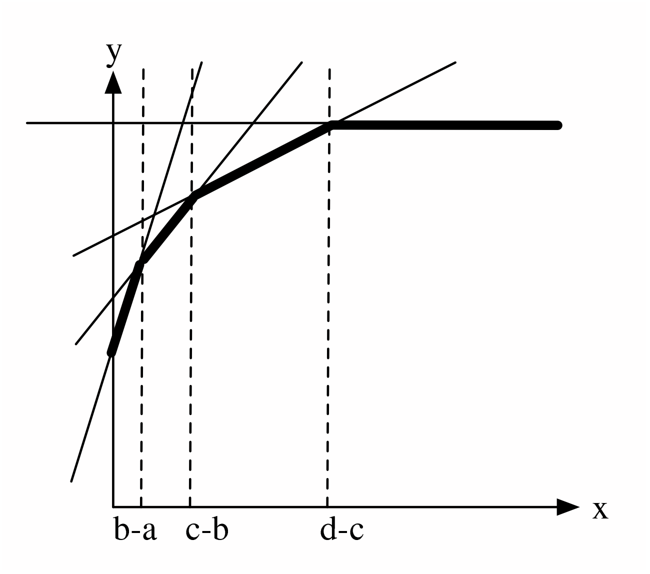

,

Fig. 3.2. The graph of a tropical cubic polynomial and its roots

A tropical polynomial function $g : \mathbb{R}^m \to \mathbb{R}$ is given as the minimum of a finite set of linear functions. We define the *tropical hypersurface* $\mathcal{T}(g)$ to be the set of all points $q \in \mathbb{R}^m$ at which this minimum is attained at least twice at q. Equivalently, a point $q \in \mathbb{R}^m$ lies in the hypersurface $\mathcal{T}(g)$ if and only if g is not linear at q. For example, if $m = 1$ and p is the cubic in (3.30) with the assumption (3.31), then $\mathcal{T}(g)$ is the set of breakpoints, $\{ b - a,\, c - b,\, d - c \}$.

We next consider the case $m = 2$ of a tropical polynomial in two variables:

$$g(q_1, q_2) \quad = \quad \bigoplus_{(i,j)} c_{ij} \odot q_1^i \odot q_2^j.$$

Proposition 3.36 *The tropical curve $\mathcal{T}(g)$ is a finite graph which is embedded in the plane $\mathbb{R}^2$. It has both bounded and unbounded edges, all edge directions are rational, and $\mathcal{T}(g)$ satisfies the* zero tension condition.

The zero tension condition means the following. Consider any node p of the graph. Then the edges adjacent to p lie on lines with rational slopes. For each such line emanating from the origin consider the first non-zero lattice vector on that line. *Zero tension* at p means that the sum of these vectors is zero.

Here is a general method for drawing a tropical curve $\mathcal{T}(g)$ in the plane. Consider any term $\gamma \odot q_1^i \odot q_2^j$ appearing in the polynomial p. We represent this term by the point (γ, i, j) in $\mathbb{R}^3$, and we compute the convex hull of these points in $\mathbb{R}^3$. Now project the lower envelope of that convex hull into the plane under the map $\mathbb{R}^3 \to \mathbb{R}^2$, $(\gamma, i, j) \mapsto (i, j)$. The image is a planar convex

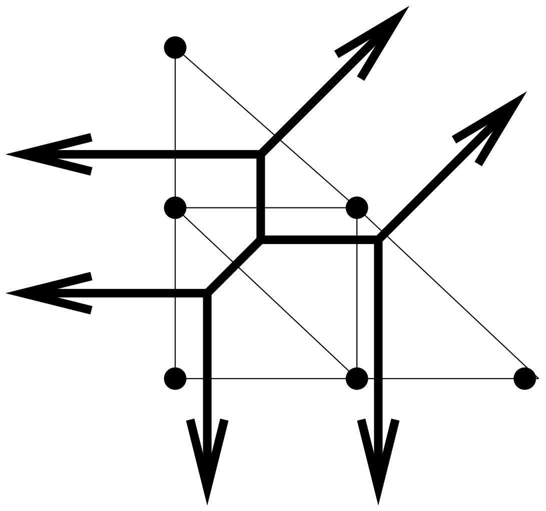

Fig. 3.3. The subdivision of Δ and the tropical curve

polygon together with a distinguished subdivision Δ into smaller polygons. The tropical curve $\mathcal{T}(g)$ is a graph which is dual to this subdivision.

Example 3.37 Consider the general quadratic polynomial

$$g(q_1, q_2) \quad = \quad a \odot q_1^2 \;\oplus\; b \odot q_1 q_2 \;\oplus\; c \odot q_2^2 \;\oplus\; d \odot q_1 \;\oplus\; e \odot q_2 \;\oplus\; f.$$

Then Δ is a subdivision of the triangle with vertices $(0, 0)$, $(0, 2)$ and $(2, 0)$. The lattice points $(0, 1)$, $(1, 0)$, $(1, 1)$ are allowed to be used as vertices in these subdivisions. Assuming that $a, b, c, d, e, f \in \mathbb{R}$ satisfy

$$2b < a + c\,,\; 2d < a + f\,,\; 2e < c + f,$$

the subdivision Δ consists of four triangles, three interior edges and six boundary edges. The tropical quadratic curve $\mathcal{T}(g)$ has four vertices, three bounded edges and six half-rays (two northern, two eastern and two southwestern). In Figure 3.4, $\mathcal{T}(g)$ is shown in bold and the subdivision of Δ is in thin lines.

It is known that tropical hypersurfaces $\mathcal{T}(g)$ intersect and interpolate like algebraic hypersurfaces do. For instance, two lines in the plane meet in one point, a line and a quadric meet in two points, two quadrics meet in four points, etc.... Also, two general points lie on a unique line, five general points lie on a unique quadric, etc... For a general discussion of Bézout's Theorem in tropical algebraic geometry, and for pictures illustrating these facts we refer to [Sturmfels, 2002, §9] and [Richter-Gebert *et al.*, 2003].

It is tempting to define tropical varieties as intersections of tropical hypersurfaces. But this is not quite the right definition to retain the desired properties from classical algebraic geometry. What we do instead is to utilize the field $\mathbb{Q}(\epsilon)$ of rational functions in one variable ϵ. We think of ϵ as a positive infinitesimal. Any non-zero rational function $c(\epsilon) \in \mathbb{Q}(\epsilon)$ has a series expansion

$$c(\epsilon) \;=\; \alpha_0\epsilon^{i_0} + \alpha_1\epsilon^{i_1}\alpha_2\epsilon^{i_2} + \cdots \quad (\text{where } i_0, i_1, \ldots \in \mathbb{Z},\ \alpha_0, \alpha_1, \ldots \in \mathbb{Q}\,, \alpha_0 \neq 0)$$

This series is unique. The *order* of the rational function $c(\epsilon)$ is the integer i_0.

Example 3.38 The following rational function in $\mathbb{Q}(\epsilon)$ has $\operatorname{order}(c(\epsilon)) = -2$:

$$c(\epsilon) \quad = \quad \frac{3\epsilon^4 + 8\epsilon^5 + \epsilon^7 - \epsilon^{10}}{17\epsilon^6 - 11\epsilon^9 + 2\epsilon^{13}} \quad = \quad \frac{3}{17}\epsilon^{-2} + \frac{8}{17}\epsilon^{-1} + \frac{50}{289}\epsilon^{1} + \frac{88}{289}\epsilon^{2} + \cdots$$

Let $\mathbb{Q}(\epsilon)[p_1, \ldots, p_m]$ be the ring of polynomials in m unknowns with coefficients in $\mathbb{Q}(\epsilon)$. For any (classical) polynomial

$$f \quad = \quad \sum_{i=1}^{s} c_i(\epsilon) \cdot p_1^{a_{1i}} p_2^{a_{2i}} \cdots p_m^{a_{mi}} \qquad \in \quad \mathbb{Q}(\epsilon)[p_1, \ldots, p_m], \tag{3.33}$$

we define the *tropicalization* $g = \operatorname{trop}(f)$ to be the tropical polynomial

$$g \quad = \quad \bigoplus_{i=1}^{s} \operatorname{order}(c_i(\epsilon)) \odot q_1^{a_{1i}} \odot q_2^{a_{2i}} \odot \cdots \odot q_m^{a_{mi}}. \tag{3.34}$$

In this manner, every polynomial f defines a tropical hypersurface $\mathcal{T}(g) = \mathcal{T}\big(\operatorname{trop}(f)\big)$ in $\mathbb{R}^m$. Recall that the function $g : \mathbb{R}^m \to \mathbb{R}$ is given as the minimum of s linear functions. The hypersurface $\mathcal{T}(g)$ consists of all points $q = (q_1, \ldots, q_m) \in \mathbb{R}^m$ where this minimum is attained at least twice, i.e.,

$$\begin{aligned} & \operatorname{order}(c_i(\epsilon)) + a_{1i}q_1 + \cdots + a_{mi}q_m \;=\; \operatorname{order}(c_j(\epsilon)) + a_{1j}q_1 + \cdots + a_{mj}q_m \\ \leq \quad & \operatorname{order}(c_k(\epsilon)) + a_{1k}q_1 + \cdots + a_{mk}q_m \quad \text{for } i \neq j \text{ and } k \in \{1, \ldots, s\} \backslash \{i, j\}. \end{aligned}$$

If, in addition to this condition, the leading coefficients α_0 of the series $c_i(\epsilon)$ and $c_j(\epsilon)$ are rational numbers of opposite signs then we say that q is a *positive point* of $\mathcal{T}(g)$. The subset of all positive points in $\mathcal{T}(g)$ is denoted $\mathcal{T}_+(g)$ and called the *positive tropical hypersurface* of the polynomial f.

If the polynomial f in (3.33) does not depend on ϵ at all, i.e., if $f \in \mathbb{Q}[p_1, \ldots, p_m]$, then $\operatorname{order}(c_i(\epsilon)) = 0$ for all coefficients of its tropicalization g in (3.34), and the function $g : \mathbb{R}^m \to \mathbb{R}$ is given as the minimum of s linear functions with zero constant terms. Here is an example where this is the case.

Example 3.39 Let $m = 9$ and consider the determinant of a 3×3-matrix

$$f \quad = \quad p_{11}p_{22}p_{33} - p_{11}p_{23}p_{32} - p_{12}p_{21}p_{33} + p_{12}p_{23}p_{31} + p_{13}p_{21}p_{32} - p_{13}p_{22}p_{31}.$$

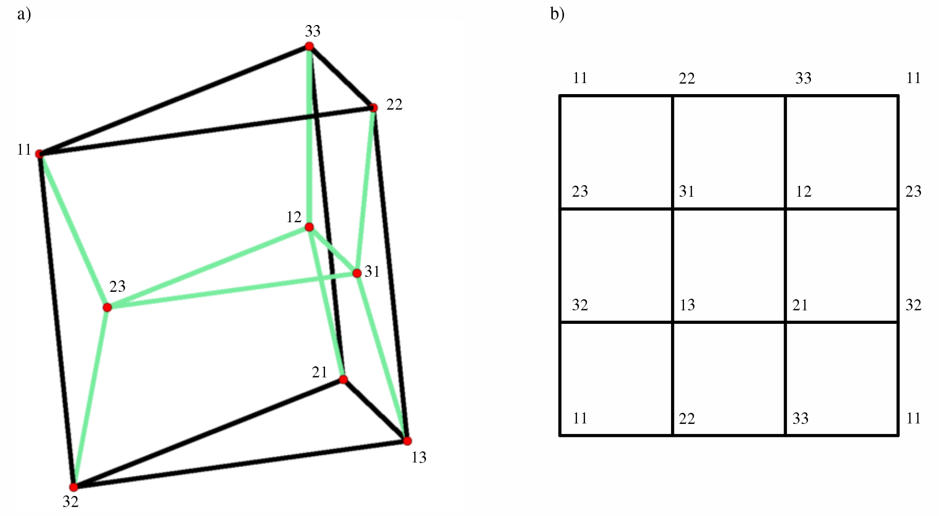

Fig. 3.4. The tropical 3×3 determinant

Its tropicalization is the *tropical determinant*

$$
\begin{aligned}
g \quad = \quad & q_{11} \odot q_{22} \odot q_{33} \;\oplus\; q_{11} \odot q_{23} \odot q_{32} \;\oplus\; q_{12} \odot q_{21} \odot q_{33} \\
\oplus\; & q_{12} \odot q_{23} \odot q_{31} \;\oplus\; q_{13} \odot q_{21} \odot q_{32} \;\oplus\; q_{13} \odot q_{22} \odot q_{31}.
\end{aligned}
$$

Evaluating g at a 3×3-matrix (q_{ij}) means solving the *assignment problem* of finding a permutation σ of $\{1,2,3\}$ whose weight $q_{1\sigma_1} + q_{2\sigma_2} + q_{3\sigma_3}$ is minimal (Remark 2.6). The tropical hypersurface $\mathcal{T}(g)$ consists of all matrices $q \in \mathbb{R}^{3\times 3}$ for which the minimum weight permutation is not unique. Working modulo the five-dimensional space of all 3×3-matrices (q_{ij}) with zero row sums and zero column sums, the tropical hypersurface $\mathcal{T}(g)$ is a three-dimensional polyhedral fan sitting in a four-dimensional space. If we intersect this fan with a 3-sphere around the origin, then we get a two-dimensional polyhedral complex consisting of six triangles and nine quadrangles. This complex consists of all 2-faces of the product of two triangles, labeled as in Figure 3.4. This complex is a bouquet of five 2-spheres. The positive tropical variety $\mathcal{T}^+(g)$ is the subcomplex consisting of the nine quadrangles shown in Figure 3.4. Note that $\mathcal{T}^+(g)$ is a torus.

Every *tropical algebraic variety* is derived from an ideal I in the polynomial ring $\mathbb{Q}(\epsilon)[p_1, \ldots, p_m]$. Namely, we define $\mathcal{T}(I)$ as the intersection of the tropical hypersurfaces $\mathcal{T}\big(\mathrm{trop}(f)\big)$ where f runs over the ideal I. Likewise, the *positive tropical variety* $\mathcal{T}_+(I)$ is the intersection of the positive tropical hypersurfaces $\mathcal{T}_+\big(\mathrm{trop}(f)\big)$ where f runs over I. In these definitions it suffices to let f run over a certain finite subset of the ideal I. Such a subset is called a *tropical basis* of I. From this finiteness property, it follows that $\mathcal{T}(I)$ and $\mathcal{T}_+(I)$ are *finite unions of convex polyhedra*. This means they are characterized by finite Boolean combinations of linear inequalities. Finding a tropical basis from given generators of an ideal I and computing the polyhedra that make up its tropical variety is an active topic of research in tropical geometry.

Example 3.40 We consider the tropicalization of DiaNA's model in Example 1.16. The 3×3-minors of a 4×4-matrix of unknowns form a tropical basis for the ideal they generate. This follows from results in [Develin *et al.*, 2003]. The tropical variety $\mathcal{T}(I)$ consists of all 4×4-matrices of tropical rank at most two. The positive tropical variety $\mathcal{T}_+(I)$ consists of all 4×4-matrices of Barvinok rank at most two. See [Develin and Sturmfels, 2004] for a topological study of these spaces and their generalizations to larger matrices.

Let $\mathbf{f} : \mathbb{C}^d \to \mathbb{C}^m$ be a polynomial map with coordinates $f_1, \ldots, f_m \in \mathbb{Q}[\theta_1, \ldots, \theta_d]$. We say that the map $\mathbf{f}$ is *positive* if each coefficient of each polynomial f_i is a positive real number. If this holds then $\mathbf{f}$ maps positive vectors in $\mathbb{R}^d$ to positive vectors in $\mathbb{R}^m$. We say that the map $\mathbf{f}$ is *surjectively positive* if $\mathbf{f}$ is positive and, in addition, $\mathbf{f}$ maps the positive orthant surjectively onto the positive points in the image, in symbols,

$$\mathbf{f}\big(\mathbb{R}^d_{>0}\big) \quad = \quad \mathrm{image}(\mathbf{f}) \cap \mathbb{R}^m_{>0}. \tag{3.35}$$

Example 3.41 Let $d = 1, m = 2$ and $\mathbf{f} : \mathbb{R}^1 \mapsto \mathbb{R}^2$, $\theta \mapsto (\,\theta + 2,\, 2\theta + 1\,)$. The map $\mathbf{f}$ is positive. But $\mathbf{f}$ is not surjectively positive: for instance, the point $(7/4, 1/2)$ is in $\mathrm{image}(\mathbf{f}) \cap \mathbb{R}^2_{>0}$ but not in $\mathbf{f}(\mathbb{R}^1_{>0})$.

On the other hand, if we take $\mathbf{f}' : \mathbb{R}^1 \mapsto \mathbb{R}^2$, $\theta \mapsto (\,\frac{1}{2}\theta + \frac{3}{2}\,,\, \theta\,)$ then $\mathbf{f}'$ is surjectively positive. Both maps have the same image, namely, $\mathrm{image}(\mathbf{f}) = \mathrm{image}(\mathbf{f}')$ is the line $V(I_\mathbf{f}) \subset \mathbb{R}^2$ which is specified by the ideal

$$I_\mathbf{f} \;=\; I_{\mathbf{f}'} \;=\; \langle\, 2p_1 - p_2 - 3\,\rangle.$$

The tropical variety $\mathcal{T}(I_\mathbf{f})$ is the curve defined by the tropical linear form

$$\mathrm{trop}(2p_1 - p_2 - 3) \quad = \quad q_1 \oplus q_2 \oplus 0.$$

This tropical line is the union of three half-rays:

$$\mathcal{T}(I_\mathbf{f}) \;=\; \big\{(\varphi, 0) : \varphi \in \mathbb{R}_{\geq 0}\big\} \,\cup\, \big\{(0, \varphi) : \varphi \in \mathbb{R}_{\geq 0}\big\} \,\cup\, \big\{(-\varphi, -\varphi) : \varphi \in \mathbb{R}_{\geq 0}\big\}.$$

Let $\mathbf{g} : \mathbb{R}^1 \to \mathbb{R}^2$ be the tropicalization of the linear map $\mathbf{f} : \mathbb{R}^1 \to \mathbb{R}^2$, and let $\mathbf{g}'$ be the tropicalization of $\mathbf{f}'$. These piecewise-linear maps are given by

$$\mathbf{g}(w) = \big(\mathrm{trop}(f_1)(w), \mathrm{trop}(f_2)(w)\big) = (w \oplus 0, w \oplus 0) = (\min(w,0), \min(w,0))$$

$$\text{and} \quad \mathbf{g}'(w) \;=\; \big(\mathrm{trop}(f_1')(w), \mathrm{trop}(f_2')(w)\big) \;=\; \big(w \oplus 0,\, w\,\big) \;=\; \big(\min(w,0),\, w\,\big).$$

These map $\mathbb{R}^1$ onto one or two of the three halfrays of the tropical line $\mathcal{T}(I_{\mathbf{f}})$:

$$\begin{aligned} \mathrm{image}(\mathbf{g}) \quad &= \quad \big\{(-\varphi, -\varphi) : \varphi \in \mathbb{R}_{\geq 0}\big\}, \\ \mathrm{image}(\mathbf{g}') \quad &= \quad \big\{(0, \varphi) : \varphi \in \mathbb{R}_{\geq 0}\big\} \;\cup\; \big\{(-\varphi, -\varphi) : \varphi \in \mathbb{R}_{\geq 0}\big\} \;=\; \mathcal{T}_+(I_{\mathbf{f}}). \end{aligned}$$

The tropicalization $\mathbf{g}'$ of the surjectively positive map $\mathbf{f}'$ maps onto the positive tropical variety. This is an example for the result in Theorem 3.42 below.

Returning to our general discussion, consider an arbitrary polynomial map $\mathbf{f} : \mathbb{C}^d \to \mathbb{C}^m$. The *tropicalization* of $\mathbf{f}$ is the piecewise-linear map

$$\mathbf{g} \,:\, \mathbb{R}^d \,\to\, \mathbb{R}^m\,, \quad \varphi \,\mapsto\, \big(g_1(\varphi), g_2(\varphi), \ldots, g_m(\varphi)\big), \tag{3.36}$$

where $g_i = \mathrm{trop}(f_i)$ is the tropicalization of the ith coordinate polynomial f_i of $\mathbf{f}$. To describe the geometry of the tropical polynomial map $\mathbf{g}$, we consider the Newton polytopes $\mathrm{NP}(f_1), \mathrm{NP}(f_2), \ldots, \mathrm{NP}(f_m)$ of the coordinates of $\mathbf{f}$. Recall from Section 2.3 that the *Newton polytope* $\mathrm{NP}(f_i)$ of the polynomial f_i is the convex hull of the vectors $(u_1, u_2, \ldots, u_d)$ such that $\theta_1^{u_1}\theta_2^{u_2}\cdots\theta_d^{u_d}$ appears with non-zero coefficient in f_i. The cones in the normal fan of the Newton polytope $\mathrm{NP}(f_i)$ are the domains of linearity of the piecewise-linear map $g_i : \mathbb{R}^d \to \mathbb{R}^m$. The *Newton polytope of the map* $\mathbf{f}$ is defined as the Newton polytope of the product of the coordinate polynomials:

$$\mathrm{NP}(\mathbf{f}) \;:=\; \mathrm{NP}(f_1 \cdot f_2 \cdot \cdots \cdot f_m) \;=\; \mathrm{NP}(f_1) \odot \mathrm{NP}(f_2) \odot \cdots \odot \mathrm{NP}(f_m). \tag{3.37}$$

The operation $\odot$ on the right is the Minkowski sum of polytopes (Theorem 2.25). The following theorem describes the geometry of tropicalizing polynomial maps.

Theorem 3.42 *The tropical polynomial map* $\mathbf{g} : \mathbb{R}^d \to \mathbb{R}^m$ *is linear on each cone in the normal fan of the Newton polytope* $\mathrm{NP}(\mathbf{f})$*. Its image lies inside the tropical variety* $\mathcal{T}(I_{\mathbf{f}})$*. If* $\mathbf{f}$ *is positive then* $\mathrm{image}(\mathbf{g})$ *lies in the positive tropical variety* $\mathcal{T}_+(I_{\mathbf{f}})$*. If* $\mathbf{f}$ *is surjectively positive then* $\mathrm{image}(\mathbf{g}) = \mathcal{T}_+(I_{\mathbf{f}})$*.*

Proof See [Pachter and Sturmfels, 2004c] and [Speyer and Williams, 2004]. □

This theorem is fundamental for the study of inference functions of statistical models in Chapter 9. Imagine that $w \in \mathbb{R}^d$ is a vector of weights for a dynamic programming problem which is derived from a statistical model. The relationship between the weights and the model parameters is $w_i \sim \log(\theta_i)$. Evaluating the tropical map $\mathbf{g}$ at w means solving the dynamic programs for all possible observations. As we vary the weights w, the vector of outcomes is piecewise constant. Whenever w crosses a boundary, the system undergoes a "phase transition", meaning that the outcome changes for some observation. Theorem 3.42 offers a geometric characterization of these phase transitions, taking into account all possible weights and all possible observations.

If the model has only one parameter, then the Newton polytope $\mathrm{NP}(\mathbf{f})$ is a line segment. There are only two "phases", corresponding to the two vertices of that segment. In Example 3.41 the "phase transition" occurs at $w = 0$.

One important application of this circle of ideas is sequence alignment (Section 2.2). The statistical model for alignment is the pair HMM $\mathbf{f}$ in (2.15). The tropicalization $\mathbf{g}$ of the polynomial map $\mathbf{f}$ is the tropicalized pair HMM, whose coordinates g_i are featured in (2.16). Parametric alignment is discussed in Chapters 5, 7, 8 and 9. We conclude this section with two other examples.

Example 3.43 DiaNA's model in Example 3.40 has $d = 16$ parameters

$$\theta \quad = \quad \big(\beta^1_A, \beta^1_C, \beta^1_G, \beta^1_T, \beta^2_A, \beta^2_C, \beta^2_G, \beta^2_T, \gamma^1_A, \gamma^1_C, \gamma^1_G, \gamma^1_T, \gamma^2_A, \gamma^2_C, \gamma^2_G, \gamma^2_T\big),$$

and it is specified by the homogeneous polynomial map $\mathbf{f} : \mathbb{C}^{16} \mapsto \mathbb{C}^{4\times 4}$ with

$$p_{ij} \quad = \quad \beta^1_i \beta^2_j + \gamma^1_i \gamma^2_j, \qquad \text{where } i, j \in \{\mathtt{A}, \mathtt{C}, \mathtt{G}, \mathtt{T}\}.$$

We know from the linear algebra literature [Cohen and Rothblum, 1993] that every positive 4×4-matrix of rank ≤ 2 is the sum of two positive 4×4-matrices of rank ≤ 1. This means that DiaNA's model $\mathbf{f}$ is a surjectively positive map. The tropicalization of $\mathbf{f}$ is the piecewise-linear map $\mathbf{g} : \mathbb{R}^{16} \mapsto \mathbb{R}^{4\times 4}$ given by

$$q_{ij} \;=\; \beta^1_i \odot \beta^2_j \;\oplus\; \gamma^1_i \odot \gamma^2_j \;=\; \min\big(\beta^1_i + \beta^2_j,\, \gamma^1_i + \gamma^2_j\big) \quad \text{for } i, j \in \{\mathtt{A}, \mathtt{C}, \mathtt{G}, \mathtt{T}\}.$$

Theorem 3.42 says that the image of $\mathbf{g}$ equals the positive tropical variety $\mathcal{T}_+(I_{\mathbf{g}})$. The space $\mathcal{T}_+(I_{\mathbf{g}})$ consists of all 4×4-matrices of *Barvinok rank* ≤ 2 and was studied in [Develin *et al.*, 2003] and [Develin and Sturmfels, 2004]. The Newton polytope $\mathrm{NP}(\mathbf{f})$ of the map $\mathbf{f}$ is a *zonotope*, i.e., it is a Minkowski sum of line segments. The map $\mathbf{g}$ is piecewise linear with respect to the hyperplane arrangement dual to that zonotope. For a detailed combinatorial study of the map $\mathbf{g}$ and the associated hyperplane arrangement see [Ardila, 2004].

Example 3.44 We consider the hidden Markov model of length $n = 3$ with binary states ($l = l' = 2$) but, in contrast to Example 3.19, we suppose that all eight parameters $\theta_{00}, \theta_{01}, \theta_{10}, \theta_{11}, \theta'_{00}, \theta'_{01}, \theta'_{10}, \theta'_{11}$ are independent unknowns.

Thus our model is the homogeneous map $\mathbf{f} : \mathbb{C}^8 \to \mathbb{C}^8$ with coordinates

$$\begin{aligned} f_{\sigma_1\sigma_2\sigma_3} \quad = \quad & \theta_{00}\theta_{00}\theta'_{0\sigma_1}\theta'_{0\sigma_2}\theta'_{0\sigma_3} + \theta_{00}\theta_{01}\theta'_{0\sigma_1}\theta'_{0\sigma_2}\theta'_{1\sigma_3} + \theta_{01}\theta_{10}\theta'_{0\sigma_1}\theta'_{1\sigma_2}\theta'_{0\sigma_3} \\ & + \theta_{01}\theta_{11}\theta'_{0\sigma_1}\theta'_{1\sigma_2}\theta'_{1\sigma_3} + \theta_{10}\theta_{00}\theta'_{1\sigma_1}\theta'_{0\sigma_2}\theta'_{0\sigma_3} + \theta_{10}\theta_{01}\theta'_{1\sigma_1}\theta'_{0\sigma_2}\theta'_{1\sigma_3} \\ & + \theta_{11}\theta_{10}\theta'_{1\sigma_1}\theta'_{1\sigma_2}\theta'_{0\sigma_3} + \theta_{11}\theta_{11}\theta'_{1\sigma_1}\theta'_{1\sigma_2}\theta'_{1\sigma_3}. \end{aligned}$$

The implicitization techniques of Section 3.2 reveal that $I_{\mathbf{f}}$ is generated by

$$\begin{gathered} p_{011}^2 p_{100}^2 - p_{001}^2 p_{110}^2 + p_{000}p_{011}p_{101}^2 - p_{000}p_{101}^2 p_{110} + p_{000}p_{011}p_{110}^2 \\ -p_{001}p_{010}^2 p_{111} + p_{001}^2 p_{100}p_{111} + p_{010}^2 p_{100}p_{111} - p_{001}p_{100}^2 p_{111} - p_{000}p_{011}^2 p_{110} \\ -p_{001}p_{011}p_{100}p_{101} - p_{010}p_{011}p_{100}p_{101} + p_{001}p_{010}p_{011}p_{110} - p_{010}p_{011}p_{100}p_{110} \\ +p_{001}p_{010}p_{101}p_{110} + p_{001}p_{100}p_{101}p_{110} + p_{000}p_{010}p_{011}p_{111} - p_{000}p_{011}p_{100}p_{111} \\ -p_{000}p_{001}p_{101}p_{111} + p_{000}p_{100}p_{101}p_{111} + p_{000}p_{001}p_{110}p_{111} - p_{000}p_{010}p_{110}p_{111}. \end{gathered}$$

Thus $\mathcal{T}(I_{\mathbf{f}})$ is the tropical hypersurface defined by this degree four polynomial. The tropicalized HMM is the map $\mathbf{g} : \mathbb{R}^8 \to \mathbb{R}^8$, $(w, w') \mapsto q$ with coordinates

$$q_{\sigma_1\sigma_2\sigma_3} \;=\; \min\big\{\, w_{h_1h_2} + w_{h_2h_3} + w'_{h_1\sigma_1} + w'_{h_2\sigma_2} + w'_{h_3\sigma_3} \;:\; (h_1,h_2,h_3) \in \{0,1\}^3 \,\big\}.$$

This minimum is attained by the most likely explanation $(\hat{h}_1, \hat{h}_2, \hat{h}_3)$ of the observation $(\sigma_1, \sigma_2, \sigma_3)$. *Inference* means evaluating the tropical polynomials $q_{\sigma_1\sigma_2\sigma_3}$. For instance, for the parameters $w = \left(\begin{smallmatrix} 6 & 5 \\ 8 & 1 \end{smallmatrix}\right)$ and $w' = \left(\begin{smallmatrix} 0 & 8 \\ 8 & 8 \end{smallmatrix}\right)$ we find:

The observation	$\sigma_1\sigma_2\sigma_3$	$=$	000	001	010	011	100	101	110	111
has the explanation	$\hat{h}_1\hat{h}_2\hat{h}_3$	$=$	000	001	000	011	000	111	110	111

We call $\{0,1\}^3 \to \{0,1\}^3$, $\sigma_1\sigma_2\sigma_3 \mapsto \hat{h}_1\hat{h}_2\hat{h}_3$ the *inference function* for the parameters (w, w'). There are $8^8 = 16,777,216$ functions from $\{0,1\}^3$ to itself, but only 398 of them are inference functions. In Chapter 9 it is shown that the number of inference functions is polynomial in the sequence length n, while the number of functions from $\{0,1\}^n$ to itself is doubly-exponential in n.

The inference functions are indexed by the vertices of the Newton polytope $\mathrm{NP}(\mathbf{f})$. In our example, `polymake` reveals that $\mathrm{NP}(\mathbf{f})$ is 5-dimensional and has 398 vertices, 1136 edges, 1150 two-faces, 478 ridges and 68 facets. Thus there are 398 inference functions, and we understand their phase transitions.

However, there are still many questions we do not yet know how to answer, even for small n. What is the most practical method for listing all maximal cones in the image of $\mathbf{g}$? How does the number of these cones compare to the number of vertices of $\mathrm{NP}(\mathbf{f})$? Is the hidden Markov model $\mathbf{f}$ surjectively positive? Which points of the positive tropical variety $\mathcal{T}_+(I_{\mathbf{f}})$ lie in image$(\mathbf{g})$?

3.5 The tree of life and other tropical varieties

At the 1998 International Congress of Mathematicians in Zürich, Andreas Dress presented an invited lecture titled “The tree of life and other affine buildings” [Dress and Terhalle, 1998]. Our section title is meant as a reference to that paper, which highlighted the importance and utility of understanding the geometry and structure of phylogenetic trees and networks. In Chapter 4, we return to this topic by explaining how the space of trees and its generalizations is relevant for modeling and reconstructing the tree of life.

Here we begin with a reminder of the definition of metrics and tree metrics, which were introduced in Section 2.4. A *metric* on $[n] = \{1, 2, \ldots, n\}$ is a dissimilarity map for which the triangle inequality holds. Of course, most metrics D are not tree metrics. The set of tree metrics is the *space of trees* $\mathcal{T}_n$. This is a $(2n-3)$-dimensional polyhedral fan inside $\binom{n}{2}$-dimensional cone of all metrics. Membership in $\mathcal{T}_n$ is characterized by the *Four Point Condition.* Our goal here is to derive an interpretation of $\mathcal{T}_n$ in tropical geometry.

Let $Q = (q_{ij})$ be a symmetric matrix with zeros on the diagonal whose $\binom{n}{2}$ distinct off-diagonal entries are unknowns. For each quadruple $\{i, j, k, l\} \subset \{1, 2, \ldots, n\}$ we consider the quadratic tropical polynomial

$$g_{ijkl}(Q) \quad = \quad q_{ij} \odot q_{kl} \;\oplus\; q_{ik} \odot q_{jl} \;\oplus\; q_{il} \odot q_{jk}. \tag{3.38}$$

This tropical polynomial is the tropicalization of the Plücker relation (3.14)

$$g_{ijkl}(Q) \quad = \quad \mathrm{trop}(p_{ik}p_{jl} - p_{ij}p_{kl} - p_{il}p_{jk})$$

which defines a tropical hypersurface $\mathcal{T}(g_{ijkl})$ in the space $\mathbb{R}^{\binom{n}{2}}$. In fact, the Plücker relations (3.14) form a tropical basis for the Plücker ideal $I_{2,n}$ [Speyer and Sturmfels, 2004]. This implies that the *tropical Grassmannian* $\mathcal{T}(I_{2,n})$ equals the intersection of these $\binom{n}{4}$ tropical hypersurfaces, i.e.,

$$\mathcal{T}(I_{2,n}) \quad = \bigcap_{1\le i<j<k<l\le n} \mathcal{T}(g_{ijkl}) \quad \subset \quad \mathbb{R}^{\binom{n}{2}}. \tag{3.39}$$

Theorem 3.45 *The space of trees $\mathcal{T}_n$ is (up to sign) the tropical Grassmannian $\mathcal{T}(I_{2,n})$.*

Proof A metric $D = (d_{ij})$ is a point in the space of trees $\mathcal{T}_n$ if and only if the four point condition holds. This condition states that, for all $1 \le i < j < k < l \le n$, the *maximum* of $\{d_{ij} + d_{kl},\, d_{ik} + d_{jl},\, d_{il} + d_{jk}\}$ is attained at least twice. If $Q = (q_{ij}) = -D = (-d_{ij})$ then this is equivalent to saying that the *minimum* of $\{q_{ij} + q_{kl},\, q_{ik} + q_{jl},\, q_{il} + q_{jk}\}$ is attained at least twice. This is precisely the condition for Q to be in the tropical hypersurface $\mathcal{T}(g_{ijkl})$. $\square$

Example 3.46 The space of trees on five taxa $[5] = \{1, 2, 3, 4, 5\}$ is (up to sign) a tropical variety of codimension three in $\mathbb{R}^{10}$. It is not the intersection of three tropical hypersurfaces, but it is the intersection of five hypersurfaces:

$$\begin{array}{rcrcl} \mathcal{T}(I_{2,5}) & = & -\mathcal{T}_5 & = & \mathcal{T}(q_{12} \odot q_{34} \;\oplus\; q_{13} \odot q_{24} \;\oplus\; q_{14} \odot q_{23}) \\ & & & \cap & \mathcal{T}(q_{12} \odot q_{35} \;\oplus\; q_{13} \odot q_{25} \;\oplus\; q_{15} \odot q_{23}) \\ & & & \cap & \mathcal{T}(q_{12} \odot q_{45} \;\oplus\; q_{14} \odot q_{25} \;\oplus\; q_{15} \odot q_{24}) \\ & & & \cap & \mathcal{T}(q_{13} \odot q_{45} \;\oplus\; q_{14} \odot q_{35} \;\oplus\; q_{15} \odot q_{34}) \\ & & & \cap & \mathcal{T}(q_{23} \odot q_{45} \;\oplus\; q_{24} \odot q_{35} \;\oplus\; q_{25} \odot q_{34}). \end{array}$$

The space of trees $\mathcal{T}_5$ is the union of 15 seven-dimensional cones in $\mathbb{R}^{10}_{\geq 0}$. Each cone is the solution set to a system of linear inequalities such as

$$\begin{array}{rrcrcl} & q_{12} + q_{34} & \geq & q_{13} + q_{24} & = & q_{14} + q_{23}, \\ & q_{12} + q_{35} & \geq & q_{13} + q_{25} & = & q_{15} + q_{23}, \\ & q_{12} + q_{45} & \geq & q_{14} + q_{25} & = & q_{15} + q_{24}, \\ & q_{13} + q_{45} & \geq & q_{14} + q_{35} & = & q_{15} + q_{34}, \\ \text{and} & q_{23} + q_{45} & \geq & q_{24} + q_{35} & = & q_{25} + q_{34}. \end{array}$$

The seven-dimensional cone specified by this linear system is isomorphic to $\mathbb{R}^{7}_{\geq 0}$, and corresponds to the tree with splits $(12, 345)$ and $(123, 45)$.

The combinatorial structure of the space $\mathcal{T}_5$ is that of the *Petersen graph*, shown in Figure 3.5. Vertices of the Petersen graph correspond to trees with *polytomy*, i.e trees with internal vertices of degree at least 4. The edges correspond to the seven-dimensional cones in $\mathcal{T}_5$. Two cones share a six-dimensional facet if and only if the two edges share a node in the Petersen graph.

The interpretation of the space of trees as a tropical Grassmannian opens up the possibility of modeling a wide range of problems in phylogenetics using tropical geometry. We shall demonstrate this by tropicalizing the *higher Grassmannian* $G_{d,n} = V(I_{d,n})$ and the *Pfaffian varieties* $V(I_{2,n,k})$ which we encountered towards the end of Section 3.2. We begin with a discussion of tropical linear spaces. These are relevant for evolutionary biology because:

- Trees are tropical lines.
- Higher-dimensional trees are tropical linear spaces.

The second statement will be made precise in Theorem 3.47.

A *tropical hyperplane* in $\mathbb{R}^n$ is any subset of $\mathbb{R}^n$ which has the form $\mathcal{T}(\ell)$, where ℓ is a tropical linear form in n unknowns q_i:

$$\ell(q) \quad = \quad a_1 \odot q_1 \;\oplus\; a_2 \odot q_2 \;\oplus\; \cdots \;\oplus\; a_n \odot q_n.$$

Here $a_1, \ldots a_n$ are arbitrary constants in $\mathbb{R} \cup \{\infty\}$. Solving linear equations

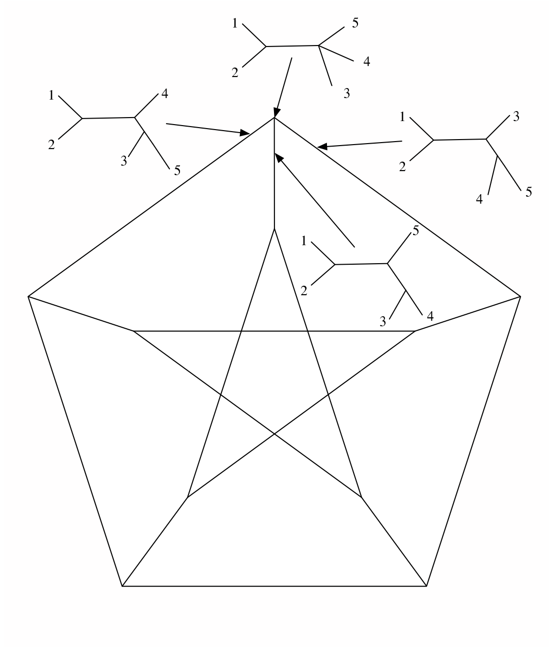

Fig. 3.5. A tropical Grassmannian of lines: the space of trees $\mathcal{T}_5$.

in tropical mathematics means computing the intersection of finitely many hyperplanes $\mathcal{H}(\ell)$. It is tempting to define tropical linear spaces simply as intersections of tropical hyperplanes. However, this would not be a good definition because such arbitrary intersections are not always pure dimensional, and they do not behave the way linear spaces do in classical geometry. A better notion of tropical linear space is derived by allowing only those intersections of hyperplanes which are "sufficiently complete". In what follows we offer a definition which generalizes the geometric relationship between tree metrics and the Grassmannian $G_{2,n}$ which underlies Theorem 3.45. The idea is that phylogenetic trees are lines in tropical projective space, and the negated pairwise distances d_{ij} are the Plücker coordinates q_{ij} of these tropical lines.

We consider the $\binom{n}{d}$-dimensional space $\mathbb{R}^{\binom{n}{d}}$ whose coordinates $q_{i_1\cdots i_d}$ are indexed by d-element subsets $\{i_1, \ldots, i_d\}$ of $\{1, 2, \ldots, n\}$. Let S be any $(d-2)$-element subset of $\{1, 2, \ldots, n\}$ and let i, j, k and l be any four distinct indices in $\{1, \ldots, n\}\backslash S$. The corresponding *three-term Grassmann Plücker relation* $g_{S,ijkl}$ is the following tropical polynomial of degree two:

$$g_{S,ijkl} \quad = \quad q_{Sij} \odot q_{Skl} \;\oplus\; q_{Sik} \odot q_{Sjl} \;\oplus\; q_{Sil} \odot q_{Sjk}. \tag{3.40}$$

We define the *space of d-trees* to be the intersection of these hypersurfaces,

$$\mathcal{T}_{d,n} \quad := \quad \bigcap_{S,i,j,k,l} \mathcal{T}(g_{S,ijkl}) \quad \subset \quad \mathbb{R}^{\binom{n}{d}}, \tag{3.41}$$

where the intersection is over all S, i, j, k, l as above. If $d = 2$ then $S = \emptyset$, the polynomial (3.40) is the four point condition (3.38), and $\mathcal{T}_{2,n}$ is the space of trees $\mathcal{T}_n = \mathcal{T}(I_{2,n})$. For $d \geq 3$, the tropical Grassmannian $\mathcal{T}(I_{d,n})$ is contained in the space of d-trees $\mathcal{T}_{d,n}$, and this containment is proper for $n \geq d+4$. However, $\mathcal{T}_{d,n}$ is a good combinatorial approximation for $\mathcal{T}(I_{d,n})$.

The points $Q = (q_{i_1 \cdots i_d})$ in $\mathcal{T}_{d,n} \subset \mathbb{R}^{\binom{n}{d}}$ are called *d-trees*. Fix a d-tree Q. For any $(d{+}1)$-subset $\{j_0, j_1, \ldots, j_d\}$ of $\{1, 2, \ldots, n\}$ we consider the hyperplane specified by the following tropical linear form in the unknowns $x_1, \ldots, x_n$:

$$\ell^{Q}_{j_0 j_1 \cdots j_d} \quad = \quad \bigoplus_{r=0}^{d} q_{j_0 \cdots \widehat{j_r} \cdots j_d} \odot x_r. \tag{3.42}$$

The *tropical linear space* associated with the d-tree Q is the intersection

$$L_Q \quad = \quad \bigcap \mathcal{T}(\ell^{Q}_{j_0 j_1 \cdots j_n}) \qquad \subset \quad \mathbb{R}^n. \tag{3.43}$$

Here the intersection is over all $(d+1)$-subsets $\{j_0, j_1, \ldots, j_d\}$ of $\{1, 2, \ldots, n\}$. The "sufficient completeness" referred to above means that we need to solve linear equations using *Cramer's rule*, in all possible ways, in order for the intersection of hyperplanes to be a linear space. The definition of linear space given here is more inclusive than the notion one would get by tropicalizing linear spaces over the field $\mathbb{Q}(\epsilon)$. The latter are the tropical linear spaces L_Q where Q is any point in the subset $\mathcal{T}(I_{d,n})$ of $TG_{d,n}$. [Speyer, 2004] proved that all tropical linear spaces L_Q are pure-dimensional polyhedral fans.

Theorem 3.47 (Speyer's Theorem) *Let $Q \in \mathcal{T}_{d,n}$ be a d-tree. Then every maximal cone of the tropical linear space L_Q is d-dimensional.*

Tropical linear spaces have many of the properties of ordinary linear spaces. First, they have the correct dimension d. Second, every tropical linear space L_Q determines its vector of tropical Plücker coordinates Q uniquely up to tropical multiplication (= classical addition) by a common scalar. If L and L' are tropical linear spaces of dimensions d and d' with $d + d' \geq n$, then L and L' meet. It is not quite true that two tropical linear spaces intersect in a tropical linear space but it is almost true. If L and L' are tropical linear spaces of dimensions d and d' with $d + d' \geq n$ and $v \in \mathbb{R}^n$ is generic then $L \cap (L' + v)$ is a tropical linear space of dimension $d + d' - n$. One then defines the *stable intersection* of L and L' by taking the limit of $L \cap (L' + v)$ as v goes to zero.

Not every d-dimensional tropical linear space in $\mathbb{R}^n$ is the intersection of

$n - d$ tropical hyperplanes. It is an open problem to determine the minimum number of tropical hyperplanes needed to cut out any tropical linear space of dimension d in $\mathbb{R}^n$. From (3.43) we see that $\binom{n}{d+1}$ hyperplanes suffice.

Theorem 3.47 is relevant for phylogenetics because tropical linear spaces can be regarded as "higher-dimensional phylogenetic trees". Indeed, suppose we have n taxa and we are given a dissimilarity measurement $-q_{i_1 i_2 \cdots i_d}$ for any d-tuple $\{i_1, i_2, \ldots, i_d\}$ of taxa in $[n]$. These $\binom{n}{d}$ real numbers form a d-dimensional dissimilarity matrix $Q = (q_{i_1 i_2 \cdots i_d}) \in \mathbb{R}^{\binom{n}{d}}$. Such a dissimilarity matrix Q is the input for the Generalized Neighbor Joining Algorithm in Section 2.4

The tropical linear space L_Q is a geometric model which plays the role of the tree for the data Q. Indeed, passing from $\mathbb{R}^n$ to the $(n-1)$-dimensional *tropical projective space* $\mathbb{R}^n/\mathbb{R}(1, 1, \ldots, 1)$, the tropical linear space L_Q is a contractible polyhedral complex of pure dimension $d - 1$. In the classical case $d = 2$, the linear space L_Q is a pure-dimensional contractible polyhedral complex of dimension 1, namely, it is precisely the tree with tree metric $-Q$.

Example 3.48 Fix $d = 3$ and $n = 6$. The *dissimilarity* of any triple $\{i, j, k\}$ of taxa in $[6] = \{1, 2, 3, 4, 5, 6\}$ is denoted by d_{ijk}, and we set $q_{ijk} = -d_{ijk}$. A point $Q = (q_{ijk}) \in \mathbb{R}^{20}$ is a 3-tree if and only if the map $(i, j) \mapsto d_{ijk}$ is a tree metric on $[6]\backslash\{k\}$ for all $k \in [6]$. Suppose this holds. Then the intersection of the $\binom{6}{4} = 15$ tropical hyperplanes $\mathcal{T}(\ell^Q_{j_0 j_1 j_2 j_3})$, is a 3-dimensional tropical linear subspace $L_Q \subset \mathbb{R}^6$. Each of the 15 defining linear forms has four terms:

$$\ell^Q_{j_0 j_1 j_2 j_3} \;=\; q_{j_0 j_1 j_2} \odot x_{j_3} \;\oplus\; q_{j_0 j_1 j_3} \odot x_{j_2} \;\oplus\; q_{j_0 j_2 j_3} \odot x_{j_1} \;\oplus\; q_{j_1 j_2 j_3} \odot x_{j_0}.$$

If we work in tropical projective 5-space, i.e. modulo the equivalence relation

$$(x_1, x_2, x_3, x_4, x_5, x_6) \quad \equiv \quad \lambda \odot (x_1, x_2, x_3, x_4, x_5, x_6),$$

then L_Q is a union of planar polygons. We call L_Q a *phylogenetic surface*.

A phylogenetic surface is a two-dimensional geometric representation of the dissimilarities among triples of taxa, just like a phylogenetic tree is a two-dimensional geometric representation of the dissimilarities among pairs of taxa. Embedded in the unbounded part of the phylogenetic surface L_Q, we find the six phylogenetic trees representing the tree metrics $(i, j) \mapsto d_{ijk}$ for fixed k.

There are 1035 combinatorial types of phylogenetic surfaces on six taxa [Speyer and Sturmfels, 2004]. They correspond to the maximal cones of the tropical Grassmannian $\mathcal{T}(I_{3,6}) = \mathcal{T}_{3,6}$, just like the 15 binary trees on five taxa correspond to the edges of the Petersen graph $\mathcal{T}_{2,5}$. If we replace $\mathbb{R}^{20}$ by its quotient modulo the subspace of dissimilarity maps of the particular form $d_{ijk} = \omega_i + \omega_j + \omega_k$, then $\mathcal{T}_{3,6}$ is a three-dimensional simplicial complex consisting of 65 vertices, 550 edges, 1395 triangles and 1035 tetrahedra. For the topologically inclined, we note that the space $\mathcal{T}_{3,6}$ of phylogenetic surfaces (i.e., the space of 3-trees on 6 taxa) is a bouquet of 126 three-dimensional spheres, just like the Petersen graph is a bouquet of 6 one-dimensional spheres.

We next discuss the tropical variety of the Pfaffian ideal $I_{2,n,k}$ and we offer a phylogenetic interpretation which generalizes the space of tree $\mathcal{T}_n$ (the special case $k = 2$). Suppose that $D^{(1)}, \ldots, D^{(r)}$ are $n \times n$-matrices which represent metrics. We define a new metric, denoted $D^{(1)} \vee \cdots \vee D^{(r)}$ and called the *mixture* of the given metrics, by taking the maximum distance for each pair:

$$(D^{(1)} \vee \cdots \vee D^{(r)})_{ij} \quad := \quad \max(D^{(1)}_{ij}, \ldots, D^{(r)}_{ij}).$$

Equivalently, using tropical matrix addition, the mixture of the r metrics is

$$D^{(1)} \vee \cdots \vee D^{(r)} \quad := \quad -\big((-D^{(1)}) \oplus \cdots \oplus (-D^{(r)})\big) \tag{3.44}$$

The term “mixture” conveys the idea that each metric $D^{(\nu)}$ corresponds to a random variable $X^{(\nu)}$ on the pairs of taxa with probability distribution

$$\mathrm{Prob}(X^{(\nu)} = \{i,j\}) \;\sim\; \exp(-\tau D^{(\nu)}_{ij}).$$

Consider a mixture of these r random variables where $\tau \gg 0$ and the mixing probabilities $p_1, \ldots, p_r$ are positive. Then the mixed distribution satisfies

$$\mathrm{Prob}(X^{(\nu)} = \{i,j\}) \;\sim\; \sum_{\nu=1}^{r} p_\nu \cdot \exp(-\tau D^{(\nu)}_{ij}) \;\sim\; \exp\big(-\tau (D^{(1)} \oplus \cdots \oplus D^{(r)})_{ij}\big),$$

Thus defining the mixture of metrics as their sum in *max-plus-algebra* is a natural thing to do in the context of tropical geometry of statistical models.

We say that a metric D has *tree rank* $\leq r$ if there exist tree metrics $D^{(1)}$, $\ldots, D^{(r)}$ such that $D = D^{(1)} \vee \cdots \vee D^{(r)}$. Let $\mathcal{T}^r_n$ denote the subset of $\mathbb{R}^{\binom{n}{2}}$ consisting of all metrics of tree rank $\leq r$. This is a polyhedral fan, generalizing the space of trees (the case $r = 1 = k-1$). We propose the following problem: *characterize membership in $\mathcal{T}^r_n$ and study the structure of this space.*

This problem may be relevant for the following issue in comparative genomics. If we are given an alignment of genomes then different regions (e.g. different genes) may give rise to different trees. It is desirable to create some consensus among the conflicting tree metrics. The resulting consensus object may no longer be tree-like, for instance, if we apply the refined techniques of Chapter 17. Mixtures of tree metrics may be useful models for such situations.

Fix a metric D and consider an even subset $\{i_1, \ldots, i_{2m}\}$ of $\{1, 2, \ldots, n\}$. This subset defines a complete graph K_{2m} with edge weights $d_{i_j i_k}$. A *matching* is a 1-regular subgraph of K_{2m}. The *weight* of a matching is the sum of the weights of its m edges. We are interested in the condition on D that each complete subgroup K_{2m} has more than one matching of maximum weight.

Proposition 3.49 *If a metric D has tree rank $\leq r$ then for every subset of $2r+2$ taxa, the maximum matching among these taxa is not unique.*

For $r = 1$ this is precisely the Four-Point Condition. In view of (3.16), we can rephrase Proposition 3.49 by tropicalizing the Pfaffians of order $2r+2$. For instance, for $r = 2$, tropicalizing (3.17) yields the tropical 6×6-Pfaffian

$$\begin{aligned} & q_{14} \odot q_{25} \odot q_{36} \;\oplus\; q_{15} \odot q_{24} \odot q_{36} \;\oplus\; q_{14} \odot q_{26} \odot q_{35} \;\oplus\; q_{15} \odot q_{26} \odot q_{34} \\ \oplus\; & q_{16} \odot q_{24} \odot q_{35} \;\oplus\; q_{16} \odot q_{25} \odot q_{34} \;\oplus\; q_{13} \odot q_{26} \odot q_{45} \;\oplus\; q_{12} \odot q_{36} \odot q_{45} \\ \oplus\; & q_{16} \odot q_{23} \odot q_{45} \;\oplus\; q_{13} \odot q_{25} \odot q_{46} \;\oplus\; q_{12} \odot q_{35} \odot q_{46} \;\oplus\; q_{15} \odot q_{23} \odot q_{46} \\ \oplus\; & q_{13} \odot q_{24} \odot q_{56} \;\oplus\; q_{12} \odot q_{34} \odot q_{56} \;\oplus\; q_{14} \odot q_{23} \odot q_{56}. \end{aligned}$$

Evaluating this tropical polynomial means finding the minimum weight matching in the complete graph K_6. We see that Proposition 3.49 is equivalent to

Proposition 3.50 *If a metric D has tree rank $\leq r$ then $-D$ lies in the intersection of the tropical hypersurfaces defined by the subpfaffians of order $2r+2$.*

Proof Theorem 3.45 implies that, for each $i \in \{1, 2, \ldots, r\}$, there exists a skew-symmetric $n \times n$-matrix $P^{(i)}$ over the field $\mathbb{Q}(\epsilon)$ such that $P^{(i)}$ has rank 2 and $\text{order}(P^{(i)}) = -D^{(i)}$. These matrices can be chosen so that there is no cancellation of leading terms when forming the sum $P := P^{(1)} + \cdots + P^{(r)}$. Then $\text{order}(P) = -D$ and $\text{rank}(P) \leq 2r$. Every Pfaffian of order $2r+2$ vanishes for P. Hence $-D$ lies on these tropical Pfaffian hypersurfaces. □

This proof shows how algebraic geometry in conjunction with tropicalization can suggest combinatorial constructions which may be useful for phylogenetics. We are not claiming that algebraic geometry is needed for the proof; indeed, it is easy to prove Proposition 3.49 without algebra. That is not the point.

Unfortunately, our necessary condition for membership in $\mathcal{T}_n^r$ is not sufficient. The following counterexample for $n = 6, r = 2$ is due to David Bryant.

Example 3.51 Consider the path metric of K_6 with a cycle removed:

$$D \quad = \quad \begin{pmatrix} 0 & 2 & 1 & 1 & 1 & 2 \\ 2 & 0 & 2 & 1 & 1 & 1 \\ 1 & 2 & 0 & 2 & 1 & 1 \\ 1 & 1 & 2 & 0 & 2 & 1 \\ 1 & 1 & 1 & 2 & 0 & 2 \\ 2 & 1 & 1 & 1 & 2 & 0 \end{pmatrix}$$

The maximum matching is attained twice, that is, $-D$ lies in the tropical hypersurface of the 6×6-Pfaffian. By examining all possible cases, one sees that D cannot be written as the mixture $D^{(1)} \vee D^{(2)}$ of two tree metrics. The tree rank of D is 3. Thus the converse to Proposition 3.50 does not hold.

At this point, it is natural to make the following conjecture: *If every restriction of a matrix D to six points is the mixture of two trees then D is a mixture of two trees.* Or, more generally: *If every restriction of D to $2r+2$ points is a mixture of r trees then D is a mixture of r trees.*

4
Biology

Lior Pachter

Bernd Sturmfels

The purpose of this chapter is to describe genome sequence data and to explain the relevance of the statistics and algebra we have discussed in Chapters 1–3 to understanding the function of genomes and their evolution. It sets the stage for the studies in biological sequence analysis in some of the later chapters.

Given that mathematics and statistics play an increasingly important role in many different aspects of biology, the question arises: why the emphasis on genome sequences? The most significant answer is that genomes are fundamental objects which carry instructions for the self-assembly of living organisms. Ultimately, our understanding of human biology will be based on an understanding of the organization and function of our genome. Also relevant to the study of genomes, is the fact that there are large quantities of high fidelity data. Current finished genome sequences have less than one error in $10,000$ bases. Statistical methods can therefore be directly applied to modeling the random evolution of genomes and to making inferences about the structure and organization of functional elements; there is no need to worry about extracting signal from noisy data. Furthermore, it is frequently possible to validate findings with laboratory experiments.

The rate of accumulation of genome sequence data has been extraordinary, far outpacing Moore's law for the density of transistors on circuit chips. This is due to breakthroughs in sequencing technologies and radical advances in automation. Thus, since the first completion of the genome of a free living organism in 1995 (Haemophilus Influenza [Fleischmann *et al.*, 1995]), there are now over 200 completely sequenced microbial genomes, and numerous complete invertebrate and vertebrate genomes. The highlight of the sequencing projects, from our *Homo sapiens* perspective, has been the completion of sequencing of the human genome which was formally announced at the end of 2004 [Human Genome Sequencing Consortium, 2004]. Our discussion of online resources in Section 4.2 explains how one reads the human genome.

4.1 Genomes

Every living organism has a genome, made up of deoxyribonucleic acids (DNA) arranged in a double helix [Watson and Crick, 1953], which encodes (in a way to be made precise) the fundamental ingredients of life. Organisms are divided into two major classes: *eukaryotes* (organisms whose cells contain a nucleus) and *prokaryotes* (for example bacteria and archaea). In this book we focus on genomes of eukaryotes, and, in particular, on genomes of vertebrates (see Chapters 21 and 22). The primary example is the human genome [Human Genome Sequencing Consortium, 2004, Venter *et al.*, 2001]. This allows for the description of ongoing genome projects at the forefront of current research interests, while limiting the scope so that some detail can be provided on how to obtain and utilize the data.

Eukaryotic genomes are divided into *chromosomes.* Each cell has two copies of each chromosome. There are 23 pairs of chromosomes: 22 *autosomes* (two copies each in both men and women) and two *sex chromosomes*, which are denoted X and Y. Women have two X chromosomes, while men have one X and one Y chromosome. Parents pass on a mosaic of their pairs of chromosomes to their children. Theoretical aspects of genetic inheritance are studied in the well-established field of *statistical genetics.* A connection between genetics and algebraic statistics was recently explored in [Hallgrimsdottir and Sturmfels, 2004].

The sequence of DNA molecules in a genome is typically represented as a sequence of letters, partitioned into chromosomes, from the four letter alphabet $\Sigma = \{\mathtt{A}, \mathtt{C}, \mathtt{G}, \mathtt{T}\}$. These letters correspond to the bases in the double helix, that is, the *nucleotides* Adenine, Cytosine, Guanine and Thymine. The four nucleotides fall into two pairs: *purines* (A and G) and *pyrimidines* (C and T). This grouping comes about because of the chemistry of the nucleotides: the purines have two rings in their structure while pyrimidines have only one. In addition to this grouping, every DNA base in the double helix is paired with a *complementary* base on the opposite helix. A is paired with T, and C with G, with hydrogen bonding serving as the main force holding the two separate chains together. Figure 4.1 illustrates these structural features of the nucleotides.

Remark 4.1 There is a natural action by the group $\mathbb{Z}_2 \times \mathbb{Z}_2$ on the alphabet $\Sigma = \{\mathtt{A}, \mathtt{C}, \mathtt{G}, \mathtt{T}\}$. This action arises by the grouping into purines and pyrimidines, and from the complementarity of the bases. Keeping in mind that finite abelian groups are (non-canonically) isomorphic to their dual groups, this leads to an identification of the nucleotides in $\Sigma = \{\mathtt{A}, \mathtt{C}, \mathtt{G}, \mathtt{T}\}$ with the group elements in $\mathbb{Z}_2 \times \mathbb{Z}_2$. This structure is the rationale behind *group based evolutionary models*, which we discuss in Section 4.4 and Chapters 15–17.

One of the consequences of DNA complementarity is *Chargaff's rule*, which

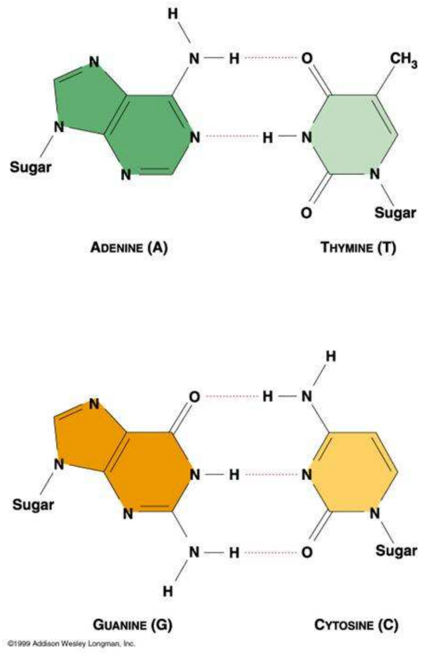

Fig. 4.1. The four DNA bases.

states that every DNA sample must contain the same number of `A`'s as `T`'s, and the same number of `G`'s as `C`'s [Chargaff, 1950]. Thus, in order to describe a genome, it suffices to list the bases in only one strand of the double helix. However, it is important to note that the two strands have a directionality. The two directions are indicated by the numbers $5'$ and $3'$ on the ends. These numbers correspond to carbon atoms in the helix backbone. The convention is to write a single strand of DNA bases in the $5' \to 3'$ direction.

Example 4.2 The DNA sequence `GATATAGAGCGGATTACAG` of length 20 is shorthand for the double stranded sequence consisting of twenty *base pairs*

```
5' GATATCAGAGCGGATTACAG 3'
3' CTATAGTCTCGCCTAATGTC 5'
```

which in turn is shorthand for the bases along the DNA double helix.

The human genome consists of approximately 2.8 billion base pairs, and has been obtained using high throughput sequencing technologies which allow for reading short fragments only hundreds of bases long. *Sequence assembly algorithms* are then necessary for piecing together the fragments [Myers, 1999].

Despite the tendency to abstract genomes as strings over the alphabet Σ,

	T	C	A	G
T	TTT $\mapsto$ Phe TTC $\mapsto$ Phe TTA $\mapsto$ Leu TTG $\mapsto$ Leu	TCT $\mapsto$ Ser TCC $\mapsto$ Ser TCA $\mapsto$ Ser TCG $\mapsto$ Ser	TAT $\mapsto$ Tyr TAC $\mapsto$ Tyr TAA $\mapsto$ *stop* TAG $\mapsto$ *stop*	TGT $\mapsto$ Cys TGC $\mapsto$ Cys TGA $\mapsto$ *stop* TGG $\mapsto$ Trp
C	CTT $\mapsto$ Leu CTC $\mapsto$ Leu CTA $\mapsto$ Leu CTG $\mapsto$ Leu	CCT $\mapsto$ Pro CCC $\mapsto$ Pro CCA $\mapsto$ Pro CCG $\mapsto$ Pro	CAT $\mapsto$ His CAC $\mapsto$ His CAA $\mapsto$ Gln CAG $\mapsto$ Gln	CGT $\mapsto$ Arg CGC $\mapsto$ Arg CGA $\mapsto$ Arg CGG $\mapsto$ Arg
A	ATT $\mapsto$ Ile ATC $\mapsto$ Ile ATA $\mapsto$ Ile ATG $\mapsto$ Met	ACT $\mapsto$ Thr ACC $\mapsto$ Thr ACA $\mapsto$ Thr ACG $\mapsto$ Thr	AAT $\mapsto$ Asn AAC $\mapsto$ Asn AAA $\mapsto$ Lys AAG $\mapsto$ Lys	AGT $\mapsto$ Ser AGC $\mapsto$ Ser AGA $\mapsto$ Arg AGG $\mapsto$ Arg
G	GTT $\mapsto$ Val GTC $\mapsto$ Val GTA $\mapsto$ Val GTG $\mapsto$ Val	GCT $\mapsto$ Ala GCC $\mapsto$ Ala GCA $\mapsto$ Ala GCG $\mapsto$ Ala	GAT $\mapsto$ Asp GAC $\mapsto$ Asp GAA $\mapsto$ Glu GAG $\mapsto$ Glu	GGT $\mapsto$ Gly GGC $\mapsto$ Gly GGA $\mapsto$ Gly GGG $\mapsto$ Gly

Table 4.1. *The genetic code.*

one must not forget that they are highly structured. For example, certain subsequences within a genome correspond to *genes*. These subsequences play the important role of encoding *proteins*. Proteins are polymers made of twenty different types of amino acids, which are described by triplets in genes known as *codons*. Thus there are 64 codons: `AAA`, `AAC`, `AAG`, ..., `GTT`, `TTT`. Each triplet codes for one amino acid, so that a DNA subsequence of length $3k$ codes for a protein with k amino acids.

The code relating DNA triplets to amino acids is known as the *genetic code*. Table 4.1 displays the genetic code, which maps the 64 possible codons to the twenty amino acids they code for. Each amino acid is represented by a three letter identifier ("Phe" = Phenylalanine, "Leu" = Leucin, ...). The code is literally translated by machinery (itself partially made of protein) that builds a protein from the linear DNA sequence of a gene. The three codons `TAA`, `TAG` and `TGA` are special: instead of coding for an amino acid, they are used to signal that translation should end.

Example 4.3 (Codon usage, GC content and genome signatures) *Codon usage* refers to the relative abundances of the different codons in a genome. Although the genetic code is universal (with a few exceptions), codon usage varies widely between genomes, and can in fact be used to distinguish genomes from each other [Campbell *et al.*, 1999, Gentles and Karlin, 2001]. Part of the difference in codon usage stems from different `G+C` content in genomes. `G` and `C` nucleotides are known to be involved in a number of genome regulation mechanisms. For example, `CpG` *sites* are locations in DNA sequences where a `C` is adjacent and upstream of a `G`. DNA methyltransferase recognizes `CpG` sites and converts the cytosine into 5-methylcytosine. Spontaneous deamination causes the 5-methylcytosine to be converted into thymine, and the mutation is not fixed by DNA repair mechanisms. This results in a gradual erosion of CpG sites in the genome. *CpG islands* are regions of DNA with many unmethylated `CpG` sites. Spontaneous deamination of cytosine to thymine in these sites is repaired, resulting in a restored `CpG` site. Such sites are associated with promoter regions of genes. `CpG` islands alone, however, do not explain the vast differences in `G+C` content seen between genomes.

A simple model for *genome signatures* that distinguish organisms is a dinucleotide model [Campbell *et al.*, 1999]. Specifically, the data consists of 16 numbers $u_{ij},\ i,j \in \{A,C,G,T\}$, where u_{ij} counts the number of times that the pair of nucleotides ij appear consecutively in that order in a genome. The independence model for dinucleotides is ...

In order to make protein, DNA is first copied into a similar molecule called RNA (this process is called *transcription*). It is the RNA that is *translated* into protein. The link between DNA, RNA and protein is the basis of molecular biology, and is sometimes referred to as the *central dogma*.

When protein is created from DNA, the gene that has been translated is said to have been *expressed*. Proteins can be structural elements, or perform complex tasks (such as regulation of expression) by interacting with the many molecules and complexes in cells. Thus, the genome is a blueprint for life. A major goal in biology, to be discussed in Section 4.3, is a complete understanding of the genes, the function of their proteins, and their expression patterns.

The human genome contains approximately 25,000 genes, although the exact number has still not been determined [Human Genome Sequencing Consortium, 2004]. While there are experimental methods for discovering and validating genes, there is still no high throughput technology for accurately identifying all the genes in a genome. The computational problem of identifying genes, the *gene finding problem*, is an active area of research [Dewey *et al.*, 2004, Korf *et al.*, 2001]. One of the main difficulties lies in the fact that only a small portion of the genome is genic; in fact, less than 5% of the genome is known to be functional. In Section 4.4 we discuss this problem, and the role of statistical models in formulating sound methods for distinguishing genes from non-genic sequence. The models of choice are the *hidden Markov models* whose mathematical characterization was discussed in Section 1.4. Hidden Markov models allow for the integration of diverse biological information (such as the genetic code and the structure of genes) and are suitable for designing efficient algorithms. In spite of much progress, the current understanding of genes is not sufficient to allow for the *ab-initio* identification of all the genes in a genome [Guigó *et al.*, 2004].

A key idea in biology has been that the comparison of multiple genome sequences can assist in identifying genes and other functional elements. The underlying premise of the *comparative genomics* approach is that although DNA sequences change over time, functional elements such as genes will tend to be conserved due to their critical role in coding for proteins or other important elements. The comparative genomics approach therefore seeks to utilize Darwin's principle of *natural selection* to sift through genome sequences for functional elements. The principle has been applied to collections of similar genomes [Boffelli *et al.*, 2003, Boffelli *et al.*, 2004b], as well as more diverged sequences [Gibbs *et al.*, 2004, Hillier *et al.*, 2004].

The different types of comparisons require an understanding of the underlying biology. For example, differences between the genomes of individuals in a population are small and are primarily due to recombination events (the process by which two copies of parental chromosomes are merged in the offspring). On the other hand, the genomes of different *species* (classes of organisms that can produce offspring together) tend to be much more diverse. Genome differences between species are a result of numerous transformations of genome sequences:

- *Genome rearrangement* – comparing chromosomes of related species reveals large segments that have been reversed and flipped (*inversions*), segments that have been moved (*transpositions*), *fusions* of chromosomes, and other large scale events. Methods of combinatorial mathematics have led to significant progress in this field [Hannenhalli and Pevzner, 1999, Tesler, 2002], but the underlying biological mechanisms are still poorly understood [Sankoff and Nadeau, 2003].
- *Duplications and loss* – some genomes have undergone whole genome duplications. This process was recently demonstrated for yeast [Kellis *et al.*, 2004]. Individual chromosomes or genes may also be duplicated. Duplication events are often accompanied by *gene loss*, as redundant genes slowly lose or adapt their function over time [Eichler and Sankoff, 2003].
- *Parasitic expansion* – large sections of genomes are repetitive, consisting of elements which can duplicate and re-integrate into a genome [Brown, 2002].
- *Point mutation, insertion and deletion* – DNA sequences mutate, and in non-functional regions these mutations accumulate over time. Such regions are also likely to exhibit deletions; for example, strand slippage during replication can lead to an incorrect copy number for repeated bases.

Biological questions about how these mechanisms operate lead directly to mathematical problems.

Example 4.4 (Sorting by reversals) Comparison of the human, mouse and rat X chromosomes reveals large blocks within which the order and orientation of genes is conserved. For example, the human genome can be divided into 16 blocks labeled consecutively $1, \ldots, 16$ which appear in different orders and orientations in the mouse and rat genomes, but within which order and orientation is preserved (not counting rearrangements less than 300kb in size). The changes in the mouse and rat can be recorded by *signed permutations.* From [Bourque *et al.*, 2004] we have:

```
Human 1 2 3 4 5 6 7 8 9 10 11 12 13 14 15 16
Mouse -5 -6 4 13 14 -15 16 1 -3 9 -10 11 12 -7 8 -2
Rat -13 -4 5 -6 -12 -8 -7 2 1 -3 9 10 11 14 -15 16
```

Inversions correspond to *reversals* of the signed permutations. These consist of selecting a subsequence of a signed permutation and reversing the order of the numbers and their sign. For example, a reversal in the mouse could be

```
Mouse -5 -6 4 13 14 -15 16 1 -3 9 -10 11 12 -7 8 -2
                        <------->
      -5 -6 4 13 14 -15 3 -1 -16 9 -10 11 12 -7 8 -2
```

An important genomics problem is to estimate the order of genes in the ancestral chromosome, so that the number of rearrangements that have occurred over time can be counted. In [Tesler, 2002] it is shown that the distance between two multichromosomal genomes, defined as the minimum number of reversals, translocations, fissions and fusions required to transform one genome to the other, can be computed in polynomial time. Genome rearrangements are important to study because they shed light on genome evolution, and also because many diseases are known to be associated with genome rearrangement (e.g. [Raphael and Pevzner, 2004]).

The problem of untangling the evolutionary history relating genome is complicated, and statistical methods are required to model the different events, many of which are inherently random. Some of the connections between statistics and evolutionary models are discussed in Section 4.5.

Two distinct DNA bases that share a common ancestor are called *homologous.* Homologous bases can be related via speciation and duplication events, and are therefore divided into two classes: *paralogous* and *orthologous.* Orthologous bases are descendant from a single base in an ancestral genome that underwent a speciation event only, whereas two paralogous bases correspond to two distinct bases in a single ancestral genome that are related via a duplication. Because we cannot sequence ancestral genomes, it is never possible to formally prove that two DNA bases are homologous. However, statistical arguments can show that it is extremely likely that two bases are homologous, or even orthologous (see Chapter 22). The problem of identifying homologous bases between genomes of related species is known as the *alignment problem*. The statistical model of choice for alignment is the pair hidden Markov model. The algebraic representation of this model and its tropicalization, which underlies the popular Needleman-Wunsch algorithm, was discussed in Section 2.2.

4.2 The data

Biology is a data-driven science. This means that progress in the field is the result of analyzing data obtained from experiments. The experiments are performed in individual laboratories, or via large scale collaborations utilizing high-throughput technologies. Data produced by scientists is often fiercely guarded, and rarely distributed before publication, however one of the attractive aspects of genomics is the availability of large amounts of high quality genome sequence data. In fact, many publicly funded projects are required to distribute their data through publicly available websites within hours of sequencing. The *Fort-Lauderdale* agreement, a result of a extensive discussions between sequence providers and sequence analyzers held in 2003, provides guidance from the NIH on how and when to publish results from genome analysis. The document can be viewed at `www.genome.gov/10506537`. Researchers are generally free to publish results derived from publicly posted genomes and in return publication right for whole genome analyses on a newly sequenced genome are reserved for those who sequenced the genome.

In this section we describe some of the data that is available for analysis, and explain how to download it from publicly accessible websites.

4.2.1 Sequence Data

Most genomes today are sequenced using the *whole genome shotgun* strategy. This strategy is based on two high-throughput technologies: the first is recombinant DNA technology which allows for the construction of *libraries*, so called because they consist of large pieces of DNA from a genome, and can be stored in a freezer. A library is made by shearing multiple copies of a genome and inserting the pieces into simple replicating molecules (or organisms) called vectors. The inserted pieces are called *inserts*. The inserts can vary in size depending on the vector: libraries may consist of inserts ranging in size from 2 kilobases up to hundreds of kilobases long. The second important technology is high-throughput sequencing which allows for the rapid sequencing of DNA from the ends of inserts. The pieces that can be sequenced accurately are typically about 500-700 base pairs long, and are called *reads*. To summarize, it is possible to sequence short segments of DNA, approximately 500-700 bp long, in pairs separated by by some predefined distances, randomly from the genome.

Example 4.5 The following is a read from the genome of the lesser Madagascar hedgehog (*Echinops telfairi*), sequenced in February 2005:

```
>gnl|ti|643153582 name:G753P82FG11.T0 mate:643161057
 mate_name:G753P82RG11.T0 template:G753P82G11 end:R
 TAATGAGTGGGGCGAAAGAATCGGCTCCGGTGATTCATCACTTGGCTGACCCAGGCCTGA
 CCCAACCCATGGAATTGTCAAGTGCCTCGTATGCATGTGGAAGTTGGACATTGATTAAGA
 AGACCAAAGAAGAATCTATGTGTTTTATTTGTGGTGCTAGAGAAGTACCTTGGACTGATA
 AAAAGACAAACCAAACTGTATTGGACGAAGTAAGGCTTCTTGGAGGCAAGGATAGGAAGA
 CTTTGTCTCACATACTTTGGACATATTGTCAGGACAGACCAGTCCCTGGCGAAGGACATC
 ATGCTTGGTCAAGTGGAGGGGCAGTGGAAAAGAGGAAGGCGCTTAATGAGATGGATGGAT
 ACAATTGCTACAATAATGGACCCAGGCATGGAAAAAAATTAAGTTTGTCACAGGACTGGG
 CAGTGTTTCCTTTTGTTGTGCACAGGGTTGCTATGGGTCGGCACAGACTCAATGGCTTCA
 AACAACAATAACAACAATCTAGTGATCCCAATAGTCAGCCTTTTATTTTTTCTCCCCCAA
 GAAGAAAATATAATGGAGAAATTACATTCTGCTTTCATATTGAGGAAGAGAATTATGTTC
 CTAATTGACCTATCATTGGCCCAGGATCCTGGATCTTCAACCCTAGTTTTTAGTGAAAGC
 GTATGCTGAACTATTGTCTCCTGCATGGCATCTTCCACCCAGTTAGCTCTTGAAATGTTG
 GGTTCTCTACATGACCTGATTCCTTCTTCTTCACACCCTAAGTCAAATATACATTGAGTC
 CCATCAGTACCATCTCCAAAATACATTACAAATAAGACCATTTATTACCAATGCATTGCT
 ATGACTCTAGACCATCTCTTCTCGTACTTGAACAATTGCAACAGCCAGTTCAATGCACCC
 AGTACCCCTGTCCTCCACCTCTTCACAGGTCTCTCTATTTACACAATGGCCAAGAAGAGG
 AAGAACACTTTTAATATATTGTGTGTCAAACAGCAAAAAACCACACAAC
```

The read was obtained by going to the NCBI trace archive (the raw output of a sequencing machine is called a *trace*), located at
`www.ncbi.nlm.nih.gov/Traces/trace.cgi`

The website allows one to browse recently deposited traces, or to perform advanced searches. Click on the `Obtaining Data` tab to learn more. Examining the read, we see that it is in `FASTA` format (see the discussion of `MAVID` in Section 2.5). Notice that the name of the read specifies which one is its pair.

In whole genome shotgun projects, enough reads are sequenced so that there is considerable overlap among them, allowing them to be merged in order to reconstruct the genome. The problem of reconstructing the genome from the reads is called the sequence assembly problem. Its difficulty depends on the amount of sequencing, and also on the repetitive nature of the genome. Reads also contain errors which complicate matters.

A few definitions are helpful in understanding sequence data, and the quality of assemblies: Reads come equipped with *quality scores.* These quality scores are estimates of the reliability of bases in a read. The estimates improve with assembly because of the redundancy of the libraries, and the fact that every base in the genome appears in many reads. Therefore, even though sequencing machines may be only 98 % accurate, there is a possibility for correcting errors during assembly, and for estimating the uncertainty in bases in assembled genomes. Quality scores are reported on a logarithmic scale, so that if a base has a $1/10^k$ chance of being incorrect then its quality score is $10k$. Sequencing standards have progressed to the point where quality scores of 40 are the norm. The *coverage* of a whole genome shotgun project is defined to be the average, taken over all bases in the genome, of the number of reads containing the base. For example, 5.1x coverage means that every base in the genome was covered, on average, by 5.1 reads (see Example 4.9). Sequence assemblies therefore typically contain gaps, and are often split into multiple pieces that cannot be pieced together.

Reads are assembled into contigs, and contigs may be linked (by paired reads) into super-contigs. Contigs are therefore made up of chains of overlapping reads, however the contigs within super-contigs do not overlap.

Example 4.6 (The Lander-Waterman model) In an important paper, [Lander and Waterman, 1988] pointed out that with a few simplifying assumptions about sequencing procedures, formulas could be derived for the expected lengths of contigs in an assembly (the original paper relates to clone fingerprinting for physical mapping, but the results apply to whole genome shotgun projects). Let G be the length of the genome being sequenced in base pairs, L the length of a read, and N the number of sequenced reads. Let T be the amount of overlap in base pairs between two reads needed to detect overlap. Set $\alpha = \frac{N}{G}$, $\theta\frac{T}{L}, \sigma = 1-\theta$ and let c be the coverage, i.e. $\frac{LN}{G}$.

Proposition 4.7 *Assuming that reads are randomly located in the genome,*

(i) *The expected number of contigs is $Ne^{-c\sigma}$.*

(ii) *The expected number of contigs consisting of j reads ($j \geq 1$) is*

$$Ne^{-2c\sigma}(1-e^{-c\sigma})^{j-1}.$$

(iii) *The expected number of reads in a contig is $e^{c\sigma}$.*

(iv) *The expected length in base pairs of a contig is*

$$L\left(\frac{e^{c\sigma}-1}{c} + (1-\sigma)\right).$$

The Lander-Waterman model is therefore just a Poisson model for the number of times a base is sequenced. The formulas can be used to calculate the amount of sequencing that is necessary for different qualities of assembly.

The quality of an assembly is measured in terms of $N50$ sizes. If c_k is defined to be the number of bases that lie in contigs of size at least k, then the $N50$ size of an assembly is the largest k such that $c_k \geq \frac{1}{2}$. $N50$ sizes can also be calculated for super-contigs.

Example 4.8 (Rice genome) The Beijing Institute of Genomics sequenced a cultivar of the *indica* subspecies of rice (*Oryza sativa*) using the whole genome shotgun strategy [Yu *et al.*, 2002]. The original publication describes an assembly from 4.2x coverage, built from $3,565,386$ reads, with reads of length 546 having quality score 20. The N50 contig size was 6.69 kb, and the N50 scaffold size was 362 Mb. Updates to the original assembly, and comparison with other subspecies are reported in [Yu *et al.*, 2005].

The whole genome shotgun strategy has certain limitations, one of which is that it is not possible to sequence long, highly repetitive portions of a genome. It is therefore not possible to sequence the *heterochromatin*. In fact, there is no existing technology for sequencing this DNA, and it is therefore impossible to completely finish sequencing any vertebrate genome. Nevertheless, the term *finished* has come into use to describe a genome whose *euchromatin* has been sequenced and for which there are very few contigs in the assembly. Unfortunately, there is no universally accepted definition of a finished genome beyond the one we have just provided.

Finished genomes are useful for a number of reasons. For example, the absence of a sequence that exists in another organisms can be certified and investigated for biological relevance, something that is not possible with a poor assembly. Furthermore, contiguity of the sequence allows for positional information of sequence to be used, something which is not always possible with draft genomes in many contigs.

Example 4.9 (Human genome) The human genome was finished in 2004 [Human Genome Sequencing Consortium, 2004]. The assembly as of January 2005 consists of 2.85 billion nucleotides interrupted by 341 gaps. It covers almost all of the euchromatic part of the genome (estimated coverage about 99%) and has only about one error in $10,000$ bases. The latest build of the human genome can be downloaded from NCBI at:
`ftp://ftp.ncbi.nih.gov/genomes/H_sapiens/`.

Another site, which is useful for browsing the genome is the UCSC genome browser. In order to retrieve part of the human genome, the following steps need to be performed:

(i) Open a browser and load the URL `genome.ucsc.edu`
(ii) Click on the `Genome Browser` tab on the left hand side.

(iii) There are three pull down menus for selecting a clade, a genome from that clade, and a specific version. Select `Vertebrate`, `Human`, `May 2004`.
(iv) The specific position to browse is entered in the `position` box. Enter the coordinates `chr17:38,451,220-38,530,912` and press `submit`.
(v) You will see a `GIF` image which depicts a region of the human genome (see Section 4.3). Click on the `DNA` tab on the top of the page.
(vi) Click on the `Get DNA` button. You should see almost 100, 000 DNA bases on the screen.

Although some assembly programs are freely distributed, they are fairly complicated software tools that require large amounts of computer memory, and until recently most assembly has been done by the sequencing centers. Thus, the sources for genome assemblies are mostly the large sequencing centers, which we summarize in the list below:

- Broad Institute at M.I.T., Cambridge, Massachusetts, USA:
  `www.broad.mit.edu/resources.html`
- DOE Joint Genome Institute, Walnut Creek, California, USA:
  `genome.jgi-psf.org`
- Human Genome Sequencing Center at the Baylor College of Medicine, Houston, Texas, USA: `www.hgsc.bcm.tmc.edu/projects`
- Wellcome Trust Sanger Institute, Cambridge, England:
  `www.sanger.ac.uk/Projects`
- Genome Sequencing Center at Washington University, St. Louis, USA:
  `www.genome.wustl.edu`
- Genoscope – the French National Sequencing Center, Evry, France:
  `www.genoscope.cns.fr/externe/English/Projets`
- Agencourt Bioscience Coorporation, Beverly, Massachusetts, USA:
  `www.agencourt.com`
- The Institute for Genomic Research, Rockville, Maryland, USA:
  `www.tigr.org/tdb`
- Beijing Genome Institute, Beijing, China:
  `www.genomics.org.cn`
- Genome Sequencing Centre, Jena, Germany:
  `genome.imb-jena.de`

We have already seen that the UCSC Genome Browser is a useful site for browsing genomes (although it is not a sequencing center). Another similar site is Project ENSEMBL at `www.ensembl.org`

The most comprehensive online resource for genomic sequence is the National Center for Biotechnology Information (NCBI) `www.ncbi.nlm.nih.gov/`. In

type	program	site
pairwise	BLASTZ	`hgdownload.cse.ucsc.edu/downloads.html`
pairwise	BLASTZ	`ecrbrowser.dcode.org`
pairwise	AVID/LAGAN	`pipeline.lbl.gov`
multiple	MAVID	`hanuman.math.berkeley.edu/genomes/`
multiple	MAUVE	`asap.ahabs.wisc.edu/mauve/index.php`

Table 4.2. *Sites for downloading genome alignments.*

addition to serving as a worldwide repository for all genome related data (maintained in a database called GENBANK `www.ncbi.nlm.nih.gov/Genbank/`), NCBI also hosts the trace archive we have mentioned. It should be noted that for some genomes, reads are not available as the sequencing centers may not have released them. Another popular trace archive is housed at `trace.ensembl.org/`.

4.2.2 Alignments

The identification of homologous components between genomes is the first step in identifying highly conserved sequences that point to the small fraction of the genome that is under selection, and therefore likely to be functional. The recognition of homologous components requires two separate steps:

(i) *Sequence matching.* The identification of similar sequence elements between genomes.

(ii) *Homology mapping.* The separation of matches into homologous components and sequences that match by chance.

The combined problem of finding matching sequence elements and then sorting them into homologous components is called the *alignment problem*. Both these problems are difficult, and are active areas of research in genomics. The homology mapping problem is the topic of Chapter 13.

Alignments of genomes are available for download from a number of places, the web sites and types of alignments available are summarized in Table 4.2.2

Genome alignments should be used with caution. Results are very dependent on choices of parameters in the programs, and the multiple genome alignment problem is particularly difficult due to the combinatorial explosion of the possible number of alignments. The dependence of alignments on parameters is the topic of Chapter 7.

4.3 The questions

Biology is the study of living organisms. Living organisms are complex, and although there are no known simple principles that completely explain their function, there are fundamental components whose organization and interaction form the basis of life. These components are distinguished by scale. At one end of the spectrum are populations of species, whose interactions may be governed by certain ecological constraints. Organs within individual species are composed of tissues and cells. And at the microscopic level there is DNA, itself composed of organic precursors and which is organized into genomes. Genomes and cells are related by a series of intermediary biomolecules: RNA and proteins, coded for by DNA, together form metabolites and organelles which make up cells, and in turn cells are the structure which house DNA and allow for its replication.

Mathematical biology is a general term that, in principle, encapsulates the parts of mathematics relevant to the study of biology. Typically however, mathematical biology usually refers to the mathematics relevant for studying biological systems at a macroscopic scale. This is because it is only recently that molecular biology has become an integral part of biological investigation. Even more recent is the emergence of *genomics*, or the study of genomes, as a discipline in its own right. Even though genomics is only a tiny piece of the complex puzzle of biology, a complete understanding of genomes is an essential step for learning more about the cell, which in turn is the stepping stone to higher level systems.

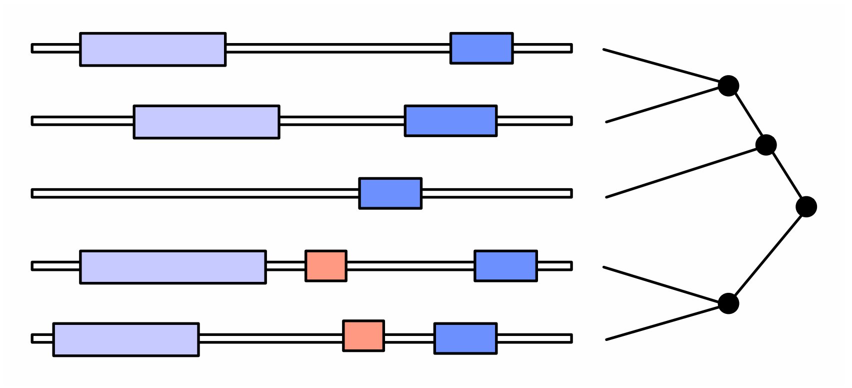

Fig. 4.2. Comparative genomics via annotation and phylogeny.

There are two important aspects to genome analysis. On the one hand, a key problem is to understand the organization and function of individual genomes. On the other hand, there is an equally interesting problem of understanding the evolution of genomes and the mechanisms of natural selection [Darwin, 1859]. The relationship between these problems is the central theme of comparative genomics, and is illustrated pictorially in Figure 4.3. Our aim in this section is to explain this figure, and survey some of the key problems in comparative genomics.

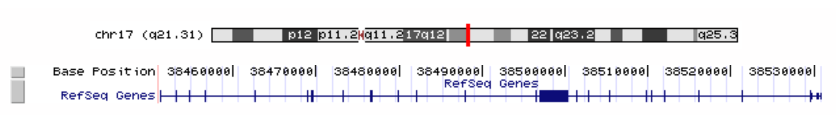

Fig. 4.3. Breast cancer type I early-onset gene: snapshot from the UCSC browser.

We begin by elaborating on the structure of a (eukaryotic) gene, which is represented in Figure 4.3 by the boxes on a single horizontal line. Note that the horizontal line is a cartoon for a genome sequence, and represents a sequence of DNA. In order to understand the meaning of the boxes it is necessary to know a bit about the structure of genes.

First, we recall that a gene is a subsequence of the genome that codes for a protein. More precisely, a gene consists of a subsequence of transcribed DNA, a subsequence of which is translated. In Figure 4.3 the top line is DNA, which is transcribed into *pre-mRNA*. Only parts of the pre-mRNA are translated; in fact, parts of it are cut out resulting in *mRNA*, which is the substrate used for translation. The untranslated parts of genes are known as UTRs (untranslated regions); typically both the $5'$ and $3'$ ends of genes contain UTRs. In Figure 4.3 they are the light blue exons, and the introns between them. One of the main features of Eukaryotic genes is that they are *spliced* . Splicing is a biological process applied to pre-mRNA from a transcribed gene, where certain subsequences called *introns* are removed. The remaining subsequences, called *exons* are spliced together to form a new RNA molecule called mRNA, a subsequence of which is then translated. The splicing junctions feature sequence signals, for example $5'$ splice sites, also called *donor sites* and which are at the $5'$ end of an intron (almost) always begins with the nucleotides `GT`. Similarly $3'$ splice sites, also known as *acceptor sites* and which are at the $3'$ end of introns are (almost) always `AG`.

The boxes along the top line shown in Figure 4.3 represent exons. If the cartoon is showing just one gene, then it has two exons, and it is their concatenation which is relevant for determining the protein they code for. An example of a real gene is shown in Figure 4.3. The figure shows a screenshot from the UCSC browser, obtained for the sequence described in Example 4.9. The region displayed in the bottom panel is quite long (almost 100 kb) but contains only one gene. The gene is called `BRCA1`, which stands for the breast

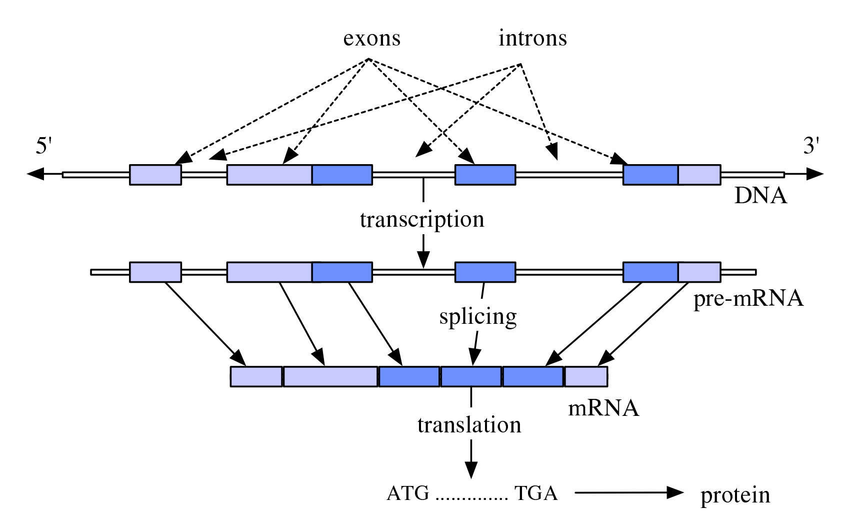

Fig. 4.4. Structure of a gene.

cancer type I early-onset gene. The top panel shows the location of the region on chromosome 17. Each of the boxes correspond to an exon. Mutations in exons of the BRCA1 gene lead to truncated proteins, and studies have confirmed that patients with early-onset breast cancer are much more likely than the general population to have mutations in this gene. One of the interesting effects of splicing is that may different possible proteins may be coded by a finite piece of DNA. This can be seen in Example 4.9 by selecting `full` for the `RefSeq` genes which shows different variants of the protein. Mathematically, the statement that a gene can have many alternative splicings is evident from the following proposition:

Proposition 4.10 *Suppose that a given DNA sequence contains n locations that could be possible active $5'$ splice sites and m locations that could be possible active $3'$ splice sites. In principle, the number of possible gene structures may be as high as the Fibonacci number F_{n+m+1}.*

There are many outstanding biology questions related to genes. For example, it is unknown if there is a functional role for all intronic sequence (sometimes called "junk" DNA). Furthermore, it is still unclear if there are organizing principles that explain in simple terms the regulation of genes. The connection between the gene finding problem and hidden Markov models is explained in Section 4.4.

Returning to Figure 4.3, we see that the tree on the right hand side shows the evolutionary relationships between the sequences. This leads us to the alignment and evolutionary modeling components of comparative genomics. In order to identify functional elements in the sequences, it is useful to identify conserved regions in the alignments. Conversely, the alignment problem is easier if one knows ahead of time the functional elements in each sequence. Statistical models for alignment and evolutionary models are based on these biological considerations, and we discuss them in more detail in Section 4.5.

It is important to note that comparative genomics is not only a computational endeavor. There are many experimental techniques being developed that can be used to identify functional elements in genomes, and that also shed light on genome evolution. In this regard it is important to mention the he ENCyclopedia of DNA Elements (ENCODE) Project [Consortium, 2004] which is an NHGRI organized international consortium working towards the goal of identifying all functional elements in the human genome sequence. The pilot phase of the project is focused on 1% of the human genome sequence. Initial efforts include the development of high-throughput technologies for detecting functional elements, as well as the sequencing of orthologous regions from multiple primates, mammals and other vertebrates. The available sequence from multiple organisms complements additional sequence extracted from whole genome sequencing projects, and serves as a testbed for comparative genomics approaches to detecting functional elements. Thus, the ENCODE project is aimed at fostering interaction between computational and experimental scientists, and at identifying promising research avenues and scalable technologies. Preliminary analysis of some ENCODE regions is discussed in Chapters 22 and 21.

The ENCODE consortium sequence and analysis repository is housed at `genome.ucsc.edu/encode`

4.4 Statistical models for a biological sequence

In Chapter 1 we introduced DiaNA, a strange fictional character who flips coins and generates words on the alphabet $\{\mathtt{A}, \mathtt{C}, \mathtt{G}, \mathtt{T}\}$. Although DiaNA does not seem to have anything to do with real biological DNA sequences, the principle of imagining DNA to have been generated by fictional entities like DiaNA who flip coins has proved to be extremely useful for biological sequence analysis. In order to see this, suppose that we would like to analyze 1 million bases of DNA from the human genome and identify CpG islands within them. One approach is to count, for each contiguous subsequence of length 100, the number of `C`s and `G`s, and to call a 100bp segment a CpG island if there are more than 70 `C`s and `G`s. There are a number of problems with such an approach. First, the segment size 100 is arbitrary; perhaps some biologists prefer working with segments of length 50, or 200. For such different segment sizes, what should be the cutoff for deciding when the number of `C`s and `G`s indicates a CpG island?

Again, there may be different intuitive guesses as to what constitutes "random looking sequence." A statistical approach to the problem helps to resolve such issues, by carefully and precisely specifying the parameters and the model, thus allowing for a mathematically rigorous description of "random." This leads to sensible approaches for deciding when a region is a CpG island.

Example 4.11 DiaNA serves as the statistical surrogate for our biological intuition and understanding of CpG islands. In searching for CpG islands, we begin with specifying what non-CpG random DNA should look like (DiaNA's fair die). When she chooses to toss this die, she makes a "non-CpG DNA base". Next, our biological knowledge suggests that CpG islands should have an excess of `C`'s and `G`'s. The CpG island die therefore has higher probabilities for those. Finally, a third die may represent DNA sequences that are poor in `C`'s and `G`'s. Returning to Example 1.1 we recall that the probabilities were:

	A	C	G	T
first die	0.15	0.33	0.36	0.16
second die	0.27	0.24	0.23	0.26
third die	0.25	0.25	0.25	0.25

(4.1)

These probabilities reflect the actual properties of CpG islands; they were computed from the table in [Durbin *et al.*, 1998, page 50]. Once a model is specified, statistical inference procedures can be applied to DNA for finding CpG islands.

One of the original applications which highlighted the use of discrete statistical models for biological sequence analysis is the gene finding problem. Hidden Markov models (HMMs) have been successfully applied to this problem. They have also been used for finding other functional elements.

Maximum a posteriori (MAP) inference with such models has become the method of choice for ab initio gene finding. To give a precise definition of MAP inference, let us recall the set-up of Section 1.3. The hidden model is the map $F : \mathbb{R}^d \to \mathbb{R}^{m\times n}$ specified by a matrix of polynomials $F = \big(f_{ij}(\theta)\big)$, while the observed model is the map $\mathbf{f} : \mathbb{R}^d \to \mathbb{R}^m$ whose coordinates are the row sums of the matrix F, that is, $f_i(\theta) = \sum_{j=1}^{n} f_{ij}(\theta)$. In MAP inference we assume that one particular observation $i \in [m]$ has been made. The problem is to identify an index $j \in [n]$ which maximizes $f_{ij}(\theta)$. In other words, we wish to find the best explanation j for the given observation i. Traditionally, the parameters θ are assumed to be known and fixed, but here we also consider the parametric version where some or all of the parameters are unknowns.

For many models used in computational biology, including the Markov models discussed in Section 1.3, the hidden model F will be a toric model (or very close to a toric model). This means that the entries of the matrix F are monomials in the parameters, say $f_{ij}(\theta) = \theta^{a_{ij}}$ for some $a_{ij} = (a_{ij1}, \ldots, a_{ijd}) \in \mathbb{N}^d$. Then the probability of observing state $i \in [m]$ in the model $\mathbf{f}$ equals $f_i(\theta) = \sum_{j=1}^{n} \theta^{a_{ij}}$. The tropicalization of this polynomial is the tropical polynomial

$$g_i(w) \;=\; \bigoplus_{j=1}^{n} w^{\odot a_{ij}} \;=\; \min\bigl\{a_{ij1}w_1 + a_{ij2}w_2 + \cdots + a_{ijd}w_d\bigr\}.$$

If we introduce logarithmic parameters $w_i = -\log(\theta_i)$ then our problem is to evaluate the tropical polynomial $g_i(w)$. We summarize this as a remark.

Example 4.12 (Google) A useful example to keep in mind when thinking of MAP inference is the Google "did you mean..." feature. A web search for the words `topicaal geom try` leads Google to respond with `Did you mean:` <u>`tropical geometry`</u>. In this case, the observed sequence (or the index i in the discussion above) is `topicaal geom try`. The MAP inference problem is to find the set of words (index j) that maximizes $f_{ij}(\theta)$. The model can be specified in many ways, perhaps taking advantage of patterns in the English language or among commonly used web sites. Below we replace the English language by DNA, and patterns of usage in the English language by features of genes.

We emphasize in a separate remark below the connection between MAP inference and tropical arithmetic. Implications of this connection are discussed in Chapters 5–9.

Remark 4.13 MAP inference is tropical evaluation of a coordinate polynomial.

In the context of biological sequence analysis, hidden Markov models can be used to model splice sites of eukaryotic genes. The underlying biology was explained in the previous section. Our model incorporates two fixed sizes for the $5'$ and $3'$ splice sites (k and k' respectively), and distinguishes exons from introns. Our HMM has length n where n is the length of the DNA sequences we wish to model. The alphabet of hidden states is $\Sigma = \{E, 1, \ldots, k, I, 1', \ldots, k'\}$, where E is a state for "exon" sequence preceding the first splice site and I a state for "intron" after the first splice site. The alphabet of observed states is $\Sigma' = \{\mathtt{A}, \mathtt{C}, \mathtt{G}, \mathtt{T}\}$.

The parameters of this model consist of a pair of matrices θ, θ' where

$$\theta \quad = \quad \begin{array}{c} \\ E \\ 1 \\ 2 \\ \vdots \\ k-1 \\ k \\ I \\ 1' \\ \vdots \\ k'-1 \\ k' \end{array} \begin{array}{c} \begin{array}{cccccccccccc} E & 1 & 2 & 3 & \cdots & k & I & 1' & 2' & \cdots & k' \end{array} \\ \begin{pmatrix} \theta_1 & 1-\theta_1 & 0 & 0 & \cdots & 0 & 0 & 0 & 0 & \cdots & 0 \\ 0 & 0 & 1 & 0 & \cdots & 0 & 0 & 0 & 0 & \cdots & 0 \\ 0 & 0 & 0 & 1 & \cdots & 0 & 0 & 0 & 0 & \cdots & 0 \\ & & & & \ddots & & & & & & \\ 0 & 0 & 0 & 0 & \cdots & 1 & 0 & 0 & 0 & \cdots & 0 \\ 0 & 0 & 0 & 0 & \cdots & 0 & 1 & 0 & 0 & \cdots & 0 \\ 0 & 0 & 0 & 0 & \cdots & 0 & \theta_2 & 1-\theta_2 & 0 & \cdots & 0 \\ 0 & 0 & 0 & 0 & \cdots & 0 & 0 & 0 & 1 & \cdots & 0 \\ & & & & & & & & & \ddots & \\ 0 & 0 & 0 & 0 & \cdots & 0 & 0 & 0 & 0 & \cdots & 1 \\ 1 & 0 & 0 & 0 & \cdots & 0 & 0 & 0 & 0 & \cdots & 0 \end{pmatrix} \end{array}$$

and θ' is a $(k+2) \times 4$ matrix specifying the output probabilities. The latter matrix is known as a *position specific scoring matrix* (PSSM) or a *weight matrix*. When describing a PSSM, the output probabilities for the states I and E are typically not represented, as they are assumed to either be 0.25 for all observed possibilities, or else easily obtainable for the problem at hand.

Example 4.14 Using 139 different splice site junction sequences, [Mount, 1982] estimated the parameters for a ($k = 12$) PSSM for donor sites :

$$\begin{array}{c} \\ \mathtt{G} \\ \mathtt{A} \\ \mathtt{T} \\ \mathtt{C} \end{array} \begin{array}{c} \begin{array}{cccccccccccc} 1 & 2 & 3 & 4 & 5 & 6 & 7 & 8 & 9 & 10 & 11 & 12 \end{array} \\ \begin{pmatrix} 0.2 & 0.09 & 0.11 & 0.74 & 1 & 0 & 0.29 & 0.12 & 0.84 & 0.09 & 0.18 & 0.2 \\ 0.3 & 0.4 & 0.64 & 0.09 & 0 & 0 & 0.61 & 0.67 & 0.09 & 0.16 & 0.39 & 0.24 \\ 0.2 & 0.07 & 0.13 & 0.12 & 0 & 1 & 0.07 & 0.11 & 0.05 & 0.63 & 0.22 & 0.27 \\ 0.3 & 0.44 & 0.11 & 0.06 & 0 & 0 & 0.02 & 0.09 & 0.02 & 0.12 & 0.2 & 0.28 \end{pmatrix} \end{array}$$

This particular PSSM played a key role in helping to find splice sites in genomes, although the availability of much more data has revealed additional structure in splice sites which can be modeled and used to improve their identification [Abril *et al.*, 2005].

The transition matrix θ is typically sparse, and so it is convenient to represent the sparsity pattern with a directed graph. This graph is known as the *state space diagram*. In our HMM for two splice sites, that graph is a directed cycle of length of $k + k' + 2$ with two special nodes (namely, "E" and "I") which have self-loops. We shall explain MAP inference for this model. For simplicity we assume that numerical values (perhaps those in Example 4.14) have been fixed for all entries in the PSSM θ', and that the initial distribution on Σ is the distribution which is uniform on the two states "E" and "I".

Suppose we are considering DNA sequences of length n. Then our HMM is a polynomial map $\mathbf{f} : \mathbb{R}^2 \to \mathbb{R}^{4^n}$. The coordinates of the map $\mathbf{f}$ are indexed by DNA sequences $\sigma \in (\Sigma')^n$. Each coordinate f_σ is a polynomial in the two model parameters θ_1 and θ_2 which is naturally written in the form

$$f_\sigma(\theta_1, \theta_2) \quad = \quad \sum_{i,j,k,l} \alpha_{ijkl} \cdot \theta_1^i \cdot (1-\theta_1)^j \cdot \theta_2^k \cdot (1-\theta_2)^l,$$

where $\alpha_{ijkl} \in \mathbb{R}_{\geq 0}$ depends polynomially on the entries in the PSSM θ'. Each sequence in Σ^n that is a walk in the directed cycle described above will contribute to one of the summands of $f_\sigma(\theta_1, \theta_2)$. In that summand, i is the number of adjacent pairs "EE" in the sequence, j is the number of pairs "$E1$", k is the number of pairs "II", and l is the number of pairs "$I1'$".

For instance, if $n = 10, k = k' = 2$ and the observation is $\sigma = \mathtt{ACGTGGTGCA}$ then the sequence of hidden states $EE12III1'2'E$ contributes the term

$$\big((\theta'_{E\mathtt{A}})^2\theta'_{C\mathtt{A}}(\theta'_{I\mathtt{G}})^2\theta'_{I\mathtt{T}}\theta'_{\mathtt{1G}}\theta'_{\mathtt{1T}}\theta'_{\mathtt{1'G}}\theta'_{\mathtt{2'C}}\big) \cdot \theta_1 \cdot (1-\theta_1) \cdot \theta_2^2 \cdot (1-\theta_2),$$

where the parenthesized product is a constant real number.

For MAP inference in this model it is convenient to think of θ_i and $1-\theta_i$ as independent parameters. We thus introduce four different logarithmic weights:

$$w_{11} = -\log(\theta_1),\ w_{12} = -\log(1-\theta_1),\ w_{21} = -\log(\theta_2),\ w_{22} = -\log(1-\theta_2).$$

Then the tropicalization of $f_\sigma(\theta_1, \theta_2)$ has the form

$$g_\sigma(w) \quad = \quad \min_{i,j,k,l}\big\{\beta_{ijkl} + iw_{11} + jw_{12} + kw_{21} + lw_{22}\big\}.$$

MAP inference for this model means evaluating this piecewise-linear function for fixed w_{ij}. Parametric inference means precomputing $g_\sigma(w)$ by polyhedral geometry. Using the techniques discussed in Section 3.3, this can be done easily for any given PSSM θ' and observation σ. The output of that computation is a complete list of all the *Viterbi sequences*, by which we mean a sequence in Σ^n whose corresponding linear form $\beta_{ijkl} + iw_{11} + jw_{12} + kw_{21} + lw_{22}$ attains the unique minimum for some choice of weights w_{ij}. Each Viterbi sequence represents the optimal splice site locations for a range of numerical values of θ_1 and θ_2. The list of Viterbi sequences produced by parametric inference also include a characterization of all boundaries between these ranges in the (θ_1, θ_2)-plane. Such an output may provide valuable information about the robustness of a specific Viterbi sequence to changes in the parameters.

In order to predict genes in a genome, a more sophisticated HMM than the splice site model given above needs to be used. Indeed, more recent approaches to gene finding make use of much more sophisticated HMMs that not only model splice sites, but also ensure that predicted structures contain an open reading frame (ORF). This means that the translated part of the mRNA must be of length 0 mod 3, and must contain a stop codon only at the very end. In addition, exon lengths, which are not geometrically distributed, are modeled explicitly using a modification of hidden Markov models known as *semi-hidden Markov models* or *generalized HMMs*. In Example 4.15 we describe a model that ensures the correct length for open reading frames, but that does not explicitly model splice sites or exon lengths. For a description of more complete models see [Burge and Karlin, 1997, Kulp *et al.*, 1996, Alexandersson *et al.*, 2003, Pachter *et al.*, 2002].

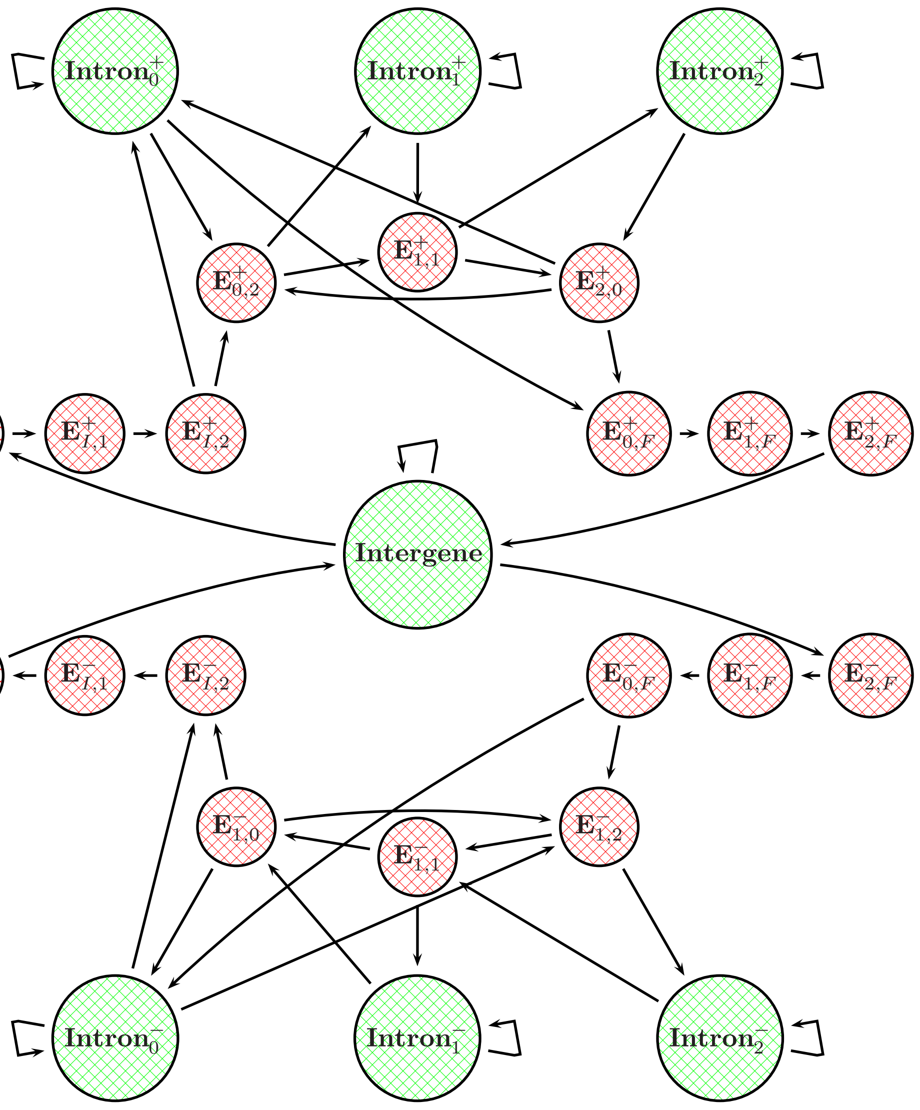

Fig. 4.5. State space diagram for a simple gene finding HMM.

Example 4.15 [Gene finding HMM] The model consists of a pair of matrices, θ, θ', one of which is a 25×25 matrix θ (transition probabilities) , and the other a 25×4 matrix (output probabilities). In total, there can therefore be up to 725 parameters. In practice, biological considerations simplify matters, leading to matrices θ that are very sparse. In fact, the specific model we have in mind has only 41 non-zero entries for the matrix θ. There is also additional structure in θ, for example many entries are set to 1. Models with so many parameters are summarized with a *state transition diagram* (see Figure 4.5). The state transition diagram is a graph with one node for every state in Σ. There is an edge for every nonzero entry in the matrix θ. Notice that the bottom half of the state transition diagram is a mirror image of the top half (with the directions of the arrows reversed). This reflects the fact that genes can be found on either strand of the DNA sequence.

Proposition 4.16 *The probability of any hidden path in the model in Example 4.15 that does not use* $0 \bmod 3$ *exon states is* 0*.*

The parameters θ' in a gene finding HMM are derived from known observed frequencies of codons in known genes, and from the overall frequencies of the bases in intergenic and intronic DNA. In other words, the maximum likelihood estimates for these parameters can be obtained from the fully observed model using Proposition 1.9 and Theorem 1.10. The parameters in θ relate biologically to lengths of introns, exons, and the distance between genes. These are also derived from known genes (for how this is done see the final section below). In principle, one could estimate the parameters using MLE with the hidden model, however this is typically not done in practice.

The model we have described in Example 4.15 has a number of limitations. As we have discussed, it does not model splice sites at all and there is no explicit modeling of exon lengths. There are also other gene elements that are simply not possible to model at all with current methods. For example, different cell types in an organism have different genes transcribed (and therefore translated) at different times. This process is largely regulated through enhancement or suppression of transcription, and is referred to as *regulation*. *Transcription factor binding sites* (TFBS), also called *cis-regulatory elements* are small sequences, typically in the neighborhood of genes that are bound to by proteins that mediate transcription (called *trans-acting*). A complete solution to the gene finding problem therefore requires annotation of TFBSs. Despite some encouraging results for TFBS identification with hidden Markov models, the problem problem is much harder and has traditionally been tackled separately.

4.5 Statistical models of mutation

Point mutations in DNA sequences are well modeled by continuous Markov processes on trees. This point of view, pioneered by Joe Felsenstein [Felsenstein, 2003], has been extensively explored and developed during the past thirty years. The relevant algebraic statistics involves the hidden tree models of Subsection 1.4.4. In what follows we offer a derivation of biologically relevant hidden tree models. We also return to our discussion of pair hidden Markov models for sequence alignment, with a biological discussion of insertions and deletions, and by explaining what exactly DiaNA is doing in the diagram on the book cover.

4.5.1 Evolutionary Models

Although the biology of point mutation is complicated, the use of Markov processes on trees is motivated by underlying principles which capture, to some degree, the complexities of mutation. These are:

- Mutations occur at random, although possibly with different probabilities at different places in the genome.
- Mutations occur independently in different species.
- In genome locations where mutations can occur, there is, at any given time, a nonzero probability that mutation occurs.

The first two requirements leads naturally to hidden tree models. The tree T corresponds to a species tree, with different species labeling the leaves of the tree. Thus, we have the structure of a phylogenetic tree appearing naturally, and associating a hidden tree model with the point mutation process is equivalent to specifying that bases observed at the leaves of the tree are a result of a stochastic process of mutation between "hidden" interior vertices of the tree.

The third requirement leads to a further restriction of hidden tree models, specifically to *evolutionary models* . We now define this class of models.

A *rate matrix* (or *Q-matrix*) is a square matrix $Q = (q_{ij})_{i,j\in\Sigma}$, with rows and columns indexed by $\Sigma = \{\mathtt{A},\mathtt{C},\mathtt{G},\mathtt{T}\}$ (note that the twenty letter alphabet of amino acids may also be used). Rate matrices must satisfy the following requirements:

$$q_{ij} \geq 0 \quad \text{for} \quad i \neq j,$$

$$\sum_{j\in\Sigma} q_{ij} = 0 \quad \text{for all} \quad i \in \Sigma,$$

$$q_{ii} < 0 \quad \text{for all} \quad i \in \Sigma.$$

Rate matrices capture the notion of *instantaneous rate of mutation*. From a given rate matrix Q one computes the *substitution matrices* $\theta(t)$ by exponentiation. The entry of $\theta(t)$ in row i and column j equals the probability that the substitution $i \to \cdots \to j$ occurs in a time interval of length t.

Theorem 4.17 *Let Q be any rate matrix and $\theta(t) = e^{Qt} = \sum_{i=0}^{\infty} \frac{1}{i!} Q^i t^i$. Then*

(i) $\theta(s+t) = \theta(s) \cdot \theta(t)$ *(Chapman-Kolmogorov equations),*
(ii) $\theta(t)$ *is the unique solution to the forward differential equation* $\theta'(t) = \theta(t) \cdot Q$, $\theta(0) = \mathbf{1}$ *for* $t \geq 0$, *(here* $\mathbf{1}$ *is the identity matrix)*
(iii) $\theta(t)$ *is the unique solution to the backward differential equation* $\theta'(t) = Q \cdot \theta(t)$, $\theta(0) = \mathbf{1}$ *for* $t \geq 0$.
(iv) $\theta^{(k)}(0) = Q^k$.

Furthermore, a matrix Q is a rate matrix if and only if the matrix $\theta(t) = e^{Qt}$ is a stochastic matrix (nonnegative with row sums equal to one) for every $t \geq 0$.

Proof For any matrix A, the matrix exponential e^A is defined by

$$e^A := \sum_{k=0}^{\infty} \frac{A^k k}{k!}.$$

The matrix exponential is well defined because the series on the right hand side converges componentwise for any A. A standard identity that can be derived directly from the definition is that $e^{A+B} = e^A e^B$ provided that A and B are matrices that commute. Since sQ and tQ commute for any s, t, it follows that $\theta(s+t) = \theta(s) \cdot \theta(t)$. In order to derive (ii) and (iii), we need to differentiate $\theta(t)$ term-by-term, which is possible because the power series $\theta(t)$ has infinite radius of convergence. We find that

$$\theta'(t) \;=\; \sum_{k=1}^{\infty} \frac{t^{k-1} Q^k}{(k-1)!} \;=\; \theta(t) \cdot Q \;=\; Q \cdot \theta(t).$$

Iterated differentiation leads to the identity (iv), which says that the kth derivative of $\theta(t)$ evaluated at 0 is just the matrix Q^k. The uniqueness in parts (ii) and (iii) is a standard result on systems of ordinary linear differential equations.

The last part of the theorem provides the crucial connection between rate matrices and substitution matrices. One direction of the theorem is easy: if $\theta(t)$ is a substitution matrix for every $t \geq 0$, then $\sum_j \theta_{ij}(t) = 1$ for all $t \geq 0$. Using identity (iv) with $k = 1$, we have that

$$\sum_j q_{ij}(t) \;=\; \sum_j \theta'_{ij}(0) \;=\; 0.$$

This says that the row sums of Q are 0, i.e., Q is a rate matrix. To prove the other direction, we note that as $t \to 0$, the Taylor series expansion gives $\theta(t) = I + tQ + O(t^2)$ which immediately implies that $q_{ij}(t) \geq 0$ for $i \neq j$ if and only if $\theta_{ij}(t) \geq 0$ for all i, j when t is sufficiently small. But $\theta(t) = \theta(t/m)^m$ for all m, so in fact $q_{ij} \geq 0$ iff $\theta_{ij}(t) \geq 0$ for all $t \geq 0$. Finally, it is easy to check that since Q has row sums equal to zero, so does Q^m for all m, and so the result follows directly from the definition of $\theta(t)$ in terms of Q. □

A standard example is the *Jukes-Cantor rate matrix*

$$Q \quad = \quad \begin{pmatrix} -3\alpha & \alpha & \alpha & \alpha \\ \alpha & -3\alpha & \alpha & \alpha \\ \alpha & \alpha & -3\alpha & \alpha \\ \alpha & \alpha & \alpha & -3\alpha \end{pmatrix},$$

where $\alpha \geq 0$ is a parameter. The corresponding substitution matrix equals

$$\theta(t) \quad = \quad \frac{1}{4}\begin{pmatrix} 1+3e^{-4\alpha t} & 1-e^{-4\alpha t} & 1-e^{-4\alpha t} & 1-e^{-4\alpha t} \\ 1-e^{-4\alpha t} & 1+3e^{-4\alpha t} & 1-e^{-4\alpha t} & 1-e^{-4\alpha t} \\ 1-e^{-4\alpha t} & 1-e^{-4\alpha t} & 1+3e^{-4\alpha t} & 1-e^{-4\alpha t} \\ 1-e^{-4\alpha t} & 1-e^{-4\alpha t} & 1-e^{-4\alpha t} & 1+3e^{-4\alpha t} \end{pmatrix}.$$

The expected number of substitutions over time t is the quantity

$$3\alpha t \quad = \quad -\frac{1}{4}\cdot \operatorname{trace}(Q)\cdot t \quad = \quad -\frac{1}{4}\cdot \log\det\bigl(\theta(t)\bigr). \tag{4.2}$$

This number is called the *branch length*. It can be computed from the substitution matrix $\theta(t)$ and is used to weight the edges in a phylogenetic tree.

One way to specify an evolutionary model is to give a phylogenetic tree T together with a rate matrix Q and an initial distribution for the root of T (which we here assume to be the uniform distribution on Σ). The branch lengths of the edges are unknown parameters, and the objective is to estimate these branch lengths from data. Thus if the tree T has r edges, then such a model has r free parameters, and, according to the philosophy of algebraic statistics, we would like to regard it as an r-dimensional algebraic variety.

Such an algebraic representation does indeed exist, This is not entirely obvious since the probabilities in the substitution $\theta(t)$ do not depend polynomially on the parameters α and t. We shall explain the (algebraic representation of) the Jukes-Cantor DNA model on an arbitrary finite rooted tree T. Suppose that T has r edges and the leaves are indexed by $[n] = \{1, 2, \ldots, n\}$. Let $\theta_i(t)$ denote the substitution matrix associated with the i-th edge of the tree.

We make the following change of variables in the space of parameters. Instead of using α_i and t_i as in (4.2), we introduce the new two parameters

$$\pi_i = \frac{1}{4}(1 - e^{-4\alpha_i t_i}) \quad \text{and} \quad \mu_i = \frac{1}{4}(1 + 3e^{-4\alpha_i t_i}).$$

These parameters satisfy the linear constraint

$$\mu_i + 3\pi_i \quad = \quad 1,$$

and the branch length of the i-th edge can be recovered as follows:

$$3\alpha_i t_i \quad = \quad -\frac{1}{4}\cdot \log\det\bigl(\theta^i\bigr) \quad = \quad -\frac{3}{4}\cdot \log(1-4\pi_i).$$

Indeed, the parameters are simply the entries in the substitution matrix

$$\theta^i \quad = \quad \begin{pmatrix} \mu_i & \pi_i & \pi_i & \pi_i \\ \pi_i & \mu_i & \pi_i & \pi_i \\ \pi_i & \pi_i & \mu_i & \pi_i \\ \pi_i & \pi_i & \pi_i & \mu_i \end{pmatrix}.$$

The *Jukes-Cantor model* is a submodel of the general Hidden Tree Model which was introduced in Section 1.4. Namely, the Jukes-Cantor model on the tree T with r edges and n leaves is the polynomial map

$$\mathbf{f} \,:\, \mathbb{R}^r \;\to\; \mathbb{R}^{4^n}$$

which is obtained by specializing the transition matrices to the specific 4×4 matrices θ^i above.

Remark 4.18 Each coordinate polynomial $f_{u_1u_2\cdots u_n}$ of the Jukes-Cantor model is a multilinear polynomial in the model parameters $(\mu_1, \pi_1), \ldots, (\mu_n, \pi_n)$, i.e., $f_{u_1u_2\cdots u_n}$ is linear in (μ_i, π_i) when the other parameters are fixed.

As an illustration we derive the model which was featured in Example 1.7.

Example 4.19 Let $n = r = 3$, and let T be the tree with three leaves, labeled by $\{1,2,3\}$, directly branching off the root of T. We consider the Jukes-Cantor DNA model with uniform root distribution on T. This model is a three-dimensional algebraic variety, given as the image of a trilinear map

$$\mathbf{f} \;:\; \mathbb{R}^3 \;\to\; \mathbb{R}^{64}.$$

The number of states in $\{\mathtt{A},\mathtt{C},\mathtt{G},\mathtt{T}\}^3$ is $4^3 = 64$ but there are only five distinct polynomials occurring among the coordinates of the map $\mathbf{f}$. Let p_{123} be the probability of observing the same letter at all three leaves, p_{ij} the probability of observing the same letter at the leaves i, j and a different one at the third leaf, and p_{dis} the probability of seeing three distinct letters. Then

$$\begin{aligned}
p_{123} &= \mu_1\mu_2\mu_3 \;+\; 3\pi_1\pi_2\pi_3,\\
p_{dis} &= 6\mu_1\pi_2\pi_3 \;+\; 6\pi_1\mu_2\pi_3 \;+\; 6\pi_1\pi_2\mu_3 \;+\; 6\pi_1\pi_2\pi_3,\\
p_{12} &= 3\mu_1\mu_2\pi_3 \;+\; 3\pi_1\pi_2\mu_3 \;+\; 6\pi_1\pi_2\pi_3,\\
p_{13} &= 3\mu_1\pi_2\mu_3 \;+\; 3\pi_1\mu_2\pi_3 \;+\; 6\pi_1\pi_2\pi_3,\\
p_{23} &= 3\pi_1\mu_2\mu_3 \;+\; 3\mu_1\pi_2\pi_3 \;+\; 6\pi_1\pi_2\pi_3.
\end{aligned}$$

All 64 coordinates of $\mathbf{f}$ are given by these five trilinear polynomials, namely,

$$\begin{aligned}
f_{\texttt{AAA}} = f_{\texttt{CCC}} = f_{\texttt{GGG}} = f_{\texttt{TTT}} &= \frac{1}{4}\cdot p_{123},\\
f_{\texttt{ACG}} = f_{\texttt{ACT}} = \cdots = f_{\texttt{GTC}} &= \frac{1}{24}\cdot p_{dis},\\
f_{\texttt{AAC}} = f_{\texttt{AAT}} = \cdots = f_{\texttt{TTG}} &= \frac{1}{12}\cdot p_{12},\\
f_{\texttt{ACA}} = f_{\texttt{ATA}} = \cdots = f_{\texttt{TGT}} &= \frac{1}{12}\cdot p_{13},\\
f_{\texttt{CAA}} = f_{\texttt{TAA}} = \cdots = f_{\texttt{GTT}} &= \frac{1}{12}\cdot p_{23}.
\end{aligned}$$

This means that our Jukes-Cantor model is the image of the simplified map

$$\mathbf{f}' : \mathbb{R}^3 \to \mathbb{R}^5,\ \big((\mu_1,\pi_1),(\mu_2,\pi_2),(\mu_3,\pi_3)\big) \mapsto (p_{123},p_{dis},p_{12},p_{13},p_{23}).$$

There are only three parameters since $\mu_i+3\pi_i = 1$. Algebraists prefer the above representation with $(\mu_i : \pi_i)$ as homogeneous coordinates on the projective line.

To characterize the image of $\mathbf{f}'$ algebraically, we perform the following linear change of coordinates:

$$\begin{aligned}
q_{111} &= p_{123} + \tfrac{1}{3}p_{dis} - \tfrac{1}{3}p_{12} - \tfrac{1}{3}p_{13} - \tfrac{1}{3}p_{23} = (\mu_1-\pi_1)(\mu_2-\pi_2)(\mu_3-\pi_3)\\
q_{110} &= p_{123} - \tfrac{1}{3}p_{dis} + p_{12} - \tfrac{1}{3}p_{13} - \tfrac{1}{3}p_{23} = (\mu_1-\pi_1)(\mu_2-\pi_2)(\mu_3+3\pi_3)\\
q_{101} &= p_{123} - \tfrac{1}{3}p_{dis} - \tfrac{1}{3}p_{12} + p_{13} - \tfrac{1}{3}p_{23} = (\mu_1-\pi_1)(\mu_2+3\pi_2)(\mu_3-\pi_3)\\
q_{011} &= p_{123} - \tfrac{1}{3}p_{dis} - \tfrac{1}{3}p_{12} - \tfrac{1}{3}p_{13} + p_{23} = (\mu_1+3\pi_1)(\mu_2-\pi_2)(\mu_3-\pi_3)\\
q_{000} &= p_{123} + p_{dis} + p_{12} + p_{13} + p_{23} = (\mu_1+3\pi_1)(\mu_2+3\pi_2)(\mu_3+3\pi_3)
\end{aligned}$$

This reveals that our model is the hypersurface in Δ_4 whose ideal equals

$$I_T = \langle\, q_{000}q_{111}^2 - q_{011}q_{101}q_{110}\,\rangle$$

If we set $\mu_i = 1-3\pi_i$ then we get the additional constraint $q_{000} = 1$.

The construction in this example generalizes to arbitrary trees T. There exists a change of coordinates, simultaneously on the *parameter space* $(\mathbb{P}^1)^r$ and on the *probability space* $\mathbb{P}^{4^n-1}$, such that the map $\mathbf{f}$ becomes a monomial map in the new coordinates. This change of coordinates is known as the *Fourier transform* or as the *Hadamard conjugation* (see [Evans and Speed, 1993, Hendy and Penny, 1993, Semple and Steel, 2003]).

We regard the Jukes-Cantor DNA model on a tree T with n leaves and r edges as an algebraic variety of dimension r in $\mathbb{P}^{4^n-1}$, namely, it is the image of the map $\mathbf{f}$. Its homogeneous prime ideal I_T is generated by differences of monomials $q^a - q^b$ in the Fourier coordinates. In the phylogenetics literature (including the books [Felsenstein, 2003, Semple and Steel, 2003]), the polynomials in the ideal I_T are known as *phylogenetic invariants* of the model. The following result was shown in [Sturmfels and Sullivant, 2004].

Theorem 4.20 *The ideal I_T which defines the Jukes-Cantor model on a binary tree T is generated by monomial differences $q^a - q^b$ of degree at most three.*

If we allow Q to be an arbitrary rate matrix then $P(t)$ is an arbitrary stochastic matrix. The resulting model is the *general Markov model* on the tree T. Allman and Rhodes [Allman and Rhodes, 2003] determined an almost-complete system of phylogenetic invariants for the general Markov model on a tree T.

An important problem in phylogenomics is to identify the maximum likelihood branch lengths, given a phylogenetic X-tree T, a rate matrix Q and an alignment of sequences. For the Jukes-Cantor DNA model on three taxa, described in Example 4.19, the exact "analytic" solution of this optimization problem leads to an algebraic equation of degree 23. See Section 3.3 for details.

The *Felsenstein hierarchy* is the cumulative result of experimentation and development of many special continuous time Markov models with rate matrices that incorporate biologically meaningful parameters. The models are summarized in Figure 4.6, with arrows indicating the nesting of the models, and the more general models on top. Each matrix shown is a rate matrix Q, and it is assumed that $\pi_A + \pi_C + \pi_G + \pi_T = 1$. The diagonal entries (marked by a dot) are forced, by the definition of a rate matrix, to equal the negative of the sum of the other entries in their row.

The simplest model is the Jukes-Cantor model [Jukes and Cantor, 1969] which is highly structured and imposes a uniform root distribution, together with equal probabilities for transitions and transversions. On the other end of the spectrum is the general time reversible (REV) model which only imposes the requirement of time reversibility. The drawback of the REV model is that it lacks the group structure of the Jukes-Cantor model, and maximum likelihood estimation is also complicated by the added parameters. A number of compromises have been studied, one of the most popular being the Hasegawa-Kishino-Yano (HKY) model. This model allows for different transition and

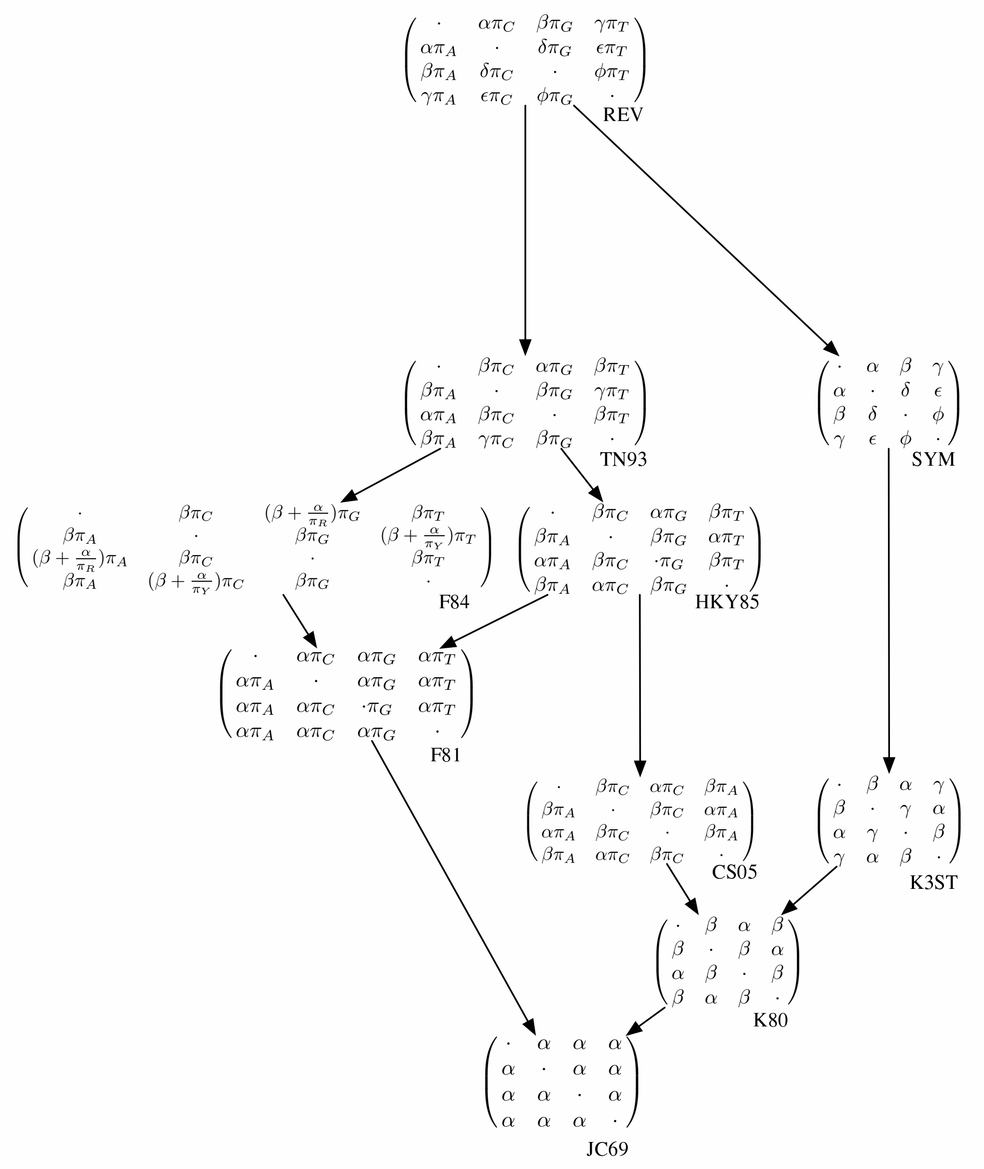

Fig. 4.6. The Felsenstein Hierarchy

transversion rates, a requirement which is dictated by the chemistry of DNA (Figure 4.1).

Strand symmetric models are specializations of the REV model in which it is assumed that $\pi_A = \pi_T$, and $\pi_C = \pi_G$. In [Yap and Pachter, 2004] it is shown that REV rate matrices estimated from human, mouse and rat alignments indicate that strand symmetry is a reasonable assumption. This is the basis for the study of the strand symmetric model in Chapter 16 by Casanellas and Sullivant.

We conclude with two examples: one that shows how mutation models are used in distance based tree reconstruction methods, and another which illustrates the use of evolutionary models for identifying conserved positions in genomes.

Example 4.21 (Jukes-Cantor correction) Suppose that we are given a multiple alignment from which we would like to infer a tree:

Human:	`ACAATGTCATTAGCGAT...`
Mouse:	`ACGTTGTCAATAGAGAT...`
Rat:	`ACGTAGTCATTACACAT...`
Chicken:	`GCACAGTCAGTAGAGCT...`

If there are many taxa, it is not feasible to search through all trees (Section 2.4), so instead a metric is constructed and then projected onto a tree metric. The neighbor joining algorithm 2.40 is the most widely used projection.

In order to obtain a metric, mutation models are used to compute the maximum likelihood distance between each pair of taxa. In the case of the Jukes-Cantor model this is known as the *Jukes-Cantor correction*. More generally, such estimates are called *pairwise distance estimates*. Here the tree T has only two leaves, labeled by $X = \{1, 2\}$, directly branching off the root of T. The model is given by a surjective bilinear map

$$\phi \ : \ \mathbb{P}^1 \times \mathbb{P}^1 \ \to \ \mathbb{P}^1\,, \quad ((\mu_1, \pi_1), (\mu_2, \pi_2)) \ \mapsto \ (\, p_{12}, p_{dis}\,). \tag{4.3}$$

The coordinates of the map ϕ are

$$\begin{aligned} p_{12} \quad &= \quad \mu_1\mu_2 \ + \ 3\pi_1\pi_2, \\ p_{dis} \quad &= \quad 3\mu_1\pi_2 \ + \ 3\mu_2\pi_1 \ + \ 6\pi_1\pi_2. \end{aligned}$$

As before, we pass to affine coordinates by setting $\mu_i = 1 - 3\pi_i$ for $i = 1, 2$.

One crucial difference between the model (4.3) and Example 4.19 is that the parameters in (4.3) are *not identifiable*. Indeed, the inverse image of any point in $\mathbb{P}^1$ under the map ϕ is a curve in $\mathbb{P}^1 \times \mathbb{P}^1$. Suppose we are given data consisting of two aligned DNA sequences of length n where k of the bases are different. The corresponding point in $\mathbb{P}^1$ is $u = (n - k, k)$. The inverse image of u under the map ϕ is the curve in the affine plane with the equation

$$12n\pi_1\pi_2 \ - \ 3n\pi_1 \ - \ 3n\pi_2 \ + \ k \quad = \quad 0.$$

Every point (π_1, π_2) on this curve is an *exact fit* for the data $u = (n - k, k)$. Hence this curve equals the set of all maximum likelihood parameters for this model and the given data. We rewrite the equation of the curve as follows:

$$(1-4\pi_1)(1-4\pi_2) \quad = \quad 1-\frac{4k}{3n}. \tag{4.4}$$

Recall from (4.2) that the branch length from the root to leaf i equals

$$3\alpha_i t_i \quad = \quad -\frac{1}{4}\cdot \log\det\bigl(\theta^i(t)\bigr) \quad = \quad -\frac{3}{4}\cdot\log(1-4\pi_i).$$

By taking logarithms on both sides of (4.4), we see that the curve of all maximum likelihood parameters becomes a line in the branch length coordinates:

$$3\alpha_1 t_1 \ + \ 3\alpha_2 t_2 \quad = \quad -\frac{3}{4}\cdot\log\bigl(1-\frac{4k}{3n}\bigr). \tag{4.5}$$

The sum on the left hand side equals the distance from leaf 1 to leaf 2 in the tree T. We summarize our discussion of the two-taxa model as follows:

Proposition 4.22 *Given an alignment of two sequences of length n, with k differences between the bases, the ML estimate of the branch length equals*

$$\delta_{12} \quad = \quad -\frac{3}{4}\cdot\log\left(1-\frac{4k}{3n}\right).$$

Similar results exist for other models in the Felsenstein hierarchy.

Example 4.23 (Phylogenetic shadowing) Suppose we are given a column in a multiple alignment and we would like to know whether it is conserved or not. One way to answer this question is to perform a likelihood ratio test with two different points on an evolutionary model. That is, for a fixed observation $\sigma=\sigma_1\sigma_2\cdots\sigma_n$ of nucleotides at the leaves of a tree T, for a fixed model in the hierarchy, and for two different rate matrices Q_S (slow model) and Q_F (fast model), we compute

$$\frac{\log p^F_\sigma}{\log p^S_\sigma} \tag{4.6}$$

where p^F_σ is the probability of σ with rate matrix Q_F, and p^S_σ is the probability of σ with rate matrix Q_S. Such a test is especially sensible if the species being compared to each are at nearby evolutionary distances, so that the multiple alignment is reliable without many insertions and deletions [Boffelli *et al.*, 2003]. *Phylogenetic hidden Markov models* are extensions of hidden Markov models to more general tree models that take advantage of this idea. More details can be found in [Siepel and Haussler, 2004, McAuliffe *et al.*, 2004].

4.5.2 Insertion and Deletion

One of the main mechanisms by which DNA sequences change is insertion and deletion. Insertions and deletions can happen, for example, during DNA replication. Repetitive sequences are particularly prone to a phenomenon known as *strand slippage*, during which non-pairing of the complementary strand results in small insertions or deletions [Levinson and Gutman, 1987]. In order to correctly align sequences, it is therefore necessary to accurately model insertions and deletion, as well as point mutation.

The description of how pair hidden Markov models are parameterized based on biological considerations and subsequently used for inference takes us back to DiaNA, and her picture on the cover of the book. DiaNA is again our surrogate for biological intuition, and what follows is an exact description of what she is doing:

Example 4.24 (DiaNA hopping on the alignment graph) The graph on which DiaNA walks is the alignment graph $\mathcal{G}_{n,m}$ (Section 2.2). This is a square grid which includes diagonal edges. DiaNA begins at one corner and will walk along edges of the graph until she reaches the opposite corner. She must always walk towards the far corner; so in particular she cannot backtrack her steps. She walks randomly, which means that at every vertex, she decides at random which of the three directions to take. When she is on a boundary however, she is constrained to walk in only one direction since she must always progress towards the far corner.

Each time she takes a step she crosses an edge, and as she does so she tosses two tetrahedral die. Each of these die has the letters `A`,`C`,`G`,`T` written on the four sides. The die land (at random) and we, the result is recorded for us, the observers. Unfortunately, we are blindfolded so we cannot see DiaNA as she hops along the graph, but fortunately, her tetrahedral die tosses are recorded for us and we read them after she is done hopping. Our gaol is to guess which path she took on the graph.

Recall from Chapter 2 that a pair hidden Markov model is specified by two matrices, θ and θ'. DiaNA's random walk on the graph is determined by the matrix θ'. It is therefore $theta'$ which models insertions and deletions, with the probabilities associated to the length distributions. Suppose that DiaNA makes an insertion move. The probability that she repeats an insertion is $\theta'_{I,I}$. It follows that the probability that she remains walking in the same direction (i.e., keeps making insertions) for k steps is therefore $(\theta'_{I,I})^k$. The insertions generated by DiaNA are therefore geometrically distributed in length, with expected length $\frac{1}{1-(\theta'_{I,I})^k}$. The average length of observed insertions and deletions can therefore be used to set the parameters $\theta'_{I,I}$ and $\theta'_{D,D}$. Similarly, the frequency of insertions and deletions determines the parameters $\theta'_{H,I}$ and $\theta'_{H,D}$. Unfortunately, to date there has not been enough data to carefully measure these quantities, however it should be possible in the near future thanks to the extraordinary amount of new sequence data, much of it from closely related species pairs.

DiaNA's pair hidden Markov model also consists of a matrix θ, which contains the probabilities for pairs of nucleotides. It is therefore necessary to select a model for mutation, and to this end the models described in the point mutation section are very reasonable. Thus, DiaNA's pair hidden Markov model contains an evolutionary model as an ingredient (albeit with two taxa in the case of pairwise sequence alignment).

In Chapter 7, the question is explored of whether pair hidden Markov models are sufficient for modeling insertion and deletion. In particular, it is shown that there are genomic sequences for which no choice of parameters yields the correct alignment, thus indicating that there is lots of room for improvement in the modeling of sequences and their mutations. In other words, we do not yet understand exactly what it is that DiaNA is doing.

Our goal, of which we must not lose sight, is to find the best alignment, which means guessing how DiaNA hopped along the graph. Recalling Remark 4.13 this is precisely MAP inference, which is the tropical evaluation of a coordinate polynomial of the model.

Part II
Studies on the four themes

The contributions in this part of the book were all written by students, postdocs and visitors who in some way were involved in the graduate course *Algebraic Statistics for Computational Biology* that we taught in in the mathematics department at UC Berkeley during the fall of 2004. The chapters range in scope from specialized case studies, further developing some of the themes in Part 1, to full-blown research article on topics of current interest.

Many of the eighteen chapters contain original research that has not been published elsewhere. Some of the highlights among new results include:

- Theorem 6.7 which states that polytope propagation on a graph runs in polynomial time, even if the number of parameters is not fixed (Chapters 6). This is accompanied by theoretical investigations into exact bounds (Chapter 8) and the impact of specializing parameters (Chapter 5).
- An example of a biologically correct alignment which is not the optimal alignment for any choice of parameters in the pair HMM (Chapter 7).
- Theorem 9.1 which states that the number of inference functions of a graphical model grows polynomially for fixed number of parameters.
- Theorem 10.5 which states that, for alphabets with four or more letters, every toric Viterbi sequence is a Viterbi sequence.
- Explicit calculations of phylogenetic invariants for the strand symmetric model (Chapter 16) which highlight connections between the general reversible model and group based models.
- A novel method for tree reconstruction based on singular value decomposition (Chapter 19).

The other chapters also include either interesting new results, or in some cases important methodological advances. Chapter 15 introduces a standardized framework for working with small trees. Even results on the smallest nontrivial tree (with three leaves) are interesting, and are discussed in Chapter 18. Similarly, Chapter 14 presents a unified algebraic statistical view of mutagenic tree models. In terms of tools, Chapters 11 and 20 describe novel numerical approaches to solving long-standing problems. Chapter 12 is a thorough exposition of the Baum-Welch algorithm, and addresses some of the pitfalls to beware of when applying it. Chapters 13, 21 and 22 focus on some of the immediate challenges we face in working with and interpreting genomic data.

We present a brief biography for each of our twenty-seven contributors that summarizes their backgrounds, and explains their connection to our class.

- **Jameel Al-Aidroos** is a Ph.D. student in mathematics at UC Berkeley. He has worked on algebraic geometry (supervised by Tom Graber), and was first introduced to computational biology during our course in fall 2004.
- **Niko Beerenwinkel** received his Ph.D. in computer science in 2004 from the University of Saarbrücken, Germany (supervised by Thomas Lengauer). His thesis was on computational biology using machine learning methods. Upon graduation, he was awarded the prestigious Emmy Noether fellowship which he is using to pursue postdoctoral research at UC Berkeley.
- **Nicolas Bray** graduated with a B.S. in mathematics from UC Berkeley in 2004, and continues now as a Ph.D. student in the same department (supervised by Lior Pachter). He is the developer of the `MAVID` multiple alignment program, and continues to work on comparative genomics.
- **David Bryant** is an assistant professor of mathematics and computer science at McGill University in Montreal, Canada, and also holds a faculty position at the University of Auckland, New Zealand. An expert on phylogenetic analysis, he is a co-developer of the software package `SplitsTree`. David Bryant was invited to lecture in our course during the fall of 2004.
- **Marta Casanellas** is an assistant professor at the Universitat Politécnica de Catalunya in Barcelona, Spain. She is an expert in algebraic geometry, and became interested in computational biology in 2004, in the course of visiting Roderic Guigó and his computational biology group at the Institut Municipal d'Investigació Médical in Barcelona. Marta came to Berkeley in the fall of 2004 for an extended visit, and now works on phylogenetics.
- **Anat Caspi** is a Ph.D. student in the joint UC San Francisco/UC Berkeley graduate group in bioengineering (supervised by Lior Pachter). She has a Masters degree in computer science from Stanford University, and is interested in machine learning applications to computational biology.
- **Mark Contois** is an undergraduate student in mathematics at San Francisco State University (supervised by Serkan Hoşten). He has also working on computational biology in the laboratory of Eric Routman.
- **Colin Dewey** studied biology and computer science as an undergraduate at UC Berkeley, and is now a Ph.D. student in computer science (supervised by Lior Pachter). He has worked on homology mapping and parametric sequence alignment, and is the developer of the `Mercator` mapping program.
- **Mathias Drton** received his Ph.D. in statistics from the University of Washington in 2004 (supervised by Michael Perlman and Thomas Richardson). He has worked on maximum likelihood estimation in graphical models, and is a postdoctoral researcher at UC Berkeley. In Fall 2005 he will start a

tenure track position in the Department of Statistics at the University of Chicago.

- **Sergi Elizalde** received his Ph.D. in applied mathematics from M.I.T. in 2004 (supervised by Richard Stanley) where he worked on combinatorics and enumeration. He is currently a postdoctoral fellow at the Mathematical Sciences Research Institute at Berkeley (MSRI). Starting in Fall 2005, he will be a John Wesley Instructor in Mathematics at Dartmouth College.
- **Nicholas Eriksson** is a Ph.D. student in mathematics at UC Berkeley (supervised by Bernd Sturmfels). He has worked on on algebraic statistics and is the first mathematics graduate student at UC Berkeley to enroll in the designated emphasis in computational biology interdisciplinary program.
- **Luis David Garcia** received his Ph.D. in mathematics from Virginia Polytechnic Institute in 2004 (supervised by Reinhard Laubenbacher), where he worked at the Virginia Bioinformatics Institute. After spending a postdoctoral semester in the fall 2004 program on *Hyperplane Arrangements* at MSRI, he is now a Visiting Assistant Professor at Texas A & M University.
- **Ingileif B. Hallgrímsdóttir** will receive her Ph.D. in statistics from UC Berkeley in June 2005 (supervised by Terence Speed). She works in statistical genetics, a topic which she had already pursued while working at DeCODE Genetics in Iceland, and for her Masters in Gothenburg, Sweden.
- **Michael Joswig** is an expert in mathematical software and polyhedral geometry. He developed the software `POLYMAKE`. Michael holds a professorship in Mathematics at the Technische Universität Darmstadt, Germany.
- **Eric Kuo** will receive his Ph.D. in computer science from UC Berkeley in June 2005 (supervised by Lior Pachter). His interests range from theoretical computer science to convex polytopes and discrete mathematics.
- **Fumei Lam** will receive her Ph.D. in applied mathematics from M.I.T. in June 2005 (supervised by Michel Goemans). She has worked on graph theory, approximation algorithms and computational biology.
- **Garmay Leung** is a Ph.D. student in the joint UC San Francisco/UC Berkeley graduate group in bioengineering and is doing rotations (currently with Michael B. Eisen). She did research on computational biology and cell biology as an undergraduate at Cornell University.
- **Dan Levy** is receiving his Ph.D. in mathematics during the summer of 2005 (supervised by Lior Pachter and Rainer Sachs), and will stay in Berkeley for one more postdoctoral year. His research is in mathematical biology.
- **Radu Mihaescu** has a B.A. from Princeton University and is now a Ph.D. student in mathematics at UC Berkeley (supervised by Lior Pachter and Satish Rao). He is interested in theoretical computer science.
- **Alex Milowski** received his M.A. in mathematics from San Francisco State University in May 2004 (supervised by Serkan Hoşten). He was one of the

developers of the Extensible Markup Language (XML) and related standards.

- **Jason Morton** is a second-year Ph.D. student in mathematics at UC Berkeley (supervised by Bernd Sturmfels). He is interested in algebraic statistics.
- **Raazesh Sainudiin** will receive his Ph.D. in statistics from Cornell University in May 2005 (supervised by Rick Durett). His research is on statistical inference in population penetics, phylogenetics and molecular evolution.
- **Sagi Snir** received his Ph.D. in computer science in May 2004 from the Technion - Israel Institute of Technology (supervised by Benny Chor). He has worked on analytic maximum likelihood solutions for phylogenetic reconstruction, and on convex recoloring. He is a postdoc at UC Berkeley. mathematics department at UC Berkeley.
- **Seth Sullivant** received his M.A. from San Francisco State University in 2002 (supervised by Serkan Hoşten) and his Ph.D. from UC Berkeley in 2005 (supervised by Bernd Sturmfels). Both degrees are in mathematics. He works on algebraic statistics. Starting in July 2005, Seth will be a junior fellow with the Society of Fellows at Harvard University.
- **Kevin Woods** received his Ph.D. in mathematics from the University of Michigan in May 2004 (supervised by Alexander Barvinok). He is interested in combinatorics, specifically topics in discrete and computational geometry, and is an NSF postdoc in the Mathematics Department at UC Berkeley.
- **Ruriko Yoshida** received her Ph.D. in mathematics from UC Davis in May 2004 (supervised by Jesus DeLoera). She has worked on phylogeny reconstruction, combinatorics, contingency tables and integer programming. After visiting the Berkeley math department during the summer of 2004, she is now an Assistant Research Professor of Mathematics at Duke University.
- **Josephine Yu** was an undergraduate at UC Davis and is now a Ph.D. student in mathematics at UC Berkeley (supervised by Bernd Sturmfels). She has worked on matrix integrals, finite metric spaces and tropical geometry.

The results in this part of the book only begin to hint at the vast number of mathematical, computational, statistical and biological challenges that will need to be overcome in order to understand the function and organization of genomes. In a future version of our graduate course we imagine numerous new class projects on a wide range of topics including Bayesian statistics, graphical models with cycles, aspects of real algebraic geometry, information geometry, multiple sequence alignment, motif finding, RNA structure, whole genome phylogeny, and protein sequence analysis, to name a few.

5
Parametric Inference

Radu Mihaescu

Inference in graphical models is one of the most frequent and important statistical problems today. These models involve two kinds of random variables: hidden and observed. In computational biology applications, the *observed random variables* correspond to known biological data, such as a sequence of nucleotides, while the *hidden random variables* correspond to unknown biological information, such as which segments of DNA are coding regions or how two sequences align. The problem of inference in graphical models is concerned with finding an *explanation* for the observed data: the most likely set of values for the hidden variables given the set of observations. We refer the reader to Chapter I for a self-contained description of graphical models and inference.

Clearly, inference of hidden data is highly dependent on the characteristics of the graphical model, such as its topology and the transition matrices associated to its edges. But very often, the models we use do not come with specific transition matrices. Usually, the assumptions one can make about the nature of evolution, site mutation and other such biological phenomena allow us to place these transition matrices on some parameterized families.

This raises several questions. If our choice of parameters is slightly off, will the explanation change? What other choices of parameters will give the same explanation? Can we find all possible explanations and what parameters will yield them? These are the sorts of questions we will answer, using the tools of *parametric inference*, which solves the inference problem for all possible sets of parameters simultaneously.

In this chapter we present the *polytope propagation algorithm* for parametric inference, which was first introduced in [Pachter and Sturmfels, 2004a]. This algorithm is nothing more than the polytope algebra version (see Section 2.3) of a classical method in the theory of graphical models, known as *sum-product decomposition*. We examine the polytope propagation algorithm in Section 5.2, and, in particular, we describe the details of the algorithm in the context of two very important problems in computational biology: the hidden Markov model for gene annotation and the pair-hidden Markov model for gene alignment. The analysis relies heavily on the theory developed in Sections 1.4, 2.2 and 2.3, and the reader is strongly urged to become familiar with those sections before reading this chapter.

Unfortunately, the running time of polytope propagation is exponential in the number of parameters. Therefore, in applications where the number of parameters is very large it is of practical interest to specialize most of them to fixed values and study the dependence of the explanation upon variations of the remaining few parameters. In Section 5.4 we give an explicit presentation of an algorithm that does this efficiently, together with an analysis of its running time. As we will see, the complexity of the algorithm is, as one would hope, polynomial in the length of the sequences, for a fixed number of unspecialized parameters.

5.1 Tropical sum-product decompositions

In general, the problem of inference (for fixed parameters) can be regarded as the tropical version of computing the marginal probability of the observed data. Indeed, let us consider a graphical model and let the vector of values for the hidden and observed variables be denoted by σ and τ respectively. Then

$$\mathrm{Prob}(\tau) = \sum_{\sigma} p_{\sigma,\tau}, \tag{5.1}$$

where $p_{\sigma,\tau}$ is the probability of having states σ at the hidden nodes and states τ at the observed nodes of the model. This is the probability of the observed data marginalized over all possible values for the hidden data. On the other hand, the task of finding an explanation corresponds to identifying the set of hidden states $\bar{\sigma}$ with maximum a-posteriori probability of generating the observed data τ. In other words:

$$\bar{\sigma} = \mathrm{argmax}_{\sigma}\{p_{\sigma,\tau}\}.$$

Now following the notation of Chapter 2, let $w_* = -\ln(p_*)$. Then the above equation turns into

$$\bar{\sigma} = \mathrm{argmin}_{\sigma}\{w_{\sigma,\tau}\}.$$

This is exactly the marginalization in (5.1), performed in tropical algebra:

$$w_{\bar{\sigma}} = \bigodot_{\sigma} w_{\sigma,\tau} \tag{5.2}$$

The reader is referred to Section 2.1 for more details on the tropical algebra.

In general, marginal probabilities for acyclic graphical models can be computed in time polynomial in the size of the model using the *sum-product decomposition*, which is a recursive representation of a polynomial in terms of smaller polynomials. Such a decomposition is very useful for computing values of polynomial expressions with a large number of monomials, where a direct symbolic computation would be very costly. This is known in the literature as the *forward algorithm*.

As we can see from the above analysis, "tropicalizing" the operation of marginalization is equivalent to solving the inference problem. Therefore, the sum-product decomposition of marginal probabilities, when it exists, naturally yields efficient algorithms for inference with fixed parameters. In the following subsections we exemplify this with the *Viterbi algorithm* for hidden Markov models and the *Needleman-Wunsch algorithm* for sequence alignment (see Section 2.2).

5.1.1 The sum-product algorithm for HMM's

The hidden Markov model is one of the simplest and most popular models used in computational biology. In this subsection we will use the notation of Section 1.4, to which we also refer the reader unfamiliar with the model. Suppose that we have an HMM of length n, with hidden states σ_i, $i \in [n]$, taking values in an alphabet Σ with l letters, and observed variables τ_i, $i \in [n]$, taking values in the alphabet Σ' of size l'. The model parameters are the "horizontal" transition matrix $\theta \in \mathbb{R}^{l \times l}$ and the "vertical" transition matrix $\theta' \in \mathbb{R}^{l \times l'}$. The probability of occurrence of a full vector of states (σ, τ) is therefore

$$p_{\sigma,\tau} = \frac{1}{l}\theta'_{\sigma_1,\tau_1}\theta_{\sigma_1,\sigma_2}\theta'_{\sigma_2,\tau_2}\theta_{\sigma_2,\sigma_3}\dots\theta'_{\sigma_n,\tau_n}$$

Given an observation $\tau = \tau_1\tau_2\dots\tau_n$, the marginal probability of τ is:

$$p_\tau = \sum_\sigma p_{\sigma,\tau} \tag{5.3}$$

By tropicalizing and maintaining the notation from the beginning of the section we get that the explanation for the sequence of observations τ is given by

$$\begin{aligned} \bar{\sigma} &= \mathrm{argmin}_\sigma\{w_{\sigma,\tau}\} \\ w_{\bar{\sigma}} &= \bigoplus_\sigma w_{\sigma,\tau} \end{aligned} \tag{5.4}$$

The problem of computing (5.3) can be easily solved by noticing that the probability p_τ has the following decomposition:

$$p_\tau = \sum_{\sigma_n=1}^{l} \theta'_{\sigma_n,\tau_n}\Big(\sum_{\sigma_{n-1}=1}^{l} \theta_{\sigma_{n-1},\sigma_n}\theta'_{\sigma_{n-1},\tau_{n-1}}(\ldots(\sum_{\sigma_1=1}^{l} s_{\sigma_1,\sigma_2}\theta'_{\sigma_1,\tau_1})\ldots)\Big) \tag{5.5}$$

Computing p_τ using this decomposition is known as the *forward algorithm* for HMM's. Its time complexity is $O(l^2n)$, as can be easily checked.

We now observe that tropicalizing this algorithm gives us a way of efficiently solving equation (5.4). By taking $u_{i,j} = -\log(\theta_{i,j})$ and $v_{i,j} = -\log(\theta'_{i,j})$, we obtain

$$\bigoplus_{\sigma}(v_{\sigma_1\tau_1} \odot u_{\sigma_1\sigma_2} \odot v_{\sigma_2\tau_2} \ldots \odot u_{\sigma_{n-1}\sigma_n} \odot v_{\sigma_n\tau_n}) = \tag{5.6}$$

$$\bigoplus_{\sigma_n}(v_{\sigma_n\tau_n} \odot (\bigoplus_{\sigma_{n-1}}(v_{\sigma_{n-1}\tau_{n-1}} \odot u_{\sigma_{n-1}\sigma_n} \ldots \odot (\bigoplus_{\sigma_1}(v_{\sigma_1\tau_1} \odot u_{\sigma_1\sigma_2}))\ldots)))$$

Evaluating this quantity by recursively computing the parentheses in the above formula is known as the *Viterbi algorithm*, and has the same time complexity as its non-tropical version, the forward algorithm.

5.1.2 The Sum-Product Algorithm for Sequence Alignment

The sequence alignment problem asks for the best possible alignment between two words $\sigma^1 = \sigma^1_1\sigma^1_2\ldots\sigma^1_n$ and $\sigma^2 = \sigma^2_1\sigma^2_2\ldots\sigma^2_n$ over the alphabet $\Sigma = \{A, C, G, T\}$ that have evolved from a common ancestor via insertions, deletions or mutations of sites in the genetic sequence. A full description of the problem can be found in Section 2.2, whose notation we maintain in the subsequent analysis. As in Section 2.2, we represent an alignment by an edit string h over the alphabet $\{H, I, D\}$ such that $\#H + \#D = n$ and $\#H + \#I = m$. Let $\mathcal{A}_{n,m}$ be the set of all strings.

Each element $h \in \mathcal{A}_{n,m}$ corresponds naturally to a pair of words (μ^1, μ^2) over the alphabet $\Sigma \cup \{-\}$ such that μ^1 consists of a copy of σ^1 together with inserted "$-$" characters, and similarly μ^2 is a copy of σ^2 with inserted "$-$" characters. See (2.8).

Now consider the pair-hidden Markov model for sequence alignment presented in Section 2.2. Equation (2.15) gives us the marginal probability f_{σ^1,σ^2} of observing the pair of sequences σ^1 and σ^2:

$$f_{\sigma^1,\sigma^2} \quad = \quad \sum_{h\in\mathcal{A}_{n,m}} \prod_{i=1}^{|h|} \theta_{\mu^1_i,\mu^2_i} \cdot \prod_{i=2}^{|h|} \theta'_{h_{i-1},h_i}. \tag{5.7}$$

Here the parameters θ and θ' are as in Section 2.2.

Just as before, we will be interested in the tropical version of the above formula, which gives the alignment with the largest a posteriori probability, given the parameters of the model and the observed sequences. Letting $w_{i,j} = -ln(\theta_{i,j})$ and $w'_{i,j} = -ln(\theta'_{i,j})$, equation (5.7) yields:

$$\mathrm{trop}(f_{\sigma^1,\sigma^2}) \quad = \quad \bigoplus_{h\in\mathcal{A}_{n,m}} \bigodot_{i=1}^{|h|} w_{\mu_i^1,\mu_i^2} \cdot \bigodot_{i=2}^{|h|} w'_{h_{i-1},h_i}. \tag{5.8}$$

The above relation computes the negative logarithm of the maximum a-posteriori probability over the set of possible alignments.

This is equivalent to finding a minimum path in the alignment graph of Section 2.2, which can be solved through the Needleman-Wunsch algorithm, a version of the sum-product algorithm, based on the recursive decomposition of (5.8) described below.

Let $\sigma^1_{\le i}$ denote the sequence $\sigma^1_1\sigma^1_2\dots\sigma^1_i$. Let $\sigma^2_{\le j}$ be defined in the same way. Also define $\Phi^X(i,j)$ to be the maximum negative log probability among alignments of $\sigma^1_{\le i}$ and $\sigma^2_{\le j}$ such that the last character in the corresponding edit string is X. Equation (5.8) then gives us the following recursive formula(s):

$$\begin{aligned}
\Phi^I(i,j) &= w_{-,\sigma_j^2} \odot \bigoplus_X (\Phi^X(i,j-1) \odot w'_{X,I}) \\
\Phi^D(i,j) &= w_{\sigma_i^1,-} \odot \bigoplus_X (\Phi^X(i-1,j) \odot w'_{X,D}) \\
\Phi^H(i,j) &= w_{\sigma_i^1,\sigma_j^2} \odot \bigoplus_X (\Phi^X(i-1,j-1) \odot w'_{X,H})
\end{aligned} \tag{5.9}$$

where

$$\begin{aligned}
\Phi^X(0,0) &= 0 \ \forall X \\
\Phi^X(0,j) &= 0 \ \forall X \neq I \\
\Phi^X(i,0) &= 0 \ \forall X \neq D \\
\Phi^I(0,j) &= w_{-,\sigma_1^2} \odot \bigodot_{k=2}^{j} (w'_{I,I} \odot w_{-,\sigma_k^2}) \\
\Phi^D(i,0) &= w_{\sigma_1^1,-} \odot \bigodot_{k=2}^{i} (w'_{D,D} \odot w_{\sigma_k^1,-})
\end{aligned}$$

Finally we have

$$\mathrm{trop}(f_{\sigma^1,\sigma^2}) = \bigoplus_X \Phi^X(n,m). \tag{5.10}$$

The running time of the Needleman-Wunsch algorithm is $O(nm)$ as we perform a constant number of $\oplus$ and $\odot$ operations for each pair of indices (i,j).

5.2 The Polytope Propagation Algorithm

In this section we will describe parametric emphmaximum a-posteriori probability (MAP) estimation for probabilistic models. Our goal is to explain how parametric MAP estimation is related to linear programming and polyhedral geometry. The parametric MAP estimation problem comes in two different versions. First there is the local version: given a particular choice of parameters determine the set of all parameters which have the same MAP estimate. The local version is an important problem because it can be used to decide how sensitive the MAP estimate is to perturbations in the parameters. The global version of parametric MAP estimation problem asks for a partition of the space of parameters such that any choice of two parameters lie in the same part if and only if they yield the same MAP estimate. We will show that for arbitrary statistical models, the local problem is solved by computing a certain polyhedral cone (the normal cone at a vertex of the Newton polytope) and the global problem is solved by computing a certain polyhedral fan (the normal fan of the Newton polytope). In the case that the underlying statistical model has a sum-product decomposition, there is a natural extension of the tropical sum-product algorithm which replaces numbers with polyhedra and solves the parametric MAP estimation problem.

We will now show how to perform the tropical sum-product algorithm in a general fashion, finding an explanation for all choices of parameters. Let us consider the polynomial

$$f(p) = \sum_{j=1}^{d} p_1^{e_{j1}} \cdots p_k^{e_{jk}}.$$

and suppose that f comes from some statistical model where $p = (p_1, \ldots, p_k)$ is the vector of parameters, and each possible sequence of hidden states corresponds to some monomial (note that some of these monomials may in fact be equal). We maintain this assumption throughout the rest of this chapter. For a fixed value of p, finding an explanation is equivalent to finding the monomial of f whose value $p_1^{e_{j1}} \cdots p_k^{e_{jk}}$ is maximum. If we let $w_i = -\log p_i$, then this amounts to finding the index j of the monomial of f which minimizes the linear expression $e_j \cdot w = \sum_{i=1}^{k} w_i e_{j,i}$. We observe that e_j can be an explanation for some choice of parameters if and only if the point $P_j = (e_{j1}, \ldots, e_{jk})$ is on the convex hull of the set $\{(e_{i1}, \ldots, e_{ik}) : i \in [d]\}$, i.e it is a vertex of the Newton polytope of f, $\mathrm{Newt}(f)$.

The optimization problem of finding an explanation for a fixed set of parameters w can therefore be interpreted geometrically as a linear programming problem in the Newton polytope $\mathrm{Newt}(f)$. In the notation of Section 2.3, the optimization problem described above means finding $(e_{j,1}, e_{j,2}, \ldots, e_{j,k}) =$

$\text{face}_w(\text{Newt}(f))$. Conversely, the parametric version of this problem asks for the set of parameter vectors w for which a vertex P_j gives the explanation. In Section 2.3 it is shown that this is the cone in the normal fan of the polytope $\text{Newt}(f)$ which corresponds to the vertex P_j: $\mathcal{N}_{\text{Newt}(f)}(P_j)$. Constructing the normal fan $\mathcal{N}_{\text{Newt}(f)}$ therefore amounts to partitioning the parameter space into regions such that the explanation for all sets of parameters in a given region is given by the polytope vertex associated to that region. We can obtain $\text{Newt}(f)$ and $\mathcal{N}_{\text{Newt}(f)}$ through the *polytope propagation algorithm*, which is nothing more than the polytope algebra version of the sum-product decomposition. We refer the reader to Section 2.3 for details on Newton polytopes, normal fans and the polytope algebra.

To exemplify, solving the parametric version of (5.4) for hidden Markov models or (5.8) for sequence alignment amounts to finding the normal fan of the Newton polytopes $\text{Newt}(p_\tau)$ and $\text{Newt}(f_{\sigma^1,\sigma^2})$. As can be easily observed, in both examples our polynomials will have an exponential number of monomials. It is thus not feasible to compute the Newton polytope by first computing the polynomial explicitly. We will therefore make use of the recursive representations given by (5.6) and (5.9). Theorem 2.25 immediately gives us a recursive representation of the needed Newton polytopes: simply translate (5.6) and (5.9) into the polytope algebra of Section 2.3.

For the hidden Markov model we obtain the following:

$$\text{Newt}(p_\tau) = \bigoplus_{\sigma_n}(\text{Newt}(\theta'_{\sigma_n\tau_n}) \odot$$
$$\bigoplus_{\sigma_{n-1}}(\text{Newt}(\theta'_{\sigma_{n-1}\tau_{n-1}}\theta_{\sigma_{n-1}\sigma_n}) \ldots \odot \bigoplus_{\sigma_1}(\text{Newt}(\theta'_{\sigma_1\tau_1}\theta_{\sigma_1\sigma_2})) \ldots)).$$

For the sequence alignment example, take $\mathcal{P}^I(i,j)$ to be the Newton polytope of the sum of the scores of all alignments of the two partial sequences $\sigma^1_{\leq i}$ and $\sigma^2_{\leq j}$ which end with an insertion. This corresponds to the sum of the weights of all paths from the origin to the insertion vertex of the $K_{3,3}$ corresponding to position (i,j) in the alignment graph of Figure 2.2. Define $\mathcal{P}^D(i,j)$ and $\mathcal{P}^H(i,j)$ similarly and (5.9) gives us:

$$\begin{aligned}
\mathcal{P}^I(i,j) &= \text{Newt}(\theta_{-,\sigma^2_j}) \odot \bigoplus_X(\mathcal{P}^X(i,j-1) \odot \text{Newt}(\theta'_{X,I}))\\
\mathcal{P}^D(i,j) &= \text{Newt}(\theta_{\sigma^1_i,-}) \odot \bigoplus_X(\mathcal{P}^X(i-1,j) \odot \text{Newt}(\theta'_{X,D}))\\
\mathcal{P}^H(i,j) &= \text{Newt}(\theta_{\sigma^1_i,\sigma^2_j}) \odot \bigoplus_X(\mathcal{P}^X(i-1,j-1) \odot \text{Newt}(\theta'_{X,H})) \quad (5.11)
\end{aligned}$$

where

$$\begin{aligned}
\mathcal{P}^X(0,0) &= \operatorname{conv}\{(0,\ldots,0)\}\ \forall X\\
\mathcal{P}^X(0,j) &= \operatorname{conv}\{(0,\ldots,0)\}\ \forall X \neq I\\
\mathcal{P}^X(i,0) &= \operatorname{conv}\{(0,\ldots,0)\}\ \forall X \neq D\\
\mathcal{P}^I(0,j) &= \operatorname{Newt}(\theta_{-,\sigma^2_1}\prod_{k=2}^{j}(\theta'_{I,I}\theta_{-,\sigma^2_k}))\\
\mathcal{P}^D(i,0) &= \operatorname{Newt}(\theta_{\sigma^1_1,-}\prod_{k=2}^{i}(\theta'_{D,D}\theta_{\sigma^1_k,-}))
\end{aligned}$$

And finally

$$\operatorname{Newt}(f_{\sigma^1,\sigma^2}) = \bigoplus_X \mathcal{P}^X(n,m). \tag{5.12}$$

The above decompositions naturally yield straightforward algorithms for computing the Newton polytopes $\operatorname{Newt}(p_\mathcal{T})$ and $\operatorname{Newt}(f_{\sigma^1,\sigma^2})$, and one can easily extend this method to any polynomial f with a sum-product decomposition. Once the polytope $\operatorname{Newt}(f)$ has been computed, the final step of our algorithm is to compute the normal fan $\mathcal{N}_{\operatorname{Newt}(f)}$.

5.2.1 A small alignment example

To illustrate our algorithm, we give below a very small example of parametric sequence alignment under a highly simplified version of the scoring scheme of Section 2.2. Under our model, the same "reward" is assigned to all matches and the same "penalty" is assigned to all mismatches and gaps. We disregard completely the scores assigned to horizontal transitions. In the language of Section 2.2, this is equivalent to $w'_{X,Y} = 0\ \forall X, Y$, $w_{a,a} = x\ \forall a \in \{A, C, G, T\}$ and $w_{a,b} = y\ \forall a, b \in \{A, C, G, T, -\}$, $a \neq b$. This model is commonly known as the *2-parameter model for sequence alignment*.

Notice that the absence of horizontal transition probabilities eliminates the need for the triple recurrence present in the sum-product decomposition of the generalized scoring scheme. Letting $\Phi(i,j)$ denote the score of the best alignment of the sequences $\sigma^1_{\leq i}$ and $\sigma^2_{\leq j}$, we have:

$$\Phi(i,j) = (\Phi(i-1,j-1)\odot w_{\sigma^1_i,\sigma^2_j}) \oplus (\Phi(i-1,j)\odot y) \oplus (\Phi(i,j-1)\odot y) \tag{5.13}$$

In the polytope algebra, letting $\mathcal{P}(i,j)$ denote the convex hull of all the points associated with alignments of $\sigma^1_{\leq i}$ and $\sigma^2_{\leq j}$, the above relation becomes:

$$\mathcal{P}(i,j) = (\mathcal{P}(i-1,j-1) \odot \mathrm{Newt}(w_{\sigma_i^1,\sigma_j^2})) \oplus (\mathcal{P}(i-1,j) \odot (y)) \oplus (\mathcal{P}(i-1,j-1) \odot (y)) \tag{5.14}$$

where for simplicity of notation we will denote by (x) the Newton polytope with the single vertex $(1,0)$ and by (y) the Newton polytope with the single vertex $(0,1)$. Figure 5.1 illustrates the polytope propagation algorithm for the alignment of two very short sequences.

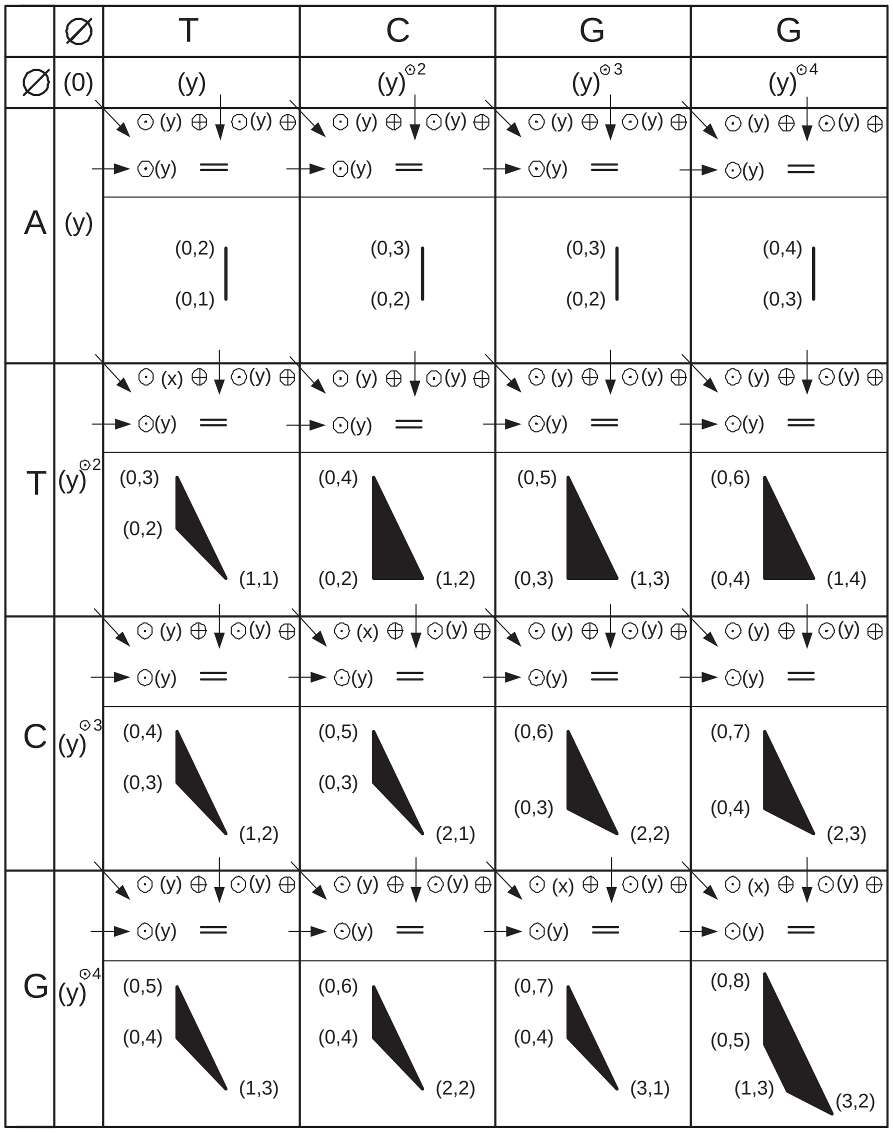

Fig. 5.1. Polytope propagation for sequence alignment.

5.3 Algorithm Complexity

In this section we analyze the time complexity of the polytope propagation algorithm. Given a polynomial f together with a sum-product decomposition, we want to compute $\mathrm{Newt}(f)$ and $\mathcal{N}_{\mathrm{Newt}(f)}$. The questions we will have to answer are the following:

(i) How many polytope algebra computations do we have to perform?
(ii) What is the individual time complexity of these operations?
(iii) What is the complexity of computing the normal fan of $\mathcal{N}_{\mathrm{Newt}(f)}$?

Let us consider the first question. In the examples of the previous section, the only multiplicative (Minkowski sum) operations we needed to perform were multiplication by a single point, i.e. shifting a polytope by a given vector. For a D-dimensional polytope with N vertices, this takes $O(ND)$ time and is strongly dominated by the additive operations. In this section we will limit our analysis to models where the only multiplicative operations are the trivial ones, as this turns out to be the case with most acyclic graphical models.

In general, the number of polytope algebra computations we need to perform will be the product of the number of levels in the sum-product decomposition of f and the number of operations per level. This is exactly the time complexity of computing the explanation for a *given* set of parameters, using the sum-product decomposition. For instance, in the case of the hidden Markov model of the previous section, the total number of polytope algebra operations will be $O(l^2n)$. In the sequence alignment example, at each step we compute three sums of exactly three polynomials, therefore the total number of operations is $O(nm)$.

In order to answer question (2), we need to settle on an efficient representation for our Newton polytopes. Section 2.3 provides us with two options: the V-representation and the H-representation. In general, the two are roughly equivalent in terms of computational versatility, due to the principle of duality. However, in the context of parametric inference, the V-representation will prove more natural, as we are able to prove upper bounds on the number of vertices of the Newton polytopes we find.

To facilitate our subsequent discussion, let us denote by $\nu_D(K)$ the computational complexity of finding the V-representation of the convex hull of K points in D dimensions. Also let N be the maximum number of vertices among all the polytopes encountered by the algorithm. It is clear that the additive polytope algebra operation will have a time complexity of at most $O(\nu_D(2N))$.

The next step is providing upper bounds for the number N. Since we are dealing with Newton polytopes of polynomials, all vertices will have integer coordinates. Now suppose that the degree of f is n. Then at every intermediate step of the algorithm, the degree of any variable will always be at most n.

We can therefore assert that all polytopes created by the algorithm will lie inside the D-dimensional hypercube of side-length n. We will make use of the following theorem of Andrews:

Theorem 5.1 *([Andrews, 1963]) For every fixed integer D there exists a constant C_D such that the number of vertices of any convex lattice polytope P in $\mathbb{R}^D$ is bounded above by $C_D \cdot \mathrm{vol}(P)^{(D-1)/(D+1)}$.*

Unfortunately, Theorem 5.1 only applies to full dimensional polytopes: the polytope cannot be contained in a lower-dimensional subspace of $\mathbb{R}^D$. As it turns out, this will almost always be the case. Now suppose that the final polytope we compute has dimension d. It is easy to see that the polytope algebra operations can only result in an increase of the dimension of the polytopes, i.e. $\dim(\mathcal{P} \oplus \mathcal{Q}) \geq \max\{\dim(\mathcal{P}), \dim(\mathcal{Q})\}$ and $\dim(\mathcal{P} \odot \mathcal{Q}) \geq \max\{\dim(\mathcal{P}), \dim(\mathcal{Q})\}$ for any two polytopes $\mathcal{P}$ and $\mathcal{Q}$. Then all of the intermediate polytopes will have dimension at most d. We call d the *true dimension* of the model (assuming that the polynomial f comes from some statistical model, as in the HMM and sequence alignment case).

Let us illustrate. In the HMM example, each monomial $p_{\sigma,\tau}$ is a product of n variables θ'_{ij} and $n-1$ variables θ_{ij}. Thus, for each point in $\mathrm{Newt}(p_\tau)$, the sum of the ll' coordinates corresponding to the θ'_{ij} variables is n and the sum of the l^2 coordinates corresponding to the θ_{ij} variables is $n-1$. These two inherent constraints of the model mean that $d \leq D-2$. In fact, the true dimension may be even smaller, but since there is no general recipe for finding the true dimension d of a model, we will limit our discussion to this simple example.

The following lemma will be essential in the derivation of our running time bounds.

Lemma 5.2 *Let $\mathcal{S}$ be a d-dimensional linear subspace of $\mathbb{R}^D$. Then among the set of D coordinate axes of $\mathbb{R}^D$, there exists a subset $\{i_1, i_2, ..., i_d\}$ such that the projection $\phi : \mathcal{S} \to \mathbb{R}^d$ given by $\phi((x_1, x_2, \ldots, x_D)) = (x_{i_1}, x_{i-2}, \ldots, x_{i_D})$ is injective.*

Proof Let $v^1, \ldots v^d \in \mathbb{R}^D$ be a basis for the subspace $\mathcal{S}$. Let A be the $D \times d$ matrix with columns $v^1, \ldots v^d$. Then the rank of the matrix A is exactly d. Now suppose that for any choice of indices $\{i_1, i_2, ..., i_d\}$ the projection $\phi((x_1, x_2, \ldots, x_D)) = (x_{i_1}, x_{i-2}, \ldots, x_{i_D})$ is not injective on $\mathcal{S}$. Let u be a non-zero vector in the kernel of the projection. Then u can be written as a linear combination of the vectors $v^1, \ldots v^d$ and its projection $\phi(u) = (u_{i_1}, u_{i-2}, \ldots, u_{i_D})$ is the 0 vector. This means that for any choice of d rows of the matrix A, the restrictions of the columns of A to those d rows are linearly dependent, in other words all $d \times d$ minors of A cancel. But A was of rank d, and we have a contradiction. $\square$

Now suppose that the true dimension of our model is d and let $\mathcal{S}$ be the affine span of the final polytope $\mathcal{P}$. By the lemma, there is a set of d coordinate axes such that the projection ϕ of the linear subspace $\mathcal{S}$ onto the space determined by those d axes is injective. Then $\phi(\mathcal{P}$ is also a d-dimensional polytope, whose vertices have integer coordinates and are in 1-1 correspondence with the vertices of $\mathcal{P}$. Moreover, $\phi(\mathcal{P})$ lies inside a d-dimensional hypercube with edge length n (all the exponents are at most n). Therefore the volume of $\phi(\mathcal{P})$ is at most n^d. Applying Andrews' result, we infer that $\mathcal{P}$ has at most $N = C_d \cdot n^{d(d-1)/(d+1)}$ vertices. Since all intermediate polytopes have dimension at most d, the above upper bound on the number of vertices will hold for all intermediate polytopes as well.

We obtain the following theorem:

Theorem 5.3 *Given a polynomial f of degree n in D variables such that the dimension of* Newt(f) *is d, then all the polytopes computed by the polytope propagation algorithm will have at most $c_d \cdot n^{d(d-1)/(d+1)}$ vertices.*

We still have not elucidated the mystery surrounding the function ν_D. If $D = 2$ or $D = 3$, computing the V-representation of the convex hull of D points is comparable to computing the entire convex hull (including edges and faces), and it can be done in time $O(Nlog(N))$.

We now turn our attention to the case $D \geq 4$. A point $v_j \in \mathbb{R}^D$ is on the convex hull of the set $\mathcal{A} = \{v_1, \ldots, v_N\}$ if and only if there is a hyperplane of $\mathbb{R}^D$ separating v_j from the rest of the points in $\mathcal{A}$. In turn, the existence of such a hyperplane is equivalent to the feasibility of a linear program. In general, a linear program has the following representation:

$$\begin{aligned} \text{Minimize} \quad & \bar{c} \cdot \bar{x}, \\ \text{subject to} \quad & A \cdot \bar{x} = \bar{b}, \\ \text{and} \quad & \bar{x} \geq 0, \end{aligned}$$

where $c \in \mathbb{R}^D$, $A \in \mathbb{R}^{N \times D}$ and $b \in \mathbb{R}^N$ are the parameters of the program. We refer the reader to [Grötschel *et al.*, 1993] for more details on linear programming and polytopes.

We can therefore solve the problem of computing the extremal points of a set of N points in $\mathbb{R}^D$ by solving N linear programs, each with D variables and N constraints. Linear programming, however, is one of the most interesting and controversial areas of theoretical computer science. If one regards the dimension D as fixed, then solving a linear program with N constraints takes

$O(N)$ time. However, the constant of proportionality is exponential in D, namely $O(2^{D\log(D)})$ [Chazelle, 1991].

On the other hand, Khachiyan's algorithm [Khachiyan, 1980] solves a linear program in time polynomial in the length of the bit representation of the program parameters. For our purposes, this implies a strongly polynomial algorithm, since all the points of our polytopes have integer coordinates of size at most n, therefore the linear programs will have integer parameters of size linear in n. The length of the representation of the linear programs will therefore be polynomial in n. Finally, it is worth mentioning that, although it has no theoretical running time guarantees, the well-known simplex method is most often the fastest way to solve linear programs.

Theorem 5.4 *Let f be a polynomial of degree n in D variables, and suppose that f has a sum-product decomposition into k steps with at most l additions and l multiplications by a monomial per step. Also let $d = \dim(\mathrm{Newt}(f))$ and let $N = c_d n^{d(d-1)/(d+1)}$. Then if $D = 2, 3$, we can compute the V-representation of $\mathrm{Newt}(f)$ in time $O(klN\log(N))$. If $D \geq 4$, we can compute the V-representation of $\mathrm{Newt}(f)$ in time $O(klN\nu_D(2N))$, where $\nu_D(2N)$ is either $O(2^{O(D\log(D))}N)$ or polynomial in both N and D.*

Finally, we need to address our third question, the complexity of computing the normal fan of $\mathrm{Newt}(f)$. Note that if one is only interested in the set of extremal vertices of $\mathrm{Newt}(f)$, together with a single parameter vector for which each such vertex is optimal, then the V-representation of $\mathrm{Newt}(f)$ suffices and the computation of the normal fan is not needed. Linear programming provides us with a certificate for each vertex, i.e. a direction in which that vertex is optimal. If one is interested in the full set of parameter vectors associated to each vertex, then one needs to compute the normal fan $\mathcal{N}_{\mathrm{Newt}(f)}$. This requires the computation of the full convex hull of the polytope $\mathrm{Newt}(f)$ and its running time is in fact dominated by this computation. For $D \leq 3$, the convex hull can be computed in time $O(N\log(N)$, as mentioned above. For $D > 3$, the best known algorithm for computing the convex hull of a D-dimensional polytope with N vertices is given in [Chazelle, 1993] and has a time complexity of $O(N^{[D/2]})$. Unfortunately, the constant of proportionality is again exponential in D.

Theorem 5.5 *Let f be a polynomial of degree n in D variables, and suppose that f has a sum-product decomposition into k steps with at most l additions and l multiplications by a monomial per step. Also let $d = \dim(\mathrm{Newt}(f))$ and let $N = c_d n^{d(d-1)/(d+1)}$. Then if $D = 2, 3$, we can compute $\mathcal{N}_{\mathrm{Newt}(f)}$ in time $O(klN\log(N))$. If $D \geq 4$, we can compute $\mathcal{N}_{\mathrm{Newt}(f)}$ in time $O(klN^2 + N^{[D/2]})$, where the constant of proportionality is exponential in D.*

5.4 Specialization of Parameters

5.4.1 Polytope Propagation with Specialized Parameters

In this section we present a variation of the polytope propagation algorithm in which we may specialize the values of some of the parameters. Let us return to the generic example

$$f(p) = \sum_{j=1}^{n} p_1^{e_{j1}} \dots p_k^{e_{jk}}.$$

Now let us assume that we assign the values $\theta_i = a_i$ for $h < i \leq k$. Our polynomial becomes

$$f_a(p) = \sum_{j=1}^{n} p_1^{e_{1j}} \dots p_h^{e_{hj}} a_{h+1}^{e_{(h+1)j}} \dots a_k^{e_{kj}},$$

which we can write as

$$f_a(p) = \sum_{j=1}^{n} p_1^{e_{1j}} \dots p_h^{e_{hj}} e^{ln(a_{h+1})e_{(h+1)j} + \dots ln(a_k)e_{kj}} \tag{5.15}$$

We can now treat the number e as a general free parameter and this new representation of f_a as a polynomial with only $h+1$ free parameters, with the only generalization that the exponent of the last parameter need not be an integer, but an integer combination of the logarithms of the specialized parameters.

But suppose that the polynomial f has a sum-product decomposition. It is clear that such a decomposition automatically translates into a decomposition for f_a by setting p_i^x to $e^{x \cdot ln(p_i)}$. Furthermore, a monomial $p_1^{e_{j1}} \dots p_k^{e_{jk}}$ gives an explanation for some parameter specialization $p = b$ such that $b_i = a_i$ for $i > h$ if and only if $b \cdot e_j = \max_i b \cdot e_i$, so if and only if the corresponding vertex $(e_1, \dots, e_h, \sum_{i=h+1}^{k} ln(a_i)e_i)$ is on the Newton polytope $\mathrm{Newt}(f_a)$ of f_a.

We have reduced the problem to that of computing $\mathrm{Newt}(f_a)$ given the sum-product decomposition of f_a induced by that of f.

Finally, we have to give an association of each set of parameters $(e_1, \dots, e_h)$ with a vertex of $\mathrm{Newt}(f_a)$. We can do this in two ways, both of which have comparable time complexity.

The first method involves computing the normal fan of $\mathrm{Newt}(f_a)$, just as before. This gives a decomposition of the plane into cones, each of which corresponds to a vertex of $\mathrm{Newt}(f_a)$. For all vectors of parameters with negative logarithm lying inside a certain cone, the corresponding explanation vertex is the one associated with that cone. However, the last parameter in the expression of f_a is the number e, therefore the only relevant part of the parameter hyperspace $\mathbb{R}^{h+1}$ is the hyperplane given by $p_{h+1} = e$, so $-\log(p_{h+1}) = -1$. The decomposition G_{f_a} of this hyperplane induced by the normal fan of Newt(f_a) in $\mathbb{R}^{h+1}$ is what we are interested in. Every region in this decomposition is associated with a unique vertex on the upper half of Newt(f_a) (with respect to the $(h+1)$'st coordinate).

Alternatively we can compute the decomposition G_{f_a} directly. First we project the upper side of the polytope Newt(f_a) onto the first h coordinates. This gives a regular subdivision R_{f_a} of an h-dimensional polytope. The reason for projecting the upper side alone is that we are looking for minima of linear functionals given by the negative logarithms of the parameter vectors. However, the last parameter is e, so the corresponding linear coefficient is -1. Taking the real line in $\mathbb{R}^{h+1}$ corresponding to a fixed set of values for the first h coordinates, we can see that the point on the intersection of this line with the polytope Newt(f_a) which minimizes the linear functional is the one with the highest $h+1$'st coordinate. Thus when projecting on the first h coordinates we will only be interested in the upper half of Newt(f_a).

In order to partition the hyperplane $\mathbb{R}^h$ into regions corresponding to vertices of R_{f_a}, we need to identify the dividing hyperplanes in $\mathbb{R}^h$. Each such hyperplane is given by the intersection of the hyperplanes in the normal fan of Newt(f_a) with the h-dimensional space given by setting the last coordinate in $\mathbb{R}^{h+1}$ to -1. Therefore, each dividing hyperplane corresponds uniquely to an edge (v_i, v_j) in R_{f_a}, and is given by the set of solutions $(x_1, \ldots x_h)$ to the following linear equation:

$$\begin{aligned} x_1 e_{i1} + \ldots + x_h e_{ih} - [ln(a_{h+1}) e_{(h+1)i} + \ldots ln(a_k) e_{ki}] &= \\ x_1 e_{j1} + \ldots + x_h e_{jh} - [ln(a_{h+1}) e_{(h+1)j} + \ldots ln(a_k) e_{kj}] & \end{aligned} \tag{5.16}$$

The subdivision of $\mathbb{R}^h$ induced by these hyperplanes will be geometrically dual to R_{f_a}, with each region uniquely associated to a vertex of R_{f_a}, so of Newt(f_a). This is the object which we are interested in, as it gives a unique monomial of f for every set of values for the first h parameters of f, given the specialization of the last $k-h$ parameters.

5.4.2 Complexity of Polytope Propagation with Parameter Specialization

Let us now compute the running time of the algorithm described above. Much of the discussion in the previous section will carry through and we will only stress the main differences. As before, the key operation is taking convex hulls of unions of polytopes. Let N be the maximum number of vertices among all the intermediate polytopes we encounter. We again define the function $\nu_{h+1}(N)$ to be the complexity of finding the vertices of the convex hull of a set of N points in $\mathbb{R}^{h+1}$. Note that in the case of parameter specialization, the last coordinate of the vertices of our polytopes is not necessarily integer.

This last observation implies that we will not be able to use Khachiyan's algorithm for linear programming to get a strongly polynomial algorithm for finding the extremal points. However, in practice this will not be a drawback, as one is nevertheless forced to settle for a certain floating point precision. Assuming that the values a_i we assign to the parameters θ_i for $h < i \leq k$ are bounded, we may still assume that the binary representation of the linear programs needed to find the extremal points is still polynomial in N. On the other hand, Chazelle's algorithm is strongly polynomial in N and will still run in time $O(2^{O(h \log(h)}N)$.

But what is an upper bound on N? Our polytopes have vertices with coordinate vectors $(e_1, \ldots, e_h, \sum_{i=h+1}^{k} \log(a_i)e_i)$. By projecting on the first h coordinates, we see that each vertex must project onto a lattice point $(e_1, \ldots, e_h)$ in $\mathbb{Z}^h_{\geq 0}$ such that $e_1, \ldots, e_h \leq n$, where n is the degree of f. There are n^h such points. Moreover, at most two vertices of the polytope can project to the same point in $\mathbb{R}^h$. Therefore, $N \leq 2n^h$ and we have the following theorem:

Theorem 5.6 *Let f be a polynomial of degree n in D variables, and suppose that f has a sum-product decomposition into k steps with at most l additions and l multiplications by a monomial per step. Also suppose that all but h of f's variables are specialized. Then the running time required to compute a V-representation of the Newton polytope of f with all but h parameters specialized is $O(klN\nu_{h+1}(N))$, where $N = 2n^h$ and $\nu_{h+1}(N) = O(2^{O(h \log(h)}N)$.*

For the last part of our task, computing the normal fan $\mathcal{N}_{\mathrm{Newt}(f_a)}$ and the regular subdivision it induces on the hyperplane $-\log(e_{h+1}) = -1$, we remark that the dominant part of the computation is in fact the computation of the convex hull of $\mathrm{Newt}(f_a)$. Again, if we consider h fixed, Chazelle's algorithm solves this in $O(N^{[(h+1)/2]})$ time, where the constant of proportionality is exponential in h.

Theorem 5.7 *Let f be a polynomial of degree n in D variables, and suppose that f has a sum-product decomposition into k steps with at most l additions and l multiplications by a monomial per step. Also suppose that all but h of f's variables are specialized. Then the running time required to compute all extremal vertices of* $\mathrm{Newt}(f_a)$*, together with their associated sets of parameter vectors, is $O(klN\nu_{h+1}(N) + N^{[(h+1)/2]})$, where $N = 2n^h$, $\nu_{h+1}(N) = O(N)$ and all constants of proportionality are exponentials in h.*

Note: One crucial observation is that if one disregards the preprocessing step of transforming a sum-product decomposition of f into a sum-product decomposition of f_a, the running time of our algorithm will generally not depend on the total number of parameters, but only on the number of unspecialized parameters. This may prove a very useful feature when one is interested in the dependence of explanations on only a small subset of the parameters.

6
Polytope Propagation on Graphs

Michael Joswig

6.1 Introduction

Polytope propagation associated with hidden Markov models or, more generally, arbitrary tree models can be carried to a further level of abstraction. This is instructive because this allows for a clearer view on the algorithmic complexity issues involved. The simple observation which starts this game is that a graphical model associated with a model graph G, which may or may not be a tree, defines another directed graph, call it $\Gamma(G)$, which can roughly be seen as a product of G with the state space of the model (considered as a graph with an isolated node for each state). Polytope propagation actually takes place on this product graph $\Gamma(G)$: at its nodes there are the polytopes propagated while each arcs carries a vector which represents the multiplication with a monomial in the parameters of the model. The purpose of this chapter is to collect some information about what happens if $\Gamma(G)$ is replaced by an arbitrary (acyclic) directed graph and to explain how this general form of polytope propagation is implemented in `polymake`.

`polymake` is a software system designed for the study of convex polytopes. Very many existing algorithms on polytopes are implemented. Additionally, there is a large array of interfaces to other software packages. This integration via interfaces is entirely transparent to the user. This way it does not make much of a difference whether a function is built into the system's core or whether it is actually realized by calling an external package. A key feature of the `polymake` system is that polytopes (and a few other things) are seen by the system as objects with a set of opaque functions which implement the polytope's properties known to the system. Calling such a function automatically triggers the construction of a sequence of steps to produce information about the desired property from the data which defines the polytope object. In this way `polymake` behaves similar to an expert system for polytopes.

As far as the implementation is concerned, `polymake` is a Perl/C++ hybrid. Both languages can be used to extend the system's functionality. The modular design allows for extensions by the user which are technically indistinguishable from the built-in functions. The polytope propagation algorithm is implemented in C++ and it is part of `polymake`'s current version 2.1 as the client `sum-product`. The annotated full source code of this program is listed below. Since it combines many of the system's features, while it is still a fairly short program, it should give a good idea how `polymake` can be extended in other ways, too.

6.2 Polytopes from Directed Acyclic Graphs

Let Γ be a finite directed graph with node set V and arc set A, and let $\alpha : A \to \mathbb{R}^d$ be some function. We assume that Γ does not have any directed cycles. Clearly, Γ has at least one *source*, that is, a node of in-degree zero, and also at least one *sink*, that is, a node of out-degree zero.

Such a pair (Γ, α) inductively defines a convex polytope $P_v \subset \mathbb{R}^d$ at each node $v \in V$ as follows: For each *source* $q \in V$ let $P_q = 0 \in \mathbb{R}^d$. For all non-source nodes v let P_v be the joint convex hull of suitably translated polytopes, more precisely,

$$P_v = \operatorname{conv}(P_{u_1} + \alpha(u_1, v), \ldots, P_{u_k} + \alpha(u_k, v)),$$

where $u_1, \ldots, u_k$ are the *predecessors* of v, that is, $(u_1, v), \ldots, (u_k, v) \in A$ are the arcs of Γ pointing to v. This polytope P_v is the polytope *propagated* by (Γ, α) at v. Often we will be concerned with graphs which have only one sink s, in which case we will write $P(\Gamma, \alpha) = P_s$.

It is a key feature of polytope propagation that each vertex of a propagated polytope corresponds to a (not necessarily unique) directed path from one of the sinks.

Example 6.1 Let $\Gamma = (V, A)$ have a unique source q, and assume that there is a function $\nu : V \to \mathbb{R}^d$ with $\nu(q) = 0$ such that $\alpha(u, v) = \nu(v) - \nu(u)$. Then the polytope P_n at each node n is the point $\nu(n) - \nu(q) = \nu(n)$.

If Γ has exactly one source and exactly one sink we call it *standard*. The following observation is immediate.

Proposition 6.2 *Let Γ be standard. Then the propagated polytope $P(\Gamma, \alpha)$ is a single point if and only if there is a function $\nu : V \to \mathbb{R}^d$ with $\alpha(u, v) = \nu(v) - \nu(u)$ for all arcs (u, v) of Γ.*

The following example shows that propagated polytopes are not restricted in any way.

Example 6.3 Let $x_1, \ldots, x_n \in \mathbb{R}^d$ be a finite set of points. We define a directed graph with the $n+2$ nodes $0, 1, \ldots, n+1$ as follows: We have arcs from 0 to the nodes $1, 2, \ldots, n$, and we have arcs from each of the nodes $1, 2, \ldots, n$ to $n+1$. Further we define $\alpha(0, k) = x_k$ and $\alpha(k, n+1) = 0$, for $1 \leq k \leq n$. Clearly, 0 is the unique source, and the propagated polytope at the unique sink $n+2$ is $\operatorname{conv}(x_1, \ldots, x_n)$.

Example 6.4 Let Γ be a (standard) directed graph on the nodes $0, 1, \ldots, 7$ with arcs as shown in Figure 6.1. The node 0 is the unique source, and the node 7 is the unique sink in Γ. The black arrows indicate the lengths and the directions of the vectors in $\mathbb{R}^2$ associated with each arc: $\alpha(0,1) = \alpha(1,3) = \alpha(3,5) = (1,0)$, $\alpha(1,4) = \alpha(3,6) = (0,1)$, $\alpha(2,4) = \alpha(4,6) = (0,2)$, and the vectors on the remaining arcs are zero. The propagated polytope is the pentagon

$$P(\Gamma, \alpha) = \operatorname{conv}((0,1), (0,4), (1,0), (1,3), (3,0)).$$

Note that, for instance, the point $(2,1)$ corresponding to the path $0 \to 1 \to 3 \to 6 \to 7$ is contained in the interior.

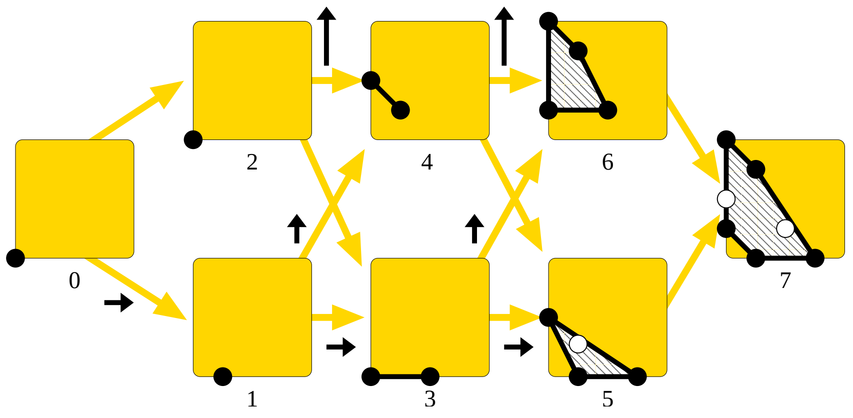

Fig. 6.1. Propagated pentagon in $\mathbb{R}^2$.

Remark 6.5 Suppose that $p \in K[x_1^{\pm}, \ldots, x_d^{\pm}]$ is a Laurent polynomial, over some field K, which is given as a sequence of sums and products with a monomial, starting from the trivial monomial 1. Then the computation of the Newton polytope of p can be paralleled to the computation of p itself by means of polytope propagation. The nodes of the corresponding graph correspond to the Newton polytopes of Laurent polynomials which arise as sub-expressions. For instance, Figure 6.1 can be interpreted as the computation of the Newton polytope of $p = x + x^3 + xy + xy^3 + x^2y + y + y^2 + y^4$. Denoting by $p(i)$ the polynomial associated with node i, we have $p(0) = p(2) = 1$, $p(2) = x$, $p(3) = 1+x^2$, $p(4) = xy+y^2$, $p(5) = x+x^3+xy+y^2$, $p(6) = x^2y+xy^3+y+y^4$, and $p(7) = p$. Note that, since we keep adding polynomials with non-negative coefficients, cancellation does not occur.

Example 6.6 A *zonotope* Z is the Minkowski sum of k line segments $[p_i, q_i] \subset \mathbb{R}^d$ or, equivalently, an affine projection of the regular k-cube. Each zonotope can be obtained by polytope propagation as follows: Take the vertex edge graph Γ_k of the regular cube $[0,1]^k$ and direct its edges according to the linear objective function $\sum x_i$. Let $\alpha(x, x+e_i) = q_i - p_i$ for each arc $(x, x+e_i)$, where x and $x+e_i$ are neighboring vertices of $[0,1]^k$. Like in Example 6.1 the propagated polytope at each node of Γ_k is a point. Now construct a (standard) directed graph Γ_k^* from Γ_k by adding one additional node ∞ and arcs, with the zero vector associated, from each node of Γ_k to ∞. Up to a translation by the vector $\sum p_i$ the propagated polytope at ∞ is the zonotope Z. Figure 6.2 shows the construction of a centrally symmetric hexagon.

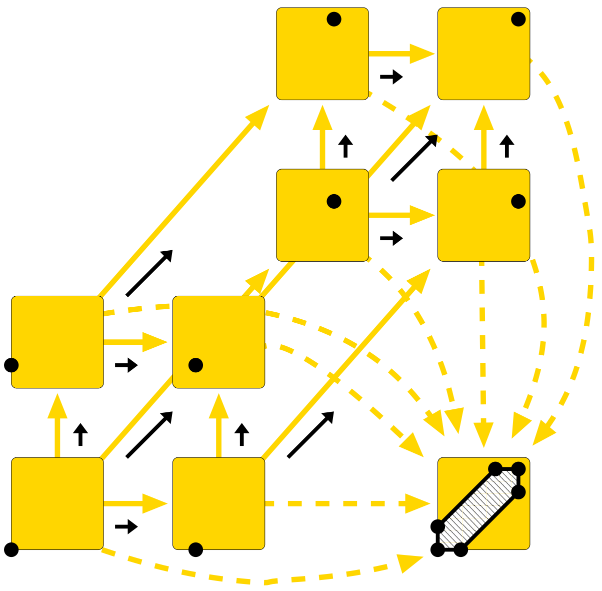

Fig. 6.2. Zonotope with three zones (here corresponding to the three parallel classes of solid arcs) in $\mathbb{R}^2$ as propagated polytope. The arcs of the graph Γ_3^* which are not arcs of Γ_3 are dashed; see Example 6.6.

Theorem 6.7 *Let Γ be a standard directed acyclic graph. Then the vertices of the polytope propagated by Γ can be computed in time which is polynomially bounded in the size of Γ.*

Proof Let s be the unique sink of Γ. By induction we can assume that the vertices of the polytopes propagated to the nodes which have an arc to s can be computed in polynomial time. In particular, their total number is bounded by a polynomial in the size of Γ.

If $P = \operatorname{conv}\{x_1, \dots, x_n\}$ is a polytope in $\mathbb{R}^d$ then a point x_k is a vertex if and only if it can be separated from $x_1, \dots, x_{k-1}, x_{k+1}, \dots, x_n$ by an affine hyperplane. The linear optimization problem:

$$\begin{aligned} \text{maximize } \epsilon \quad & \text{subject to} \\ & \lambda_0, \dots, \lambda_d \in \mathbb{R},\ \epsilon \geq 0, \\ & \sum_{j=1}^{d} \lambda_j x_{ij} \leq \lambda_0 - \epsilon, \text{ for each } i \neq k, \\ & \sum_{j=1}^{d} \lambda_j x_{kj} \geq \lambda_0 + \epsilon \end{aligned} \tag{6.1}$$

has a solution with $\epsilon > 0$ if and only if x_i is a vertex of P. Since linear optimization is solvable in polynomial time, see [Hačijan, 1979, Grötschel *et al.*, 1993], the claim follows. □

The above rough estimation of the complexity of polytope propagation is slightly incomplete. The linear optimization problem 6.1 can be solved in $O(n)$ time if d is fixed, see [Megiddo, 1984], and hence finding all the vertices of $P = \operatorname{conv}\{x_1, \dots, x_n\}$ takes $O(n^2)$ time in fixed dimension. Moreover, computing convex hulls in $\mathbb{R}^2$ or $\mathbb{R}^3$ only takes at most $O(n \log n)$ time, see [Seidel, 2004]. Hence computing convex hulls directly is superior to the approach described above, for the special case of $d \leq 3$.

6.3 Specialization to Hidden Markov Models

We consider a finite Markov process with l states and transition matrix $\theta' = (\theta'_{ij}) \in \mathbb{R}^{l \times l}$ satisfying the conditions $\theta'_{ij} \geq 0$ and $\sum_j \theta'_{ij} = 1$. The value θ'_{ij} is the transition probability of going from state i into state j. In the hidden Markov model we additionally take into account that the observation itself may be a probabilistic function of the state. That is to say, there are l' possible observations (where l' may even be different from l) and a non-negative matrix $\theta'' = (\theta''_{ij}) \in \mathbb{R}^{l \times l'}$ satisfying $\sum_j \theta''_{ij} = 1$. The entry θ''_{ij} expresses the probability that j has been observed provided that the actual state was i. In the following we will be concerned with parameterized hidden Markov models as in Chapter 1.

Example 6.8 The simplest possible (non-trivial) HMM occurs for $l = l' = 2$

and $\theta' = \begin{pmatrix} \theta'_{00} & \theta'_{01} \\ \theta'_{10} & \theta'_{11} \end{pmatrix}$, $\theta'' = \begin{pmatrix} \theta''_{00} & \theta''_{01} \\ \theta''_{10} & \theta''_{11} \end{pmatrix}$. If, for instance, we observe our primary process for three steps, the sequence of observations is some bit-string $\beta_0\beta_1\beta_2 \in \{0,1\}^3$. There are eight possible sequences of states which may have led to this observation. As in Chapter 1 we assume that the initial state of the primary process attains both states with equal probability $\frac{1}{2}$. Then we have that

$$\mathrm{Prob}[Y_0 = \beta_0, Y_1 = \beta_1, Y_2 = \beta_2] = \frac{1}{2} \sum_{\sigma \in \{0,1\}^3} \theta'_{\sigma_0\sigma_1}\theta'_{\sigma_1\sigma_2}\theta''_{\sigma_0\beta_0}\theta''_{\sigma_1\beta_1}\theta''_{\sigma_2\beta_2}.$$

Now let us have a look at the parameterized model, where —for the sake of simplicity— we assume that $\theta' = \theta'' = \begin{pmatrix} u & v \\ v & w \end{pmatrix}$ is symmetric. Since otherwise our primary process would be stationary, we can additionally assume $v \neq 0$. Neglecting the probabilistic constraints and re-scaling then allows to study the parameterized HMM of

$$\eta' = \eta'' = \begin{pmatrix} x & 1 \\ 1 & y \end{pmatrix} \in \mathbb{R}[x,y]^{2\times 2}.$$

The probability to make the specific observation 011 in the parameterized model yields

$$\mathrm{Prob}[Y_0 = 0, Y_1 = 1, Y_2 = 1] = \frac{1}{2}(x^3 + x^2y + xy + xy^3 + x + y + y^2 + y^4),$$

which happens to be the polynomial p in Remark 6.5 (up to the constant factor $\frac{1}{2}$), and whose Newton polytope is the pentagon in Figure 6.1.

The fixed observation $\beta_1 \cdots \beta_n$ of a hidden Markov model $\theta = (\theta', \theta'')$ for n steps gives rise to the standardized acyclic directed graph Γ^n_θ with node set $[n]\times[l]\cup\{-\infty,+\infty\}$ as follows: There is an arc from $-\infty$ to all nodes $(1,j)$, and there is an arc from (n,j) to $+\infty$ for all $j \in [l]$; further, there is an arc between (i,j) and $(i+1,k)$ for any i,j,k. The directed paths from the unique source $-\infty$ to the unique sink $+\infty$ directly correspond to the l^n possible sequences of states of the primary process that may or may not have led to the given observation $\beta_1 \cdots \beta_n$. Such a path passes through the node (i,j) if and only if the i-th primary state X_i has been j.

The probability that $X_{i-1} = j$ and $X_i = k$ under the condition that $Y_i = \beta_i$ is the monomial $\theta'_{jk}\theta''_{k,\beta_i} \in \mathbb{R}[\theta'_{11}, \ldots, \theta'_{ll}, \theta''_{11}, \ldots, \theta''_{ll'}]$. We associate its (integral) exponent vector with the arc $(i-1,j) \to (i,k)$. Likewise, we associate the exponent vector of θ''_{k,β_0} with the arc $-\infty \to (0,k)$ and 0 to all arcs $(l-1,k) \to +\infty$.

The graph Γ^n_θ gives rise to a propagated polytope whose vertices correspond to most likely explanations for the observation made for some choice of parameters.

This schema can be modified by specializing some of the parameters as in Example 6.8. The associated graph is given as Example 6.4, and its propagated polytope is the Newton polytope of the polynomial $p(7)$ in Remark 6.5, a pentagon.

In our scheme of polytope propagation we chose to restrict the information on the arcs to be single points (which are 0-dimensional polytopes). For this reason we chose our parametric HMM to have monomials for the transition probabilities. It is conceivable (but not implemented in `polymake`) to allow for arbitrary polynomials for the transition probabilities. This would then require to iteratively compute Minkowski sums of higher dimensional polytopes. For Minkowski sum algorithms for general polytopes see [Fukuda, 2004].

6.4 An Implementation in `polymake`

We give a complete listing of the program `sum_product`, which implements the algorithm described. In order to increase the legibility the code has been re-arranged and shortened slightly.

6.4.1 Main Program and the `polymake` Template Library

The main program sets up the communication with the `polymake` server for the polytope object `p`, which is contains the propagation graph Γ and the function α. The graph Γ is assumed to be standard, and the polytope object `p` corresponds to the propagated polytope $P(\Gamma, \alpha)$. The class `Poly` is derived from `iostream`. The actual function which does the job is `sum_product` in the namespace `polymake::polytope`.

```
using namespace polymake;

int main(int argc, char *argv[]) {
   if (argc != 2) {
      cerr << "usage: " << argv[0] << " <file>" << endl;
      return 1;
   }
   try {
      Poly p(argv[1], ios::in | ios::out);
      polytope::sum_product(p);
   }
   catch (const std::exception& e) {
      cerr << e.what() << endl;
      return 1;
   }
   return 0;
}
```

The `polymake` system comprises a rich template library which complies with the Standard Template Library (STL). This includes a variety of container template classes, such as `Array` (which is a variation of STL's `vector` class) and template classes for doing linear algebra, such as `Vector` and `Matrix`. Additionally, there are several classes which special functionality useful in algorithmic polytope theory, for example, `Graph` and `IncidenceMatrix`.

A common feature of `polymake`'s container classes is a memory management based on reference counting (with copy-on-write). Hence copying a non-altered `Array`, for example, costs next to nothing. Further all these classes provide a range of features useful for debugging. The reader is referred to the `polymake`'s documentation for a detailed description.

The arithmetic operations use exact representations of rational numbers. Our class `Rational` wraps the corresponding implementation from the GNU Multiprecision Library.

The rest of this section lists the function `sum_product` in the namespace `polymake::polytope`.

```
namespace polymake { namespace polytope { ... } }
```

6.4.2 The core of the implementation

The graph that the client reads already comes with a (translation) vector specified for each edge. This is the second template parameter. The first template parameter is set to an artificial type `nothing` which means that do not have any data at the nodes The third template parameter (again some artificial type) indicates that our graph is directed. We assume that the graph is acyclic with a unique sink. Arbitrarily many sources are allowed.

```
typedef Graph< nothing, Vector<Rational>, directed > graph;
```

We now start to describe the actual polytope propagation algorithm. It operates on a single `Poly` object from which the `SUM_PRODUCT_GRAPH` is read. It writes the `VERTICES` and `VERTEX_NORMALS` of the polytope corresponding to the unique sink in the graph.

```
void sum_product(Poly& p) { ... }
```

Read the graph and the dimension of the ambient space. The member function `give()` of the `Poly` class induces the polymake server to deliver the named property of the object `p`; if necessary the server triggers further computations, as defined by an extensible set of rules, to answer the request made. There is a reciprocal function `take()` to be used further below.

```
   const graph G=p.give("SUM_PRODUCT_GRAPH");
   const int n(G.nodes());
   if (n==0)
      throw std::runtime_error("SUM_PRODUCT_GRAPH must be non-empty");

   const int d=p.give("AMBIENT_DIM");
```

Below is given the description of the origin as a 0-dimensional polytope (living in d-space). It has one vertex and en empty vertex-facet incidence matrix. This is used to define the initial objects of type `Poly` for the sources of the graph.

```
   const Matrix<Rational> single_point_vertices(vector2row(
                                 unit_vector<Rational>(d+1,0)));
   const IncidenceMatrix<> single_point_vif;
```

The following defines an array where all the intermediate polytopes are stored. The nodes in the graph are consecutively numbered, starting with 0. The corresponding polytope can be accessed by indexing the array `pa` with the node number. In the beginning the `Poly` objects are undefined.

```
   Array<Poly> pa(n);
   std::list<int> next_nodes;
```

Initialize by assigning a single point (origin) to each source in the graph.

```
   for (int v=0; v<n; ++v) {
      if (G.in_degree(v)==0) {
         pa[v].init(0, ios::in | ios::out | ios::trunc,
                                          "RationalPolytope");
         pa[v].take("VERTICES") << single_point_vertices;
         pa[v].take("VERTICES_IN_FACETS") << single_point_vif;
         add_next_generation(next_nodes,v,G,pa);
      }
   }
```

At each node of the graph recursively define a polytope as the convex hull of the translated predecessors. We also try to find the sink on the way.

```
   int sink=-1;
```

The number -1 does not correspond to any valid node number; it indicates that no sink has been found yet.

```
   while(!next_nodes.empty()) {
```

Get some node `w` for which we already know all its predecessors. Initialize the client-server communication for that node's polytope. Until now it was undefined.

```
      const int w=next_nodes.front(); next_nodes.pop_front();
      pa[w].init(0, ios::in | ios::out, "RationalPolytope");
```

The polytope will be specified as the convex hull of points, which will be collected from other polytopes. The special data type `ListMatrix` is efficient in terms of concatenating rows (which correspond to points) but it is not efficient in terms of matrix operations (although all operations are defined). This is acceptable, since we do not compute anything in this step. The C++ operator `/` takes care of the concatenation of compatible matrix blocks on top of one another.

```
      ListMatrix< Vector<Rational> > points(0,d+1);
      for (Entire<graph::in_edge_list>::const_iterator
                 e=entire(G.in_edges(w)); !e.at_end(); ++e) {
```

The node `v` is the current predecessor to process. The arc from `v` to `w` is `e`. The operator `*` extracts the associated vector from an arc.

```
         const int v=e.from_node();
         const Vector<Rational> vec=*e;
```

Next we read the vertices of the predecessor polytope. `polymake`'s rule basis by default uses `cdd`'s implementation to check for redundant (= non-vertex) points among the input by solving linear programs. No convex hull computation is necessary. What is going on behind the scene is hidden from the user. The `polymake` server decides how to produce the `VERTICES` of the polytope object `pa[v]`. Note that this is the same behavior as if `polymake` would asked for these vertices via the command line interface.

```
         const Matrix<Rational> these_vertices=pa[v].give("VERTICES");
```

Now concatenate the translated matrix (where the rows correspond to the vertices of the predecessor) to what we already have. The final `}` closes the for-loop through all the predecessors of `w`.

```
         points /= these_vertices*translation_by(vec);
      }
```

Define the polytope object as the convex hull of all those points collected and proceed.

```
      pa[w].take("POINTS") << points;
      if (G.out_degree(w)==0) sink=w;
      else add_next_generation(next_nodes,w,G,pa);
   }
```

This will be just any sink; it is indeterministic if the graph does have several sinks.

```
   if (sink<0)
      throw std::runtime_error("no sink found in digraph");
```

The `sink` defines the polytope we are after and this is going to be defined as the polytope object `p`. The vertex normals serve as certificates that the claimed points are indeed vertices.

```
   const Matrix<Rational>
      sink_vertices = pa[sink].give("VERTICES"),
      sink_normals  = pa[sink].give("VERTEX_NORMALS");

   p.take("VERTICES") << sink_vertices;
   p.take("VERTEX_NORMALS") << sink_normals;
}
```

6.4.3 Two auxiliary functions

The first one gathers the next generation of graph nodes which can be defined at that stage, since all predecessors known. It is one step in a common breadth first search. The graph nodes which can be processed (because all their predecessors are known) are stored in a doubly linked list, that is STL's type `list`.

```
void add_next_generation(std::list<int>& next_nodes, const int v,
                         const graph& G, const Array<Poly>& pa)
{
   for (Entire<graph::out_edge_list>::const_iterator
            e=entire(G.out_edges(v)); !e.at_end(); ++e) {
      const int x=e.to_node();
      Entire<graph::in_edge_list>::const_iterator
            f=entire(G.in_edges(x));
      for( ; !f.at_end() && pa[f.from_node()].get_mode(); ++f);
      if (f.at_end())
         next_nodes.push_back(x);
   }
}
```

The following function returns a translation matrix (to be applied to row vectors from the right) for given vector. The C++ operators `|` and `/` are overloaded for the `Matrix` class: They define the concatenation of two matrix blocks side by side and one on top of the other, respectively.

```
Matrix<Rational> translation_by(const Vector<Rational>& vec)
{
   const int d=vec.dim();
   return unit_vector<Rational>(d+1,0) |
          (vec / unit_matrix<Rational>(d));
}
```

6.5 Returning to Our Example

There is another standard client program `binary-markov-graph` which produces the polytope propagation graphs for the special HMM discussed in Example 6.8. It can be called from the command line as follows:

```
> binary-markov-graph b011.poly 011
```

Here the argument `011` specifies the observation. The command yields a file `b011.poly` which contains a description of the polytope propagation suitable as input for the `sum_product` client.

```
> sum_product b011.poly
```

This defines a polytope object, which is accessible to all of `polymake`'s functions. For example, this is how to list all the vertices of the propagated polytope. Each row corresponds to a vertex of our pentagon (first column used for homogenization of the coordinates).

```
> polymake b011.poly VERTICES
VERTICES
1 3 0
1 1 0
1 0 1
1 1 3
1 0 4
```

7
Parametric Sequence Alignment

Colin Dewey

Kevin Woods

The alignment of DNA and protein sequences is one of the most fundamental problems in computational biology. Section 2.2 introduced some scoring schemes and algorithms used for global alignment of two biological sequences. Each scoring scheme is dependent on a set of parameters, and, as Example 2.14 showed, the optimal alignment can change significantly as these parameters are varied. Users of alignment algorithms would like to know how their results are affected by the values of the parameters and how confident they can be in a given optimal alignment. Such questions are answered using *parametric sequence alignment* methods. In this chapter, the techniques of parametric sequence alignment are introduced and later applied to characterize a couple of simple scoring schemes. As parametric alignment algorithms can be implemented almost as efficiently as algorithms for normal sequence alignment, parametric sequence alignment methods are powerful and important components of the computational biologist's toolbox.

7.1 Few alignments are optimal

The primary goal of biological sequence alignment is to match up positions in the input sequences that are *homologous*. Two sequence positions are homologous if the characters at those positions are derived from the same position in some ancestral sequence. It is important to note that two positions can be homologous even though the states of the positions are different. For example, position 5 in σ^1 and position 9 in σ^2 may be homologous despite the fact that $\sigma^1_5 = \mathtt{A}$ and $\sigma^2_9 = \mathtt{C}$. Alignments indicate that positions in two sequences are homologous by matching up the characters at those positions. An alignment is *biologically correct* if it matches up all positions that are truly homologous and no others. Because this chapter focuses on the *global* alignment problem for two sequences, we will ignore cases in which a duplication event causes one position to be homologous to multiple positions in the other sequence.

What does it mean for a global alignment to be "optimal"? If our goal is to discover the biological truth, we should say that an "optimal" global alignment is one that is biologically correct. Having biologically correct alignments is critical because other analyses, such as phylogenetic tree construction, are heavily dependent on sequence alignments. Unfortunately, in most cases, we do not know what the biological truth is. We must therefore use a scoring scheme to rank the alignments and take the highest-ranking alignment as our best guess of the truth. Which scoring scheme should we use to make such a guess? Once we have chosen our parameter values, how confident can we be that the resulting alignment is a good guess? It could be the case that, if we vary our chosen parameter values just slightly, we will obtain very different alignments. Even worse, it could be that no values for the parameters of our chosen scoring scheme will give the biologically correct alignment as being optimal.

The methods of parametric sequence alignment help to answer these questions, for specific input sequences, by analyzing a scoring scheme over all possible parameter values. Specifically, parametric sequence alignment subdivides the parameter space into regions such that parameter values in the same region give rise to the same optimal alignments. Such a subdivision tells us which of the exponentially-many possible alignments can be optimal for some choice of parameter values and how many classes of optimal alignments there can be. In addition, if we find that the point in the parameter space corresponding to our current choice of values for the parameters is close to the boundary of a region in the subdivision, we may be less confident in our results. This is because varying the parameter values slightly is likely to move the point to a different region in the subdivision and thus produce different optimal alignments. Lastly, we may wish to take a Bayesian approach and place a prior distribution on the parameters. In this case, we can determine what the most likely optimal alignments are by integrating over the different regions in the subdivision (note that this is different from finding the *most likely alignment*) [Pachter and Sturmfels, 2004b].

Parametric sequence alignment is feasible, because, although two given sequences have exponentially-many possible alignments, there are only a few subsets of these alignments (corresponding to regions of the parameter space subdivision) that can be optimal for some choice of parameters. For two sequences of length at most n, it has been shown that for a simple scoring scheme with 2 parameters allowed to vary, the number of regions in the subdivision is $\mathcal{O}(n^{\frac{2}{3}})$ [Gusfield *et al.*, 1994]. This bound corresponds exactly with the bound given in Section 5.3 for the number of vertices of a sequence alignment Newton polytope with $d = 2$. In fact, for a scoring scheme with any number of parameters, the number of regions is bounded by a polynomial in n (see Section 5.3).

The bound on the number of regions in the subdivision allows for the subdivision to be determined in just slightly more time than it takes to simply align the sequences in question. For the simple scoring scheme just mentioned, the subdivision can be found in $\mathcal{O}(n^{\frac{8}{3}})$ time, as opposed to $\mathcal{O}(n^2)$ time for aligning the sequences with a fixed set of parameter values.

The concept of parametric sequence alignment is not a new one, and there are several programs available to perform parametric analysis [Gusfield, 1997]. Existing methods are restricted to the analysis of scoring schemes with at most 2 parameters allowed to vary at one time, whereas we may also like to analyze scoring schemes that have many parameters, such as the general 33-parameter scoring scheme described in Section 2.2. In this chapter, we apply the techniques of parametric inference described in Chapter 5 to the problem of sequence alignment and thus give a general method for parametric sequence analysis with scoring schemes involving any number of parameters.

7.2 Polytope propagation for alignments

In this section, we will describe how to efficiently compute a parametric sequence alignment of two sequences, σ^1 and σ^2, with lengths n and m, respectively. While the method we describe can be used to analyze a fully-parameterized scoring scheme (with the 33 parameters comprising the matrices shown in Equations 2.11 and 2.12), we will concentrate on a simple 4-parameter scoring scheme, with parameters M, X, S, and G, corresponding to the weights for matches, mismatches, spaces (- symbols in the alignment), and gaps (contiguous sets of spaces), respectively. This scoring scheme is just a special case of the general scoring scheme with

$$\begin{array}{rcll} w_{\pi,\pi} & = & M & \forall \pi \in \Sigma \\ w_{\pi_1,\pi_2} & = & X & \forall \pi_1, \pi_2 \in \Sigma, \pi_1 \neq \pi_2 \\ w_{\pi,-} = w_{-,\pi} & = & S & \forall \pi \in \Sigma \\ w'_{H,I} = w'_{H,D} = w'_{I,D} = w'_{D,I} & = & G & \\ w'_{H,H} = w'_{I,H} = w'_{D,H} = w'_{I,I} = w'_{D,D} & = & 0 & . \end{array}$$

An even simpler scoring scheme, which we will refer to as the 3-parameter scoring scheme, has $G = 0$. We shall present a method for parametric alignment with the 3-parameter scoring scheme, but it should be noted that this method easily generalizes to the 4-parameter and 33-parameter scoring schemes.

With the 3-parameter scoring scheme, the weight of an alignment, h, is

$$W_{\sigma^1,\sigma^2}(h) = Mm_h + Xx_h + Ss_h, \tag{7.1}$$

where m_h, x_h, and s_h denote the number of matches, mismatches, and spaces in h, respectively. We define the monomial

$$f_{\sigma^1,\sigma^2,h} = \theta_M^{m_h} \theta_X^{x_h} \theta_S^{s_h} \tag{7.2}$$

and the polynomial

$$f_{\sigma^1,\sigma^2} = \sum_{h \in \mathcal{A}_{n,m}} f_{\sigma^1,\sigma^2,h}. \tag{7.3}$$

The weight, $W(h)$, is simply $\log f_{\sigma^1,\sigma^2,h}(e^M, e^X, e^S)$. As we saw in Section 2.2, finding the alignment, h, that minimizes $W(h)$ is equivalent to evaluating f_{σ^1,σ^2} tropically. Following with tradition, we will choose to maximize $W(h)$ in this chapter, but these are equivalent problems.

The parametric alignment problem for this scoring scheme, then, is to compute which values of M, X, and S result in which optimal alignments. The key object in our parametric alignment of σ^1 and σ^2 is the Newton polytope of the polynomial f_{σ^1,σ^2}. The Newton polytope of f_{σ^1,σ^2} is the convex hull of all points (m_h, x_h, s_h), for $h \in \mathcal{A}_{n,m}$. Recall from Section 2.3 that each vertex of $\mathrm{NP}(f_{\sigma^1,\sigma^2})$ corresponds to an alignment (or set of alignments, all having the same number of matches, mismatches, and spaces) that will be optimal for a certain set of values for the parameters, M, X, and S. For a vertex, v, of $\mathrm{NP}(f_{\sigma^1,\sigma^2})$, the set of parameters for which the alignments corresponding to v are all optimal is given by its normal cone $N(v)$. The normal fan of the Newton polytope, $\mathcal{N}(\mathrm{NP}(f_{\sigma^1,\sigma^2}))$ is thus a subdivision of the parameter space with the property that, for all parameter values in the same region (normal cone), the same alignments are optimal. This subdivision is exactly the desired output of parametric sequence alignment.

Having shown that the Newton polytope of f_{σ^1,σ^2} and its corresponding normal fan solve the parametric alignment problem, we now turn to how to compute these objects efficiently using the polytope propagation algorithm of Chapter 5. First, however, we make two remarks that will make our presentation cleaner.

Remark 7.1 For an alignment, h, of σ^1 and σ^2, we must have that $2m_h + 2x_h + s_h = n + m$.

Proof Recall from Section 2.2 that h is a string over the alphabet $\{H, I, D\}$. Matches and mismatches correspond to H characters in the alignment, while spaces correspond to I and D characters. The remark follows from combining the equalities in Equation 2.7. □

Remark 7.2 Any 3-parameter scoring scheme (M, X, S) is equivalent to another scoring scheme (M', X', S'), where $M' = 0$, $X' = X - M$, and $S' = S - \frac{M}{2}$.

Proof Using Remark 7.1, we have that

$$W'(h) = M'm_h + X'x_h + S's_h = W(h) - \frac{M}{2}(n+m) = W(h) - C,$$

where $C = \frac{M}{2}(n+m)$ is a constant with respect to the alignment h. Since all scores are shifted by the same constant, the rankings of possible alignments under the two scoring schemes are the same. □

Having made this remark, we now assume that $M = 0$ for the remainder of this section. With this specialization (and setting $\theta_M = e^M = 1$), we have

$$f_{\sigma^1,\sigma^2} = \sum_{h \in \mathcal{A}_{n,m}} \theta_X^{x_h} \theta_S^{s_h},$$

and our Newton polytope and normal fan will be two-dimensional.

Let us briefly recall the Needleman-Wunsch algorithm, which, given specific parameter values X and S and sequences σ^1 and σ^2, computes the optimal global alignment. Let $\sigma^1 = \sigma^1_1\sigma^1_2\cdots\sigma^1_n$ and $\sigma^2 = \sigma^2_1\sigma^2_2\cdots\sigma^2_m$. For $0 \le i \le n$, define

$$\sigma^1_{\le i} = \sigma^1_1\sigma^1_2\cdots\sigma^1_i,$$

and similarly define $\sigma^2_{\le j}$ to be the first j characters in σ^2. Define $M[i,j]$ to be the score of the optimal alignment of $\sigma^1_{\le i}$ and $\sigma^2_{\le j}$. We would like to find $M[n,m]$, and we do this recursively as follows. For characters π_1 and π_2 in Σ, define $w(\pi_1,\pi_2)$ to be 0 if $\pi_1 = \pi_2$ and X if $\pi_1 \ne \pi_2$. For the base cases of the recursion, we have that $M[i,0] = i \cdot S$ and $M[0,j] = j \cdot S$ (since the only alignments have i spaces and j spaces, respectively). Then we recursively apply the formula

$$M[i,j] = \max \begin{cases} M[i-1,j-1] + w(\sigma^1_i, \sigma^2_j) \\ M[i-1,j] + S \\ M[i,j-1] + S \end{cases} \tag{7.4}$$

for $1 \le i \le n$ and $1 \le j \le m$.

Example 7.3 Suppose that $\sigma^1 = \texttt{CAA}$ and $\sigma^2 = \texttt{AAC}$, and we have parameter values $M = 0$, $X = -2$, and $S = -3$. Then Figure 7.1 shows $M[i,j]$ for $0 \le i,j \le 3$. In particular, the optimal alignment for σ^1 and σ^2 is $\substack{\texttt{CAA}\\\texttt{AAC}}$ with score $M[3,3] = -4$.

In the recursive formula for the Needleman-Wunsch algorithm, we use two operations, max and +. In other words, the recursion takes place in the (max, +) algebra (which is equivalent to the tropical algebra). The polytope propagation algorithm is the exact same recursion, but in the polytope algebra (Section 2.3), where addition is the convex hull of the union of two polytopes

$$\begin{array}{c|c|c|c|c|}
 & & \mathsf{A} & \mathsf{A} & \mathsf{C} \\
\hline
 & 0 & -3 & -6 & -9 \\
\hline
\mathsf{C} & -3 & -2 & -5 & -6 \\
\hline
\mathsf{A} & -6 & -3 & -2 & -5 \\
\hline
\mathsf{A} & -9 & -6 & -3 & -4 \\
\hline
\end{array}$$

Fig. 7.1. Matrix showing $M[i, j]$ with $M = 0$, $X = -2$, and $S = -3$.

and multiplication is the Minkowski sum of two polytopes. To be precise, let $P[i, j]$ be the Newton polytope for aligning the two strings $\sigma^1_{\leq i}$ and $\sigma^2_{\leq j}$, and define $v(\pi_1, \pi_2)$ to be $\{(1, 0)\}$ (the Newton polytope of the monomial θ^1_X) if $\pi_1 \neq \pi_2$ and $\{(0, 0)\}$ if $\pi_1 = \pi_2$. Then, if $\oplus$ is the Minkowski sum operation, we have the recursion

$$P[i, j] = \operatorname{conv}\left(\begin{array}{l} P[i-1, j-1] \oplus v(\sigma^1_i, \sigma^2_j) \quad \cup \\ P[i-1, j] \oplus \{(0, 1)\} \quad \cup \\ P[i, j-1] \oplus \{(0, 1)\} \end{array} \right) \tag{7.5}$$

for $1 \leq i \leq n$ and $1 \leq j \leq m$. Compare this to (7.4). We must also describe the base cases for the recursion: $P[i, 0] = \{(0, i)\}$, because the only possible alignment has 0 mismatches and i spaces, and similarly $P[0, j] = \{(0, j)\}$. This recursion is exactly the polytope propagation algorithm run on a directed acyclic graph (Chapter 6), namely, the alignment graph $\mathcal{G}_{n,m}$ (Section 2.2).

Example 7.4 Using the same sequences as in Example 7.3, Figure 7.2 shows $P[i, j]$ for $0 \leq i, j \leq 3$, including an illustration of how to determine $P[3, 3]$ from $P[2, 2]$, $P[2, 3]$, and $P[3, 2]$. Table 7.1 lists, for each vertex of the polytope $P[3, 3]$, an optimal alignment corresponding to that vertex, and the parameter values for which this alignment is optimal (these parameters are obtained by taking the normal fan of $P[3, 3]$). Note that $(0, 6)$ and $(2, 2)$ do not correspond to biologically reasonable parameters, because their corresponding alignments are optimal for $S \geq 0 = M$.

As we noted before, the parametric alignment method we have described generalizes to scoring schemes of any number of parameters by translating the extended Needleman-Wunsch algorithm to the polytope algebra. The algorithm presented runs efficiently for small numbers of parameters. It runs in $\mathcal{O}(n^{\frac{8}{3}})$ and $\mathcal{O}(n^{\frac{7}{2}})$ time for the 3 and 4-parameter scoring schemes, respectively (Section 5.3). For a large number of parameters, however, the algorithm

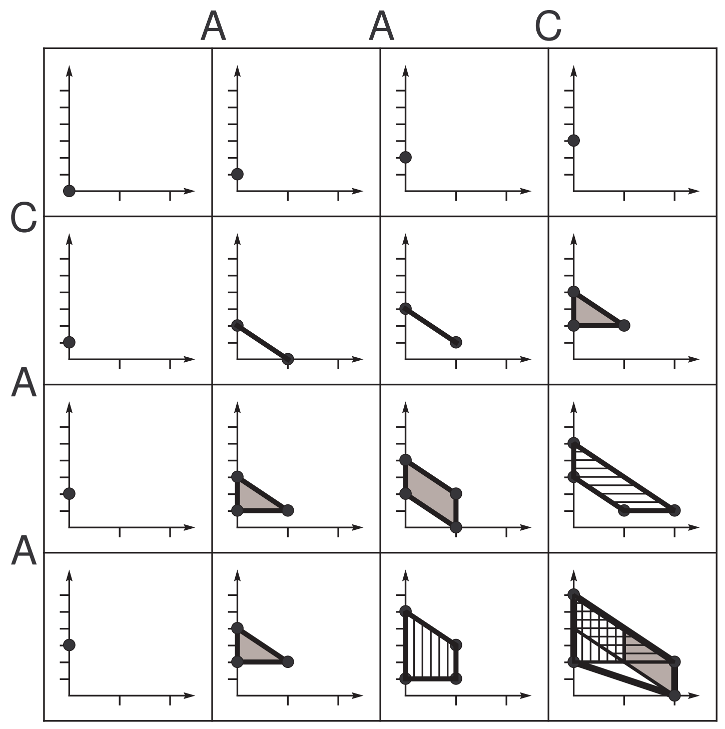

Fig. 7.2. P[i,j] for $0 \leq i, j \leq 3$.

is quite computationally expensive, as the convex hull operation is much more costly in higher dimensions. In practice, for scoring schemes with many parameters, one would fix all but a few of the parameters using the methods outlined in Section 5.4. If one is only concerned with computing the normal cone containing given parameter values, this can also be done efficiently by simply keeping track of the relevant vertices of the Newton polytope.

7.3 Retrieving alignments from polytope vertices

Parametric alignment is made feasible by the fact that the number of vertices of the Newton polytope is fairly small. In fact, for the 3-parameter scoring scheme, the number of vertices is bounded by

$$\text{constant} \cdot n^{\frac{2}{3}},$$

a polynomial in n, where n is the length of the longer of the two sequences (see Section 5.3). The total number of possible alignments, in contrast, is

vertex	alignment	parameter values
(2,0)	`CAA` `AAC`	$S \leq 0$ and $S \leq X$
(0,2)	`CAA-` `-AAC`	$X \leq S \leq 0$
(0,6)	`CAA---` `---AAA`	$S \geq 0$ and $S \geq \frac{1}{2}X$
(2,2)	`-CAA` `AAC-`	$0 \leq S \leq \frac{1}{2}X$

Table 7.1. *Vertices of* $P[3,3]$*, a corresponding optimal alignment, and the parameter values for which it is optimal.*

exponential in n (see Proposition 2.9), which becomes unmanageable for large n.

However, the bound on the number of vertices of the Newton polytope does not imply a bound on the number of actual optimal alignments that each vertex may correspond to. Is this number also small, that is, bounded by a polynomial in n?

Unfortunately, in our 3-parameter scoring scheme, this is easily seen not to be the case.

Example 7.5 Assuming that $M > S$ (a natural assumption), the optimal alignments of

$$\underbrace{\texttt{CC}\cdots\texttt{CC}}_{2n} \text{ and } \underbrace{\texttt{C}\cdots\texttt{C}}_{n}$$

would look like

```
CCCCCCCC
-CC--C-C
```

and there are $\binom{2n}{n}$ of these, which is exponential in n.

One would hope that a more robust scoring scheme would not have this problem. For example, let us look at the 4-parameter scoring scheme discussed at the beginning of Section 7.2. Further, we will restrict our attention to "biologically reasonable" parameter values. A good first approximation of this is to require $M > S$, $M > X$, and $G < 0$. Note that if we do not restrict our attention to biologically reasonable parameter values, then it is easy to get exponentially-many optimal alignments. For example, if $G = 0$, then we are reduced to the 3-parameter scoring scheme, and Example 7.5 shows sequences with $\binom{2n}{n}$ optimal alignments.

Small experiments do lead one to believe that, if the parameters are biologically reasonable, then there are not "too many" optimal alignments. Unfortunately, for each such choice of parameters, there are sequences with exponentially many optimal alignments.

Proposition 7.6 *Given parameters M, X, G, and S such that $M > X$, $M > S$, and $G < 0$, choose any $k \in \mathbb{Z}_+$ such that*

$$k > \frac{-G}{M - \max\{X, S\}}.$$

For a given $m \in \mathbb{Z}_+$, define the sequences σ^1 and σ^2 of lengths $4km$ and $3km$, respectively, as follows: σ^1 is

$$\underbrace{\mathtt{AA}\cdots\mathtt{AA}}_{2k}\underbrace{\mathtt{CC}\cdots\mathtt{CC}}_{2k}$$

repeated m times, and σ^2 is

$$\underbrace{\mathtt{AA}\cdots\mathtt{AA}}_{2k}\underbrace{\mathtt{C}\cdots\mathtt{C}}_{k}$$

also repeated m times.

Then there are exactly $(k+1)^m$ optimal alignments, which is exponential in the lengths of σ^1 and σ^2.

Proof The obvious choice for optimal alignments are ones like

```
AAAACCCCAAAACCCCAAAACCCC
AAAACC--AAAAC--CAAAA--CC
```

(in this example, $k = 2$ and $m = 3$) with all of the A's aligned and with one gap in each block of C's in σ^2. Since there are m blocks of C's and $k+1$ choices of where to place the gap in each block, there are $(k+1)^m$ of these alignments. Let O denote the set of such alignments. We must prove that there are no alignments better than those in O.

Note that these alignments have the greatest possible number of matches ($3km$) and the least possible number of mismatches (zero). Therefore, the only way to improve the alignment is to have fewer gaps. Suppose we have a new alignment, h, with a better score than those in O. We will divide the alignment scores into 2 parts:

(i) score from gaps in σ^2, and
(ii) score from gaps in σ^1, and from matches and mismatches in the alignment.

Let n be the number of gaps in h appearing in σ^2 (there may also be gaps in σ^1). Then $n < m$, because having fewer gaps is the only way to improve on the score of the alignments in O. Part 1 of the score is increased by at most

$$(m-n)(-G),$$

since the alignments in O have m gaps and km spaces, and h has n gaps and at least km spaces in σ^2.

To see how much part 2 of the score is decreased by changing from an alignment in O to the alignment h, we partition σ^2 into $m+1$ blocks

$$\underbrace{\mathtt{A}\cdots\mathtt{A}}_{k} \;\Big|\; \overbrace{\underbrace{\mathtt{A}\cdots\mathtt{A}}_{k}\underbrace{\mathtt{C}\cdots\mathtt{C}}_{k}\underbrace{\mathtt{A}\cdots\mathtt{A}}_{k} \;\Big|\; \cdots \;\Big|\; \underbrace{\mathtt{A}\cdots\mathtt{A}}_{k}\underbrace{\mathtt{C}\cdots\mathtt{C}}_{k}\underbrace{\mathtt{A}\cdots\mathtt{A}}_{k}}^{m-1} \;\Big|\; \underbrace{\mathtt{A}\cdots\mathtt{A}}_{k}\underbrace{\mathtt{C}\cdots\mathtt{C}}_{k}.$$

Ignoring the first block, we concentrate on the last m blocks. In the alignment h, at least $m-n$ of these blocks have no gaps inside them. No matter what part of σ^1 is aligned to one of these blocks, there must be at least k total of mismatches or spaces (each placed at the expense of a match); for example,

```
AACCCC          AACC--          AA--AA
AACCAA          AACCAA          AACCAA
```

are possibilities. Then part 2 of the score must be decreased by at least

$$(m-n)\cdot k\big(M - \max\{X,S\}\big)$$

by changing from an alignment in O to the alignment h.

Since we have assumed that the alignment h has a better score, we combine parts 1 and 2 of the score and have that

$$(m-n)(-G) - (m-n)k\big(M - \max\{X,S\}\big) \geq 0.$$

But then

$$k \leq \frac{-G}{M - \max\{X,S\}},$$

contradicting our choice of k. Therefore, the alignments in O must have been optimal (and, in fact, must have been the only optimal alignments), and the proof follows. □

A few comments are in order. Sequences with exponentially many alignments might often appear in reality. The key condition yielding this exponential behavior is that there are large regions that are well aligned (the blocks of `A`'s) interspersed with regions with more than one optimal alignment (the blocks of `C`'s). In situations like this, however, there is some consolation: consensus alignment would work very well (in the example, the consensus alignment would have all of the `A`'s aligned perfectly).

7.4 Achieving biological correctness

The scoring schemes that we have discussed thus far attempt to produce biologically correct alignments by modeling the evolutionary events undergone by biological sequences. The 3-parameter scoring scheme introduced in Section 7.2 models evolution by simply assigning weights to the events of mutation, deletion, and insertion. The hope is that a suitable choice of values for the parameters of this scoring scheme will lead to biologically correct alignments. In this section, we explore the capability of the 3-parameter scoring scheme to produce correct alignments. Through the use of the parametric inference machinery that we have discussed, we may characterize the optimal alignments determined by this scoring scheme over the entire parameter space.

As in Section 7.3, we restrict ourselves to biologically reasonable parameters ($M > X$ and $M > S$). As the following remark shows, parameters that are not biologically reasonable are not worth considering.

Remark 7.7 For the 3-parameter scoring scheme with parameter values $(M, X, S) = (2\alpha, 2\alpha, \alpha)$, for $\alpha \in \mathbb{R}$, all possible alignments of two sequences, σ^1 and σ^2, are optimal.

Proof With this scoring scheme, we have that

$$\begin{aligned} W_{\sigma^1,\sigma^2}(h) &= 2\alpha(m_h + x_h) + \alpha s_h \\ &= \alpha(2m_h + 2x_h + s_h) \\ &= \alpha(n + m), \end{aligned}$$

where in the second step we have used Remark 7.1. Note that this weight is independent of the specific alignment h. Under this scoring scheme all alignments receive the same weight and are thus all considered to be optimal. □

Given any two biological sequences, can the correct alignment be obtained using biologically reasonable parameters? The hope is that the answer to this question is "yes", but, unfortunately, for the 3-parameter scoring scheme, this is not the case.

Theorem 7.8 *There exist two biological sequences, σ^1 and σ^2, such that the biologically correct alignment of these sequences is not optimal for any choice of biologically reasonable parameter values under the 3-parameter scoring scheme.*

Proof The first coding exon of the human gene *UBE1DC1*, which codes for a ubiquitin-activating enzyme, is particularly hard to align to its ortholog in the *Takifugu rubripes* genome. This exon is found in the human genome

(NCBI assembly build 35) on chromosome 3 at bases 133,862,080-133,862,238. The corresponding exon in the *Takifugu rubripes* genome is found at bases 151,556,461-151,556,622 of the chrUn sequence (as constructed from unordered scaffolds of the JGI v3.0 assembly by the UCSC Genome Browser, found at `genome.ucsc.edu`).

Here we consider the problem of aligning just the first 57 bases of the human exon to the first 54 bases of the fugu exon. The sequences of the prefixes of the two exons are shown below in a hand-made alignment guided by the amino acid sequences coded for by these exons.

```
   HUMAN AA   M  A  E  S  V  E  R  L  Q  Q  R  V  Q  E  L  E  R  E  L
  HUMAN DNA  ATGGCGGAGTCTGTGGAGCGCCTGCAGCAGCGGGTCCAGGAGCTGGAGCGGGAACTT
    FUGU AA   M  A  -  T  V  E  E  L  K  L  R  V  R  E  L  E  N  E  L
   FUGU DNA  ATGGCG---ACAGTCGAGGAACTGAAGCTGCGGGTGCGAGAATTAGAGAATGAATTA
DNA MATCHES  ******    * ** ***   *** *** ****** *  **  * ***   *** *
     REGION  111111222222333333333333333333333333333333333333333333333
```

Based on the amino acid sequence, it is clear that regions 1 and 3 are aligned correctly in this hand-made alignment. The alignment of region 2 is somewhat less clear, although it is likely that the codon coding for `S` is homologous to the codon coding for `T`, as is suggested by this alignment. Since it is unclear what the correct alignment of region 2 is, we consider the problem of aligning the two sequences with the first 9 bases of the fugu exon removed. The biologically correct alignment should be

```
   HUMAN AA   M  A  E  S  V  E  R  L  Q  Q  R  V  Q  E  L  E  R  E  L
  HUMAN DNA  ATGGCGGAGTCTGTGGAGCGCCTGCAGCAGCGGGTCCAGGAGCTGGAGCGGGAACTT
    FUGU AA   -  -  -  -  V  E  E  L  K  L  R  V  R  E  L  E  N  E  L
   FUGU DNA  ------------GTCGAGGAACTGAAGCTGCGGGTGCGAGAATTAGAGAATGAATTA
DNA MATCHES              ** ***   *** *** ****** *  **  * ***   *** *
```

We now show that the 3-parameter scoring scheme does not yield the correct alignment for any biologically reasonable parameter values.

The correct alignment has 28 matches, 17 mismatches, and 12 spaces. Running the parametric alignment algorithm (as described in Section 7.2) with these sequences as input (and without M fixed to zero), we obtain a 2-dimensional polygon in 3-space with vertices shown in Table 7.2.

The optimal alignments correspond to vertices of this polytope or points on its boundary whose coordinates are integers. None of the vertices correspond to an alignment with 28 matches, 17 mismatches, and 12 spaces. However, the point (28, 17, 12) does lie on the edge between vertices 4 and 5, so it is an optimal alignment for the parameter values in the intersection of the normal cones at vertices 4 and 5. In this intersection, we have that $M = X$, which is not a biologically reasonable parameter constraint. Therefore, no biologically

vertex number	(matches, mismatches, spaces)
1	(0, 0, 102)
2	(32, 0, 38)
3	(32, 11, 16)
4	(30, 15, 12)
5	(2, 43, 12)
6	(0, 43, 16)

Table 7.2. *Vertices of the alignment polytope (listed in counterclockwise order around the polygon, looking in the $-z$ direction).*

reasonable parameter values for the 3-parameter scoring scheme allow us to align these sequences correctly. □

Theorem 7.8 shows that the 3-parameter scoring scheme is inadequate for correctly aligning some biological sequences. Simply using the 4-parameter scoring scheme is sufficient for obtaining the correct alignment of these particular sequences. However, we conjecture that 4 parameters is still not sufficient to correctly align all biological sequences.

Conjecture 7.9 *There exist two biological sequences, σ^1 and σ^2, such that the biologically correct alignment of these sequences is not optimal for any choice of biologically reasonable parameter values under the 4-parameter scoring scheme.*

As in the 3-parameter case, parametric sequence alignment should be an invaluable tool in proving this conjecture.

8
Bounds for Optimal Sequence Alignment

Sergi Elizalde

Fumei Lam

One of the most frequently used techniques in determining the similarity between biological sequences is optimal sequence alignment. In the standard instance of the sequence alignment problem, we are given two sequences (usually DNA sequences) that have evolved from a common ancestor via a series of mutations, insertions and deletions. The goal is to find the best alignment between the two sequences. The definition of "best" here depends on the choice of scoring scheme and there is often disagreement about the correct choice. In [Fitch and Smith, 1983], it is shown that optimizing an inappropriately chosen alignment objective function can miss a biologically accepted homologous alignment. In *parametric sequence alignment*, this problem is avoided by instead computing the optimal alignment as a function of *variable* scores. In this chapter, we address one such scheme, in which all matches are equally rewarded, all mismatches are equally penalized and all gaps are equally penalized. For a detailed treatment on the subject of sequence alignment, we refer the reader to [Gusfield, 1997].

8.1 Alignments and optimality

We first review some notation from Section 2.2. In this chapter, all alignments will be *global alignments* between two sequences of the same length, denoted by n. An *alignment* between two sequences σ^1 and σ^2 of length n is specified either by a string over $\{H, I, D\}$ satisfying $\#H + \#D = \#H + \#I = n$, or by a pair (μ^1, μ^2) obtained from σ^1, σ^2 by possibly inserting "$-$" characters, or by a path in the alignment graph $\mathcal{G}_{n,n}$. A *match* is a position in which μ^1 and μ^2 have the same character, a *mismatch* is a position in which μ^1 and μ^2 have different characters, and a *space* (or *indel*) is a position in which exactly one of μ^1 or μ^2 has a space.

In the general sequence alignment problem, the number of parameters in a scoring scheme is 33 (see Section 2.2). In this chapter, we consider the special case in which the score of any mismatch is $-\alpha$ and the score of any space is $-\beta$. Without loss of generality, we fix the reward for a match to be 1. We then have only two parameters and the following pair (w, w') represents our scoring scheme.

$$w = \begin{pmatrix} 1 & -\alpha & -\alpha & -\alpha & -\beta \\ -\alpha & 1 & -\alpha & -\alpha & -\beta \\ -\alpha & -\alpha & 1 & -\alpha & -\beta \\ -\alpha & -\alpha & -\alpha & 1 & -\beta \\ -\beta & -\beta & -\beta & -\beta & \end{pmatrix}, \quad w' = \begin{pmatrix} 0 & 0 & 0 \\ 0 & 0 & 0 \\ 0 & 0 & 0 \end{pmatrix}$$

Observe that in any alignment of two sequences of equal length, the number of spaces inserted in each sequence is the same. For convenience, we will define the number of *gaps* of an alignment to be half the total number of spaces (note that this is not the same terminology used in [Fernández-Baca *et al.*, 2002]). The score of an alignment $\mathcal{A}$ with z matches, x mismatches, and y gaps (i.e., $2y$ spaces) is then

$$score(\mathcal{A}) = z - x\alpha - y\beta.$$

The vector (x, y, z) will be called the *type* of the alignment. Note that for sequences of length n, the type always satisfies $x + y + z = n$.

8.2 Geometric Interpretation

For two fixed sequences, different choices of parameters α and β may yield different optimal alignments. If two alignments have the same score as a function of α and β, we call them *equivalent alignments*. Observe that there may be alignments that are not optimal for any choice of α and β. When α, β are not fixed, an alignment will be called *optimal* if there is some choice of the parameters that makes it optimal for those values of the parameters. Given two sequences, it is an interesting problem to determine how many different equivalence classes of alignments can be optimal for some value of α and β.

For each of these classes, consider the region in the $\alpha\beta$-plane corresponding to the values of the parameters for which the alignments in the given equivalence class are optimal. This gives a decomposition of the $\alpha\beta$-plane into *optimality regions*. Such regions are convex polyhedra; more precisely, they are translates of cones. To see this, note that the score of an alignment with z matches, x mismatches, and y gaps is $z-x\alpha-y\beta = n-x(\alpha+1)-y(\beta+1)$ (since $x + y + z = n$). To each such alignment, we can associate a point $(x, y) \in \mathbb{R}^2$. The convex hull of all such points is a polygon, which we denote P_{xy}. Then, an alignment is optimal for those values of α and β such that the corresponding point (x, y) minimizes the product $(x, y) \cdot (\alpha + 1, \beta + 1)$ among all the points

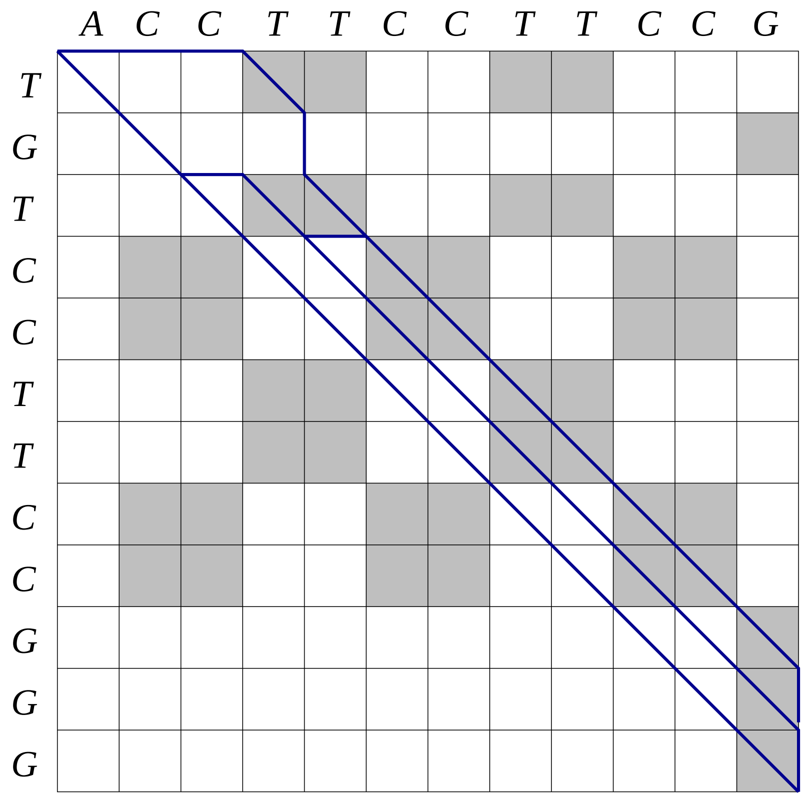

Fig. 8.1. Shaded squares denote the positions in which σ^1 and σ^2 agree. The four alignments shown and corresponding scores are

```
ACCTTCCTTCCG   ACCTTCCTTCCG-   ACCTTCCTTCCG--   ACCT-TCCTTCCG--
TGTCCTTCCGGG   TG-TCCTTCCGGG   TG-T-CCTTCCGGG   ---TGTCCTTCCGGG
```

$1 - 11\alpha$ $\quad$ $5 - 6\alpha - \beta$ $\quad$ $8 - 2\alpha - 2\beta$ $\quad$ $9 - 3\beta$

(x, y) associated to alignments of the two given sequences. Thus, an alignment with x mismatches and y gaps is optimal if and only if (x, y) is a vertex of P_{xy}. From this, we see that the decomposition of the $\alpha\beta$-plane into optimality regions is a translation of the normal fan of P_{xy}.

We are interested in the number of optimality regions, or equivalently, the number of vertices of P_{xy}. The parameters are only biologically meaningful for $\alpha, \beta \geq 0$, the case in which gaps and mismatches are penalized. Thus, we will only consider the optimality regions intersecting this quadrant. Equivalently, we are concerned only with the vertices of P_{xy} along the lower-left border.

Note that for $\alpha = \beta = -1$, the score of *any* alignment is $z-(-1)x-(-1)y = z + x + y = n$; therefore, the lines bounding each optimality region are either coordinate axes or lines passing through the point $(-1, -1)$. This shows that

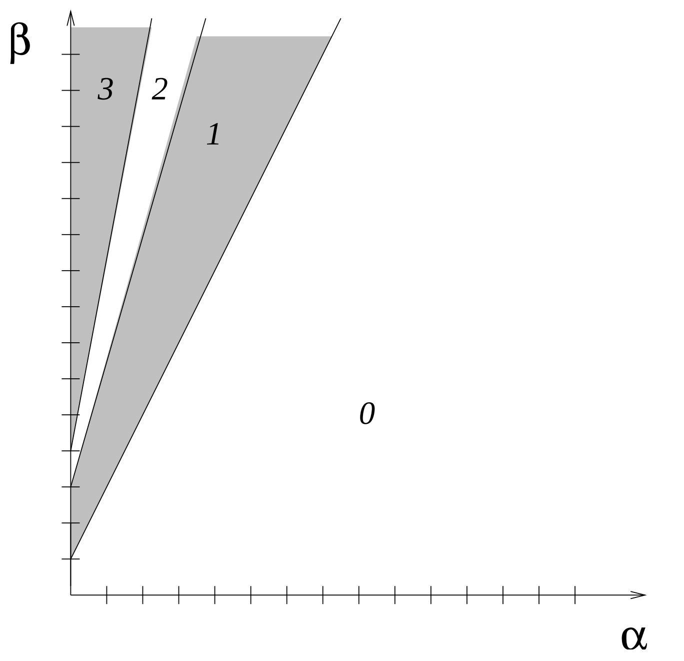

Fig. 8.2. Decomposition of the parameter space by sequences ACCTTCCTTCCG and ACCTTCCTTCCG from Figure 8.1. The boundaries of the regions are given by the coordinate axes and the lines $\beta = 1 + 2\alpha$, $\beta = 3 + 4\alpha$ and $\beta = 4 + 5\alpha$.

all boundary lines of optimality regions are either coordinate axes or lines of the form $\beta = c + (c + 1)\alpha$ for some constant c ([Gusfield *et al.*, 1994]).

The polygon P_{xy} is a projection of the convex hull of the points (x, y, z) giving the number of mismatches, gaps and matches of each alignment. All these points lie on the plane $x + y + z = n$ and their convex hull is a polygon which we denote P. We call P the *alignment polygon*. One obtains polygons combinatorially equivalent to P and P_{xy} by projecting onto the xz-plane or the yz-plane instead. It will be convenient for us to consider the projection onto the yz-plane, which we denote P_{yz}.

8.2.1 The structure of the alignment polygon

The polygon P_{yz} is obtained by taking the convex hull of the points (y, z) whose coordinates are the number of gaps and the number of matches of each alignment of the two given sequences. Note that any mismatch of an alignment can be replaced with two spaces, one in each sequence, without changing the rest of the alignment. If we perform such a replacement in an alignment of type (x, y, z), we obtain an alignment of type $(x - 1, y + 1, z)$. By replacing all mismatches with gaps we obtain an alignment of type $(0, x+y, z) = (0, n-z, z)$.

Similarly, replacing a match with two spaces in an alignment of type (x, y, z) yields one of type $(x, y+1, z-1)$, and performing all such replacements results in an alignment of type $(x, n-x, 0)$. Note however that the replacement of a match with spaces never gives an optimal alignment for nonnegative values of α and β.

From this, we see that if a point (y, z) inside P_{yz} comes from an alignment, then the points $(y+1, z)$ and $(y+1, z-1)$ must also come from alignments. A natural question is whether all lattice points (i.e., points with integral coordinates) inside P_{yz} come from alignments. We will see in the construction of Proposition 9.2 that this is not the case in general. This means that there are instances in which a lattice point (y', z') lies inside the convex hull of points corresponding to alignments, but there is no alignment with y' gaps and z' matches.

From the above observation, it follows that P has an edge joining the vertices $(0, n, 0)$ and $(0, n - z_{\max}, z_{\max})$, where $z_{\max}$ is the maximum number of matches in any alignment of the two given sequences. Similarly, P has an edge joining $(0, n, 0)$ and $(x_{\max}, n - x_{\max}, 0)$, where $x_{\max}$ is the maximum number of mismatches in any alignment. The alignment with no gaps also gives a vertex of P, which we denote $v_0 = (x_0, 0, z_0)$. Going around P starting from v_0 in the direction where z increases, we label the vertices $v_1, v_2, \ldots, v_r = (0, n - z_{\max}, z_{\max}), v_{r+1} = (0, n, 0), v_{r+2} = (x_{\max}, n - x_{\max}, 0), \ldots$

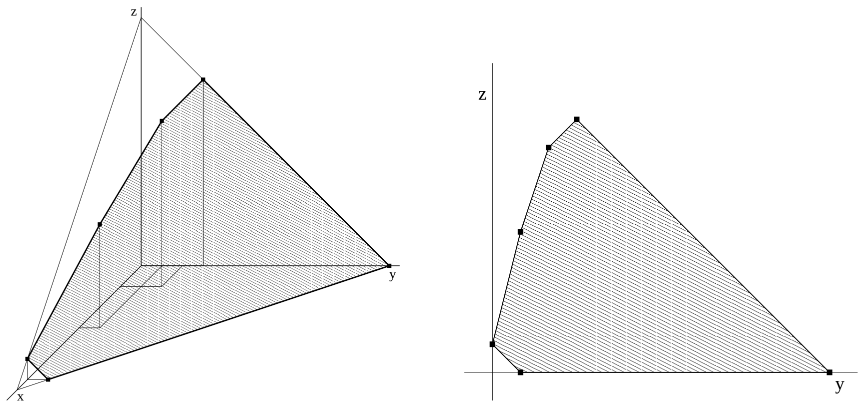

Fig. 8.3. The alignment polygon P for the sequences in Figure 8.1 and its projection P_{yz}.

For the meaningful values of the parameters, optimal alignments correspond to the vertices $v_0, v_1, \ldots, v_r$. We call them *relevant vertices* of P. For $v_i = (x_i, y_i, z_i)$, we have

$$z_0 < z_1 < \cdots < z_{r-1} \leq z_r = z_{\max},$$

$$0 = y_0 < y_1 < \cdots < y_{r-1} < y_r = n - z_{\max},$$

$$x_0 > x_1 > \cdots > x_{r-1} > x_r = 0.$$

Each vertex corresponds to an optimality region in the first quadrant of the $\alpha\beta$-plane. For sequences σ^1, σ^2, we define $g(\sigma^1, \sigma^2) = r+1$ to be the number of such optimality regions. Note that $g(\sigma^1, \sigma^2)$ also equals the number of relevant vertices of P, and the number of equivalence classes of optimal alignments of σ^1 and σ^2 for nonnegative values of α and β.

Let Σ be a fixed alphabet (which can be finite or infinite). We define

$$f_\Sigma(n) = \max_{\sigma^1, \sigma^2 \in \Sigma^n} g(\sigma^1, \sigma^2).$$

In other words, $f_\Sigma(n)$ is the maximum number of optimality regions in the decomposition of the first quadrant induced by a pair of sequences of length n in the alphabet Σ. We are interested in bounds on $f_\Sigma(n)$.

8.3 Known bounds

The first nontrivial upper bound on $f_\Sigma(n)$ was given in [Gusfield *et al.*, 1994], where it was shown that $f_\Sigma(n) = O(n^{2/3})$ for any alphabet Σ (finite or infinite). The more precise bound $f_\Sigma(n) = 3(n/2\pi)^{2/3} + O(n^{1/3} \log n)$ is shown in [Fernández-Baca *et al.*, 2002], and an example is given for which the bound is tight if Σ is an infinite alphabet.

The idea used in [Fernández-Baca *et al.*, 2002] to establish the upper bound uses the fact that the slopes of the segments connecting pairs of consecutive relevant vertices of P_{yz} must be all different. The bound is obtained by calculating the maximum number of different rational numbers such that the sum of all the numerators and denominators is at most n. To show that this bound is tight for an infinite alphabet, for every n, they construct a pair of sequences of length n for which the above bound on the number of different slopes between consecutive vertices of P_{yz} is attained. In their construction, the number of different symbols that appear in the sequences of length n grows linearly in n. It is an interesting question whether a similar $\Omega(n^{2/3})$ bound can be achieved using fewer symbols, even if the number of symbols tends to infinity as n increases.

This lower bound example only works when the alphabet Σ is infinite. However, biological sequences encountered in practice are over a finite alphabet, usually the 4-letter alphabet $\{\mathtt{A}, \mathtt{C}, \mathtt{G}, \mathtt{T}\}$. For finite alphabets Σ, the asymptotic behavior of $f_\Sigma(n)$ is not known. The upper bound $f_\Sigma(n) \leq 3(n/2\pi)^{2/3} + O(n^{1/3} \log n)$ seems to be far from the actual value in the case of a finite alphabet Σ.

8.4 The Square Root Conjecture

In the case of a binary alphabet $\Sigma = \{0,1\}$, for any n, there is a pair of sequences of length n over Σ such that the number of equivalence classes of optimal alignments is $\Omega(\sqrt{n})$ ([Fernández-Baca *et al.*, 2002]). More precisely, if we let $s(n) = s$ be the largest integer such that $s(s-1)/2 \leq n$, then the number of relevant vertices of the polygon P corresponding to the constructed sequences of length n is $s(n)$. This shows that $f_{\{0,1\}}(n) \geq s(n) = \Omega(\sqrt{n})$. Clearly, for any alphabet Σ of size $|\Sigma| \geq 2$, the same construction using only two symbols also shows $f_\Sigma(n) \geq s(n) = \Omega(\sqrt{n})$. For a finite alphabet, the best known bounds are $f_\Sigma(n) = \Omega(\sqrt{n})$ and $f_\Sigma(n) = O(n^{2/3})$. It is an open problem to close this gap. We believe that the actual asymptotic behavior of $f_{\{0,1\}}(n)$ is given by the lower bound.

Conjecture 8.1 $f_{\{0,1\}}(n) = \Theta(\sqrt{n})$.

It is clear that increasing the number of symbols in the alphabet Σ creates a larger number of possible pairs of sequences. In particular, we have that $f_{\Sigma'}(n) \geq f_\Sigma(n)$ whenever $|\Sigma'| \geq |\Sigma|$. Intuitively, a larger alphabet gives more freedom on the different alignment polygons that arise, which potentially increases the upper bound on the number of relevant vertices.

This is indeed the case in practice, as the following example shows. Let $\Sigma = \{0,1\}$ be the binary alphabet, and let $\Sigma' = \{w_1, w_2, \ldots, w_6\}$. Take a pair of sequences of length $n = 9$ over Σ' as follows: $\sigma^1 = w_1w_2w_3w_4w_5w_5w_5w_5w_5$, $\sigma^2 = w_6w_1w_2w_6w_3w_6w_6w_4w_6$ (note that this construction is similar to the one in Figure 8.4). Then, the alignment polygon has 5 relevant vertices, namely $v_0 = (9,0,0)$, $v_1 = (6,1,2)$, $v_2 = (4,2,3)$, $v_3 = (1,4,4)$ and $v_4 = (0,5,4)$. It is not hard to see that in fact $f_{\Sigma'}(n) = 5$. However, one can check by exhaustive computer search that there is no pair of binary sequences of length 9 such that their alignment polytope has 5 relevant vertices. Thus, $f_{\{0,1\}}(n) = 4 < f_{\Sigma'}(n)$.

In contrast to this result, the construction that gives the best known lower bound $\Omega(\sqrt{n})$ for finite alphabets is in fact over the binary alphabet. Thus, one interesting question is whether the bounds on $f_\Sigma(n)$ are asymptotically the same for all finite alphabets. In particular, it is an open question whether an improved upper bound in the case of the binary alphabet would imply an improved upper bound in the case of a finite alphabet.

One possible approach to reduce from the finite alphabet case to the binary alphabet case is to consider the sequences σ^1 and σ^2 under all maps $\pi : \Sigma \to \{0,1\}$. There are 2^k such maps, which we denote by π_j, $j = 1, \ldots, 2^k$. For each j, let P^j_{xy} be the convex hull of the points (x,y) giving the number of mismatches and gaps of the alignments of sequences $\pi(\sigma^1)$ and $\pi(\sigma^2)$. We would like to relate the vertices of P_{xy} to the vertices of P^j_{xy}.

Conjecture 8.2 *For each relevant vertex (x_i, y_i) of P_{xy}, there exists a map $\pi_j : \Sigma \to \{0,1\}$ such that P^j_{xy} has a relevant vertex whose second coordinate is y_i.*

Let Σ be a finite alphabet on at least two symbols and let $k = |\Sigma|$. If this conjecture is true, then $f_\Sigma(n) \leq 2^k f_{\{0,1\}}(n)$ for every n, implying the following stronger version of Conjecture 8.1.

Conjecture 8.3 *For any finite alphabet Σ, $f_\Sigma(n) = \Theta(\sqrt{n})$.*

Note that the case of $\Sigma = \{\mathtt{A}, \mathtt{C}, \mathtt{G}, \mathtt{T}\}$ is particularly interesting since most biological sequences are in this 4-letter alphabet.

Instead of finding a relationship between the vertices of P_{xy} and the vertices of P^j_{xy}, another approach would be to try to find a relationship between the optimality regions in the decomposition of the $\alpha\beta$ parameter space under all mappings to the binary alphabet. For sequences σ^1 and σ^2, let $A_0, A_1, \dots A_m$ denote the optimality regions of the decomposition of the parameter space, and for any map $\pi : \Sigma \to \{0,1\}$, let $B^\pi_0, B^\pi_1, \dots B^\pi_{i_\pi}$ denote the optimality regions for alignments of $\pi(\sigma^1)$ and $\pi(\sigma^2)$. If for every A_i, $0 \leq i \leq m$, there exists a mapping π such that $B^\pi_j \subseteq A_i$ for some j, $0 \leq j \leq i_\pi$, then this would imply $f_\Sigma(n) \leq 2^k f_{\{0,1\}}(n)$ for every n, proving Conjecture 8.3. However, this is not true for the example in Figure 8.4.

The construction of two binary sequences of length n with $s = s(n)$ optimal alignments used to obtain the lower bound in [Fernández-Baca *et al.*, 2002] has the following peculiarity. The number of gaps in the alignments giving relevant

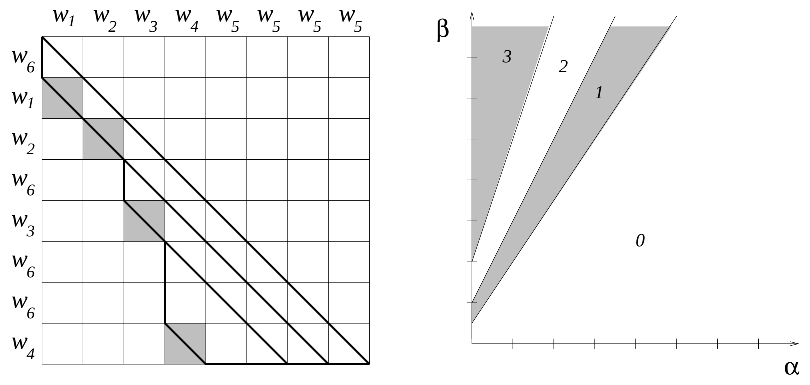

w_1 w_2 w_3 w_4 w_5 w_5 w_5 w_5
w_6 w_1 w_2 w_6 w_3 w_6 w_6 w_4
β
3
2
1
0
α

Fig. 8.4. Optimal alignments for $\sigma^1 = w_1w_2w_3w_4w_5w_5w_5w_5$ and $\sigma^2 = w_6w_1w_2w_6w_3w_6w_6w_4$, and corresponding optimality regions A_0, A_1, A_2 and A_3 given by lines $\beta = \frac{1}{2} + \frac{3}{2}\alpha, \beta = 1 + 2\alpha$ and $\beta = 2 + 3\alpha$. . In this example, for any mapping $\pi : \{w_1, w_2, \dots, w_6\} \to \{0,1\}$ and any region B^π_j in the resulting decomposition, $B^\pi_j \not\subseteq A_1$ and $B^\pi_j \not\subseteq A_2$.

vertices of the alignment polygon P are $y_0 = 0,\ y_1 = 1,\ y_2 = 2,\ \ldots,\ y_{s-2} = s-2$ (see Figure 8.5).

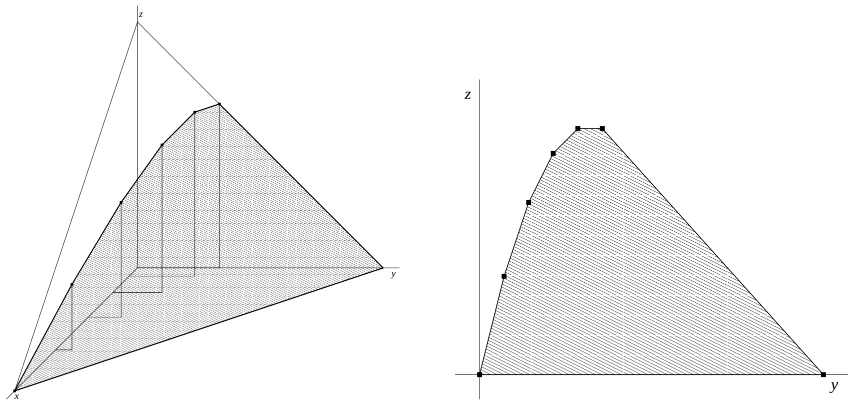

Fig. 8.5. The alignment polygon P for binary sequences of length $n = 15$ with $s(n) = 6$ relevant vertices.

The slopes between consecutive relevant vertices in the projected alignment polygon P_{yz} are then $s, s-1, s-2, \ldots, 1, 0$. In particular, all the slopes are integral. If this was true of all alignment polytopes coming from binary sequences, then Conjecture 8.1 would follow, because the maximum number of different integral slopes in P_{yz} is $s(n)$. However, it is not the case in general that the slopes obtained from binary sequences are always integral.

The smallest counterexample is given by the pair of sequences $\sigma^1 = 001011$ and $\sigma^2 = 111000$. The vertices of the corresponding polytope P_{yz} are $(0, 2)$, $(3, 3)$, $(6, 0)$ and (10). The slope between the first two vertices is $1/3$, which shows that not all slopes are integral. In fact, it follows from the proof of Proposition 9.3 that the situation is quite the opposite. We will see in the next chapter that for any positive integers u, v with $u < v$, one can construct a pair of binary sequences of length at most $6v - 2u$ such that the corresponding (projected) alignment polytope P_{yz} has a slope u/v between two consecutive relevant vertices.

9
Inference Functions

Sergi Elizalde

Some of the statistical models introduced in Chapter 1 have the feature that, aside from the observed data, there is hidden information that cannot be determined from an observation. These are called observed models, and particular examples of them are the hidden Markov model and the hidden tree model. A natural problem in such models is to determine, given a particular observation, what is the most likely hidden data (which is called *explanation*) for that observation. Any fixed values of the parameters determine a way to assign an explanation to each possible observation. A map obtained in this way is called an *inference function.*

Examples of inference functions include *gene finding functions.* These are used to determine what parts of a DNA sequence correspond to exons, which will be translated into proteins, and what parts are introns, which will get spliced out before the translation. They are inference functions of the hidden Markov model described in Section 4.4. An observation in this model is a sequence in the alphabet $\Sigma' = \{\texttt{A}, \texttt{C}, \texttt{G}, \texttt{T}\}$.

9.1 What is an inference function?

Let us introduce some notation and make the definition more formal. Consider a graphical model (as defined in Section 1.5) with n observed random variables $Y_1, Y_2, \ldots, Y_n$, and q hidden random variables $X_1, X_2, \ldots, X_q$. To simplify the notation, we make the assumption, which is often the case in practice, that all the observed variables are on the same finite alphabet Σ', and that all the hidden variables are on the finite alphabet Σ. The state space is then $(\Sigma')^n$. Let $l = |\Sigma|$ and $l' = |\Sigma'|$. Let d be the number of parameters of the model, which we denote $\theta_1, \theta_2, \ldots, \theta_d$. They express transition probabilities between states. The model is represented by a positive polynomial map $\mathbf{f} : \mathbb{R}^d \longrightarrow \mathbb{R}^{(l')^n}$. For each observation $\tau \in (\Sigma')^n$, the corresponding coordinate f_τ is a polynomial in $\theta_1, \theta_2, \ldots, \theta_d$ which gives the probability of making the particular observation τ.

Thus, we have $f_\tau = \mathrm{Prob}(\mathbf{Y} = \tau) = \sum_{\mathbf{h}\in\Sigma^q} \mathrm{Prob}(\mathbf{X} = \mathbf{h}, \mathbf{Y} = \tau)$, where each summand $\mathrm{Prob}(\mathbf{X} = \mathbf{h}, \mathbf{Y} = \tau)$ is a monomial in the parameters $\theta_1, \theta_2, \ldots, \theta_d$.

For fixed values of the parameters, the basic inference problem is to determine, for each given observation τ, the value $\mathbf{h} \in \Sigma^q$ of the hidden data that maximizes $\mathrm{Prob}(\mathbf{X} = \mathbf{h}|\mathbf{Y} = \tau)$. A solution to this optimization problem is denoted $\widehat{\mathbf{h}}$ and is called an *explanation* of the observation τ. Each choice of parameters $(\theta_1, \theta_2, \ldots, \theta_d)$ defines an *inference function* $\tau \mapsto \widehat{\mathbf{h}}$ from the set of observations $(\Sigma')^n$ to the set of explanations Σ^q. A brief discussion of inference functions and their geometric interpretation in terms of the tropicalization of the polynomial map $\mathbf{f}$ was given at the end of Section 3.4.

It is possible that there is more than one value of $\widehat{\mathbf{h}}$ attaining the maximum of $\mathrm{Prob}(\mathbf{X} = \mathbf{h}|\mathbf{Y} = \tau)$. In this case, for simplicity, we will pick only one such explanation, according to some consistent tie-breaking rule decided ahead of time. For example, we can pick the least such $\widehat{\mathbf{h}}$ in some given total order of the set Σ^q of hidden states. Another alternative would be to define inference functions as maps from $(\Sigma')^n$ to subsets of Σ^q. This would not affect the results of this chapter, so for the sake of simplicity we consider only inference functions as defined above.

It is important to observe that the total number of functions $(\Sigma')^n \longrightarrow \Sigma^q$ is $(l^q)^{(l')^n} = l^{q(l')^n}$, which is doubly-exponential in the length n of the observations. However, most of these are not inference functions for any value of the parameters. In this chapter we give an upper bound on the number of inference functions of a graphical model.

We finish this section with some more notation that will be used in the chapter. We denote by E the number of edges of the underlying graph of the graphical model. The logarithms of the model parameters will be denoted by $v_i = \log(\theta_i)$.

The coordinates of our model are polynomials of the form $f_\tau(\theta_1, \theta_2, \ldots, \theta_d) = \sum_i \theta_1^{a_{1,i}}\theta_2^{a_{2,i}}\cdots\theta_d^{a_{d,i}}$. Recall from Section 2.3 that the *Newton polytope* of such a polynomial is defined as the convex hull in $\mathbb{R}^d$ of the exponent vectors $(a_{1,i}, a_{2,i}, \ldots, a_{d,i})$. We denote the Newton polytope of f_τ by $\mathrm{NP}(f_\tau)$, and its *normal fan* by $\mathcal{N}(\mathrm{NP}(f_\tau))$.

Recall also that that the *Minkowski sum* of two polytopes P and P' is $P \odot P' := \{\mathbf{x} + \mathbf{x}' : \mathbf{x} \in P, \mathbf{x}' \in P'\}$. The Newton polytope of the map $\mathbf{f} : \mathbb{R}^d \longrightarrow \mathbb{R}^{(l')^n}$ is defined as the Minkowski sum of the individual Newton polytopes of its coordinates, namely $\mathrm{NP}(\mathbf{f}) := \bigodot_{\tau\in(\Sigma')^n} \mathrm{NP}(f_\tau)$.

9.2 The Few Inference Functions Theorem

For fixed parameters, the inference problem of finding the explanation $\widehat{\mathbf{h}}$ that maximizes $\mathrm{Prob}(\mathbf{X} = \mathbf{h}|\mathbf{Y} = \tau)$ is equivalent to identifying the monomial

$\theta_1^{a_{1,i}}\theta_2^{a_{2,i}}\cdots\theta_d^{a_{d,i}}$ of f_τ with maximum value. Since the logarithm is a monotone increasing function, the sought monomial also maximizes the quantity

$$\begin{aligned}\log(\theta_1^{a_{1,i}}\theta_2^{a_{2,i}}\cdots\theta_d^{a_{d,i}}) &= a_{1,i}\log(\theta_1)+a_{2,i}\log(\theta_2)+\ldots+a_{d,i}\log(\theta_d)\\ &= a_{1,i}v_1+a_{2,i}v_2+\ldots+a_{d,i}v_d.\end{aligned}$$

This is equivalent to the fact that the corresponding vertex $(a_{1,i},a_{2,i},\ldots,a_{d,i})$ of the Newton polytope $\mathrm{NP}(f_\tau)$ maximizes the linear expression $v_1x_1+\ldots+v_dx_d$. Thus, the inference problem for fixed parameters becomes a linear programming problem.

Each choice of the parameters $\theta=(\theta_1,\theta_2,\ldots,\theta_d)$ determines an inference function. If $\mathbf{v}=(v_1,v_2,\ldots,v_d)$ is the vector in $\mathbb{R}^d$ with coordinates $v_i=\log(\theta_i)$, then we denote the corresponding inference function by

$$\Phi_{\mathbf{v}}:(\Sigma')^n\longrightarrow\Sigma^q.$$

For each observation $\tau\in(\Sigma')^n$, its explanation $\Phi_{\mathbf{v}}(\tau)$ is given by the vertex of $\mathrm{NP}(f_\tau)$ that is maximal in the direction of the vector $\mathbf{v}$. Note that for certain values of the parameters there may be more than one vertex attaining the maximum, if $\mathbf{v}$ is perpendicular to a face of $\mathrm{NP}(f_\tau)$. It is also possible that the same point $(a_{1,i},a_{2,i},\ldots,a_{d,i})$ in the polytope corresponds to several different values of the hidden data. In both cases, we pick the explanation according to the tie-braking rule decided ahead of time. This simplification does not affect the asymptotic number of inference functions.

Different values of θ yield different directions $\mathbf{v}$, which give possibly different inference functions. We are interested in bounding the number of different inference functions that a graphical model can have. The next theorem states that the number of inference functions grows polynomially in the complexity of the graphical model. In particular, very few of the $l^{q(l')^n}$ functions $(\Sigma')^n\longrightarrow\Sigma^q$ are inference functions.

Theorem 9.1 (The Few Inference Functions Theorem) *Let d be a fixed positive integer. Consider a graphical model with d parameters, and let E be the number of edges of the underlying graph. Then, the number of inference functions of the model is at most*

$$O(E^{d^2(d-1)/2}).$$

Before proving this theorem, observe that the number E of edges depends on the number n of observed random variables. In most graphical models, E is a linear function of n, so the bound becomes $O(n^{d^2(d-1)/2})$. For example, the hidden Markov model has $E=2n-1$ edges.

Proof We have seen that an inference function is specified by a choice of the parameters, which is equivalent to choosing a vector $\mathbf{v} \in \mathbb{R}^d$. The function is denoted $\Phi_{\mathbf{v}} : (\Sigma')^n \longrightarrow \Sigma^q$, and the explanation $\Phi_{\mathbf{v}}(\tau)$ of a given observation τ is determined by the vertex of $\mathrm{NP}(f_\tau)$ that is maximal in the direction of $\mathbf{v}$. Thus, cones of the normal fan $\mathcal{N}(\mathrm{NP}(f_\tau))$ correspond to sets of vectors $\mathbf{v}$ that give rise to the same explanation for the observation τ. Non-maximal cones correspond to directions $\mathbf{v}$ for which more than one vertex is maximal. Since ties are broken using a consistent rule, we disregard this case for simplicity. Thus, in what follows we consider only maximal cones of the normal fan.

Let $\mathbf{v}' = (v'_1, v'_2, \ldots, v'_d)$ be another vector corresponding to a different choice of parameters. By the above reasoning, $\Phi_{\mathbf{v}}(\tau) = \Phi_{\mathbf{v}'}(\tau)$ if and only if $\mathbf{v}$ and $\mathbf{v}'$ belong to the same cone of $\mathcal{N}(\mathrm{NP}(f_\tau))$. Thus, $\Phi_{\mathbf{v}}$ and $\Phi_{\mathbf{v}'}$ are the same inference function if and only if $\mathbf{v}$ and $\mathbf{v}'$ belong to the same cone of $\mathcal{N}(\mathrm{NP}(f_\tau))$ for all observations $\tau \in (\Sigma')^n$. Denote by $\bigwedge_{\tau \in (\Sigma')^n} \mathcal{N}(\mathrm{NP}(f_\tau))$ the common refinement of all these normal fans. Then, $\Phi_{\mathbf{v}}$ and $\Phi_{\mathbf{v}'}$ are the same function exactly when $\mathbf{v}$ and $\mathbf{v}'$ lie in the same cone of this common refinement.

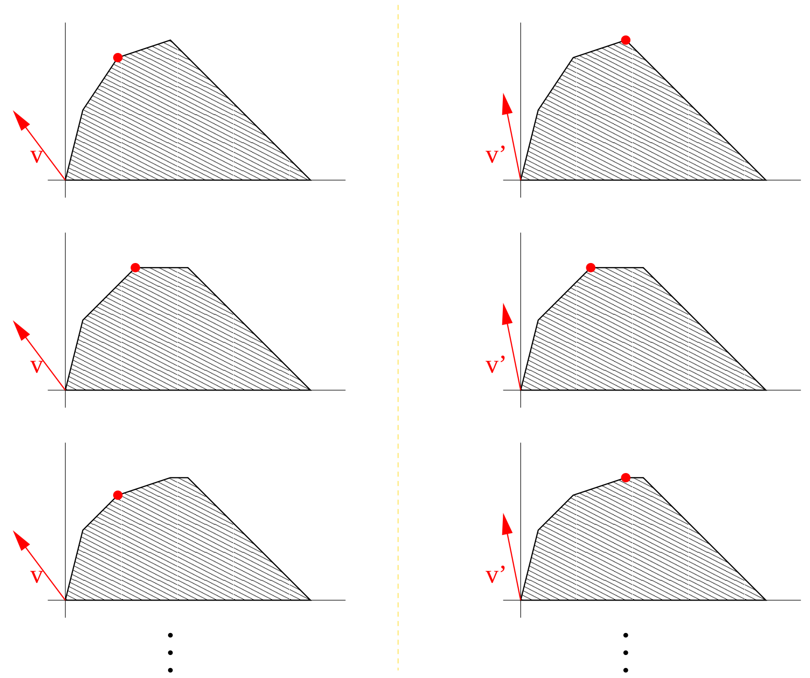

Fig. 9.1. Two different inference functions $\Phi_{\mathbf{v}}$ and $\Phi_{\mathbf{v}'}$. Each row depicts the Newton polytope of an observation, and the respective explanations are given by the marked vertices.

Therefore, the number of inference functions equals the number of cones in $\bigwedge_{\tau \in (\Sigma')^n} \mathcal{N}(\mathrm{NP}(f_\tau))$. It is well known that the normal fan of a Minkowski sum of polytopes is the common refinement of the individual fans (see [Ziegler, 1995, Proposition 7.12]). In our case, the common refinement is the normal fan of $\mathrm{NP}(\mathbf{f}) = \bigodot_{\tau\in(\Sigma')^n} \mathrm{NP}(f_\tau)$, the Minkowski sum of the polytopes $\mathrm{NP}(f_\tau)$ for all observations τ. Thus, our goal is to bound the number of vertices of $\mathrm{NP}(\mathbf{f})$.

Note that for each τ, the polytope $\mathrm{NP}(f_\tau)$ is contained in the cube $[0, E]^d$. This is because each parameter θ_i can appear as a factor of a monomial of f_τ at most E times. Besides, the vertices of $\mathrm{NP}(f_\tau)$ have integral coordinates, because they are exponent vectors. Polytopes whose vertices have integral coordinates are called *lattice polytopes*. It follows that the edges of $\mathrm{NP}(f_\tau)$ are given by vectors where each coordinate is an integer between $-E$ and E. Each edge of $\mathrm{NP}(\mathbf{f})$ has the same direction as an edge of one of its summands $\mathrm{NP}(f_\tau)$. Therefore, the normal vector of any facet of $\mathrm{NP}(\mathbf{f})$ is obtained as the vector perpendicular to $d-1$ linearly independent vectors in $[-E, E]^d$ with integral coordinates. Since there are only $O(E^d)$ such vectors, the normal vectors of the facets of $\mathrm{NP}(f_\tau)$ can take at most $O(E^{d(d-1)})$ different directions.

This implies that $\mathrm{NP}(\mathbf{f})$ has at most $O(E^{d(d-1)})$ facets. By the Upper Bound Theorem (see [McMullen, 1971]), a d-dimensional polytope with N facets can have at most $O(N^{d/2})$ vertices. Thus, the number of vertices of $\mathrm{NP}(\mathbf{f})$, and hence the number of inference functions of the graphical model, is bounded from above by $O(E^{d^2(d-1)/2})$. □

9.3 Inference functions for sequence alignment

We now show how Theorem 9.1 can be applied to give a tight bound on the number of inference functions of the model for sequence alignment used in Chapter 8. Recall the sequence alignment problem from Section 2.2, which consists in finding the best alignment between two sequences. Given two strings σ^1 and σ^2 of lengths n_1 and n_2 respectively, an *alignment* is a pair of equal length strings (μ^1, μ^2) obtained from σ^1, σ^2 by inserting "$-$" characters in such a way that there is no position in which both μ^1 and μ^2 have a "$-$". A *match* is a position where μ^1 and μ^2 have the same character, a *mismatch* is a position where μ^1 and μ^2 have different characters, and a *space* is a position in which one of μ^1 and μ^2 has a space. A simple scoring scheme consists of two parameters α and $\widetilde{\beta}$ denoting mismatch and space penalties respectively. The score of an alignment with z matches, x mismatches, and $\widetilde{y}$ spaces is then $z - x\alpha - \widetilde{y}\widetilde{\beta}$. Observe that these numbers always satisfy $2z + 2x + \widetilde{y} = n_1 + n_2$. For pairs of sequences of equal length, this is the same scoring scheme used in Chapter 8, with $\widetilde{y} = 2y$ and $\widetilde{\beta} = \beta/2$. In this case, y is called the number of gaps, which is half the number of spaces, and β is the penalty for a gap.

This 2-parameter model for sequence alignment is a particular case of the pair hidden Markov model discussed in Section 2.2. The problem of determining the highest scoring alignment for given values of α and $\widetilde{\beta}$ is equivalent to the inference problem in the pair hidden Markov model, with some parameters set to functions of α and $\widetilde{\beta}$, or to 0 or 1. In this setting, an observation is a pair of sequences $\tau = (\sigma^1, \sigma^2)$, and the number of observed variables is $n = n_1 + n_2$. An explanation is then an optimum alignment, since the values of the hidden variables indicate the positions of the spaces.

For each pair of sequences τ, the Newton polytope of the polynomial f_τ is the convex hull of the points $(x, \widetilde{y}, z)$ whose coordinates are, respectively, the number of mismatches, spaces and matches of each possible alignment of the pair. This polytope lies on the plane $2z+2x+\widetilde{y} = n_1+n_2$, so no information is lost by considering its projection onto the $x\widetilde{y}$-plane instead. This projection is just the convex hull of the points $(x, \widetilde{y})$ giving the number of mismatches and spaces of each alignment. For any alignment of sequences of lengths n_1 and n_2, the corresponding point $(x, \widetilde{y})$ lies inside the square $[0, n]^2$, where $n = n_1 + n_2$. Therefore, since we are dealing with lattice polygons inside $[0, n]^2$, it follows from Theorem 9.1 that the number of inference functions of this model is $O(n^2)$.

Next we show that this quadratic bound on the number of inference functions of the model is tight. We first consider the case in which the alphabet Σ' of the observed sequences is allowed to be large enough.

Proposition 9.2 *Consider the* 2*-parameter model for sequence alignment described above. Assume for simplicity that the two observed sequences have the same length* n_1*, and let* $n = 2n_1$*. Let* $\Sigma' = \{\omega_0, \omega_1, \ldots, \omega_{n_1}\}$ *be the alphabet of the observed sequences. Then, the number of inference functions of this model is* $\Theta(n^2)$*.*

Proof The above argument shows that $O(n^2)$ is an upper bound on the number of inference functions of the model. To prove the proposition, we will argue that there are at least $\Omega(n^2)$ such functions.

Since the two sequences have the same length, we will use y to denote the number of gaps, where $y = \widetilde{y}/2$, and $\beta = 2\widetilde{\beta}$ to denote the gap penalty. For fixed values of α and β, the explanation of an observation $\tau = (\sigma^1, \sigma^2)$ is given by the vertex of $\mathrm{NP}(f_\tau)$ that is maximal in the direction of the vector $(-\alpha, -\beta, 1)$. In this model, $\mathrm{NP}(f_\tau)$ is the convex hull of the points (x, y, z) whose coordinates are the number of mismatches, spaces and matches of the alignments of σ^1 and σ^2.

The argument in the proof of Theorem 9.1 shows that the number of inference functions of this model is the number of cones in the common refinement of the normal fans of $\mathrm{NP}(f_\tau)$, where τ runs over all pairs of sequences of length n_1 in the alphabet Σ'. Since the polytopes $\mathrm{NP}(f_\tau)$ lie on the plane $x + y + z = n_1$, it is equivalent to consider the normal fans of their projections onto the yz-

plane. These projections are lattice polygons contained in the square $[0, n_1]^2$. We denote by P_τ the projection of $\mathrm{NP}(f_\tau)$ onto the yz-plane.

We claim that for any two integers a and b such that $a, b \geq 1$ and $a+b \leq n_1$, there is a pair $\tau = (\sigma^1, \sigma^2)$ of sequences of length n_1 in the alphabet Σ' so that the polygon P_τ has an edge of slope b/a.

Before proving the claim, let us show that it implies the statement of the proposition. First note that the number of different slopes b/a obtained by numbers a and b satisfying the above conditions is $\Theta(n_1^2)$. Indeed, this follows from the fact that the proportion of relative prime pairs of numbers in $\{1, 2, \ldots, m\}$ tends to a constant (namely $6/\pi^2$) as m goes to infinity (see for example [Apostol, 1976]). Now, in the normal fan, each slope of P_τ becomes a 1-dimensional ray perpendicular to it. Different slopes give different rays in $\bigwedge_{\tau \in (\Sigma')^n \times (\Sigma')^n} \mathcal{N}(P_\tau)$, the common refinement of fans. In two dimensions, the number of maximal cones equals the number of rays. Thus, $\bigwedge_\tau \mathcal{N}(P_\tau)$ has at least $\Omega(n_1^2) = \Omega(n^2)$ cones. Equivalently, the model has $\Omega(n^2)$ inference functions.

Let us now prove the claim. Given a and b as above, construct the sequences σ^1 and σ^2 as follows:

$$\sigma^1 = \omega_1 \omega_2 \cdots \omega_b \underbrace{\omega_{b+1} \cdots \omega_{b+1}}_{n_1 - b \,\text{times}},$$

$$\sigma^2 = \underbrace{\omega_0 \cdots \omega_0}_{a \,\text{times}} \omega_1 \omega_2 \cdots \omega_b \underbrace{\omega_{b+2} \cdots \omega_{b+2}}_{n_1 - a - b \,\text{times}}.$$

Then, it is easy to check that for $\tau = (\sigma^1, \sigma^2)$, P_τ has an edge between the vertex $(0, 0)$, corresponding to the alignment with no spaces, and the vertex (a, b), corresponding to the alignment

$$\begin{array}{l} \mu^1 = - \;\cdots\; - \;\omega_1\, \omega_2 \cdots \omega_b\, \omega_{b+1} \cdots \omega_{b+1}\, \omega_{b+1} \cdots \omega_{b+1} \\ \mu^2 = \omega_0 \cdots \omega_0\, \omega_1\, \omega_2 \cdots \omega_b\, \omega_{b+2} \cdots \omega_{b+2} \;\; - \;\cdots\; - \end{array}$$

The slope of this edge is b/a. In fact, the four vertices of P_τ are $(0, 0)$, (a, b), $(n_1 - b, b)$ and $(n_1, 0)$. This proves the claim.

Figure 9.2 shows a pair of sequences for which P_τ has an edge of slope $4/3$. □

Chapter 8 raised the question of whether all the lattice points inside the projected alignment polygon P_τ come from alignments of the pair of sequences τ. The construction in the proof of Proposition 9.2 gives instances for which some lattice points inside P_τ do not come from any alignment.

For example, take P_τ to be the projection of the alignment polygon corresponding to the pair of sequences in Figure 9.2. The points $(1, 1)$, $(2, 1)$ and $(2, 2)$ lie inside P_τ. However, there is no alignment of these sequences with

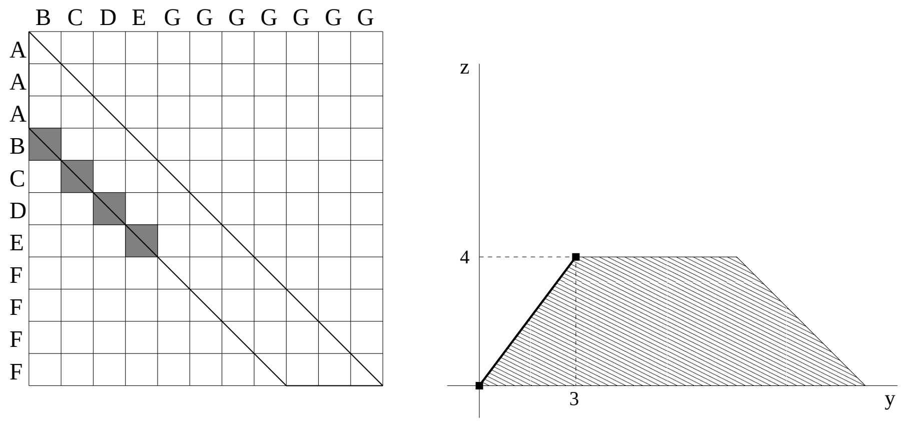

Fig. 9.2. Two sequences of length 11 giving the slope 4/3 in their alignment polytope.

less than 3 gaps having at least one match, so these points do not correspond to alignments. Figure 9.3 shows exactly which lattice points in P_τ come from alignments of the pair.

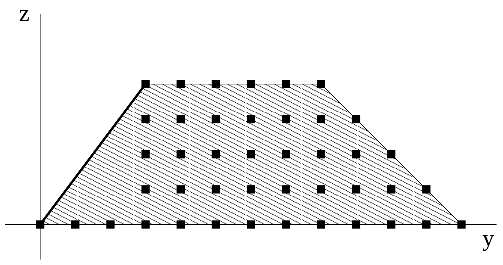

Fig. 9.3. The thick dots are the points (y, z) giving the number of gaps and matches of alignments of the sequences in Figure 9.2.

Next we will show that, even in the case of the binary alphabet, our quadratic upper bound on the number of inference functions of the 2-parameter model for sequence alignment is tight as well. Thus, the large alphabet Σ' from Proposition 9.2 is not needed to obtain $\Omega(n^2)$ slopes in the alignment polytopes.

Proposition 9.3 *Consider the 2-parameter model for sequence alignment as before, where the two observed sequences have length n_1. Let $n = 2n_1$, and let $\Sigma' = \{0, 1\}$ be the binary alphabet. The number of inference functions of this model is $\Theta(n^2)$.*

Proof We follow the same idea as in the proof of Proposition 9.2. We will construct a collection of pairs of binary sequences $\tau = (\sigma^1, \sigma^2)$ so that the total number of different slopes of the edges of the polygons $\mathrm{NP}(f_\tau)$ is $\Omega(n^2)$. This will imply that the number of cones in $\bigwedge_\tau \mathcal{N}(\mathrm{NP}(f_\tau))$, where τ ranges over all pairs of binary sequences of length n_1, is $\Omega(n^2)$.

Recall that P_τ denotes the projection of $\mathrm{NP}(f_\tau)$ onto the yz-plane, and that it is a lattice polygon contained in $[0, n_1]^2$.

We claim that for any positive integers u and v with $u < v$ and $6v - 2u \leq n_1$, there exists a pair τ of binary sequences of length n_1 such that P_τ has an edge of slope u/v. This will imply that the number of different slopes created by the edges of the polygons P_τ is $\Omega(n^2)$.

Thus, it only remains to prove the claim. Given positive integers u and v as above, let $a := 2v$, $b := v - u$. Assume first that $n_1 = 6v - 2u = 2a + 2b$. Consider the sequences

$$\sigma^1 = 1^a 0^b 1^b 0^a, \qquad \sigma^2 = 0^a 1^b 0^b 1^a,$$

where 0^a indicates that the symbol 0 is repeated a times. Let $\tau = (\sigma^1, \sigma^2)$. Then, it is not hard to see that the polygon P_τ for this pair of sequences has four vertices: $v_0 = (0, 0)$, $v_1 = (b, 3b)$, $v_2 = (a + b, a + b)$ and $v_3 = (n_1, 0)$. The slope of the edge between v_1 and v_2 is $\frac{a-2b}{a} = \frac{u}{v}$.

If $n_1 > 6v - 2u = 2a + 2b$, we just append $0^{n_1 - 2a - 2b}$ to both sequences σ^1 and σ^2.

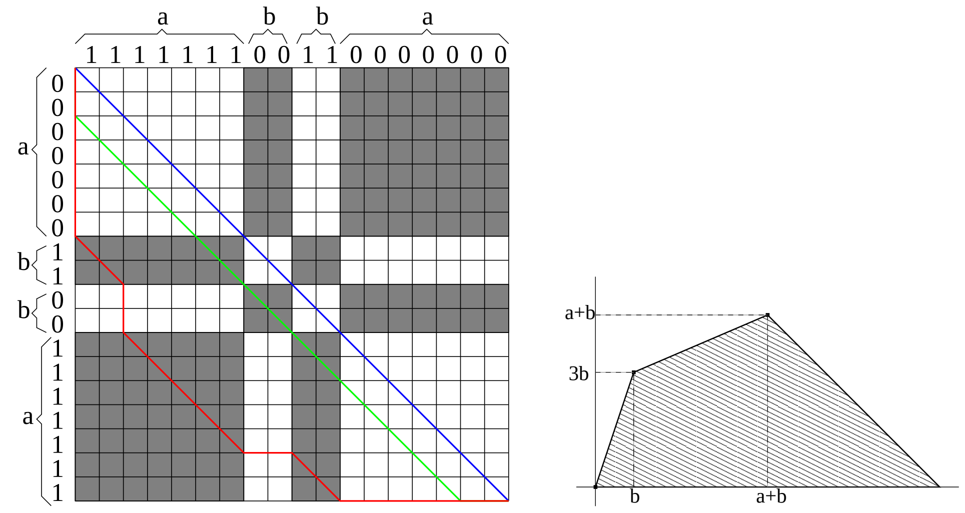

Fig. 9.4. Two binary sequences of length 18 giving the slope 3/7 in their alignment polytope.

Note that if $v - u$ is even, the construction can be done with sequences of length $n_1 = 3v - u$ by taking $a := v$, $b := \frac{v-u}{2}$. Figure 9.4 shows the alignment graph and the polygon P_τ for $a = 7$, $b = 2$. $\square$

In most cases, one is interested only in those inference functions that are biologically meaningful. In our case, meaningful values of the parameters occur when $\alpha, \beta \geq 0$, which means that mismatches and spaces are penalized, instead of rewarded. Sometimes one also requires that $\alpha \leq \beta$, which means that a mismatch should be penalized less than two spaces. It is interesting to observe that our constructions in the proofs of Propositions 9.2 and 9.3 not only show that the total number of inference functions is $\Omega(n^2)$, but also that the number of biologically meaningful ones is still $\Omega(n^2)$. This is because the different rays created in our construction have a biologically meaningful direction in the parameter space.

Let us now relate the results from this section with the bounds given in the previous chapter. In Chapter 8 we saw that in the 2-parameter model for sequence alignment, if τ is a pair of sequences of length n in an arbitrarily large alphabet, then the polygon P_τ can have $\Theta(n^{2/3})$ vertices in the worst case. In Proposition 9.2 we have shown that the Minkowski sum of these polygons for all possible such observations τ, namely $\bigodot_\tau P_\tau$, has $\Theta(n^2)$ vertices.

In the case where the alphabet for the sequences is binary (or more generally, finite), in Chapter 8 we conjectured that the polygon P_τ can only have $\Theta(\sqrt{n})$ vertices at most. In Proposition 9.3 we have proved that the polygon $\bigodot_\tau P_\tau$, where τ runs over all pairs of binary sequences of length n, has $\Theta(n^2)$ vertices as well.

Having shown that the number of inference functions of a graphical model is polynomial in the size of the model, an interesting next step would be to find a way to precompute all the inference functions for given models and store them in the memory. This would allow us to answer queries about a given observation very efficiently.

10
Geometry of Markov Chains

Eric Kuo

This chapter discusses the differences between Viterbi sequences of Markov chains and toric Markov chains. When the chains have 2 or 3 states, there are some sequences that are Viterbi for a toric Markov chain, but not for any Markov chain. However, when the chain has 4 or more states, the sets of Viterbi sequences are identical for both Markov chains and toric Markov chains. We also discuss maximal probability sequences for fully observed Markov models.

10.1 Viterbi Sequences

In this chapter, we number the states of an l-state Markov chain from 0 to $l-1$. Given a Markov chain M, the probability of a sequence is the product of the initial probability of the first state and all the transition probabilities between consecutive states. There are l^n possible sequences of length n. A *Viterbi path of length* n is a sequence of n states (containing n transitions) with the highest probability. Viterbi paths of Markov chains can be computed in polynomial time [Forney, 1973, Viterbi, 1967]. A Markov chain may have more than one Viterbi path of length n; for instance, if 012010 is a Viterbi path of length 6, then 010120 must also be a Viterbi path since both sequences have the same initial state and the same set of transitions, only that they appear in a different order. Two sequences are *equivalent* if their set of transitions are the same. The Viterbi paths of a Markov chain might not be all equivalent. Consider the Markov chain on l states that has a uniform initial distribution and a uniform transition matrix (i.e. $\theta_{ij} = \frac{1}{l}$ for all states i, j). Since each sequence of length n has the same probability $\frac{1}{l^n}$, every sequence is a Viterbi path for this Markov chain.

If a sequence S and all others equivalent to S are the only Viterbi paths of a Markov chain, then we call S a *Viterbi sequence.* A simple example of a Viterbi sequence of length 4 is 0000 since it is the only Viterbi path for the two-state Markov chain with transition matrix

$$\theta = \begin{pmatrix} 1 & 0 \\ 0 & 1 \end{pmatrix}.$$

An example of a sequence that is not a Viterbi sequence is 0011. If 0011 were a Viterbi sequence, then its probability must be greater than those of sequences 0001 and 0111. Since $p_{0011} > p_{0001}$,

$$\theta_{00}\theta_{01}\theta_{11} > \theta_{00}^2\theta_{01},$$

from which we conclude $\theta_{11} > \theta_{00}$. But from $p_{0011}p_{0111}$, we get

$$\theta_{00}\theta_{01}\theta_{11} > \theta_{01}\theta_{11}^2,$$

from which we get $\theta_{00} > \theta_{11}$, a contradiction.

We can similarly define Viterbi paths and sequences for toric Markov chains. Recall that the transition matrix for a toric Markov chain is not necessarily stochastic. Because of this fact, the set T_l of Viterbi sequences of l-state toric Markov chains may be different from the set V_l of Viterbi sequences of l-state (regular) Markov chains. Note that V_l is a subset of T_l since every Markov chain is a toric Markov chain. We call the sequences in the set difference $T_l - V_l$ *pseudo-Viterbi sequences*. (For the rest of this article, the term *Viterbi path* and *sequence* will refer to regular Markov chains; for toric Markov chains, we call them *toric Viterbi paths* and *sequences*.

The main result in this article is that for $l = 2$ and 3, pseudo-Viterbi sequences exist. When $l \geq 4$, there are no pseudo-Viterbi sequences; the sets of Viterbi sequences and toric Viterbi sequences are equal.

To help prove these results, we will need to prove some general properties about Viterbi sequences.

Proposition 10.1 *If a Viterbi sequence S has two subsequences T_1 and T_2 of length t that both begin with state q_1 and end with state q_2, then T_1 and T_2 are equivalent sequences.*

Proof Suppose that T_1 and T_2 are not equivalent subsequences. Then let S_1 be the sequence obtained by replacing T_2 with T_1 in S so that $p_{S_1} = p_S p_{T_1}/p_{T_2}$. Similarly, let S_2 be the sequence obtained by replacing T_1 with T_2 in S so that $p_{S_2} = p_S p_{T_2}/p_{T_1}$. Since S is Viterbi and not equivalent to S_1, we must have $p_S > p_{S_1}$, which implies $p_{T_2} > p_{T_1}$. But since S is also not equivalent to S_2, we also have $p_S > p_{S_2}$, which implies $p_{T_1} > p_{T_2}$. This is a contradiction, so T_1 and T_2 must be equivalent. □

As an example, 01020 is not a Viterbi sequence since 010 and 020 are non-

$A*$	0^{2m+1}	$(2m, 0, 0, 0)$	$A*$	0^{2m+2}	$(2m+1, 0, 0, 0)$
B	$0^{2m}1$	$(2m-1, 1, 0, 0)$	B	$0^{2m+1}1$	$(2m, 1, 0, 0)$
C	$0(01)^m$	$(1, m, m-1, 0)$	$C*$	$0(01)^m0$	$(1, m, m, 0)$
$D*$	$(01)^m1$	$(0, m, m-1, 1)$	D	$(01)^m10$	$(0, m, m, 1)$
$E*$	$(01)^m0$	$(0, m, m, 0)$	$E*$	$(01)^{m+1}$	$(0, m+1, m, 0)$
F	$01^{2m-1}0$	$(0, 1, 1, 2m-2)$	F	$01^{2m}0$	$(0, 1, 1, 2m-1)$
$G*$	01^{2m}	$(0, 1, 0, 2m-1)$	$G*$	01^{2m+1}	$(0, 1, 0, 2m)$

Table 10.1. *Left: Toric Viterbi sequences of length* $2m+1$. *Right: Toric Viterbi sequences of length* $2m+2$. *Starred sequences are Viterbi, unstarred are pseudo-Viterbi.*

equivalent subsequences of the same length beginning and ending with 0. Either p_{01010} or p_{02020} will be greater than or equal to p_{01020}.

The next proposition was illustrated with an earlier example, 0011.

Proposition 10.2 *If a transition ii exists in a Viterbi sequence S, then no other transition jj can appear in S, where $j \neq i$.*

Proof Suppose S did contain transitions ii and jj. Consider the sequences S_1 where subsequence ii is replaced by i and jj is replaced by jjj. Since S is Viterbi, we must have $p_S > p_{S_1}$, from which we conclude $p_{ii} > p_{jj}$. However, we can also create another sequence S_2 in which ii is replaced with iii and jj is replaced with j. Once again, $p_S > p_{S_2}$, so $p_{jj} > p_{ii}$, giving us a contradiction. □

10.2 Two- and Three-State Markov Chains

For toric Markov chains on $l = 2$ states, there are seven toric Viterbi sequences with initial state 0 when the length $n \geq 5$. They are listed in Table 10.1.

Not all toric Viterbi sequences are Viterbi sequences. In fact, for each $n > 3$, three sequences are pseudo-Viterbi because of the following proposition.

Proposition 10.3 *No Viterbi sequence on two states can end with 001 or 110.*

Proof Suppose that 001 is a Viterbi sequence. Then since $p_{001} > p_{010}$, we must have $\theta_{00} > \theta_{10}$. Also, $p_{001} > p_{000}$, so $\theta_{01} > \theta_{00}$. Finally, $p_{001} > p_{011}$, so $\theta_{00} > \theta_{11}$. But then

$$1 = \theta_{00} + \theta_{01} > \theta_{10} + \theta_{00} > \theta_{10} + \theta_{11} = 1,$$

which is a contradiction. Thus no Viterbi sequence can end with 001 (or by symmetry, 110). □

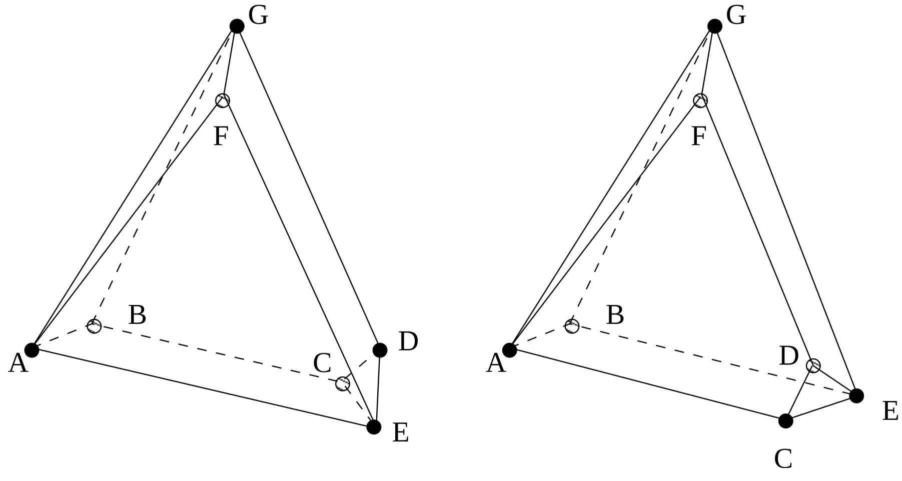

Fig. 10.1. Polytopes of two-state toric Viterbi sequences.

The remaining four toric Viterbi sequences are actual Viterbi sequences. Stochastic transition matrices are easily constructed to produce these Viterbi sequences.

We can view each two-state toric Viterbi sequence of length n as the vertex of the Newton polytope of the polynomial $\sum p_S$ where S ranges over all sequences of length n that start with 0. These polytopes are shown in Figure 10.1. The left and right polytopes are for odd and even length sequences, respectively. The vertices share the labels listed in Table 10.1. Black vertices represent Viterbi sequences, and white vertices represent pseudo-Viterbi sequences.

When $l = 3$ states, the number of toric Viterbi sequences that start with state 0 is 93 for even n and 95 for odd n, when $n \geq 12$. Of these sequences, only four are pseudo-Viterbi. Specifically, these pseudo-Viterbi sequences end in 11210 or some symmetric variant such as 00102.

Proposition 10.4 *A Viterbi sequence (or an equivalent sequence) cannot end in 11210, or equivalently, 12110.*

Proof Suppose that a Viterbi sequence did end in 11210. Since the sequence ends with 10, we must have $\theta_{10} > \theta_{11}$. Since 110 is a Viterbi subsequence with higher probability than 100, we also have $\theta_{11} > \theta_{00}$. Thus

$$\theta_{10} > \theta_{00}. \tag{10.1}$$

Moreover, $p_{110} > p_{101}$, we must have $\theta_{11}\theta_{10} > \theta_{10}\theta_{01}$, which means

$$\theta_{11} > \theta_{01}. \tag{10.2}$$

Finally, 112 has higher probability than 102, so $\theta_{11}\theta_{12} > \theta_{10}\theta_{02}$. Then

$$\theta_{12} > \frac{\theta_{10}\theta_{02}}{\theta_{11}} > \theta_{02} \tag{10.3}$$

where we use the fact that $\theta_{10} > \theta_{11}$. Thus

$$1 = \theta_{10} + \theta_{11} + \theta_{12} > \theta_{00} + \theta_{01} + \theta_{02} = 1 \tag{10.4}$$

which is a contradiction. □

However, 0212110 is a toric Viterbi sequence for the toric Markov chain with the following transition matrix:

$$\begin{pmatrix} 0 & 0 & 0.1 \\ 0.5 & 0.3 & 0.2 \\ 0 & 0.6 & 0 \end{pmatrix}.$$

10.3 Markov Chains with Many States

Of the seven two-state toric Viterbi sequences of length n that start with state 0, three are pseudo-Viterbi sequences. Out of the 93 or 95 (depending on the parity of n) three-state toric Viterbi sequences of length n starting with state 0, only four of them are pseudo-Viterbi sequences. So we might ask, how many pseudo-Viterbi sequences exist as the number of states increases? The answer lies in the following theorem:

Theorem 10.5 *Every toric Viterbi sequence on $l \geq 4$ states is a Viterbi sequence.*

Proof In order to show that a min-weight sequence S (of length n) is Viterbi, we need the following facts:

(i) For each state i, there exists another state j (which may be the same as i) for which transition ij does not appear in S.
(ii) If the previous statement is true, then we can find a stochastic matrix of transition probabilities whose Viterbi sequence of length n is S.

To prove the first fact, we assume there is a state q for which each transition $q0, q1, \ldots, q(l-1)$ exists at least once in S. Let's assume q is state 0 (for we could merely relabel the states in S). We can rearrange S so that the final l appearances of state 0 take the form $001x_1 02x_2 03x_3 \ldots 0(l-1)x_{l-1}$, where each x_i is a (possibly empty) string of states. Thus each transition $00, 01, \ldots, 0(l-1)$ appears exactly once in this subsequence, and we assume that $l-1$ is the state that follows the last 0.

Since $l \geq 4$, strings x_1 and x_2 must be followed by state 0. Strings x_1 and x_2 cannot both be empty, for then $p_{010} = p_{020}$, violating Proposition 10.1.

(Note that for $l \leq 3$, this proof fails since x_1 and x_2 could both be empty.) So suppose x_1 is nonempty. The first state of x_1 (immediately following state 1) cannot be state 1, for then $p_{00} = p_{11}$, violating Proposition 10.2. So it must be some state other than 0 or 1; call it state r. We could rearrange S so that transition 00 precedes transition $0r$. Then within S we have two subsequences $00r$ and $01r$, violating Proposition 10.1. This is a contradiction. Thus there must be at least one state s that never follows state 0 in S.

To prove the second statement, we construct a stochastic transition matrix for which S is a Viterbi sequence. Because of the first fact, we can assign every transition ij in S a probability θ_{ij} greater than $1/l$. (Note that this would be impossible in the cases 001 for $l = 2$ and 11210 for $l = 3$.) For each transition ij that appears in S, we assign a probability θ_{ij} between $\frac{1}{l} + \epsilon$ and $\frac{1}{l} + \alpha\epsilon$, where

$$\frac{1}{l} < \frac{1}{l} + \epsilon < \frac{1}{l} + \alpha\epsilon < \frac{1}{l-1}.$$

If ij is in S, then for the transitions ij' that are not in S, we can still let $0 < \theta_{ij'} < 1/l$.

Now if state i does not appear in S or only appears as the final state of S, then each transition ij is assigned a probability θ_{ij} not exceeding $\frac{1}{l} + \eta$, where $0 < \eta < \epsilon$. We attempt to choose α, ϵ, and η so that they satisfy the inequality

$$\left(\frac{1}{l} + \eta\right)\left(\frac{1}{l} + \alpha\epsilon\right)^{n-2} < \left(\frac{1}{l} + \epsilon\right)^{n-2}\left(\frac{1}{l} + \alpha\epsilon\right). \qquad (10.5)$$

The right hand side represents the minimum possible value for the probability of S, for it has at least one transition with the maximum probability $\frac{1}{l} + \alpha\epsilon$ while all the others have at least the minimum probability $\frac{1}{l} + \epsilon$. The left hand side represents the maximum probability any other sequence S' can attain in which S' contains a transition not in S. At least one transition has probability at most $\frac{1}{l} + \eta$, while the rest may have maximum probability $\frac{1}{l} + \alpha\epsilon$.

We show that we can choose values for α, ϵ, and η that satisfies the inequality. If we set $\alpha = 1$ and $\eta = 0$, the inequality is automatically satisfied, and thus we can increment α and η very slightly and still satisfy the inequality.

Since S is a toric Viterbi sequence, there is a matrix θ^T for which S is the toric Viterbi sequence. We then take logarithms so that $w_{ij} = \log \theta^T_{ij}$ for each transition ij for which $\theta^T_{ij} \neq 0$. Let w_1 and w_2 be the minimum and maximum values of w_{ij}, respectively, of all the transitions ij that appear in S. We then let $L(w) = aw + b$ (where $a > 0$) be the linear transformation that maps w_1 to $-\log(\frac{1}{l} + \alpha\epsilon)$ and w_2 to $-\log(\frac{1}{l} + \epsilon)$. For each transition ij that appears in S, we set θ_{ij} such that

$$-\log \theta_{ij} = L(w_{ij}) = aw_{ij} + b. \qquad (10.6)$$

In particular, if all of the transition in another sequence S' appears in S, we have

$$\begin{aligned}\sum_{i=1}^{n-1} L(w_{S_iS_{i+1}}) &= b(n-1) + a\sum w_{S_iS_{i+1}} \\ &< b(n-1) + a\sum_{i=1}^{n-1} w_{S'_iS'_{i+1}} \\ &= \sum_{i=1}^{n-1} L(w_{S'_iS'_{i+1}})\end{aligned}$$

Note how for each ij in S,

$$\frac{1}{l} + \epsilon = \exp(-L(w_2)) \leq \theta_{ij} = \exp(-L(w_{ij})) \leq \exp(-L(w_1)) = \frac{1}{l} + \alpha\epsilon.$$

If ij is a transition in S, then each transition starting with i that is not in S is assigned a probability not exceeding $\frac{1}{l} - \frac{\epsilon}{l-1}$. The remaining probabilities are assigned so that none of them exceed $\frac{1}{l} + \eta$.

We now demonstrate that θ is a stochastic matrix for which S is the only Viterbi path. If sequence S' has a transition not in S, then p_S is at least the right-hand side of 10.5, and $p_{S'}$ is at most the left-hand side of 10.5. Thus $p_S > p_{S'}$. If all the transitions in S' are in S, then

$$\begin{aligned}-\log p_S &= -\sum_{i=1}^{n-1} \log \theta_{S_iS_{i+1}} = \sum_{i=1}^{n-1} L(w_{S_iS_{i+1}}) \\ &< \sum_{i=1}^{n-1} L(w_{S'_iS'_{i+1}}) \\ &= -\sum_{i=1}^{n-1} \log \theta_{S'_iS'_{i+1}} = -\log p_{S'}.\end{aligned}$$

□

10.4 Fully Observed Markov Models

We turn our attention to the *fully observed Markov model.* The states of a fully observed Markov model are represented by two alphabets Σ and Σ' of l and l' letters, respectively. We parameterize the fully observed Markov model by a pair of matrices (θ, θ') with dimensions $l \times l$ and $l \times l'$. The entry θ_{ij} is the transition probability from state $i \in \Sigma$ to state $j \in \Sigma$. Entry θ'_{ij} represents a transition probability from $i \in \Sigma$ to $j \in \Sigma'$.

The fully observed Markov model generates a pair of sequences $S \in \Sigma^*$

and $T \in \Sigma'^*$. Sequence S is generated just the same way that a regular Markov chain with transition matrix θ would. Each state in T is generated individually from the corresponding state in S with the transition matrix θ'. Thus if $S_i = \sigma$ is the ith state in S, then the ith state of T would be $T_i = \sigma'$ with probability $\theta'_{\sigma\sigma'}$. We will call S the *state sequence* and T the *output sequence* of a *fully observed sequence* (S, T). A fully observed sequence (S, T) of length n is generated by a fully observed Markov model with transitions (θ, θ') with probability

$$p_{S,T} = \pi_1 \theta'_{S_1T_1} \prod_{i=2}^{n} \theta_{S_{i-1}S_i} \theta'_{S_iT_i} \tag{10.7}$$

where π_1 is the probability of the initial state S_1.

In a fully observed Markov model, both transition matrices (θ, θ') are stochastic. When we don't require either matrix to be stochastic, we call it a *fully observed toric Markov model.*

We now define some terms referring to fully observed sequences of maximal likelihood. A *fully observed Viterbi path of length* n of a fully observed Markov model is the fully observed sequence (S, T) of length n that the fully observed Markov model generates with the highest probability. If (S, T) and (S', T') are two fully observed sequences for which each transition $(i, j) \in \Sigma \times \Sigma$ or $(i, j') \in \Sigma \times \Sigma'$ appears in each sequence pair an equal number of times, then we say that (S, T) and (S', T') are *equivalent.* If the only fully observed Viterbi paths for a fully observed Markov model are (S, T) and any equivalent sequences, then (S, T) is a *fully observed Viterbi sequence.* The pair (S, T) will usually represent the entire equivalence class of sequences. We analogously define a *fully observed toric Viterbi paths* and *sequences* for fully observed toric Markov models.

We make an immediate observation about fully observed Viterbi sequences:

Lemma 10.6 *Let (S, T) be a fully observed (toric) Viterbi sequence. If S_i and S_j are the same state in Σ, then T_i and T_j are the same state in Σ'.*

Proof Suppose that $S_i = S_j$, but $T_i \neq T_j$. We can create two additional output sequences T' and T'' in which we set $T'_i = T'_j = T_i$ and $T''_i = T''_j = T_j$. Then since $p_{S,T} > p_{S,T'}$, we must have

$$\theta'_{S_iT_i} > \theta'_{S_iT'_i} = \theta'_{S_iT_j}. \tag{10.8}$$

Since we also have $p_{S,T} > p_{S,T''}$, we must also have

$$\theta'_{S_jT_j} > \theta'_{S_jT''_j}. \tag{10.9}$$

Since $S_i = S_j$ and $T''_j = T_i$, we get

$$\theta'_{S_i T_j} > \theta'_{S_i T_i}, \tag{10.10}$$

contradicting (10.8). □

So if state $j \in \Sigma'$ appears with state $i \in \Sigma$ in a fully observed Viterbi sequence (S, T), then j appears in T with every instance of i in S.

We now prove some properties about the state sequence of a fully observed toric Viterbi sequence.

Lemma 10.7 *The state sequence of every fully observed toric Viterbi sequence is a toric Viterbi sequence.*

Proof Let S be the state sequence for the fully observed toric Viterbi sequence (S, T) of a fully observed Markov model M with matrices (θ, θ'). Now create a new toric Markov chain M' with transition matrix ϕ such that

$$\phi_{ij} = \max_k \theta_{ij} \theta'_{jk}. \tag{10.11}$$

Now we show that S is also the only toric Viterbi path of M'. Its probability is greater than that of any other sequence S' since the probability of S' in the Markov chain is equal to the maximum probability $p_{S',T'}$ of all fully observed sequences with state sequence S'. The value $p_{S',T'}$ is less than $p_{S,T}$. □

We finally deduce a criterion for determining whether a fully observed sequence is a fully observed Viterbi sequence.

Theorem 10.8 *The state sequence S for a fully observed toric Viterbi sequence (S, T) is a Viterbi sequence if and only if (S, T) is also a fully observed Viterbi sequence.*

Proof Let S be a Viterbi sequence. Then there is a stochastic matrix θ for which S is the only Viterbi path. We also create another stochastic matrix θ' in which $\theta'_{ij} = 1$ whenever transition ij appears in (S, T). (Recall from Lemma 10.6 that for each i, at most one output state j matches with i.) So for all other fully observed Viterbi sequences (S', T'),

$$p_{S,T} = p_S > p_{S'} \geq p_{S',T'}. \tag{10.12}$$

Thus (S, T) is a fully observed Viterbi sequence for the fully observed Markov model with matrices (θ, θ').

To show the other direction, we assume that the state sequence S is not a Viterbi sequence. However, we know that S is a toric Viterbi sequence by Lemma 10.7. Thus S is a pseudo-Viterbi sequence. So there are two cases to consider:

Case I: $\Sigma = \{0, 1\}$, and S (or an equivalent sequence) ends with 001 (or symmetrically, 110). Let $A, B \in \Sigma'$, and θ'_{0A} and θ'_{1B} are the maximal probability transitions from states 0 and 1 in θ'. (Note that A and B need not be distinct.) Then since $p_{001,AAB} > p_{010,ABA}$, we must have $\theta_{00} > \theta_{10}$. Also, $p_{001,AAB} > p_{000,AAA}$, so $\theta_{01}\theta'_{1B} > \theta_{00}\theta'_{0A}$. Finally, $p_{001,AAB} > p_{011,ABB}$, so $\theta_{00}\theta'_{0A} > \theta_{11}\theta'_{1B}$. Thus $\theta_{01}\theta'_{1B} > \theta_{11}\theta'_{1B}$, so $\theta_{01} > \theta_{11}$. But then

$$1 = \theta_{00} + \theta_{01} > \theta_{10} + \theta_{11} = 1,$$

which is a contradiction. Thus S is not the state sequence of a fully observed Viterbi sequence.

Case II: $\Sigma = \{0, 1, 2\}$, and S (or an equivalent sequence) ends with 11210 (or any symmetric variant like 00102). Let $A, B, C \in \Sigma'$ such that $\theta'_{0A}, \theta'_{1B}$, and θ'_{2C} are the greatest probabilities for transitions from states 0, 1, and 2 in θ'. (Once again, A, B, and C need not be distinct.) Since the sequence ends with 10, we must have

$$\theta_{10}\theta'_{0A} > \theta_{11}\theta'_{1B}. \tag{10.13}$$

We also have $p_{11210,BBCBA} > p_{12100,BCBAA}$, which implies that

$$\theta_{11}\theta'_{1B} > \theta_{00}\theta'_{0A} \tag{10.14}$$

From inequalities 10.13 and 10.14, we conclude $\theta_{10}\theta'0A > \theta_{00}\theta'_{0A}$, which means

$$\theta_{10} > \theta_{00}. \tag{10.15}$$

And since $p_{11210,BBCBA} > p_{12101,BCBAB}$, we must also have

$$\theta_{11} > \theta_{01}. \tag{10.16}$$

Finally, $p_{11210,BBCBA} > p_{10210,BABCA}$, so

$$\theta_{11}\theta_{12}\theta'_{1B} > \theta_{10}\theta_{02}\theta'_{0A}. \tag{10.17}$$

Combining inequalities 10.17 and 10.13, we get

$$\theta_{12} > \frac{\theta_{10}\theta_{02}\theta'_{0A}}{\theta_{11}\theta'_{1B}} > \theta_{02}. \tag{10.18}$$

Finally, by combining inequalities 10.15, 10.16, 10.18, we conclude

$$1 = \theta_{10} + \theta_{11} + \theta_{12} > \theta_{00} + \theta_{01} + \theta_{02} = 1, \tag{10.19}$$

which is a contradiction. □

11
Equations Defining Hidden Markov Models

Nicolas Bray

Jason Morton

In this chapter, we investigate the ideal of equations involving the probabilities of observing particular sequences in the hidden Markov model. Two main techniques for computing this ideal are employed. First, elimination using Gröbner bases is only feasible for small models and yields invariants which may not be easy to interpret. Second, a technique using linear algebra refined by two gradings of the ideal of relations. Finally, we interpret and classify some of the invariants found in this way.

11.1 The Hidden Markov Model

The *hidden Markov model* was described in Section 1.4.3 as the algebraic statistical model defined by composing the fully observed Markov model F with the marginalization ρ, giving a map $\rho \circ F : \Theta_1 \subset \mathbb{C}^d \longrightarrow \mathbb{C}^{(l')^n}$, where Θ_1 is the subset of Θ defined by requiring row sums equal to one. Here we will write the hidden Markov model as a composition of three maps, $\rho \circ F \circ g$, beginning in a coordinate space $\Theta^{''} \subset \mathbb{R}^d$ which parameterizes the $l(l-1) + l(l'-1)$-dimensional linear subspace Θ_1 lying in the $l^2 + ll'$-dimensional space Θ, so that $\Theta_1 = g(\Theta^{''})$. These maps are shown in the following diagrams:

$$\begin{tikzcd}\mathbb{C}^{l(l-1)+l(l'-1)} \arrow[r, "g"] & \mathbb{C}^{l^2+ll'} \arrow[r, "F"] & \mathbb{C}^{l^n l'^n} \arrow[r, "\rho"] & \mathbb{C}^{l'^n}\end{tikzcd}$$

$$\begin{tikzcd}\mathbb{C}[\theta_i^{''}] & \mathbb{C}[\theta_{ij}, \theta_{ij}^{'}] \arrow[l, "g^*"'] & \mathbb{C}[p_{\sigma,\tau}] \arrow[l, "F^*"'] & \mathbb{C}[p_\sigma] \arrow[l, "\rho^*"']\end{tikzcd}$$

In the bottom row of the diagram, we have phrased the hidden Markov model in terms of rings by considering the ring homomorphism g^*, F^* and ρ^*. The marginalization map $\rho : \mathbb{C}[p_\tau] \to \mathbb{C}[p_{\sigma,\tau}]$ expands p_τ to a sum across hidden states, $p_\tau \mapsto \sum_\sigma p_{\sigma,\tau}$. The fully observed Markov model ring map $F^* : \mathbb{C}[p_{\sigma,\tau}] \to \mathbb{C}[\theta_{ij}, \theta_{ij}^{'}]$ expands each probability in terms of the parameters,

$p_{\sigma,\tau} \mapsto \theta_{\sigma_1\sigma_2} \dots \theta_{\sigma_{n-1}\sigma_n}\theta'_{\sigma_1\tau_1} \dots \theta'_{\sigma_n\tau_n}$. The map g^* gives the Θ'' coordinates of the Θ parameters, $g^* : \theta_{ij} \mapsto \theta''_k$; for example, in the binary case our final parameter ring will be $\mathbb{C}[x, y, z, w]$ with the map g^* from $\mathbb{C}[\theta_{ij}, \theta'_{ij}]$ given by,

$$(\theta_{ij}) \quad \overset{g^*}{\mapsto} \quad \begin{array}{c|cc} & \sigma = 0 & \sigma = 1 \\ \hline \sigma = 0 & x & 1-x \\ \sigma = 1 & 1-y & y \end{array} \qquad \text{and}$$

$$(\theta'_{ij}) \quad \overset{g^*}{\mapsto} \quad \begin{array}{c|cc} & \tau = 0 & \tau = 1 \\ \hline \sigma = 0 & z & 1-z \\ \sigma = 1 & 1-w & w \end{array}$$

As discussed in Section 3.2, the Zariski closure of the image of $\mathbf{f} := \rho \circ F \circ g$ is a variety in the space of probability distributions. We are interested in the ideal $I_{\mathbf{f}}$ of invariants (polynomials) in $\mathbb{C}[p_\tau]$ which vanish on this variety. By plugging observed data into these invariants (even if we don't know all of them) and observing if the result is close to zero, it can be checked whether a hidden Markov model might be appropriate model. In addition, since this ideal captures the geometry and the restrictions imposed by the choice of model, it may be useful for inference. For more on parameter inference for the hidden Markov model, see Chapter 12.

The equations defining the hidden Markov model are precisely the elements of the kernel of the composed ring map $g^* \circ F^* \circ \rho^*$, so one way to investigate this kernel is to look at the kernels of these maps separately. In other words, if we have an invariant f in the ring $\mathbb{C}[p_\tau]$, and we trace it to its image in $\mathbb{C}[\theta''_i]$, at which point does it become zero? In particular we distinguish invariants which are in the kernel of $F^* \circ \rho^*$ as they have a helpful multigraded structure not shared by all of the invariants of the constrained model. Mihaescu [Mihaescu, 2004] has investigated the map F^*. In section 11.4 we trace how some of the invariants of this map become invariants of the hidden Markov model map.

11.2 Gröbner Bases

Elimination theory provides an algorithm for computing the implicitization of a polynomial map such as the one corresponding to the hidden Markov model. We recall the method from Section 3.2.

Let $\mathbb{C}[\theta''_i, p_\tau]$ be the ring containing both the parameter and probability variables, where the θ''_i are the variables is the final parameter ring. Now let I be the ideal $I = (p_\tau - (g^* \circ F^* \circ \rho^*)(p_\tau))$, where $(g^* \circ F^* \circ \rho^*)(p_\tau)$ is p_τ expanded as a polynomial in the final parameters, considered as an element of $\mathbb{C}[\theta''_i, p_\tau]$.

Then the ideal of the hidden Markov model is just the elimination ideal consisting of elements of I involving only the p_τ, $I_e = I \cap \mathbb{C}[p_\tau]$, and $V(I_e)$ is the smallest variety in probability space containing the image of the hidden Markov model map. To actually compute I_e, we compute a Gröbner basis G for I under a term ordering (such as lexicographic) which makes the parameter indeterminates "expensive." Then the elements of G not involving the parameters form a basis for I_e; see Example 3.19.

The computer packages `Macaulay 2` [Grayson and Stillman, 2002] as well as `Singular` [Greuel *et al.*, 2003] contain optimized routines for computing such Gröbner bases, and so can be used to find the ideal of the implicitization. These packages are discussed in Section 2.5. However, Gröbner basis computations suffer from intermediate expression swell. In the worst case, the degree of the polynomials appearing in intermediate steps of the computation is doubly exponential in the degree of the polynomials defining I [Cox *et al.*, 1997]. Thus, these methods are only feasible for small models. Perhaps more importantly, the basis obtained this way tends to involve complex expressions and many redundant elements, which makes interpretation of the generators' statistical meaning difficult.

The three node binary model is the largest model which has succumbed to a direct application of the Gröbner basis method. For the binary, unconstrained model ($F^* \circ \rho^*$, no g^*), the computation takes about seven hours on a dual 2.8GHz, 4 GB RAM machine running `Singular` and yields the single polynomial, reported in [Pachter and Sturmfels, 2004a]:

$$p_{011}^2 p_{100}^2 - p_{001}p_{011}p_{100}p_{101} - p_{010}p_{011}p_{100}p_{101} + p_{000}p_{011}p_{101}^2$$

$$+p_{001}p_{010}p_{011}p_{110} - p_{000}p_{011}^2 p_{110} - p_{010}p_{011}p_{100}p_{110} + p_{001}p_{010}p_{101}p_{110}$$

$$+p_{001}p_{100}p_{101}p_{110} - p_{000}p_{101}^2 p_{110} - p_{001}^2 p_{110}^2 + p_{000}p_{011}p_{110}^2$$

$$-p_{001}p_{010}^2 p_{111} + p_{000}p_{010}p_{011}p_{111} + p_{001}^2 p_{100}p_{111} + p_{010}^2 p_{100}p_{111}$$

$$-p_{000}p_{011}p_{100}p_{111} - p_{001}p_{100}^2 p_{111} - p_{000}p_{001}p_{101}p_{111} + p_{000}p_{100}p_{101}p_{111}$$

$$+p_{000}p_{001}p_{110}p_{111} - p_{000}p_{010}p_{110}p_{111}$$

Note that the polynomial is homogeneous. It is also homogeneous with respect to a multigrading by the total number of ones and zeros appearing among the τs in a given monomial. An implicitization program using linear algebraic techniques and a multigrading of the kernel (to be discussed in section 11.3) computes this polynomial in 45 seconds. The relevant commands for the `Singular`-based implementation would be:

```
makemodel(4,2,2); setring R_0; find_relations(4,1);
```

The Gröbner basis method is very sensitive to the number of ring variables. Consequently, adding in the constraining map g^* makes the 3-node binary Gröbner basis computation much faster, taking only a few seconds.

The variety obtained has dimension 4, as expected, and has degree 11. The computation yields fourteen generators in the reduced Gröbner basis for graded reverse lexicographic order, though the ideal is in fact generated by a subset of five generators. One of them (homogenized using the sum of the p_τ; see section 11.3) is the following:

$$\begin{aligned} g_4 \;=\;& 2p_{010}p_{100}^2 + 2p_{011}p_{100}^2 - p_{000}p_{100}p_{101} - p_{001}p_{100}p_{101} + 3p_{010}p_{100}p_{101} \\ &+3p_{011}p_{100}p_{101} - p_{100}^2p_{101} - p_{000}p_{101}^2 - p_{001}p_{101}^2 + p_{010}p_{101}^2 + p_{011}p_{101}^2 \\ &-2p_{100}p_{101}^2 - p_{101}^3 - p_{000}p_{010}p_{110} - p_{001}p_{010}p_{110} - p_{010}^2p_{110} \\ &-p_{000}p_{011}p_{110} - p_{001}p_{011}p_{110} - 2p_{010}p_{011}p_{110} - p_{011}^2p_{110} - p_{000}p_{100}p_{110} \\ &-p_{001}p_{100}p_{110} + 2p_{010}p_{100}p_{110} + 2p_{011}p_{100}p_{110} + p_{100}^2p_{110} - 2p_{000}p_{101}p_{110} \\ &-2p_{001}p_{101}p_{110} + p_{010}p_{101}p_{110} + p_{011}p_{101}p_{110} - p_{101}^2p_{110} - 2p_{000}p_{110}^2 \\ &-2p_{001}p_{110}^2 - p_{010}p_{110}^2 - p_{011}p_{110}^2 + p_{100}p_{110}^2 + p_{000}^2p_{111} + 2p_{000}p_{001}p_{111} \\ &+p_{001}^2p_{111} + p_{000}p_{010}p_{111} + p_{001}p_{010}p_{111} + p_{000}p_{011}p_{111} + p_{001}p_{011}p_{111} \\ &+3p_{010}p_{100}p_{111} + 3p_{011}p_{100}p_{111} + p_{100}^2p_{111} - p_{000}p_{101}p_{111} - p_{001}p_{101}p_{111} \\ &+2p_{010}p_{101}p_{111} + 2p_{011}p_{101}p_{111} - p_{101}^2p_{111} - 3p_{000}p_{110}p_{111} \\ &-3p_{001}p_{110}p_{111} - p_{010}p_{110}p_{111} - p_{011}p_{110}p_{111} + 2p_{100}p_{110}p_{111} - p_{000}p_{111}^2 \\ &-p_{001}p_{111}^2 + p_{100}p_{111}^2 \end{aligned}$$

Unfortunately, these generators remain a bit mysterious. We would like to be able to write down a more intuitive set, which has clear statistical and geometric meaning. To this end, we turn to alternative methods of finding the invariants of the model.

11.3 Linear Algebra

We may also consider the implicitization problem as a linear algebra problem by limiting our search to those generators of the ideal which have degree less than some bound. As we speculate that the ideal of a binary hidden Markov model of any length is generated by polynomials of low degree (see Conjecture 11.7) this approach is not too unreasonable. Our implementation in `Singular` and C++ is available at `www.math.berkeley.edu/~mortonj`. In it, we make use of `NTL`, a number theory library, for finding exact kernels of integer matrices [Shoup, 2004], which is in turn made quicker by the `GMP` library [Swox, 2004] .

11.3.1 Finding the relations of a statistical model

Turning for a moment to the general implicitization problem, given a polynomial map $\mathbf{f}$ with ring map $\mathbf{f}^* : \mathbb{C}[p_1 \dots p_r] \to \mathbb{C}[\theta_j]$, we are interested in calculating the ideal $I_\mathbf{f}$ of relations among the p_i. If we denote $\mathbf{f}(p_i)$ by f_i, $\prod_i p_i^{a_i}$ by p^a, and $\mathbf{f}(p^a)$ by f^a, these are all the expressions $\sum_a \alpha_a p^a$ such that $\sum_a \alpha_a f^a = 0$.

The Gröbner basis methods discussed in the previous section will generate a basis for $I_\mathbf{f}$ but as we have stated these computations quickly become intractable. However by restricting our attention to $I_{\mathbf{f},\delta}$, the ideal of relations generated by those of degree at most δ, there are linear-algebraic methods which are more practical. As $I_\mathbf{f}$ is finitely generated, there is some δ such that we in fact have that $I_\mathbf{f} = I_{\mathbf{f},\delta}$ so eventually these problems coincide. Deciding which δ will suffice is a difficult question but some degree bounds are available in Gröbner basis theory.

We begin with the simplest case, namely that of $\delta = 1$. Let $\mathcal{P} = \{f_0 := 1, f_1, \dots, f_{l'^n}\}$. A polynomial relation of degree at most $\delta = 1$ is a linear relation among the f_i.

Let $\mathcal{M} = \{m_i\}_{i=1}^k$ is the collection of all monomials in the θ_j occurring in $\mathcal{P}$, so we can write each f_i in the form $f_i = \sum_j \beta)ijm_j$. An invariant then becomes a relation

$$\sum_{i=1}^n \alpha_i (\sum_{j=1}^k \beta_{ij} m_j) = \sum_{i=1}^n \sum_{j=1}^k \alpha_i \beta_{ij} m_j = \sum_{j=1}^k (\sum_{i=1}^n \beta_{ij} \alpha_i) m_i = 0$$

This polynomial will equal the zero polynomial if and only if the coefficient of each monomial is zero. Thus all linear relations between the given polynomials are given by the common solutions to the relations $\sum_{i=1}^n \beta_{ij} \alpha_i = 0$ for $j \in \{1, \dots, k\}$. To say that such a vector $\alpha = (\alpha_i)$ satisfies these relations is to say it belongs to the kernel of $B = (\beta_{ij})$, the matrix of monomial coefficients, and so a set of generators for $I_{\mathbf{f},1}$ can be found by computing a linear basis for the kernel of B. A straightforward method for computing a set of generators for $I_{\mathbf{f},\delta}$ now presents itself: a polynomial relation of degree at most δ is a linear relation between the products of the p_is of degree at most δ, and so we can simply compute all the polynomials f^a and then find linear relations among them as above.

As exactly computing the kernel of a large matrix is difficult ($O(n^3)$), we will introduce some refinements to this technique. Some of these are applicable to any statistical model, while some depend on the structure of the hidden Markov model in particular.

Suppose we increment the maximum degree, compute the generators of at most this degree by taking the kernel as above, and repeat. Call the resulting list of generators, in the order in which they are found, $\mathcal{L}$. There will be many generators in $\mathcal{L}$ which, while linearly independent of preceding generators, lie in the ideal of those generators. We can save steps and produce a shorter list of generators by eliminating those monomials p^a in higher degree that can be expressed, using previous relations in $\mathcal{L}$, in terms of monomials of lower degree. This elimination can be accomplished, after each addition of a generator g to the list $\mathcal{L}$, by deleting all columns which correspond to monomials p^a which are multiples of leading terms of relations so far included in $\mathcal{L}$. In fact, we can delete all columns whose corresponding monomials lie in the initial ideal of the ideal generated by the entries of $\mathcal{L}$.

Since $\mathbf{f}$ is an algebraic statistical model, we automatically have the trivial invariant $1 - \sum_{i=1}^{n} p_i$. If the constant polynomial 1 is added to our set of polynomials then this invariant will automatically be found in the degree one step of the above procedure, and one of the p_is (depending on how they are ordered) will then be eliminated from all subsequent invariants. However, there is a better use for this invariant.

Proposition 11.1 *Suppose* $\mathbf{f}$ *is an algebraic statistical model, and* $I_{\mathbf{f}}$ *is its ideal of invariants. Then there exists a set* $\mathcal{L}$ *of homogeneous polynomials in the* p_i *such that* $\{1 - \sum_i p_i\} \cup \mathcal{L}$ *is a basis for* $I_{\mathbf{f}}$.

Proof By Hilbert's basis theorem (Theorem 3.2), $I_{\mathbf{f}}$ has a finite basis $\mathcal{B}$. For $g \in \mathcal{B}$, let δ be the smallest degree occurring in g; if δ is the smallest degree occurring in g, it is homogeneous. If not, let g_δ be the degree δ part of g. Since $1 - \sum_i p_i \in I_{\mathbf{f}}$, so is $(1 - \sum_i p_i)g_d$. Then if we replace $g \in \mathcal{B}$ with $g - (1 - \sum_i p_i)g_d$, $\mathcal{B}$ still generates $I_{\mathbf{f}}$, but g has no degree δ part. Repeating this finitely many times, we have the required $\mathcal{L}$. □

Thus we may restrict our search for invariants to homogeneous polynomials. We summarize the method we have described in Algorithm 11.6. Let $m(\delta)$ be the the set of all degree δ monomials in $\mathbb{C}[p_i]$.

Algorithm 11.2

```
Input: An algebraic statistical model f and a degree bound DB.
Output: Generators for the ideal I_f up to degree DB.

Step 1: Compute ker(f) by letting I = find-relations(DB)

Subroutine: find-relations(delta):
    If delta=1, return(find-linear-relations(m(1), (0));
      else I_R = find-relations(delta-1, I_R)
    Return(find-linear-relations(m(delta), I_R)

Subroutine: find-linear-relations(m,J):
    Delete the monomials in m which lie in the initial ideal of J to form a list P
    Write the coefficient matrix M by mapping P to the parameter ring, using the given f
    Return the kernel of M as relations among the monomials in P
```

11.3.2 Hidden Markov model refinements

In the hidden Markov model, both $\mathbb{C}[p_\tau]$ and $\mathbb{C}[\theta_{ij}, \theta'_{ij}]$ can be $\mathbb{N}^{l'}$-multigraded by assigning an indeterminate a weight $(c_1, \ldots c_{l'})$ where c_k is the number of occurrences of output state k in its subscript. So θ_{ij} will have a weight vector of all zeros while θ'_{ij} will have $c_j = 1$ and all other vector entries zero. The key fact is that this multigrading is preserved by the map $F^* \circ \rho^*$.

Proposition 11.3 *If $f \in \mathbb{C}[p_\tau]$ is homogeneous with weight $(c_1, \ldots c_{l'})$ then so is $(F^* \circ \rho^*)(f)$. Thus the kernel of $F^*\rho^*$ is also multigraded by this grading.*

Proof It will suffice to assume that f is a monomial. Each monomial in the p_τ has an image of the form $\prod \sum_\sigma \theta_{\sigma_1\sigma_2} \ldots \theta_{\sigma_{n-1}\sigma_n} \theta'_{\sigma_1\tau_1} \ldots \theta'_{\sigma_n\tau_n}$ and expanding the product, the same multiset of τ_i appear in the subscripts of each resulting monomial. If $f \in \ker F^*\rho^*$ the images of its terms in $\mathbb{C}[\theta_{ij}, \theta'_{ij}]$ must cancel. As there are no relations among the θ'_{ij}, this means that each monomial must cancel only with others possessed of the same multiset of τ_i. Then the ideal decomposes according to the multigrading. $\square$

In particular note that if f is homogeneous with weight $(c_1, \ldots, c_{l'})$ then $\sum_k c_k$ is n times the degree of f and so the kernel of $F^*\rho^*$ is homogeneous in the usual sense. When we move to the constrained model $g^*F^*\rho^*$ the above multigrading is no longer preserved, but by Proposition 11.1, the grading by degree nearly is. Moreover, any invariants of $g^* \circ F^* \circ \rho^*$ which fail to be multigraded must contain all output symbols, since otherwise there will still be no relations among the appearing θ''_{ij} and the proof of Proposition 11.3 goes through.

Using the multigrading to find the kernel of $F^* \circ \rho^*$ yields an immense advantage in efficiency. For example in the binary case, in degree δ, instead of finding the kernel of a matrix with $\binom{2^n+\delta-1}{\delta}$ columns, we can instead use $n\delta$ matrices with at most $\binom{n\delta}{n\delta/2} = \frac{(n\delta)!}{(n\delta/2)!^2}$ columns. Computing the ideal of the four node unconstrained $(F^* \circ \rho^*)$ binary hidden Markov model, intractable for the Gröbner basis method, takes only a few minutes to find the invariants up to degree 4 using the multigrading. The method yields 43 invariants, 9 of degree 2, 34 of degree 3, and none of degree 4; the coefficients are small, just 1s and 2s. After building the multigraded kernel for $F^* \circ \rho^*$, the full kernel of $g^* \circ F^* \circ \rho^*$ up to degree 3 can be computed, yielding 21 additional relations in degree 2 and 10 in degree 3.

A stronger condition on the output letters also holds: the count of each letter in each position is the same for the positive and negative terms of any invariant. Thanks to Radu Mihaescu for suggesting the proof.

Proposition 11.4 *For a monomial p_τ^a, let $C(p_\tau^a)$ be the matrix of counts with* *rows are labeled by output symbols, columns by node number, and entry c^i_j the number of times symbol i appears in position j among the factors of the monomial. Then if $f = \sum_a \beta_a p^a_\tau$ is an invariant of the unconstrained hidden Markov model, $\sum_a \beta_a C(p^a_\tau) = 0$*

Proof We assume the hidden Markov model has at least two hidden states. Let f be an invariant, and expand f by the map ρ^* to obtain a sum of terms in $\mathbb{C}[p_{\sigma,\tau}]$. The kernel of the fully observed Markov model is graded by the multiset T of hidden state transitions, as the image of each T-graded piece f_T in $\mathbb{C}[\theta_{ij}, \theta^{'}_{ij}]$ must be zero. Moreover, every possible T appears in the expansion of each monomial in f, since we sum over all hidden states.

Consider the T in which are hidden state transitions are $1, 1$ except for a single $0, 1$ transition. Then the factors of any monomials in the T-graded piece f_T must have hidden states consisting of all 1s, except for exactly one factor which must have a 0 in position 1 and 1 everywhere else. In degree δ, the expansion of each monomial of f has δ such terms, one for each factor; hence the image under F^* of each term has exactly one $\theta^{'}_{0j}$, with j the output symbol in position 1 in the corresponding factor. Then the positive and negative parts f_T must have the same count of each output symbol in position 1. But the counts of output symbols in position one is the same for all T.

Now let T be all $1, 1$ transitions except for a single $0, 1$ transition and a single $0, 0$ transition. Again the only possibility is that the factors of any monomials in the T-graded piece have hidden states consisting of all 1s, except one with its first two hidden states 0. Now the positive and negative parts of f_T have the same multiset of output symbols in the union over positions 1 and 2. But the contents of position 1 are already accounted for, so it must be that the positive and negative parts have the same count of output symbols in position 2. Proceeding by induction, we have the result for a model of length n. □

To further reduce the number of invariants we must consider, we can also show that once we have found an invariant, we have found a whole class of invariants which result from permuting the output alphabet Σ'. We first show that in the binary case the complement of an invariant will also be an invariant. Let $\bar{\tau}$ be the complement of τ (e.g. $\overline{01101} = 10010$). Given that $\theta_\sigma(x, y)$ is the product of the transition probabilities within σ where $x = \theta_{00}$ and $y = \theta_{11}$, we can express $\theta_{\bar{\sigma}}(x, y) = \theta_\sigma(y, x)$ since we are swapping θ_{00} with θ_{11} and θ_{01} with θ_{10}. Similarly, if $\theta'_{\sigma,\tau}(z, w)$ is the product of the transitions between hidden and observed nodes (and $z = \theta'_{00}$, $w = \theta'_{11}$), then $\theta'_{\bar{\sigma},\bar{\tau}}(z, w) = \theta'_{\sigma,\tau}(w, z)$. Then

$$\begin{aligned} p_{\bar{\tau}}(x,y,z,w) &= \sum_{\sigma} \theta_{\sigma}(x,y)\theta'_{\sigma,\bar{\tau}}(z,w) \\ &= \sum_{\sigma} \theta_{\bar{\sigma}}(x,y)\theta'_{\bar{\sigma},\bar{\tau}}(z,w) \\ &= \sum_{\sigma} \theta_{\sigma}(y,x)\theta'_{\sigma,\tau}(w,z) \\ &= p_{\tau}(y,x,z,w). \end{aligned}$$

Thus by swapping variables x with y and w with z in an invariant relation, we produce another invariant that is the complement to the original invariant.

We can generalize the idea of complementation to arbitrarily many states. The key idea behind complementation is that a particular permutation of the output state alphabet can be induced by a relabeling of the final parameters. In fact, any permutation of the output alphabet preserves invariants.

Proposition 11.5 *Let $\pi \in S_{\Sigma'}$ be a permutation of the output alphabet, and let π^* be the automorphism of $\mathbb{C}[p_\tau]$ induced by $\pi^*(p_\tau) = p_{\pi(\tau)}$. Then if f is in the kernel of $\mathbf{f}^* = g^* \circ F^* \circ \rho^*$, so is $\pi^*(f)$.*

Proof We have two maps from $\mathbb{C}[p_\tau]$ to $\mathbb{C}[\theta_i'']$, namely $\mathbf{f}^*$ and $\mathbf{f}^* \circ \pi^*$. If there exists an automorphism ϕ^* of $\mathbb{C}[p_\tau]$ such that $\phi^* \circ \mathbf{f}^* \circ \pi^* = \mathbf{f}^*$, then if $\mathbf{f}^*(f) = 0$, so does $\mathbf{f}^* \circ \pi^*(f)$ as ϕ is injective.

$$\begin{tikzcd} \mathbb{C}[p_\tau] \arrow[r, "\mathbf{f}^*"] \arrow[dr, "\mathbf{f}^*\circ\pi^*"'] & \mathbb{C}[\theta_i''] \\ & \mathbb{C}[\theta_i''] \arrow[u, dashed, "\phi^*"'] \end{tikzcd}$$

Thus we need only show that for any $\pi \in S_{\Sigma'}$, there exists such a ϕ^*. But π is equivalent to simply permuting the columns of the matrix $g^*(\theta')$, which are labeled by Σ'. Thus we define ϕ^* to be the map induced by π as a permutation of the columns of $g^*(\theta')$. Note that ϕ^* is a ring homomorphism, and in fact an automorphism of $\mathbb{C}[\theta'']$, as required. $\square$

As an example of the map induced by π as a permutation of the columns in the occasionally dishonest casino, let $\pi = (12345)$. Then ϕ^* would be $f_1 \mapsto f_2, f_2 \mapsto f_3, \ldots f_5 \mapsto 1 - \sum f_i$, which implies $1 - \sum f_j \mapsto f_1$, and similarly for the l_j. Note that in the multigraded case, we now need only look at a representative of each equivalence class (given by partitions of $n\delta$ objects into at most l' places); the proof of Proposition 11.5 works for the unconstrained case as well. We now revise the algorithm to take into account these refinements.

Algorithm 11.6

```
Input: A hidden Markov model f(n,l,l')=g* F* rho* and a degree bound DB.
Output: Generators for the ideal I_f up to degree DB.

Step 1: Compute ker(F* rho*) by letting I_u = find-relations(DB, (0), multigraded)

Step 2: Compute ker(g* F* rho*) by letting I = find-relations(DB,I_u,Z-graded)

Subroutine: find-relations(bound delta, ideal I, grading):
    If delta=1, return(find-linear-relations(m(1), (0), grading);
     else {
          I_R = find-relations(delta-1, I_R, grading)
          return(find-linear-relations(m(delta), I_R, grading)
          }

Subroutine: find-linear-relations(m, J, grading):
    Delete the monomials in m which lie in the initial ideal of J to form a list P
    If grading=multigrading {
         For each multigraded piece P_w of P, modulo permutations of the output alphabet
         Write the coefficient matrix M_w by mapping P_w to the parameter ring by F* rho*
         Append to a list K the kernel of M_w as relations among the monomials in P_w
         }
     else {
          Write the coefficient matrix M by mapping P to the parameter ring by f
          Let K be the kernel of M as relations among the monomials in P
          }
     Return K
```

While the above suffices as an algorithm to calculate $I_{\mathbf{f},\delta}$, our goal is to calculate all of $I_{\mathbf{f}}$. One could simply calculate $I_{\mathbf{f},\delta}$ for increasing δ, but this would require a stopping criterion to yield an algorithm. One approach is to bound the degree using a conjecture based on the linear algebra. We strongly suspect that the ideals of hidden Markov models of arbitrary length are generated in low degree, perhaps as low as 3. We can observe directly that this is true of the 3-node binary model, and the following conjecture of Sturmfels suggests why long models might be generated in degree 2.

Conjecture 11.7 *The ideal of invariants of the binary hidden Markov model of length n is generated by linear and quadric polynomials if $n \geq 14$.*

Proof [Idea] Let $\mathcal{M}$ be the vector of all monomials occurring in the hidden Markov model map $\mathbf{f}^*$, i.e., the monomials in the support of $\{\mathbf{f}^*(p_\tau)\}$. $\#(\mathcal{M}) \leq \binom{n+1}{2}\binom{n+2}{2} = \mathcal{O}(n^4)$, and fourteen is the first n for which $2^n \geq \binom{n+1}{2}\binom{n+2}{2}$.

Represent $\mathbf{f}^*$ by a matrix B with rows indexed by the coordinates of $\mathcal{M}$ and columns indexed by output strings τ. Then $\mathbf{f}^* = \mathcal{M}B$.

Hope 1 The rows of B are linearly independent. Then we may choose a square submatrix A of B which is invertible, corresponding to a set of columns C. Then $\mathbf{f}^* |_C = \mathcal{M}A$ so $\mathbf{f} |_C A^{-1} = \mathcal{M}I$, and every monomial which occurs in $\mathbf{f}$ can in fact be written as a linear combination of the probabilities p_τ.

Hope 2 The toric ideal of the map given by expansion of the row labels is generated by quadrics. These are the the relations that hold on the row labels, for example, $(xy)^2 - (x^2)(y^2)$ which we would write as $m_7^2 - m_6 m_{10}$ if our row labels began $1, x, y, z, w, x^2, xy, xz, xw, y^2, \dots$

If Hopes 1 and 2 hold, we have that the ideal of the hidden Markov model I_f is generated by the kernel of B acting on the right and the quadrics from Hope 2. $\square$

Another conjecture is that there are 'no holes' in the generating sets:

Conjecture 11.8 *If $I_{\mathbf{f},\delta} \neq 0$ is the ideal of invariants in $I_{\mathbf{f}}$ generated by the invariants of $\mathbf{f}$ of degree less than or equal to δ, and $I_{\mathbf{f},\delta} = I_{\mathbf{f},\delta+1}$ then $I_{\mathbf{f}} = I_{\mathbf{f},\delta}$.*

While this does not provide an absolute bound on the degree in which $I_{\mathbf{f}}$ is generated, it would provide an algorithmic stopping criterion.

11.4 Invariant Interpretation

We discuss two types of invariants of the hidden Markov model, found by the linear algebra technique, and which admit a statistical interpretation. They are *Permutation Invariants* and *Determinantal Invariants*

As discussed in [Mihaescu, 2004], the unhidden Markov model has certain simple invariants called *shuffling invariants*. These are invariants of the form $p_{\sigma,\tau} - p_{\sigma,t(\tau)}$ where t is a permutation of τ which preserves which hidden state each symbol is output from (clearly such an invariant can be non-trivial only if there are repeated hidden states in σ). To translate these invariants to the hidden Markov model, it is tempting to try to simply sum over σ. However, this is not possible unless every σ has repeated hidden states, and even then the permutation t will depend on σ and so one would end up with $p_\tau - \sum_\sigma p_{\sigma,t_\sigma(\tau)}$. However, if we also sum over certain permutations of τ then this problem can be avoided.

Proposition 11.9 *If σ has two identical states then for any τ, the polynomial*

$$\sum_{\pi \in S_\tau} (-1)^\pi p_{\sigma,\pi(\tau)} \qquad (11.1)$$

is an invariant of the unhidden Markov model.

Proof Suppose that $\sigma_i = \sigma_j$ and let $t_\sigma = (ij)$. We now have that

$$\sum_{\pi \in S_n} (-1)^\pi p_{\sigma,\pi(\tau)} = \sum_{\pi \in A_n} p_{\sigma,\pi(\tau)} - p_{\sigma,(t_\sigma \pi)(\tau)}$$

The result now follows from the fact that each $p_{\sigma,\pi(\tau)} - p_{\sigma,t_\sigma(\pi(\tau))}$ is a shuffling invariant. $\square$

Corollary 11.10 *If $l < n$ then*

$$\sum_{\pi \in S_\tau} (-1)^\pi p_{\pi(\tau)}$$

is an invariant of the hidden Markov model.

Proof If $l < n$ then any σ for the n-node model with l hidden states will have some repeated hidden state and so we can choose a t_σ for every σ and sum over σ to get an invariant of the hidden Markov model. $\square$

However, if $l' < n$ then for any τ, there will be two repeated output states. If $\tau_i = \tau_j$ and $t = (ij)$ then we have $\sum_{\pi \in S_n} (-1)^\pi p_{\pi(\tau)} = \sum_{\pi \in A_n} p_{\pi(\tau)} - p_{(\pi t)(\tau)} = \sum_{\pi \in A_n} p_{\pi(\tau)} - p_{\pi(\tau)} = 0$. So the above corollary gives non-trivial invariants only when $l < n \leq l'$ in which case there are $\binom{l'}{n}$ such invariants, each corresponding to the set of unique output letters occurring in the subscripts.

Note, however, that we did not actually have to sum over the full set of permutations of τ in the above. In Proposition 11.9, any set $B \subset S_\tau$ which is closed under multiplication by t_σ would suffice and in the corollary, we need B to be closed under multiplication by every t_σ for some choice of t_σ for every σ. In particular, if we let F be a subset of the nodes of our model and let B be all permutations fixing F then we will have permutation invariants so long as $l < n - \#(F)$, since we will then have repeated hidden states outside of F allowing us to choose t_σ to transpose two identical hidden states outside of F. This will imply that $t_\sigma B = B$. Again these permutation invariants will be non-trivial only if the output states outside of F are unique and so we will have permutation invariants for every F such that $l < n - \#(F) \leq l'$. In particular, we will have permutation invariants for every model with $l < \min(n, l')$.

All the linear invariants of the 3-node occasionally dishonest casino ($l = 2, l' = 6$) are of the type described in Corollary 11.10 while the 4 node ODC exhibits permutation invariants with fixed nodes. For example,

$$-p_{0253} + p_{0352} + p_{2053} - p_{2350} - p_{3052} + p_{3250}$$

is the sum over permutations of $0, 2, 3$ with the third letter, 5, fixed.

11.4.1 Determinantal Invariants

Among the degree three invariants of the binary hidden Markov model discovered using the linear algebra method described in the previous section is the invariant

$$\begin{gathered} p_{0000}p_{0101}p_{1111} + p_{0001}p_{0111}p_{1100} + p_{0011}p_{0100}p_{1101} \\ -p_{0011}p_{0101}p_{1100} - p_{0000}p_{0111}p_{1101} - p_{0001}p_{0100}p_{1111} \end{gathered}$$

Consider the length n hidden Markov model with l hidden states and l' observed states. For $i, j \in \Sigma$, $\tau_1 \in \Sigma'^k$, and $\tau_2 \in \Sigma'^{n-k}$, let $p_{\tau_1,i}$ be the total probability of outputting τ_1 and ending in hidden state i and p_{j,τ_2} be the total probability of starting in state j and outputting τ_2. Conditional independence for the hidden Markov model then implies that

$$p_{\tau_1\tau_2} = \sum_{i=1}^{l}\sum_{j=1}^{l} p_{\tau_1,i}\theta_{ij}p_{j,\tau_2}$$

Let P be the l^k by l^{n-k} matrix whose entries are indexed by pairs (τ_1, τ_2) with $P_{\tau_1,\tau_2} = p_{\tau_1\tau_2}$, let F be the l^k by l matrix with $F_{\tau_1,i} = p_{\tau_1,i}$ and let G be the l by l^{n-k} matrix with $G_{j,\tau_2} = p_{j,\tau_2}$. Then the conditional independence statement says exactly that $P = F\theta G$.

Since $\operatorname{rank}(\theta) = l$, this factorization implies that $\operatorname{rank}(P) \leq l$ or, equivalently, that all of its $l+1$ by $l+1$ minors vanish. These minors provide another class of invariants which we call *determinantal invariants*. For example, the invariant above is the determinant of the matrix

$$\begin{pmatrix} p_{0000} & p_{0001} & p_{0011} \\ p_{0100} & p_{0101} & p_{0111} \\ p_{1100} & p_{1101} & p_{1111} \end{pmatrix}$$

which occurs as a minor when the four node model is split after the second node. See Chapter 19 for more on invariants from flattenings along splits.

12
The EM Algorithm for Hidden Markov Models

Ingileif B. Hallgrímsdóttir

R. Alexander Milowski

Josephine Yu

In this chapter we study the EM algorithm for hidden Markov models (HMMs). As discussed in Chapter 1 the EM is an iterative procedure used to obtain maximum likelihood estimates (MLEs) for the parameters of a statistical model when only a part of the data is observed and direct estimation of the model parameters is not possible. An HMM is an example of such a model. The Baum-Welch algorithm is an efficient way of implementing the EM algorithm for HMMs. After showing that the Baum-Welch algorithm is equivalent to the EM algorithm for HMMs we discuss some issues regarding its implementation. For a few examples of two-state HMMs with binary output we study the exact form of the likelihood function and look at the paths taken by the EM algorithm from a number of different starting points.

12.1 The Baum-Welch algorithm

The hidden Markov model was derived in section 1.4.3 from the fully observed Markov model in section 1.4.2. We will use the same notation as in these sections, so $\sigma = \sigma_1\sigma_2\ldots\sigma_n \in \Sigma^n$ is a sequence of states and $\tau = \tau_1\tau_2\ldots\tau_n \in (\Sigma')^n$ a sequence of output variables. We assume that we observe N sequences of output variables from an HMM of length n, $\tau^1, \tau^2, \ldots, \tau^N$ where $\tau^j \in (\Sigma')^n, j = 1, \ldots, N$, but that the corresponding state sequences $\sigma^1, \sigma^2, \ldots, \sigma^N$, where $\sigma^j \in \Sigma^n, j = 1, \ldots, N$, are not observed (hidden).

The parameters of both the fully observed and hidden Markov models are an $l \times l$ matrix θ of transition probabilities and an $l \times l'$ matrix of emission probabilities. The entry θ_{rs} represents the probability of transitioning from state $r \in \Sigma$ to state $s \in \Sigma$, and θ'_{rt} represents the probability of emitting the symbol $t \in \Sigma'$ when in state $r \in \Sigma$. In Section 1.4.2 it is assumed that there is a uniform distribution on the first state in each sequence, i.e. $\text{Prob}(\sigma_1 = r) = 1/l, \forall r \in \Sigma$. We will allow an arbitrary distributions on the initial state. The initial probability θ_{0r} where $r \in \Sigma$ is the probability of starting in state r, i.e., $\mathrm{Prob}(\sigma_1 = r) = \theta_{0r}, \forall r \in \Sigma$, we require that $\sum_{r\in\Sigma} \theta_{0r} = 1$. In Proposition 1.18 it is shown that it is easy to solve the maximum likelihood problem for the fully observed Markov model and the maximum likelihood estimates for the θ_{rs} and θ'_{rt} are given. We will now describe in some detail how they are calculated, and derive the maximum likelihood estimates for θ_{r0}. Let w be an $l^2 \times l^n$ matrix such that there is one row corresponding to every combination rs, where $r \in \Sigma$ and $s \in \Sigma$, and one column corresponding to each path $\sigma \in \Sigma^n$. The entry $w_{rs,\sigma}$ in row rs and column σ equals the number of indices i such that $\sigma_i\sigma_{i+1} = rs$ in the path σ. Recall that the data matrix is $u \in \mathbb{N}^{(l')^n \times l^n}$ where $u_{(\tau,\sigma)}$ is the number of times the pair (τ, σ) was observed. Let $\tilde{u}$ be a vector of length l^n such that $\tilde{u}_\sigma = \sum_{\tau\in\Sigma'} u_{(\tau,\sigma)}$, i.e. $\tilde{u}_\sigma$ equals the number of times the path σ was used in the dataset. Let $v = w \cdot \tilde{u}$ then v_{rs} is the number of times a transition from state r to s was made in the data. The MLE for θ_{rs} is the proportion of times a transition from state r to state s was used out of all transitions starting in state r,

$$\widehat{\theta}_{rs} \quad = \quad \frac{v_{rs}}{\sum_{s'\in\Sigma} v_{rs'}}, \quad r \in \Sigma, s \in \Sigma \tag{12.1}$$

The maximum likelihood estimates for the initial probabilities are obtained similarly. Let $w_{0r,\sigma}$ be a $l \times (l')^n$ matrix such that $w_{0r,\sigma}$ is 1 if $\sigma_1 = r$ and 0 otherwise. Also let $v_{0r} = w_{0r,\sigma} \cdot \tilde{u}_\sigma$. The maximum likelihood estimator for θ_{0r} is the proportion of times we started in the state r:

$$\widehat{\theta}_{0r} \quad = \quad \frac{v_{0r}}{N}, \quad r \in \Sigma \tag{12.2}$$

The MLEs for θ' are obtained similarly. Let w' be an $(l \cdot l') \times (l^n \cdot (l')^n)$ matrix such that there is one row corresponding to each pair rt where $r \in \Sigma$ and $t \in \Sigma'$ and there is one column for each pair (τ, σ) of an output sequence $\tau \in (\Sigma')^n$ and a path $\sigma \in \Sigma^n$. An entry in the matrix, $w'_{rt,\tau\sigma}$ equals the number of times the symbol t is emitted from state r for the pair (τ, σ). Now let $\tilde{u}'$ be a vector of length $l^n \cdot (l')^n$ which is obtained by concatenating the rows of u into a vector. Then $v' = w' \cdot \tilde{u}'$ is a column vector of length $l \cdot l'$ and each entry v'_{rt} equals the number of times the symbol t was emitted from r in the dataset. The MLE for θ'_{rt} is the proportion of times the symbol t was emitted when in state r,

$$\widehat{\theta}'_{rt} \quad = \quad \frac{v'_{rt}}{\sum_{t'\in\Sigma'} v'_{rt'}}, \quad r \in \Sigma, t \in \Sigma' \tag{12.3}$$

To calculate the MLEs the full data matrix u is needed, it is however not available when only the output sequences have been observed. To estimate the parameters of a HMM we therefore need to use the EM algorithm. In the E-step the expected value of each entry in u, $u_{\tau,\sigma} = \frac{u_\tau}{f_\tau(\theta,\theta')} f_{\tau,\sigma}(\theta, \theta')$, is calculated and in the M-step these expected counts are used to obtain updated parameter values based on the solution of the maximum likelihood problem for the fully observed Markov model. Running the EM algorithm the way it is stated in Section 1.4. involves evaluating (and storing) the matrix f where each entry $f_{\tau,\sigma}(\theta,\theta')$ is the joint probability of using the path σ and observing the output sequence τ. The matrix is of size $(l')^n \times l^n$ and each entry is a monomial of degree $n(n-1)$ in $l^2 + l \cdot l'$ variables. This is computationally intensive and requires a lot of memory. We will now write the entries v_{rs} and v'_{rt} in a way that is much less compact, but will lead us to a more efficient way of implementing the EM algorithm using dynamic programming, namely the Baum-Welch algorithm. In the following derivation we write $w_{rs,\sigma} = \sum_{i=1}^{n-1} I_{(\sigma_i\sigma_{i+1}=rs)}$ where I_A is the indicator function which takes the value 1 if the statement A is true and 0 otherwise.

$$\begin{aligned}
v_{rs} &= \sum_{\sigma\in\Sigma} w_{rs,\sigma}\cdot \tilde{u}_\sigma \\
&= \sum_{\sigma\in\Sigma} w_{rs,\sigma}\cdot \sum_{\tau\in\Sigma'} u_{\tau,\sigma} \\
&= \sum_{\sigma\in\Sigma} w_{rs,\sigma}\cdot \sum_{\tau\in\Sigma'} u_\tau \frac{f_{\tau,\sigma}(\theta,\theta')}{f_\tau(\theta,\theta')} \\
&= \sum_{\tau\in\Sigma'} \frac{u_\tau}{f_\tau(\theta,\theta')} \sum_{\sigma\in\Sigma} w_{rs,\sigma}\cdot f_{\tau,\sigma}(\theta,\theta') \\
&= \sum_{\tau\in\Sigma'} \frac{u_\tau}{f_\tau(\theta,\theta')} \sum_{i=1}^{n-1}\sum_{\sigma\in\Sigma} I_{(\sigma_i\sigma_{i+1}=rs)}\cdot f_{\tau,\sigma}(\theta,\theta') \\
&= \sum_{\tau\in\Sigma'} \frac{u_\tau}{f_\tau(\theta,\theta')} \sum_{i=1}^{n-1} \mathrm{Prob}(\tau,\sigma_i=r,\sigma_{i+1}=s) \\
&= \sum_{\tau\in\Sigma'} \frac{u_\tau}{f_\tau(\theta,\theta')} \sum_{i=1}^{n-1} \mathrm{Prob}(\tau_1,\ldots,\tau_i,\sigma_i=r)\cdot \mathrm{Prob}(\sigma_{i+1}=s|\sigma_i=r) \\
&\qquad\qquad \cdot\mathrm{Prob}(\tau_{i+1}|\sigma_{i+1}=s)\cdot \mathrm{Prob}(\tau_{i+2},\ldots,\tau_n|\sigma_{i+1}=s) \\
&= \sum_{\tau\in\Sigma'} \frac{u_\tau}{f_\tau(\theta,\theta')} \sum_{i=1}^{n-1} \mathrm{Prob}(\tau_1,\ldots,\tau_i,\sigma_i=r)\cdot\theta_{rs}\cdot\theta'_{s\tau_{i+1}} \\
&\qquad\qquad \cdot\mathrm{Prob}(\tau_{i+2},\ldots,\tau_n|\sigma_{i+1}=s) \\
&= \sum_{\tau\in\Sigma'} \frac{u_\tau}{f_\tau(\theta,\theta')} \sum_{i=1}^{n-1} \tilde{f}_{\tau,r}(i)\cdot\theta_{rs}\cdot\theta'_{s\tau_{i+1}}\cdot \tilde{b}_{\tau,s}(i+1)
\end{aligned}$$

In the last step we introduced two new quantities,

Definition 12.1 The **forward probability** $\tilde{f}_{\tau,r}(i) = \mathrm{Prob}(\tau_1,\ldots,\tau_i,\sigma_i=r)$

is the probability of the observed sequence τ up to and including τ_i, requiring that we are in state r at position i. The **backward probability** $\tilde{b}_{\tau,r}(i) = \text{Prob}(\tau_{i+1}, \ldots, \tau_n | \sigma_i = r)$ is the probability of the observed sequence τ from τ_{i+1} to the end of the sequence, requiring that we are in state r at position i.

We will return to the forward and backward probabilities later but first we show how the v'_{rs} can be written in terms of the forward and backward probabilities. We use that $w'_{rt,(\tau,\sigma)} = \sum_{i=1}^{n} I_{(\sigma_i=r,\tau_i=t)}$.

$$
\begin{aligned}
v'_{rt} &= \sum_{\sigma\in\Sigma}\sum_{\tau\in\Sigma'} w'_{rt,(\tau,\sigma)} \cdot \tilde{u}'_{(\tau,\sigma)} \\
&= \sum_{\sigma\in\Sigma}\sum_{\tau\in\Sigma'} w'_{rt,(\tau,\sigma)} \cdot u_{(\tau,\sigma)} \\
&= \sum_{\sigma\in\Sigma}\sum_{\tau\in\Sigma'} w'_{rt,(\tau,\sigma)} \cdot u_\tau \frac{f_{\tau,\sigma}(\theta,\theta')}{f_\tau(\theta,\theta')} \\
&= \sum_{\tau\in\Sigma'} \frac{u_\tau}{f_\tau(\theta,\theta')} \sum_{\sigma\in\Sigma} w'_{rt,(\tau,\sigma)} \cdot f_{\tau,\sigma}(\theta,\theta') \\
&= \sum_{\tau\in\Sigma'} \frac{u_\tau}{f_\tau(\theta,\theta')} \sum_{i=1}^{n}\sum_{\sigma\in\Sigma} I_{(\sigma_i=r,\tau_i=t)} \cdot f_{\tau,\sigma}(\theta,\theta') \\
&= \sum_{\tau\in\Sigma'} \frac{u_\tau}{f_\tau(\theta,\theta')} \sum_{i=1}^{n} \text{Prob}(\tau_1,\ldots,\tau_{i-1},\tau_i=t,\tau_{i+1},\ldots,\tau_n,\sigma_i=r) \\
&= \sum_{\tau\in\Sigma'} \frac{u_\tau}{f_\tau(\theta,\theta')} \sum_{i=1}^{n} \text{Prob}(\tau_1,\ldots,\tau_{i-1},\tau_i=t,\sigma_i=r) \cdot \text{Prob}(\tau_{i+1},\ldots,\tau_n|\sigma_i=r) \\
&= \sum_{\tau\in\Sigma'} \frac{u_\tau}{f_\tau(\theta,\theta')} \sum_{i=1}^{n} \tilde{f}_{\tau,r}(i) \cdot \tilde{b}_{\tau,r}(i) I_{(\tau_i=t)}
\end{aligned}
$$

Finally

$$\begin{aligned}
v_{0r} &= \sum_{\sigma\in\Sigma} w_{0r,\sigma}\cdot\tilde{u}_\sigma \\
&= \sum_{\sigma\in\Sigma} w_{0r,\sigma}\cdot\sum_{\tau\in\Sigma'} u_{\tau,\sigma} \\
&= \sum_{\sigma\in\Sigma} w_{0r,\sigma}\cdot\sum_{\tau\in\Sigma'} u_\tau\frac{f_{\tau,\sigma}(\theta,\theta')}{f_\tau(\theta,\theta')} \\
&= \sum_{\tau\in\Sigma'}\frac{u_\tau}{f_\tau(\theta,\theta')}\sum_{\sigma\in\Sigma} w_{0r,\sigma}\cdot f_{\tau,\sigma}(\theta,\theta') \\
&= \sum_{\tau\in\Sigma'}\frac{u_\tau}{f_\tau(\theta,\theta')}\sum_{\sigma\in\Sigma} I_{(\sigma_1=r)}\cdot f_{\tau,\sigma}(\theta,\theta') \\
&= \sum_{\tau\in\Sigma'}\frac{u_\tau}{f_\tau(\theta,\theta')}\text{Prob}(\tau,\sigma_1=r) \\
&= \sum_{\tau\in\Sigma'}\frac{u_\tau}{f_\tau(\theta,\theta')}\text{Prob}(\sigma_1=r)\cdot\text{Prob}(\tau_1|\sigma_1=r)\cdot\text{Prob}(\tau_2,\ldots,\tau_n|\sigma_1=r) \\
&= \sum_{\tau\in\Sigma'}\frac{u_\tau}{f_\tau(\theta,\theta')}\theta_{0r}\theta'_{r\tau_1}\cdot\text{Prob}(\tau_2,\ldots,\tau_n|\sigma_1=r) \\
&= \sum_{\tau\in\Sigma'}\frac{u_\tau}{f_\tau(\theta,\theta')}\theta_{0r}\theta'_{r\tau_1}\cdot\tilde{b}_{\tau,r}(1)
\end{aligned}$$

The forward and backward probabilities can be calculated recursively in an efficient manner. It is easy to show [Durbin *et al.*, 1998] that:

$$\begin{aligned}
\tilde{f}_{\tau,r}(1) &= \theta'_{r\tau_i}\theta_{0r} \quad \text{for } r\in\{1,2,\ldots,l\}, \\
\tilde{f}_{\tau,r}(i) &= \theta'_{r\tau_i}\sum_s \tilde{f}_{\tau,s}(i-1)\theta_{sr} \quad \text{for } i\in\{1,2,\ldots,n\} \text{ and } r\in\{1,2,\ldots,l\}
\end{aligned}$$

and

$$\begin{aligned}
\tilde{b}_{\tau,r}(n) &= 1 \quad \text{for } r\in\{1,2,\ldots,l\} \\
\tilde{b}_{\tau,r}(i) &= \sum_s \theta_{rs}\theta'_{s\tau_{i+1}}\tilde{b}_{\tau,s}(i+1) \quad \text{for } i\in\{2,\ldots,n\} \text{ and } r\in\{1,2,\ldots,l\}
\end{aligned}$$

The probability of the whole sequence can be calculated based on the forward probabilities, $f_\tau(\theta,\theta') = \sum_{r\in\Sigma}\tilde{f}_{\tau,r}(n)$. The matrices $\tilde{f}_\tau$ and $\tilde{b}_\tau$ of forwards and backwards probabilities are of size $l\times n$ (a total of $2\cdot(l')^n\cdot l\cdot n$ values), and each entry can be efficiently obtained based on the values in the previous/subsequent column. This results in a great saving of both computer memory and processor time, compared to evaluating the $(l')^n \times l^n$ matrix f where, as was stated before, each entry is a monomial of degree $n(n-1)$. Recall that in the EM algorithm one calculates the expected counts $u_{\tau,\sigma}$ in the E-step and the MLEs for θ and θ' in the M-step. However, in each iteration of the Baum-Welch algorithm the parameters $\hat{\theta}$ and $\hat{\theta}'$ are updated in the following steps:

Algorithm 12.2 (Baum-Welch)

Initialization: Pick arbitrary model parameters $\widehat{\theta}_{rs}$ and $\widehat{\theta'}_{rt}$.
Recurrence:

```
        Calculate $\tilde{f}_{\tau,r}(i)$ and $\tilde{b}_{\tau,r}(i)$.
        Calculate $v_{rs}$ and $v'_{rt}$.
        Calculate new $\widehat{\theta}_{rs}$ and $\widehat{\theta'}_{rt}$.
```

Termination: Stop if change in ℓ_{obs} is less than some predefined threshold.

Below we provide pseudo-code for implementing the Baum-Welch algorithm, it includes the following functions:

forwards_array implements a dynamic programming algorithm to calculate the forward probabilities (in log-space) for a given output sequence τ, each position i in the sequence, and each possible state σ_i.
backwards_array calculates the backward probabilities in a similar way.
count_transitions calculates v_{rs} using forward and backward probabilities.
count_emissions calculates v'_{rt} using forward and backward probabilities.
Baum_Welch implements the Baum_Welch algorithm. Explain?

The values $\tilde{f}_{\tau,r}(i)$ and $\tilde{b}_{\tau,r}(i)$ are in general very small, small enough to cause underflow problems on most computer systems. Thus it is necessary to either scale the values or work with logarithms. It is convenient to work with logarithms and in fact all calculations in the pseudo-code below are performed in log-space. To evaluate the sum $x + y$ based on $\log x$ and $\log y$ without converting back to x and y we use,

$$\log(x + y) = \log x + \log(1 + e^{\log y - \log x})$$

which is codified in the utility function `add_logs`. In the implementation of the Baum-Welch algorithm below the matrices $\tilde{f}_\tau$ and $\tilde{b}_\tau$ are calculated at the beginning of each iteration (note that we only need to keep one $\tilde{f}_\tau$ and one $\tilde{b}_\tau$ matrix in memory at any time). One can also use the recursive property of the forward and backward probabilities to calculate them for each position r and output sequence τ, as they are needed in the evaluation of v_{rs} and v'_{rt}. This adds computation time but removes the need for storing the matrices $\tilde{f}_\tau$ and $\tilde{b}_\tau$. In the code we use S to denote the transition matrix θ and T to denote the emission matrix θ'.

```
add_logs(x, y):
    return $x + \log(1 + \exp(y - x))$


forwards_array(S, T, sequence, end):
    // Allocate memory for matrix of forwards probabilities, of size $n \times l$
    $result \leftarrow$ allocate_matrix($length[sequence], row\_count[S]$)
    for $state \leftarrow 1$ to $row\_count[S]$
    do
        // Start with initial transitions
        $result[0][state] \leftarrow S[0][state] + T[state][sequence[0]]$
    // Calculate the value forwards from the start of the sequence
    for $pos \leftarrow 0$ to $end$
    do
        // Calculate the next step in the forwards chain
        for $state \leftarrow 1$ to $row\_count[S] - 1$
        do
            // Traverse all the paths to the current state
            $result[pos][state] \leftarrow result[pos - 1][1] + S[1][state]$
            for $from \leftarrow 2$ to $row\_count[S] - 1$
            do
                // log formula for summation chains
                $result[pos][state] \leftarrow$ add_logs($result[pos][state], result[pos-1][from]+S[from][state]$)
            // Add in the probability of emitting the symbol
            $result[pos][state] \leftarrow result[pos][state] + T[state][sequence[pos]]$
    return $result$


backwards_array(S, T, sequence, start):
    // Allocate matrix of length of sequence vs states
    $result \leftarrow$ allocate_matrix($length[sequence], row\_count[S]$)
    for $state \leftarrow 1$ to $row\_count[S]$
    do
        // Start with end transitions
        $result[length[sequence]][state] \leftarrow S[state][0]$
    // Calculate the value backwards from end
    for $pos \leftarrow length[sequence] - 1$ to $start$
    do
        for $state \leftarrow 1$to$row\_count[S] - 1$
        do
            $result[pos][state] \leftarrow result[pos + 1][1] + (S[state][1] + T[1][sequence[pos]])$
            for $to \leftarrow 2$ to $row\_count[S] - 1$
            do
                // log formula for summation chains
                $result[pos][state] \leftarrow$ add_logs($result[pos][state], result[pos + 1][to] + (S[state][to] +
T[to][sequence[pos]])$)
    return $result$


count_transitions(S_counts, S, T, forwards, backwards, sequence):
    // Count initial transitions 0-¿n
    for $to \leftarrow 1$ to $row\_count[S] - 1$
    do
        $S\_counts[0][to] \leftarrow S[0][to] + (T[to][sequence[0]] + backwards[to][1])$
    // Count final transitions n-¿0
    for $from \leftarrow 1$ to $row\_count[S] - 1$
    do
        $S\_counts[from][0] \leftarrow S[from][0] + forwards[from][length[sequence] - 1]$
    // Count transitions k-¿l where k,l!=0
    for $from \leftarrow 1$ to $row\_count[S] - 1$
    do
        for $to \leftarrow 1$ to $row\_count[S] - 1$
```

```
      do
         $S\_counts[from][to] \leftarrow forwards[from][0]+(S[from][to]+(T[to][sequence[1]]+backwards[to][1]))$
         for $pos \leftarrow 1$ to $length[sequence]-2$
         do
            $v \leftarrow forwards[from][pos]+(S[from][to]+(T[to][sequence[pos]]+backwards[to][pos+1]))$
            $S\_counts[from][to] \leftarrow \text{add\_logs}(S\_counts[from][to], v)$
   return $S\_counts$
```

```
count_emissions(T_counts, T, forwards, backwards, sequence):
   // Count initial transitions 0-¿n
   for $state \leftarrow 1$ to $row\_count[S]-1$
   do
      $T\_counts[state][sequence[0]] \leftarrow forwards[state][0]+backwards[state][0]$
   for $state \leftarrow 1$ to $row\_count[S]-1$
   do
      for $pos \leftarrow 1$ to $length[sequence]-1$
      do
         $T\_counts[state][sequence[pos]] \leftarrow \text{add\_logs}(T\_counts[state][sequence[pos]], forwards[state][pos]+backwards[state][pos])$
   return $T\_counts$
```

```
Baum_Welch(S, T, sequences, limit):
   $lastLogLikelihood \leftarrow -\infty$
   repeat
      $logLikelihood \leftarrow 0$
      // These are matrices
      $S\_counts \leftarrow \text{zero\_matrix}(S)$
      $new\_S \leftarrow \text{zero\_matrix}(S)$
      $T\_counts \leftarrow \text{zero\_matrix}(T)$
      $new\_T \leftarrow \text{zero\_matrix}(T)$
      for $s \leftarrow 0$ to $length[sequences]-1$
      do
         $sequence \leftarrow sequences[s]$
         // Get the forwards/backwards values for the current sequence & model parameters
         $forwards \leftarrow \text{forwards\_array}(S, T, sequence, length[sequence]-1)$
         $backwards \leftarrow \text{backwards\_array}(S, T, sequence, 0)$
         // Calculate sequence probability
         $seqprob \leftarrow forwards[1][length[sequence]]+S[1][0]$
         for $state \leftarrow 2$ to $row\_count[S]-1$
         do
            $seqprob \leftarrow \text{add\_logs}(seqprob, forwards[state][length[sequence]]+S[state][0])$
         // Add contribution to log-likelihood
         $logLikelihood \leftarrow logLikelihood + seqprob$
         // Calculate the "counts" for this sequence
         $S\_counts \leftarrow \text{count\_transitions}(S\_counts, S, T, forwards, backwards, sequence)$
         $T\_counts \leftarrow \text{count\_emissions}(T\_counts, T, forwards, backwards, sequence)$
         // Calculate contribution for this sequence to the transitions
         for $from \leftarrow 0$ to $row\_count[S]-1$
         do
            for $to \leftarrow 1$ to $row\_count[S]-1$
            do
               if $s = 0$
               then
                  $new\_S[from][to] \leftarrow S\_counts[from][to] - seqprob$
               else
                  $new\_S[from][to] \leftarrow \text{add\_logs}(new\_S[from][to], S\_counts[from][to] - seqprob)$
            // Calculate contribution for this sequence to the transitions
            for $sym \leftarrow 0$ to $row\_count[T]-1$
            do
               if $s = 0$
            then
                $new\_T[from][sym] \leftarrow T\_counts[from][sym] - seqprob$
            else
                $new\_T[from][sym] \leftarrow \text{add\_logs}(new\_T[from][sym], T\_counts[from][sym] - seqprob)$
    // We'll stop when the log-likelihood changes a small amount
    $change \leftarrow logLikelihood - lastLogLikelihood$
until $change < limit$
return $S, T$
```

12.2 Evaluating the likelihood function

The likelihood function for a hidden Markov model is

$$L_{obs} = \prod_{\tau \in (\Sigma')^n} f_\tau(\theta, \theta')^{u_\tau}.$$

Hence L_{obs} is a polynomial of degree $Nn(n-1)$ whose variables are the unknown parameters in the matrices θ and θ'. It is in general not possible to obtain the MLEs, $\hat{\theta}$ and $\hat{\theta}'$, directly, so the Baum-Welch algorithm is used. However, for short Markov chains with few states and output variables it is possible to obtain the MLEs directly. We will look at a few examples of likelihood functions that arise from two state HMMs of length 3 with binary output (so $l = 2, n = 3, l' = 2$). If we fix the initial probabilities at 0.5 the model has 4 free parameters. For simplicity, we will denote the transition and emission probabilities by

$$\theta = \begin{pmatrix} x & 1-x \\ 1-y & y \end{pmatrix} \quad \text{and} \quad \theta' = \begin{pmatrix} z & 1-z \\ 1-w & w \end{pmatrix}.$$

For a fixed set of observed data, the likelihood function L_{obs} is a polynomial in the variables $x, y, z,$ and w. We are interested in maximizing L_{obs} over the region $0 \leq x, y, z, w \leq 1$. More generally, we want to study how many critical points L_{obs} typically has. We make the following observation; $L_{obs}(x, y, 0.5, 0.5)$ is constant with respect to x and y and also $L_{obs}(x, y, z, w) = L_{obs}(y, x, 1-w, 1-z)$ for any x, y, z, w. Therefore the critical points and global maxima of L_{obs} occur in pairs for the four parameter model.

In the rest of this section, we will look at the likelihood functions for the six examples listed in the following table. In each example we either fix one or two of the emission probabilities or impose symmetry constraints on the transition probabilities, thereby reducing the number of free parameters to 2 or 3 and allowing visualization in 3 dimensions. For each model a data vector

u_τ is given.

	000	001	010	011	100	101	110	111	N	z	w
Example 1	113	102	80	59	53	32	28	33	500	12/17	12/17
Example 2	26	31	44	4	9	16	40	35	205	12/17	12/17
Example 3	37	20	35	46	29	13	50	33	263	0.635	0.635
Example 4	73	56	49	51	70	53	67	81	500	free	0.1
Example 5	116	88	67	85	51	37	31	25	500	$z = w$	$z = w$
Example 6	37	20	35	46	29	13	50	33	263	$z = w$	$z = w$

In the first three examples we specialize z and w to a constant, so there are only two free parameters, x and y. Using a Singular implementation, by Luis Garcia, of the algebraic method for obtaining maximum likelihood estimates described in Section 3.3, we find that the likelihood function in the first example has a single critical point $(0.68838697, 0.33743958)$, which is a local and global maximum.

We can plot the likelihood as a function of x and y using MATHEMATICA, which was introduced in Chapter 2. For simplicity and better precision, we use 1 instead of 0.5 for the initial probabilities. This only scales the likelihood function by a constant and does not change the critical points. The MATHEMATICA code is:

```
s[0,0] := x; s[0,1] := 1-x; s[1,0] := 1-y; s[1,1] := y;
t[0,0] := 12/17; t[0,1] := 5/17; t[1,0] := 5/17; t[1,1] := 12/17;
f[i_,j_,k_]:=Sum[t[a,i]*Sum[s[a,b]*t[b,j]*Sum[s[b,c]*t[c,k],{c,0,1}],{b,0,1}],{a,0,1}];
L := Product[Product[Product[f[i,j,k]^u[i,j,k], {k,0,1}], {j,0,1}], {i,0,1}];
u[0,0,0] = 113; u[0,0,1] = 102; u[0,1,0] = 80; u[0,1,1] = 59;
u[1,0,0] = 53; u[1,0,1] = 32; u[1,1,0] = 28; u[1,1,1] = 33;
Plot3D[L,{x,0,1}, {y,0,1}, PlotPoints -> 60, PlotRange -> All];
```

The resulting plot can be viewed in the first panel of Figure 12.1. This is a typical likelihood function for this model. In fact we randomly generated several hundred data vectors u_τ and for each of them we examined the likelihood as a function of x and y for various values of $z = w$. There was almost always only one local maxima. We did find a handful of more interesting examples, including the ones in Example 2 and Example 3. The following code was used to generate the data in MATHEMATICA:

```
<< Graphics`Animation`
s[0, 0] := x; s[0, 1] := 1-x; s[1, 0] := 1-y; s[1, 1] := y;
t[0, 0] := z; t[0, 1] := 1-z; t[1, 0] := 1-z; t[1, 1] := z;
f[i_,j_,k_]:=Sum[t[a,i]*Sum[s[a,b]*t[b,j]*Sum[s[b,c]*t[c,k],{c,0,1}],{b,0,1}],{a,0,1}];
L := Product[Product[Product[f[i, j, k]^u[i, j, k], {k, 0, 1}], {j, 0, 1}], {i, 0, 1}];
For[n = 1, n <= 3, n++,
   u[0, 0, 0] = Random[Integer, {1, 50}];  u[0, 0, 1] = Random[Integer, {1, 50}];
   u[0, 1, 0] = Random[Integer, {1, 50}];  u[0, 1, 1] = Random[Integer, {1, 50}];
   u[1, 0, 0] = Random[Integer, {1, 50}];  u[1, 0, 1] = Random[Integer, {1, 50}];
   u[1, 1, 0] = Random[Integer, {1, 50}];  u[1, 1, 1] = Random[Integer, {1, 50}];
   Print[u[0, 0, 0], ",", u[0, 0, 1], ",", u[0, 1, 0], ",",u[0, 1, 1], ",",
   u[1, 0, 0], ",", u[1, 0, 1], ",", u[1, 1, 0], ",", u[1, 1, 1]];
   MoviePlot3D[L, {x, 0, 1},{y, 0, 1}, {z, 0, 1}, PlotPoints -> 40, PlotRange -> All]
]
```

We obtained the critical points for the likelihood functions as before. For Example 2 there are three critical points in the unit square $0 \leq x, y \leq 1$, namely a local and global maximum at $(0.13511114, 0.31536773)$, a local maximum at $(0.7828824, 0.72776217)$, and a saddle point at $(0.61297887, 0.61172163)$. In Example 3, the unique global maximum occurs on the boundary of the unit square but there is also a local maximum at $(0.65116323, 0.7092192)$ and a saddle point at $(0.27783904, 0.55326519)$. In section 12.3 we will return to these three examples.

In Examples 4-6 we look at models with three free parameters. It is no longer possible to obtain the critical values analytically as before, and we cannot plot a function in three variables. However we can look at level surfaces (3 dimensional contours) of the log-likelihood. For example, the following MATHEMATICA code can be used to plot the level surface of the log-likelihood function in Example 6 at the value -363.5.

```
<< Graphics`ContourPlot3D`
s[0, 0] := x; s[0, 1] := 1 - x; s[1, 0] := 1 - y; s[1, 1] := y;
t[0, 0] := z; t[0, 1] := 1 - z; t[1, 0] := 1 - z; t[1, 1] := z;
f[i_,j_,k_]:=Sum[t[a,i]*Sum[s[a,b]*t[b,j]*Sum[s[b,c]*t[c,k],{c,0,1}],{b,0,1}],{a,0,1}];
logL := Sum[Sum[Sum[u[i, j, k]*Log[f[i, j, k]], {k, 0, 1}], {j, 0, 1}], {i, 0, 1}];
u[0, 0, 0] = 37; u[0, 0, 1] = 20; u[0, 1, 0] = 35; u[0, 1, 1] = 46;
u[1, 0, 0] = 29; u[1, 0, 1] = 13; u[1, 1, 0] = 50; u[1, 1, 1] = 33;
ContourPlot3D[logL, {x, 0.01, 0.99}, {y, 0.01, 0.99}, {z, 0.01, 0.99},
    Contours -> {-363.5}, PlotPoints -> {10, 6}, Axes -> True];
```

In Example 4, we specialize w to a constant and let z vary. The level surface at -686 can be seen in Figure 12.1. In Examples 5 and 6 we impose the condition that the emission matrix $\hat{\theta}$ is symmetric, i.e. $z = w$. The symmetry $L_{obs}(x, y, z, w) = L_{obs}(y, x, 1-w, 1-z)$ then becomes $L_{obs}(x, y, z) = L_{obs}(y, x, 1-z)$. We can estimate the global and local maxima by picking the log likelihood value using binary search and checking if the corresponding level surface is empty. A weakness of this method is that sometimes MATHEMATICA mistakenly outputs an empty level surface if the resolution is not high enough. For Example 5 and 6, the level surfaces gets closer to the boundaries $z = w = 0$ and $z = w = 1$ as we gradually increase the likelihood value. Hence there seem to be two global maxima on the boundaries $z = w = 0$ and $z = w = 1$ in each example. In Example 6, there are also two local maxima on the boundaries $x = 0$ and $y = 0$. Example 3 has the same data vector as Example 6, so it is a "slice" of Example 6.

We did not find any examples where there are local maxima inside the (hyper)cube, but do not know whether that is true in general. For the two state HMMs with binary output of length 3 and 4, the coordinate functions $f_{(\tau,\sigma)}(\theta, \theta')$ have global maxima on the boundaries $z = 0, z = 1, w = 0, w = 1$.

We do not know if this will hold true for longer HMMs. This is a question worth pursuing because we would like to know whether the information about the location of global maxima of coordinate functions is useful in determining the location of critical points of likelihood function L_{obs}.

12.3 A general discussion about the EM algorithm

The EM algorithm is usually presented in two steps, the E-step and the M-step. However for the forthcoming discussion it is convenient to view the EM algorithm as a map from the parameter space onto itself,

$$M : \Theta \mapsto \Theta, \quad \theta^t \to \theta^{t+1}$$

where

$$\theta^{t+1} = M(\theta^t) = \text{argmax}_\theta E\left[l_{obs}(\theta|\tau,\sigma) \mid \sigma, \theta^t\right].$$

Where in this section we use θ to denote the pair (θ, θ'). By applying the mapping repeatedly we get a sequence of parameter estimates $\theta^1, \theta^2, \theta^3, \ldots$ s.t. $\theta^{t+1} = M^t(\theta^1)$. Local maxima of the likelihood function are fixed points of the mapping M. If $\theta^1, \theta^2, \theta^3, \cdots \to \theta^*$ then, by a Taylor expansion,

$$\theta^{t+1} - \theta^* \approx M'(\theta^*)(\theta^t - \theta^*)$$

in the neighborhood of θ^*, where $M'(\theta^*)$ is the first derivative of M evaluated at θ^* [Salakhutdinov *et al.*, 2003]. This implies that the EM is a linear iteration algorithm with convergence rate matrix $M'(\theta^*)$, and the convergence behavior is controlled by the eigenvalues of $M'(\theta^*)$. The convergence speed is a matter of great practical importance and there is a vast literature available on the subject, but that discussion is outside the scope of this chapter. More important than the speed of convergence is where the algorithm converges to. The EM algorithm is typically run from a number of different starting points in the hope of finding as many critical points as possible. We can ask questions such as: in what direction (in the parameter space) does the EM algorithm move in each step, how does the choice of starting value affect where it converges to and along what path does it travel. Most optimization algorithms move in the direction of the gradient at each step, so it is natural to compare the step direction to the direction of the gradient. In fact the updated parameter estimates can be written as a function of the parameter estimates from the previous step of the EM as [Salakhutdinov *et al.*, 2004]:

$$\theta^{t+1} = \theta^t + P(\theta^t)\nabla_{l_{obs}}(\theta^t) \tag{12.4}$$

where $\nabla_{l_{obs}}(\theta^t)$ is the gradient of the log-likelihood function evaluated at θ^t. The symmetric positive definite matrix P depends on the model, and its form for HMMs was derived in [Salakhutdinov *et al.*, 2004]. Note that each step of the EM algorithm has positive projection onto the gradient of the likelihood function.

The Baum-Welch algorithm was run from 121 different starting points for the three examples of 2 parameter models seen above. In the interest of space we only show the paths that the EM algorithm took for the second example, see figure 12.3. Each starting value is indicated by a dot and the two local maxima and the saddle point are indicated with filled circles. None of the paths end at the saddle point, in about one third of the runs Baum-Welch converges to the local maxima at $(0.783, 0.728)$ and in the other two thirds to the (larger) local maxima at $(0.135, 0.315)$. There seems to be a border going from (0,1) to (1,0) through the saddle point partitioning the parameter space so that if we start the Baum-Welch algorithm from any point in the lower section it converges to $(0.135, 0.315)$ but to $(0.783, 0.728)$ if we start at any point in the top section. The Baum-Welch was run from each starting point until the change in log-likelihood was $< 10^{-8}$. The number of iterations ranged from 66 to 2785 with an average of 1140. The change in the value of the log-likelihood in each step gets smaller and smaller, in fact for all starting points the ridge was reached in 10 to 75 steps (usually between 20 and 30). The change in log-likelihood in each step along the ridge is very small, usually on the order of $10^{-4} - 10^{-5}$. It is thus important to set the limit for the change of the log-likelihood low enough, or we would in this case think that we had reached convergence while still somewhere along the ridge. In figure 12.3 the direction of the gradient has been indicated with a black line at steps $1, 3, 5, 10, 20, \ldots, 100, 300, 500, 750, 1000, \ldots, 5000$. For comparison a contour plot of the likelihood is provided. It is clear that although the projection of the EM path onto the gradient is always positive, the steps of the EM are sometimes close to perpendicular to it, especially near the boundary of the parameter space. However, after reaching the ridge all paths are in the direction of the gradient. It is worth noting that since the EM algorithm does not move in the direction of the gradient of the log-likelihood it will not always converge to the same local maxima as a method based on gradient ascent run from the same starting point, and that the EM algorithm does in general display slower convergence than such methods. However the EM does have the distinct advantage that the updated parameters guaranteed to stay within the probability simplex. The above discussion also applies to the first and third examples.

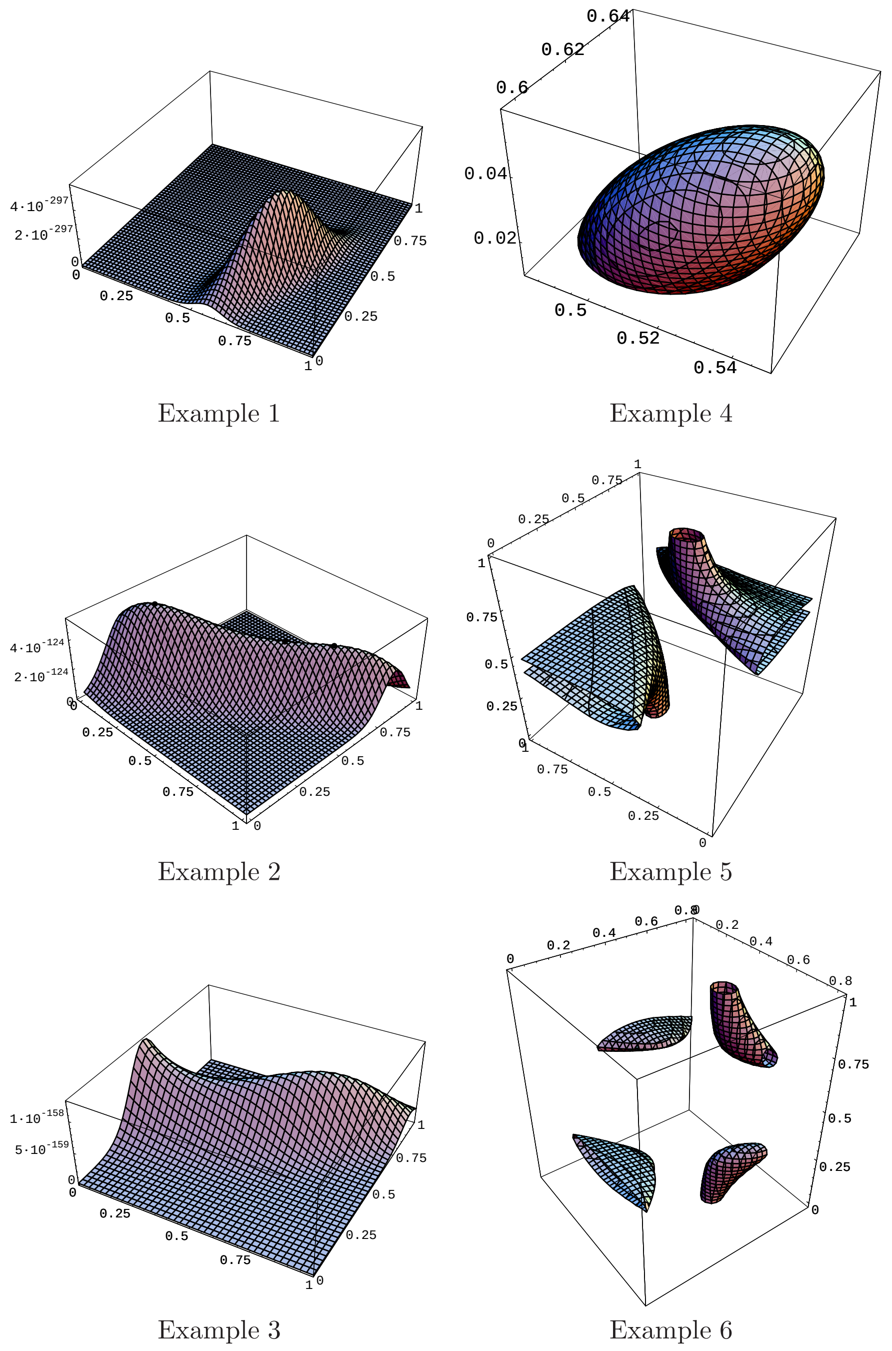

Fig. 12.1. The three figures on the left show graphs of likelihood functions for the 2−parameter models. The figures on the right show the level surfaces of the likelihood function for the 3− parameter models.

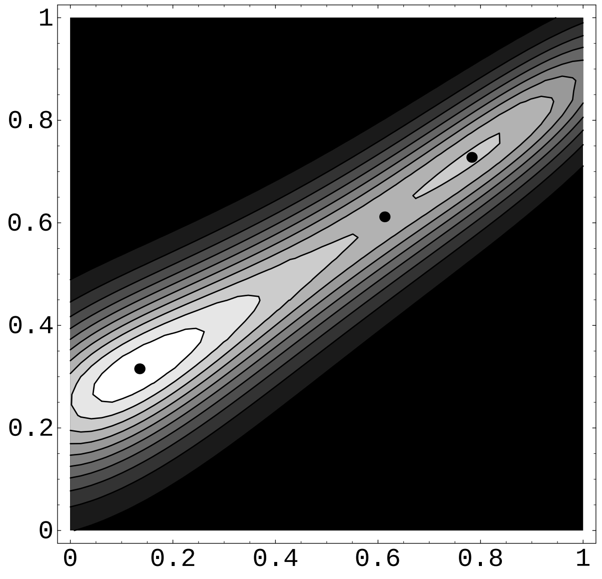

Fig. 12.2. Contour plot of the likelihood function for Example 2.

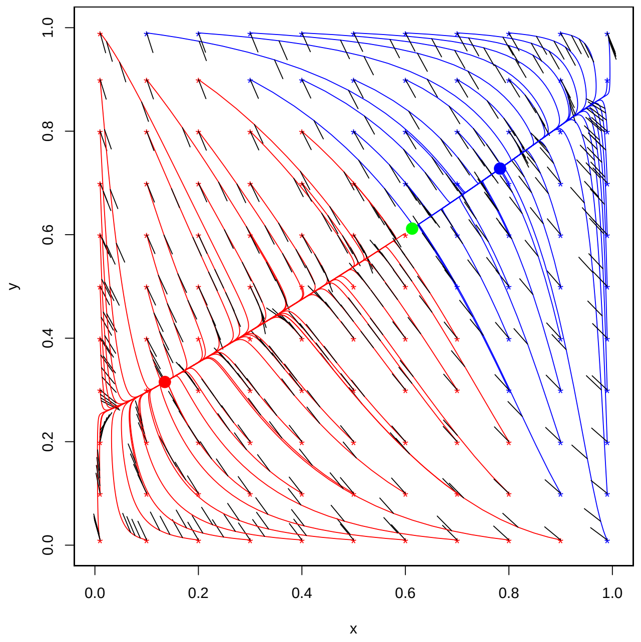

Fig. 12.3. The paths of the EM algorithm for Example 2. The direction of the gradient is indicated with black lines.

13
Homology mapping with Markov Random Fields

Anat Caspi

In this chapter we take a different approach to biological sequence comparison. We look for portions of the sequences that diverged from the same genomic region in the closest common ancestor, that is, *homologous* sequences. We explore this question as a structured data labelling problem, and offer a toric model formulation. The exact solution in the general toric model is intractable. However, for a very relevant subclass of this class of models, we find a linear (non-integer) formulation that can give us the exact integer solution in polynomial time. This is an encouraging result: for a specific, though widely useful, subclass of toric models in which the joint probability density is structured, MAP inference is tractable.

13.1 Genome mapping

Evolution through divergence gives rise to different, though related, present-day genomes that shared common ancestors. Portions of genomes could also be seen as genomic entities spawned through some pattern of evolutionary events from a single entity in the ancestral genome. Such genomic portions (be they gene-coding regions, conserved non-coding regions, etc) that are related through divergence from a common region in the ancestral genome are termed *homologs*. *Homology* is therefore a relational term asserting the common ancestry of two genomic components. Since much of our understanding of phylogeny and evolution comes from a comparative framework, it is important to accurately identify those homologous genomic entities in order to compare components that are actually linked by common ancestry. Additional, more specific, relational descriptors exist to delineate the evolutionary events that occurred to initiate the divergence between *homologs*; we leave those outside the scope of this discussion. Our objective is to create a *homology mapping*: a mapping between compared sequences in which an element in one sequence mapping to an element in another sequence indicates a homologous relationship between the two.

Earlier comparative studies aimed to map homology at different levels of resolution. At low resolution, gene markers, BAC fingerprints, or chromosomal locations were used to map entire genes on long genomic regions like chromosomes. At high resolution, nucleotide sequence mapping was designed for the available genomic sequences: usually short regions coding for one or two genes. Alignment models such as those discussed in chapter 7 were introduced . Note that the pair hidden Markov model introduced assumed collinearity (i.e., that the sequences compared can be mapped sequentially). This was a result of adopting local alignment models to align relatively short sequences. This model design primarily intended to deal with point mutations, rather than large-scale mutations (like gene inversions, or chromosomal duplication) which are more likely to be found in longer sequences. Assuming collinearity places an ordering constraint on the mapping produced.

As entire genome sequences are available, we are interested in mapping longer sequence regions, and must offer a model that does not imbed the ordering constraint. However, biological evidence (see [Marcotte *et al.*, 1999], [P. and G., 2003]) suggests that as genomes diverge, functional constraints apply pressure against genome shuffling, inversions, and duplications. As a result, homologs are more likely to occur in sequential syntenic clumps in the genome. That is, although we shouldn't constrain our maps to be ordered, we should look at genomic context and prefer locally collinear homologs. The model suggested here expresses dependencies among locally interacting portions of the genome, thereby having an affinity towards locally collinear alignments, but allows mappings that contain rearrangements like duplications and inversions.

The suggested output is a mapping between the genomic sequences that is not constrained to preserve the order of the sequences if the most likely mapping contains a rearrangement. Additionally, the mapping may not be one-to-one: a single component in one sequence may be mapped non-uniquely to several components in a second sequence, indicating a genomic duplication event. Due to these differences from the traditional meaning of a *sequence alignment*, we use the term *homology mapping* to describe the desired output.

We can pose the *homology mapping* problem as a graph assignment problem. Let us consider a homolog pair as a single entity, representing a single divergence occurrence from a particular component in an ancestral sequence. We call a proposed homolog pair a *match*– a match i, postulates homology between component a in one sequence, $a \in S1$, with component b in another sequence, $b \in S2$. The *components*, a and b, matched by a *match* need not be atomic subunits of the sequence (such as a single base-pair), matches could be proposed between regions of genomic sequences, or even entire structural domains.

Given genomic sequences for comparison, we introduce a graph in which proposed homolog pairs (matches) are nodes. We represent the local context dependencies among matches in our graph by introducing edges among match nodes whose components are located within a specified base-pair distance in the genomic sequence of at least one of the two paired components. This introduces a notion of locality of a node in the graph- where locality denotes a neighborhood of genome location.

We can choose to attribute weights to the dependencies among the matches. Edge weights can quantify associations among matches based on proximity or genomic distance, match density, orientation, or whether considering both matches homologs would necessitate particular genomic events (like inversions, duplications or shuffling) in their divergence pattern. Our objective is to choose a graph coloring for all the nodes in such a way that the sum of the weights on the edges connecting like-colored nodes is minimized. A discrete binary coloring scheme (for example, black and white) is natural to this problem since there are no partial homologs– components either did (black) or did not (white) share a common ancestor.

We are interested in solving this discrete labelling task probabilistically. Assuming a common ancestor between two sequences, we treat evolutionary events as part of a stochastic biological process that results in many pairs of homologous diverged genomic components that are distributed according to stochastically defined local spatial relations. To summarize: the model ought to capture context-dependent interactions among locally-interacting objects in a probabilistic manner. This is a an instance of a *structured labelling problem*.

Markov random fields (MRF) are a stochastic approach to modelling structured labelling problems. In MRFs, the label class (in our case homolog/non-homolog) pattern is generated by a random process. The parameters of the process induce the particular configuration of the correct labelling of the nodes. The random processes modelled by MRFs provide properties of local dependencies whereby the probability of a specific label (in our case, the probability that a match is or is not a homolog) is entirely dependent on a local subset of neighboring labels (in our case, a match is dependent on its immediate genomic context).

13.2 Markov random fields

Our goal here is to introduce the log-linear Markov Random Field model using algebraic notation (for a more general exposition of MRFs in algebraic statistics refer to [Geiger *et al.*, 2002]). The model consists of an underlying topology specified by an undirected graph $\mathcal{G} \equiv (\mathbf{Y}, E)$ (like the one introduced in example 1.), and a strictly positive probability distribution which factors according to the graph. $\mathbf{Y} = \{Y_1, \ldots, Y_N\}$ contains N nodes representing random variables. A node i has an assignment σ_i from a finite alphabet Σ_i of $l_i = |\Sigma_i|$ values or states. For example, if our nodes are binary random variables (for instance, indicating *not homolog* or *homolog*), then $\Sigma_{\mathbf{Y}} = \{0, 1\}$, as there are two possible values for each node factors, and $|\Sigma_{\mathbf{Y}}| = l_{\mathbf{Y}} = 2$. The state space is the finite and enumerable product space of all possible assignments $\mathbf{Y} = \prod_{Y_i \in \mathbf{Y}} \Sigma_{Y_i}$. In the case of a uniform alphabet of size $l_{\mathbf{Y}}$ for all the nodes in the graph, this state space comprises of $m = |\Sigma_{\mathbf{Y}}|^N = l_{\mathbf{Y}}^N$ possible assignments.

We turn our attention to the set of edges in the graph. E is a subset of $\mathbf{Y} \times \mathbf{Y}$. Each edge, denoted e_{ij}, is an undirected edge between nodes i and j in $\mathbf{Y}$. The edges define neighborhood associations in the form of direct dependencies among nodes. We define the neighborhood of node i as the set of all nodes j to which i is connected by an edge, $N_i = \{j \mid i, j \in \mathbf{Y}, i \neq j, e_{i,j} \in E\}$. The neighborhood of i is sometimes referred to as the *Markov blanket* of i. While Markov blankets describe the web of associations for a particular node, the entire graph could be factorized into subsets of maximally connected subgraphs in $\mathcal{G}$, known as cliques. Cliques vary in size. The set of cliques of size one, $\mathcal{C}(\mathcal{G})_1 = \{i \mid i \in \mathbf{Y}, N_i = \varnothing\}$ is a subset of the nodes in the graph; the set of cliques of size two is a subset of the adjacent nodes (or *pair-matches*), $\mathcal{C}(\mathcal{G})_2 = \{(i, j) \mid j \in N_i, i \in \mathbf{Y}\}$; the set of cliques of size three enumerates triples of neighboring nodes, $\mathcal{C}(\mathcal{G})_3 = \{(i, j, k) \mid i, j, k \in \mathbf{Y}, e_{ij}, e_{jk}, e_{ik} \in E\}$, etc. The collection of all cliques in the graph is $\mathcal{C}(\mathcal{G}) = \mathcal{C}(\mathcal{G})_1 \bigcup \mathcal{C}(\mathcal{G})_2 \bigcup \mathcal{C}(\mathcal{G})_3 \bigcup \cdots$. $\mathcal{C}(\mathcal{G})$ induces a decomposition of the graph into *factors*. Decomposing a graph in this way is instrumental both in understanding dependencies among the nodes, and in performing efficient inference as will be described below.

Each clique factor of a general Markov random field has a *potential function* which associates a non-negative value with each possible assignment of the nodes in that clique. In the log-linear class of models, the positivity constraint is imposed on the probability density function which in turn restricts the potential functions to be strictly positive. This restriction is enforced by expressing the potential valued functions in the exponential family form $e^{(T(\sigma))}$, where $T(\sigma)$ is the sufficient statistic for the family. We denote the potential value of a particular instance of a clique by $\phi_{c_i}(\sigma_{c_i})$, where σ_{c_i} is an instantiation of all the nodes in clique c_i. In the discrete case, the potential function for each clique $c_i \in \mathcal{C}(\mathcal{G})$ could be represented by a contingency matrix, θ^{c_i}, of k dimensions (where k is the [size of the clique vs. cardinality of c_i], $|c_i| = k$). θ^{c_i} is indexed by a k-tuple, $(\sigma_1, \sigma_2, \ldots \sigma_k)$ where $\sigma_j \in \Sigma_j$, the finite alphabet from which node $j \in c_i$ takes its value. This contingency matrix associates a positive value with each possible assignment for all nodes in the clique. As noted, positive valued potential functions induce strict positivity on the distributions generated by the cliques. *Positivity* is one of the two main properties of the random processes that log-linear MRFs model, and is a requirement of the Hamemrsley-Clifford theorem.

The random processes addressed by all MRFs preserve the Markov property. Specifically, as noted above, each edge association is a conditional independence statement which the probability distribution must satisfy. (Let σ_i denote the state (or: a particular assignment) for the node $i \in \mathbf{Y}$.)

$$\mathbf{P}(\sigma_i|\sigma_{\mathbf{Y}\backslash\{i\}}) = \mathbf{P}(\sigma_i|\sigma_{N_i}) \tag{13.1}$$

The Markov property states that the probability of a particular labelling for node i (given the rest of the labelled graph nodes) is only conditioned on the local Markov blanket of node i. That is, to assess a node's conditional probability, we only need the specification of its local neighborhood. Additionally, we see that two nodes, i and j, that do *not* share an edge in E must be conditionally independent because their Markov blankets are disjoint,

$$\mathbf{P}(\sigma_i, \sigma_j|\sigma_{\mathbf{Y}\backslash\{i,j\}}) = \mathbf{P}(\sigma_i|\sigma_{N_i})\mathbf{P}(\sigma_j|\sigma_{N_j}) \;\; \forall i, j \,|\, e_{ij}$$

By definition, every node j *not* in the Markov blanket of i is conditionally independent of i given the other nodes in the graph:

$$i \perp\!\!\!\perp j \,|\, \mathbf{Y}\backslash\{i,j\} \; \forall j \nsubseteq N_i, i, j \in \mathbf{Y}$$

Note that the set of Markov statements applied to each node $i \in \mathbf{Y}$, is the full set of conditional independence statements $\mathcal{M}_G$ (previously introduced in (1.63)) necessary and sufficient to specify the undirected graphical model in its quadratic form.

When the individual node probabilities and their Markov blankets are put together, the graph factorizes as the maximally connected subgraphs in the graph, introduced above as $\mathcal{C}(\mathcal{G})$. In this class of models, specifying the factorization and the potential function for each factor is tantamount to specifying the joint probability distribution of all variables for the Markov random field. Specifically, the log linear probability distribution on a full assignment to the graph labels, σ, is defined as:

$$P(\sigma) = \frac{1}{Z} \prod_{c_i \in \mathcal{C}(\mathcal{G})} \phi_{c_i}(\sigma_{c_i})$$

where Z is the *partition function* given by $Z = \sum_{\sigma \in \Sigma^n} \prod_{c_i \in \mathcal{C}(\mathcal{G})} \phi_{c_i}(\sigma_{c_i})$.

The probability is only dependent on the exponential family potential functions, and the node assignments in σ. We can therefore equivalently parameterize the model by the collection of contingency matrices, θ^{c_i}, one for each maximally connected subgraph, $c_i \in \mathcal{C}(\mathcal{G})$. The probability distribution over the state space is then defined to be proportional to the product of the parameters relevant to the particular model instantiation,

$$P_\theta(\sigma) \propto \prod_{c_i \in \mathcal{C}(\mathcal{G})} \theta^{c_i}_{\sigma'_{c_i}} I(\sigma'_{c_i} \equiv \sigma_{c_i}) \tag{13.2}$$

where $I(\cdot)$ is the boolean indicator function. The proportionality constant is the partition function as above. The components of θ are enumerable. For instance, in a Markov random field whose nodes take value assignments from the same alphabet, Σ such that $|\Sigma| = l$, the number of (potential values vs. potential valued functions) in the graph is

$$d = \sum_{c_i \in \mathcal{C}(\mathcal{G})} l^{|c_i|}.$$

We call the cliques in the factorized graph $\mathcal{C}(\mathcal{G})$ the model *generators*, defining d unknown, positive, model parameters $\theta = \{\theta_1, \ldots, \theta_d\}$.

We have characterized a class of *undirected graphical models* which is log-linear in the parameter values. Given the finite state space Σ^n, we can define an associated monomial mapping in θ for each assignment $\sigma \in \Sigma^n$.

$$f_\sigma(\theta) = P_\theta(\sigma) = \frac{1}{Z} \prod_{j=1}^{d} \theta_j I(j \in \sigma)$$

Recall that θ is indexed by a generator and its possible instantiation. Hence, the degree of each θ_j is determined by the state of the associated factors in the assignment. Since every factor must take on one and only one state label, the degree of all m monomials associated with a valid assignment is the same. Pooling all such monomials into a single map $\mathbf{f}$, we have specified a toric model parametrically (for definition of a *toric model* see 1.26).

$$\mathbf{f} \, : \, \mathbb{R}^d \to \mathbb{R}^m \, , \quad \theta \, \mapsto \, \frac{1}{\sum_{j=1}^m f_j(\theta)} \cdot \big(f_1(\theta), f_2(\theta), \ldots, f_m(\theta)\big).$$

We can express each of the monomials, f_i, as a column vector, thereby constructing a design $d \times m$ integer matrix, A. As before, the toric model of A is the image of the orthant $\theta = \mathbb{R}^d_{>0}$ under the map:

$$\mathbf{f} : \mathbb{R}^d \to \mathbb{R}^m, \theta \to \frac{1}{\sum_{j=1}^m \theta^{a_j}} (\theta^{a_1}, \theta^{a_2}, \ldots \theta^{a_m})$$

where $\sum_{j=1}^m \theta^{a_j}$ is the partition function. By construction, the joint probability distribution, P, is in the image of the mapping $\mathbf{f}$, and we say that P factors according to the model A. Once again we see that Hammersley-Clifford Theorem holds since that a toric model specified by A coincides with any log-linear MRF as defined above.

13.3 MRFs in homology assignment

We return to the homology assignment problem and illustrate the application of the MRF model with a simple example.

Example 13.1 Example 2.1 We are given two sequences, $S1$ and $S2$, for which we are to construct a log-linear MRF model.

pos	1	2	3	4	5	6	7	8	9	10	11	12	13	14	15	16	17
$S1:$	A	A	G	A	C	C	G	C	T	T	G	A	C	T	C	G	G
$S2:$	C	C	G	C	T	A	A	G	A	C	T	C	T	A	T	A	T

pos	18	19	20	21	22	23	24	25	26	27	28	29	30
$S1:$	A	A	A	A	G	G	G	G	C	T	C	–	–
$S2:$	A	T	A	G	G	C	T	C	C	C	G	C	C

Let us propose a match for every pair of perfectly matching 5-mers in the sequences. We denote a match node as $Y_i = (S1_j, S2_k)$, where i enumerates the nodes, and j, k are the indices pointing to the center of the 5-mer in the sequences $S1$ and $S2$, respectively. Let us define an edge between any two proposed matches whose center indices are within 14 base-pairs of one another on either of the two sequences. Four matches are proposed for the given sequences. Let $Y_1 = (S1_3, S2_8)$, $Y_2 = (S1_{13}, S2_{10})$, $Y_3 = (S1_7, S2_3)$, $Y_4 = (S1_{26}, S2_{23})$. The full node set is $\mathbf{Y} = \{Y_1, Y_2, Y_3, Y_4\}$, as depicted in Figure (Figure 13.1). The graph has four nodes, each taking its values from $\Sigma = \{0, 1\}$, and has a finite enumerable state space with $m = 2^4 = 16$ possible outcomes. We introduce four edges among matches whose centers are within 14 base-paris of one-another: $E = \{e_{\{1,2\}}, e_{\{2,3\}}, e_{\{1,3\}}, e_{\{2,4\}}\}$. $\mathcal{G}(\mathbf{Y}, E)$ is a four-node, four-edge graph, as depicted in (Figure 13.2).

Note the representation of the local context dependencies among matches in our graph. Match nodes whose assignments are likely to influence each other (those within a specified base-pair distance), are connected by an edge. Each node has its own locality, or neighborhood on the graph

$$\begin{aligned} N_1 &= \{Y_2, Y_3\} \\ N_2 &= \{Y_1, Y_3, Y_4\} \\ N_3 &= \{Y_1, Y_2\} \\ N_4 &= \{Y_2\} \end{aligned}$$

This induces a factorization on the graph of two maximally connected cliques,

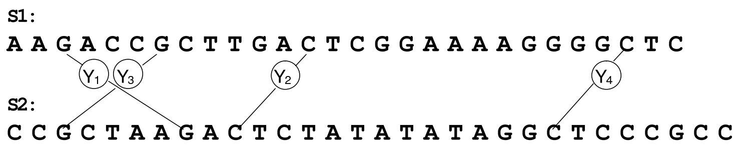
S1:
A A G A C C G C T T G A C T C G G A A A A G G G G C T C
Y1
Y3
Y2
Y4
S2:
C C G C T A A G A C T C T A T A T A T A G G C T C C C G C C

Fig. 13.1. Example of two sequences, S_1 and S_2. Match nodes are proposed between every perfectly matched 5-mers in the sequences.

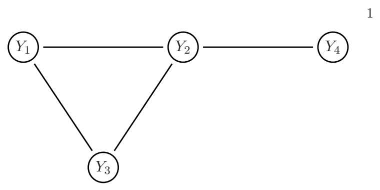

Fig. 13.2. Graph of a Markov random field with two maximal cliques.

one of size three ($c_1 = (Y_1, Y_2, Y_3)$), and another of size two ($c_2 = (Y_2, Y_4)$). The complete set of clique factors in the graph is $\mathcal{C}(\mathcal{G}) = \{c_1, c_2\} = \{(Y_1, Y_2, Y_3), (Y_2, Y_4)\}$. We expect to parameterize the model with 12 parameters:

$$d = \sum_{c_i \in \mathcal{C}(\mathcal{G})} l^{|c_i|} = 2^{|c_1|} + 2^{|c_2|} = 2^3 + 2^2 = 12$$

The parameter space consists of the contingency matrices for each clique in the graph. Each contingency matrix associates a positive value with each possible assignment on the nodes in the cliques. The parameters contributed by the two-node clique c_2 is denoted θ^{c_2} and is a subset of $\mathbb{R}^{2\times 2}_{>0}$ the space of 2×2 matrices whose four entries are positive. Similarly, the parameters contributed by the three-node clique c_1 is denoted θ^{c_1} and is a subset of $\mathbb{R}^{2\times 2\times 2}_{>0}$ the space of $2 \times 2 \times 2$ matrices whose eight entries are positive. The parameter space for the entire model $\Theta \subset \mathbb{R}^{(2\times 2\times 2)+(2\times 2)}$ consists of all matrices θ whose twelve entries t_i are positive. We associate the clique parameters with the model parameters as follows.

$$\theta^{c_1} = \begin{array}{cccccccc} t_1 & t_2 & t_3 & t_4 & t_5 & t_6 & t_7 & t_8 \\ \big(\theta^{c_1}_{000} & \theta^{c_1}_{001} & \theta^{c_1}_{010} & \theta^{c_1}_{011} & \theta^{c_1}_{100} & \theta^{c_1}_{101} & \theta^{c_1}_{110} & \theta^{c_1}_{111}\big) \end{array}$$

$$\theta^{c_2} = \begin{array}{cccc} t_9 & t_{10} & t_{11} & t_{12} \\ \big(\theta^{c_2}_{00} & \theta^{c_2}_{01} & \theta^{c_2}_{10} & \theta^{c_2}_{11}\big) \end{array}.$$

Using this factorization, we can fully characterizes the conditional independence relationships among the match nodes. Specifically, we have

$$\begin{aligned} P(\sigma_1|\sigma_2,\sigma_3,\sigma_4) &= P(\sigma_1|\sigma_2,\sigma_3) \\ P(\sigma_2|\sigma_1,\sigma_3,\sigma_4) &= P(\sigma_2|\sigma_1,\sigma_3,\sigma_4) \\ P(\sigma_3|\sigma_1,\sigma_2,\sigma_4) &= P(\sigma_3|\sigma_1,\sigma_2) \\ P(\sigma_4|\sigma_1,\sigma_2,\sigma_3) &= P(\sigma_4|\sigma_2)\,\cdot \end{aligned}$$

There are only 2 pairs of nodes not connected by an edge; the rendered model is

$$\mathcal{M}_{\mathcal{G}} = \{Y_1 \perp\!\!\!\perp Y_4 \,|\, \{Y_2, Y_3\}, Y_3 \perp\!\!\!\perp Y_4 \,|\, \{Y_1, Y_2\}, \}$$

Each such conditional independence statement can be translated into a system of quadratic polynomials in $\mathbb{R}^{[\mathbf{Y}]}$. The representation of independence statements as polynomial equations is an implicit representation of the toric model, where the common zero set of the polynomials represent the model.

For binary alphabets Σ_i the following eight quadric forms compose the set $\mathcal{Q}_{\mathcal{M}_G}$ representing the probability distribution from the example above.

$$\begin{gathered} p_{0001}p_{1000} - p_{0000}p_{1001}\,,\ p_{0001}p_{0010} - p_{0000}p_{0011}\,, \\ p_{0011}p_{1010} - p_{0010}p_{1011}\,,\ p_{0101}p_{0110} - p_{0100}p_{0111}\,, \\ p_{0101}p_{1100} - p_{0100}p_{1101}\,,\ p_{1001}p_{1010} - p_{1000}p_{1011}\,, \\ p_{0111}p_{1110} - p_{0110}p_{1111}\,,\ p_{1101}p_{1110} - p_{1100}p_{1111}. \end{gathered}$$

This set specifies a model which is a subset of the 15-dimensional simplex Δ with coordinates $p_{\sigma_1\sigma_2\sigma_3\sigma_4}$. The non-negative points on the variety defined by this set of polynomials represent probability distributions which satisfy the conditional independence statements in $\mathcal{M}_{\mathcal{G}}$.

The same quadric polynomials can also be determined by the vectors in the kernel of the parametric matrix $d \times m$ model $A_{\mathcal{G}}$. Each quadric form corresponds to a vector in the kernel of the design matrix $A_{\mathcal{G}}$. The columns of $A_{\mathcal{G}}$ are indexed by the m states in the state space, and the rows represent the potential values, indexed by a pair consisting of a maximal clique and a particular assignment possible on that clique, with a separate potential value for each possible assignment on the clique; 12 parameters in all. Each column in $A_{\mathcal{G}}$ represents a possible assignment of the graph.

$$\begin{array}{c|cccccccccccccccc}
 & 0000 & 0001 & 0010 & 0011 & 0100 & 0101 & 0110 & 0111 & 1000 & 1001 & 1010 & 1011 & 1100 & 1101 & 1110 & 1111 \\
000\cdot & 1 & 1 & 0 & 0 & 0 & 0 & 0 & 0 & 0 & 0 & 0 & 0 & 0 & 0 & 0 & 0 \\
001\cdot & 0 & 0 & 1 & 1 & 0 & 0 & 0 & 0 & 0 & 0 & 0 & 0 & 0 & 0 & 0 & 0 \\
010\cdot & 0 & 0 & 0 & 0 & 1 & 1 & 0 & 0 & 0 & 0 & 0 & 0 & 0 & 0 & 0 & 0 \\
011\cdot & 0 & 0 & 0 & 0 & 0 & 0 & 1 & 1 & 0 & 0 & 0 & 0 & 0 & 0 & 0 & 0 \\
100\cdot & 0 & 0 & 0 & 0 & 0 & 0 & 0 & 0 & 1 & 1 & 0 & 0 & 0 & 0 & 0 & 0 \\
101\cdot & 0 & 0 & 0 & 0 & 0 & 0 & 0 & 0 & 0 & 0 & 1 & 1 & 0 & 0 & 0 & 0 \\
110\cdot & 0 & 0 & 0 & 0 & 0 & 0 & 0 & 0 & 0 & 0 & 0 & 0 & 1 & 1 & 0 & 0 \\
111\cdot & 0 & 0 & 0 & 0 & 0 & 0 & 0 & 0 & 0 & 0 & 0 & 0 & 0 & 0 & 1 & 1 \\
\cdot 0 \cdot 0 & 1 & 0 & 1 & 0 & 0 & 0 & 0 & 0 & 1 & 0 & 1 & 0 & 0 & 0 & 0 & 0 \\
\cdot 0 \cdot 1 & 0 & 1 & 0 & 1 & 0 & 0 & 0 & 0 & 0 & 1 & 0 & 1 & 0 & 0 & 0 & 0 \\
\cdot 1 \cdot 0 & 0 & 0 & 0 & 0 & 1 & 0 & 1 & 0 & 0 & 0 & 0 & 0 & 1 & 0 & 1 & 0 \\
\cdot 1 \cdot 1 & 0 & 0 & 0 & 0 & 0 & 1 & 0 & 1 & 0 & 0 & 0 & 0 & 0 & 1 & 0 & 1
\end{array}$$

The geometry of the model is imbedded in this simplex. Each of the m columns of $A_{l,n}$ represents a distinct point in the d-dimensional space. The convex hull of these points define the polytope $f_{l,n}(\theta)$. Referring back to the toric Markov chain of chapter 1, we saw that the map $f_{l,n}$ was a k dimensional object inside the $(m-1)$ dimensional simplex Δ which consisted of all probability distributions in the state space l^n. The dimension k of the polytope is dependent on the conditionally dependent components, or cliques in the model. In the modeling literature this is referred to as graph partitions and separators on the graph.

The equivalence of the expressions of the log-linear Markov distributions is guaranteed by the important result of the Hammersley-Clifford theorem. In general, however, without the constraint on strictly positive probability density functions, $p_x > 0$, the class of toric models is larger than the general MRF exponential model.

13.4 Tractable MAP Inference in a subclass of MRFs

We return to the homology assignment problem. We wished to find the optimal factor assignment for $\mathbf{Y}$. In the case we presented, we have a binary assignment, designating *homolog* or *not homolog*. We note that the graph topology, conditional dependencies among its factors and potential functions on the graph (the θ vector) were obtained by incorporating observations about the given biological sequences for which we want homology assignments. In this case, we are interested in the label assignment to the factors in $\mathbf{Y}$ that maximizes the joint probability of the assignments given the parameter values. Specifically, we would like to find the mode (peak) of the distribution. This is called the Maximum A Posteriori (MAP) assignment of the model.

We have already specified the joint probabilities of the assignments $P_\theta(\sigma)$, given the parameters of the model in 13.2. In terms of the parameters, the probability of observing σ is the product of the parameters that correspond to the instantiation of these maximal cliques on the graph normalized by the partition function. The partition function enumerates ($m = |\Sigma_{\mathbf{Y}}|^N$) possible assignments, and despite the model factorizing as the graph, calculating the joint probability is computationally nontrivial. Various mechanisms for estimating the partition function have been suggested. For instance, using Gibbs distributions, we can obtain a global probability of a labelling by sampling from the distribution ([Geman and Geman, 1984]). We're interested in an exact MAP solution that is tractable. Tractable MAP computation is possible for a specific subclass of toric models which is very relevant to the homology assignment problem and other discrete labelling problems.

First, let us try to simplify the MAP inference computation. We transform the problem to logarithmic coordinates $\log(\Theta)$, where the joint probability density calculation for every assignment becomes a linear sum:

$$log(P_\theta(\sigma)) = \sum_{c_i \in \mathcal{C}(\mathcal{G})} \theta^{c_i}_{\sigma'_{c_i}} I(\sigma'_{c_i} \equiv \sigma_{c_i}) - log(Z)$$

This is the polytope calculated from the m columns of matrix $-\log(A_{\mathcal{G}})$. Computing a vertex on the convex hull of this matrix is the same as tropicalizing the partition function. This reduces the problem to calculating the convex hull of $-\log(P_\theta(\sigma))$ and finding the maximal vertex. Evaluating the partition function is intractable beyond small sized problems because the computation is exponential in the number of nodes on the graph (for a more detailed discussion, see chapter 9). This makes computation of the entire joint probability very difficult. There exists a subclass of log-linear models for which MAP inference can be computed exactly by reformulating the problem as a problem for which we already have efficient algorithms.

For many integer and combinatorial optimization problem, some very successful approximation algorithms are based on linear relaxations, such as branch-and-cut. In general, these are approximation algorithms. However, for a certain subclass of the log-linear models called *ferromagnetic Ising models*, solving the integer programming problem based on a linear relaxation gives an exact solution to the problem [Besag, 1986, Kolmogorov and Zabih, 2003]. This subclass encodes situations in which locally related variables (nodes in the same Markov blanket) tend to have the same labelling. In this subclass, the contingency matrix for each generator of the model (maximal clique) is constrained to have all of the off-diagonal terms be identically one, and all the diagonal terms be greater than one. When we take the logarithm of these terms, the off-diagonal terms vanish, and the diagonal terms are strictly positive. Those familiar with computer vision or physics literature would recognize this is akin to the *generalized Potts*, but with no penalty for assignments that do not have the same label across edges in the graph.

Recall that the diagonal terms are those which assign the same label to all the nodes in the same maximal clique. This type of value assignment is known as *guilt by association*, since being in the same clique (local neighborhood) has a positive potential value (hence increasing the likelihood) associated with being assigned the same value. In the context of the homology assignment, this is a way of representing an underlying evolutionary process in which homologous matches are related objects whose homology assignment should be consistent with other local matches. This kind of attractive assignment is important in many domains in which different labels have structures of affinities within local neighborhoods. In our formulation, the different labels can have different affinities.

To formulate the linear relaxation for solving this problem, we must leave the realm of toric varieties. The state space now comprises of continuous vectors. In the implicitization of the model, we maintain the quadric polynomials we had before (that is, the conditional independence statements remain the same). We present new polynomials that ensure that a particular value assignment, $(\sigma_{c_i}) = k$, on a clique is only possible when all the component nodes $j \in \{c_i\}$ are assigned the same value, k. The new model is represented by the non-negative set of the added quadric polynomials (a set of inequalities) rather than the common zero set of all the polynomials as before. These new constraints did not add points to the model outside the convex hull of the original toric model. Hence, the polytope remains the same, only the linear formulation incorporates more than just the integer lattice vertices in the set of feasible solutions. Importantly, it has been shown that in the binary case, when a solution exists, the linear relaxation is guaranteed to produce the same integer solution as the integer model [Besag, 1986, Kolmogorov and Zabih, 2003]. In practice, this problem conveniently reduces to a problem known as graph min-cut, which can be solved exactly in polynomial time only in the number of nodes on the graph.

This is an encouraging result: for a specific, though widely applicable, sub-class of toric models in which the joint probability density is structured, MAP inference is tractable.

13.5 The Cystic Fibrosis Transmembrane Regulator

The 'greater Cystic Fibrosis Transmembrane Regulator (CFTR) region' is a DNA dataset of 12 megabases (Mb) of high-quality sequences from 12 vertebrate genomes. The data was collected by Thomas et. al. [Thomas *et al.*, 2003], targeting a genomic region orthologous to a segment of about 1.8 Mb on human chromosome 7, which encodes 10 genes. One of the genes encodes CFTR, which is the gene mutated in cystic fibrosis.

The original comparative study successfully identified 98% of the exons as well as many conserved noncoding sequences. The gene number and order were found to be mostly conserved across the 12 species, with strikingly variable amount of noncoding sequences mainly interspersed repeats. Additionally, the authors identified three insertions (transposons) that are shared between the primates and rodents, which confirms the close relationship of the two lineages and highlights the opportunity such data provides for refining species phylogenies and characterizing the evolutionary process of genomes.

To demonstrate the use of our method, we took the greater CFTR region from four currently sequenced vertebrate genomes: human, chicken, rat and mouse.

In practice, our method delineates the *sequence matching* (see chapter 7) from the *homology mapping* aspects of alignment. To produce homolog mappings among multiple sequences, we proceed as follows:

(i) Obtain matches (not necessarily identical) between multiple sequences in advance of the homology mapping: these matches may be pairs of single base pairs, larger `BLAT` hits[Kent, 2002], exons, or even complete genes.
(ii) Construct the constrained Ising model based on the matches (as above).
(iii) Find the MAP assignment using linear programming.
(iv) Output the nodes that were assigned a value of 1 as homologous matches.

Figure 13.3 displays the CFTR dataset for the four selected genomes. Horizontal shaded bars represent the CFTR region in a fully sequenced chromosome. The lines between chromosome bars connecting small segments represent `BLAT`[Kent, 2002] output matches.

Our method takes these matches as nodes, and constructs a Markov network from them. In this particular instance, there are 169 nodes and our network has nearly six thousand edges. On a (machine spec here) it took 12.18 seconds to solve the corresponding linear program formulation. The results (that is, the nodes that were assigned a value of 1, designated as *homolog*) are depicted in figure 13.4.

Overall, we have performed this operation on much larger sets of data, with

Fig. 13.3. BLAT output

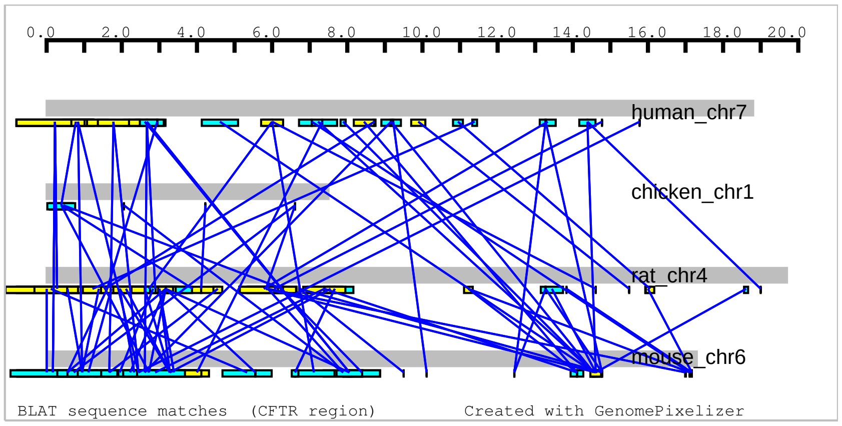

Fig. 13.4. our MRF MAP output

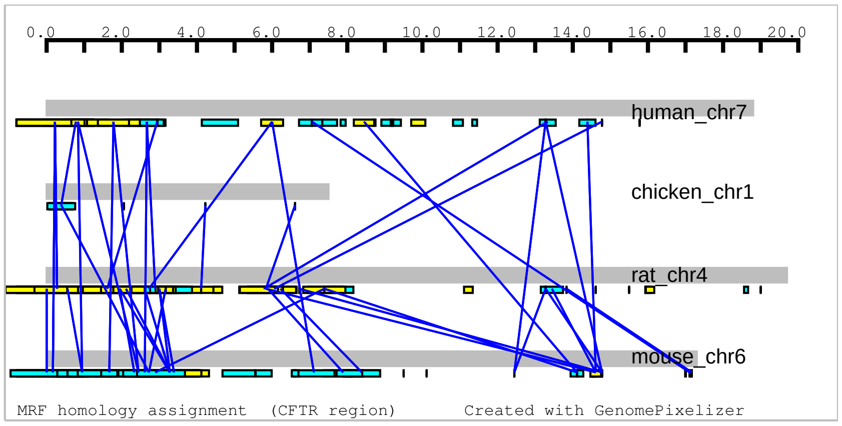

networks as large as three hundred thousand nodes, and two million edges. Solution time scales polynomially with the number of nodes.

14
Mutagenetic Tree Models

Niko Beerenwinkel

Mathias Drton

Mutagenetic trees are a class of graphical models designed for accumulative evolutionary processes. We determine the algebraic invariants of mutagenetic trees and discuss the geometry of mixture models.

14.1 Accumulative Evolutionary Processes

Some evolutionary processes can be described as the accumulation of non-reversible genetic changes. For example, the progression of tumor development of several cancer types can be regarded as the accumulation of chromosomal alterations [Vogelstein *et al.*, 1988, Zang, 2001]. This clonal evolutionary process starts from the set of complete chromosomes and is characterized by subsequent chromosomal gains and losses or by losses of heterozygosity. Mutagenetic trees (also called *oncogenetic trees* in the context of oncogenesis) have been applied to model the occurrence of chromosome alterations in patients with renal cancer [Desper *et al.*, 1999, von Heydebreck *et al.*, 2004], ovarian adenocarcinoma [Simon *et al.*, 2000], and melanoma [Radmacher *et al.*, 2001]. For glioblastoma and prostate cancer, tumor progression along the oncogenetic tree model has been shown to be an independent marker of patient survival [Rahnenführer *et al.*, 2005].

Amino acid substitutions may also be modeled as permanent under certain conditions, such as a very strong selective pressure. For example, the evolution of human immunodeficiency virus (HIV) under antiviral drug therapy exhibits this behavior. The development of drug resistance can be regarded as the accumulation of resistance-conferring mutations. Mixtures of mutagenetic trees have been applied to data sets obtained from HIV infected patients under different antiviral drug regimens [Beerenwinkel *et al.*, 2004, Beerenwinkel *et al.*, 2005a]. This modeling approach has revealed different evolutionary pathways the virus can take to become resistant, which is important for the design of effective therapeutic protocols.

In general, we consider clonal evolutionary processes on a finite set of events. An event can be a genetic alteration, such as the loss of a chromosome arm in a tumor cell or an amino acid substitution in a protein. We assume that these changes are permanent. Mutagenetic trees aim at modeling the order and rate of occurrence of these changes. A software package for statistical inference with mutagenetic trees and mixtures of these is described in [Beerenwinkel *et al.*, 2005b].

14.2 Mutagenetic Trees

Consider n binary random variables $X_1, \ldots, X_n$ each indicating the occurrence of an event. We will represent an observation of $X := (X_1, \ldots, X_n)$ as a binary vector $i = (i_1, \ldots, i_n) \in \mathcal{I} := \{0,1\}^n$, but sometimes use the equivalent representation by the subset $S_i \subset [n] = \{1, \ldots, n\}$ of occurred events, i.e. $S_i = \{v \in [n] \mid i_v = 1\}$. The inverse of this bijection is simply $i_S = (1_S, 0_{V \setminus S})$. For a subset $A \subset [n]$ we denote by $X_A = (X_v)_{v \in A}$ the correponding subvector of random variables taking values in $\mathcal{I}_A := \{0,1\}^{|A|}$.

A *mutagenetic tree* T on n events is a connected branching on the set of nodes $V = V(T) = \{0\} \cup [n]$, rooted at node 0. The set of edges in T is denoted by $E(T)$. There are $(n+1)^{n-1}$ different mutagentic trees on n events. Indeed, the set of connected rooted branchings on V is in one-to-one correspondence with the set of undirected labeled trees on $n+1$ nodes, and Cayley's theorem states that this set has cardinality $(n+1)^{n-1}$ [Stanley, 1999]. A subbranching of T is a directed subtree of T with the same root node 0. For any subset $V' \subset V$ we denote by $T_{V'}$ the induced subgraph. In particular, each state $i \in \mathcal{I}$ induces a subgraph $T_i := T_{S_i}$ of the mutagenetic tree T. Every node $v \in [n]$ has exactly one entering edge $(u, v) \in E(T)$. We call u the *parent* of v, denoted $\mathrm{pa}(v) = u$. For $V' \subset V$, $\mathrm{pa}(V')$ is the vector $(\mathrm{pa}(v))_{v \in V'}$. Finally, the outgoing edges of a node u are called the *children* of u, and this set is denoted $\mathrm{ch}(u)$.

For $n = 3$ events, there are $4^2 = 16$ mutagenetic trees, which fall into four distinct groups according to the tree topology. Figure 14.1 shows one mutagenetic tree from each of the four topology classes.

14.2.1 Statistical Model

With each edge $(\mathrm{pa}(v), v)$, $v \in [n]$, in a mutagenetic tree T, associate a probability $\theta^v_{11} \in [0,1]$ and a matrix

$$\theta^v = \theta^{\mathrm{pa}(v),v} = \begin{pmatrix} 1 & 0 \\ 1 - \theta^v_{11} & \theta^v_{11} \end{pmatrix}. \tag{14.1}$$

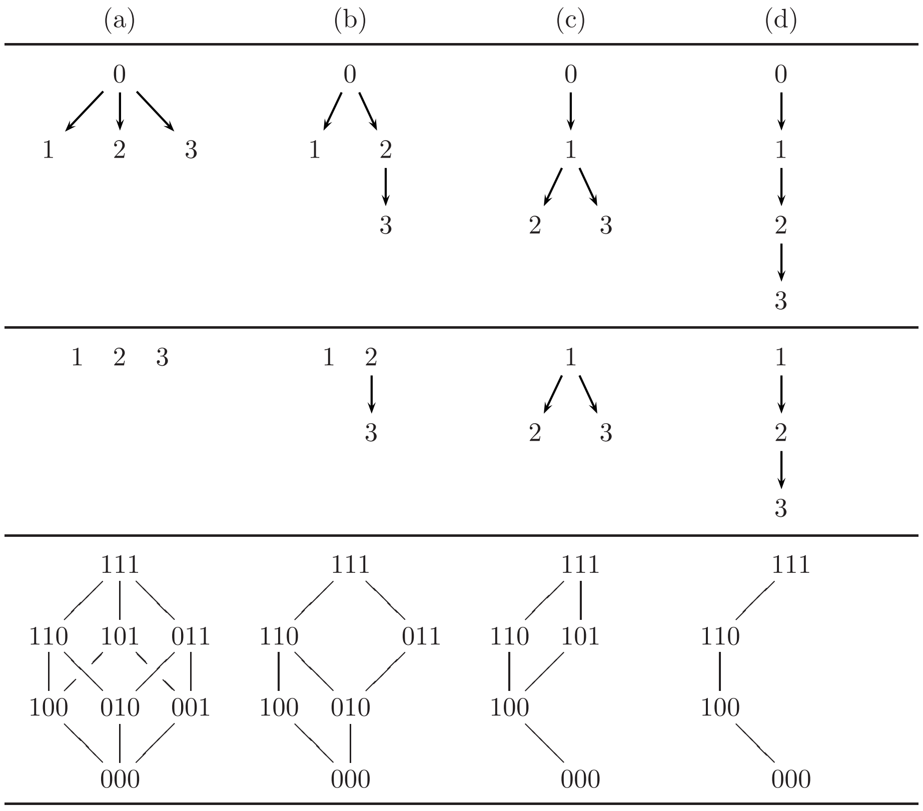

Fig. 14.1. Mutagenetic trees for $n = 3$ events (first row), their induced directed forests (second row) and lattices of compatible states (third row).

Let $\Theta = [0,1]^n$, and let $\Delta = \Delta_{2^n-1}$ be the $2^n - 1$ dimensional probability simplex in $\mathbb{R}^{2^n}$. Let $\theta = (\theta^1_{11}, \dots, \theta^n_{11})$ and consider the polynomial map

$$\mathbf{f}^{(T)} : \Theta \to \Delta, \quad \theta \mapsto (f_i(\theta))_{i \in \mathcal{I}}, \quad \text{defined by } \; f_i(\theta) = \prod_{v=1}^{n} \theta^v_{i_{\mathrm{pa}(v)}, i_v}, \qquad (14.2)$$

where we set $i_0 = 1$; compare (1.52).

Definition 14.1 The n-dimensional *mutagenetic tree model* $\mathcal{T} := \mathbf{f}^{(T)}(\Theta) \subset \Delta$ is the fully observed tree model given by the map $\mathbf{f}^{(T)}$. This algebraic statistical model has parameter space Θ and state space $\mathcal{I}$.

In the model $\mathcal{T}$ an event can occur only if all of its ancestor events have already occurred.

Example 14.2 Let T be the mutagenetic tree in Figure 14.1(b). Then the map $\mathbf{f}^{(T)}$ has coordinates

$$\begin{aligned} f_{000}(\theta) &= (1-\theta^1_{11})(1-\theta^2_{11})(1-\theta^3_{11}), & f_{100}(\theta) &= \theta^1_{11}(1-\theta^2_{11}),\\ f_{001}(\theta) &= 0, & f_{101}(\theta) &= 0,\\ f_{010}(\theta) &= (1-\theta^1_{11})\theta^2_{11}(1-\theta^3_{11}), & f_{110}(\theta) &= \theta^1_{11}\theta^2_{11}(1-\theta^3_{11}),\\ f_{011}(\theta) &= (1-\theta^1_{11})\theta^2_{11}\theta^3_{11}, & f_{111}(\theta) &= \theta^1_{11}\theta^2_{11}\theta^3_{11}. \end{aligned}$$

From the form of the matrix of transition probabilities in (14.1) and Example 14.2, it is apparent that not all states $i \in \mathcal{I}$ may occur with positive probability in a mutagenetic tree model $\mathcal{T}$.

Definition 14.3 Let $\Gamma \subset \Delta$ be a statistical model with state space $\mathcal{I}$. A state $i \in \mathcal{I}$ is *compatible* with Γ if there exists $p \in \Gamma$ such that $p_i > 0$. Otherwise, i is said to be *incompatible* with Γ. The set of all states compatible with Γ is denoted $\mathcal{C}(\Gamma)$.

Lemma 14.4 *Let T be a mutagenetic tree. For a state $i \in \mathcal{I}$ the following are equivalent:*

(i) *$i \in \mathcal{C}(\mathcal{T})$, i.e. i is compatible with $\mathcal{T}$,*
(ii) *for all $v \in S_i$, $\mathrm{pa}(v) \in S_i \cup \{0\}$,*
(iii) *T_i is a subbranching of T.*

Hence, all states $i \in \mathcal{I}$ are compatible with $\mathcal{T}$ if and only if T is a star, i.e. $\mathrm{pa}(T) = 0_{[n]}$.

Proof By (14.2) and (14.1),

$$p_i = \left[\prod_{v:\mathrm{pa}(v)\in S_i\cup\{0\}} (\theta^v_{11})^{i_v}(1-\theta^v_{11})^{1-i_v}\right] \times \left[\prod_{v:\mathrm{pa}(v)\notin S_i} 0^{i_v}1^{1-i_v}\right], \qquad (14.3)$$

from which the stated claims follow immediately; see also [Beerenwinkel *et al.*, 2004]. □

The following algorithm efficiently generates the set $\mathcal{C}(\mathcal{T})$ of compatible states.

Algorithm 14.5 (Compatible states)
Input: A mutagenetic tree T.
Output: The set $\mathcal{C}(\mathcal{T})$ of states compatible with $\mathcal{T}$.
Step 1: Sort the nodes of T in any reverse topological order $v_n, v_{n-1}, \ldots, v_1, 0$. (For example, use the reverse breadth-first-search order.)

Step 2: For $v = v_n, v_{n-1}, \ldots, v_1$:
Let $T(v)$ be the subtree of T rooted at v and set

$$\mathcal{C}_v = \begin{cases} \{0,1\} & \text{if } v \text{ is a leaf,} \\ \{0_{V(T(v))}\} \cup \left(\{1_v\} \times \prod_{u \in \mathrm{ch}(v)} \mathcal{C}_u\right) & \text{else.} \end{cases}$$

Step 3: Return the Cartesian product $\mathcal{C}(\mathcal{T}) = \prod_{u: u \in \mathrm{ch}(v)} \mathcal{C}_u$.

The correctness of the algorithm follows from the fact that the states $\mathcal{I}_{T(v)}$ compatible with $\mathcal{T}(v)$ are $i = (0, \ldots, 0)$ and those states i with $i_v = 1$ and as remaining components the free combinations of all states compatible with the subtree models $\mathcal{T}(u)$ for each $u \in \mathrm{ch}(v)$. For all mutagenetic trees on $n = 3$ events, the sets of compatible states can be read off from the first eight rows of Table 14.1, in which the symbol $\bullet$ marks incompatible states.

The following Theorem 14.6 connects mutagenetic tree models to directed graphical models (Bayesian networks) and yields, in particular, that maximum likelihood estimates of the parameters θ_{11}^v are rational functions of the data [Lauritzen, 1996]. The theorem is an immediate consequence of the model defining equation (14.2) and the theory of graphical models (compare Theorem 1.33 and Remark 1.34). Figure 14.1 illustrates the theorem.

Theorem 14.6 *Let T be a mutagenetic tree and $p \in \Delta$ a probability distribution. Then, $p \in \mathcal{T}$ if and only if p is in the directed graphical model based on the induced directed forest $T_{[n]}$, and $p_i = 0$ for all incompatible states $i \notin \mathcal{C}(\mathcal{T})$. In particular, if $X = (X_1, \ldots, X_n)$ is distributed according to $\mathbf{f}^{(T)}(\theta)$, $\theta \in \Theta$, i.e. if*

$$\mathrm{Prob}(X = i) = f_i(\theta), \qquad \forall\, i \in \mathcal{I},$$

then

$$\theta_{11}^v = \begin{cases} \mathrm{Prob}(X_v = 1) & \textit{if } \mathrm{pa}(v) = 0, \\ \mathrm{Prob}(X_v = 1 \mid X_{\mathrm{pa}(v)} = 1) & \textit{else.} \end{cases}$$

14.2.2 Algebraic Invariants

The power set of $[n]$, which can be written as $\{S_i\}_{i \in \mathcal{I}}$, forms a poset ordered by inclusion. Moreover, $(\{S_i\}_{i \in I}, \cup, \cap)$ is a finite distributive lattice. The corresponding join and meet operations in $\mathcal{I}$ are

$$\begin{aligned} i \vee j :=& \big(\max(i_v, j_v)\big)_{v \in [n]} = i_{S_i \cup S_j} \in \mathcal{I}, \\ i \wedge j :=& \big(\min(i_v, j_v)\big)_{v \in [n]} = i_{S_i \cap S_j} \in \mathcal{I}, \quad i, j \in \mathcal{I}, \end{aligned}$$

and we will subsequently work with the isomorphic lattice $(\mathcal{I}, \vee, \wedge)$.

Lemma 14.7 *For any mutagenetic tree T, the compatible states $(\mathcal{C}(\mathcal{T}), \vee, \wedge)$ form a sublattice of $\mathcal{I}$.*

Proof We need to verify that $i, j \in \mathcal{C}(\mathcal{T})$ implies that both $i \vee j$ and $i \wedge j$ are elements of $\mathcal{C}(\mathcal{T})$. This follows from Lemma 14.4 and the fact that $0 \in V(T_i)$ for all $i \in \mathcal{I}$. □

See Figure 14.1 for examples of lattices of compatible states.

Consider now the polynomial ring $R := \mathbb{R}[p_i,\ i \in \mathcal{I}]$ generated by the states $i \in \mathcal{I}$. The statistical model $\mathcal{T}$ is an algebraic variety in Δ. Let $I_{\mathcal{T}} \subset R$ be the ideal of polynomials that vanish on $\mathcal{T}$. Clearly, the monomial ideals $\langle p_i,\ i \notin \mathcal{C}(\mathcal{T})\rangle$ lie in $I_{\mathcal{T}}$. In addition, Lemma 14.6 implies that certain polynomials encoding conditional independence statements of $\mathcal{T}$ lie in $I_{\mathcal{T}}$.

Consider an independence statement $X_A \perp\!\!\!\perp X_B \mid X_C$, or $A \perp\!\!\!\perp B \mid C$ for short. According to Proposition 1.26 in Chapter 1, its ideal of invariants $I_{A \perp\!\!\!\perp B|C}$ is generated by the 2×2 minors

$$p_{i_A i_B i_C} p_{j_A j_B i_C} - p_{i_A j_B i_C} p_{j_A i_B i_C} = \det \begin{pmatrix} p_{i_A i_B i_C} & p_{i_A j_B i_C} \\ p_{j_A i_B i_C} & p_{j_A j_B i_C} \end{pmatrix}, \qquad (14.4)$$

for all $(i_A, i_B, i_C), (j_A, j_B, i_C) \in \mathcal{I}$.

The *global Markov property* [Lauritzen, 1996] on the mutagenetic tree T states that $A \perp\!\!\!\perp B \mid C$ if and only if A is separated from B by $C \cup \{0\}$ in T, i.e. if every path from a node $u \in A$ to a node $v \in B$ intersects $C \cup \{0\}$. Let $I_{\mathrm{global}(T)}$ be the sum of the independence ideals $I_{A \perp\!\!\!\perp B|C}$ over all statements $A \perp\!\!\!\perp B \mid C$ induced by T. It turns out that $I_{\mathrm{global}(T)}$ is already generated by the *saturated* independence statements, i.e. by all $A \perp\!\!\!\perp B \mid C$ with $A \dot\cup B \dot\cup C = [n]$; see also [Geiger *et al.*, 2005]. Note that saturated independence statements translate into quadratic binomials.

Drawing on previous work on independence ideals in graphical models we can characterize the ideal $I_{\mathcal{T}}$ of invariants of $\mathcal{T}$ as follows.

Proposition 14.8

$$I_{\mathcal{T}} = I_{\mathrm{global}(T)} + \big\langle\, p_i,\ i \notin \mathcal{C}(\mathcal{T}) \big\rangle + \Big\langle \sum_{i \in \mathcal{I}} p_i - 1 \Big\rangle.$$

Proof Note that A is separated from B by $C \cup \{0\}$ in T if and only if A is separated from B by C in the induced forest $T_{[n]}$. The claim follows from Theorems 6 and 8 in [Garcia *et al.*, 2004] together with Theorem 14.6. □

Using the lattice structure from Lemma 14.7, we can find a much smaller set of the generators for $I_{\mathcal{T}}$. Table 14.1 illustrates the generators for the trees on $n = 3$ events.

Invariant \ pa(T)	0 1 2	0 3 1	2 0 1	3 0 2	3 1 0	2 3 0	0 1 1	2 0 2	3 3 0	0 0 2	0 3 0	0 0 1	3 0 0	0 1 0	2 0 0	0 0 0
p_{000}	·	·	·	·	·	·	·	·	·	·	·	·	·	·	·	·
p_{001}	●	●	●	●	·	·	●	●	·	●	·	●	·	·	·	·
p_{010}	●	●	·	·	●	●	●	·	●	·	●	·	·	●	·	·
p_{011}	●	●	●	·	●	·	●	·	·	·	·	●	·	●	·	·
p_{100}	·	·	●	●	●	●	·	●	●	·	·	·	●	·	●	·
p_{101}	●	·	●	●	·	●	·	●	·	●	·	·	·	·	●	·
p_{110}	·	●	·	●	●	●	·	·	●	·	●	·	●	·	·	·
p_{111}	·	·	·	·	·	·	·	·	·	·	·	·	·	·	·	·
$p_{001}p_{010} - p_{000}p_{011}$	○	○	○	·	○	·	○	·	·	·	·	○	●	●	●	●
$p_{001}p_{100} - p_{000}p_{101}$	○	·	○	○	·	○	·	○	·	○	●	·	·	●	○	●
$p_{001}p_{110} - p_{000}p_{111}$	·	·	·	·	·	·	·	·	·	·	·	·	·	●	●	●
$p_{010}p_{100} - p_{000}p_{110}$	·	○	·	○	○	○	·	·	○	●	○	●	○	·	·	●
$p_{010}p_{101} - p_{000}p_{111}$	·	·	·	·	·	·	·	·	·	·	·	●	●	·	·	●
$p_{011}p_{100} - p_{000}p_{111}$	·	·	·	·	·	·	·	·	·	●	●	·	·	·	·	●
$p_{011}p_{101} - p_{001}p_{111}$	○	○	○	○	·	·	○	○	●	○	●	○	●	·	·	●
$p_{011}p_{110} - p_{010}p_{111}$	○	○	·	·	○	○	○	●	○	●	○	·	·	○	●	●
$p_{101}p_{110} - p_{100}p_{111}$	·	·	○	○	○	○	●	○	○	·	·	●	○	●	○	●
Figure 1.1 and 1.2	(d)						(c)			(b)						(a)

Table 14.1. *Algebraic invariants for the 16 mutagenetic tree models on $n = 3$ events. Polynomials in the Gröbner basis of the ideal of invariants are indicated by "●", polynomials that lie in the ideal are indicated by "○".*

Theorem 14.9 *Let $\mathcal{T}$ be a mutagenetic tree model. Then its ideal of invariants $I_{\mathcal{T}}$ is generated by the following polynomials:*

(i) *the monomials p_i, i incompatible with $\mathcal{T}$,*
(ii) *the squarefree quadratic binomials $p_i p_j - p_{i \vee j} p_{i \wedge j}$, i and j compatible with $\mathcal{T}$, and*
(iii) *the sum $\sum_{i \in \mathcal{I}} p_i - 1$.*

Proof Consider $i, j \in \mathcal{C}(\mathcal{T})$, $i \neq j$. By Lemma 14.4, the induced subgraphs T_i and T_j are subbranchings of T. If we define $A := S_i \setminus S_j$, $B := S_j \setminus S_i$, and

$$C := [n] \setminus (A \dot\cup B) = (S_i \cap S_j) \dot\cup ([n] \setminus (S_i \cup S_j)),$$

then A and B are separated by $C \cup \{0\}$ in T, hence $A \perp\!\!\!\perp B \mid C$. Setting

$$(i_A, i_B, i_C) = (1_A, 0_B, 1_{S_i \cap S_j}, 0_{[n] \setminus (S_i \cup S_j)}),$$
$$(j_A, j_B, i_C) = (0_A, 1_B, 1_{S_i \cap S_j}, 0_{[n] \setminus (S_i \cup S_j)}),$$

we find that

$$p_i p_j - p_{i \vee j} p_{i \wedge j} = p_{i_A i_B i_C} p_{j_A j_B i_C} - p_{i_A j_B i_C} p_{j_A i_B i_C} \in I_{\text{global}(T)}.$$

This establishes the inclusion $\langle p_i p_j - p_{i\vee j} p_{i\wedge j},\ i,j \in \mathcal{C}(\mathcal{T})\rangle \subset I_{\mathcal{T}}$.

To prove that the stated list of polynomials generates $I_{\mathcal{T}}$, it suffices to consider a saturated conditional independence statement $A \perp\!\!\!\perp B \mid C$, and to show that

$$I_{A\perp\!\!\!\perp B|C} \subset \big\langle\, p_i p_j - p_{i\vee j} p_{i\wedge j},\ i,j \in \mathcal{C}(\mathcal{T})\big\rangle + \big\langle\, p_i,\ i \notin \mathcal{C}(\mathcal{T})\big\rangle.$$

So consider a generator g of $I_{A\perp\!\!\!\perp B|C}$,

$$g = p_{i_A i_B i_C} p_{j_A j_B i_C} - p_{i_A j_B i_C} p_{j_A i_B i_C}, \quad (i_A, i_B, i_C), (j_A, j_B, i_C) \in \mathcal{I}.$$

First, note that

$$p_{i_A i_B i_C} p_{j_A j_B i_C} \in \langle p_i \mid i \notin \mathcal{C}(\mathcal{T})\rangle \iff p_{i_A j_B i_C} p_{j_A i_B i_C} \in \langle p_i \mid i \notin \mathcal{C}(\mathcal{T})\rangle\,.$$

Indeed, by Lemma 14.4, $k \notin \mathcal{C}(\mathcal{T})$ if and only if there exists $(u,v) \in E(T)$ with $v \in V(T_k)$, but $u \notin V(T_k)$. Since A and B are separated by $C \cup \{0\}$, such an edge cannot connect A and B. Therefore, it can only appear in both sets $E(T_{i_A i_B i_C}) \cup E(T_{j_A j_B i_C})$ and $E(T_{i_A j_B i_C}) \cup E(T_{j_A i_B i_C})$.

Assume now that all four states defining g are compatible with $\mathcal{T}$. Then Lemma 14.7 implies that their joins and meets are also compatible. Moreover,

$$\begin{aligned} i_A i_B i_C \vee j_A j_B i_C &= i_A j_B i_C \vee j_A i_B i_C =: i \vee j \\ i_A i_B i_C \wedge j_A j_B i_C &= i_A j_B i_C \wedge j_A i_B i_C =: i \wedge j \end{aligned}$$

and we can write

$$g = (p_{i_A i_B i_C} p_{j_A j_B i_C} - p_{i\vee j} p_{i\wedge j}) + (p_{i\vee j} p_{i\wedge j} - p_{i_A j_B i_C} p_{j_A i_B i_C})$$

as an element of $\langle p_i p_j - p_{i\vee j} p_{i\wedge j},\ i,j \in \mathcal{C}(\mathcal{T})\rangle$. □

Example 14.10 Let $\mathcal{S}$ be the mutagenetic tree model defined by the star topology, i.e. the model of complete independence; cf. Figures 14.1(a). Then $\mathcal{S}$ is the intersection of the probability simplex with the Segre variety

$$V_{\text{Segre}} = \bigcap_{k=1}^{n} V(p_{i_1 \dots i_n} p_{j_1 \dots j_n} - p_{i_1 \dots i_{k-1} j_k i_{k+1} \dots i_n} p_{j_1 \dots j_{k-1} i_k j_{k+1} \dots j_n},\ i,j \in \mathcal{I}),$$

i.e. the image of the n-fold Segre embedding $\mathbb{P}^1 \times \dots \times \mathbb{P}^1 \to \mathbb{P}^{2^n - 1}$. To see this note that the minors defining the Segre variety lie in

$$\langle p_i p_j - p_{i\vee j} p_{i\wedge j},\ i,j \in \mathcal{I}\rangle\,,$$

because both products of the binomials defining V_{Segre} have the same join and meet. Conversely, let $i,j \in \mathcal{I}$, $i \neq j$. Then there is a sequence of pairs of states

$$(i,j) = (i^{(0)}, j^{(0)}),\ \dots,\ (i^{(m+1)}, j^{(m+1)}) = (i \vee j, i \wedge j)$$

such that for all $l = 1, \dots, m$, both $i^{(l+1)}$ and $j^{(l+1)}$ are obtained from $i^{(l)}$ and $j^{(l)}$, respectively, by exchanging at most one index. Hence, the telescoping sum

$$p_i p_j - p_{i\vee j} p_{i\wedge j} = \sum_{l=0}^{m} (p_{i^{(l)}} p_{j^{(l)}} - p_{i^{(l+1)}} p_{j^{(l+1)}})$$

lies in I_{Segre}.

Our goal is to find a subset of the generators in Theorem 14.9 that forms a Gröbner basis (compare Chapter 3). More precisely, we seek a Gröbner basis for the ideal

$$P_{\mathcal{T}} := \langle p_i p_j - p_{i\wedge j} p_{i\vee j},\ i, j \in \mathcal{C}(\mathcal{T}) \rangle + \langle p_i \mid i \notin \mathcal{C}(\mathcal{T}) \rangle$$

generated by the homogeneous polynomials in $I_{\mathcal{T}}$. The lexicographic order of binary vectors in the state space $\mathcal{I}$ induces the order

$$p_{0\dots0000} > p_{0\dots0001} > p_{0\dots0010} > p_{0\dots0011} > p_{0\dots0100} > \cdots > p_{1\dots1111}$$

among the p_i, $i \in \mathcal{I}$. With this order of the indeterminates we use a monomial order in $\mathbb{R}[p_i,\, i \in \mathcal{I}]$ that selects the underlined terms in the set

$$\mathcal{G}_{\mathcal{T}} = \{\underline{p_i p_j} - p_{i\vee j} p_{i\wedge j},\ i, j \in \mathcal{C}(\mathcal{T}),\ (i \wedge j) < i < j < (i \vee j)\} \qquad (14.5)$$

as the leading monomials, for example the reverse or the degree-reverse lexicographic order. This monomial order is fixed for the rest of this chapter and underlies all subsequent results. We first consider the case of the star $\mathcal{S}$.

Lemma 14.11 *The polynomials $\mathcal{G}_{\mathcal{S}}$ form a Gröbner basis for $P_{\mathcal{S}}$.*

Proof Let $i, j, k, l \in \mathcal{C}(\mathcal{S}) = \mathcal{I}$ such that $i \neq j$ and $k \neq l$. Then (possibly after relabeling the four states) there exists $u \in S_i \setminus S_j$ and $v \in S_k \setminus S_l$. Set $A := \{u, v\}$ and $B := [n] \setminus A$ and consider the generic matrix

$$\left(p_{(i_A, i_B)}\right)_{i_A \in \mathcal{I}_A,\, i_B \in \mathcal{I}_B} .$$

All 2×2 minors of this matrix are elements of $\mathcal{G}_{\mathcal{S}}$, and they enjoy the Gröbner basis property. In particular, the S-polynomial

$$S(p_i p_j - p_{i\vee j} p_{i\wedge j},\ p_k p_l - p_{k\vee l} p_{k\wedge l})$$

reduces to zero modulo $\mathcal{G}_{\mathcal{S}}$. So, $\mathcal{G}_{\mathcal{S}}$ is a Gröbner basis for $P_{\mathcal{S}}$ by Buchberger's criterion (Theorem 3.10). □

Lemma 14.12 *The polynomials $\mathcal{G}_{\mathcal{T}}$ form a Gröbner basis for $\langle \mathcal{G}_{\mathcal{T}} \rangle = \langle \mathcal{G}_{\mathcal{S}} \rangle \cap \mathbb{R}[p_i,\, i \in \mathcal{C}(\mathcal{T})]$.*

Proof We first show the Gröbner basis property

$$\langle \mathrm{LT}(\mathcal{G}_\mathcal{T}) \rangle = \langle \mathrm{LT}(\langle \mathcal{G}_\mathcal{S} \rangle \cap \mathbb{R}[p_i,\, i \in \mathcal{C}(\mathcal{T})]) \rangle \,.$$

Since $\mathcal{G}_\mathcal{T} \subset \mathcal{G}_\mathcal{S} \cap \mathbb{R}[p_i,\, i \in \mathcal{C}(\mathcal{T})]$, one inclusion is obvious. For the other one, let $f \in \langle \mathcal{G}_\mathcal{S} \rangle \cap \mathbb{R}[p_i,\, i \in \mathcal{C}(\mathcal{T})]$. By Lemma 14.11, $\mathrm{LT}(f)$ is divisible by $\mathrm{LT}(g)$ for some

$$g = p_i p_j - p_{i \wedge j} p_{i \vee j} \;\in\; \mathcal{G}_\mathcal{S}.$$

Since $\mathrm{LT}(f) \in \mathbb{R}[p_i,\, i \in \mathcal{C}(\mathcal{T})]$, also $\mathrm{LT}(g) \in \mathbb{R}[p_i,\, i \in \mathcal{C}(\mathcal{T})]$, i.e. i and j are compatible with $\mathcal{T}$. But then, by Lemma 14.7, $i \wedge j$ and $i \vee j$ are also compatible with $\mathcal{T}$. Hence, $g \in \mathcal{G}_\mathcal{S} \cap \mathbb{R}[p_i,\, i \in \mathcal{C}(\mathcal{T})] = \mathcal{G}_\mathcal{T}$.

It remains to show that $\langle \mathcal{G}_\mathcal{S} \rangle \cap \mathbb{R}[p_i,\, i \in \mathcal{C}(\mathcal{T})] = \langle \mathcal{G}_\mathcal{T} \rangle$ but this follows from the Gröbner basis property of $\mathcal{G}_\mathcal{T}$. □

Theorem 14.13 *For any mutagenetic tree $\mathcal{T}$, the set $\mathcal{G}_\mathcal{T} \cup \{p_i \mid i \notin \mathcal{C}(\mathcal{T})\}$ is a reduced Gröbner basis for the ideal $P_\mathcal{T}$ generated by the homogeneous invariants of $\mathcal{T}$.*

Proof By Buchberger's criterion we need to show that all S-polynomials $S(f, g)$ of elements from $\mathcal{G}_\mathcal{T} \cup \{p_i \mid i \notin \mathcal{C}(\mathcal{T})\}$ reduce to zero. If both f and g are elements of $\mathcal{G}_\mathcal{T}$, this follows from Lemma 14.12. Otherwise, the leading terms of f and g are relatively prime, and hence the S-polynomial reduces to zero.

The Gröbner basis is reduced, because for any $f \in \mathcal{G}_\mathcal{T} \cup \{p_i \mid i \notin \mathcal{C}(\mathcal{T})\}$, no monomial of f lies in $\langle \mathrm{LT}((\mathcal{G}_\mathcal{T} \cup \{p_i \mid i \notin \mathcal{C}(\mathcal{T})\}) \setminus \{f\}) \rangle$ by the definition (14.5) of $\mathcal{G}_\mathcal{T}$. □

We note that these results can also be derived from work of [Hibi, 1987] on algebras with straightening laws on distributive lattices. However, the self-contained derivation given here emphasizes the unexpected relation to independence statements and Bayesian networks.

Theorem 14.13 together with Algorithm 14.5 provides an efficient method for computing a reduced Gröbner basis for the ideal of invariants of a mutagenetic tree model. This approach does not require implicitization (cf. Section 3.2) and the computational complexity is linear in the size of the output, i.e. the size of the Gröbner basis.

Proposition 14.14 *Let $\mathcal{T}$ be a mutagenetic tree on n events.*

(i) *The number of incompatible states is bounded from above by $2^n - n - 1$. This bound is attained if and only if $\mathcal{T}$ is a chain.*
(ii) *The cardinality of $\mathcal{G}_\mathcal{T}$ is bounded from above by $\binom{2^n+1}{2} - 3^n$. This bound is attained if and only if $\mathcal{T}$ is the star $\mathcal{S}$.*

Therefore, the cardinality of the Gröbner basis in Theorem 14.13 is at most of order $O(4^n)$.

Proof The number of compatible states is $n + 1$ for the chain model; cf. Fig. 14.1(d). Any other tree topology has stricly more compatible states; cf. Algorithm 14.5. This proves (i).

The polynomials in $\mathcal{G}_\mathcal{S}$ are indexed by the set of pairs $(i, j) \in \mathcal{I}^2$ with $(i \wedge j) < i < j < (i \vee j)$. We write this index set as the difference

$$\{(i, j) \in \mathcal{I}^2 \mid i \leq j\} \setminus \{(i, j) \in \mathcal{I}^2 \mid i \leq j,\ S_i \subset S_j\}. \tag{14.6}$$

The cardinality of the first set is $\binom{2^n+1}{2}$. For the second set, we group subsets according to their cardinality. A subset of cardinality k has 2^{n-k} supersets. Hence, the second set has cardinality

$$\sum_{k=0}^{n} \binom{n}{n-k} 2^{n-k} = \sum_{k=0}^{n} \binom{n}{k} 2^k 1^{n-k} = (1+2)^n.$$

Since the second set in (14.6) is contained in the first one, the bound in (ii) follows. For the tightness note that if (u, v), $u \neq 0$, is an edge of T, then the polynomial indexed by (i, j) with $S_i = \{u\}$ and $S_j = \{v\}$ is not in $\mathcal{G}_\mathcal{T}$, because j is not a compatible state. □

14.3 Mixture Models

Let $K \in \mathbb{N}_{>0}$ and $(T_1, \ldots, T_K)$ be a family of K mutagenetic trees. Define the map

$$\begin{aligned} \mathbf{f}^{(T_1,\ldots,T_K)} : \Delta_{K-1} \times \Theta^K &\to \Delta = \Delta_{2^n-1} \\ (\lambda, \theta^{(1)}, \ldots, \theta^{(K)}) &\mapsto \sum_{k=1}^{K} \lambda_k \, \mathbf{f}^{(T_k)}(\theta^{(k)}). \end{aligned} \tag{14.7}$$

Definition 14.15 The *K-mutagenetic trees mixture model* $(\mathcal{T}_1, \ldots \mathcal{T}_K) := \mathbf{f}^{(T_1,\ldots,T_K)}(\Delta_{K-1} \times \Theta^K) \subset \Delta$ is given by the map $\mathbf{f}^{(T_1,\ldots,T_K)}$. This algebraic statistical model has parameter space $\Delta_{K-1} \times \Theta^K$ and state space $\mathcal{I}$.

A state $i \in \mathcal{I}$ is *compatible* with the K-mutagenetic trees mixture model $(\mathcal{T}_1, \ldots, \mathcal{T}_K)$ if it is compatible with at least one of the mutagenetic tree models $\mathcal{T}_k = \mathbf{f}^{(T_k)}(\Theta)$, i.e. $\mathcal{C}(\mathcal{T}_1, \ldots, \mathcal{T}_K) = \bigcup_{k=1}^{K} \mathcal{C}(\mathcal{T}_k)$.

Example 14.16 Consider the family (S, T), where S is the star in Figure 14.1(a) and T the tree in Figure 14.1(b). All states $i \in \mathcal{I}$ are compatible with the resulting mixture model $(\mathcal{S},\mathcal{T})$. Two example coordinates of the map $\mathbf{f}^{(S,T)}$ are

$$f_{101}(\lambda,\theta,\bar{\theta}) = \lambda\theta^1_{11}(1-\theta^2_{11})\theta^3_{11},$$
$$f_{100}(\lambda,\theta,\bar{\theta}) = \lambda\theta^1_{11}(1-\theta^2_{11})(1-\theta^3_{11}) + (1-\lambda)\bar{\theta}^1_{11}(1-\bar{\theta}^2_{11}).$$

The coordinates of the map $\mathbf{f}^{(T_1,\ldots,T_K)}$ defining a mutagenetic trees mixture model are multilinear (cf. Example 1.7). The EM algorithm described in Chapter 1 permits to compute the maximum likelihood estimates for mixture models of mutagenetic trees [Beerenwinkel *et al.*, 2004].

Mutagenetic trees mixture models are, like mixture models in general, difficult to study algebraically. Let us consider an example.

Example 14.17 Let (T_1,T_2) be the family of mutagenetic trees defined by the parent vectors $\mathrm{pa}(T_1) = (2,0,0,3)$ and $\mathrm{pa}(T_2) = (0,0,2,3)$. The resulting mixture model $(\mathcal{T}_1,\mathcal{T}_2)$ is of dimension 8. The reduced degree-reverse lexicographic Gröbner basis for the ideal of invariants contains the 6 polynomials p_i, $i \notin \mathcal{C}(\mathcal{T}_1,\mathcal{T}_2) = \mathcal{C}(\mathcal{T}_1)\cup\mathcal{C}(\mathcal{T}_2)$, the sum $\sum_{i\in\mathcal{I}} p_i - 1$, and the degree-5 polynomial

$$p_{0011}p_{0110}p_{0111}p_{1000}p_{1110} - p_{0010}p^2_{0111}p_{1000}p_{1110} - p^2_{0011}p_{0110}p_{1100}p_{1110} + \ldots$$

with 51 terms.

14.3.1 Secant Varieties

Consider the family (T,T) of two mutagenetic trees, in which a single tree is repeated. Then every distribution $p \in (\mathcal{T},\mathcal{T})$ is a convex combination of two distributions $p_T, p'_T \in \mathcal{T}$, i.e. $p = \lambda p_T + (1-\lambda)p'_T$, $\lambda \in [0,1]$. Therefore, $(\mathcal{T},\mathcal{T})$ is a subset of the intersection of the probability simplex Δ with the first secant variety of $\mathbf{f}^{(T)}(\mathbb{C}^{\mathcal{I}})$, i.e. the Zariski closure of the set $\{\lambda p_T + (1-\lambda)p'_T \mid \lambda \in \mathbb{C},\ p_T \neq p'_T \in \mathbb{C}^{\mathcal{I}}\}$. This is the correspondence between mixture models and secant varieties mentioned on page 1; see also Chapter 3.

If T is a chain, then every node in T has at most one child and $|\mathcal{C}(\mathcal{T})| = n+1$. The chain model $\mathcal{T}$ is equal to the n-dimensional variety obtained by intersecting the probability simplex Δ with the $2^n - n - 1$ hyperplanes $p_i = 0$, $i \notin \mathcal{C}(\mathcal{T})$. Since $\mathcal{C}(\mathcal{T},\mathcal{T}) = \mathcal{C}(\mathcal{T})$ and $\mathcal{T} \subset (\mathcal{T},\mathcal{T})$ it follows that the chain mixture model is trivial in the sense that $(\mathcal{T},\mathcal{T}) = \mathcal{T}$.

If $T = S$ is the star, then the mixture model $(\mathcal{S},\mathcal{S})$ is also known as a naive Bayes model (compare Proposition 14.19). In algebraic terms it is the first secant variety of the Segre variety. It has been shown that $\dim(\mathcal{S},\mathcal{S}) = \min(2n+1, 2^n-1)$ in this case [Catalisano *et al.*, 2002, Garcia, 2004].

Let us consider an example of a tree that is neither a chain nor the star.

Example 14.18 Let T be the tree over $n = 4$ events with vector of parents $\mathrm{pa}(T) = (2, 0, 0, 3)$. Then $\dim(\mathcal{T}, \mathcal{T}) = 7$, whereas $\dim(\mathcal{T}) = 4$. The reduced degree-reverse lexicographic Gröbner basis for the ideal of invariants of $\mathcal{M}$ contains the 7 polynomials p_i, $i \notin \mathcal{C}(\mathcal{T}, \mathcal{T}) = \mathcal{C}(\mathcal{T})$, the sum $\sum_{i \in \mathcal{I}} p_i - 1$, as well as a polynomial of degree 3 with 22 terms.

The K-mutagenetic trees mixture models resulting from repeating a single tree K times correspond algebraically to the K-th secant variety of the single tree model. The following proposition and its proof are in analogy to Theorem 14.6.

Proposition 14.19 *Let T be a mutagenetic tree and $K \in \mathbb{N}_{>0}$. Let M be the directed acyclic graph obtained from T by adding the edges $(0, v)$, $v \in [n]$, from the root 0 to every node v. Associating a hidden random variable X_0 with K levels with the root node 0 induces a directed graphical model $\mathcal{M}$ with one hidden variable. Then a probability distribution $p \in \Delta$ is in the K-mutagenetic trees mixture model $(T, \ldots, T)$ if and only if $p \in \mathcal{M}$ and $p_i = 0$ for all $i \notin \mathcal{C}(\mathcal{T})$.*

14.3.2 The Uniform Star as an Error Model

If the observations contain a state that is incompatible with a tree model $\mathcal{T}$, then the likelihood function of $\mathcal{T}$ is constant and equal to zero. Thus, in the presence of false positives and false negatives the maximum likelihood tree will often be the star or have a star-like topology despite the fact that other pathways may be significantly overrepresented in the data. One way to account for such states is to mix a mutagenetic tree with a uniform star model; see [Szabo and Boucher, 2002] for an alternative approach.

Definition 14.20 Let S be the star over n events. The 1-dimensional *uniform star model* $\mathcal{S}_{\mathrm{uni}} := \mathbf{f}^{(S_{\mathrm{uni}})}([0, 1]) \subset \Delta$ is given by the specialization map $\mathbf{f}^{(S_{\mathrm{uni}})}(\theta_{11}) = \mathbf{f}^{(S)}(\theta_{11}, \ldots, \theta_{11})$.

Note that in the uniform star model the n events occur independently with the same probability. This is our error model.

Algebraically the uniform star model is the intersection of the probability simplex with the rational normal curve of degree n, i.e. the image of the Veronese map $\mathbb{P}^1 \to \mathbb{P}^n$. To see this note that the coordinates of $\mathbf{f}$ only depend on the number $k = |S_i|$ of occurred events: $f_i(\theta_{11}) = \theta_{11}^k (1 - \theta_{11})^{n-k}$. This means that we can identify the ideal $I_{\mathcal{S}_{\mathrm{uni}}}$ with its image in the ring $\mathbb{R}[p_k,\, k = 0, \ldots, n]$ under the ring homomorphism induced by $i \mapsto |S_i|$. In this ring, $I_{\mathcal{S}_{\mathrm{uni}}}$ is generated by the quadrics (Theorem 14.9)

$$p_{i_1}^{k_1}p_{i_2}^{k_2} - p_{j_1}^{l_1}p_{j_2}^{l_2}, \quad k_1i_1 + k_2i_2 = l_1j_1 + l_2j_2,$$
$$0 \le k_1, k_2, l_1, l_2 \le 2, \quad 0 \le i_1, i_2, j_1, j_2 \le n.$$

These terms are exactly the 2×2 minors of the $2 \times n$ matrix

$$\begin{pmatrix} p_0 & p_1 & p_2 & \cdots & p_{n-1} \\ p_1 & p_2 & p_3 & \cdots & p_n \end{pmatrix},$$

the defining polynomials of the rational normal curve of degree n.

Proposition 14.21 *Let $n \ge 3$. Then for any n-dimensional mutagenetic tree model $\mathcal{T}$ the mixture model $(\mathcal{S}_{\mathrm{uni}}, \mathcal{T})$ has dimension $n+2$.*

Proof Clearly, $\dim(\mathcal{S}_{\mathrm{uni}}, \mathcal{T}) \le n+2$ because $\dim(\mathcal{T}) = n$ and $\dim(\mathcal{S}_{\mathrm{uni}}) = 1$. Thus, we have to show that the dimension may not drop below $n+2$.

Consider first a tree $T \ne S$. It is easy to see that $|\mathcal{I} \setminus \mathcal{C}(\mathcal{T})| \ge 2$, because $n \ge 3$. Choosing two states $j, j' \notin \mathcal{C}(\mathcal{T})$ such that $p_j = p_{j'} = 0$ for all $p \in \mathcal{T}$, we obtain that the Jacobian matrix J of the map $\mathbf{f}^{(S_{\mathrm{uni}},T)}$ is upper triangular

$$J = \begin{pmatrix} \lambda \times J_T & * \\ 0 & J_{j,j'} \end{pmatrix}, \quad \text{where} \quad J_T = \left(\frac{\partial f_i}{\partial \theta_{11}^v}\right)_{i \in \mathcal{C}(\mathcal{T}) \setminus \{j,j'\},\, v \in [n]}.$$

The matrix J_T depends only on $(\theta_{11}^1, \ldots, \theta_{11}^n)$ and up to deletion of two rows of zeros it is the Jacobian matrix of the map $\mathbf{f}^{(T)}$ and, thus, of full rank in the interior of the parameter space of $(\mathcal{S}_{\mathrm{uni}}, \mathcal{T})$. The matrix

$$J_{j,j'} = \begin{pmatrix} \frac{\partial f_j}{\partial \lambda} & \frac{\partial f_j}{\partial \theta_{11}} \\ \frac{\partial f_{j'}}{\partial \lambda} & \frac{\partial f_{j'}}{\partial \theta_{11}} \end{pmatrix}$$

depends only on (λ, θ_{11}) and its determinant equals $1 - \lambda$ times a univariate polynomial $g(\theta_{11})$. Since g has only finitely many roots, it holds almost everywhere that the matrix $J_{j,j'}$ is of full rank 2 and the Jacobian J of full rank $n+2$. Therefore, $\dim(\mathcal{S}_{\mathrm{uni}}, \mathcal{T}) = n+2$; compare [Geiger *et al.*, 2001].

If $T = S$ is the star, then we know that the mixture model $(\mathcal{S}_{\mathrm{uni}}, \mathcal{S})$ is obtained by parameter specialization from $(\mathcal{S}, \mathcal{S})$. As mentioned in Section 14.3.1, $\dim(\mathcal{S}, \mathcal{S}) = 2n+1$ and thus the Jacobian of the map $\mathbf{f}^{(S,S)}$ is of full rank $2n+1$ almost everywhere. Now it follows from the chain rule that

$$\frac{\partial f_i^{(S_{\mathrm{uni}},S)}}{\partial \theta_{11}} = \sum_{v \in [n]} \frac{\partial f_i^{(S,S)}}{\partial \theta_{11}^v}\Big|_{\theta_{11}^v = \theta_{11}},$$

which implies that the Jacobian of the map $\mathbf{f}^{(S_{\mathrm{uni}},S)}$ is of full rank $n+2$. □

15
Catalog of Small Trees

Marta Casanellas

Luis David Garcia

Seth Sullivant

This chapter is concerned with the description of the Small Trees website which can be found at the following web address:

`http://www.math.tamu.edu/∼lgp/small-trees/small-trees.html`

The goal of the website is to make available in a unified format various algebraic features of different phylogenetic models. In the first section, we describe a detailed set of notational conventions for describing the phylogenetic models on trees which are listed on this website. This includes conventions for writing down the parameterizations given a tree as well as describing the Fourier transform and writing down phylogenetic invariants in Fourier coordinates. The second section gives a brief description of each of the types of algebraic information which are associated to a model and a tree on the Small Trees website. The third section contains an example of a page on the website. The final section is concerned with simulation studies of using algebraic invariants to recover phylogenies using the invariants for the Kimura 3–parameter model.

15.1 Notational Conventions

15.1.1 Labeling trees

We assume that each phylogenetic model is presented with a particular tree T together with a figure representing that tree. The figures of trees with up to five leaves will be the ones that can be found on the Small Trees website.

15.1.1.1 Rooted trees

If T is a rooted tree, there is a distinguished vertex of T called the root and labeled by the letter r. The tree T should be drawn with the root r at the top of the figure and the edges of the tree below the root. Each edge in the tree is labeled with a lowercase letter $a, b, c, \ldots$. The edges are labeled in alphabetical order starting at the upper left hand corner, proceeding left to right and top to bottom. The leaves are labeled with the numbers $1, 2, 3, \ldots$ starting with the left–most leaf and proceeding left to right. Figure 15.1 shows the "giraffe" tree with four leaves and its labeling.

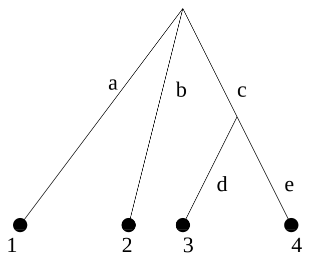

Fig. 15.1. The giraffe tree on four leaves

15.1.1.2 Unrooted trees

If T is an unrooted tree, it should be drawn with the leaves in a circle. The edges of T are labeled with lower–case letters $a, b, c, \ldots$ in alphabetical order starting at the upper left–hand corner of the figure and proceeding left to right and top to bottom. The leaves are labeled with the numbers $1, 2, 3, \ldots$ starting at the first leaf "left of 12 o'clock" and proceeding counterclockwise around the perimeter of the tree. Figure 15.2 illustrates this on the "quartet" tree.

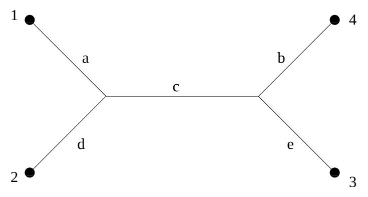

Fig. 15.2. The quartet tree on four leaves

15.1.2 Parameterizations

Associated to each node in a model is a random variable with two or four states depending on whether we are looking at binary data or DNA data. In the case of binary data these states are $\{0, 1\}$ and for DNA data they are $\{A, C, G, T\}$ in this order.

15.1.2.1 Root Distribution

The root distribution is a vector of length two or four depending on whether the model is for binary or DNA sequences. The name of this vector is r. Its entries are parameters $r_0, r_1, r_2, \ldots$ and are filled in from left to right and are recycled as the model requires.

Example 15.1 In the general strand symmetric model r always denotes the vector

$$r = (r_0, r_1, r_1, r_0).$$

We tacitly assume that the entries in r sum to 1, though we do not eliminate a parameter to take this into account. If the model assumes a uniform root distribution, then r has the form $r = (1/2, 1/2)$ or $r = (1/4, 1/4, 1/4, 1/4)$ according to whether the model is for binary or DNA data.

15.1.2.2 Transition Matrices

In each type of model, the letters $a, b, c, \ldots$ which label the edges are also the transition matrices in the model. These are either 2×2 or 4×4 matrices depending on whether the model is a model for binary data or DNA data. In each case, the matrix is filled from left to right and top to bottom with unknown parameters, recycling a parameter whenever the model requires it. For the transition matrix of the edge labeled with x these entries are called $x_0, x_1, x_2, \ldots$.

Example 15.2 For example, in the Kimura 3–parameter model the letter a represents the matrix

$$a = \begin{pmatrix} a_0 & a_1 & a_2 & a_3 \\ a_1 & a_0 & a_3 & a_2 \\ a_2 & a_3 & a_0 & a_1 \\ a_3 & a_2 & a_1 & a_0 \end{pmatrix}.$$

The Kimura 2–parameter and Jukes–Cantor models give rise to specializations of the parameters in the Kimura 3–parameter model, and hence the letters denoting the parameters are recycled. For instance, the letter c in the Jukes–Cantor DNA model and the letter d in the Kimura 2–parameter model represent the following matrices

$$c = \begin{pmatrix} c_0 & c_1 & c_1 & c_1 \\ c_1 & c_0 & c_1 & c_1 \\ c_1 & c_1 & c_0 & c_1 \\ c_1 & c_1 & c_1 & c_0 \end{pmatrix}, \qquad d = \begin{pmatrix} d_0 & d_1 & d_2 & d_1 \\ d_1 & d_0 & d_1 & d_2 \\ d_2 & d_1 & d_0 & d_1 \\ d_1 & d_2 & d_1 & d_0 \end{pmatrix}.$$

In the general strand symmetric model the letter e always represents the matrix

$$e = \begin{pmatrix} e_0 & e_1 & e_2 & e_3 \\ e_4 & e_5 & e_6 & e_7 \\ e_7 & e_6 & e_5 & e_4 \\ e_3 & e_2 & e_1 & e_0 \end{pmatrix}.$$

We assume that the entries of these matrices satisfy additional linear constraints which make them into transition matrices. For instance, in the Jukes-Cantor DNA model, this constraint is $c_0 + 3c_1 = 1$ and in the general strand symmetric model the two linear relations are $e_0 + e_1 + e_2 + e_3 = 1$ and $e_4 + e_5 + e_6 + e_7 = 1$. We do not, however, use these linear relations to eliminate parameters.

15.1.2.3 Molecular Clock Assumption

The molecular clock (MC) assumption for a rooted tree T is defined as the assumption that, for each subtree, along each path from the root of that subtree to any leave i the product of the transition matrices corresponding to the edges are identical. As the edges in the path are read down the tree, the matrices are multiplied left to right.

Example 15.3 For the giraffe tree in Figure 15.1 the MC assumption translates into the following identities:

$$a = b = cd = ce \text{ and } d = e.$$

These equalities of products of parameter matrices suggest that some parameter matrices should be replaced with products of other parameter matrices and their inverses. This makes the parameterization involve rational functions (instead of just polynomials).

Here is a systematic rule for making these replacements. Starting from the bottom of the tree, make replacements for transition matrices. Each vertex in the tree induces equalities among products of transition matrices along all paths emanating downward from this vertex. Among the edges emanating downward from a given vertex, all but one of the transition matrices for these edges will be replaced by a product of other transition matrices and their inverses. When choosing replacements, always replace the transition matrix which belongs to the shorter path to a leaf. If all such paths have the same length, replace the matrices which belong to the left most edges emanating from a vertex.

Example 15.4 In the 4–leaf giraffe tree from the previous example, we replace the matrix d with e and we replace the matrices a and b with ce. Thus, when we write the parameterization in probability coordinates only the letters c and e will appear in the parameterizing polynomials.

15.1.2.4 Specifying the Joint Distribution

The probabilities of the leaf colorations of a tree with n leaves are denoted by p_W where W is a word of length n in the alphabet $\{0,1\}$ or $\{A,C,G,T\}$. Every probability indeterminate p_W is a polynomial in the parameters of the model. Two of these probabilities p_W and p_U are equivalent if their defining polynomials are identical. This divides the 2^n or 4^n probabilities into equivalence classes. The elements of each class are ordered lexicographically, and the classes are ordered lexicographically by their lexicographically first elements.

Example 15.5 For the Jukes–Cantor DNA model with uniform root distribution on a three taxa claw tree there are five equivalence classes:

- **Class 1:** $p_{AAA}\ p_{CCC}\ p_{GGG}\ p_{TTT}$
- **Class 2:** $p_{AAC}\ p_{AAG}\ p_{AAT}\ p_{CCA}\ p_{CCG}\ p_{CCT}\ p_{GGA}\ p_{GGC}\ p_{GGT}\ p_{TTA}\ p_{TTC}\ p_{TTG}$
- **Class 3:** $p_{ACA}\ p_{AGA}\ p_{ATA}\ p_{CAC}\ p_{CGC}\ p_{CTC}\ p_{GAG}\ p_{GCG}\ p_{GTG}\ p_{TAT}\ p_{TCT}\ p_{TGT}$
- **Class 4:** $p_{ACC}\ p_{AGG}\ p_{ATT}\ p_{CAA}\ p_{CGG}\ p_{CTT}\ p_{GAA}\ p_{GCC}\ p_{GTT}\ p_{TAA}\ p_{TCC}\ p_{TGG}$
- **Class 5:** $p_{ACG}\ p_{ACT}\ p_{AGC}\ p_{AGT}\ p_{ATC}\ p_{ATG}\ p_{CAG}\ p_{CAT}\ p_{CGA}\ p_{CGT}\ p_{CTA}\ p_{CTG}\ p_{GAC}\ p_{GAT}\ p_{GCA}\ p_{GCT}\ p_{GTA}\ p_{GTC}\ p_{TAC}\ p_{TAG}\ p_{TCA}\ p_{TCG}\ p_{TGA}\ p_{TGC}$

For each class i there will be an indeterminate p_i which denotes the sum of the probabilities in the class i. For these N probabilities the expression for the probability p_i as a polynomial or rational function in the parameters appears on the webpage (if these expressions are small enough) or in a separate linked page for longer expressions.

Example 15.6 In the 3–taxa claw tree with Jukes–Cantor model and uniform root distribution these indeterminates are:

$$\begin{aligned}
p_1 &= a_0b_0c_0 + 3a_1b_1c_1 \\
p_2 &= 3a_0b_0c_1 + 3a_1b_1c_0 + 6a_1b_1c_1 \\
p_3 &= 3a_0b_1c_0 + 3a_1b_0c_1 + 6a_1b_1c_1 \\
p_4 &= 3a_1b_0c_0 + 3a_0b_1c_1 + 6a_1b_1c_1 \\
p_5 &= 6a_0b_1c_1 + 6a_1b_0c_1 + 6a_1b_1c_0 + 6a_1b_1c_1
\end{aligned}$$

Note that $p_1+p_2+p_3+p_4+p_5 = 1$ after substituting $a_0 = 1-3a_1$, $b_0 = 1-3b_1$ and $c_0 = 1-3c_1$.

15.1.3 Fourier Coordinates

Often we will describe these phylogenetic models in an alternate coordinate system called the Fourier coordinates. This change of coordinates happens simultaneously on the parameters and on the probability coordinates themselves.

15.1.3.1 Full Fourier Transform

Each of the 2^n or 4^n Fourier coordinate are denoted by q_W where W is a word in either $\{0,1\}$ or $\{A,C,G,T\}$.

The Fourier transform from p_U to q_W is given by the following rule:

$$p_{i_1\cdots i_n} = \sum_{j_1,\dots,j_n} \chi^{j_1}(i_1)\cdots\chi^{j_n}(i_n) q_{j_1\cdots j_n},$$
$$q_{i_1\cdots i_n} = \frac{1}{k^n}\sum_{j_1,\dots,j_n} \chi^{i_1}(j_1)\cdots\chi^{i_n}(j_n) p_{i_1\cdots i_n}.$$

Here χ^i is the character of the group associated to the ith group element. The character tables of the groups we use, namely $\mathbb{Z}_2$ and $\mathbb{Z}_2\times\mathbb{Z}_2$ are:

	0	1
0	1	1
1	1	−1

and

	A	C	G	T
A	1	1	1	1
C	1	−1	1	−1
G	1	1	−1	−1
T	1	−1	−1	1

In other words, $\chi^i(j)$ is the (i,j) entry in the appropriate character table. One special feature of this transformation is that the Fourier transform of the joint distribution has a parameterization that can be written in product form; we refer to [Evans and Speed, 1993, Sturmfels and Sullivant, 2004, Székely *et al.*, 1993] for a detailed treatment of the subject. Equivalently, the Fourier transform simultaneously diagonalizes all transition matrices. Therefore, we replace the transition matrices $a, b, c, \dots$ for diagonal matrices denoted $A, B, C, \dots$, where A has diagonal elements A_1, A_2, A_3, A_4; B has diagonal elements B_1, B_2, B_3, B_4; etc. Since we will only use the entries of the previous diagonal matrices, there will be no confusion, for example, between the matrix A and the base A. Furthermore, these parameters must satisfy the relations imposed by the corresponding model and the Molecular Clock assumption. For instance, in the Jukes–Cantor model we have the relations $A_2 = A_3 = A_4$, $B_2 = B_3 = B_4$.

The q_W are polynomials or rational functions in the transformed parameters.

They are given parametrically as

$$q_{i_1 \cdots i_n} := \begin{cases} \prod_{e \in E} M_e(k_e) & \text{if } i_n = i_1 + i_2 + \cdots + i_{n-1} \text{ in the group} \\ 0 & \text{otherwise} \end{cases}$$

where M_e is the corresponding diagonal matrix associated to edge e, and k_e is the sum (in the corresponding group) of the labels at the leaves that are "beneath" the edge e.

We say that q_W and q_U are equivalent if they represent the same polynomial in terms of these parameters. These Fourier coordinates are grouped into equivalence classes. The elements in the equivalence classes are ordered lexicographically. Most of the Fourier coordinates q_W are zero and these are grouped in class 0. The others are ordered Class 1, Class 2, lexicographically by their lexicographically first element.

Example 15.7 Here we display the classes of Fourier coordinates for the Jukes–Cantor DNA model on the 3 leaf claw tree.

- **Class 0:** $q_{AAC}\ q_{AAT}\ \ldots$
- **Class 1:** q_{AAA}
- **Class 2:** $q_{ACC}\ q_{AGG}\ q_{ATT}$
- **Class 3:** $q_{CAC}\ q_{GAG}\ q_{TAT}$
- **Class 4:** $q_{CCA}\ q_{GGA}\ q_{TTA}$
- **Class 5:** $q_{CGT}\ q_{CTG}\ q_{GCT}\ q_{GTC}\ q_{TCG}\ q_{TGC}$

We replace each of the Fourier coordinates in class i by the new Fourier coordinate q_i. We take q_i to be the *average* of the q_W in class i since this operation is better behaved with respect to writing down invariants.

15.1.3.2 Specialized Fourier Transform

We also record explicitly the linear transformation between the p_i and the q_i by recording a certain rational matrix which describes this transformation. This is the *specialized Fourier transform.* In general, this matrix will not be a square matrix. This is because there may be additional linear relations among the p_i which are encoded in the different q_i classes. Because of this ambiguity, we also explicitly list the inverse map.

It is possible to obtain the matrix that represents the specialized Fourier transform from the matrix that represents the full Fourier transform. If M represents the matrix of the full Fourier transform and N the matrix of the specialized Fourier transform, then N_{ij}, (the entry indexed by the ith Fourier class and the jth probability class) is given by the formula:

$$N_{ij} = \frac{1}{|C_i||D_j|} \sum_{U \in C_i} \sum_{W \in D_j} M_{UW}$$

where C_i is the ith equivalence class of Fourier coordinates and D_j is the jth equivalence class of probability coordinates. We do not include the 0th equivalence class of Fourier coordinates in the previous formula.

Example 15.8 In the Jukes–Cantor DNA model on the 3 leaf claw tree the specialized Fourier transform matrix is

$$\begin{pmatrix} 1 & 1 & 1 & 1 & 1 \\ 1 & 1 & -\frac{1}{3} & -\frac{1}{3} & -\frac{1}{3} \\ 1 & -\frac{1}{3} & 1 & -\frac{1}{3} & -\frac{1}{3} \\ 1 & -\frac{1}{3} & -\frac{1}{3} & 1 & -\frac{1}{3} \\ 1 & -\frac{1}{3} & -\frac{1}{3} & -\frac{1}{3} & \frac{1}{3} \end{pmatrix}.$$

15.2 Description of website features

We give a brief description of the various items described on the website.

Dimension (D): The dimension of the model.

Degree (d): The degree of the model. Algebraically, this is defined as the number of points in the intersection of the model and a generic (i.e. “random”) subspace of dimension 4^n minus the dimension of the model.

Maximum Likelihood Degree (mld): The maximum likelihood degree of the model. See section 3.

Number of Probability Coordinates (np): Number of equivalences classes of the probability coordinates. See the preceding section.

Number of Fourier Coordinates (nq): Number of equivalence classes of Fourier coordinates without counting Class 0 (see the preceding section). This is also the dimension of the smallest linear space that contains the model.

Specialized Fourier Transform: See the preceding section for a description.

Phylogenetic Invariants: A list of generators of the prime ideal of phylogenetic invariants. These are given in the Fourier coordinates.

Singularity Dimension (sD): The dimension of the set of singular points on the model.

Singularity Degree (sd): The algebraic degree of the set of singular points on the model.

15.3 Example

Here we describe the Jukes–Cantor model on the quartet tree (see Figure 15.2) in more detail.

Dimension: $D = 5$ (note that there are only 5 independent parameters, one for each transition matrix.)

Degree: $d = 34$.

Number of Probability Coordinates: $np = 15$ and the classes are represented by:

$$\begin{aligned}
p_1 &= a_0b_0c_0d_0e_0 + 3a_1b_0c_1d_1e_0 + 3a_0b_1c_1d_0e_1 + 3a_1b_1c_0d_1e_1 + 6a_1b_1c_1d_1e_1,\\
p_2 &= 3(a_0b_1c_0d_0e_0 + 3a_1b_1c_1d_1e_0 + a_0b_0c_1d_0e_1 + 2a_0b_1c_1d_0e_1\\
&\quad + a_1b_0c_0d_1e_1 + 2a_1b_1c_0d_1e_1 + 2a_1b_0c_1d_1e_1 + 4a_1b_1c_1d_1e_1),\\
p_3 &= 3(a_0b_1c_1d_0e_0 + a_1b_1c_0d_1e_0 + 2a_1b_1c_1d_1e_0 + a_0b_0c_0d_0e_1\\
&\quad + 2a_0b_1c_1d_0e_1 + 2a_1b_1c_0d_1e_1 + 3a_1b_0c_1d_1e_1 + 4a_1b_1c_1d_1e_1),\\
p_4 &= 3(a_0b_0c_1d_0e_0 + a_1b_0c_0d_1e_0 + 2a_1b_0c_1d_1e_0 + a_0b_1c_0d_0e_1\\
&\quad + 2a_0b_1c_1d_0e_1 + 2a_1b_1c_0d_1e_1 + 7a_1b_1c_1d_1e_1),\\
p_5 &= 6(a_0b_1c_1d_0e_0 + a_1b_1c_0d_1e_0 + 2a_1b_1c_1d_1e_0 + a_0b_1c_0d_0e_1 + a_0b_0c_1d_0e_1\\
&\quad + a_0b_1c_1d_0e_1 + a_1b_0c_0d_1e_1 + a_1b_1c_0d_1e_1 + 2a_1b_0c_1d_1e_1 + 5a_1b_1c_1d_1e_1),\\
p_6 &= 3(a_1b_0c_1d_0e_0 + a_0b_0c_0d_1e_0 + 2a_1b_0c_1d_1e_0 + a_1b_1c_0d_0e_1\\
&\quad + 2a_1b_1c_1d_0e_1 + 2a_1b_1c_0d_1e_1 + 3a_0b_1c_1d_1e_1 + 4a_1b_1c_1d_1e_1),\\
p_7 &= 3(a_1b_1c_1d_0e_0 + a_0b_1c_0d_1e_0 + 2a_1b_1c_1d_1e_0 + a_1b_0c_0d_0e_1 + 2a_1b_1c_1d_0e_1\\
&\quad + 2a_1b_1c_0d_1e_1 + a_0b_0c_1d_1e_1 + 2a_1b_0c_1d_1e_1 + 2a_0b_1c_1d_1e_1 + 2a_1b_1c_1d_1e_1),\\
p_8 &= 6(a_1b_1c_1d_0e_0 + a_0b_1c_0d_1e_0 + 2a_1b_1c_1d_1e_0 + a_1b_1c_0d_0e_1\\
&\quad + a_1b_0c_1d_0e_1 + a_1b_1c_1d_0e_1 + a_1b_0c_0d_1e_1 + a_1b_1c_0d_1e_1\\
&\quad + a_0b_0c_1d_1e_1 + a_1b_0c_1d_1e_1 + 2a_0b_1c_1d_1e_1 + 3a_1b_1c_1d_1e_1),\\
p_9 &= 3(a_1b_1c_0d_0e_0 + a_0b_1c_1d_1e_0 + 2a_1b_1c_1d_1e_0 + a_1b_0c_1d_0e_1 + 2a_1b_1c_1d_0e_1\\
&\quad + a_0b_0c_0d_1e_1 + 2a_1b_1c_0d_1e_1 + 2a_1b_0c_1d_1e_1 + 2a_0b_1c_1d_1e_1 + 2a_1b_1c_1d_1e_1),\\
p_{10} &= 3(a_1b_0c_0d_0e_0 + a_0b_0c_1d_1e_0 + 2a_1b_0c_1d_1e_0 + 3a_1b_1c_1d_0e_1\\
&\quad + a_0b_1c_0d_1e_1 + 2a_1b_1c_0d_1e_1 + 2a_0b_1c_1d_1e_1 + 4a_1b_1c_1d_1e_1),\\
p_{11} &= 6(a_1b_1c_0d_0e_0 + a_0b_1c_1d_1e_0 + 2a_1b_1c_1d_1e_0 + a_1b_0c_1d_0e_1\\
&\quad + 2a_1b_1c_1d_0e_1 + a_1b_0c_0d_1e_1 + a_0b_1c_0d_1e_1 + a_1b_1c_0d_1e_1\\
&\quad + a_0b_0c_1d_1e_1 + a_1b_0c_1d_1e_1 + a_0b_1c_1d_1e_1 + 3a_1b_1c_1d_1e_1),\\
p_{12} &= 6(a_1b_1c_1d_0e_0 + a_1b_1c_0d_1e_0 + a_0b_1c_1d_1e_0 + a_1b_1c_1d_1e_0\\
&\quad + a_1b_1c_0d_0e_1 + a_1b_0c_1d_0e_1 + a_1b_1c_1d_0e_1 + a_0b_0c_0d_1e_1\\
&\quad + a_1b_1c_0d_1e_1 + 2a_1b_0c_1d_1e_1 + 2a_0b_1c_1d_1e_1 + 3a_1b_1c_1d_1e_1),\\
p_{13} &= 6(a_1b_1c_1d_0e_0 + a_1b_1c_0d_1e_0 + a_0b_1c_1d_1e_0 + a_1b_1c_1d_1e_0\\
&\quad + a_1b_0c_0d_0e_1 + 2a_1b_1c_1d_0e_1 + a_0b_1c_0d_1e_1 + a_1b_1c_0d_1e_1\\
&\quad + a_0b_0c_1d_1e_1 + 2a_1b_0c_1d_1e_1 + a_0b_1c_1d_1e_1 + 3a_1b_1c_1d_1e_1),
\end{aligned}$$

$$\begin{aligned}
p_{14} = 6(&a_1b_0c_1d_0e_0 + a_1b_0c_0d_1e_0 + a_0b_0c_1d_1e_0 + a_1b_0c_1d_1e_0 + a_1b_1c_0d_0e_1 \\
&+ 2a_1b_1c_1d_0e_1 + a_0b_1c_0d_1e_1 + a_1b_1c_0d_1e_1 + 2a_0b_1c_1d_1e_1 + 5a_1b_1c_1d_1e_1), \\
p_{15} = 6(&a_1b_1c_1d_0e_0 + a_1b_1c_0d_1e_0 + a_0b_1c_1d_1e_0 + a_1b_1c_1d_1e_0 + a_1b_1c_0d_0e_1 \\
&+ a_1b_0c_1d_0e_1 + a_1b_1c_1d_0e_1 + a_1b_0c_0d_1e_1 + a_0b_1c_0d_1e_1 + a_0b_0c_1d_1e_1 \\
&+ a_1b_0c_1d_1e_1 + a_0b_1c_1d_1e_1 + 4a_1b_1c_1d_1e_1).
\end{aligned}$$

Number of Fourier Coordinates: $nq = 13$. The classes are:

$$\begin{aligned}
q_1 &= q_{AAAA}, \\
q_2 &= q_{AACC}, q_{AAGG}, q_{AATT}, \\
q_3 &= q_{ACAC}, q_{AGAG}, q_{ATAT}, \\
q_4 &= q_{ACCA}, q_{AGGA}, q_{ATTA}, \\
q_5 &= q_{ACGT}, q_{ACTG}, q_{AGCT}, q_{AGTC}, q_{ATCG}, q_{ATGC}, \\
q_6 &= q_{CAAC}, q_{GAAG}, q_{TAAT}, \\
q_7 &= q_{CACA}, q_{GAGA}, q_{TATA}, \\
q_8 &= q_{CAGT}, q_{CATG}, q_{GACT}, q_{GATC}, q_{TACG}, q_{TAGC}, \\
q_9 &= q_{CCAA}, q_{GGAA}, q_{TTAA}, \\
q_{10} &= q_{CCCC}, q_{CCGG}, q_{CCTT}, q_{GGCC}, q_{GGGG}, q_{GGTT}, \\
&\quad\ q_{TTCC}, q_{TTGG}, q_{TTTT}, \\
q_{11} &= q_{CGAT}, q_{CTAG}, q_{GCAT}, q_{GTAC}, q_{TCAG}, q_{TGAC}, \\
q_{12} &= q_{CGCG}, q_{CGGC}, q_{CTCT}, q_{CTTC}, q_{GCCG}, q_{GCGC}, \\
&\quad\ q_{GTGT}, q_{GTTG}, q_{TCCT}, q_{TCTC}, q_{TGGT}, q_{TGTG}, \\
q_{13} &= q_{CGTA}, q_{CTGA}, q_{GCTA}, q_{GTCA}, q_{TCGA}, q_{TGCA}.
\end{aligned}$$

Specialized Fourier Transform:

$$\begin{array}{rrrrrrrrrrrrrrr}
1 & 1 & 1 & 1 & 1 & 1 & 1 & 1 & 1 & 1 & 1 & 1 & 1 & 1 & 1 \\
1 & -\frac{1}{3} & -\frac{1}{3} & 1 & -\frac{1}{3} & 1 & -\frac{1}{3} & -\frac{1}{3} & -\frac{1}{3} & 1 & -\frac{1}{3} & -\frac{1}{3} & -\frac{1}{3} & 1 & -\frac{1}{3} \\
1 & -\frac{1}{3} & 1 & -\frac{1}{3} & -\frac{1}{3} & -\frac{1}{3} & 1 & -\frac{1}{3} & -\frac{1}{3} & 1 & -\frac{1}{3} & -\frac{1}{3} & 1 & -\frac{1}{3} & -\frac{1}{3} \\
1 & 1 & -\frac{1}{3} & -\frac{1}{3} & -\frac{1}{3} & -\frac{1}{3} & -\frac{1}{3} & -\frac{1}{3} & 1 & 1 & 1 & -\frac{1}{3} & -\frac{1}{3} & -\frac{1}{3} & -\frac{1}{3} \\
1 & -\frac{1}{3} & -\frac{1}{3} & -\frac{1}{3} & \frac{1}{3} & -\frac{1}{3} & -\frac{1}{3} & \frac{1}{3} & -\frac{1}{3} & 1 & -\frac{1}{3} & \frac{1}{3} & -\frac{1}{3} & -\frac{1}{3} & \frac{1}{3} \\
1 & -\frac{1}{3} & 1 & -\frac{1}{3} & -\frac{1}{3} & 1 & -\frac{1}{3} & -\frac{1}{3} & 1 & -\frac{1}{3} & -\frac{1}{3} & 1 & -\frac{1}{3} & -\frac{1}{3} & -\frac{1}{3} \\
1 & 1 & -\frac{1}{3} & -\frac{1}{3} & -\frac{1}{3} & 1 & 1 & 1 & -\frac{1}{3} & -\frac{1}{3} & -\frac{1}{3} & -\frac{1}{3} & -\frac{1}{3} & -\frac{1}{3} & -\frac{1}{3} \\
1 & -\frac{1}{3} & -\frac{1}{3} & -\frac{1}{3} & \frac{1}{3} & 1 & -\frac{1}{3} & -\frac{1}{3} & -\frac{1}{3} & -\frac{1}{3} & \frac{1}{3} & -\frac{1}{3} & \frac{1}{3} & -\frac{1}{3} & \frac{1}{3} \\
1 & 1 & 1 & 1 & 1 & -\frac{1}{3} & -\frac{1}{3} & -\frac{1}{3} & -\frac{1}{3} & -\frac{1}{3} & -\frac{1}{3} & -\frac{1}{3} & -\frac{1}{3} & -\frac{1}{3} & -\frac{1}{3} \\
1 & -\frac{1}{3} & -\frac{1}{3} & 1 & -\frac{1}{3} & -\frac{1}{3} & 1 & -\frac{1}{3} & 1 & -\frac{1}{3} & -\frac{1}{3} & -\frac{1}{3} & -\frac{1}{3} & -\frac{1}{3} & 1 \\
1 & -\frac{1}{3} & 1 & -\frac{1}{3} & -\frac{1}{3} & -\frac{1}{3} & -\frac{1}{3} & \frac{1}{3} & -\frac{1}{3} & -\frac{1}{3} & \frac{1}{3} & -\frac{1}{3} & -\frac{1}{3} & \frac{1}{3} & \frac{1}{3} \\
1 & -\frac{1}{3} & -\frac{1}{3} & -\frac{1}{3} & \frac{1}{3} & -\frac{1}{3} & 1 & -\frac{1}{3} & -\frac{1}{3} & -\frac{1}{3} & \frac{1}{3} & \frac{1}{3} & -\frac{1}{3} & \frac{1}{3} & -\frac{1}{3} \\
1 & 1 & -\frac{1}{3} & -\frac{1}{3} & -\frac{1}{3} & -\frac{1}{3} & -\frac{1}{3} & -\frac{1}{3} & -\frac{1}{3} & -\frac{1}{3} & -\frac{1}{3} & \frac{1}{3} & \frac{1}{3} & \frac{1}{3} & \frac{1}{3}
\end{array}$$

Phylogenetic Invariants: We computed the phylogenetic invariants using the results of [Sturmfels and Sullivant, 2004]. The invariants of degree 2 are:

$$\begin{aligned}
&q_1q_{10} - q_2q_9, \quad q_3q_7 - q_4q_6, \quad q_3q_8 - q_5q_6,\\
&q_4q_8 - q_5q_7, \quad q_3q_{13} - q_4q_{11}, \quad q_3q_{12} - q_5q_{11},\\
&q_4q_{12} - q_5q_{13}, \quad q_6q_{13} - q_7q_{11}, \quad q_6q_{12} - q_8q_{11},\\
&q_7q_{12} - q_8q_{13}.
\end{aligned}$$

The invariants of degree 3 associated to the left interior vertex are:

$$\begin{aligned}
&q_1q_{11}q_{11} - q_3q_6q_9, q_1q_{11}q_{13} - q_3q_7q_9, q_1q_{11}q_{12} - q_3q_8q_9,\\
&q_1q_{13}q_{11} - q_4q_6q_9, q_1q_{13}q_{13} - q_4q_7q_9, q_1q_{13}q_{12} - q_4q_8q_9,\\
&q_1q_{12}q_{11} - q_5q_6q_9, q_1q_{12}q_{13} - q_5q_7q_9, q_1q_{12}q_{12} - q_5q_8q_9,\\
&q_2q_{11}q_{11} - q_3q_6q_{10}, q_2q_{11}q_{13} - q_3q_7q_{10}, q_2q_{11}q_{12} - q_3q_8q_{10},\\
&q_2q_{13}q_{11} - q_4q_6q_{10}, q_2q_{13}q_{13} - q_4q_7q_{10}, q_2q_{13}q_{12} - q_4q_8q_{10},\\
&q_2q_{12}q_{11} - q_5q_6q_{10}, q_2q_{12}q_{13} - q_5q_7q_{10}, q_2q_{12}q_{12} - q_5q_8q_{10}.
\end{aligned}$$

The invariants of degree 3 associated to the right interior vertex are:

$$\begin{aligned}
&q_1q_5q_5 - q_3q_4q_2, q_1q_5q_8 - q_3q_7q_2, q_1q_5q_{12} - q_3q_{13}q_2,\\
&q_1q_8q_5 - q_6q_4q_2, q_1q_8q_8 - q_6q_7q_2, q_1q_8q_{12} - q_6q_{13}q_2,\\
&q_1q_{12}q_5 - q_{11}q_4q_2, q_1q_{12}q_8 - q_{11}q_7q_2, q_1q_{12}q_{12} - q_{11}q_{13}q_2,\\
&q_9q_5q_5 - q_3q_4q_{10}, q_9q_5q_8 - q_3q_7q_{10}, q_9q_5q_{12} - q_3q_{13}q_{10},\\
&q_9q_8q_5 - q_6q_4q_{10}, q_9q_8q_8 - q_6q_7q_{10}, q_9q_8q_{12} - q_6q_{13}q_{10},\\
&q_9q_{12}q_5 - q_{11}q_4q_{10}, q_9q_{12}q_8 - q_{11}q_7q_{10}, q_9q_{12}q_{12} - q_{11}q_{13}q_{10}.
\end{aligned}$$

The maximum likelihood degree, the singularity dimension and the singularity degree are computationally difficult to achieve and we have not been able to compute them using computer algebra programs.

15.4 Using the invariants

In this section we report some of the experiments we have made for inferring small trees using phylogenetic invariants. These experiments were made using the invariants for trees with 4 taxa on the Kimura 3–parameter model that can be found in our website [Casanellas *et al.*, 2004] which were computed using the Sturmfels–Sullivant theorem [Sturmfels and Sullivant, 2004]. The results obtained show that phylogenetic invariants are an efficient method for tree reconstruction.

We implemented an algorithm that performs the following tasks. Given 4 DNA sequences s_1, s_2, s_3, s_4, it first counts the number of occurrences of each pattern for the topology $((s_1, s_2), s_3, s_4)$. Then it changes these absolute frequencies to Fourier coordinates. From this, we have the Fourier transforms in the other two possible topologies for trees with 4 species. We then evaluate all the phylogenetic invariants for the Kimura 3–parameter model in the Fourier coordinates of each tree topology. We call s_f^T the absolute value of this evaluation for the polynomial f and tree topology T. From these values $\{s_f^T\}_f$, we produce a score for each tree topology T, namely $s(T) = \sum_f |s_f^T|$. The algorithm then chooses the topology that has minimum score.

There was an attempt to define the score as the Euclidean norm of the values s_f^T, but from our experiments, we deduced that the 1–norm chosen above performs better.

We then tested this algorithm for different sets of sequences. We used the program *evolver* from the package PAML [Yang, 1997] to generate sequences according to the Kimura 2–parameter model with transition/transversion ratio equal to 2 (typical value of mammalian DNA). In what follows we describe the different tests we made and the results we obtained.

We generated 4–taxa trees with random branch lengths uniformly distributed between 0 and 1. We performed 600 tests for sequences of lengths between 1000 and 10,000. The percentage of trees correctly reconstructed can be seen in Figure 15.3.

We observed that our method fails to reconstruct the right tree mainly when the length of the interior edge of the tree is small compared to the other branch lengths. More precisely, in the trees that cannot be correctly inferred, the length of the interior edge is about 10% the average length of the other edges.

Our method was also tested by letting the edge lengths be normally distributed with a given mean μ. We chose the values $0.25, 0.05, 0.005$ for the mean μ, following [John *et al.*, 2003]. We also let the standard deviation be 0.1μ. In this case, we tested DNA sequences of lengths ranging from 50 to 10,000. Here, we only display the results for sequences of length up to 1000, because we checked that for larger sequences, we always infer the correct tree. For each sequence length in $\{50, 100, 200, 300, 400, 500, 600, 700, 800, 900, 1000\}$, we generated edge lengths normally distributed with mean μ using the data analysis program *R* [R Development Core Team, 2004]. Consequently, we generated 100 sequences for each mean and sequence length. The results are presented in Figure 15.4.

From Figure 15.4, we see that for $\mu = 0.25$ or $\mu = 0.05$, it is enough to consider sequences of length 200 to obtain a 100% efficiency. A much smaller mean such as $\mu = 0.0005$ was also tested. In this case, an efficiency over 90% was only obtained for sequences of length ≥ 3000.

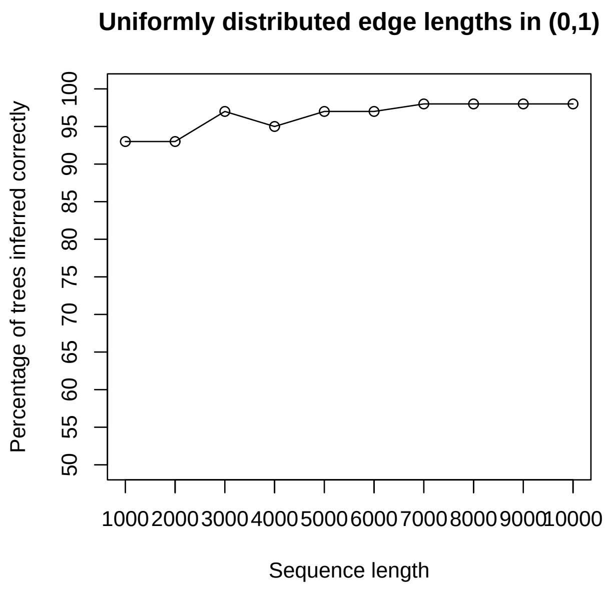

Fig. 15.3. Percentage of trees correctly reconstructed with random branch lengths uniformly distributed between 0 and 1.

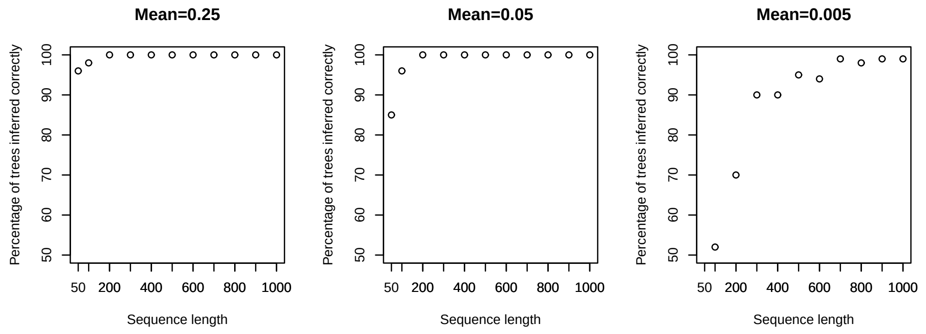

Fig. 15.4. Percentage of trees correctly reconstructed with edge lengths normally distributed with mean equal to 0.25, 0.05, 0.005.

The method presented here is by no means the unique form of using these invariants, so different ways of using them can even improve the tests.

Acknowledgments

Marta Casanellas was partially supported by RyC program of "Ministerio de Ciencia y Tecnologia", BFM2003-06001 and BIO2000-1352-C02-02 of "Plan

Nacional I+D" of Spain. Luis David Garcia was a postdoctoral fellow at the Mathematical Science Research Institute. Seth Sullivant was supported by a NSF graduate research fellowship. Much of the research in this chapter occurred during a visit to University of California, Berkeley, and we are grateful for their hospitality. We like to thank Serkan Hoşten for all his help and guidance throughout this project.

16
The Strand Symmetric Model

Marta Casanellas

Seth Sullivant

16.1 Introduction

This chapter is devoted to the study of strand symmetric Markov models on trees from the standpoint of algebraic statistics. By a strand symmetric Markov model, we mean one whose mutation structure reflects the symmetry induced by the double-stranded structure of DNA. In particular, a strand symmetric model for DNA must have the following equalities of probabilities in the root distribution:

$$\pi_A = \pi_T \text{ and } \pi_C = \pi_G$$

and the following equalities of probabilities in the transition matrices (θ_{ij})

$$\theta_{AA} = \theta_{TT}, \theta_{AC} = \theta_{TG}, \theta_{AG} = \theta_{TC}, \theta_{AT} = \theta_{TA},$$

$$\theta_{CA} = \theta_{GT}, \theta_{CC} = \theta_{GG}, \theta_{CG} = \theta_{GC}, \theta_{CT} = \theta_{GA}.$$

Important special cases of strand symmetric Markov models are the group-based phylogenetic models including the Jukes-Cantor model and the Kimura 2 and 3 parameter models. The *general strand symmetric model* or in this chapter just the *strand symmetric model* (SSM) has only these eight equalities of probabilities in the transition matrices and no further restriction on the transition probabilities. Thus, for each edge in the corresponding phylogenetic model, there are 6 free parameters.

For the standard group-based models (i.e. Jukes-Cantor and Kimura), the transition matrices and the entire parametrization can be simultaneously diagonalized by means of the Fourier transform of the group $\mathbb{Z}_2 \times \mathbb{Z}_2$ [Evans and Speed, 1993, Székely *et al.*, 1993]. Besides the practical uses of the Fourier transform for group based models (see for example [Semple and Steel, 2003]), this diagonalization of the group-based models makes it possible to compute phylogenetic invariants for these models, by reducing the problem to the claw tree $K_{1,3}$ [Sturmfels and Yu, 2004]. Our goal in this chapter is to extend the Fourier transform from group-based models to the strand symmetric model. This is carried out in Section 16.2.

In Section 16.3 we focus in on the case of the three taxa tree. The computation of phylogenetic invariants for the SSM in the Fourier coordinates is still not complete, though we report on what is known about these invariants. In particular, we describe all invariants of degree three and four. Section 16.5 is concerned with extending known invariants from the three taxa tree to an arbitrary tree. In particular, we describe how to extend the given degree three and four invariants from Section 16.3 to an arbitrary binary tree. To do this, we introduce *G-tensors* and explore their properties in Section 16.4.

In Section 16.6, we take up the task of extending the "gluing" results for phylogentic invariants which appear both in the work of Allman and Rhodes [Allman and Rhodes, 2004a] and Sturmfels and Sullivant [Sturmfels and Sullivant, 2004]. Our exposition and inspiration mainly comes from the work of Allman and Rhodes and we deduce that the problem of determining *defining* phylogenetic invariants for the strand symmetric model reduces to finding phylogenetic invariants for the claw tree $K_{1,3}$. Here *defining* means a set of polynomials which generate the ideal of invariants up to radical; that is, defining invariants have the same zero set as the whole ideal of invariants. This result is achieved by proving some "block diagonal" versions of results which appear in the Allman and Rhodes paper. This line of attack is the heart of Sections 16.4 and 16.6.

16.2 Matrix-Valued Fourier Transform

In this section we introduce the matrix-valued group-based models and show that the strand symmetric model is a matrix-valued group-based model. Then we describe the matrix-valued Fourier transform and the resulting simplification in the parametrization of these models. We make special emphasis on the strand symmetric model.

Let T be a rooted tree with n taxa. First, we wish to describe the random variables associated to each vertex in the tree in the matrix-valued group-based models. Each random variable X_v takes on kl states where k is the cardinality of a finite abelian group G. The states of the random variable are 2-ples $\binom{j}{i}$ where $j \in G$ and $i \in \{0, 1, \ldots, l-1\}$.

Associated to the root node R in the tree is the root distribution $R_{i_1}^{j_1}$. For each edge E of T the double indexed set of parameters $E_{i_1 i_2}^{j_1 j_2}$ is the transition matrix associated to this edge. We use the convention that E is both the edge and the transition matrix associated to that edge, to avoid the need for introducing a third index on the matrices. Thus $E_{i_1 i_2}^{j_1 j_2}$ is the conditional probability of making a transition from state $\binom{j_1}{i_1}$ to state $\binom{j_2}{i_2}$ along the edge E.

Definition 16.1 A phylogenetic model is a *matrix-valued group-based model* if for each edge, the matrix transition probabilities satisfy

$$E^{j_1 j_2}_{i_1 i_2} = E^{j_3 j_4}_{i_1 i_2}$$

when $j_1 - j_2 = j_3 - j_4$ (where the difference is taken in G) and the root distribution probabilities satisfy $R^{j_1}_i = R^{j_2}_i$.

Example 16.2 Consider the strand symmetric model and make the identification of the states $A = \binom{0}{0}$, $G = \binom{0}{1}$, $T = \binom{1}{0}$, and $C = \binom{1}{1}$. One can check directly from the definitions that the strand symmetric model is a matrix-valued group-based model with $l = 2$ and $G = \mathbb{Z}_2$.

To avoid some even more cumbersome notation, we will restrict attention to binary trees T and to the strand symmetric model for DNA. While the results of Section 16.3 and 16.5 are exclusive to the case of the SSM, all our other results can be easily extended to arbitrary matrix-valued group-based models with the introduction of the more general Fourier transform, though we will not explain these generalizations here.

We assume all edges of T are directed away from the root R. Given an edge E of T let $s(E)$ denote the initial vertex of E and $t(E)$ the trailing vertex. Then the parametrization of the phylogenetic model is given as follows. The probability of observing states ${}^{j_1 j_2 \ldots j_n}_{i_1 i_2 \ldots i_n}$ at the leaves is

$$p^{j_1 j_2 \ldots j_n}_{i_1 i_2 \ldots i_n} = \sum_{(\binom{j_v}{i_v}) \in H} R^{j_R}_{i_R} \prod_E E^{j_{s(E)} j_{t(E)}}_{i_{s(E)} i_{t(E)}}$$

where the product is taken over all edges E of T and the sum is taken over the set

$$H = \{(\begin{pmatrix} j_v \\ i_v \end{pmatrix})_{v \in IntV(T)} | j_v, i_v \in \{0, 1\}\}.$$

Here $IntV(T)$ denotes the interior or nonleaf vertices of T.

Example 16.3 For the three leaf claw tree, the parametrization is given by the expression:

$$p^{lmn}_{ijk} = R^0_0 A^{0l}_{0i} B^{0m}_{0j} C^{0n}_{0k} + R^1_0 A^{1l}_{0i} B^{1m}_{0j} C^{1n}_{0k} + R^0_1 A^{0l}_{1i} B^{0m}_{1j} C^{0n}_{1k} + R^1_1 A^{1l}_{1i} B^{1m}_{1j} C^{1n}_{1k}.$$

The study of this particular tree will occupy a large part of the paper.

Because of the role of the group in determining the symmetry in the parame-trization, the Fourier transform can be applied to make the parametri-zation simpler. We will not define the Fourier transform in general, only in the specific case of the group $\mathbb{Z}_2$. The Fourier transform applies to all of the probability coordinates, the transition matrices and the root distribution.

Definition 16.4 The *Fourier transform of the probability coordinates is*

$$q^{j_1 j_2 \ldots j_n}_{i_1 i_2 \ldots i_n} = \sum_{k_1, k_2, \ldots, k_n \in \{0,1\}} (-1)^{k_1 j_1 + k_2 j_2 + \cdots + k_n j_n} p^{k_1 k_2 \ldots k_n}_{i_1 i_2 \ldots i_n}.$$

The Fourier transform of the transition matrix E is

$$e^{j_1 j_2}_{i_1 i_2} = \frac{1}{2} \sum_{k_1, k_2 \in \{0,1\}} (-1)^{k_1 j_1 + k_2 j_2} E^{k_1 k_2}_{i_1 i_2}.$$

The Fourier transform of the root distribution is

$$r^j_i = \sum_{k \in \{0,1\}} (-1)^{kj} R^k_i.$$

It is easy to check that $e^{j_1 j_2}_{i_1 i_2} = 0$ if $j_1 + j_2 = 1 \in \mathbb{Z}_2$ and similarly that $r^j_i = 0$ if $j = 1$. In particular, writing e as a matrix, we see that the Fourier transform replaces the matrix E with a matrix e that is block diagonal. Generally, when working with our "hands on" the parameters (in particular in Section 16.3) we will write the transition matrices with only one superscript: $e^j_{i_1 i_2}$ and the transformed root distribution r_i with no superscript at all, though at other times it will be more convenient to have the extra superscript around, in spite of their redundancy.

Lemma 16.5 *In the Fourier coordinates the parametrization is given by the rule*

$$q^{j_1 j_2 \ldots j_n}_{i_1 i_2 \ldots i_n} = \sum_{(i_v) \in H} r^{j_r}_{i_r} \prod_e e^{j_{s(e)}}_{i_{s(e)} i_{t(e)}}$$

where $j_{s(e)}$ is the sum of j_l such that l is a leaf below $s(e)$ in the tree, $j_r = j_1 + \cdots + j_n$ and H denotes the set

$$H = \{(i_v)_{v \in IntV(T)} \text{ and } i_v \in \{0,1\}\}.$$

Proof We can rewrite the parametrization in the probability coordinates as

$$p^{k_1 k_2 \ldots k_n}_{i_1 i_2 \ldots i_n} = \sum_{(i_v) \in H} \left(\sum_{(k_v) \in H'} R^{k_R}_{i_R} \prod_E E^{k_{s(E)} k_{t(E)}}_{i_{s(E)} i_{t(E)}} \right)$$

where H is the set defined in the lemma and

$$H' = \{(k_v)_{v \in IntV(T)} \text{ and } k_v \in \mathbb{Z}_2\}.$$

The crucial observation is that for any fixed values of $i_1, \dots, i_n$ and $(i_v) \in H$, the expression inside the parentheses is a standard group-based model for $\mathbb{Z}_2$. Applying the Fourier transform we have the following expression for $q^{j_1 j_2 \dots j_n}_{i_1 i_2 \dots i_n}$:

$$\sum_{k_1,k_2,\dots,k_n \in \{0,1\}} (-1)^{k_1 j_1 + k_2 j_2 + \cdots + k_n j_n} \sum_{(i_v) \in H} \left(\sum_{(k_v) \in H'} R^{k_R}_{i_R} \prod_E E^{k_{s(E)} k_{t(E)}}_{i_{s(E)} i_{t(E)}} \right)$$

and interchanging summations

$$\sum_{(i_v) \in H} \left(\sum_{k_1,k_2,\dots,k_n \in \{0,1\}} (-1)^{k_1 j_1 + k_2 j_2 + \cdots + k_n j_n} \sum_{(k_v) \in H'} R^{k_R}_{i_R} \prod_E E^{k_{s(E)} k_{t(E)}}_{i_{s(E)} i_{t(E)}} \right).$$

By our crucial observation above, the expression inside the large parentheses is the Fourier transform of a group-based model and hence by results in [Evans and Speed, 1993] and [Székely *et al.*, 1993] the expression inside the parentheses factors in terms of the Fourier transforms of the transition matrices and root distribution in precisely the way illustrated in the statement of the lemma. □

Definition 16.6 Given a tree T, the projective variety of the SSM given by the tree T is denoted by $V(T)$. The notation $CV(T)$ denotes the affine cone over $V(T)$.

Proposition 16.7 (Linear Invariants)

$$q^{j_1 j_2 \dots j_n}_{i_1 i_2 \dots i_n} = 0$$

if $j_1 + j_2 + \cdots + j_n = 1 \in \mathbb{Z}_2$.

Proof The equation $j_1 + j_2 + \cdots + j_n = 1 \in \mathbb{Z}_2$ implies that in the parametrization every summand involves $r^1_{i_r}$ for some i_r. However, all of these parameters are zero. □

The linear invariants in the previous lemma are equivalent to the fact that

$$p^{j_1 j_2 \dots j_n}_{i_1 i_2 \dots i_n} = p^{\bar{j}_1 \bar{j}_2 \dots \bar{j}_n}_{i_1 i_2 \dots i_n}$$

where $\bar{j} = 1 - j \in \mathbb{Z}_2$.

Up until now, we have implicitly assumed that all the matrices E involved were actually matrices of transition probabilities and that the root distribution R was an honest probability distribution. If we drop these conditions and look at the parametrization in the Fourier coordinates, we can, in fact, drop r from this representation altogether. That is, the variety parametrized by dropping the transformed root distribution r is the cone over the Zariski closure of the probabilistic parametrization.

Lemma 16.8 *In the Fourier coordinates there is an open subset of $CV(T)$, the cone over the strand symmetric model, that can be parametrized as*

$$q^{j_1 j_2 \dots j_n}_{i_1 i_2 \dots i_n} = \sum_{(i_v) \in H} \prod_e e^{j_{s(e)}}_{i_{s(e)} i_{t(e)}}$$

when $j_1 + \cdots + j_n = 0 \in \mathbb{Z}_2$, where $j_{s(e)}$ is the sum of j_l such that l is a leaf below $s(e)$ in the tree and H denotes the set

$$H = \{(i_v)_{v \in IntV(T)} \text{ and } i_v \in \{0,1\}\}.$$

Proof Due to the structure of the reparametrization of the SSM which we will prove in Section 16.4, it suffices to prove the lemma when T is the 3-leaf claw tree $K_{1,3}$. In this case, we are comparing the parametrizations

$$\phi : \; q^{mno}_{ijk} = r_0 a^m_{0i} b^n_{0j} c^o_{0k} + r_1 a^m_{1i} b^n_{1j} c^o_{1k}$$

and

$$\psi : \; q^{mno}_{ijk} = d^m_{0i} e^n_{0j} f^o_{0k} + d^m_{1i} e^n_{1j} f^o_{1k}.$$

In the second case, there are no conditions on the parameters. In the first parametrization, the stochastic assumption on the root distribution and transition matrices translates into the following restrictions on the Fourier parameters

$$r_0 = 1, a^0_{l0} + a^0_{l1} = 1, b^0_{l0} + b^0_{l1} = 1, c^0_{l0} + c^0_{l1} = 1$$

for $l = 0, 1$. We must show that for d, e, f belonging to some open subset U we can choose r, a, b, c with the prescribed restrictions which realize the same Q tensor up to scaling. To do this, define

$$\delta_l = d^0_{l0} + d^0_{l1}, \gamma_l = e^0_{l0} + e^0_{l1}, \lambda_l = f^0_{l0} + f^0_{l1}$$

for $l = 0, 1$ and take U the subset where these numbers are all non-zero. Set

$$a^m_{li} = \delta_l^{-1} d^m_{li}, b^n_{lj} = \gamma_l^{-1} e^n_{lj}, c^o_{lk} = \lambda_l^{-1} f^o_{lk}, r_0 = 1, \text{ and } r_1 = \frac{\delta_1 \gamma_1 \lambda_1}{\delta_0 \gamma_0 \lambda_0}.$$

Clearly, all the parameters r, a, b, c satisfy the desired prescription. Furthermore, the parameterization with this choice of r, a, b, c differs from the original parametrization by a factor of $(\delta_0 \gamma_0 \lambda_0)^{-1}$. This proves that $\psi(U) \subset Im(\psi) \subset CV(T)$. On the other hand we have that $V(T) \subset Im(\psi)$ because we can always take $d^m_{li} = r_l a^m_{li}$, $e^n_{lj} = b^n_{lj}$, $f^o_{lk} = c^o_{lk}$. Moreover it is clear that $Im(\psi)$ is a cone and hence $CV(T) \subset Im(\psi)$. The proof of the lemma is completed by taking the Zariski closure. □

Example 16.9 In the particular instance of the three leaf claw tree the Fourier parametrization of the model is given by the formula

$$q_{ijk}^{mno} = a_{0i}^{m} b_{0j}^{n} c_{0k}^{o} + a_{1i}^{m} b_{1j}^{n} c_{1k}^{o}.$$

16.3 Invariants for the 3 taxa tree

In this section, we will describe the degree 3 and degree 4 phylogenetic invariants for the claw tree $K_{1,3}$ on the strand symmetric model. We originally found these polynomial invariants using the computational algebra package Macaulay2 [Grayson and Stillman, 2002] though we will give a combinatorial description of these invariants and proofs that they do, in fact, vanish on the strand symmetric model.

It is still an open problem to decide whether or not the 32 cubics and 18 quartics described here generate the ideal of invariants, or even describe the SSM set theoretically. Computationally, we determined that they generate the ideal up to degree 4. Furthermore, one can show that neither the degree 3 nor the degree 4 invariants alone are sufficient to describe the variety set theoretically.

16.3.1 Degree 3 Invariants

Proposition 16.10 *For each $l = 1, 2, 3$ let $m_l, n_l, o_l, i_l, j_l, k_l$ be indices in $\{0, 1\}$ such that $m_l + n_l + o_l = 0$, $m_1 = m_2$, $m_3 = 1 - m_1$, $n_1 = n_3$, $n_2 = 1 - n_1$, $o_2 = o_3$, and $o_1 = 1 - o_2$ in $\mathbb{Z}_2$. Let $f(m_\bullet, n_\bullet, o_\bullet, i_\bullet, j_\bullet, k_\bullet)$ be the polynomial in the Fourier coordinates described as*

$$\begin{vmatrix} q_{i_1 j_1 k_1}^{m_1 n_1 o_1} & q_{i_2 j_1 k_1}^{m_2 n_1 o_1} & 0 \\ q_{i_1 j_2 k_2}^{m_1 n_2 o_2} & q_{i_2 j_2 k_2}^{m_2 n_2 o_2} & q_{i_3 j_3 k_2}^{m_3 n_3 o_2} \\ q_{i_1 j_2 k_3}^{m_1 n_2 o_3} & q_{i_2 j_2 k_3}^{m_2 n_2 o_3} & q_{i_3 j_3 k_3}^{m_3 n_3 o_3} \end{vmatrix} - \begin{vmatrix} q_{i_1 j_3 k_1}^{m_1 n_3 o_1} & q_{i_2 j_3 k_1}^{m_2 n_3 o_1} & 0 \\ q_{i_1 j_2 k_2}^{m_1 n_2 o_2} & q_{i_2 j_2 k_2}^{m_2 n_2 o_2} & q_{i_3 j_1 k_2}^{m_3 n_1 o_2} \\ q_{i_1 j_2 k_3}^{m_1 n_2 o_3} & q_{i_2 j_2 k_3}^{m_2 n_2 o_3} & q_{i_3 j_1 k_3}^{m_3 n_1 o_3} \end{vmatrix}.$$

Then $f(m_\bullet, n_\bullet, o_\bullet, i_\bullet, j_\bullet, k_\bullet)$ is a phylogenetic invariant for $K_{1,3}$ on the SSM.

Remark 16.11 The only nonzero cubics invariants for $K_{1,3}$ arising from Proposition 1 are those satisfying $i_2 = 1 - i_1$, $i_3 = i_2$,$j_2 = j_1$, $j_3 = 1 - j_1$, $k_2 = 1 - k_1$ and $k_3 = k_1$. We maintain all the indices because they are necessary when we extend invariants to larger trees in section 16.5. In total, we obtain 32 invariants in this way and we verified in Macaulay2 [Grayson and Stillman, 2002] that these 32 invariants generate the ideal in degree 3.

Proof In order to prove this result it is very useful to write the parametrization in Fourier coordinates as:

$$q_{ijk}^{mno} = \begin{vmatrix} a_{0i}^{m} b_{0j}^{n} & -c_{1k}^{o} \\ a_{1i}^{m} b_{1j}^{n} & c_{0k}^{o} \end{vmatrix}.$$

In $f(m_\bullet, n_\bullet, o_\bullet, i_\bullet, j_\bullet, k_\bullet)$ we substitute the Fourier coordinates by their parametrization and we call D_1 the first determinant and D_2 the second one so that

$$D_1 = \begin{vmatrix} \begin{vmatrix} a_{0i_1}^{m_1} b_{0j_1}^{n_1} & -c_{1k_1}^{o_1} \\ a_{1i_1}^{m_1} b_{1j_1}^{n_1} & c_{0k_1}^{o_1} \end{vmatrix} & \begin{vmatrix} a_{0i_2}^{m_2} b_{0j_1}^{n_1} & -c_{1k_1}^{o_1} \\ a_{1i_2}^{m_2} b_{1j_1}^{n_1} & c_{0k_1}^{o_1} \end{vmatrix} & 0 \\ \begin{vmatrix} a_{0i_1}^{m_1} b_{0j_2}^{n_2} & -c_{1k_2}^{o_2} \\ a_{1i_1}^{m_1} b_{1j_2}^{n_2} & c_{0k_2}^{o_2} \end{vmatrix} & \begin{vmatrix} a_{0i_2}^{m_2} b_{0j_2}^{n_2} & -c_{1k_2}^{o_2} \\ a_{1i_2}^{m_2} b_{1j_2}^{n_2} & c_{0k_2}^{o_2} \end{vmatrix} & \begin{vmatrix} a_{0i_3}^{m_3} b_{0j_3}^{n_3} & -c_{1k_2}^{o_2} \\ a_{1i_3}^{m_3} b_{1j_3}^{n_3} & c_{0k_2}^{o_2} \end{vmatrix} \\ \begin{vmatrix} a_{0i_1}^{m_1} b_{0j_2}^{n_2} & -c_{1k_3}^{o_3} \\ a_{1i_1}^{m_1} b_{1j_2}^{n_2} & c_{0k_3}^{o_3} \end{vmatrix} & \begin{vmatrix} a_{0i_2}^{m_2} b_{0j_2}^{n_2} & -c_{1k_3}^{o_3} \\ a_{1i_2}^{m_2} b_{1j_2}^{n_2} & c_{0k_3}^{o_3} \end{vmatrix} & \begin{vmatrix} a_{0i_3}^{m_3} b_{0j_3}^{n_3} & -c_{1k_3}^{o_3} \\ a_{1i_3}^{m_3} b_{1j_3}^{n_3} & c_{0k_3}^{o_3} \end{vmatrix} \end{vmatrix}.$$

Now we observe that the indices in the first position are the same for each column in both determinants involved in $f(m_\bullet, n_\bullet, o_\bullet, i_\bullet, j_\bullet, k_\bullet)$. Similarly, the indices in the third position are the same for each row in both determinants. Using recursively the formula

$$\begin{vmatrix} \begin{vmatrix} x_{1,1} & y \\ x_{2,1} & z \end{vmatrix} & \begin{vmatrix} x_{1,2} & y \\ x_{2,2} & x \end{vmatrix} & \begin{vmatrix} x_{1,3} & y \\ x_{2,3} & z \end{vmatrix} \\ x_{3,1} & x_{3,2} & x_{3,3} \\ x_{4,1} & x_{4,2} & x_{4,3} \end{vmatrix} = \begin{vmatrix} x_{1,1} & x_{1,2} & x_{1,3} & y \\ x_{2,1} & x_{2,2} & x_{2,3} & z \\ x_{3,1} & x_{3,2} & x_{3,3} & 0 \\ x_{4,1} & x_{4,2} & x_{4,3} & 0 \end{vmatrix}$$

it is easy to see that D_1 can be written as the following 6×6 determinant:

$$D_1 = \begin{vmatrix} a_{0i_1}^{m_1} b_{0j_1}^{n_1} & a_{0i_2}^{m_2} b_{0j_1}^{n_1} & 0 & -c_{1k_1}^{o_1} & 0 & 0 \\ a_{1i_1}^{m_1} b_{1j_1}^{n_1} & a_{1i_2}^{m_2} b_{1j_1}^{n_1} & 0 & c_{0k_1}^{o_1} & 0 & 0 \\ a_{0i_1}^{m_1} b_{0j_2}^{n_2} & a_{0i_2}^{m_2} b_{0j_2}^{n_2} & a_{0i_3}^{m_3} b_{0j_3}^{n_3} & 0 & -c_{1k_2}^{o_2} & 0 \\ a_{1i_1}^{m_1} b_{1j_2}^{n_2} & a_{1i_2}^{m_2} b_{1j_2}^{n_2} & a_{1i_3}^{m_3} b_{1j_3}^{n_3} & 0 & c_{0k_2}^{o_2} & 0 \\ a_{0i_1}^{m_1} b_{0j_2}^{n_2} & a_{0i_2}^{m_2} b_{0j_2}^{n_2} & a_{0i_3}^{m_3} b_{0j_3}^{n_3} & 0 & 0 & -c_{1k_3}^{o_3} \\ a_{1i_1}^{m_1} b_{1j_2}^{n_2} & a_{1i_2}^{m_2} b_{1j_2}^{n_2} & a_{1i_3}^{m_3} b_{1j_3}^{n_3} & 0 & 0 & c_{0k_3}^{o_3} \end{vmatrix}.$$

Now using Laplace expansion for the last 3 columns we obtain:

$$D_1 = -c^{o_1}_{0k_1} c^{o_2}_{1k_2} c^{o_3}_{0k_3} \begin{vmatrix} a^{m_1}_{0i_1} b^{n_1}_{0j_1} & a^{m_2}_{0i_2} b^{n_1}_{0j_1} & 0 \\ a^{m_1}_{1i_1} b^{n_2}_{1j_2} & a^{m_2}_{1i_2} b^{n_2}_{1j_2} & a^{m_3}_{1i_3} b^{n_3}_{1j_3} \\ a^{m_1}_{0i_1} b^{n_2}_{0j_2} & a^{m_2}_{0i_2} b^{n_2}_{0j_2} & a^{m_3}_{0i_3} b^{n_3}_{0j_3} \end{vmatrix} -$$

$$c^{o_1}_{0k_1} c^{o_2}_{0k_2} c^{o_3}_{1k_3} \begin{vmatrix} a^{m_1}_{0i_1} b^{n_1}_{0j_1} & a^{m_2}_{0i_2} b^{n_1}_{0j_1} & 0 \\ a^{m_1}_{0i_1} b^{n_2}_{0j_2} & a^{m_2}_{0i_2} b^{n_2}_{0j_2} & a^{m_3}_{0i_3} b^{n_3}_{0j_3} \\ a^{m_1}_{1i_1} b^{n_2}_{1j_2} & a^{m_2}_{1i_2} b^{n_2}_{1j_2} & a^{m_3}_{1i_3} b^{n_3}_{1j_3} \end{vmatrix} +$$

$$c^{o_1}_{1k_1} c^{o_2}_{1k_2} c^{o_3}_{0k_3} \begin{vmatrix} a^{m_1}_{1i_1} b^{n_1}_{1j_1} & a^{m_2}_{1i_2} b^{n_1}_{1j_1} & 0 \\ a^{m_1}_{1i_1} b^{n_2}_{1j_2} & a^{m_2}_{1i_2} b^{n_2}_{1j_2} & a^{m_3}_{1i_3} b^{n_3}_{1j_3} \\ a^{m_1}_{0i_1} b^{n_2}_{0j_2} & a^{m_2}_{0i_2} b^{n_2}_{0j_2} & a^{m_3}_{0i_3} b^{n_3}_{0j_3} \end{vmatrix} +$$

$$c^{o_1}_{1k_1} c^{o_2}_{0k_2} c^{o_3}_{1k_3} \begin{vmatrix} a^{m_1}_{1i_1} b^{n_1}_{1j_1} & a^{m_2}_{1i_2} b^{n_1}_{1j_1} & 0 \\ a^{m_1}_{0i_1} b^{n_2}_{0j_2} & a^{m_2}_{0i_2} b^{n_2}_{0j_2} & a^{m_3}_{0i_3} b^{n_3}_{0j_3} \\ a^{m_1}_{1i_1} b^{n_2}_{1j_2} & a^{m_2}_{1i_2} b^{n_2}_{1j_2} & a^{m_3}_{1i_3} b^{n_3}_{1j_3} \end{vmatrix}.$$

Doing the same procedure for D_2 we see that its Laplace expansion has exactly the same 4 nonzero terms.

□

16.3.2 Degree 4 Invariants

Now we wish to explain the derivation of some nontrivial degree 4 invariants for the SSM on the $K_{1,3}$ tree. Each of the degree 4 invariants involves 16 of the nonzero Fourier coordinates which come from choosing two possible distinct sets of indices for the group-based indices. Up to symmetry, we may suppose these are from the tensors

$$q^{mn_1o_1} \text{ and } q^{mn_2o_2}.$$

Choose the ten indices $i_1, i_2, j_1, j_2, j_3, j_4, k_1, k_2, k_3, k_4$. Define the four matrices $q^{mn_1o_1}_i$ and $q^{mn_2o_2}_i$, $i \in \{i_1, i_2\}$ by

$$q^{mn_1o_1}_i = \begin{pmatrix} q^{mn_1o_1}_{ij_1k_1} & q^{mn_1o_1}_{ij_1k_2} \\ q^{mn_1o_1}_{ij_2k_1} & q^{mn_1o_1}_{ij_2k_2} \end{pmatrix} \text{ and } q^{mn_2o_2}_i = \begin{pmatrix} q^{mn_2o_2}_{ij_3k_3} & q^{mn_2o_2}_{ij_3k_4} \\ q^{mn_2o_2}_{ij_4k_3} & q^{mn_2o_2}_{ij_4k_4} \end{pmatrix}$$

For any of these matrices, adding an extra subindex j means taking the j-th row of the matrix, e.g. q^{011}_{1j} is the vector $(q^{011}_{1j0}\ q^{011}_{1j1})$.

Theorem 16.12 *The* 2×2 *minors of the following* 2×3 *matrix are all degree*

4 invariants of the SSM model on the 3 leaf claw tree:

$$\begin{pmatrix} \left|q_{i_1}^{mn_1o_1}\right| & \begin{vmatrix} q_{i_1j_1}^{mn_1o_1} \\ q_{i_2j_2}^{mn_1o_1} \end{vmatrix} + \begin{vmatrix} q_{i_1j_2}^{mn_1o_1} \\ q_{i_2j_1}^{mn_1o_1} \end{vmatrix} & \left|q_{i_2}^{mn_1o_1}\right| \\ & & \\ \left|q_{i_1}^{mn_2o_2}\right| & \begin{vmatrix} q_{i_1j_3}^{mn_2o_2} \\ q_{i_2j_4}^{mn_2o_2} \end{vmatrix} + \begin{vmatrix} q_{i_1j_4}^{mn_2o_2} \\ q_{i_2j_3}^{mn_2o_2} \end{vmatrix} & \left|q_{i_2}^{mn_2o_2}\right| \end{pmatrix}.$$

These degree 4 invariants are not in the radical of the ideal generated by the degree 3 invariants above. Up to symmetry, of the SSM on $K_{1,3}$ the 18 degree 4 invariants which arise this way are the only minimal generators of the ideal of degree 4.

Proof The third claim was proven computationally using Macaulay 2 [Grayson and Stillman, 2002]. The second claim follows by noting that all of the degree 3 invariants above use 3 different superscripts whereas the degree 4 invariants use only 2 different superscripts and the polynomials are multi-homogeneous in these indices. Hence, for example, an assignment of arbitrary values to the tensors q^{000} and q^{011} and setting $q^{101} = q^{110} = 0$ creates a set of Fourier values which necessarily satisfies all degree 3 invariants but does not satisfy the degree 4 polynomials described in the statement of the theorem.

Now we will prove that these polynomials are, in fact, invariants of the SSM on $K_{1,3}$. The parametrization of $q_i^{mn_1o_1}$ and $q_i^{mn_2o_2}$ can be rewritten as

$$q_i^{mn_1o_1} = a_{0i}^m M_0^0 + a_{1i}^m M_1^0 \text{ and } q_i^{mn_2o_2} = a_{0i}^m M_0^1 + a_{1i}^m M_1^1$$

where each of the four matrices M_0^0, M_1^0, M_0^1, and M_1^1 are arbitrary 2×2 matrices of rank 1. This follows by noting that the $q^{mn_1o_1}$ uses b^{n_1} and c^{o_1} in its description, $q^{mn_2o_2}$ uses b^{n_2} and c^{o_2} in its description, and simply reforming these descriptions into matrix notation.

In particular, $q_{i_1}^{mn_1no_1}$ and $q_{i_2}^{mn_1o_1}$ lie in the plane spanned by the rank 1 matrices M_0^0 and M_1^0 and $q_{i_1}^{mn_2o_2}$ and $q_{i_2}^{mn_2o_2}$ lie in the plane spanned by the rank 1 matrices M_0^1 and M_1^0 . Furthermore, the coefficients used to write these linear combinations are the same for pair $q_{i_1}^{mn_1o_1}$ and $q_{i_1}^{mn_2o_2}$ and for the pair $q_{i_2}^{mn_1o_1}$ and $q_{i_2}^{mn_2o_2}$.

If we are given a general point on the variety of the SSM, none of the matrices $q_{i_1}^{mn_1o_1}$, $q_{i_2}^{mn_1o_1}$, $q_{i_1}^{mn_2o_2}$ or $q_{i_2}^{mn_2o_2}$ will have rank 1. This implies that, generically, the set of matrices

$$\mathcal{M}_1 = \{\lambda q_{i_1}^{mn_1o_1} + \gamma q_{i_2}^{mn_1o_1} | \lambda, \gamma \in \mathbb{C}\}$$

$$\mathcal{M}_2 = \{\lambda q_{i_1}^{mn_2o_2} + \gamma q_{i_2}^{mn_2o_2} | \lambda, \gamma \in \mathbb{C}\}$$

each contain precisely 2 lines of rank 1 matrices. This is because the variety of

2×2 rank 1 matrices has degree 2. The set of values of λ and γ which produce these lines of rank 1 matrices are the same because of the way that $q_{i_1}^{mn_1o_1}$, $q_{i_2}^{mn_1o_1}$, $q_{i_1}^{mn_2o_2}$ or $q_{i_2}^{mn_2o_2}$ were written in terms of M_0^0, M_1^0, M_0^1 and M_1^1. In the first case, this set of λ and γ is the solution set of the quadratic equation

$$\left|\lambda q_{i_1}^{mn_1o_1} + \gamma q_{i_2}^{mn_1o_1}\right| = 0$$

and in the second case this set is the solution to the quadratic equation

$$\left|\lambda q_{i_1}^{mn_2o_2} + \gamma q_{i_2}^{mn_2o_2}\right| = 0.$$

To say that these two quadrics have the same zero set is equivalent to the vanishing of the three 2×2 minors in the statement of the theorem. Since the minors in the statement of the theorem vanish for a general point on the parametrization they must vanish on the entire variety and hence are invariants of the SSM. □

16.4 G-tensors

In this section we introduce the notion of a G-tensor which should be regarded as a multidimensional analog of a block diagonal matrix. We describe G-tensor multiplication and a certain variety defined for G-tensors which will be useful for extending invariants from the 3-leaf claw tree to arbitrary trees. This variety ${}^{G}V(4^{r_1}, 4^{r_2}, 4^{r_3})$ generalizes in a natural way the SSM on the claw tree $K_{1,3}$.

Notation. Let G be a group. For an n-tuple $\mathbf{j} = (j_1, \ldots, j_n) \in G^n$ we denote by $\sigma(\mathbf{j})$ the sum $j_1 + \cdots + j_n \in G$.

Definition 16.13 Let $q_{\mathbf{i_1}\cdots\mathbf{i_n}}^{\mathbf{j_1}\cdots\mathbf{j_n}}$ define a $4^{r_1}\times\cdots\times 4^{r_n}$ tensor Q where the upper indices are r_i-tuples in the group $G = \mathbb{Z}_2$. We say that Q is *G-tensor* if whenever $\sigma(\mathbf{j_1}) + \cdots + \sigma(\mathbf{j_n}) \neq 0$ in G, $q_{\mathbf{i_1}\cdots\mathbf{i_n}}^{\mathbf{j_1}\cdots\mathbf{j_n}} = 0$. If $n = 2$ then Q is called a G-matrix.

Lemma 16.14 *If Q is a $4\times\cdots\times 4$ tensor arising from the SSM in the Fourier coordinates, then Q is a G-tensor. All the Fourier parameter matrices $e_{i_1i_2}^{j_1j_2}$ are G-matrices.*

Proof This is immediate from Proposition 16.7 and the comments following Definition 16.4. □

Convention. Henceforth, we order any set of indices $\{\left(\begin{smallmatrix} j_1 & \cdots & j_t \\ i_1 & \cdots & i_t \end{smallmatrix}\right)\}_{j_1,\ldots,j_t,i_1,\ldots,i_t}$ so that we put first those indices whose upper sum $\sigma(\mathbf{j}) = j_1 + \cdots + j_t$ is equal to zero.

¿From now on we are going to use only Fourier coordinates and we will refer to the corresponding tensor as Q.

An operation on tensors that we will use frequently is the tensor multiplication $*$ which is defined as follows. If R and Q are n-dimensional and m-dimensional tensors so that R (resp. Q) has κ states at the last index (resp. first index), the $(m+n-2)$-dimensional tensor $R * Q$ is defined as

$$(R * Q)_{i_1,\ldots,i_{n+m-2}} = \sum_{j=1}^{\kappa} R_{i_1,\ldots,i_{n-1},j} \cdot Q_{j,i_n,\ldots,i_{n+m-2}} .$$

If R and Q are matrices this is the usual matrix multiplication. Note that if R and Q are G-tensors then $R * Q$ is also a G-tensor. We can also perform the $*$ operation on two varieties: if V and W are varieties of tensors then $V * W = \overline{\{R * Q | R \in V, Q \in W\}}$. If T' is a tree with taxa $v_1, \ldots, v_n$ and T'' is a tree with taxa $w_1, \ldots, w_m$ we call $T' * T''$ the tree obtained by identifying the vertices v_n and w_1, deleting this new vertex, and replacing the two corresponding edges by a single edge. This construction is a useful tool for constructing a reparametrization of the variety associated to an n-leaf tree T_n in terms of the parametrization for two smaller trees.

Proposition 16.15 *Let T_n be an n-leaf tree. Let $T_n = T_{n-1} * T_3$ be a decomposition of T_n into an $n-1$ leaf tree and a 3 leaf tree at a cherry. Then*

$$CV(T_n) = CV(T_{n-1}) * CV(T_3).$$

Proof Consider the parametrization for T_{n-1} written in the usual way as

$$q^{j_1 j_2 \ldots j_{n-2} l}_{i_1 i_2 \ldots i_{n-2} k} = \sum_{(i_v) \in H} \prod_e e^{j_{s(e)}}_{i_{s(e)} i_{t(e)}} .$$

and the parameterization for the 3 leaf tree T_3

$$r^{l j_{n-1} j_n}_{k i_{n-1} i_n} = \sum_{i_u \in \{0,1\}} \prod_f f^{j_{s(f)}}_{i_{s(f)} i_{t(f)}}$$

where u is the interior vertex of T_3. Writing the first tensor as Q and the second as R, we have an entry of $P = Q * R$ given by the formula

$$p^{j_1 j_2 \ldots j_n}_{i_1 i_2 \ldots i_n} = \sum_{k \in \{0,1\}} q^{j_1 j_2 \ldots j_{n-2} l}_{i_1 i_2 \ldots i_{n-2} k} r^{l j_{n-1} j_n}_{k i_{n-1} i_n}$$

where l satisfies $\sum j_{n-1} + j_n + l = 0 \in \mathbb{Z}_2$. Let $\mathbf{e}$ and $\mathbf{f}$ denote the distinguished edges of T_{n-1} and T_3 respectively which are joined to make the tree

T_n. Expanding the expression and regrouping yields

$$= \sum_{k\in\{0,1\}} \left(\sum_{(i_v)\in H} \prod_{e} e^{j_{s(e)}}_{i_{s(e)}i_{t(e)}} \right) \left(\sum_{i_v\in\{0,1\}} \prod_{f} f^{j_{s(f)}}_{i_{s(f)}i_{t(f)}} \right)$$

$$= \sum_{(i_v)\in H} \sum_{i_u\in\{0,1\}} \sum_{k\in\{0,1\}} \prod_{e} e^{j_{s(e)}}_{i_{s(e)}i_{t(e)}} \prod_{f} f^{j_{s(f)}}_{i_{s(f)}i_{t(f)}}.$$

$$= \sum_{(i_v)\in H} \sum_{i_u\in\{0,1\}} \prod_{e\neq \mathbf{e}} e^{j_{s(e)}}_{i_{s(e)}i_{t(e)}} \prod_{f\neq \mathbf{f}} f^{j_{s(f)}}_{i_{s(f)}i_{t(f)}} \left(\sum_{k\in\{0,1\}} \mathbf{e}^{l}_{i_{s(\mathbf{e})}i_k} \mathbf{f}^{l}_{i_k i_{t(\mathbf{f})}} \right).$$

The parenthesized expression is the product of the G-matrices $\mathbf{e}$ and $\mathbf{f}$. Replacing this expression with a new single G-matrix of parameters along the conjoined edge $\mathbf{ef}$ proves that $CV(T_{n-1}) * CV(T_3) \subseteq CV(T_n)$. Now expanding the paramaterization given in Lemma 16.8 as a sum on the vertex u we obtain the other inclusion. $\square$

Now we define a variety ${}^{G}V(4^{r_1}, 4^{r_2}, 4^{r_3})$ which plays a large role when we extend invariants.

Definition 16.16 For $l = 1, 2, 3$ let $\binom{\mathbf{j_l}}{\mathbf{i_l}}$ be a string of indices of length r_l. Let ${}_lM$ be an arbitrary G-matrix of size 4^{r_l} where the rows are indexed by $\{\binom{0}{0}, \binom{0}{1}, \binom{1}{0}, \binom{1}{1}\}$ and the columns are indexed by the 4^{r_l} indices $\binom{\mathbf{j_l}}{\mathbf{i_l}}$. Define the parametrization $Q = \psi_{r_1,r_2,r_3}({}_1M, {}_2M, {}_3M)$ by

$$Q^{\mathbf{j_1 j_2 j_3}}_{\mathbf{i_1 i_2 i_3}} = \sum_{i\in\{0,1\}} {}_1M^{\sigma(\mathbf{j_1})\mathbf{j_1}}_{i\mathbf{i_1}} \, {}_2M^{\sigma(\mathbf{j_2})\mathbf{j_2}}_{i\mathbf{i_2}} \, {}_3M^{\sigma(\mathbf{j_3})\mathbf{j_3}}_{i\mathbf{i_3}}$$

if $\sigma(\mathbf{j_1}) + \sigma(\mathbf{j_2}) + \sigma(\mathbf{j_3}) = 0$ and $Q^{\mathbf{j_1 j_2 j_3}}_{\mathbf{i_1 i_2 i_3}} = 0$ if $\sigma(\mathbf{j_1}) + \sigma(\mathbf{j_2}) + \sigma(\mathbf{j_3}) = 1$. The projective variety that is the Zariski closure of the image of ψ_{r_1,r_2,r_3} is denoted ${}^{G}V(4^{r_1}, 4^{r_2}, 4^{r_3})$. The affine cone over this variety is $C^{G}V(4^{r_1}, 4^{r_2}, 4^{r_3})$.

Remark 16.17 By the definition of ${}^{G}V(4^{r_1}, 4^{r_2}, 4^{r_3})$ any $Q \in {}^{G}V(4^{r_1}, 4^{r_2}, 4^{r_3})$ is a G-tensor. Furthermore ${}^{G}V(4, 4, 4)$ is equal to the variety defined by the SSM on the three leaf claw tree $K_{1,3}$.

Besides the fact that ${}^{G}V(4^{r_1}, 4^{r_2}, 4^{r_3})$ is equal to the SSM when $r_1 = r_2 = r_3 = 1$ the importance of this variety for the strand symmetric model comes from the fact that ${}^{G}V(4^{r_1}, 4^{r_2}, 4^{r_3})$ contains the SSM for any binary tree as illustrated by the following proposition.

Proposition 16.18 *Let T by a binary tree and v an interior vertex. Suppose that removing v from T partitions the leaves of T into the three sets $\{1,\ldots,r_1\}$, $\{r_1+1,\cdots,r_1+r_2\}$, and $\{r_1+r_2+1\ldots,r_1+r_2+r_3\}$. Then the SSM on T is a subvariety of ${}^{G}V(4^{r_1},4^{r_2},4^{r_3})$.*

In the proposition, the indices in the Fourier coordinates for the SSM are grouped in the natural way according to the tripartition of the leaves.

Proof In the parametric representation

$$q^{j_1j_2\ldots j_n}_{i_1i_2\ldots i_n} = \sum_{(i_v)\in H}\prod_e e^{j_{s(e)}}_{i_{s(e)}i_{t(e)}}$$

perform the sum associated to the vertex v first. This realizes the G-tensor Q as the sum over the product of entries of three G-tensors. $\square$

Our goal for the remainder of this section is to prove a result analogous to Theorem 7 in Allman and Rhodes [Allman and Rhodes, 2004a]. This theorem will provide a method to explicitly determine the ideal of invariants for ${}^{G}V(4^{r_1},4^{r_2},4^{r_3})$ from the ideal of invariants for ${}^{G}V(4,4,4)$. Denote by ${}^{G}M(2l,2m)$ the set of $2l\times 2m$ G-matrices. A fundamental observation is that if ${r_3}'\geq r_3$ then

$$C^{G}V(4^{r_1},4^{r_2},4^{r_3'}) = C^{G}V(4^{r_1},4^{r_2},4^{r_3}) * {}^{G}M(4^{r_3},4^{r_3'}).$$

Thus, we need to understand the $*$ operation when V and W are "well-behaved" varieties.

Lemma 16.19 *Let $V\subset {}^{G}M(2l,4)$ be a variety and suppose that $V*{}^{G}M(4,4)=V$. Let I be the vanishing ideal of V. Let K be the ideal of 3×3 G-minors of the $2l\times 2m$ G-matrix of indeterminates Q. Let Z be $2m\times 4$ G-matrix of indeterminates and*

$$L = \langle \mathrm{coeff}_Z(f(Q*Z))|f\in \mathrm{gens}(I)\rangle\,.$$

Then $K+L$ is the vanishing ideal of $W=V*{}^{G}M(4,2m)$.

By a *G-minor* we mean a minor which involves only the nonzero entries in the G-matrix Q.

Proof A useful fact is that

$$L =< f(Q*A)|f\in I, A\in {}^{G}M(2m,4) > \ .$$

Let J be the vanishing ideal of W. By the definition of W, all the polynomials in K must vanish on it. Moreover if $f(Q*A)$ is a polynomial in L, then it vanishes at all the points of the form $P*B$, for any $P\in V$ and $B\in {}^{G}M(4,2m)$.

Indeed, as $P*B*A \in V$ and $f \in I$ we have $f(P*B*A) = 0$. As all the points of W are of this form, we obtain the inclusion $K + L \subseteq J$. Our goal is to show that $J \subseteq K + L$.

Since $V * {}^{G}M(4,4) = V$, we must also have $W * {}^{G}M(2m, 2m) = W$. This implies that there is an action of $Gl(\mathbb{C}, m) \times Gl(\mathbb{C}, m)$ on W and hence, any graded piece of J, the vanishing ideal of W, is a representation of $Gl(\mathbb{C}, m) \times Gl(\mathbb{C}, m)$. Let J_d be the d-th graded piece of J. Since $Gl(\mathbb{C}, m) \times Gl(\mathbb{C}, m)$ is reductive, we just need to show each irreducible subspace M of J_d belongs to $K+L$. By construction, $K+L$ is also invariant under the action of $Gl(\mathbb{C}, m) \times Gl(\mathbb{C}, m)$ and, hence, it suffices to show that there exists a polynomial $f \in M$ such that $f \in K + L$.

Let $f \in M$ be an arbitrary polynomial in the irreducible representation M. Let P be a $2l \times 4$ G-matrix of indeterminates. Suppose that for all $B \in {}^{G}M(4, 2m)$, $f(P * B) \equiv 0$. This implies that f vanishes when evaluated at any G-matrix Q which has rank 2 in both components. Hence, $f \in K$.

If $f \notin K$ there exists a $B \in {}^{G}M(4, 2m)$ such that $f_B(P) := f(P * B) \not\equiv 0$. Renaming the P indeterminates we can take D a matrix in ${}^{G}(2m, 4)$ formed by ones and zeroes such that $f_B(Q * D) \not\equiv 0$. Since $f \in J$, we must have $f_B(P) \in I$. Therefore $f_B(Q * D) \in L$. Let $B' = D * B \in {}^{G}M(2m, 2m)$. Although $B' \notin Gl(\mathbb{C}, m) \times Gl(\mathbb{C}, m)$, the representation M must be closed and hence $f(Q * B') = f_B(Q * D) \in M$ which completes the proof. □

Proposition 16.20 *Generators for the vanishing ideal of* ${}^{G}V(4^{r_1}, 4^{r_2}, 4^{r_3})$ *are explicitly determined by generators for the vanishing ideal of* ${}^{G}V(4, 4, 4)$.

Proof Starting with ${}^{G}V(4, 4, 4)$, apply the preceding lemma three times. Now we will explain how to compute these polynomials explicitly. For $l = 1, 2, 3$ let Z_l be a $4^{r_l} \times 4$ G-matrix of indeterminates. This G-matrix Z_l acts on the $4^{r_1} \times 4^{r_2} \times 4^{r_3}$ tensor Q by G-tensor multiplication in the l-th coordinate. For each $f \in \text{gens}(I)$, where I is the vanishing ideal of ${}^{G}V(4, 4, 4)$, we construct the polynomials $\text{coeff}_Z f(Q * Z_1 * Z_2 * Z_3)$. That is, we construct the $4 \times 4 \times 4$ G-tensor $Q * Z_1 * Z_2 * Z_3$, plug this into f and expand, and extract, for each Z monomial, the coefficient, which is a polynomial in the entries of Q. Letting f range over all the generators of I determines an ideal L.

We can also flatten the 3-way G-tensor Q to a G-matrix in three different ways. For instance, we can flatten in to a $4^{r_1} \times 4^{r_2+r_3}$ G-matrix grouping the last two coordinates together. Taking the ideal generated by the 3×3 G-minors in these three flattenings yields an ideal K. The ideal $K + L$ generates the vanishing ideal of ${}^{G}V(4^{r_1}, 4^{r_2}, 4^{r_3})$. □

16.5 Extending invariants

In this section we will show how to derive invariants for arbitrary trees from the invariants introduced in section 16.3. We also introduce the degree 3 determinantal flattening invariants which arise from flatting the n-way G-tensor associated to a tree T under the SSM along an edge of the tree. The idea behind all of our results is to use the embedding of the SSM into the variety ${}^{G}V(4^{r_1}, 4^{r_2}, 4^{r_3})$.

Let T be a tree with n taxa on the SSM and let v be any interior vertex. Removing v creates a tripartition of the leaves into three sets of cardinalities r_1, r_2 and r_3, which we may suppose, without loss of generality, are the sets $\{1, \dots, r_1\}$, $\{r_1 + 1, \dots, r_1 + r_2\}$, and $\{r_1 + r_2 + 1, \dots, r_1 + r_2 + r_3\}$.

Proposition 16.21 *Let $f(m_\bullet, n_\bullet, o_\bullet, i_\bullet, j_\bullet, k_\bullet)$ be one of the degree 3 invariants for the 3 taxa tree $K_{1,3}$ introduced in Proposition 16.10. For each $l = 1, 2, 3$ we choose sets of indices $\mathbf{m_l}, \mathbf{i_l} \in \{0,1\}^{r_1}$, $\mathbf{n_l}, \mathbf{j_l} \in \{0,1\}^{r_2}$, and $\mathbf{o_l}, \mathbf{k_l} \in \{0,1\}^{r_3}$ such that $\sigma(\mathbf{m_l}) = m_l$ $\sigma(\mathbf{n_l}) = n_l$ and $\sigma(\mathbf{o_l}) = o_l$. Then $f(\mathbf{m_\bullet}, \mathbf{n_\bullet}, \mathbf{o_\bullet}, \mathbf{i_\bullet}, \mathbf{j_\bullet}, \mathbf{k_\bullet})$*

$$= \begin{vmatrix} q^{\mathbf{m_1n_1o_1}}_{\mathbf{i_1j_1k_1}} & q^{\mathbf{m_2n_1o_1}}_{\mathbf{i_2j_1k_1}} & 0 \\ q^{\mathbf{m_1n_2o_2}}_{\mathbf{i_1j_2k_2}} & q^{\mathbf{m_2n_2o_2}}_{\mathbf{i_2j_2k_2}} & q^{\mathbf{m_3n_3o_2}}_{\mathbf{i_3j_3k_2}} \\ q^{\mathbf{m_1n_2o_3}}_{\mathbf{i_1j_2k_3}} & q^{\mathbf{m_2n_2o_3}}_{\mathbf{i_2j_2k_3}} & q^{\mathbf{m_3n_3o_3}}_{\mathbf{i_3j_3k_3}} \end{vmatrix} - \begin{vmatrix} q^{\mathbf{m_1n_3o_1}}_{\mathbf{i_1j_3k_1}} & q^{\mathbf{m_2n_3o_1}}_{\mathbf{i_2j_3k_1}} & 0 \\ q^{\mathbf{m_1n_2o_2}}_{\mathbf{i_1j_2k_2}} & q^{\mathbf{m_2n_2o_2}}_{\mathbf{i_2j_2k_2}} & q^{\mathbf{m_3n_1o_2}}_{\mathbf{i_3j_1k_2}} \\ q^{\mathbf{m_1n_2o_3}}_{\mathbf{i_1j_2k_3}} & q^{\mathbf{m_2n_2o_3}}_{\mathbf{i_2j_2k_3}} & q^{\mathbf{m_3n_1o_3}}_{\mathbf{i_3j_1k_3}} \end{vmatrix}$$

is a phylogenetic invariant for T.

Proof The polynomial $f(\mathbf{m_\bullet}, \mathbf{n_\bullet}, \mathbf{o_\bullet}, \mathbf{i_\bullet}, \mathbf{j_\bullet}, \mathbf{k_\bullet})$ must vanish on the variety ${}^{G}V(4^{r_1}, 4^{r_2}, 4^{r_3})$. This is because choosing $\mathbf{m_1}$, $\mathbf{m_2}$, … in the manner specified corresponds to choosing a $3 \times 3 \times 3$ subtensor of Q which belongs to a $4 \times 4 \times 4$ G-subtensor of Q (after flattening to a 3-way tensor). Since ${}^{G}V(4, 4, 4)$ arises as a projection of ${}^{G}V(4^{r_1}, 4^{r_2}, 4^{r_3})$ onto this G-subtensor, $f(\mathbf{m_\bullet}, \mathbf{n_\bullet}, \mathbf{o_\bullet}, \mathbf{i_\bullet}, \mathbf{j_\bullet}, \mathbf{k_\bullet})$ belongs to the corresponding elimination ideal. Since the variety of the SSM for T is contained in the variety ${}^{G}V(4^{r_1}, 4^{r_2}, 4^{r_3})$, $f(\mathbf{m_\bullet}, \mathbf{n_\bullet}, \mathbf{o_\bullet}, \mathbf{i_\bullet}, \mathbf{j_\bullet}, \mathbf{k_\bullet})$ is an invariant for the SSM on T. □

Similarly, we can extend the construction of degree four invariants to arbitrary trees T by replacing the indices in their definition with vectors of indices. We omit the proof which follows the same lines as the preceding proposition.

Proposition 16.22 *Let $\mathbf{m}, \mathbf{i_l} \in \{0,1\}^{r_1}$, $\mathbf{n_l}, \mathbf{j_l} \in \{0,1\}^{r_2}$, and $\mathbf{o_l}, \mathbf{k_l} \in \{0,1\}^{r_3}$. Then the three 2×2 minors of the following matrix are all degree 4 invariants* *of the SSM model on the tree T:*

$$\begin{pmatrix} \begin{vmatrix} q_{\mathbf{i_1}}^{\mathbf{mn_1o_1}} \end{vmatrix} & \begin{vmatrix} q_{\mathbf{i_1j_1}}^{\mathbf{mn_1o_1}} \\ q_{\mathbf{i_2j_2}}^{\mathbf{mn_1o_1}} \end{vmatrix} + \begin{vmatrix} q_{\mathbf{i_1j_2}}^{\mathbf{mn_1o_1}} \\ q_{\mathbf{i_2j_1}}^{\mathbf{mn_1o_1}} \end{vmatrix} & \begin{vmatrix} q_{\mathbf{i_2}}^{\mathbf{mn_1o_1}} \end{vmatrix} \\ \\ \begin{vmatrix} q_{\mathbf{i_1}}^{\mathbf{mn_2o_2}} \end{vmatrix} & \begin{vmatrix} q_{\mathbf{i_1j_3}}^{\mathbf{mn_2o_2}} \\ q_{\mathbf{i_2j_4}}^{\mathbf{mn_2o_2}} \end{vmatrix} + \begin{vmatrix} q_{\mathbf{i_1j_4}}^{\mathbf{mn_2o_2}} \\ q_{\mathbf{i_2j_3}}^{\mathbf{mn_2o_2}} \end{vmatrix} & \begin{vmatrix} q_{\mathbf{i_2}}^{\mathbf{mn_2o_2}} \end{vmatrix} \end{pmatrix}.$$

Now we wish to describe the determinantal edge invariants which arise by flattening the G-tensor Q to a matrix along each edge of the tree. As we shall see, there existence is already implied by our previous results, namely Proposition 16.20. We make the special point of describing them here because they will be useful in the next section.

Let e be an edge in the tree T. Removing this edge partitions the leaves of T into two sets of size r_1 and r_2. The G-tensor Q flattens to a $4^{r_1} \times 4^{r_2}$ G-matrix R. Denote by $\mathcal{F}_e$ the set of 3×3 G-minors of R.

Proposition 16.23 *The 3×3 G-minors $\mathcal{F}_e$ are invariants of the SSM on T.*

Proof The edge e is incident to some interval vertex v of T. These 3×3 G-minors are in the ideal of say ${}^{G}V(4^{r_1}, 4^{r_2'}, 4^{r_3'})$ associated to flattening the tensor Q to a 3-way G tensor at this vertex. Then by Proposition 16.18 $\mathcal{F}_e$ are invariants of the SSM on T. □

16.6 Reduction to $K_{1,3}$

In this section, we explain how the problem of computing defining invariants for the SSM on a tree T reduces to the problem of computing defining invariants on the claw tree $K_{1,3}$. Our statements and proof are intimately related to the results of Allman and Rhodes [Allman and Rhodes, 2004a] and we draw much inspiration from their work.

Given an internal vertex v of T, denote by ${}^{G}V_v$ the variety ${}^{G}V(4^{r_1}, 4^{r_2}, 4^{r_3})$ associated to flattening the G-tensor Q to a 3-way tensor according to the tripartiiton induced by v.

Theorem 16.24 *Let T be a binary tree. For each $v \in IntV(T)$ let $\mathcal{F}_v$ be a set of invariants which define the variety ${}^{G}V_v$ set theoretically. Then*

$$CV(T) = \cap_{v \in IntV(T)} {}^{G}V_v$$

and hence

$$\mathcal{F}_{flat}(T) = \cup_{v \in IntV(T)} \mathcal{F}_v$$

are a defining set of invariants for the SSM on T.

The theorem reduces the computation of defining invariants to $K_{1,3}$ since a defining set of invariants for ${}^G V(4^{r_1}, 4^{r_2}, 4^{r_3})$ can be determined from a set of defining invariants for ${}^G V(4, 4, 4) = V(K_{1,3})$. Given the reparametrization result of Section 16.4, it will suffice to show the following lemma, about the $*$ operation on G-matrix varieties.

Lemma 16.25 *Let $V \subseteq {}^G M(2l, 4)$ and $W \subseteq {}^G M(4, 2m)$ be two varieties such that $V = V * {}^G M(4, 4)$ and $W = {}^G M(4, 4) * W$. Then*

$$V * W = \left(V * {}^G M(4, 2m)\right) \cap \left({}^G M(2l, 4) * W\right).$$

Proof Call the variety on the right hand side of the equality U. Since both of the component varieties of U contain $V * W$, we must have $V * W \subseteq U$. Our goal is to show the reverse inclusion. Let $Q \in U$. This matrix can be visualized as a block diagonal matrix:

$$Q = \begin{pmatrix} Q_0 & 0 \\ 0 & Q_1 \end{pmatrix}.$$

Since $Q \in U$ it must be the case that the rank of Q_0 and Q_1 are both less than or equal to 2. Thus we can factorize Q as $Q = R * S$ where $R \in {}^G M(2l, 4)$ and $S \in {}^G M(4, 2m)$. Without loss of generality, we may suppose that the factorization $Q = R * S$ is nondegenerate in the sense that the rank of each of the matrices R and S has only rank(Q) nonzero rows. Our goal is to show that $R \in V$ and $S \in W$ as this will imply the theorem.

By our assumption that the factorization $Q = R * S$ is nondegenerate, there exists a G-matrix $A \in {}^G M(2m, 4)$ such that $Q * A = R * S * A = R$ (A is called the pseudo-inverse of S). Augmenting the matrix A with extra 0-columns, we get a G-matrix $A' \in {}^G M(2m, 2m)$. Then $Q * A' \in V * {}^G M(4, 2m)$ since Q is and $V * {}^G M(4, 2m)$ is closed under multiplication by G-matrices on the right. On the other hand, the natural projection of $Q * A'$ to ${}^G M(2l, 4)$ is $Q * A = R$. Since the projection $V * {}^G M(4, 2m) \to {}^G M(2l, 4)$ is the variety V because $V = V * {}^G M(4, 4)$, we have $R \in V$. A similar argument yields $S \in W$ and completes the proof. □

Now we are in a position to give the proof the Theorem 16.24.

Proof We proceed by induction on n the number of leaves of T. If $n = 3$ there is nothing to show since this is the three leaf claw tree $K_{1,3}$. Let T by a binary n taxa tree. The tree T has a cherry T_3, and thus we can represent the tree $T = T_{n-1} * T_3$ and the resulting variety as $V(T) = V(T_{n-1}) * V(T_3)$ by the reparametrization. Now we apply the induction hypothesis to T_{n-1} and T_3. The varieties $V(T_{n-1})$ and $V(T_3)$ have the desired representation as intersections of ${}^G V_v$. By the preceding Lemma, it suffices to show that this representation extends to the variety $V(T_{n-1}) * {}^G M(4,16)$ and ${}^G M(4^{n-1},4) * V(T_3)$. This is almost immediate, since

$$ {}^G V(4^{r_1}, 4^{r_2}, 4^{r_3}) * {}^G M(4, 4^s) = {}^G V(4^{r_1}, 4^{r_2}, 4^{r_3+s-1}) $$

where ${}^G M(4,4^s)$ acts on a *single index* of ${}^G V(4^{r_1}, 4^{r_2}, 4^{r_3})$ (recall that ${}^G V(4^{r_1}, 4^{r_2}, 4^{r_3})$ can be considered as either a 3-way tensor or an n-way $4 \times \cdots \times 4$ tensor). This equation of varieties applies to each of the component varieties in the intersection representation of $V(T_{n-1})$ and $V(T_3)$ and completes the proof. □

Acknowledgments

We would like to thank Bernd Sturmfels for some useful conversations about this problem. Marta Casanellas was partially supported by RyC program of "Ministerio de Ciencia y Tecnologia", BFM2003-06001 and BIO2000-1352-C02-02 of "Plan Nacional I+D" of Spain. Seth Sullivant was supported by a NSF graduate research fellowship. Much of the research in this chapter occurred during visits to University of California, Berkeley, and to the Universitat de Barcelona (2001SGR-00071), and we are grateful for their hospitality.

17
Extending Tree Models to Split Networks

David Bryant

17.1 Introduction

In this chapter take statistical models designed for trees and generalize them to more general constructions. In Chapter 2 we saw that phylogenetic trees can be viewed as collections of pair-wise compatible splits (Theorem 2.34), where each split corresponds to an edge in the tree. Thus a statistical model on a tree is a statistical model on a collection of pair-wise compatible splits with weights (or lengths). Our approach here is to drop the condition of pair-wise compatibility and consider statistical models based on general collections of splits and the split networks that represent them (Section 17.2).

Geometrically, the models we propose fill in the gaps between statistical models for different trees. We show how we can *relax* the constraint that limits analyses to tree-space. A relaxation of tree models can be used to test statistically whether or not the data actually supports a tree. Split networks provide natural swing-bridges between trees which could be used to compare likelihood ratios or, in a Bayesian setting, used to estimate the ratio of Bayes factors for two trees. The potential to relax the tree constraint also opens up a huge range of new search techniques.

One of the more appealing applications of models based on split networks is the representation of phylogenetic uncertainty. At present, the only widely used way to represent uncertainty in an estimated phylogeny is to place confidence values (such as posterior probabilities or bootstrap P-values) on the branches of the phylogeny. A tree with confidence measures shows which part of the phylogeny is less certain, but gives no indication of the nature of the conflicting signal. Split networks, on the other hand, provide a means to represent confidence sets of trees in a single diagram, indicating both the uncertain parts of the tree and any conflicting secondary signal.

A confusing aspect of split network models is that they are not explicit representations of evolutionary history. Rather, they represent *summary statistics*, statistics that are more informative than trees contain only a subset of the information present in a complete recombination history [Griffiths and Marjoram, 1996]. They are can therefore be more reliably estimated than complete reticulation histories, and perhaps provide a stepping stone in the analysis. On the whole, population geneticists don't even dream to think that explicit recombination histories can be reconstructed exactly. Instead they integrate out over different histories and take summary statistics. Split networks are a particularly informative and graphically appealing set of summary statistics to infer.

The outline of this chapter is:

- In section 17.2 we review the definitions of splits and split networks.
- In section 17.3 we discuss statistical models for split networks based on distance data.
- In section 17.4 we briefly discuss, and critique, the application of graphical models to split networks.
- In sections 17.5 to 17.7 we develop a character based model for splits networks based on the Fourier calculus for evolutionary trees studied by [Székely *et al.*, 1993].
- We conclude with open problems and some baseless speculation.

17.2 Trees, splits and split networks

Splits are the foundation of phylogenetic combinatorics, and they will be the building blocks of our general statistical model. Recall (from Chapter 2) that a *split* $S = \{A, B\}$ of a finite set X is an unordered partition of X into two non-empty blocks. An X-*tree* is a pair $\mathcal{T} = (T, \phi)$ such that T is a tree and $\phi : X \to V(T)$ is a map for which $\phi^{-1}(v)$ is empty whenever v has degree less than three. We say that $\mathcal{T}$ is a *phylogenetic tree* if T has no vertices of degree two and ϕ is a bijection from X to the leaves of $\mathcal{T}$.

Removing an edge e from an X-tree divides the tree into two connected component, thereby inducing a split of X that we say is the *split associated to* e. We use *splits*$(\mathcal{T})$ to denote the sets associated to edges of T. The X-tree $\mathcal{T}$ can be reconstructed from the collection *splits*$(\mathcal{T})$. The *Splits Equivalence Theorem* (Theorem 2.34) tells us that a collection $\mathcal{S}$ of splits equals *splits*(T) for some X-tree T if and only if the collection is *pairwise compatible*, that is, for all pairs of splits $\{A, B\}, \{A', B'\}$ at least one of the intersections

$$A \cap A',\ A \cap B',\ B \cap A',\ B \cap B'$$

is empty.

If we think of X-trees as collections of compatible splits then it becomes easy to generalize trees: we simply consider collections of splits that are not necessarily pairwise compatible. This is the approach taken by Split Decomposition [Bandelt and Dress, 1992], Median Networks [Bandelt *et al.*, 1995], SpectroNet [Huber *et al.*, 2002], Neighbor-Net [Bryant and Moulton, 2004], Consensus Networks [Holland *et al.*, 2004] and Z-networks [Huson *et al.*, 2004], many of which are implemented in the SplitsTree package[Huson, 1998, Huson and Bryant, 2005]. The usefulness of these methods is due to a particularly elegant graphical representation for general collections of splits: the splits network.

To define splits networks, we first need to discuss splits graphs. These graphs have multiple characterizations. We will work with three of these here.

In a graph G let d_G denote the (unweighted) shortest path metric. A map ψ from a graph H to a graph G is an *isometric embedding* if $d_H(u,v) = d_G(\psi(u),\psi(v))$ for all $u, v \in V(H)$. A graph G is a *partial cube* if there exists an isometric embedding from G to a hypercube. Wetzel [Wetzel, 1995] called these graphs *splits graphs.* This terminology has persisted in the phylogenetics community, despite the potential for confusion with the graph-theoretic term 'split graph' (a special class of perfect graphs). Refer to [Imrich and Klavžar, 2000] for a long list of characterizations for partial cubes.

Wetzel [Wetzel, 1995] (see also Dress and Huson [Dress and Huson, 2004]) characterized splits graphs in terms of isometric colorings. Let σ be an edge coloring of the graph. For each pair $u, v \in V(G)$ let $C_\sigma(u,v)$ denote the set of colors appearing on *all* shortest paths between u and v. We say that σ is an *isometric coloring* if $d_G(u,v) = |C_\sigma(u,v)|$ for all pairs $u, v \in V(G)$. In other words, σ is isometric if the edges along any shortest path all have different colors, while any two shortest paths between the same pair of vertices have the same set of edge colors. A connected graph is a splits graph if and only if it has an isometric coloring [Wetzel, 1995].

A third characterization of splits graphs is due to [Winkler, 1984]. We define a relation Θ on pairs off edges $e_1 = \{u_1, v_1\}$ and $e_2 = \{u_2, v_2\}$ in a graph G by

$$e_1 \Theta e_2 \Leftrightarrow d_G(u_1,u_2) + d_G(v_1,v_2) \neq d_G(u_1,v_2) + d_G(v_1,u_2). \tag{17.1}$$

This relation is an equivalence relation if and only if G is a splits graph.

Two edges e_1 and e_2 in a splits graph have the same color an isometric coloring if and only if the isometric embedding of the splits graph maps e_1 and e_2 to edges in the same dimension, if and only if $e_1 \Theta e_2$. Thus, a splits graph has, essentially, a unique isometric coloring and a unique isometric embedding into the hypercube. The partition of edges into color classes is completely determined by the graph.

Suppose now that we have a splits graph G and a map $\phi : X \to V(G)$. Using the isometric embedding, one can quickly prove that removing all edges in a particular color class partitions the graph into exactly two connected (and convex) components. This in turn induces a split of X, via the map ϕ. A *splits network* is a pair $\mathcal{N} = (G, \phi)$ such that

(i) G is a splits graph.

(ii) ϕ is a map from X to $\phi(G)$.

(iii) Each color class induces a distinct split of X.

The set of splits induced by the different color classes is denoted $splits(\mathcal{N})$.

Time for two examples. The split network on the left of figure 17.1 corresponds to a collection of compatible splits - it is a tree. In this network, every edge is in a distinct color class. If we add the split $\{\{2,6\},\{1,3,4,5\}\}$ we get the split network on the right. There are four color classes in this graph that contain more than a single edge. These are the three horizontal pairs of parallel edges and the four edges marked in bold that induce the extra split.

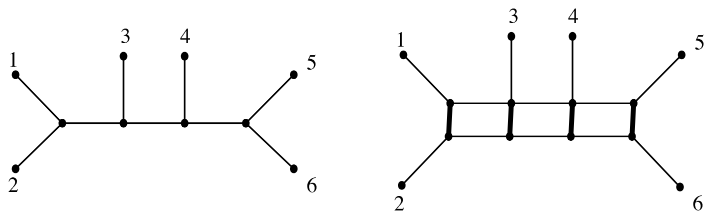

Fig. 17.1. Two splits networks. On the left, a split network for compatible splits (i.e. a tree). On the right, the same network with the split $\{\{2,6\},\{1,3,4,5\}\}$ included.

It is important to realize that the split network for a collection of splits may not be unique. Figure 17.2 reproduces an example in [Wetzel, 1995]. Both graphs are split networks for the set

$$\mathcal{S} = \Big\{\{\{1,2,3\},\{4,5,6,7\}\},\{\{2,3,4\},\{1,5,6,7\}\},\{\{1,2,7\},\{3,4,5,6\}\},\{\{1,2,6,7\},\{3,4,5\}\}\Big\}.$$

Each is minimal, in the sense that no subgraph of either graph is also a splits network. In both graphs, the edges in the color class inducing the split $\{\{1,2,3\},\{4,5,6,7\}\}$ are in bold.

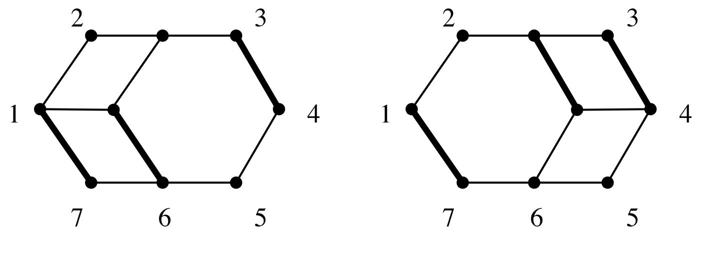

Fig. 17.2. Two different, and minimal, split networks for the same set of splits

17.3 Distance based models for trees and splits graphs

In molecular phylogenetics, the length of an edge in a tree is typically measured in terms of the average (or expected) number of mutations that occurred, per site, along that edge. The *evolutionary distance* between two sequences equals the sum of the lengths of the edges along the unique path the connects them in the unknown 'true' phylogeny. There is a host of methods for estimating the evolutionary distance starting from the sequences alone. These form the basis of distance based approaches to phylogenetics.

The oldest statistical methods for phylogenetics use models of how evolutionary distances estimated from pairwise comparisons of sequences differ from the true evolutionary distances (or *phyletic distances*) in the true, but unknown, phylogenetic tree [Cavalli-Sforza and Edwards, 1967, Farris, 1972, Bulmer, 1991]. It is assumed that the pairwise estimates were distributed, at least approximately, according to a multi-variate normal density centered on the true distances. The variance-covariance matrix for the density, here denoted by V, can be estimated from the data [Bulmer, 1991, Susko, 2003], though early papers used a diagonal matrix, or the identity, for V.

Once we have a variance covariance matrix, and the observed distances, we can begin maximum likelihood estimation of the true distances δ_T, from which we can construct the maximum likelihood tree. Note that the term maximum likelihood here refers only to our approximate distance based model, not to the maximum likelihood estimation introduced by Felsenstein [Felsenstein, 1981]. The maximum likelihood estimator is the tree metric $\widehat{\delta_T}$ that maximizes the likelihood function

$$L(\widehat{\delta_T}) = \Phi_{\binom{n}{2}}(d - \delta_T | V)$$

where Φ_m is the probability density function for the m dimensional multivariate normal:

$$\Phi_m(x|V) = \frac{1}{(2\pi)^{\frac{m}{2}}\sqrt{\det(V)}} e^{-\frac{1}{2}x^T V^{-1} x}.$$

Equivalently, we can minimize the least squares residue

$$\sum_{w<x}\sum_{y<z} \big(\widehat{\delta_T}(w,x) - d(w,x)\big) \mathbf{V}^{-1}_{(wx)(yz)} \big(\widehat{\delta_T}(y,z) - d(y,z)\big).$$

In either formulation, the optimization is carried out over all tree metrics in $\mathcal{T}_X$, the space of X-trees (Chapter 2).

We can describe tree metrics in terms of linear combinations of split metrics. The split metric for a split $\{A, B\}$ is the pseudo-metric on X given by

$$\delta_{\{A,B\}}(x,y) = \begin{cases} 0 & \text{if } \{x,y\} \subseteq A \text{ or } \{x,y\} \subseteq B; \\ 1 & \text{otherwise.} \end{cases}$$

Let $w_{\{A,B\}}$ denote the length of the edge associated to a split $\{A, B\} \in splits(T)$. Then

$$\delta_T = \sum_{\{A,B\} \in splits(T)} w_{\{A,B\}} \delta_{\{A,B\}}. \tag{17.2}$$

This formulation is used when we want to estimate edge lengths on a fixed topology.

Equation (17.2) generalizes immediately to split networks. Suppose that the lengths of the edges in a split network $\mathcal{N}$ are given by the split weights $w_{\{A,B\}}$. Hence, all edges in the same color class have the same length. The distance between two labeled vertices x, y is the length of the shortest path between them, which in turn equals the sum of the weights of the splits separating x and y. We can therefore define a *network metric* $\mathcal{N}$ by

$$\delta_{\mathcal{N}} = \sum_{\{A,B\} \in splits(\mathcal{N})} w_{\{A,B\}} \delta_{\{A,B\}}.$$

The statistical model for distances from splits networks then works exactly as it did for phylogenetic trees. We assume that the observed distances d are distributed according to a multi-variate normal centered on the network metric $\delta_{\mathcal{N}}$. The covariance matrix can be estimated using the non-parametric method of Susko [Susko, 2003]. The likelihood of a network metric $\widehat{\delta_{\mathcal{N}}}$ is, as before, given by $L(\widehat{\delta_{\mathcal{N}}}) = \Phi_{\binom{n}{2}}(d - d_{\mathcal{N}})$.

We immediately come across the problem of identifiability. Phylogenetic trees, together with their edge lengths, are determined uniquely from their tree metrics. The same does not apply for network distances. The split metrics $\delta_{\{A,B\}}$ associated to splits of a network will not, in general, be linearly independent.

In practice, identifiability has not been too much of a problem. Split decomposition produces *weakly compatible* collections of splits. These have linearly independent and are uniquely determined from their network metrics [Bandelt and Dress, 1992]. Neighbor-Net produces networks based on *circular collections of splits* which, as a subclass of weakly compatible splits, are also uniquely determined from their network metrics.

However the most important shortcoming of distance based methods, for either trees of networks, is that they lack the statistical efficiency of likelihood methods based on full stochastic models (see, e.g. Felsenstein [Felsenstein, 2003]). When we estimate distances from pair-wise sequence comparisons we are effectively ignoring the joint probabilities of larger sets of sequences. What we gain in speed, we lose in accuracy.

17.4 A graphical model on a splits network?

The Markov model for trees outlined in Chapter 2 and Chapter 4 is just a special case in a general class of graphical models (Section 1.5). Given the vast literature on graphical models, it seems that the logical generalization of the hidden tree model would be a graphical model defined on the splits network. This was the approach taken by [Strimmer and Moulton, 2000, Strimmer *et al.*, 2001]. We review this approach here, and point out why it doesn't really work.

Let $\mathcal{N}$ be a splits network. The first step is to choose a root and direct all edges away from the root (Figure 17.3). We now can apply a directed graphical model. The probability that a node is assigned a particular state depends on the states assigned to its parents: Strimmer and Moulton suggest several ways that this may be done.

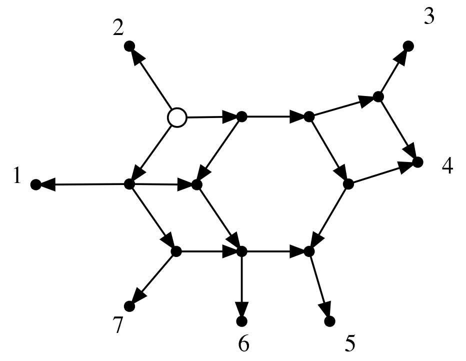

Fig. 17.3. Edge directions induced by placing the root at the white vertex.

There are several problems with this general approach. Firstly, the probability of observing the data changes for different positions of the root, even when the mutation process is a time reversible model. It was claimed that this permitted estimation of the root, but there is no indication that the differences in distributions corresponded to any evolutionary phenomenon.

Secondly, different split networks for the *same* set of splits give different pattern probabilities, even though the networks represent exactly the same information.

Thirdly, the internal nodes in split networks do not represent hypothetical ancestors, they are products of an embedding in a hypercube.

Strimmer et al. eventually concluded that split networks may not provide a suitable underlying graph for a stochastic network [Strimmer *et al.*, 2001]. It is true that graphical model technology can not be applied 'straight-off-the-shelf' to split networks. We need to be more sensitive to the particular properties of split networks. In the following section we will develop a model for split networks that avoids the problems encountered in the graphical model approach. The downside, however, is that we must first restrict ourselves to a special class of mutation models: group based models.

17.5 Group based mutation models

A mutation model on state space $\{1, 2, \ldots, r\}$ is said to be a *group based model* if there exists an abelian group G with elements $g_1, \ldots, g_r$ and a function $\psi : G \to \Re$ such that the instantaneous rate matrix Q satisfies

$$Q_{ij} = \psi(g_j - g_i)$$

for all i, j. The group operation on G is denoted using addition and we will use 0 for the identity element.

Let f be a function from G to the set of complex numbers $\mathbb{C}$ such that $f(g + g') = f(g)f(g')$ for all $g, g' \in G$. Then f is a *homomorphism* from G to $\mathbb{C}$. The set of these homomorphisms forms a group $\widehat{G}$ that is isomorphic to G. We label the elements of $\widehat{G}$ so that the map $g \to \widehat{g}$ taking $g \in G$ to $\widehat{g} \in \widehat{G}$ is an isomorphism. If $g = 0$ then $\widehat{g}$ is the function taking every element of G to 1.

Lemma 17.1 *Suppose that $g, h, h' \in G$, $a \in \mathbb{Z}$. Then we have the following identities:*

$$\begin{aligned}
\widehat{g}(-h) &= \overline{\widehat{g}(h)};\\
\widehat{g}(h + h') &= \widehat{g}(h)\widehat{g}(h');\\
(\widehat{h + h'})(g) &= \widehat{h}(g)\widehat{h'}(g);\\
\widehat{ag}(h) &= \widehat{g}(ah);\\
\sum_{h \in G} \widehat{g}(h) &= \begin{cases} |G| & \textit{if } g = h;\\ 0 & \textit{otherwise.}\end{cases}
\end{aligned}$$

Proof See, for example, [Körner, 1989]. □

Some indexing conventions will make our life easier. Since the elements of G are in one to one correspondence with $\{1, 2, \ldots, r\}$ we will index Q and $P(t)$ by group elements. So $Q_{g_i g_j}$ is equivalent to Q_{ij}.

We start with some basic observations about group valued models.

Lemma 17.2 *(i) The eigenvalues of Q are given by*

$$\lambda_g = \sum_{h \in G} \overline{\widehat{g}(h)}\psi(h).$$

(ii) *The transition probabilities are given by*

$$P_{gg'}(t) = \frac{1}{r}\sum_{h\in G}\widehat{h}(g'-g)e^{\lambda_h t}.$$

(iii) *The uniform distribution is a stationary distribution.*

(iv) *If the process is ergodic and time reversible then $\psi(g) = \psi(-g)$ for all $g \in G$.*

Proof Define the $r \times r$ matrix K by $K_{ij} = \widehat{g_i}(g_j)$. Then

$$\begin{aligned}(KQ)_{gg'} &= \sum_{h\in G}\widehat{g}(h)\psi(g'-h)\\ &= \sum_{h\in G}\widehat{g}(g'-h)\psi(h) \qquad\qquad [\text{replacing } h \text{ by } g'-h]\\ &= \widehat{g}(g')\sum_{h\in G}\overline{\widehat{g}(h)}\psi(h)\\ &= K_{gg'}\lambda_g.\end{aligned}$$

Thus the rows of K are left-eigenvectors for Q. This proves (i). Let Λ be the diagonal matrix with $\Lambda_{gg} = \lambda_g$. Then $Q = K^{-1}\Lambda K$. By the orthogonality property in Lemma 17.1 we have $K^{-1} = \frac{1}{|G|}K^*$. Thus

$$\begin{aligned}P_{gg'}(t) &= (e^{Qt})_{gg'}\\ &= \frac{1}{|G|}(K^* e^{\Lambda t}K)_{gg'}\\ &= \frac{1}{r}\sum_{h\in G}\overline{\widehat{h}(g)}e^{\lambda_h t}\widehat{h}(g')\\ &= \frac{1}{r}\sum_{h\in G}\widehat{h}(g'-g)e^{\lambda_h t}\end{aligned}$$

proving (*ii*). For (*iii*), observe that the first row of K gives a left-eigenvector that is all ones. Finally, if the process is ergodic then the uniform distribution is the unique stationary distribution. This, together with the assumption that the process is time reversible, implies that both Q and $P(t)$ are symmetric and that $\psi(g) = \psi(-g)$ for all g. □

We define

$$\phi_t(g) = \frac{1}{r}\sum_{h\in G}\widehat{h}(g)e^{\lambda_h t}$$

so that $P_{gg'}(t) = \phi_t(g'-g)$ for all $g, g' \in G$ and $t \geq 0$.

As an example, consider the case when $r = 4$. There are two (up to isomorphism) abelian groups on four elements, $\mathbb{Z}_4$ and $\mathbb{Z}_2 \times \mathbb{Z}_2$. If $G = \mathbb{Z}_4$ then the condition that $\psi(g) = \psi(-g)$ implies that Q must have the form

$$Q = \begin{pmatrix} -2a-b & a & b & a \\ a & -2a-b & a & b \\ b & a & -2a-b & a \\ a & b & a & -2a-b \end{pmatrix}$$

so the mutation model is a sub-class of the K2P model (Chapter 4). If $G = \mathbb{Z}_2 \times \mathbb{Z}_2$ then we always have $g = -g$ so there are three parameters available for Q:

$$Q = \begin{pmatrix} -a-b-c & a & b & c \\ a & -a-b-c & c & b \\ b & c & -a-b-c & a \\ c & b & a & -a-b-c \end{pmatrix}.$$

In this case, the mutation models are a subclass of Kimura's three parameter model [Kimura, 1981].

17.6 Group based models on trees and splits

Suppose that we have an ergodic, time reversible, group based mutation model with state set $\Sigma = \{1, 2, \ldots, r\}$ and abelian group G, where $Q_{ij} = \psi(g_j - g_i)$ for all i, j. Let $P(t) = e^{Qt}$ denote the corresponding transition probabilities. Let T be a phylogenetic tree with n leaves. We use $t_e = t_{kl}$ to denote the length of an edge $e = kl \in E(T)$. In terms of the tree model of Chapter 2, $\theta^{kl} = P(t_{kl})$ for all $kl \in E(T)$.

Lemma 17.3 *Let σ be a map from $N(T)$ to Σ. For each edge $e = kl$ define $x_e = g_{\sigma_l} - g_{\sigma_k}$. Then*

$$p_\sigma = \frac{1}{r} \prod_{e \in E(T)} \phi(x_e).$$

Proof By Lemma 17.2 the mutation model has a uniform stationary distribution. We can therefore apply (1.53), giving

$$\begin{aligned} p_\sigma &= \frac{1}{|\Sigma|} \prod_{kl \in E(T)} \theta^{kl}_{\sigma_k \sigma_l} \\ &= \frac{1}{r} \prod_{kl \in E(T)} \phi_{t_{kl}}(g_{\sigma_l} - g_{\sigma_k}) \\ &= \frac{1}{r} \prod_{e \in E(T)} \phi_{t_e}(x_e). \end{aligned}$$

□

Let χ be a map from the leaves of T to Σ. We say that $\sigma : N(T) \to \Sigma$ extends χ if $\sigma_i = \chi_i$ for all leaves i. Under the *hidden tree model* the probability of observing χ is defined

$$p_\chi = \sum_{\sigma:\sigma \text{ extends } \chi} p_\sigma.$$

Suppose that $E(T) = \{e_1, e_2, \ldots, e_q\}$, let $\{A_k, B_k\}$ be the split associated to edge k and let A be the $(n-1) \times q$ matrix defined by

$$(A)_{ik} = \begin{cases} 1 & i \text{ and } n \text{ are on opposite sides of } \{A_k, B_k\} \\ 0 & \text{otherwise.} \end{cases} \tag{17.3}$$

The next observation is crucial.

Theorem 17.4 *Define the vector $y = y[\chi] \in G^{n-1}$ by $y_i = \chi_i - \chi_n$. Then*

$$p_\chi = \sum_{\substack{x:Ax=y \\ x \in G^q}} \prod_{e \in E(T)} \phi_{t_e}(x_e). \tag{17.4}$$

Proof Suppose that x is defined from σ as in Lemma 17.3. We prove that $Ax = y$ if and only if σ extends χ, so that the result follows from Lemma 17.3.

For each leaf i, let E_i be the edges on the path from leaf n to leaf i. We will assume that T is rooted at leaf n, so all edges in E_i are directed away from n. Then

$$\begin{aligned} (Ax)_i &= \sum_{kl \in E_i} x_{kl} \\ &= \sum_{kl \in E_i} (g_{\sigma_l} - g_{\sigma_k}) \\ &= g_{\sigma_i} - g_{\sigma_n}. \end{aligned}$$

Thus $Ax = y$ if and only if $g_{\sigma_i} = \chi_i$ for all leaves i, if and only if σ extends χ.
□

The importance of Theorem 17.4 so far as we are concerned is that p_χ is not expressed in terms of the tree structure: it is defined in terms of splits. We can therefore generalize the definition of pattern probabilities to any collection of splits.

Let $\mathcal{N}$ be a weighted split network with splits $\{A_1, B_1\}, \{A_2, B_2\}, \ldots, \{A_q, B_q\}$ and let t_k be the length assigned to split $\{A_k, B_k\}$. Let A be the matrix defined by Equation 17.3. The *probability of a phylogenetic character χ given $\mathcal{N}$* is then defined by

$$p_\chi = \sum_{\substack{x:Ax=y\\ x\in G^q}} \prod_{k=1}^{q} \phi_{t_k}(x_k). \tag{17.5}$$

Astute readers will notice an uncanny similarity between (17.4) and (17.5).

Theorem 17.5 *Let $\mathcal{N}$ be a weighted split network. If the splits of $\mathcal{N}$ are compatible then the character probabilities correspond to exactly those given by the tree based model.*

We can rephrase this model in terms of graphical models on the splits network. We say that a map $\sigma : V(\mathcal{N}) \to \Sigma$ is *concordant* if $\sigma_l - \sigma_k = \sigma_j - \sigma_i$ for all pairs of edges $ij, kl \in E(\mathcal{N})$ in the same color class. The probability of a map σ is just the product of $P_{\sigma_k \sigma_l}(t_{kl})$ over all edges $kl \in E(T)$, where t_{kl} is the length of the edge. We then have that p_χ equals the probability that a map σ extends χ, conditional on σ being concordant.

17.7 A Fourier calculus for split networks

Szekely et al. [Székely *et al.*, 1993] describe a *Fourier calculus on evolutionary trees* that generalizes the Hadamard transform of [Hendy and Penny, 1989, Steel *et al.*, 1992]. Using their approach, we can take the observed character frequencies, apply a transformation, and obtain a vector of values from which we can read off the support for different splits. They show that if the observed character frequencies correspond exactly to the character probabilities determined by some phylogenetic tree then the split supports will correspond exactly to the splits and branch lengths in the phylogenetic tree. Conversely, the inverse transformation gives a single formula for the character probabilities in any tree.

This theory generalizes seamlessly from trees to split networks—in fact so seamlessly that the proofs of [Székely *et al.*, 1993] require almost no modifications to establish the general case. Their approach was prove that their transform worked when applied to character probabilities from a tree. The correctness of the inverse formula then followed by applying a Fourier transformation. In this section we will prove the same results but working in the opposite direction. We show that, starting with weights on the splits, a single invertible formula gives the character probabilities. Our rationale is that, at some point in the future, we will need to generalize these results beyond Abelian group models, and the elegant Fourier inversion formula may not exist in this context.

First a little more algebra. For $x, y \in G^m$ we define

$$\widehat{y}(x) = \prod_{i=1}^{m} \widehat{y_i}(x_i).$$

The set $\{\widehat{y} : y \in G^m\}$ forms a group under multiplication that is isomorphic to G^m.

The following can (and should) be proved directly using an elegant result in algebra, but I could only come up with a low-technology proof.

Lemma 17.6 *Suppose that $z \in G^q$ and $y \in G^{n-1}$. Let A be an $(n-1) \times q$ integer matrix with linearly independent rows. Either*

$$\sum_{x \in G^q : Ax = y} \widehat{z}(x) = 0$$

or there is $u \in G^{n-1}$ such that $z = A^T u$ and so

$$\sum_{x \in G^q : Ax = y} \widehat{z}(x) = r^{q-(n-1)} \widehat{z}(u)$$

Proof Suppose that $\sum_{x \in G^q : Ax = y} \widehat{z}(x) \neq 0$. For any v such that $Av = 0$ we have

$$\sum_{x \in G^q : Ax = y} \widehat{z}(x) = \sum_{x \in G^q : Ax = y} \widehat{z}(x + v) = \widehat{z}(v) \sum_{x \in G^q : Ax = y} \widehat{z}(x)$$

so $\widehat{z}(v) = 1$.

For every $x, y \in G^{n-1}$ we have

$$Ax = Ay \Leftrightarrow A(x - y) = 0 \Leftrightarrow \widehat{z}(x - y) = 1 \Leftrightarrow \widehat{z}(x) = \widehat{z}(y).$$

We can thus define a map $f : G^{n-1} \to \mathbb{C}$ by setting $f(Ax) = \widehat{z}(x)$ for all $x \in G^q$. This is a homomorphism, since $f(Ax+Ay) = f(A(x+y)) = \widehat{z}(x+y) = \widehat{z}(x)\widehat{z}(y) = f(Ax)f(Ay)$. Thus there is u such that $f = \widehat{u}$ and, for all $x \in G^q$, $\widehat{z}(x) = \widehat{u}(Ax)$. The result now follows by expanding $\widehat{u}(Ax)$. □

We will assume that $\mathcal{N}$ contains all the trivial splits $\{\{i\}, X - \{i\}\}$ since these can be added and assigned weight zero. Let H be the matrix with rows and columns indexed by G^{n-1} and $H_{gg'} = \widehat{g}(g)$. Define the vector b by

$$b_z = \begin{cases} \psi(h)t_k & \text{if there is } h \in G \text{ and } k \text{ such that } z = A_{ikh} \text{ for all } i \\ -\sum_{v \in G^{n-1}-\{0\}} b_v & \text{if } z = 0 \\ 0 & \text{otherwise.} \end{cases}$$

Theorem 17.7 *Let $y \in G^{n-1}$ be the vector such that $y_i = g_{\chi_n} - g_{\chi_i}$ for all leaves i. Then*

$$p_\chi = \left[H^{-1}\exp[Hb]\right]_y . \tag{17.6}$$

Proof ¿From (17.5) we have

$$\begin{aligned} p_\chi &= \sum_{\substack{x:Ax=y\\ x\in G^q}} \prod_{k=1}^{q} \phi_{t_k}(x_k) \\ &= \sum_{\substack{x:Ax=y\\ x\in G^q}} \prod_{k=1}^{q} \frac{1}{r} \sum_{h\in G} \widehat{h}(x_k) e^{\lambda_h t_k} \\ &= \frac{1}{r^q} \sum_{\substack{x:Ax=y\\ x\in G^q}} \sum_{z\in G^q} \prod_{k=1}^{q} \widehat{z_k}(x_k) e^{\lambda_{z_k} t_k} \\ &= \frac{1}{r^q} \sum_{z\in G^q} \left(\sum_{\substack{x:Ax=y\\ x\in G^q}} \widehat{z}(x) \right) \exp\left[\sum_{k=1}^{q} \lambda_{z_k} t_k\right]. \end{aligned}$$

So far we have just applied the definitions, reversed a summation and product, and regrouped. From Lemma 17.6 we get that $\widehat{z}(x) = 0$ unless $z = A^T\overline{u}$ for some u (the change from u to $\overline{u}$ is not a problem). Substituting in we obtain

$$\begin{aligned} p_\chi &= \frac{1}{r^{n-1}} \sum_{u\in G^{n-1}} \widehat{\overline{u}}(y) e^{\beta_u} \\ &= H^{-1}\exp[\beta] \end{aligned}$$

where

$$\begin{aligned}
\beta_u &= \sum_{k=1}^{q} \lambda_{(A^T\overline{u})_k} t_k \\
&= \sum_{k=1}^{q} \sum_{h\in G} \widehat{A^T u_k}(h)\psi(h)t_k \\
&= \sum_{k=1}^{q} \sum_{h\in G} \widehat{u}(\eta_{kh})\psi(h)t_k \\
&= \sum_{v\in G^{n-1}} \widehat{u}(v)b_v \\
&= Hb.
\end{aligned}$$

□

We have proven, more or less, Theorem 6 of [Székely *et al.*, 1993] without any reference to trees. In the special case that $r = 2$, (17.6) becomes the classical *Hadamard transform* of [Hendy and Penny, 1989, Steel *et al.*, 1992].

Note that the formula $H^{-1}\exp[Hb$ is invertible. This means that every split network gives a different character distribution. We cannot recover split networks from their distance metrics $d_{\mathcal{N}}$ but we can recover them from their character probabilities. A maximum likelihood estimator based on (17.6) will be statistically consistent.

17.8 Discussion

We have discussed ways in which stochastic models for trees can be generalized to split networks. En route, we have rediscovered the Fourier calculus approach of [Székely *et al.*, 1993]. This is comforting: Felsenstein describes the Hadamard type approach as "one of the nicest applications of mathematics to phylogenies so far." While we have not made a substantial mathematical contribution to the theory, we have proposed a quite different way to look at these methods.

For us, the Hadamard transform is useful because it gives character probabilities for general collections of splits, not because it is invertible. A maximum likelihood method, or Bayesian method, only requires a way to compute character probabilities. The transform taking probabilities to split weights is less useful in this context, since it requires a huge number of parameters. If we use the Hadamard as a statistical model we can optimize likelihood and restrict the number of parameters appropriately.

One key problem remains. The constraint that we only use group based mutation models is too much of a restriction. For nucleotide data, and especially for protein data, a uniform stationary distribution is unrealistic. It is reasonable to believe that some reasonable generalization of these results exists for more general mutation models: after all there is no such restriction on distance based methods. What exact form these generalizations will take is, at the moment, anybody's guess.

18

Small Trees and Generalized Neighbor-Joining

Mark Contois

Dan Levy

Direct reconstruction of phylogenetic trees by maximum likelihood methods is computationally prohibitive for trees with many taxa; however, by computing all trees for subsets of taxa of size m, we can attempt to infer the entire tree. In particular, if $m = 2$, the traditional distance-based methods such as neighbor-joining [Saitou and Nei, 1987] and UPGMA [Sneath and Sokal, 1973] are applicable. Under distance-based methods, 2-leaf subtrees are completely determined by the total length between the pairs of leaves. We extend this idea to m leaves by defining the m-dissimilarity of a set $R \in \binom{X}{m}$ as the total length of the subtree spanning R. By building small subtrees of size m and finding the total length, we can obtain an m-dissimilarity map on X. We will define the Generalized Neighbor-Joining (GNJ) algorithm [Levy *et al.*, 2004] for obtaining a phylogenetic X-tree with edge lengths given an m-dissimilarity map on X.

This algorithm is consistent: given an m-dissimilarity map D^T that comes from a tree T, GNJ returns the correct tree. However, in the case of data that is "noisy", e.g., when the observed dissimilarity map does not lie in the space of X-trees, the accuracy of GNJ depends on the reliability of the subtree lengths. Numerical methods may run into trouble when models are of high degree (1.3); exact methods for computing subtrees, therefore, could only serve to improve the accuracy of GNJ. One family of such methods consists of algorithms to find critical points of the ML equations as discussed in chapter 15 and in [Hoşten *et al.*, 2004]. We explore the results of this method for the Jukes-Cantor DNA model on three taxa and conjecture that, for any 3-subtree, there is at most one critical point yielding edge lengths that are positive and real.

18.1 From Alignments to Dissimilarity

Any method for phylogenetic tree reconstruction begins with a sequence alignment. Distance-based methods then proceed by comparing pairs of taxa from this alignment to find the distances between them. Let X be the set of taxa and $\binom{X}{k}$ the set of all subsets $R \subset X$ such that $|R| = k$. Then $\binom{X}{2}$ is the set of all pairs of taxa and $D : \binom{X}{2} \to \mathbb{R}_{>0}$ assigns a distance to each pair of taxa. We call D a *dissimilarity map on* X. Where there is no confusion, we will write $D(\{a,b\})$ as $D(a,b)$.

If a and b are taxa in X, we may compare their aligned sequences to find the Jukes-Cantor corrected distance $D_{JC}(a,b)$. If the alignment has a length of L and a and b differ in k places, then

$$D_{JC}(a,b) = -\frac{3}{4}\log\left(1 - \frac{4}{3}p\right) \tag{18.1}$$

where $p = \frac{k}{L}$. It has been shown in 4.2 that $D_{JC}(a,b)$ is the maximum likelihood branch length estimate of the alignment of a and b, with respect to the JC model on the simple two-leaf tree. The conceit of distance-based methods is that the branch length estimate on the two-leaf tree is a good estimate of the total path length from a to b in the maximum likelihood tree T on X. Stated in the terms of section 2.4, distance based methods are effective when D_{JC} is close to δ_T, the tree metric on X induced by T. (Recall that $\delta_T(a,b) = \sum_{e \in P_{ab}} l_T(e)$, where P_{ab} is the path from a to b in T and l_T is the length function associated to the edges of T.)

We can extend the notion of dissimilarity maps to subsets of X larger than two. We define an *m-dissimilarity map on X* as a function $D : \binom{X}{m} \to \mathbb{R}_{>0}$. That is, D assigns a positive real value to every subset of X of size m. In particular, a dissimilarity map is a 2-dissimilarity map. Again, where there is no confusion, we will write $D(\{x_1, ..., x_m\})$ as $D(x_1, ..., x_m)$. For a subset $R \subseteq X$, we define $[R]$ as the spanning subtree of R in T: $[R]$ is the smallest subtree of T containing R. For two leaves, $a, b \in X$, the path from a to b, P_{ab}, is equivalent to the spanning subtree $[\{a,b\}]$.

Just as we defined tree metrics induced by a tree T, we can define the m-dissimilarity map induced by T, $D_m^T : \binom{X}{m} \to \mathbb{R}_{>0}$ by

$$D_m^T(R) = \sum_{e \in [R]} l_T(e)$$

for $R \subset X, |R| = m$. $D_m^T(R)$ is the sum of all the edge lengths in the spanning subtree of R. We call $D_m^T(R)$ the *m-subtree length* of $[R]$. Since $P_{ab} = [\{a,b\}]$, $D_2^T(a,b) = \delta_T(a,b)$, and the 2-dissimilarity map induced by T is a tree metric.

Just as we used the JC corrected distance to approximate δ_T, we can employ analytical or numerical methods to find maximum likelihood estimates for the total branch lengths of subtrees with m leaves. To find an approximate m-dissimilarity map, D, for all $R \in \binom{X}{m}$, we find the MLE tree for R and sum the branch lengths:

$$D(R) = \sum_{e \in T(R)} l_{T(R)}(e)$$

where $T(R)$ is the MLE tree for R.

18.2 From Dissimilarity to Trees

The neighbor-joining algorithm and its variants are examples of methods that take an approximate dissimilarity map and construct a "nearby" tree. Similarly, we would like to define an algorithm that takes as its input an m-dissimilarity map and constructs a "nearby" tree, and we would like this method to be consistent: given an m-dissimilarity map D_m^T induced by a tree T, our algorithm should return T.

The crux of our method is the construction of a 2-dissimilarity map S_D from the m-dissimilarity map D. In the case that D is induced by a tree T, then S_D will be the tree metric induced by a tree T'. Further, T' is isomorphic to a contraction of certain "deep" edges, $E_{>n-m}(T)$, of T. If $|X| > 2m-1$, then T and T' are topologically equivalent. Further, there exists an invertible linear map from edge lengths of T to the edge lengths of T'.

The deletion of an edge e in T divides T into two subtrees $T_1(e)$ and $T_2(e)$. If $L(T_1(e))$ and $L(T_2(e))$ are the leaves in each subtree, then we define the *depth of* e, $d(e)$ by

$$d(e) = \min(|L(T_1(e))|, |L(T_2(e))|).$$

Observe that the pendant edges are exactly those edges of depth 1, and, if T has n leaves, then $d(e) \leq \frac{n}{2}$ for any $e \in E(T)$. We define $E_{>k}(T) = \{e \in E : d(e) > k\}$. For example, $E_{>1}(T)$ is all the interior edges of T.

For any edge e in T, we may contract e by deleting the edge and identifying its vertices. We write the resulting tree as T/e and for a set of edges E', the contraction of each edge in that set is denoted as T/E'. For example, $T/E_{>1}(T)$ contracts all interior edges and has the star topology (figure 18.1). We may now state our claim explicitly:

Theorem 18.1 *Let D be an m-dissimilarity map on a set X of size n. We define*

$$S_D(i,j) = \sum_{R \in \binom{X \setminus \{i,j\}}{m-2}} D(i,j,R). \qquad (18.2)$$

If $D = D_m^T$ then $S_D = D^{T'}$ and T' is isomorphic to $T/E_{>n-m}$. Further, there exists an invertible linear transformation between the interior edge lengths of T' to $T/E_{>n-m}$. If $E_{>n-m}$ is empty, then there is also an invertible linear

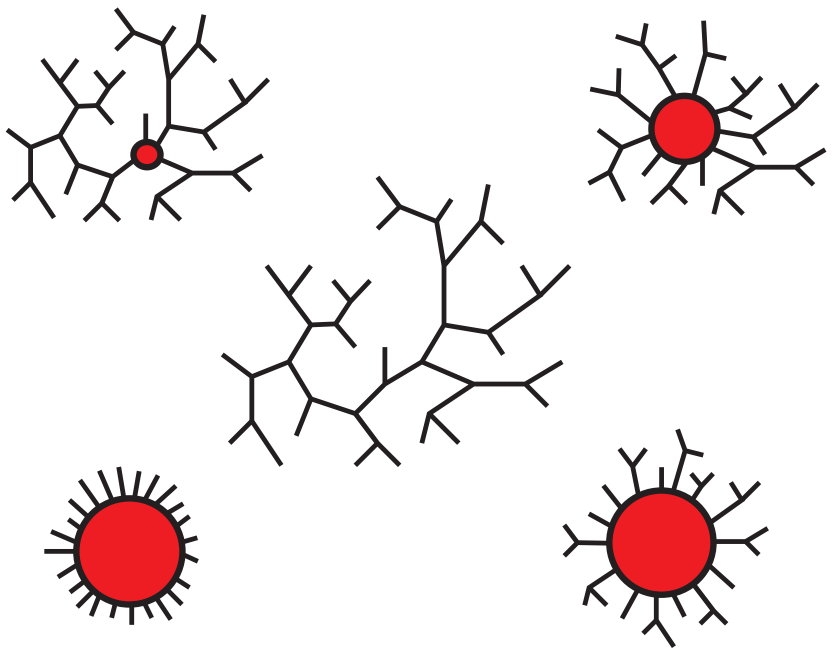

Fig. 18.1. In the center, we have a tree T surrounded by $T/E_{>k}$ for $k = 11, 4, 2$, and 1 starting at the top left and proceeding clockwise. The red circle represents the vertex to which the edges of $E_{>k}$ have collapsed. Notice that T has 24 leaves and so $E_{>12} = \emptyset$ and $T/E_{>12} = T$.

transformation between the pendant edges; otherwise, the pendant edges may not be determined uniquely.

Observe that for a phylogenetic X-tree with edge lengths, T, any linear combination of the m-subtree lengths is a linear combination of the edge lengths $l_T(e)$ in the tree. This is because $D_m^T(R) = \sum_{e \in [R]} l_T(e)$; i.e. every m-subtree length is the sum of the edge lengths in the spanning subtree. For a linear function on the m-subtree lengths $F : \mathbb{R}^{\binom{n}{m}} \to \mathbb{R}$, let $v_F(e)$ denote the coefficient of $l_T(e)$ in F. For instance, $v_{S(i,j)}(e)$ denotes the coefficient of $l_T(e)$ in $S(i,j)$. Note that $v_{F+G}(e) = v_F(e) + v_G(e)$. We will also use the notation $L_i(e)$ to denote the set of leaves in the component of $T \setminus e$ that contains leaf i.

Lemma 18.2 *Given a pair of leaves a, b and any edge e we have*

$$v_{S(a,b)}(e) = \begin{cases} \binom{n-2}{m-2} & e \in P_{ab}; \\ \\ \binom{n-2}{m-2} - \binom{|L_a(e)|-2}{m-2} & e \notin P_{ab}. \end{cases}$$

Proof If e is on the path from a to b, then it will be included in all the subtrees

$[a, b, Y]$. If e is not on the the path from a to b, then the only way it will be excluded is if all the other leaves fall on the a side of e (which is the same as the b side); that is, if $Y \subset L_a(e) \setminus \{a, b\}$. There are $\binom{|L_a(e)|-2}{m-2}$ such sets. □

Lemma 18.3 *Given a quartet* $(a_1, a_2; a_3, a_4)$ *in* T *with interior vertices* b_1 *and* b_2 *(figure 18.2),*

$$v_{S(a_1,a_2)+S(a_3,a_4)}(e) = \begin{cases} 2\binom{n-2}{m-2} - \binom{n-|L_{a_i}(e)|-2}{m-2} & e \in P_{a_i b_{\lceil i/2\rceil}}; \\ 2\binom{n-2}{m-2} - \binom{|L_{a_1}(e)|-2}{m-2} - \binom{|L_{a_3}(e)|-2}{m-2} & e \in P_{b_1 b_2}; \\ 2\binom{n-2}{m-2} - 2\binom{|L_{a_1}(e)|-2}{m-2} & e \notin [a_1, a_2, a_3, a_4]. \end{cases}$$

$$v_{S(a_1,a_3)+S(a_2,a_4)}(e) = \begin{cases} 2\binom{n-2}{m-2} - \binom{n-|L_{a_i}(e)|-2}{m-2} & e \in P_{a_i b_{\lceil i/2\rceil}}; \\ 2\binom{n-2}{m-2} & e \in P_{b_1 b_2}; \\ 2\binom{n-2}{m-2} - 2\binom{|L_{a_1}(e)|-2}{m-2} & e \notin [a_1, a_2, a_3, a_4]. \end{cases}$$

and

$$v_{S(a_1,a_4)+S(a_2,a_3)} = v_{S(a_1,a_3)+S(a_2,a_4)}$$

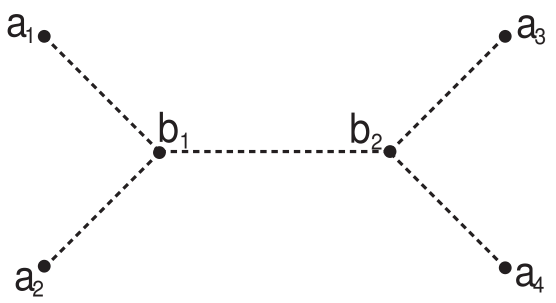

Fig. 18.2. A quartet $(a_1, a_2; a_3, a_4)$

Proof We use the fact that $v_{S(a_1,a_2)+S(a_3,a_4)} = v_{S(a_1,a_2)} + v_{S(a_3,a_4)}$ and apply the previous lemma. We also note that for $e \notin [\{a_1, a_2, a_3, a_4\}]$, $L_{a_1}(e) = L_{a_i}(e)$ for all i.

□

Corollary 18.4 *For a quartet* $(a_1, a_2; a_3, a_4)$*, we define*

$$S(a_1, a_2; a_3, a_4) = S(a_1, a_2) + S(a_3, a_4) - S(a_1, a_3) - S(a_2, a_4).$$

Then,

$$v_{S(a_1,a_2;a_3,a_4)}(e) = \begin{cases} -\binom{|L_{a_1}(e)|-2}{m-2} - \binom{n-|L_{a_1}(e)|-2}{m-2} & e \in P_{b_1b_2}; \\ \\ 0 & \textit{otherwise.} \end{cases}$$

Corollary 18.4 implies that S satisfies the four-point condition (as discussed in section 2.4 and theorem 2.35) although it may be that $v_{S(a_1a_2;a_3a_4)}(e) = 0$ which means that the edge e has been contracted in T'. In particular, this happens when $|L_{a_1}(e)| < m$ and $n - |L_{a_1}(e)| < m$ which is equivalent to $d(e) > n - m$. So for any quartet $(a_1, a_2; a_3, a_4)$, if the splitting path contains at least one edge e such that $d(e) \leq n - m$, then T' has the same quartet. However, if every edge in the splitting path has $d(e) > n - m$, then T' does not contain that quartet. Consequently, T' is isomorphic to $T/E_{>n-m}$.

It remains to show that there is an invertible linear map between the edge lengths in the T' and $T/E_{>n-m}$:

Lemma 18.5 *If* e *is an internal edge of* $T/E_{>n-m}$ *with* e' *the corresponding edge in* T' *then*

$$l_{T'}(e') = \frac{1}{2}\left(\binom{|L_a(e)|-2}{m-2} + \binom{|L_c(e)|-2}{m-2}\right) l_T(e)$$

where a *is a leaf in one component of* $T - e$ *and* c *a leaf in the other.*

Proof Since e is an internal edge, we may choose a, b, c and d such that e is the only edge on the splitting path of $(a, b; c, d)$ (figure 18.3). Then

$$\begin{aligned} l_{T'}(e') &= \frac{1}{2}S(a,b;c,d) \\ &= \frac{1}{2}\left(\binom{|L_a(e)|-2}{m-2} + \binom{|L_c(e)|-2}{m-2}\right) l_T(e) \\ &= \frac{1}{2}\left(\binom{d(e)-2}{m-2} + \binom{n-d(e)-2}{m-2}\right) l_T(e). \end{aligned}$$

□

Corollary 18.6

$$l_T(e) = \frac{2l_{T'}(e')}{\left(\binom{d(e)-2}{m-2} + \binom{n-d(e)-2}{m-2}\right)}$$

which is well defined if $d(e) \leq n - m$.

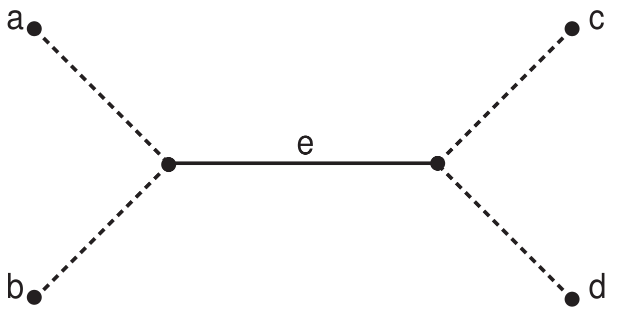

Fig. 18.3. The quartet $(a, b; c, d)$ has only the one edge e on its splitting path.

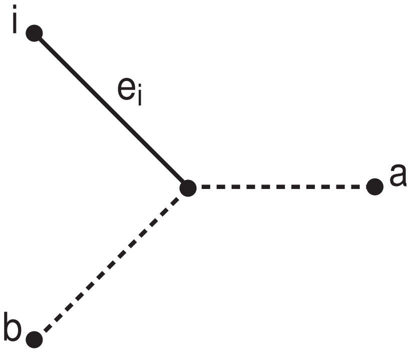

Fig. 18.4. The pendant edge e_i is incident on two other edges. We may choose leaves a and b such that $P_{ia} \cap P_{ib} = e_i$.

Lemma 18.7 *Denote the edges adjacent to the leaves by* $e_1, \ldots, e_n$ *(with corresponding edges in* T' $e'_1, \ldots, e'_n$*) and the set of internal (non-pendant) edges by* $int(T) = E_{>1}$*. Let*

$$C_i = \sum_{e \in int(T)} \left(\binom{n-2}{m-2} - \binom{|L_i(e)|-2}{m-2} \right) l_T(e)$$

and let $\mathbf{A}$ *be the matrix* $2\binom{n-3}{m-2}\mathbf{I} + \binom{n-3}{m-3}\mathbf{J}$*, where* $\mathbf{I}$ *is the identity matrix and* $\mathbf{J}$ *is the matrix with every entry equal to one. Then*

$$\begin{pmatrix} l_{T'}(e'_1) \\ \vdots \\ l_{T'}(e'_n) \end{pmatrix} = \frac{1}{2}\mathbf{A} \begin{pmatrix} l_T(e_1) \\ \vdots \\ l_T(e_n) \end{pmatrix} + \frac{1}{2} \begin{pmatrix} C_1 \\ \vdots \\ C_n \end{pmatrix}$$

Proof The interior vertex of a pendant edge e_i is incident to two other edges. Choose a leaf a such that P_{ia} intersects one of the edges, and b such that P_{ib}

intersects the other (figure 18.4). Then

$$l_{T'}(e') = \frac{1}{2}\left(S(i,a) + S(i,b) - S(a,b)\right)$$

which after some algebra gives the above lemma. □

Corollary 18.8

$$\begin{pmatrix} l_T(e_1) \\ \vdots \\ l_T(e_n) \end{pmatrix} = \mathbf{A}^{-1} \begin{pmatrix} 2l_{T'}(e_1') - C_1 \\ \vdots \\ 2l_{T'}(e_n') - C_n \end{pmatrix}$$

where $\mathbf{A}^{-1} = \frac{1}{2\binom{n-3}{m-2}}\left(\mathbf{I} - \frac{m-2}{(m-1)(n-2)}\mathbf{J}\right)$.

In order to recover $l_T(e)$ for every edge, we start by calculating the interior edge lengths, after which we can calculate the values C_i. The matrix $\mathbf{A}$ is always invertible if $m \leq n-1$; however, calculating C_i requires that $int(T) = int(T')$. If $n < 2m-1$, then while we can determine all the interior edge lengths of $T/E_{>n-m}$ from T', if $E_{>n-m}$ is nonempty, then some interior edges of T have been contracted in T'. If we delete the edges of $E_{>n-m}$ from T to form the forest $T \setminus E_{>n-m}$, then every connected component of $T \setminus E_{>n-m}$ has strictly fewer than m leaves. As a result, every m-subtree length will include at least one undetermined edge, and so there is no way to uniquely determine the lengths of the pendant edges.

18.3 The Need for Exact Solutions

These observations about S_D allow us to employ traditional distance-based methods, such as neighbor joining (algorithm 2.40), to construct trees from m-dissimilarity maps. For an alignment on a set of taxa X with $|X| = n$, we proceed as follows:

(i) For each $R \in \binom{X}{m}$ use a (ML) method to find $D(R)$.
(ii) For each pair (i,j), compute $S_D(i,j)$.
(iii) Apply neighbor joining to S_D to find a tree T'.
(iv) Apply linear transformation to the edge lengths of T' to find T.

We refer to this class of algorithm as *Generalized Neighbor-Joining* (GNJ).

In section 2.4, we encountered the neighbor-joining method and the cherry-picking matrix

$$Q_D(i,j) \quad = \quad (n-2)\cdot D(i,j) - \sum_{k\neq i} D(i,k) - \sum_{k\neq j} D(j,k). \qquad (18.3)$$

If D is a tree metric for a tree T, then the minimum entry $Q_D(x, y)$ identifies $\{x, y\}$ as a cherry in T. We also encountered the quartet split length

$$w_D(i, j; k, l) = \frac{1}{4}[2D(i, j) + 2D(k, l) - D(i, k) - D(i, l) - D(j, k) - D(j, l)]$$

which was instrumental in constructing an analogue to the cherry picking matrix. Here, we will see that it also plays a crucial rule in describing the effect of agglomeration on the cherry picking matrix.

Having chosen a pair $\{x, y\}$ that minimizes Q_D, the neighbor joining algorithm proceeds to agglomerate x and y to a single vertex z. We form a new set $X' = X \setminus \{x, y\} \cup \{z\}$ and define D' as a dissimilarity map on X' such that, for $k, l \in X' \setminus z$,

$$\begin{aligned} D'(z, k) &= \frac{1}{2}[D(x, k) + D(y, k) - D(x, y)], \\ D'(k, l) &= D(k, l). \end{aligned}$$

A brief computation allows us to explicitly relate the agglomeration update to the cherry-picking matrix. Specifically:

$$\begin{aligned} Q_{D'}(z, k) &= \frac{1}{2}[Q_D(x, k) + Q_D(y, k)] + 2D(x, y), \\ Q_{D'}(k, l) &= Q_D(k, l) + 2w_D(x, y; k, l) + 2D(x, y) \end{aligned}$$

where $Q_{D'}$ is the $(n-1) \times (n-1)$ cherry-picking matrix after agglomeration.

Given a 2-dissimilarity map D, we may construct a 3-dissimilarity map induced by D as follows:

$$D_3(i, j, k) = \frac{1}{2}[D(i, j) + D(i, k) + D(j, k)]. \qquad (18.4)$$

Theorem 18.9 *Given $D : \binom{X}{2} \to \mathbb{R}_{>0}$, define D_3 as in equation (18.4). If we let $S = S_{D_3}$, then Q_S is related to Q_D by an affine transformation. If S' and D' are the 2-dissimilarity maps on X' after agglomeration of S and D respectively, then $Q_{S'}$ and $Q_{D'}$ are also related by an affine transformation.*

Proof We first note that

$$\begin{aligned} S(i, j) &= \sum_{x \in X \setminus \{i,j\}} D_3(i, j, x) \\ &= \frac{1}{2} \sum_{x \in X \setminus \{i,j\}} D(i, j) + D(i, x) + D(j, x) \\ &= \frac{1}{2}[(n-4)D(i, j) + \sum_{x \in X \setminus \{i\}} D(i, x) + \sum_{x \in X \setminus \{j\}} D(j, x)]. \qquad (18.5) \end{aligned}$$

We substitute (18.5) into the cherry picking equation (18.3) and find that

$$Q_S = \frac{n-4}{2} Q_D - 2T,$$

where $T = \sum D(x,y)$ over all $\{x,y\} \in \binom{X}{2}$.

To compute the effect on the update function, we agglomerate x and y to a vertex z as above. We first note that

$$w_S(i,j;k,l) = \frac{n-4}{2} w_D(i,j;k,l).$$

Applying this to the update function (18.4), we obtain

$$Q_{S'} = \frac{n-4}{2} Q_{D'} - 2T + \sum_{i \in X \setminus x} D(i,x) + \sum_{y \in X \setminus x} D(i,y).$$

□

Corollary 18.10 *Given a 2-dissimilarity map D and induced 3-dissimilarity map D_3, neighbor-joining applied to D is equivalent to GNJ applied to D_3.*

Corollary 18.10 provides a means for comparing GNJ with traditional neighbor-joining. In particular, given an MLE method for generating trees on alignments of three taxa, we may compare its fidelity to the true total length with the fidelity of the 3-dissimilarity map induced by neighbor-joining's 2-dissimilarity map.

To this end, we compared the HKS method applied to Jukes-Cantor claw trees (described in the following section) with the 3-dissimilarity map D_3 constructed from Jukes-Cantor corrected 2-distances (as in equation 18.1). We used `seq-gen` [Rambaut and Grassly, 1997] to generate pseudorandom alignments of triplets evolved from the Jukes-Cantor DNA model ($\alpha = \frac{1}{4}$) on four different tree shapes over a range of total tree lengths. The total lengths varied from .125 to 7 and for each total length and each tree shape, we generated 100 alignments of length 500. Figure 18.5 shows that as the total length increases, HKS generated values, are, on average, closer to the true value than those generated from the Jukes-Cantor corrected 2-distance.

We may infer from this and corollary 18.10 that generalized neighbor-joining with the HKS claw tree will be more accurate than neighbor-joining with Jukes-Cantor corrected distances, particularly in trees with large pairwise distances. Experiments coupling GNJ with fastDNAml, a numerical approximation method, show an improvement over traditional neighbor-joining [Levy *et al.*, 2004]. If conjecture 18.12 is true, then methods such as fastDNAml which locate a biologically meaningful local maxima, will be assured to have found the only global maximum for 3-leaf trees, and therefore, are commensurate with a global maxima method such as HKS.

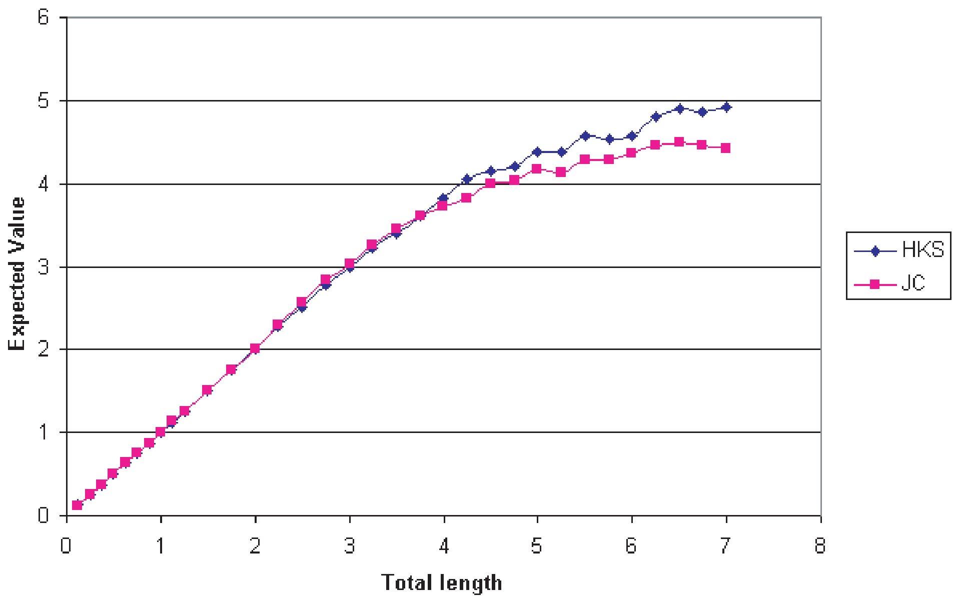

Fig. 18.5. The expected value of the total length for claw trees with edge ratios (1:1:1), (1:1:4), (1:2:4), and (1:4:4) as a function of the true total length. HKS indicates the HKS claw tree method and JC indicates D_3 computed from the Jukes-Cantor corrected 2-distance.

18.4 Jukes-Cantor Triples

Hoşten et al. [2004] describe a method (here called the *HKS method* by which local maxima of likelihood functions may be identified using computer algebra systems such as Singular and Macaulay 2. They also demonstrate the application of this method to finding an ML parameter set for the Jukes-Cantor DNA model on the three-taxon "claw" phylogenetic tree with uniform root distribution. (This tree and its model invariants are described in chapter 15 as well as in [Pachter and Sturmfels, 2004a].) The parameter θ_i represents the probability of a character's remaining the same along branch i, and $\pi_i = \frac{1}{3}(1 - \theta_i)$ the probability of its changing, according to the following transition matrix (whose rows and columns are indexed by $\{\mathtt{A}, \mathtt{C}, \mathtt{G}, \mathtt{T}\}$):

$$\begin{pmatrix} \theta_i & \pi_i & \pi_i & \pi_i \\ \pi_i & \theta_i & \pi_i & \pi_i \\ \pi_i & \pi_i & \theta_i & \pi_i \\ \pi_i & \pi_i & \pi_i & \theta_i \end{pmatrix}$$

We define the members of $K = \{[123], [dis], [12], [13], [23]\}$ to be equivalence classes of observed characters at homologous loci for our three taxa: [123] indicates that all three characters are identical, and [*dis*] that all three are distinct; [12] corresponds to identical characters at taxa 1 and 2 and a different character at taxon 3; and so on. As described in Chapter 1, an observation here is just a vector $u = (u_{123}, u_{dis}, u_{12}, u_{13}, u_{23})$ generated by tallying character similarities over some number of loci.

The probability of making an observation in class k at a given locus is denoted by p_k. For the claw tree, we may write down each of these as a trilinear form in $\theta_1, \theta_2, \theta_3, \pi_1, \pi_2, \pi_3$:

$$\begin{aligned}
p_{123} &= \theta_1\theta_2\theta_3 + 3\pi_1\pi_2\pi_3 \\
p_{dis} &= 6\theta_1\pi_2\pi_3 + 6\pi_1\theta_2\pi_3 + 6\pi_1\pi_2\theta_3 + 6\pi_1\pi_2\pi_3 \\
p_{12} &= 3\theta_1\theta_2\pi_3 + 3\pi_1\pi_2\theta_3 + 6\pi_1\pi_2\pi_3 \\
p_{13} &= 3\theta_1\pi_2\theta_3 + 3\pi_1\theta_2\pi_3 + 6\pi_1\pi_2\pi_3 \\
p_{23} &= 3\pi_1\theta_2\theta_3 + 3\theta_1\pi_2\pi_3 + 6\pi_1\pi_2\pi_3
\end{aligned}$$

Our wish, as the reader may have anticipated, is to find a parameter $\widehat{\theta} = (\widehat{\theta}_1, \widehat{\theta}_2, \widehat{\theta}_3)$ that maximizes the likelihood function $L(\theta) = \prod_{k \in K} p_k^{u_k}$, or equivalently the log-likelihood function $\ell(\theta) = \sum_{k \in K} u_k \log p_k$, given an observation u.

Algebraic statistical methods, including HKS, tend to operate in vector spaces of arbitrary dimension over algebraically closed fields such as $\mathbb{C}$. For many problems susceptible to ML methods, there is an obvious motivation to constrain the solution set to a region (or regions) of the parameter space corresponding to inputs that are in some sense “reasonable” or “meaningful”—this has already been seen in examples such as 1.6, where only parameters lying in the preimage of the probability simplex are admissible.

Specifically, for phylogenetic tree models it is natural to define the following restricted parameter space:

Definition 18.11 Given an algebraic statistical model of a phylogenetic tree T, a *biologically meaningful parameter* for the model is a parameter $\theta \in \Theta \subset \mathbb{R}^d$ that induces a tree in which all branch lengths are nonnegative real.

In the case of the claw tree, branch lengths may be determined from transition probabilities by the Jukes-Cantor corrected distance map as given in equation 18.1 (the transition probability p there is our θ_i). Now consider the inverse map:

$$\theta_i = \frac{1 + 3e^{-4b_i/3}}{4} \tag{18.6}$$

where b_i is the length of branch i. Note that $\theta_i \in \mathbb{R}$ if and only if $\mathrm{Im}(b_i) \in \{3\pi n/4 \mid n \in \mathbb{Z}\}$; when b_i is real, branch lengths in $[0, \infty)$ go to θ_i's in $(\frac{1}{4}, 1]$.

On this tree, therefore, a biologically meaningful parameterization is one in which $\frac{1}{4} < \theta_1, \theta_2, \theta_3 \leq 1$.

We applied the HKS algorithm, using MAPLE and SINGULAR code due to Garcia and Hoşten, to find local maxima of the likelihood function for this model, and found that, given some 20,000 observation vectors—half with independent randomly generated components and half derived from `seq-gen` alignments —at most one biologically meaningful solution was found for each observation.

Conjecture 18.12 *For any observation (u_k), the Jukes-Cantor DNA claw tree model admits at most one local maximum (p_k) that gives a biologically meaningful parameterization $\widehat{\theta}$.*

This conjecture, if true, would have a number of interesting consequences: even if approximate numerical methods are used to target local maxima of the likelihood function, we could be assured that any maximum occurring in the biologically meaningful region $\Theta = (\frac{1}{4}, 1]^3$ was unique. Identifying bounds on the number of biologically meaningful ML solutions for this and other models promises to be a rich area of inquiry.

19

Tree Construction Using Singular Value Decomposition

Nicholas Eriksson

We present a new, statistically consistent algorithm for phylogenetic tree construction that uses the algebraic theory of statistical models (as developed in Chapters 1 and 3). Our basic tool is the *Singular Value Decomposition* (SVD) from numerical linear algebra.

Starting with an alignment of n species, we show that the SVD allows us to quickly decide whether a split of the species occurs in their phylogenetic tree, assuming only that evolution follows a tree Markov model. Using this fact, we have developed an algorithm (jointly with Sagi Snir) to construct a phylogenetic tree by computing only n^2 SVD's.

We have implemented this algorithm using the SVDLIBC library† and have done extensive testing with simulated and real data. The algorithm is very fast in practice on trees with 20-30 taxa.

We begin by describing the general Markov model and then show how to flatten the joint probability distribution along a partition of the leaves in the tree. We give rank conditions for the resulting matrix; notably, we give a set of new rank conditions that are satisfied by non-splits in the tree. Armed with these rank conditions, we show how to use the SVD to calculate how close a matrix is to a certain rank and present the tree building algorithm. Finally, we give experimental results on the behavior of the algorithm with both simulated and real-life (ENCODE) data.

19.1 The General Markov Model

We assume that evolution follows a tree Markov model, as introduced in Section 1.4, with evolution acting independently at different sites of the genome. We do not assume that the transition matrices for the model are stochastic. Furthermore, we do not assume the existence of a global rate matrix (as in Section 4.5).

† Available at http://tedlab.mit.edu/∼dr/SVDLIBC/

This model is called the general Markov model. It is a more general model than any in the Felsenstein hierarchy (Figure 4.6). The main results in this paper therefore hold no matter what model in the Felsenstein hierarchy one works with.

Under the general dogma that statistical models are algebraic varieties, the polynomials defining the varieties are of great interest. Initially, in [Cavender and Felsenstein, 1987] and [Lake, 1987], certain linear relations for the Jukes-Cantor model were identified and named "phylogenetic invariants". These invariants have been used to infer phylogenies on four and five taxa; see [Sankoff and Blanchette, 2000]. Sturmfels and Sullivant finished the classification of the invariants for group based models ([Sturmfels and Yu, 2004]); see Chapter 15 for an application of these invariants for constructing trees on four taxa. Invariants for the general Markov model have been studied extensively by Allman and Rhodes (see [Allman and Rhodes, 2003, Allman and Rhodes, 2004b, Allman and Rhodes, 2004a]).

The main problem with invariants is that there are exponentially many polynomials in exponentially many variables to test on exponentially many trees. Because of this, they are currently considered impractical by many and have only been applied to small problems. However, we solve the problem of this combinatorial explosion by only concentrating on invariants which are given by rank conditions on certain matrices, called "flattenings".

19.2 Flattenings and Rank Conditions

Recall from Chapters 2 and 17 that a *split* A, B in a tree is a partition of the leaves obtained by removing an edge of the tree. We will say that A, B is a *partition* of the set of leaves if it is not necessarily a split but merely a disjoint partition of the set of leaves into two sets.

Throughout, all trees will be assumed to be binary with n leaves. We let m denote the number of states in the alphabet Σ. Usually $m = 4$ and $\Sigma = \{A, C, G, T\}$ or $m = 2$ and $\Sigma = \{0, 1\}$. We will write the joint probabilities of an observation on the leaves as $p_{i_1 \ldots i_n}$. That is, $p_{i_1 \ldots i_n}$ is the probability that leaf j is observed to be in state i_j. We write P for the entire probability distribution.

Although the descriptions of tree-based models in this book all deal with rooted trees, we will mostly consider unrooted tree models, which are equivalent for the general Markov model, see [Allman and Rhodes, 2004a] for details on this technical point. Our tree building algorithm actually constructs a rooted tree, but the rooting is arbitrary.

Definition 19.1 A *flattening* along a partition A, B is the $m^{|A|}$ by $m^{|B|}$ matrix where the rows are indexed by the possible states for the leaves in A and the columns are indexed by the possible states for the leaves in B. The entries of this matrix are given by the joint probabilities of observing the given pattern at the leaves. We write $\text{Flat}_{A,B}(P)$ for this matrix.

Example 19.2 (Flattening a split on 4 taxa) Let T be a tree with 4 leaves and let $m = 4$, $\Sigma = \{\texttt{A},\texttt{C},\texttt{G},\texttt{T}\}$. The split $\{1,3\},\{2,4\}$ flattens to the 16×16 matrix $\text{Flat}_{\{1,3\},\{2,4\}}(P)$ where the rows are indexed by bases of taxa 1 and 3 and the columns by bases of taxa 2 and 4:

$$\text{Flat}_{\{1,3\},\{2,4\}}(P) = \begin{array}{c} \\ \texttt{AA} \\ \texttt{AC} \\ \texttt{AG} \\ \texttt{AT} \\ \texttt{CA} \\ \vdots \end{array} \begin{array}{c} \begin{array}{ccccccc} \texttt{AA} & \texttt{AC} & \texttt{AG} & \texttt{AT} & \texttt{CA} & \texttt{CC} & \dots \end{array} \\ \begin{pmatrix} p_{\texttt{AAAA}} & p_{\texttt{AAAC}} & p_{\texttt{AAAG}} & p_{\texttt{AAAT}} & p_{\texttt{ACAA}} & p_{\texttt{ACAC}} & \cdots \\ p_{\texttt{AACA}} & p_{\texttt{AACC}} & p_{\texttt{AACG}} & p_{\texttt{AACT}} & p_{\texttt{ACCA}} & p_{\texttt{ACCC}} & \cdots \\ p_{\texttt{AAGA}} & p_{\texttt{AAGC}} & p_{\texttt{AAGG}} & p_{\texttt{AAGT}} & p_{\texttt{ACGA}} & p_{\texttt{ACGC}} & \cdots \\ p_{\texttt{AATA}} & p_{\texttt{AATC}} & p_{\texttt{AATG}} & p_{\texttt{AATT}} & p_{\texttt{ACTA}} & p_{\texttt{ACTC}} & \cdots \\ p_{\texttt{CAAA}} & p_{\texttt{CAAC}} & p_{\texttt{CAAG}} & p_{\texttt{CAAT}} & p_{\texttt{CCAA}} & p_{\texttt{CCAC}} & \cdots \\ \vdots & \vdots & \vdots & \vdots & \vdots & \vdots & \vdots \end{pmatrix} \end{array}.$$

Next we define a measure of how close a general partition of the leaves is to being a split. If A is a subset of the leaves of T, we let T_A be the subtree induced by the leaves in A. That is, T_A is the minimal set of edges needed to connect the leaves in A.

Definition 19.3 Suppose that A, B is a partition of $[n]$ and T_A is the subtree of T induced by the leaves in A (similarly for T_B). The "distance" between the partition A, B and the nearest split, written $e(A, B)$, is the number of edges that occur both in T_A and in T_B.

Notice that $e(A, B) = 0$ exactly when A, B is a split.

Example 19.4 Let T be the 6 taxa tree pictured in Figure 19.1. Then $e(\{1,2\},\{3,4,5,6\}) = 0$, but $e(\{1,2,3\},\{4,5,6\}) = 1$.

Our main theorem ties together how close a partition is to being a split with the rank of the flattening associated to that partition.

Theorem 19.5 *Let A, B be a partition of $[n]$, let T be a binary, unrooted tree with leaves labeled by $[n]$, and assume that the joint probability distribution P comes from a Markov model on T with an alphabet with m letters. Then the generic rank of the flattening* $\text{Flat}_{A,B}(P)$ *is given by*

$$m^{\min(e(A,B)+1,|A|,|B|)}$$

Proof We claim that $\text{Flat}_{A,B}(P)$ can be thought of as the joint distribution for a simple graphical model. Pick all of the nodes that are shared by the

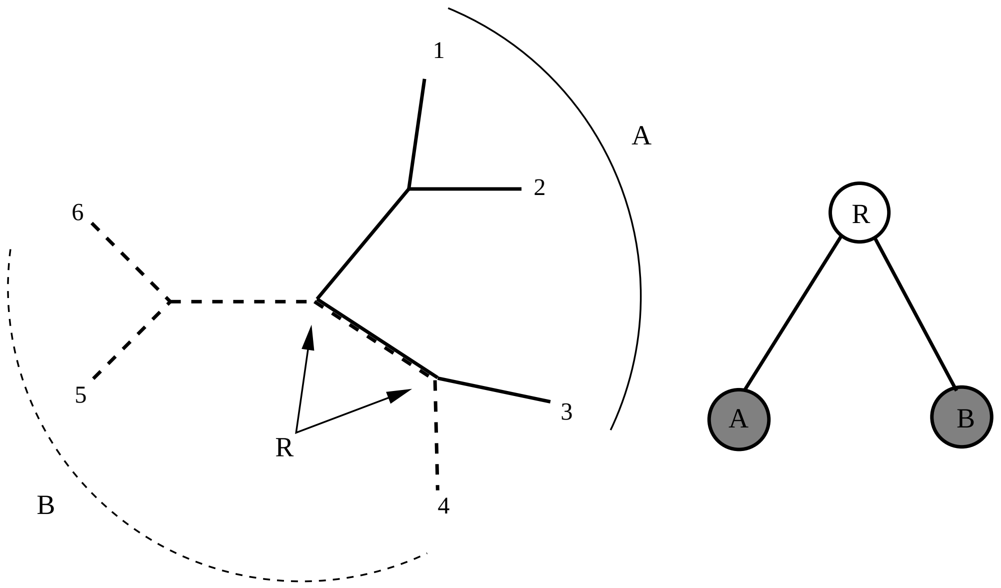

Fig. 19.1. If $A = \{1, 2, 3\}$ and $B = \{4, 5, 6\}$, then $e(A, B) = 1$ and $\mathrm{Flat}_{A,B}(P)$ is the joint distribution for a 3 state graphical model where the root R has m^2 states and the leaves A and B have m^3 states each.

induced subtrees for A and B. If this set is empty then A, B is a split, in that case pick one of the vertices of the edge separating A and B. Notice that this set has cardinality $e(A, B) + 1$. Think of these vertices as a single hidden random variable R with $m^{e(A,B)+1}$ states. Group the states of the nodes in A together into one $m^{|A|}$-state observed random variable; similarly the nodes in B are grouped into a $m^{|B|}$-state random variable. Then create the graphical model with one hidden $m^{e(A,B)+1}$-state random variable and two descendent observed variables with $m^{|A|}$ and $m^{|B|}$ states. Notice that $\mathrm{Flat}_{A,B}(P)$ is the joint distribution for this model. See Figure 19.1 for an example.

Furthermore, the distribution for this 3-state model factors as

$$\mathrm{Flat}_{A,B}(P) = M_A^T \,\mathrm{diag}(\pi(R)) M_B$$

where $\pi(R)$ is the distribution of R and M_A and M_B are the $m^{e(A,B)} \times m^{|A|}$ and $m^{e(A,B)} \times m^{|B|}$ transition matrices. That is, the (i, j) entry of M_A is the probability of transitioning from state i at the root R to state j at A.

To say the tree distribution factors like this just means that

$$\mathrm{Prob}(A = i, B = j) = \sum_k \mathrm{Prob}(R = k)\mathrm{Prob}(A = i \mid R = k)\mathrm{Prob}(B = j \mid R = k)$$

Notice that all of the terms in this expression can be written as polynomials in the edge parameters (after choosing a rooting). Therefore the flattening factors, so the rank of $\mathrm{Flat}_{A,B}(P)$ is at most $m^{\min(e(A,B)+1,|A|,|B|)}$. It is not hard to see that all matrices in this factorization generically have full rank since the monomials that appear in them are distinct. $\square$

This theorem gives rise to a well known corollary upon noticing that if A, B is a split, then $e(A, B) = 0$ (see [Allman and Rhodes, 2004a], for example).

Corollary 19.6 *If A, B is a split in the tree, the generic rank of* $\mathrm{Flat}_{A,B}(P)$ *is m.*

Example 19.7 In Example 19.2, the 16×16 matrix $\mathrm{Flat}_{\{1,3\},\{2,4\}}(P)$ has rank 4 if the split $\{1,3\}, \{2,4\}$ occurs in the tree, otherwise, it has rank 16.

In fact, if $m = 2$, it has recently been shown by Allman and Rhodes [Allman and Rhodes, 2004b] that the rank conditions in Corollary 19.6 generate the ideal of invariants for the general Markov model. However, they do not suffice if $m = 4$, in that case a polynomial of degree 9 (see [Strassen, 1983, Garcia *et al.*, 2004]) lies in the ideal of invariants and [Landsberg and Manivel, 2004] show that this polynomial is not generated by the degree 5 rank conditions.

19.3 Singular Value Decomposition

The SVD provides a method to compute the distance between a matrix and the nearest rank k matrix. In this section, we briefly introduce the basic properties of the SVD. See [Demmel, 1997] for a thorough treatment. Throughout, let A be a $m \times n$ matrix with $m \leq n$.

Definition 19.8 A *singular value decomposition* of a $m \times n$ matrix A is a factorization $A = U\Sigma V^T$ where U is $n \times n$ orthogonal, V is $m \times m$ orthogonal and $\Sigma = \begin{pmatrix}\Sigma_1 & 0\end{pmatrix}$, where $\Sigma_1 = \mathrm{diag}(\sigma_1, \sigma_2, \ldots, \sigma_m)$, with $\sigma_1 \geq \sigma_2 \geq \cdots \geq \sigma_m$.

Definition 19.9 Let a_{ij} be the (i, j) entry of A. The *Frobenius norm*, written $||A||_F$, is the root-sum-of-squares norm on $\mathbb{R}^{m\cdot n}$. That is,

$$||A||_F = \sqrt{\sum a_{ij}^2}.$$

The L_2 *norm*, written $||A||_2$, is given by

$$||A||_2 = \max_{||x||=1} \left\{ \frac{||Ax||}{||x||} \right\}$$

Theorem 19.10 *The distance from A to the nearest rank k matrix is*

$$\min_{Rank(B)=k} ||A - B||_F = \sqrt{\sum_{i=k+1}^{m} \sigma_i^2},$$

in the Frobenius norm and

$$\min_{Rank(B)=k} ||A - B||_2 = \sigma_{k+1}$$

in the L_2 norm.

One way of computing the singular values is to compute the eigenvalues of$A^T A$, the singular values are the square roots of these eigenvalues. Therefore, general techniques to solve the real symmetric eigenvalue problem can be used to compute the SVD. These various methods, both iterative and direct, are implemented by many software packages for either sparse or general matrices. We will discuss the computational issues with the SVD after we describe how to use it to construct phylogenetic trees.

19.4 Tree Construction Algorithm

Now that we know how to tell how close a matrix is to being of a certain rank, we can test if a given split comes from the underlying tree or not by using the SVD to tell how close a flattening matrix is to being rank m. However, since there are exponentially many possible splits, we must cleverly search through this space. We do this by building the tree bottom up, at each step joining cherries together, in a method reminiscent of neighbor joining (Algorithm 2.40).

It is an interesting open question whether the additional information in Theorem 19.5 about non-splits that are almost splits can be harnessed to produce an improved algorithm.

Algorithm 19.11 (Tree construction with SVD, joint with S. Snir)
Input: A multiple alignment of genome data from n species, from the alphabet Σ with m states.
Output: An unrooted binary tree with n leaves labelled by the species.

Initialization: Compute joint probabilities $p_{i_1 \dots i_n}$. That is, count occurrences of each possible column of the alignment, ignoring columns with characters not in Σ. Store the results in a sparse format.

Loop: For k from n down to 2.

For each of the $\binom{k}{2}$ pairs of species compute the SVD for the split {pair}, {other $k-2$ species}. Pick the pair that is closest to rank m according to the Frobenius norm and join this pair together in the tree. That is, consider this pair as a single element when picking pairs at the next step.

Proposition 19.12 *Algorithm 19.11 requires the computation of n^2 SVD's.*

Proof At the first step, we compute an SVD $\binom{n}{2}$ times. At each subsequent step, we only need to compute those splits involving the pair that we just joined together. Thus we compute $(n-2)+(n-3)+\cdots+1 = \binom{n-1}{2}$ total SVD's after the first step for $\binom{n}{2}+\binom{n-1}{2} = n^2$ SVD computations in total. □

The flattenings are very large (size $m^{|A|} \times m^{|B|}$), yet they are typically very sparse. If an alignment is of length L, at most L entries of the flattening and typically many fewer are non-zero. Generally, computing all singular values of a $a \times b$ matrix takes $O(a^2 b + ab^2)$ time. However, Lanczos iterative methods allow singular values to be computed quickly individually, starting with the largest. Furthermore, sparse matrix techniques allow us take advantage of this structure without having to deal with matrices of exponential size.

Since we will be comparing the SVD from different sized splits, we need to compute distances in the Frobenius norm, which does not change as the dimensions of the matrices change (as long as the number of entries is constant). This means that we should compute all singular values, however that is difficult computationally. But in practice, the singular values typically decrease very quickly, so it suffices to compute only the largest singular values to estimate the Frobenius norm.

By exploiting the sparsity and only computing singular values until they become sufficiently small, we find that we are able to very quickly compute the SVD for for flattenings coming from trees of size at most 31 with binary data ($m = 2$) and roughly size 15 with DNA data ($m = 4$). This limitation is due to limits on the size of array indices in SVDLIBC and can probably be exceeded. Furthermore, there are very good approximation algorithms (see [Frieze *et al.*, 1998]) for the SVD that could make very large problems practical.

Theorem 19.13 *Algorithm 19.11 is statistically consistent. That is, as the probability distribution converges to a distribution that comes from the general Markov model on a binary tree T, the probability that Algorithm 19.11 outputs T goes to 1.*

Proof We must show that the algorithm picks a correct split at each step, that is, that as the distribution approaches the true distribution, the probability of choosing a bad split goes to zero. By Corollary 19.6, we see that a true split will lead to a flattening that approaches a rank m matrix, while other partitions will approach a matrix of higher rank (except for partitions where one set contains only one element, however, these are never considered in the algorithm). Therefore, as the distribution approaches the true one, the distance from rank m of the split will go to zero while the distance from rank m of the non-split will not go to zero. □

Example 19.14 We start with an alignment of DNA data of length 500 for 5 species, labeled $0, \dots, 4$. For the first step, we look at all pairs of the 5 species. The score column is the distance in the Frobenius norm from the flattening to the nearest rank 4 matrix.

```
Split           Score
0 1 | 2 3 4     2.7661
2 3 | 0 1 4     3.1513
3 4 | 0 1 2     5.9997
2 4 | 0 1 3     6.0359
0 4 | 1 2 3     6.8419
1 4 | 0 2 3     6.9895
1 3 | 0 2 4     8.0600
0 2 | 1 3 4     8.0673
1 2 | 0 3 4     8.1503
0 3 | 1 2 4     8.2082
picked split 0 1 | 2 3 4
tree is 2 3 4 (0,1)
```

After the first step, we see that the split $\{0, 1\}, \{2, 3, 4\}$ is best, so we join the nodes $\{0, 1\}$ together in the tree.

```
Split           Score
2 3 | 0 1 4     3.1513
0 1 4 | 2 3     3.1513
3 4 | 0 1 2     5.9997
0 1 2 | 3 4     5.9997
0 1 3 | 2 4     6.0359
2 4 | 0 1 3     6.0359
picked split 0 1 4 | 2 3
tree is 4 (0,1) (2,3)
```

We have found another cherry in the tree, this time we join $\{2, 3\}$ together.

```
Split           Score
2 3 4 | 0 1     2.7661
0 1 4 | 2 3     3.1513
picked split 0 1 | 2 3 4
tree is ((0,1),(4,(2,3)))
```

Finally we find that node 4 should be joined with the $\{2, 3\}$ cherry, and the tree is complete.

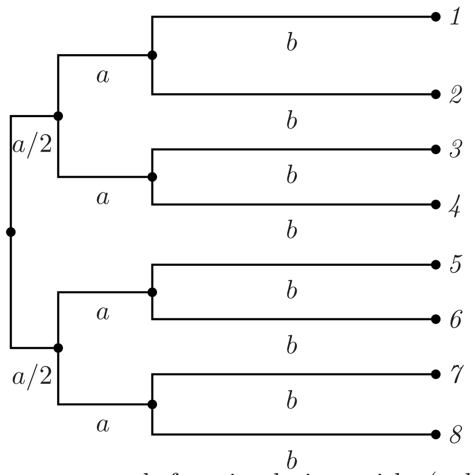

Fig. 19.2. The 8-taxa tree used for simulation with $(a, b) = (0.01, 0.07)$ and $(0.02, 0.19)$.

19.5 Performance Analysis

19.5.1 Building Trees with Simulated Data

The idea of simulation is that we first pick a tree and simulate a model on that tree to obtain aligned sequence data. Then we build a tree using Algorithm 19.11 and other methods from that data and compare the answers to the original tree.

We used the program `seq-gen` [Rambaut and Grassly, 1997] to simulate data of various lengths for the tree in Figure 19.2 with various branch lengths. This tree was chosen as a particularly difficult tree.

We simulated data under the general reversible model (the most general model supported by `seq-gen`). Random numbers uniformly distributed between 1 and 2 were chosen on each run for the six transition parameters (see Figure 4.6). The root frequencies were all set to 1/4.

Next, the data was collapsed to binary data (that is, `A` and `G` were identified, similarly `C` and `T`). We used binary data instead of DNA data because of numerical instability with the SVD using the much larger matrices from the DNA data. It should be noted that Algorithm 19.11 performed better on binary data than on DNA data. This may be due to the instability, however, it may also be because the rank conditions define the entire ideal for binary data.

We ran all tests using our Algorithm 19.11 as well as two algorithms from the `PHYLIP` package (see Section 2.5): neighbor joining (i.e., Algorithm 2.40), and a maximum likelihood algorithm (`dnaml`). All three algorithms took ap-

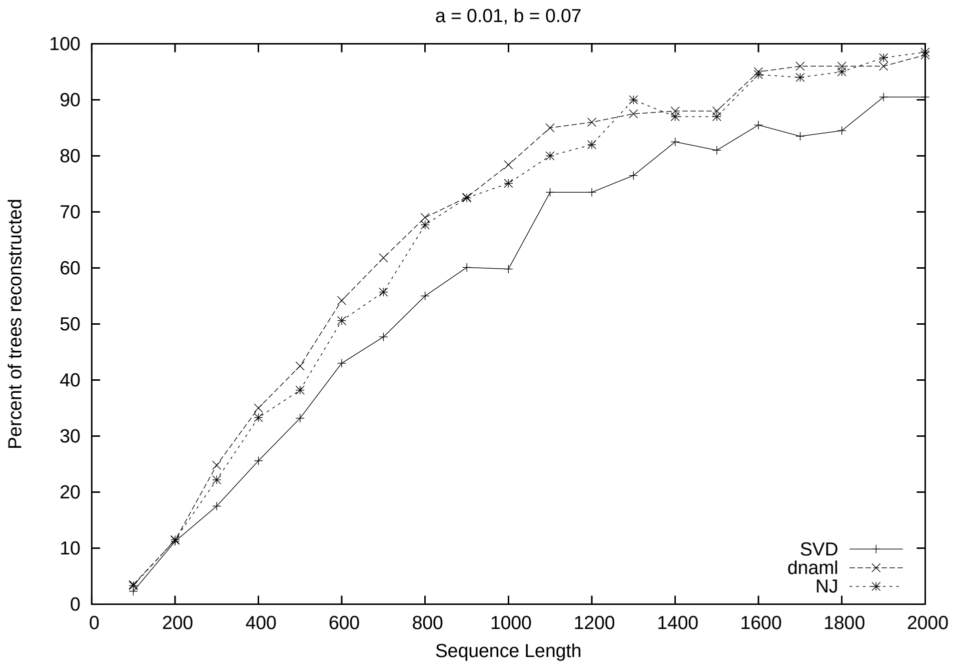

Fig. 19.3. Percent of trees reconstructed correctly (for the 8 taxa tree with branch lengths $(a, b) = (0.01, 0.07)$) using our SVD algorithm and two `PHYLIP` packages.

proximately the same amount of time, except for `dnaml`, which slowed down considerably for long sequences.

Figures 19.3 and 19.4 show the results of the simulations. Each algorithm was run 1000 times for each tree and sequence length. While the SVD performed slightly worse than the others, it showed very comparable behavior. It should be noted that this tree is very difficult, requiring much more data than a typical tree on 8 taxa.

19.5.2 Building Trees with Real Data

For data, we use the October 2004 freeze of the ENCODE alignments. For detailed information on these, see Section 4.3, Chapters 21 and 22.

As in Chapter 21, we restricted our attention to 8 species: human, chimp, galago, mouse, rat, cow, dog, and chicken. We processed each of the 44 ENCODE regions to obtain 3 data sets. First, for each region, all of the ungapped columns were chosen. Second, within each region, all ungapped columns that corresponded to refSeq annotated human genes were chosen. Third, we restricted even further to only the human exons within the genes. Bins without all 8 species and bins with less than 100 ungapped positions in the desired class

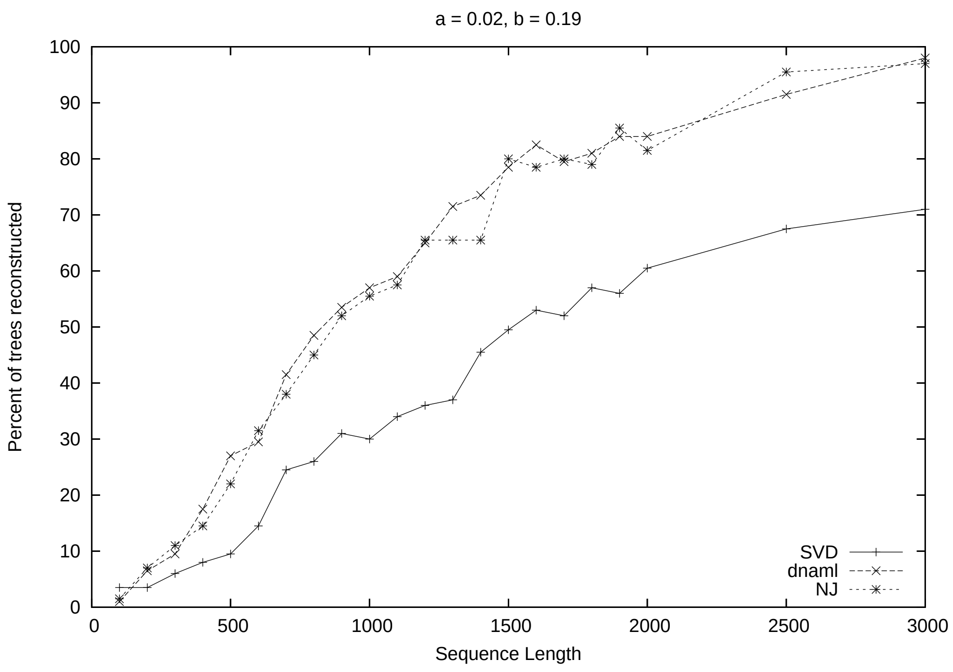

Fig. 19.4. Percent of trees reconstructed correctly (for the 8 taxa tree with branch lengths $(a, b) = (0.02, 0.019)$) using our SVD algorithm and two `PHYLIP` packages.

were removed from consideration. This left us with 33 regions for the entire alignment, and 28 for both the gene and exon regions, of lengths between 302 and over 100000 base pairs. See Chapter 21 for a more through discussion of these data sets.

As is discussed in Section 21.4, tree construction methods that use genomic data usually misplace the rodents on the tree. The reasons for this are not entirely known, but it could be because tree construction methods generally assume the existence of a global rate matrix (cf. Section 4.5) for all the species, however, rat and mouse have mutated faster than the other species. Our method does not assume anything about the rate matrix, however, and thus is promising for situations where additional assumptions beyond the Markov process of evolution at independent sites are not feasible.

In fact, Table 19.1 shows that our algorithm performs better on the ENCODE data sets. While it did not construct the correct tree a majority of the time, it came much closer on average than `dnaml`, which almost never constructed the correct tree (see Figure 21.7 for the correct tree and a common mistake).

	SVD		`dnaml`	
	Ave. distance	% correct	Ave. distance	% correct
All	2.06	5.8	3.29	2.9
Gene	1.93	10.3	3.21	0.0
Exon	2.43	21.4	3.0	3.5

Table 19.1. *Comparison of the SVD algorithm and* **`dnaml`** *on data from the ENCODE project. Distance between trees is given by the Robinson-Foulkes measure.*

s

20
Applications of Interval Methods to Phylogenetics

Raazesh Sainudiin

Ruriko Yoshida

In this chapter, we will apply interval methods to problems in phylogenetics. An interval extension of the recursive formulation for the likelihood function of the simplest Markov model of DNA evolution on unrooted phylogenetic trees with a fixed topology is used to obtain rigorous enclosure(s) of the global maximum likelihood. Thus, we can obtain the validated global maximizer(s) inside any compact set of the parameter space which is the set of all branch lengths of the tree. The algorithm is an adaptation of a widely applied global optimization method using interval analysis for the phylogenetic context. The method is applied to enclose the most likely 2, 3, and 4 taxa trees under the simplest model of DNA evolution. The method is general and can provide rigorous estimates when coupled with standard phylogenetic algorithms.

20.1 Interval methods for exact solutions

When statistical inference is conducted in a maximum likelihood (ML) framework, one is interested in the global maximum of the likelihood function over the parameter space. In practice one settles for a local optimization algorithm to numerically approximate the global solution since explicit analytical solutions for the maximum likelihood estimates (MLEs) are not available. However, statistical inference procedures that rely on finding some global optimum through any numerical approach may suffer from at least five major sources of errors. To fully appreciate the sources of errors one needs some understanding of a number screen. Computers only support a finite set of numbers that are usually represented in a semi-logarithmic manner as a set of fixed length binary floating-point numbers of the form, $x = \pm m \cdot 2^e = \pm 0.1 m_2 \cdots m_p \cdot 2^e$, where m is the signed mantissa ($m_i \in \{0,1\}, \forall i, 1 < i \leq p$) with base 2, p is the precision, and e is the exponent ($\underline{e} \leq e \leq \overline{e}$) [IEEE Task P754, 1985]. Thus, the smallest and largest machine-representable numbers in absolute value are $\underline{x} = 0.10 \cdots 0 \cdot 2^{\underline{e}}$ and $\overline{x} = 0.11 \cdots 1 \cdot 2^{\overline{e}}$, respectively. Thus, the binary floating-point system of most machines $\mathcal{R} = \mathcal{R}(2, p, \underline{e}, \overline{e})$ is said to form a screen of the real numbers in the interval $[-\overline{x}, +\overline{x}]$ with 0 uniquely represented by $0.00 \cdots 0 \cdot 2^{\underline{e}}$. Arithmetic on a machine is typically performed with such a screen in an inexact manner and may suffer from the following errors: *roundoff error* – the difference between computed and exact result [Cuyt *et al.*, 2001, Loh and Walster, 2002], *truncation error* – from having to truncate an infinite sequence of operations, *conversion error* – inability to machine-represent decimals with infinite binary expansion, and *ill-posed statistical experiment* – presence of unknown nonidentifiable subspaces.

The verified global optimization method [Hansen, 1980] sketched below rigorously encloses the global maximum of the likelihood function through interval analysis [Moore, 1967]. Such interval methods evaluate the likelihood function over a continuum of points including those that are not machine-representable and account for all sources of errors described earlier. In the sequel we will see that interval methods, in contrast to heuristic local search methods, can enclose the global optimum with guaranteed accuracy by exhaustive search within any compact set of the parameter space. We begin with a brief introduction to interval analysis.

Lower case letters denote real numbers, e.g. $x \in \mathbb{R}$. Upper case letters represent compact real intervals, e.g. $X = [\underline{x}, \overline{x}] = [\inf(X), \sup(X)]$. Any compact interval $X \in \mathbb{IR} := \{[a, b] : a \leq b,\ a, b \in \mathbb{R}\}$, the set of all compact real intervals. The diameter and the midpoint of X are $d(X) := \overline{x} - \underline{x}$ and $m(X) := (\underline{x} + \overline{x})/2$, respectively. The magnitude of X is $\langle X \rangle := \min\{|x| : x \in X\} = \min\{|\underline{x}|, |\overline{x}|\}$, if $0 \notin X$, and 0 otherwise. The magnitude of X is $|X| := \max\{|x| : x \in X\} = \max\{|\underline{x}|, |\overline{x}|\}$, while the absolute value of an interval X is $|X|_{[\,]} := \{|x| : x \in X\} = [\langle X \rangle, |X|]$. The relative diameter of an interval X, denoted by d_{rel}, is the diameter $d(X)$ itself if $0 \in X$ and $d(X)/\langle X \rangle$ otherwise. An interval X with zero diameter is called a thin interval with $\underline{x} = \overline{x} = x$. The hull of two intervals is $X \underline{\cup} Y := [\min\{\underline{x}, \underline{y}\}, \min\{\overline{x}, \overline{y}\}]$. By the notation $X \Subset Y$, it is meant that X is completely contained in Y, i.e. $\underline{x} > \underline{y}$ and $\overline{x} < \overline{y}$. No notational distinction is made between a real number $x \in \mathbb{R}$ and a real vector $x = (x_i, \cdots, x_n)^T \in \mathbb{R}^n$ and between a real interval X and a real interval vector or box $X = (X_1, \cdots, X_n)^T \in \mathbb{IR}^n$, i.e. $X_i = [\underline{x_i}, \overline{x_i}] = [\inf(X_i), \sup(X_i)] \in \mathbb{IR}$, where $i = 1, \cdots, n$. For an interval vector X, the diameter, relative diameter, midpoint, and hull operations are defined component-wise to yield vectors, while the maximum over its components is taken to obtain the maximal diameter and the maximal relative diameter, $d_\infty(X) = \max_i d(X_i)$ and $d_{rel,\infty}(X) = \max_i d_{rel}(X_i)$, respectively. Also $\mathbb{IR}$ under the metric $\mathfrak{h}$, given by $\mathfrak{h}(X, Y) := \max\{|\underline{x} - \underline{y}|, |\overline{x} - \overline{y}|\}$, is a complete metric space. Convergence of a sequence of intervals $\{X^{(i)}\}$ to an interval X under the metric $\mathfrak{h}$ is equivalent to the sequence $\mathfrak{h}(X^{(i)}, X)$ approaching 0 as i approaches ∞, which in turn is equivalent to both $\underline{x}^{(i)} \to \underline{x}$ and $\overline{x}^{(i)} \to \overline{x}$. Continuity and differentiability of a function $F : \mathbb{IR}^n \to \mathbb{IR}^k$ are defined in the usual way. An interval arithmetic (IA) operation $X \circ Y := \{x \circ y : x \in X, y \in Y\}$ thus yields the set containing the result of the operation done for every real pair $(x, y) \in (X, Y)$. Although there are uncountably many real operations to consider during an interval operation, the properties of continuity, monotonicity, and compactness imply that:

$$X + Y = [\underline{x} + \underline{y}, \overline{x} + \overline{y}],\ X \cdot Y = [\min\{\underline{x}\underline{y}, \underline{x}\overline{y}, \overline{x}\underline{y}, \overline{x}\overline{y}\}, \max\{\underline{x}\underline{y}, \underline{x}\overline{y}, \overline{x}\underline{y}, \overline{x}\overline{y}\}],$$
$$X - Y = [\underline{x} - \overline{y}, \overline{x} - \underline{y}],\ X/Y = X \cdot [1/\overline{y}, 1/\underline{y}],\ 0 \notin Y.$$

This definition of IA leads to the property of inclusion isotony which stipulates that $X \circ Y$ contains $V \circ W$ provided $V \subseteq X$ and $W \subseteq Y$. The identity elements of $+$ and $\cdot$ are the thin intervals 0 and 1, respectively. Multiplicative and additive inverses do not exist except when X is also thin. IA is commutative and associative but not distributive. However, $X \cdot (Y + Z) \subseteq (X \cdot Y) + (X \cdot Z)$. For any real function $f(x) : \mathbb{R}^n \to \mathbb{R}$ and some box $X \in \mathbb{IR}^n$, let the range of f over X be denoted by $f(X) := \{f(x) : x \in X\}$. Inclusion isotony also holds for interval evaluations that are compositions of arithmetic expressions and the elementary functions. When real constants, variables, and operations in f are replaced by their interval counterparts, one obtains $F(X) : \mathbb{IR}^n \to \mathbb{R}$, the natural interval extension of f. Guaranteed enclosures of the range $f(X)$ are obtained by $F(X)$ by the inclusion property that $x \in X \implies f(x) \in F(X)$. The natural interval extension $F(X)$ often overestimates the range $f(X)$, but can be shown under mild conditions to linearly approach the range as the maximal diameter of the box X goes to zero, i.e. $\mathfrak{h}(F(X), f(X)) \leq \alpha \cdot d_\infty(X)$ for some $\alpha \geq 0$. This implies that a partition of X into smaller boxes $\{X^{(1)}, \cdots, X^{(m)}\}$ gives better enclosures of $f(X)$ through the union $\bigcup_{i=1}^{m} F(X^{(i)})$ as illustrated in Figure 20.1.

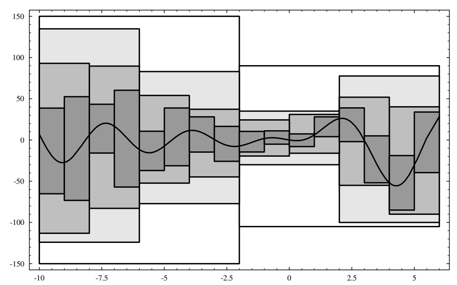

Fig. 20.1. *Range enclosure of* $-\sum_{k=1}^{5} k\, x \sin\left(\frac{k(x-3)}{3}\right)$ *linearly tightens with mesh*

Let $\bigtriangledown F(x)$ and $\bigtriangledown^2 F(x)$ represent the interval extensions of $\bigtriangledown f(x)$ and $\bigtriangledown^2 f(x)$, the gradient and Hessian of f. A better enclosure of $f(X)$ is possible for an f with the centered form,

$$f(x) = f(c) + \bigtriangledown f(b) \cdot (x - c) \in f(c) + \bigtriangledown f(X) \cdot (x - c) \subseteq F_c(X),$$

where $F_c(X) := f(c) + \bigtriangledown F(X) \cdot (X - c)$ and $b, c, x \in X$ with b between c and x. $F_c(X)$ is the interval extension of the centered form of f with center c and decays quadratically to $f(X)$ as the maximal diameter of $X \to 0$. Finally, some interval extensions of f are better at enclosing the true range than others. Although the three functions shown in Figure 20.2 are equivalent, their interval extensions yield different range enclosures. The interval extension $F^{(3)}$ is better than $F^{(1)}$ and $F^{(2)}$ as depicted in Figure 20.2. Note that $F^{(3)} \subset F^{(2)}$ since $X^2 \subset X \cdot X$ in IA. If X appears only once in the expression and all parameters are thin intervals, it was shown by [Moore, 1979] that the natural interval extension does indeed yield a tight enclosure, i.e. $F(X) = f(X)$. In general, one can obtain tighter enclosures by minimizing the occurrence of X in the expression. Next we introduce automatic differentiation (AD).

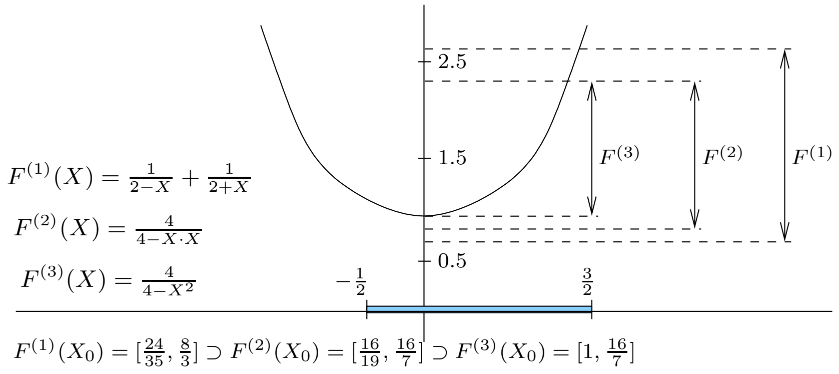

Fig. 20.2. *Extension-specific dependence of range enclosures*

When it becomes too cumbersome or impossible to explicitly compute $\bigtriangledown f(x)$ and $\bigtriangledown^2 f(x)$ of a function $f : \mathbb{R}^n \to \mathbb{R}$, or when f itself is only available as an algorithm, one may employ a Hessian differentiation arithmetic, also known as AD [Rall, 1981]. This approach defines an arithmetic on a set of ordered triples. Consider a twice-continuously differentiable function $f : \mathbb{R}^n \to \mathbb{R}$ with the gradient vector, $\bigtriangledown f(x) := (\partial f(x)/\partial x_1, \cdots, \partial f(x)/\partial x_n)^T \in \mathbb{R}^n$, and Hessian matrix $\bigtriangledown^2 f(x) := ((\partial^2 f(x)/\partial x_i \partial x_j))_{i,j=\{1,\cdots,n\}} \in \mathbb{R}^{n \times n}$. For every f, consider its corresponding ordered triple $(\, f(x),\ \bigtriangledown f(x),\ \bigtriangledown^2 f(x)\,)$. The ordered triples corresponding to a constant function, $c(x) = c : \mathbb{R}^n \to \mathbb{R}$, and a component identifying function (or variable), $I_j(x) = x_j : \mathbb{R}^n \to \mathbb{R}$, are $(\, c,\ 0,\ 0\,)$ and $(\, x_j,\ e^{(j)},\ 0\,)$, respectively, where $e^{(j)}$ is the j-th unit vector and the 0's are additive identities in their appropriate spaces. To perform an elementary operation $\circ \in \{+, -, \cdot, /\}$ with a pair of such triples to obtain another, as in

$(\,h(x),\ \triangledown h(x),\ \triangledown^2 h(x)\,) := (\,f(x),\ \triangledown f(x),\ \triangledown^2 f(x)\,)\circ(\,g(x),\ \triangledown g(x),\ \triangledown^2 g(x)\,)$, or to compose the triples of two elementary functions, we use the chain rules of Newtonian calculus. For dyadic reasons, the differentiation arithmetic was explained only in terms of reals. By replacing the real x's above by interval X's and performing all operations in the real IA with the interval extension F of f, one can rigorously enclose the components of the triple $(\,F(X),\ \triangledown F(X),\ \triangledown^2 F(X)\,)$ through an interval-extended Hessian differentiation arithmetic such that for every $x \in X \in \mathbb{IR}^n$, $f(x) \in F(X) \in \mathbb{IR}$, $\triangledown f(x) \in \triangledown F(X) \in \mathbb{IR}^n$, and $\triangledown^2 f(x) \in \triangledown^2 F(X) \in \mathbb{IR}^{n\times n}$. Next we take advantage of AD to find the roots of nonlinear functions.

The interval version of Newton method computes an enclosure of the zero x^* of a continuously differentiable function $f(x)$ in the interval X through the following dynamical system in $\mathbb{IR}$:

$$X^{(j+1)} = \left(m(X^{(j)}) - \frac{f(m(X^{(j)}))}{F'(X^{(j)})} \right) \cap X^{(j)}, \qquad j = 0, 1, 2, \cdots$$

Here, $X^{(0)} = X$, $F'(X^{(j)})$ is the enclosure of $f'(x)$ over $X^{(j)}$, and $m(X^{(j)})$ is the mid-point of $X^{(j)}$. The interval Newton method will never diverge, provided that $0 \notin F'(X^{(0)})$ or equivalently that a unique zero of f lies in $X^{(0)}$. [Moore, 1967] derived the interval Newton method. Under natural conditions on f, the sequence of compact sets $X^{(0)} \supseteq X^{(1)} \supseteq X^{(2)} \cdots$ can be shown to converge quadratically to x^* [Alefeld and Herzberger, 1983]. One can derive the above dynamical system in $\mathbb{IR}$ via the mean value theorem. Let $f(x)$ be continuously differentiable and $f'(x) \neq 0$ for all $x \in X$ such that x^* is the only zero of f in X. Then, by the mean value theorem, there exists $c \in (x, x^*)$ such that $f(x) - f(x^*) = f'(c)(x - x^*)$ for every x. Since $f'(c) \neq 0$ by assumption, and since $f(x^*) = 0$, it follows that:

$$x^* = x - \frac{f(x)}{f'(c)} \in x - \frac{f(x)}{F'(X)} =: N(X), \quad \forall x \in X.$$

$N(X)$ is called the Newton operator and it contains x^*. Since our root of interest lies in X, $x^* \in N(X) \cap X$. Note that the above dynamical system in $\mathbb{IR}$ is obtained by replacing x with $m(X)$ and X with $X^{(j)}$ in the previous expression. In a geometric interpretation of the usual Newton's method, during every j^{th} iteration, a light beam is shone upon the domain from the point $(x^{(j)}, f(x^{(j)}))$ along the tangent to $f(x)$ at $x^{(j)}$. The intersection of this beam (white line in Figure 20.3) with the domain provides $x^{(j+1)}$, which is where the next iteration is resumed. However, in the interval Newton method, a set of light beams are shone from the point $(x^{(j)}, f(x^{(j)}))$ along the directions of all the tangents to $f(x)$ on the entire interval X. The intersection of these beams (gray floodlight of Figure 20.3) with the domain is $N(X^{(j)})$. The iteration is

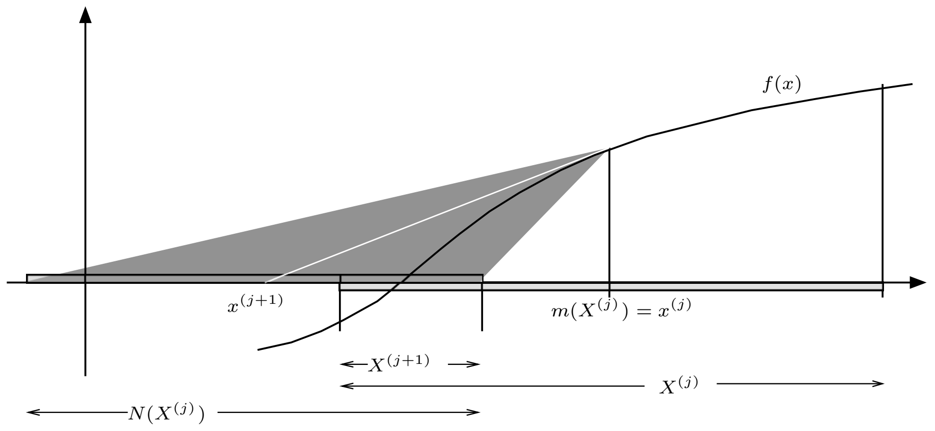

Fig. 20.3. *Geometric interpretation of the interval Newton method*

resumed with the new interval $X^{(j+1)} = N(X^{(j)}) \cap X^{(j)}$. Next we extend the interval Newton method in order to allow $F'(X)$ to contain 0.

By including two ideal points $+\infty$ and $-\infty$ to $\mathbb{R}$, it becomes possible to apply extended interval arithmetic (EIA) to $\mathbb{IR}^* := \mathbb{IR} \cup \{(-\infty, \overline{x}] : \overline{x} \in \mathbb{R}\} \cup \{[\underline{x}, +\infty) : \underline{x} \in \mathbb{R}\} \cup (-\infty, +\infty)$, the set of intervals with end points in the complete lattice $\mathbb{R}^* := \mathbb{R} \cup \{+\infty\} \cup \{-\infty\}$, with respect to the ordering relation $\leq$. Let $[\,]$ denote the empty interval. Division by intervals containing 0 becomes possible with the following rules:

$$X/Y := \begin{cases} (-\infty, +\infty) & \text{if } 0 \in X, \text{or } Y = [0,0] \\ [\,] & \text{if } 0 \notin X, \text{and } Y = [0,0] \\ [\,\overline{x}/\underline{y}, +\infty) & \text{if } \overline{x} \leq 0, \text{ and } \overline{y} = 0 \\ [\,\underline{x}/\overline{y}, +\infty) & \text{if } 0 \leq \underline{x}, \text{ and } 0 = \underline{y} < \overline{y} \\ (-\infty, \overline{x}/\overline{y}\,] & \text{if } \overline{x} \leq 0, \text{ and } 0 = \underline{y} < \overline{y} \\ (-\infty, \underline{x}/\underline{y}\,] & \text{if } 0 \leq \underline{x}, \text{ and } \underline{y} < \overline{y} = 0 \\ (-\infty, \overline{x}/\overline{y}\,] \cup [\,\overline{x}/\underline{y}, +\infty) & \text{if } \overline{x} \leq 0, \text{ and } [0,0] \Subset Y \\ (-\infty, \underline{x}/\underline{y}\,] \cup [\,\underline{x}/\overline{y}, +\infty) & \text{if } 0 \leq \underline{x}, \text{ and } [0,0] \Subset Y. \end{cases}$$

When X is a thin interval with $x = \underline{x} = \overline{x}$ and Y has $+\infty$ or $-\infty$ as one of its bounds, then extended interval subtraction is also necessary for the extended interval Newton algorithm, and is defined as follows:

$$[\,\underline{x}, \overline{x}\,] - Y := \begin{cases} (-\infty, +\infty) & \text{if } Y = (-\infty, +\infty) \\ (-\infty, x - \underline{y}] & \text{if } Y = (\,\underline{y}, +\infty) \\ [x - \overline{y}, +\infty) & \text{if } Y = (-\infty, \overline{y}\,]. \end{cases}$$

The extended interval Newton method uses the EIA described above and is a variant of the method based on [Hansen and Sengupta, 1981] with Ratz's modifications [Ratz, 1992] as implemented in [Hammer *et al.*, 1995]. It can be used to enclose the roots of a continuously differentiable $f : \mathbb{R}^n \to \mathbb{R}^n$ in a given box $X \in \mathbb{IR}^n$. Let $J_f(x) := ((\partial f_i(x)/\partial x_j))_{i,j=\{1,\cdots,n\}} \in \mathbb{R}^{n\times n}$ denote the Jacobian matrix of f at x. Let $J_F(X) \supset J_f(X)$ denote the Jacobian of the interval extension of f. The Jacobian can be computed via AD by computing the gradient of each component f_i of f. By the mean value theorem, $f(m(X)) - f(x^*) = J_f(w)\cdot(m(X) - x^*)$, for some $x^* \in X, w = (w_1, w_2, \cdots, w_n)$, where $w_i \in X, \forall i \in \{1, 2, \cdots, n\}$. Interest in x^* with $f(x^*) = 0$ yields the following relation provided that $J_F(x)\, \forall x \in X$ is invertible: $x^* \in \mathcal{N}(X) \cap X$, where $\mathcal{N}(X) := m(X) - (\, J_F(X)\,)^{-1} \cdot F(m(X))$. An iteration scheme $X^{(j+1)} := \mathcal{N}(X^{(j)}) \cap X^{(j)}$ for $j = 0, 1, \cdots$, and $X^{(0)} := X$ will enclose the zeros of f contained in X. To relax the assumption that every matrix in $J_F(X)$ be invertible, the inverse of the midpoint of $J_F(X)$, i.e. $(m(J_F(X)))^{-1} =: p \in \mathbb{R}^{n\times n}$, is used as a matrix preconditioner. The extended interval Gauss-Seidel iteration, which is also applicable to singular systems [Neumaier, 1990], is used to solve the preconditioned interval linear equation,

$$\begin{aligned} p \cdot F(m(X)) &= p \cdot J_F(X) \cdot (m(X) - x^*) \\ a &= G \cdot (c - x^*), \end{aligned}$$

where $a \in A := p \cdot F(m(X)), G := p \cdot J_F(X)$, and $c := m(X)$. Thus, the solution set $\mathbf{S} := \{x \in X : g \cdot (c - x) = a, \forall g \in G\}$ of the interval linear equation $a = G \cdot (c - x)$ has the component-wise solution set $\mathbf{S}_i = \{x_i \in X_i : \sum_{j=1}^{n} (\, g_{i,j} \cdot (c_j - x_j)\,) = a_i, \forall g \in G\}$, $\forall i \in \{1, \cdots, n\}$. Now set $Y = X$, and solve the ith equation for the ith variable iteratively for each i as follows:

$$\begin{aligned} y_i = c_i - \tfrac{1}{g_{i,i}} &\left(a_i + \textstyle\sum_{j=1, j\neq i}^{n} (\, g_{i,j} \cdot (y_j - c_j)\,)\right) \\ &\in \left(c_i - \tfrac{1}{G_{i,i}} \left(A_i + \textstyle\sum_{j=1, j\neq i}^{n} (\, G_{i,j} \cdot (Y_j - c_j)\,)\right)\right) \cap Y_i. \end{aligned}$$

The interval vector(s) Y obtained at the end of such an iteration is the set, $\mathcal{N}_{GS}(X)$, resulting from one extended interval Newton Gauss-Seidel step such that $\mathbf{S} \subseteq \mathcal{N}_{GS}(X) \subseteq X$. Thus, the roots of f are enclosed by the discrete dynamical system $X^{(j)} = \mathcal{N}_{GS}(X^{(j)})$ in $\mathbb{IR}^n$. Every 0 of f that lies in X also lies in $\mathcal{N}_{GS}(X)$. If $\mathcal{N}_{GS}(X) = [\,]$, the empty interval, then f has no solution in X. If $\mathcal{N}_{GS}(X) \Subset X$, then f has a unique solution in X [Hansen, 1992]. When $G_{ii} \supset 0$, the method is applicable with EIA that allows for division by 0. In such cases, one may obtain up to two disjoint compact intervals for Y_i subsequent to EIA and intersection with the previous compact interval X_i. In such cases, the iteration is applied to each resulting sub-interval.

All IA was done above with real intervals. However, $\mathcal{R}$, the set of floating-point numbers available on a computing machine, is finite. A machine interval is a real interval with floating-point bounds. One works with $\mathbb{I}\mathcal{R} := \{X \in \mathbb{I}\mathbb{R} : \underline{x}, \overline{x} \in \mathcal{R}\}$, the set of all machine intervals, in a computer. In spite of the finiteness of $\mathbb{I}\mathcal{R}$, the strength of IA lies in a machine interval X being able to enclose the entire continuum of reals between its machine-representable boundaries. Operations with real intervals can be tightly enclosed by the rounding directed operations, provided by the IEEE arithmetic standard, with the smallest machine intervals containing them [Hammer *et al.*, 1995, Kulisch *et al.*, 2001].

20.2 Enclosing the likelihood of a compact set of trees

Let $\mathcal{D}$ denote a homologous set of distinct DNA sequences of length v from n species. We want the MLEs of branch lengths for the most likely tree under a particular topology. Let b denote the number of branches and s denote the number of nodes of a tree with topology τ. Thus, for a given unrooted topology τ with n leaves and b branches, the unknown parameter $\theta = (\theta_1, \cdots, \theta_b)$ is the real vector of branch lengths in the positive orthant ($\theta_q \in \mathbb{R}_+$). An explicit model of DNA evolution is needed to construct the likelihood function which gives the probability of observing data $\mathcal{D}$ as a function of the parameter θ. The simplest such continuous time Markov chain model (JC69) on the state space Σ is due to [Jukes and Cantor, 1969]. One may compute $\ell^{(k)}(\theta)$, the log likelihood at site $k \in \{1, \cdots, v\}$ through the following post-order traversal [Felsenstein, 1981]:

(i) Associate with each node $q \in \{1, \cdots, s\}$ with m descendants, a partial likelihood vector, $\mathbf{l}_q := (\mathbf{l}_q^A, \mathbf{l}_q^C, \mathbf{l}_q^G, \mathbf{l}_q^T) \in \mathbb{R}^4$, and let the length of the branch leading to its ancestor be θ_q.

(ii) For a leaf node q with nucleotide i, set $\mathbf{l}_q^i = 1$ and $\mathbf{l}_q^j = 0$ for all $j \neq i$. For any internal node q, set $\mathbf{l}_q := (1, 1, 1, 1)$.

(iii) For an internal node q with descendants $s_1, s_2, \cdots, s_m$,

$$\mathbf{l}_q^i = \sum_{j_1, \cdots, j_m \in \Sigma} \{ \mathbf{l}_{s_1}^{j_1} \cdot P_{i,j_1}(\theta_{s_1}) \cdot \mathbf{l}_{s_2}^{j_2} \cdot P_{i,j_2}(\theta_{s_2}) \cdots \mathbf{l}_{s_m}^{j_m} \cdot P_{i,j_m}(\theta_{s_m}) \}.$$

(iv) Compute $\mathbf{l}_q$ for each sub-terminal node q, then those of their ancestors recursively to finally compute $\mathbf{l}_r$ for the root node r to obtain the log likelihood for site k, $\ell^{(k)}(\theta) = \mathbf{l}_r = \log \sum_{i \in \Sigma} (\pi_i \cdot \mathbf{l}_r^i)$.

Assuming independence across sites one obtains $\ell(\theta) = \sum_{k=1}^{v} \ell^{(k)}(\theta)$, the natural logarithm of the likelihood function for the data $\mathcal{D}$ by multiplying the site-specific likelihoods. The problem of finding the global maximum of this likelihood function is equivalent to finding the global minimum of $l(\theta) := -\ell(\theta)$. Replacing every constant c by its corresponding constant triple $(C, 0, 0)$, every variable θ_j by its triple $(\, \Theta_j, e^{(j)}, 0\,)$, and every real operation or elementary function by its counterpart in interval-extended Hessian differentiation arithmetic in the above post-order traversal yields a rigorous enclosure of the negative log likelihood triple $(\, \mathcal{L}(\Theta), \bigtriangledown\mathcal{L}(\Theta), \bigtriangledown^2\mathcal{L}(\Theta)\,)$ of the negative log likelihood function $l(\theta)$ over Θ.

20.3 Global Optimization

20.3.1 Branch-and-bound

The most basic strategy in global optimization through enclosure methods is to employ rigorous branch-and-bound techniques. Such techniques recursively partition (branch) the original compact space of interest into compact subspaces and discard (bound) those subspaces that are guaranteed to not contain the global optimizer(s). For the real scalar-valued multi-dimensional objective function $l(\theta)$, the interval branch-and-bound technique can be applied to its natural interval extension $\mathcal{L}(\Theta)$ to obtain an interval enclosure $\mathcal{L}^*$ of the global minimum value l^* as well as the set of minimizer(s) to a specified accuracy ϵ. Note that this set of minimizer(s) of $\mathcal{L}(\theta)$ is the set of maximizer(s) of the likelihood function for the observed data $\mathcal{D}$. The strength of such methods arises from the algorithmic ability to discard large sub-boxes from the original search region,

$$\Theta^{(0)} = (\, \Theta_1^{(0)}, \cdots, \Theta_b^{(0)}\,) := (\, [\underline{\theta}_1^{(0)}, \overline{\theta}_1^{(0)}], \cdots, [\underline{\theta}_b^{(0)}, \overline{\theta}_b^{(0)}]\,) \subset \mathbb{IR}^b,$$

that are not candidates for global minimizer(s). Four tests that help discard sub-regions are described below. Let $\mathfrak{L}$ denote a list of ordered pairs of the form $(\, \Theta^{(i)}, \underline{\mathcal{L}}_{\Theta^{(i)}}\,)$, where $\Theta^{(i)} \subseteq \Theta^{(0)}$, and $\underline{\mathcal{L}}_{\Theta^{(i)}} := \min(\, \mathcal{L}(\Theta^{(i)})\,)$ is a lower bound for the range of the negative log likelihood function l over $\Theta^{(i)}$. Let $\tilde{l}$ be an upper bound for l^* and $\bigtriangledown\mathcal{L}(\Theta^{(i)})_k$ denote the k-th interval of the gradient box $\bigtriangledown\mathcal{L}(\Theta^{(i)})$. If no information is available for $\tilde{l}$, then $\tilde{l} = \infty$.

20.3.1.1 Midpoint cut-off test

The basic idea of the *midpoint cut-off test* is to discard sub-boxes of the search space $\Theta^{(0)}$ with the lower bound for their range enclosures above $\tilde{l}$, the current best estimate of an upper bound for l^*. Figure 20.4 shows a multi-modal l as a function of a scalar valued θ over $\Theta^{(0)} = \cup_{i=1}^{16}\Theta^{(i)}$. For this illustrative example, $\tilde{l}$ is set as the upper bound of the range enclosure of l over the smallest machine interval containing the midpoint of $\Theta^{(15)}$, the interval with the smallest lower bound of its range enclosure. The shaded rectangles show the range enclosures over intervals that lie strictly above $\tilde{l}$. In this example the *midpoint cut-off test* would discard all other intervals except $\Theta^{(1)}$, $\Theta^{(2)}$, and $\Theta^{(4)}$.

- Given a list $\mathfrak{L}$ and $\tilde{l}$.

- Choose an element j of $\mathfrak{L}$, such that, $j = \underset{i}{argmin} \underline{\mathcal{L}}_{\Theta^{(i)}}$, since $\Theta^{(j)}$ is likely to contain a minimizer.
- Find its midpoint $c = m(\Theta^{(j)})$ and let C be the smallest machine interval containing c.
- Compute a possibly improved $\tilde{l} = \min \{\tilde{l}, \overline{\mathcal{L}}_C\}$, where $\overline{\mathcal{L}}_C := \max(\mathcal{L}(C))$.
- Discard any i-th element of $\mathfrak{L}$ for which $\underline{\mathcal{L}}_{\Theta^{(i)}} > \tilde{l} \geq l^*$.

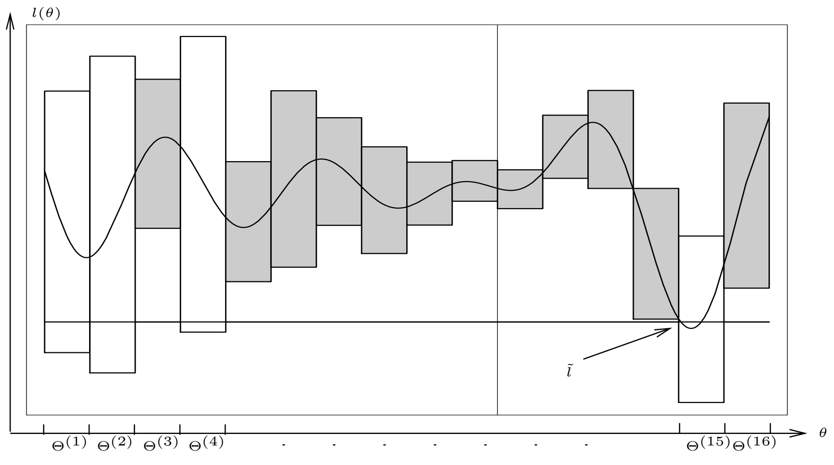
$l(\theta)$
$\tilde{l}$
θ
$\Theta^{(1)}$ $\Theta^{(2)}$ $\Theta^{(3)}$ $\Theta^{(4)}$ . . . . $\Theta^{(15)}$ $\Theta^{(16)}$

Fig. 20.4. *Midpoint Cut-off test*

20.3.1.2 Monotonicity test

For a continuously differentiable function $l(\theta)$, the *monotonicity test* determines whether $l(\theta)$ is strictly monotone over an entire sub-box $\Theta^{(i)} \subset \Theta^{(0)}$. If l is strictly monotone over $\Theta^{(i)}$, then a global minimizer cannot lie in the interior of $\Theta^{(i)}$. Therefore, $\Theta^{(i)}$ can only contain a global minimizer as a boundary point if this point also lies in the boundary of $\Theta^{(0)}$. Figure 20.5 illustrates the *monotonicity test* for the one-dimensional case. In this example the search space of interest, $\Theta^{(0)} = [\underline{\theta}^{(0)}, \overline{\theta}^{(0)}] = \cup_{i=1}^{8} \Theta^{(i)}$, can be reduced considerably. In the interior of $\Theta^{(0)}$, one may delete $\Theta^{(2)}$, $\Theta^{(5)}$, and $\Theta^{(7)}$, since $l(\theta)$ is monotone over them as indicated by the enclosure of the derivative $l'(\theta)$ being bounded away from 0. Since $l(\theta)$ is monotonically decreasing over $\Theta^{(1)}$ one can also deleted it since we are only interested in minimization. $\Theta^{(8)}$ may be pruned to its right boundary point $\theta^{(8)} = \overline{\theta}^{(8)} = \overline{\theta}^{(0)}$ due to the strictly decreasing nature of $l(\theta)$ over it. Thus, the *monotonicity test* has pruned $\Theta^{(0)}$ to the smaller candidate set $\{\overline{\theta}^{(0)}, \Theta^{(3)}, \Theta^{(4)}, \Theta^{(6)}\}$ for a global minimizer.

- Given $\Theta^{(0)}$, $\Theta^{(i)}$, and $\bigtriangledown\mathcal{L}(\Theta^{(i)})$.
- Iterate for $k = 1, \cdots, b$

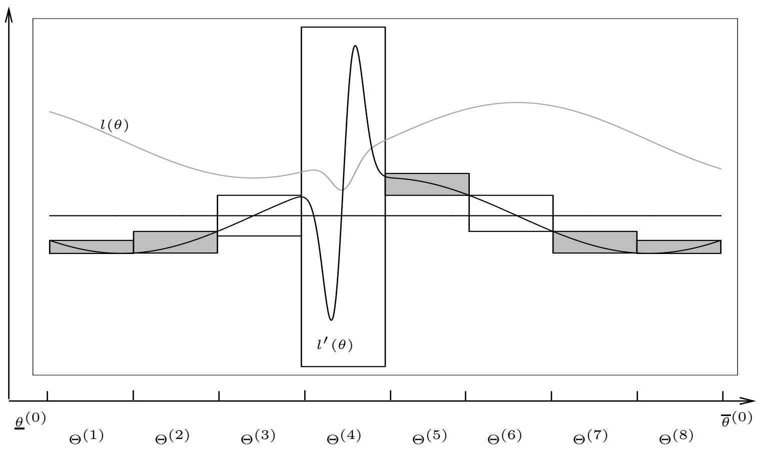

Fig. 20.5. *Monotonicity test*

– If $0 \in \bigtriangledown\mathcal{L}(\Theta^{(i)})_k$, then leave $\Theta_k^{(i)}$ unchanged, as it may contain a stationary point of l.
– Otherwise, $0 \notin \bigtriangledown\mathcal{L}(\Theta^{(i)})_k$. This implies that $\Theta^{(i)}$ can be pruned, since $l^* \notin \Theta^{(i)}$ except possibly at the boundary points, as follows:
  (i) if $\min(\bigtriangledown\mathcal{L}(\Theta^{(i)})_k) > 0$ and $\underline{\theta}_k^{(0)} = \underline{\theta}_k^{(i)}$, then $\Theta_k^{(i)} = [\underline{\theta}_k^{(i)}, \underline{\theta}_k^{(i)}]$,
  (ii) Else if $\max(\bigtriangledown\mathcal{L}(\Theta^{(i)})_k) < 0$ and $\overline{\theta}_k^{(0)} = \overline{\theta}_k^{(i)}$, then $\Theta_k^{(i)} = [\overline{\theta}_k^{(i)}, \overline{\theta}_k^{(i)}]$.
  (iii) Else, delete the i-th element of $\mathfrak{L}$ and stop the iteration.

20.3.1.3 Concavity test

Given $\Theta^{(i)} \Subset \Theta^{(0)}$, and the diagonal elements $(\bigtriangledown^2\mathcal{L}(\Theta^{(i)}))_{kk}$ of $\bigtriangledown^2\mathcal{L}(\Theta^{(i)})$, note that if $\min((\bigtriangledown^2\mathcal{L}(\Theta^{(i)}))_{kk}) < 0$ for some k, then $\bigtriangledown^2\mathcal{L}(\Theta^{(i)})$ cannot be positive semidefinite, and therefore $l(\theta)$ cannot be convex over $\Theta^{(i)}$ and thus cannot contain a minimum in its interior. In the one-dimensional example shown in Figure 20.5, an application of the *concavity test* to the candidate set $\{\underline{\theta}^{(0)}, \Theta^{(4)}, \Theta^{(6)}\}$ for a global minimizer returned by the *monotonicity test*, would result in the deletion of $\Theta^{(6)}$ due to the concavity of $l(\theta)$ over it.

- Given $\Theta^{(i)} \Subset \Theta^{(0)}$ and $\bigtriangledown^2\mathcal{L}(\Theta^{(i)})$
- If $\min((\bigtriangledown^2\mathcal{L}(\Theta^{(i)}))_{kk}) < 0$ for any $k \in \{1, \cdots, b\}$, then delete the i-th element of $\mathfrak{L}$.

20.3.1.4 Interval Newton test

Given $\Theta^{(i)} \Subset \Theta^{(0)}$, and $\bigtriangledown\mathcal{L}(\Theta^{(i)})$, attempt to solve the system, $\bigtriangledown\mathcal{L}(\theta) = 0$, in terms of $\theta \in \Theta^{(i)}$.

- Apply one extended interval Newton Gauss-Seidel step to the linear interval equation $a = G \cdot (c - \theta)$, where $a := p \cdot \mathcal{L}(m(\Theta^{(i)}))$, $G := p \cdot \bigtriangledown^2 \mathcal{L}(\Theta^{(i)})$, $c := m(\Theta^{(i)})$, and $p := (m(\bigtriangledown^2 F(X)))^{-1}$, in order to obtain $\mathcal{N}'_{GS}(\Theta^{(i)})$.
- One of the following can happen,
  - (i) If $\mathcal{N}'_{GS}(\Theta^{(i)})$ is empty, then discard $\Theta^{(i)}$.
  - (ii) If $\mathcal{N}'_{GS}(\Theta^{(i)}) \Subset \Theta^{(i)}$, then replace $\Theta^{(i)}$ by the contraction $\mathcal{N}'_{GS}(\Theta^{(i)}) \cap \Theta^{(i)}$.
  - (iii) If $0 \in G_{jj}$, and the extended interval division splits $\Theta_j^{(i)}$ into a non-empty union of $\Theta_j^{(i),1}$ and $\Theta_j^{(i),2}$, then the iteration is continued on $\Theta_j^{(i),1}$, while $\Theta_j^{(i),2}$, if non-empty, is stored in $\mathfrak{L}$ for future processing. Thus, one extended interval Newton Gauss-Seidel step can add at most $b + 1$ sub-boxes to $\mathfrak{L}$.

20.3.2 Verification

Given a collection of sub-boxes, $\{ \Theta^{(1)}, \cdots, \Theta^{(n)} \}$, each of width $\leq \epsilon$, that could not be discarded by the tests in Section 20.3.1, one can attempt to verify the existence and uniqueness of a local minimizer within each sub-box $\theta^{(i)}$ by checking whether the conditions of the following two theorems are satisfied. For proof of these two theorems see [Hansen, 1992] and [Ratz, 1992].

(i) If $\mathcal{N}'_{GS}(\Theta^{(i)}) \Subset \Theta^{(i)}$, then there exists a unique stationary point of $\mathcal{L}$, i.e. a unique zero of $\bigtriangledown\mathcal{L}$ exists in $\Theta^{(i)}$.

(ii) If $(I + \frac{1}{\kappa} \cdot (\bigtriangledown^2 \mathcal{L}(\Theta^{(i)}))) \cdot Z \Subset Z$, where $(\bigtriangledown^2 \mathcal{L}(\Theta^{(i)}))_{d,\infty} \leq \kappa \in \mathbb{R}$, for some $Z \in \mathbb{IR}^n$, then the spectral radius $\rho(s) < 1$ for all $s \in (I - \frac{1}{\kappa} \cdot (\bigtriangledown^2 \mathcal{L}(\Theta^{(i)})))$ and all symmetric matrices in $\bigtriangledown^2 \mathcal{L}(\Theta^{(i)})$ are positive definite.

If the conditions of the above two theorems are satisfied by some $\Theta^{(i)}$, then a unique stationary point exists in $\Theta^{(i)}$ and this stationary point is a local minimizer. Therefore, if exactly one candidate sub-box for minimizer(s) remained after pruning the search box $\Theta^{(0)}$ with the tests in Section 20.3.1, and if this sub-box satisfies the above two conditions for the existence of a unique local minimizer within it, then one has rigorously enclosed the global minimizer in the search interval. On the other hand, if there are two or more sub-boxes in our candidate list for minimizer(s) that satisfy the above two conditions, then one may conclude that each sub-box contains a candidate for a global minimizer which may not necessarily be unique (disconnected sub-boxes, for example). Observe that failure to verify the uniqueness of a local minimizer in a sub-box can occur if it contains two or more points or even a continuum of points that are stationary.

20.3.3 Algorithm

- *Initialization:*

Step 1 Let the search region be a single box $\Theta^{(0)}$ or a collection of not necessarily connected, but pair-wise disjoint boxes, $\Theta^{(i)}$, $i \in \{1, \cdots, r\}$.

Step 2 Initialize the list $\mathfrak{L}$ which may just contain one element $(\, \Theta^{(0)}, \underline{\mathcal{L}}_{\Theta^{(0)}} \,)$ or several elements

$$\{\, (\, \Theta^{(1)}, \underline{\mathcal{L}}_{\Theta^{(1)}} \,), (\, \Theta^{(2)}, \underline{\mathcal{L}}_{\Theta^{(2)}} \,), \cdots, (\, \Theta^{(r)}, \underline{\mathcal{L}}_{\Theta^{(r)}} \,) \,\}.$$

Step 3 Let ϵ be a specified tolerance.

Step 4 Let $\max_{\mathfrak{L}}$ be the maximal length allowed for list $\mathfrak{L}$.

Step 5 Set the noninformative lower bound for l^*, i.e. $\tilde{l} = \infty$

- *Iteration:*

Step1 Perform the following operations:

Step 1.1 Improve $\tilde{l} = \min\{\tilde{l}, \max(\mathcal{L}(m(\Theta^{(j)})))\}$, $j = \underset{i}{argmin}\{\underline{\mathcal{L}}_{\Theta^{(i)}}\}$.

Step 1.2 Perform the *midpoint cut-off test* to $\mathfrak{L}$.

Step 1.3 Set $\mathcal{L}^* = [\underline{\mathcal{L}}_{\Theta^{(j)}}, \tilde{l}]$.

Step 2 Bisect $\Theta^{(j)}$ along its longest side k, i.e. $d(\Theta_k^{(j)}) = d_\infty(\Theta^{(j)})$, to obtain sub-boxes $\Theta^{(j_q)}$, $q \in \{1, 2\}$.

Step 3 For each sub-box $\Theta^{(j_q)}$, evaluate $(\, \mathcal{L}(\Theta^{(j_q)}), \bigtriangledown\mathcal{L}(\Theta^{(j_q)}), \bigtriangledown^2\mathcal{L}(\Theta^{(j_q)}) \,)$, and do the following:

Step 3.1 Perform *monotonicity test* to possibly discard $\Theta^{(j_q)}$.

Step 3.2 *Centered form cut-off test:*
Improve the range enclosure of $\mathcal{L}(\Theta^{(j_q)})$ by replacing it with its centered form $\mathcal{L}_c(\Theta^{(j_q)}) :=$

$$\{\mathcal{L}(m(\Theta^{(j_q)})) + \bigtriangledown\mathcal{L}(\Theta^{(j_q)}) \cdot (\Theta^{(j_q)} - m(\Theta^{(j_q)}))\} \cap \mathcal{L}(\Theta^{(j_q)}),$$

and then discarding $\Theta^{(j_q)}$, if $\tilde{l} < \underline{\mathcal{L}}_{\Theta^{(j_q)}}$.

Step 3.3 Perform *concavity test* to possibly discard $\Theta^{(j_q)}$.

Step 3.4 Apply an *extended interval Newton Gauss-Seidel step* to $\Theta^{(j_q)}$, in order to either entirely discard it or shrink it into v sub-sub-boxes, where v is at most $2s - 2$.

Step 3.5 For each one of these sub-sub-boxes $\Theta^{(j_{q,u})}$, $u \in \{1, \cdots, v\}$

Step 3.5.1 Perform *monotonicity test* to possibly discard $\Theta^{(j_{q,u})}$.

Step 3.5.2 Try to discard $\Theta^{(j_{q,u})}$ by applying the *centered form cut-off test* in **Step 3.2** to it.

Step 3.5.3 Append $(\, \Theta^{(j_{q,u})}, \underline{\mathcal{L}}_{\Theta^{(j_{q,u})}} \,)$ to $\mathfrak{L}$ if $\Theta^{(j_{q,u})}$ could not be discarded by steps **Step 3.5.1** and **Step 3.5.2**.

Table 20.1. *Chimpanzee (1), Gorilla (2), and Orangutan (3).*

$\Theta^{(0)}$ and Tree	$\Theta^* \supset \theta^*$	$-\mathcal{L}(\Theta^*) \supset -l(\theta^*)$
$[1.0 \times 10^{-11}, 10.0]^{\otimes 3}$	$5.98162213840^{2}_{0} \times 10^{-2}$	
$\tau_1 = (1,2,3)$	$5.41674167940^{2}_{0} \times 10^{-2}$	
	$1.3299089685^{9}_{8} \times 10^{-1}$	$-2.150318065856^{5}_{6} \times 10^{3}$

- *Termination:*

Step 1 Terminate iteration if $d_{rel,\infty}(\Theta^{(j)}) < \epsilon$, or $d_{rel,\infty}(\mathcal{L}^*) < \epsilon$, or $\mathfrak{L}$ is empty, or Length$(\mathfrak{L}) > \max_{\mathfrak{L}}$.

Step 2 Verify uniqueness of minimizer(s) in the final list $\mathfrak{L}$ by applying algorithm of Section 20.3.2 to each of its elements.

20.4 Applications to phylogenetics

The global maximum of the log likelihood function for the JC69 model of DNA evolution on the three taxa unrooted tree with data from the mitochondria of Chimpanzee, Gorilla, and Orangutan [Brown *et al.*, 1982] is enclosed. There is only one unrooted multifurcating topology for three species with all three branches emanating from the root like a star. The data set for this problem is summarized in [Sainudiin, 2004] by 29 data patterns. The sufficient statistics for this data is $(7, 100, 42, 46, 700)$. The parameter space is three dimensional corresponding to the three branch lengths of the 3-leaved star tree τ_1. The algorithm is given a large search box $\Theta^{(0)}$. The results are summarized in Table 20.1. The notation x^b_a means the interval $[xa, xb]$ (e.g. $5.98162213840^2_0 \times 10^{-2} = [5.98162213840 \times 10^{-2}, 5.98162213842 \times 10^{-2}]$). Figure 20.6 shows the the parameter space being rigorously pruned as the algorithm progresses. When there are four taxa, the phylogeny estimation problem is more challenging as there are four distinct topologies to consider in addition to the branch lengths. A similar method was used to solve the most likely phylogeny of four primates with data from their mitochondria [Sainudiin, 2004].

The running time of the global optimization algorithm depends on where the MLEs lie in the parameter space. For trees with smaller branch lengths, the running time is faster while larger trees have a much longer running time. The Table 20.2 shows the mean and 95% confidence intervals of the number of calls to the likelihood function $\mathcal{L}$ and the CPU time in seconds for each of four trees with different weights. The results summarized in Table 20.2 are

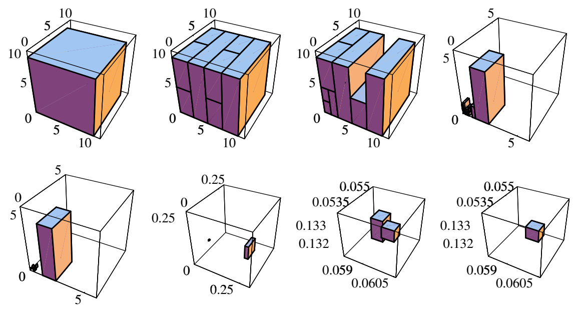

Fig. 20.6. Progress of the algorithm as it prunes $[0.001, 10.0]^{\otimes 3}$.

Table 20.2. *Computational efficiency for four different 3 taxa trees.*

True Tree	Calls to $\mathcal{L}(\Theta^*)$	CPU time
$(1 : 0.01, 2 : 0.07, 3 : 0.07)$	$1272\ [1032, 1663]$	$0.55\ [0.45, 0.72]$
$(1 : 0.02, 2 : 0.19, 3 : 0.19)$	$3948\ [2667, 6886]$	$1.75\ [1.17, 3.05]$
$(1 : 0.03, 2 : 0.42, 3 : 0.42)$	$20789\ [12749, 35220]$	$9.68\ [5.94, 16.34]$
$(1 : 0.06, 2 : 0.84, 3 : 0.84)$	$245464\ [111901, 376450]$	$144.62\ [64.07, 232.94]$

from 100 data sets, each of sequence length 1000, simulated under JC69 model upon each one of the four trees shown in the first column.

The MLEs obtained by means of interval methods are equivalent to numerical proofs for the MLEs. The method is robust in the presence of multiple local maxima or nonidentifiable manifolds with the same ML value. For example, when a time reversible Markov chain, such as JC69, is super-imposed on a rooted tree, only the sum of the branch lengths emanating from the root is identifiable. Identifiability is a prerequisite for statistical consistency of estimators. To demonstrate the ability of interval methods to enclose the nonidentifiable ridge along $\theta_1 + \theta_2$ in the simplest case of a two-leaved tree, a nonidentifiable negative log likelihood function $l(\theta_1, \theta_2)$ is formulated with its global minimizers along $\theta_1 + \theta_2 = \frac{3}{4} \log(45/17) = 0.730087$ under a fictitious dataset for which 280 out of 600 sites are polymorphic. Figure 20.7 shows the contours of $l(\theta_1, \theta_2)$ in gray scale and the solutions of the interval method (gray and black rectangles) and those of 10 Quasi-Newton searches with random initializations (10 pairs of colored ovals). Observe that the basin of attraction for each point on $\theta_1 + \theta_2 = 0.730087$ under a Quasi-Newton local search algorithm is the line running orthogonal to it.

Interval methods can be slow on currently available processors that are optimized for floating-point arithmetic, especially when applied naively. If one

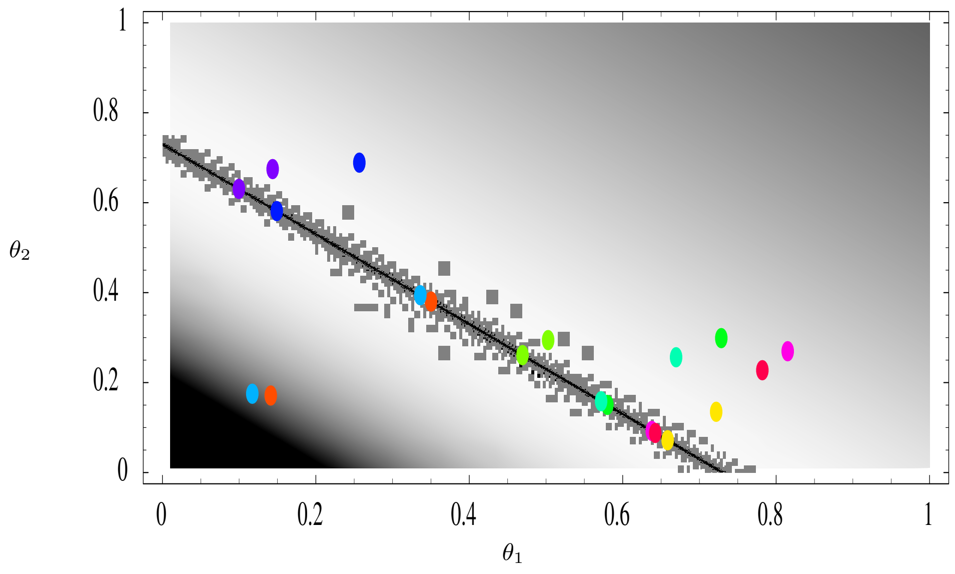

Fig. 20.7. The nonidentifiable subspace of minimizers $\theta_1 + \theta_2 = \frac{3}{4}\log(45/17)$ of $l(\theta_1, \theta_2)$ under the JC69 model evolving on a rooted two-leaved tree is enclosed by a union of up to 30,000 rectangles. The larger gray, and smaller black rectangles have tolerances of $\epsilon = 1.0 \times 10^{-4}$ and $\epsilon = 1.0 \times 10^{-6}$, respectively. The 10 pairs of colored ovals are the initial and final points of 10 local Quasi-Newton searches with random initializations.

were to pre-enclose the likelihood function over a fine mesh and use hash tables to access them, then computational efficiency can be gained. Interval methods can work efficiently when algebraic techniques are first used to reduce the data into sufficient statistics (see details in Chapter 18). Interval methods are particularly suited to methods that solve a large dimensional problem by solving a set of lower dimensional problems. For instance, one can apply the rigorously enclosed MLEs to the generalized neighbor-joining (GNJ) method discussed in Chapter 2. We call this the *rigorous neighbor-joining method*. Using `fastDNAml` which implements a gradient flow algorithm with floating-point arithmetic, [Levy *et al.*, 2004] computed dissimilarity maps that are needed for the GNJ method. The rigorous NJ method uses, instead, the rigorously enclosed MLEs. We apply this method to find the NJ tree for 21 SRK sequences [Sainudiin *et al.*, 2005] from the self/nonself discriminating self-incompatibility system of the mustard family [Nasrallah, 2002]. We sampled 10,000 trees from a Markov chain with stationary distribution proportional to the likelihood function by means of a Markov chain Monte Carlo (MCMC) algorithm implemented in `PHYBAYES` [Aris-Brosou, 2003]. We compared the tree topology of each tree generated by this MCMC method with the tree topology of the reconstructed trees via the rigorous NJ method, `fastDNAml`, `DNAml` from `PHYLIP`

$\boldsymbol{\Delta}$	Rigorous NJ	fastDNAml	DNAml(A)	DNAml(B)	TrExML
0	0	0	2	3608	0
2	0	0	1	471	0
4	171	6	3619	5614	0
6	5687	5	463	294	5
8	4134	3987	5636	13	71
10	8	5720	269	0	3634
12	0	272	10	0	652
14	0	10	0	0	5631
16	0	0	0	0	7

Table 20.3. *Symmetric difference* ($\boldsymbol{\Delta}$) *between* $10,000$ *trees sampled from the likelihood function via MCMC and the trees reconstructed by 5 methods.*

package [Felsenstein, 2004], and `TrExML` [Wolf *et al.*, 2000] under their respective default settings with the JC model. We use `treedist` [Felsenstein, 2004] to compare two tree topologies. If the symmetric difference Δ between two topologies is 0, then the two topologies are identical. Larger Δ's are reflective of a larger distance between the two compared topologies. Table 20.3 summarizes the distance between a reconstructed tree and the MCMC samples from the normalized likelihood function. For example, the first two elements in the third row of Table 20.3 mean that 171 out of the $10,000$ MCMC sampled trees are at a symmetric difference of 4 ($\Delta = 4$) from the tree reconstructed via the rigorous NJ method. DNAml was used in two ways. DNAml(A) is a basic search with no global rearrangements. DNAml(B) applies a broader search with global rearrangements and 100 jumbled inputs. The fruits of the broader search are reflected by the piling of MCMC sampled trees over small Δ values from the DNAml(B) tree. Although the rigorous NJ tree is identical to the Saito and Nei NJ tree (with pairwise distance) as well as the fastdnaml-based NJ tree with 3 leaves for this dataset, we have the guarantee from the rigorous NJ method that the global optimum for each triplet was enclosed.

21
Analysis of Point Mutations in Vertebrate Genomes

Jameel Al-Aidroos

Sagi Snir

Using biological sequence from homologs in eight vertebrates of the human ENCODE regions, we present a concrete example of the estimation of mutation rates in the models of evolution introduced in Chapter 4. We detail the process of data selection from within a multiple alignment of the vertebrates, and compare rate estimates for each of the models in the Felsenstein Hierarchy of figure 4.6. In the course of the example we also address a standing problem in vertebrate evolution, namely the resolution of the phylogeny of the Eutherian orders, and discuss some of the challenges of molecular sequence analysis in inferring the phylogeny of this subclass. In particular, we consider the question of the position of the rodents relative to the primates, carnivora and artiodactyla; a question we affectionately dub the rodent problem.

21.1 Estimating mutation rates

Given an alignment of sequence homologs from various taxa, and a choice of evolutionary model from among the models in Figure 4.6, we are naturally led to ask the question,"What tree (with what branch lengths) and what values of the parameters in the rate matrix for that model are suggested by the alignment?" One answer to this question, the so-called maximum-likelihood solution, is, "The tree and rate parameters which maximize the probability that the given alignment would be generated by the given model."

There are a number of available software packages which find, to varying degrees, this maximum-likelihood solution. For example, for a few of the most restrictive models in the Felsenstein hierarchy, the package `PHYLIP` [Felsenstein, 2004] will very efficiently search the tree space for the maximum-likelihood tree, and rate parameters. The commercially available software `PAUP*` [Swofford, 1998] effectively searches the tree space, and implements a wider range of models than `PHYLIP`. Another package, `PAML` [Yang, 1997], though it does not reliably search the tree space, is flexible enough, given a particular tree topology, to find the maximum-likelihood branch lengths and rate parameters for *any* of the models described in Chapter 4.

An evolutionary for a set of taxa consists of a tree-topology T, with an assignment of the taxa to the leaves of T, a branch length, t_e, for each edge $e \in E(T)$, and rate matrix Q. The entries of Q depend on a certain number of rate parameters $\alpha, \beta, \ldots$, and often on the base frequencies $\pi_{\mathtt{A}}, \pi_{\mathtt{C}}, \pi_{\mathtt{G}}, \pi_{\mathtt{T}}$, as described, for example, in Figure 4.6. These entries are a measure of the instantaneous rates of mutation among nucleotides. For a particular edge $e \in E(T)$, the probability of transition from nucleotide i to j along e, is the entry $[P_e]_{ij}$, of the transition matrix $P_e = e^{Qt_e}$. The probability of generating a particular alignment of sequences from a specific tree and fixed parameters is given by the likelihood function

$$\prod_{\substack{\{\mathtt{A,C,G,T}\}\text{-labeling}\\ \text{of leaves of T by}\\ \text{an alignment}\\ \text{column C}}} \left(\sum_{\substack{\text{all labelings}\\ \text{by } \{\mathtt{A,C,G,T}\}\\ \text{of internal}\\ \text{vertices}}} \left(\prod_{\substack{e=(k,l)\\ e \in E(T)}} \begin{array}{c} [P_e]_{ij} \\ \text{for label } i \text{ at } k \\ \text{and label } j \text{ at } l \end{array} \right) \right)$$

Thus, for a given tree topology, the maximum-likelihood solution consists of the values of the branch lengths, the base frequencies and the other rate parameters that maximize the likelihood function.

Figure 21.1 contains sample inputs for `PAML`, and its output of the maximum-likelihood solution for the HKY85 model. Notice that `PAML` returns one rate parameter (in the third last line of output in Figure 21.1), κ, whereas the HKY85 model in Figure 4.6 appears to have two, α and β. The product Qt_e in the likelihood function, forces the branch lengths and rate matrix to be determined only up to scaling. Thus, for example, in the HKY model of Figure 4.6 we could multiply all the branch-lengths by β, divide the rate matrix by β, and take $\kappa = \alpha/\beta$ to overcome the missing parameter. Notice also that whereas the nucleotides are ordered alphabetically in Chapter 4, `PAML` orders them `T-C-A-G` when it reports base frequencies or in columns and rows of rate matrices. The output from Figure 21.1, and the form of the HKY85 model from Figure 4.6 allow us to write the rate matrix

$$Q = \begin{bmatrix} \cdot & \pi_{\mathtt{C}} & \kappa\pi_{\mathtt{G}} & \pi_{\mathtt{T}} \\ \pi_{\mathtt{A}} & \cdot & \pi_{\mathtt{G}} & \kappa\pi_{\mathtt{T}} \\ \kappa\pi_{\mathtt{A}} & \pi_{\mathtt{C}} & \cdot & \pi_{\mathtt{T}} \\ \pi_{\mathtt{A}} & \kappa\pi_{\mathtt{C}} & \pi_{\mathtt{G}} & \cdot \end{bmatrix} = \begin{bmatrix} \cdot & 0.28929 & 1.63618 & 0.22577 \\ 0.20244 & \cdot & 0.28250 & 1.30761 \\ 1.75746 & 0.28929 & \cdot & 0.22577 \\ 0.20244 & 1.67551 & 0.28250 & \cdot \end{bmatrix}$$

`PAML` represents trees in the *newick format*. This is a recursive definition of rooted trees in which vertices (i.e species, extant or extinct) grouped in a

INPUT: the sequence file "seq.txt"

```
8 78306
chimp     GGGGAAGGGGAACCGGGGCCGGGGCCGGAACCGGAAGGGGGGTTTT...
chicken   GGGGGGGGGGGGAAGGGGCCGGGGCCGGAACCGGGGAAGGGGTTTT...
human     GGGGAAGGGGAACCGGGGCCGGGGCCGGAACCGGAAGGGGGGTTTT...
galago    GGGGAAGGGGGGTTGGGGCCGGGGCCGGAACCGGAAGGGGGGTTTT...
cow       GGGGAAGGGGAAAAGGGGCCGGGGCCGGAATTGGAAGGGGGGTTTT...
dog       GGGGAAGGGGAACCGGGGCCGGGGCCGGAACCGGAAGGGGGGTTTT...
rat       GGGGGGGGGGAAAAGGGGTTGGGGAAGGAACCGGAAGGGGGGTTTT...
mouse     GGGGGGGGGGAAAAGGGGAAAAGGGGGGAACCGGAAGGGGGGTTTT...
```

INPUT: the tree structure file "tree.txt"

```
((((human,chimp),galago),(mouse,rat)),(cow,dog),chicken);
```

INPUT: the PAML control file "baseml.ctl"

```
     model  = 4          * 0:JC69, 1:K80, 2:F81, ...
     nhomo  = 1          * 0 or 1:  homogeneous, 2:...
  treefile  = tree.txt   * tree structure file name
   seqfile  = seq.txt    * sequence data file name
 cleandata  = 0          * remove ambiguous data (1:y,0:n)
   outfile  = out.txt    * main result file
     noisy  = 3          * 0,1,2,3:  how much junk on screen
   verbose  = 1          * 1:  detailed output, 0:  concise output
     getSE  = 0          * 0:  omit; 1:  get S.E.s of estimates
   runmode  = 0          * 0:  user tree; 1 or 2:  find tree...
Small_Diff  = 1e-6       * step value for derivative estimates
    method  = 0          * 0:  simult.; 1:  one branch at a time
     clock  = 0          * 0:no clock, 1:clock; 2:local clock...
 fix_kappa  = 0          * 0:  estimate kappa; 1:  fix kappa
     kappa  = 2.5        * initial or fixed kappa
```

OUTPUT: excerpt from the PAML output file "out.txt"

```
lnL(ntime:  14 np:  18):-396419.669383 +0.000000
⋮
(((((human:  0.004484, chimp:  0.005159):  0.068015, galago:
0.102113):  0.014305, (mouse:  0.068227, rat:  0.062353):  0.182379):
0.011786, (cow:  0.114727, dog:  0.095417):  0.018334):  0.014105,
chicken:0.555154);

Detailed output identifying parameters kappa under HKY85:  5.79179
base frequency parameters
0.22577 0.28929 0.20244 0.28250
```

Fig. 21.1. PAML input and output for rate estimation in the HKY85 model.

parentheses, share a common ancestor. If two vertices are grouped in the same set of parentheses, they are sister vertices. For example the tree $((1,2),3)$ is a rooted triplet over the species $\{1,2,3\}$ with 1 and 2 are sister taxa and their most recent common ancestor (represented by the vertex $(1,2)$) is a sister of 3. This format is extended to weighted trees by attaching a number to the right of a vertex. This number is the length of the edge entering that vertex.
Note that in the example in Figure21.1, that the input tree is unweighted,

Model	`model =`	`nhomo =`
JC69	`0`	`0`
K80	`1`	`0`
F81	`2`	`1`
F84	`3`	`1`
HKY85	`4`	`1`
T92	`5`	`1`
TN93	`6`	`1`
REV	`7`	`1`
CS05	`9 [1 (AC AT CG GT)]`	`1`
SYM	`10 [5 (AC CA) (AG GA) (AT TA) (CG GC) (CT TC)]`	`0`
K3ST	`10 [2 (AC CA GT TG) (AG GA CT TC)]`	`0`

Fig. 21.2. Implementing the models of the Felsenstein Hierarchy in `PAML`.

while the tree returned by `PAML` contains the edge lengths. The probability of obtaining the input alignment with the calculated parameters and lengths is given in the output from `PAML` as a log-likelihood in the first line of the excerpt.

The next two sections of this paper discuss the ENCODE project, from which the sequence for this study is taken, information about a refinement of the alignment which isolates only synonymous substitution sites, and the results of the implementation of each of the models of the Felsenstein hierarchy in `PAML`. Figure 21.2 describes how to implement each of the models of the Felsenstein hierarchy in `PAML` by making small adjustments in the baseml.ctl file to the options `model` and `nhomo` (which controls whether the base frequencies are uniform or parameters). These examples demonstrate only some of the versatility of that software in dealing with more sophisticated models. Section 21.4 introduces the main problem addressed, namely the position of the rodents in the phylogeny of the mammals considered in this chapter.

21.2 The ENCODE data

Our analysis of mutation rates is based on alignments of the human genome from regions identified by the ENCODE Pilot Project which was described briefly in section 4.3. The Berkeley ENCODE Group, using Mercator [Dewey, 2005] and Stanford's Shuffle-Lagan[Brudno *et al.*, 2003], has mapped these regions to homologous regions from other vertebrates, and multiply-aligned the homologs with MAVID[Bray and Pachter, 2004]. We have used in this study the alignments of the Stanford re-ordering of the October 2004 freezes of the homologous regions, which are available at `bio.math.berkeley.edu/encode/`.

ENCODE's pilot project [Consortium, 2004] identifies 44 regions in the human genome for extensive study. The first 14 of these are manually selected regions, ENm001 to ENm014, chosen to include well-understood functional re-

Manual ENCODE Regions

Bin	Importance or Expected function
[ENm001]	CFTR - Cystic Fibrosis
ENm002	Interleukin Cluster - immune system regulation
ENm003	Apo Cluster - liver and intestinal function
ENm004	region from Chromosome 22
ENm005	region from Chromosome 21
ENm006	region from Chromosome X
[ENm007]	region from Chromosome 19
ENm008	α-globin - implicated in α-thalassemia (anemia)
ENm009	β-globin - implicated in Sickle Cell Anemia
ENm010	HOXA Cluster embryonic development: body axis and limb patterning
[ENm011]	IGF2/H19 - insulin growth factor: growth and early development
ENm012	FOXP2 - language and speech development
ENm013	region from Chromosome 7 - selected to balance stratification
ENm014	region from Chromosome 7 - selected to balance stratification

Random ENCODE Regions

density of conserved non-exonic bases		density of genic bases	
	low (0-50%-ile)	medium (60-80%-ile)	high (80-100%-ile)
low	ENr111, [ENr112]	ENr121, ENr122	ENr131, ENr132
(0-50%-ile)	ENr113, ENr114	ENr123	ENr133
medium	ENr211, ENr212	ENr221, ENr222	ENr231, ENr232
(50-80%-ile)	[ENr213]	ENr223	ENr233
high	ENr311, [ENr312]	ENr321, ENr322	ENr331, ENr332
(80-100%-ile)	ENr313	ENr323, ENr324	ENr333,[ENr334]

Fig. 21.3. Summary of the manual and random ENCODE regions. [..] denotes a region that was not considered in this study because a homolog was missing for at least one of the seven other vertebrates at the time the data was generated.

gions of the genome. For example, ENm001 contains the gene CFTR, associated with cystic fibrosis, which has been studied extensively since its discovery in 1989. The remaining 30 regions, the so-called "random" regions, were chosen pseudo-randomly to represent varying degrees of non-exonic conservation with respect to orthologous sequence from the mouse genome, and varying degrees of gene density. Figure 21.3 describes the manual and random ENCODE regions.

A primary goal of the Berkeley ENCODE Group is to generate mappings from the human genome in the ENCODE regions to homologous regions in assemblies of sequence from other vertebrates, and to align the homologs. Such alignments have been generated for each ENCODE region, although the set of taxa in which homologs have been identified varies from region to region. In this study, we restricted our attention to the eight vertebrates human (*Homo sapiens*), galago monkey (*Otolemur garnettii*), chimp (*Pan troglodytes*), rat (*Rattus norvegicus*), mouse (*Mus musculus*), dog (*Canis familiaris*), cow (*Bos taurus*) and chicken (*Gallus gallus*), and considered only the 37 ENCODE regions which, at the time we generated data, had alignments of homologs for all eight taxa. In Figure 21.3, the regions that appear in square braces are those for which the homolog was missing for at least one of our eight vertebrates, and which were not considered.

21.3 Synonymous substitutions

Starting with the MAVID alignment of the homologs of the human ENCODE regions, we refined the alignment by isolating only those columns corresponding to synonymous substitution sites in exons. In this section we define synonymous substitution, and describe the process for identifying these columns of the alignment.

Recall from Table 4.1 in Chapter 4 that every amino acid is coded by a sequence of three nucleotides, called a codon. As there are four (types of) nucleotides, this scheme allows for $4^3 = 64$ different codons. However, since there are only twenty amino acids, the above implies that some amino acids are encoded by a few different codons, giving some redundancy to the amino acid coding scheme. Nucleotide mutations in the gene (which necessarily change the codons in the gene) are divided into three types, depending on what amino acid is encoded by the new codon:

(i) synonymous mutations: mutations that, although they alter a particular codon, they do not alter the encoded amino acid.
(ii) missense mutations: mutations that alter the codon so as to produce an different amino acid.
(iii) nonsense mutations: mutations that change a codon that encodes an amino acid into one of the STOP codons (`TAA`, `TAG`, or `TGA`).

Because synonymous mutations do not alter the amino acid, they do not alter the protein. Such mutations produce no functional changes, and are thus considered to be free from selective pressure. By removing the selective pressure, we restrict our attention to those sites whose mutation is more likely to behave according to a random Markov process. Furthermore, by isolating these synonymous substitution sites, we impose a level of homogeneity on the data. For example, although `PAML` implements models that allow for the rate matrix to vary among sites, we believe that by selecting the neutral mutation sites, we substantially reduce the need for this introduction of extra parameters into the models.

The procedure for refinement of the data consisted of mapping annotations of human genes to the alignment, and identifying triples of columns containing synonymous codons. For each of the 37 ENCODE regions, we identified the manually verified (refSeq) annotations of genes in that region by consulting the refGene table in the UCSC annotation database

```
   a.a.  GlnMetGlnGlnLeuGlnGlnGlnGlnHisLeuLeu...LeuGln...GlnGlyLeuIle
-----------------------------------------------------------------------
  human  CAGATGCAACAACTCCAGCAGCAGCAGCATCTGCTCAGCCTTCAGCGTCAGGGACTCATC
 galago  CAGATGCAACAACTCCAGCAGCAGCAGCATCTGCTCAGCCTTCAGCGTCAGGGACTCATC
  mouse  CAAATGCAGCAGCTACAGCAGCAACAACATCTGCTCAGCCTTCAGCGCCAGGGCCTCATC
    rat  CAGATGCAGCAACTACAGCAGCAGCAGCATCTGCTCAGCCTTCAGTGTCAGGGCCTCATC
    cow  CAGATGCAACAACTCCAGCAGCAGCAGCATCTGCTCAGCCTTCAGCGTCAGGGACTCATC
chicken  CAGATGCAACAACTTCAGCAGCAGCAACATCTGCTGAACCTTCAGCGTCAGGGACTCATT
  chimp  CAGATGCAACAACTCCAGCAGCAGCAGCATCTGCTCAGCCTTCAGCGTCAGGGACTCATC
    dog  CAGATGCAACAACTCCAGCAGCAGCAGCATCTGCTCAGCCTTCAGCGTCAGGGACTCATC
-----------------------------------------------------------------------
         ..*.....*..*..*..*..*..*..*..*..*..*.....*..*.....*..*..*..*
         123123123123123123123123123123123123123123123123123123123123
```

Fig. 21.4. Excerpt of alignment from FOXP2 (RefSeq annot. NM_148900) in ENm012. The top row indicates the amino acid translation of the codon (where all there is agreement among all the taxa). The stars denote columns corresponding to the third positions in codons all coding for the same amino acid. The bottom row indicates the frame dictated by the human gene annotation, where 1 denotes the first position in a codon.

(`hgdownload.cse.ucsc.edu/downloads.html`). For each gene in the region, we mapped the annotation of its coding region to the MAVID alignment, and extracted the relevant columns. Below each codon triple in the human sequence, we identified the amino acids encoded by the triple in each of the homologs. We automatically discarded all triples which contained gaps in any of the homologs, and extracted the third column from each triple in which each homolog's codon encoded the amino acid in the human sequence. We note here that because of gaps in the alignment and because we use only the frame of the human annotation to identify coding triples, it is possible that some sites chosen correspond to a second or third position in a codon of one of the other vertebrates. The high degree of conservation in the aligned exons, and the stringent requirement of agreement in the preceding two columns, however, meant that extracted columns were very unlikely to suffer from this fault; a visual inspection of the alignments revealed that extracted columns very reliably consisted of third positions. An excerpt of the alignment from the speech and language development gene, FOXP2, is given in Figure 21.4.

With the refined sequence data in hand we used `PAML` to find the maximum-likelihood solutions for the rate parameters, base frequencies and branch lengths. However, as was indicated in the introductory chapter, `PAML` does not reliably search the tree space, so we restricted ourselves to only the two trees in Figure 21.7, namely the *tree tree* (that is, the actual tree representing the evolutionary history of those species), and the maximum likelihood tree (The tree attaining the biggest likelihood under all models studied). The rate

Fig. 21.5. The Felsenstein Hierarchy for the ML Tree.

Fig. 21.6. The Felsenstein Hierarchy for the True Tree.

matrices and log-likelihoods for each model are displayed in Figures 21.5 and 21.6.

21.4 The rodent problem

Rodents have the special characteristic that although their molecular information closely resembles that of the primates, they exhibit very different morphological features. This discrepancy has attracted a lot of attention and has formed the basis of much research.

In this section we point out the phenomenon that current tree reconstruction methods misplace the two rodents mouse and rat on the tree, with respect to other mammals. The real phylogenetic tree describing the evolution of the taxa in this study is agreed among most of the evolutionary biologists nowadays. It is supported by either fossil records or molecular data ([Madsen *et al.*, 2001, Murphy *et al.*, 2001, Phillips and Penny, 2003, Lin *et al.*, 2002, Schmitz and Zischler, 2003] to mention a few). In that tree (see Figure 21.7 up), we have the primate clade, composed of the siblings human and chimpanzee and then the galago as an outgroup to these two. The rodents clade mouse and rat, is a sister group to the primates and an artiodactyls-carnivores clade is an outgroup to the former species. By using the chicken as an outgroup to all these, we get a rooting of the tree. However, the currently available phylogenetic reconstruction methods, regardless of the evolutionary model, misplace the rodents and put them as an outgroup to the primates and artiodactyls-carnivores (see Figure 21.7 down). A partial explanation to this phenomenon is given by the fact that rodents have shorter generation time. This causes the rate of synonymous substitutions in the rodents to be 2.0 times faster than in human and the rate of non-synonymous substitutions to be 1.3 times faster [Wu and Li, 1985].

This question of rodents divergence time (and the relative location of this event on the phylogeny) has a long history and is still gaining a lot of popularity with the increasing availability of complete mammalian genomes (e.g. [International Human Genome Sequencing Consortium, 2001, Waterston *et al.*, 2002, Hillier *et al.*, 2004, Gibbs *et al.*, 2004]). Recent works ([Adkins *et al.*, 2001, Thomas *et al.*, 2003]) have also addressed the question that few methods fail to estimate correctly this event. [Adkins *et al.*, 2001] addressed the question of monophyly of the rodents order and noticed that

Model	**True Tree**	**ML Tree**
0 JC69	$\begin{bmatrix} * & 1 & 1 & 1 \\ 1 & * & 1 & 1 \\ 1 & 1 & * & 1 \\ 1 & 1 & 1 & * \end{bmatrix}$ lnL =-420359.749970	$\begin{bmatrix} * & 1 & 1 & 1 \\ 1 & * & 1 & 1 \\ 1 & 1 & * & 1 \\ 1 & 1 & 1 & * \end{bmatrix}$ lnL =-419661.571184
1 K80	$\kappa = 5.59362$ $\begin{bmatrix} * & 5.59362 & 1 & 1 \\ 5.59362 & * & 1 & 1 \\ 1 & 1 & * & 5.59362 \\ 1 & 1 & 5.59362 & * \end{bmatrix}$ lnL=-398246.156240	$\kappa = 5.60258$ $\begin{bmatrix} * & 5.60258 & 1 & 1 \\ 5.60258 & * & 1 & 1 \\ 1 & 1 & * & 5.60258 \\ 1 & 1 & 5.60258 & * \end{bmatrix}$ lnL=-397790.545395
2 F81	$\pi_T = 0.23195$ $\pi_C = 0.28483$ $\pi_A = 0.21225$ $\pi_G = 0.27097$ $\begin{bmatrix} * & 0.28483 & 0.21225 & 0.27097 \\ 0.23195 & * & 0.21225 & 0.27097 \\ 0.23195 & 0.28483 & * & 0.27097 \\ 0.23195 & 0.28483 & 0.21225 & * \end{bmatrix}$ lnL = -419290.724659	$\pi_T = 0.23193$ $\pi_C = 0.28485$ $\pi_A = 0.21268$ $\pi_G = 0.27054$ $\begin{bmatrix} * & 0.28485 & 0.21268 & 0.27054 \\ 0.23193 & * & 0.21268 & 0.27054 \\ 0.23193 & 0.28485 & * & 0.27054 \\ 0.23193 & 0.28485 & 0.21268 & * \end{bmatrix}$ lnL = -418618.222983
3 F84	$\kappa = 2.39698$ $\pi_T = 0.22193$ $\pi_C = 0.28389$ $\pi_A = 0.20583$ $\pi_G = 0.28834$ $\begin{bmatrix} * & 1.62919 & 0.20583 & 0.28834 \\ 1.27361 & * & 0.20583 & 0.28834 \\ 0.22193 & 0.28389 & * & 1.68694 \\ 0.22193 & 0.28389 & 1.20421 & * \end{bmatrix}$ lnL =-396478.578685	$\kappa = 2.40280$ $\pi_T = 0.22185$ $\pi_C = 0.28406$ $\pi_A = 0.20598$ $\pi_G = 0.28811$ $\begin{bmatrix} * & 1.63320 & 0.20598 & 0.28811 \\ 1.27552 & * & 0.20598 & 0.28811 \\ 0.22185 & 0.28406 & * & 1.68922 \\ 0.22185 & 0.28406 & 1.20769 & * \end{bmatrix}$ lnL =-396045.066120
4 HKY85	$\kappa = 5.79179$ $\pi_T = 0.22577$ $\pi_C = 0.28929$ $\pi_A = 0.20244$ $\pi_G = 0.28250$ $\begin{bmatrix} * & 1.67551 & 0.20244 & 0.28250 \\ 1.30761 & * & 0.20244 & 0.28250 \\ 0.22577 & 0.28929 & * & 1.63618 \\ 0.22577 & 0.28929 & 1.17249 & * \end{bmatrix}$ lnL = -396419.669383	$\kappa = 5.80371$ $\pi_T = 0.22563$ $\pi_C = 0.28937$ $\pi_A = 0.20264$ $\pi_G = 0.28235$ $\begin{bmatrix} * & 1.67942 & 0.20264 & 0.28235 \\ 1.30949 & * & 0.20264 & 0.28235 \\ 0.22563 & 0.28937 & * & 1.63868 \\ 0.22563 & 0.28937 & 1.17606 & * \end{bmatrix}$ lnL = -395987.273186

some of the genes investigated, returned a false tree. [Thomas *et al.*, 2003] investigated conserved regions among vertebrates and noticed by analysis of transposable elements that the true tree is supported. However, none of these works raised the question of why all existing evolutionary models fail to reconstruct the true tree, and specifically, misplace the order of rodents.

5 T92	$\kappa =$ $\pi_T =$ $\pi_C =$ $\pi_A =$ $\pi_G =$ $\begin{bmatrix} * & \pi_C & \pi_A & \pi_G \\ \pi_T & * & \pi_A & \pi_G \\ \pi_T & \pi_C & * & \pi_G \\ \pi_T & \pi_C & \pi_A & * \end{bmatrix}$ lnL =	$\pi_T =$ $\pi_C =$ $\pi_A =$ $\pi_G =$ $\begin{bmatrix} * & \pi_C & \pi_A & \pi_G \\ \pi_T & * & \pi_A & \pi_G \\ \pi_T & \pi_C & * & \pi_G \\ \pi_T & \pi_C & \pi_A & * \end{bmatrix}$ lnL =
6 TN93	$\kappa_1 = 6.29360$ $\kappa_2 = 5.28772$ $\pi_T = 0.21984$ $\pi_C = 0.28271$ $\pi_A = 0.20870$ $\pi_G = 0.28874$ $\begin{bmatrix} * & 1.77926 & 0.20870 & 0.28874 \\ 1.38359 & * & 0.20870 & 0.28874 \\ 0.21984 & 0.28271 & * & 1.52678 \\ 0.21984 & 0.28271 & 1.10355 & * \end{bmatrix}$ lnL =-396308.224349	$\kappa_1 = 6.29927$ $\kappa_2 = 5.30517$ $\pi_T = 0.21979$ $\pi_C = 0.28288$ $\pi_A = 0.20884$ $\pi_G = 0.28849$ $\begin{bmatrix} * & 1.78194 & 0.20884 & 0.28849 \\ 1.38452 & * & 0.20884 & 0.28849 \\ 0.21979 & 0.28288 & * & 1.53049 \\ 0.21979 & 0.28288 & 1.10793 & * \end{bmatrix}$ lnL =-395879.760438
7 REV	$\begin{bmatrix} * & 0.928553 & 0.153082 & 0.114229 \\ 0.719295 & * & 0.138117 & 0.117185 \\ 0.167314 & 0.194874 & * & 0.822751 \\ 0.084580 & 0.112011 & 0.557377 & * \end{bmatrix}$ lnL =-395649.076601	$\begin{bmatrix} * & 0.928911 & 0.155345 & 0.11 \\ 0.718400 & * & 0.137595 & 0.11 \\ 0.169773 & 0.194438 & * & 0.82 \\ 0.083624 & 0.111230 & 0.558110 & * \end{bmatrix}$ lnL = -395194.825177
9 CS05	$\begin{bmatrix} -1.126077 & 0.873315 & 0.105515 & 0.147247 \\ 0.681559 & -0.934321 & 0.105515 & 0.147247 \\ 0.117676 & 0.150784 & -1.121289 & 0.852828 \\ 0.117676 & 0.150784 & 0.611124 & -0.879585 \end{bmatrix}$ lnL =-396419.669383	$\begin{bmatrix} -1.126393 & 0.873994 & 0.105458 \\ 0.681474 & -0.933873 & 0.105458 \\ 0.117421 & 0.150592 & -1.120814 \\ 0.117421 & 0.150592 & 0.612049 \end{bmatrix}$ lnL = -395987.273185
10 SYM	$\begin{bmatrix} -1.066465 & 0.809931 & 0.159339 & 0.097194 \\ 0.809931 & -1.087021 & 0.158949 & 0.118141 \\ 0.159339 & 0.158949 & -0.974734 & 0.656446 \\ 0.097194 & 0.118141 & 0.656446 & -0.871780 \end{bmatrix}$ lnL =-397702.025844	$\begin{bmatrix} -1.067056 & 0.809476 & 0.161438 \\ 0.809476 & -1.085413 & 0.158448 \\ 0.161438 & 0.158448 & -0.976893 \\ 0.096143 & 0.117489 & 0.657007 \end{bmatrix}$ lnL = -397237.324766
11 K3ST	$\begin{bmatrix} -1.000000 & 0.736581 & 0.135559 & 0.127860 \\ 0.736581 & -1.000000 & 0.127860 & 0.135559 \\ 0.135559 & 0.127860 & -1.000000 & 0.736581 \\ 0.127860 & 0.135559 & 0.736581 & -1.000000 \end{bmatrix}$ lnL =-395649.076601	$\begin{bmatrix} -1.000000 & 0.736880 & 0.135950 \\ 0.736880 & -1.000000 & 0.127170 \\ 0.135950 & 0.127170 & -1.000000 \\ 0.127170 & 0.135950 & 0.736880 \end{bmatrix}$ lnL = -398241.937632

A common feature of many of the most popular models used to reconstruct the evolutionary tree is the assumption of a constant rate matrix along all branches. This leaves the time as the only free parameter between the different branches of the tree. As a consequence, it causes distortion in the

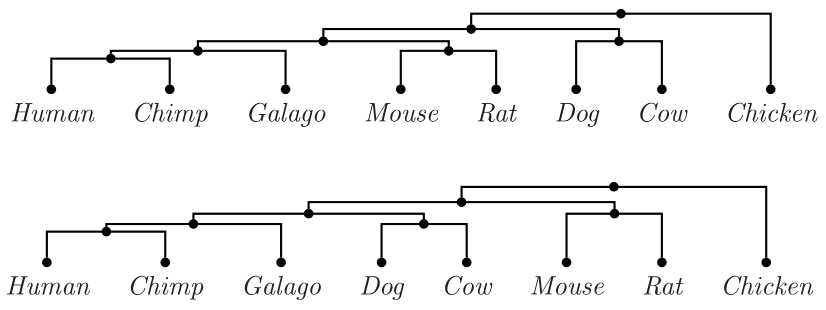

Fig. 21.7. The trees evaluated in the study: above - the actual tree representing the evolution of our eight vertebrates; below - the tree obtaining the highest likelihood in all models

tree topology that is reflected by placement of the rodents speciation event, higher in the tree closer to the root (see Figure 21.7 down). This behavior is shared among all models. However, it is not totally clear to us why the accelerated rate of evolution should change the topology of the tree, instead of stretching the rodents branch but leaving it in its place. An explanation that is sprung immediately is the phenomenon of *long branch attraction* (LBA) [Felsenstein, 1978, Hendy and Penny, 1989]. (LBA) is the phenomenon where two fast evolving taxa are grouped together although they belong to different clades. This is caused mainly when a distant species is used as an outgroup for tree rooting, or when the number of taxa is relatively small. We assert that the rodent problem can not be explained simply by the argument of LBA for three main reasons: (a) The outgroup used in our study, the chicken, is not that a far species, (b) The number of sites in the input data (over 78,000) is relatively big considering the number of species, and (c) Although [Thomas *et al.*, 2003] reported they obtained the true tree, when using ML phylogenetic reconstruction even on a larger set of species, they observed the same behavior([Siepel, 2005]). [Huelsenbeck *et al.*, 2000] examined even larger set of species, and yet arrived at a tree supporting the ML tree.

In general in nature, a rate might change (increase or decrease) during the course of evolution. The models studied in this book allow rate heterogeneity among sites. That is, different sites might exhibit different rates. However, per site, the rate along all lineages is constant. More advanced models allow in-site rate heterogeneity which accounts for rate changes throughout evolution. Some of these [Galtier and Gouy, 1998, Yang and Roberts, 1995] build on previous models such as HKY85 or TN93 by using the same rate matrices (and therefore also the assumption of evolutionary model), but enhance them by allowing the parameters at the matrix to change at every vertex. Other

Model	True Tree	ML Tree	difference
F84	397851	397388	463
HKY85	396144	395704	440
TN92	396108	395668	440

Fig. 21.8. Log-likelihoods for models allowing kappa to vary from branch to branch.

models (e.g. [Huelsenbeck *et al.*, 2000]) allow the rate to behave as a Poisson process, enabling non homogeneity even along a single tree branch. All these models strive to imitate more closely the natural mutation process. However, the more descriptive a model is, it introduces many more parameters into the estimation procedure, turning it to computationally hard task, even on a given tree.

In addition to the models outlined above, `PAML` implements some more advanced model to be detailed later. These models enable some further flexibility with different rates over the branches. In order to check if these advanced features resolve the discrepancy between the true tree and ML tree, We tested them on our data.
In the first benchmark we relaxed the homogeneity constraint prevailed in the former set of tests. We note here that even the model described by [Huelsenbeck *et al.*, 2000] which allow greater flexibility inferred an incorrect tree with respect to the rodents divergence event. For certain models, `PAML` enables to vary κ along the tree branches. Naturally, this option applies only to some of the models involving κ which are F84 HKY85 and T92. This allows for the rate matrix to variate between the branches in order to obtain optimal solution. This corresponds to the models described by Yang and Roberts [Yang and Roberts, 1995], who used F84 or HKY85, and Galtier and Gouy [Galtier and Gouy, 1998] who used T92 for their model. Since we were interested to see if the gap between the two trees is decreased, we only measured the likelihood obtained for the two trees. The results are displayed in Figure 21.8.

In the next trial we tried to partition the clades of the trees into different rate groups. This approach was motivated by [Mindell and Honeycutt, 1990] who showed that opossums artiodactyles and primates possess a very similar mutation rate while rodents are evolving at a significantly higher rate. This calls for a model that discriminates between the different branches of the tree according to their clade. The *local clock* option of `PAML` described in [Yoder and Yang, 2000] allows for such a partition. In this model, the same rate matrix is assumed along all lineages in the tree. However, when the transition matrix for branch e is computed, the rate matrix is multiplied by the branch length t_e and another scalar, the rate r_e along that branch.

Model	**True Tree**	**ML Tree**	**difference**
HKY85	396604	396339	265
T92	396711	396443	268
TN93	396493	396232	261
REV	395834	395559	275
UNREST	395646	395365	281

Fig. 21.9. Log-likelihoods for models using local clock option.

This provides the model with the property that the tree inferred satisfies the molecular clock property, while allowing rate heterogeneity. Indeed in [Douzery E. J. P. and D., 2003] this model was used with very similar grouping (as the set of taxa was different) for the study of the discrepancy between fossil calibration and estimation based on molecular data. However, in their study, only the true tree was considered as the different goals were posed. , we the leaves into 3 groups:

(i) The chicken clade (which comprise the branch from the root to the chicken)
(ii) The rodents clade (comprises all edge joining the ancestral rodent)
(iii) All the rest

the results obtained under this model are depicted in Figure 21.9. It can be seen that under this model the difference in the log likelihood is diminished, nevertheless, still the ML tree prevails.

22
Ultra-Conserved Elements in Vertebrate and Fly Genomes

Mathias Drton

Nicholas Eriksson

Garmay Leung

Ultra-conserved elements in multiple aligned genomes consist of consecutive nucleotides that are in perfect agreement across all the genomes. For aligned vertebrate and aligned fly genomes, we give descriptive statistics of ultra-conserved elements, explain their biological relevance, and calculate the probability of occurrence of ultra-conserved elements using statistical models.

22.1 The Data

Our analyses of ultra-conserved elements are based on multiple sequence alignments produced by MAVID [Bray and Pachter, 2004]. Prior to the alignment of multiple genomes, homology mappings (from Mercator [Dewey, 2005]) bin together genomic regions that are anchored together by homologous exons. A multiple sequence alignment is then produced for each of these alignment bins. MAVID is a global multiple alignment program, and therefore homologous regions with more than one homologous hit to another genome may not be found aligned together.

The vertebrate dataset consists of 10,279 bins over 9 genomes: zebra fish (*Danio rerio*), fugu fish (*Takifugu rubripes*), puffer fish (*Tetraodon nigroviridis*), dog (*Canis familiaris*), human (*Homo sapiens*), chimp (*Pan troglogytes*), mouse (*Mus musculus*), rat (*Rattus norvegicus*) and chicken (*Gallus gallus*). The genome sizes range from 260 Mbp (million base pairs) to 4.2 Gbp (billion base pairs). A total of 4,368 bins (42.5%) contain alignments across all 9 species. The evolutionary relationships between these species (which first diverged about 450 million years ago) are shown in Figure 22.1.

The fruit fly dataset consists of 8 *Drosophila* genomes: *D. melanogaster*, *D. simulans*, *D. yakuba*, *D. erecta*, *D. ananassae*, *D. pseudoobscura*, *D. virilis* and *D. mojavensis*. Each of these genomes consists of 114 to 177 Mbp, and 2,985 of the 3,731 alignment bins (80.0%) contain all 8 species, indicative of a smaller

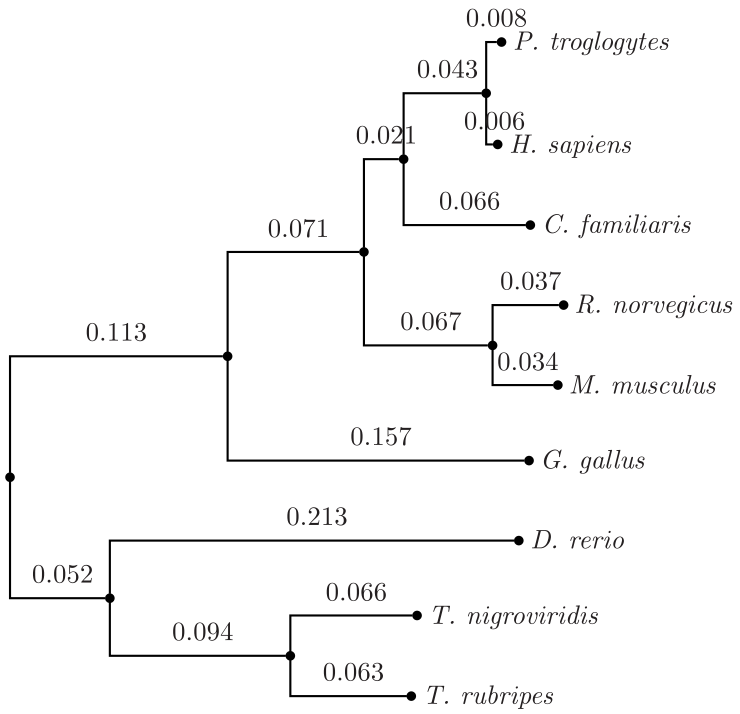

Fig. 22.1. Phylogenetic tree for whole genome alignment of 9 vertebrates.

degree of evolutionary divergence. A phylogenetic tree for these 8 species is illustrated in Figure 22.2.

The pilot phase of the ENCODE project (cf. Section 4.3 and Chapter 21) provides an additional dataset of vertebrate sequences aligned to 44 regions of the human genome. There are 14 manually selected regions of biological interest and 30 randomly selected regions with varying degrees of non-exonic conservation and gene-density. Each manually selected region consists of 0.5-1.9 Mbp, while each randomly selected region is 0.5 Mbp in length, for a total of about 30 Mbp. Varying with the region under consideration, a subset of the following 11 species is aligned to the human genome in the October 2004 freeze: chimp, baboon, marmoset, galago, mouse, rat, dog, armadillo, platypus and chicken. This collection of species lacks the three fish of the nine-vertebrate alignment. Armadillo and platypus sequences are only available for the first manually picked ENCODE region, and sequences for every region are only available for human, mouse, rat, dog and chicken. The number of species available for each region varies between 6 and 11 for manually selected regions, and between 8 and 10 for randomly selected regions. For each region, Shuffle-LAGAN [Brudno *et al.*, 2003] is applied between the human sequence and each of the other available sequences to account for rearrangements. MAVID then

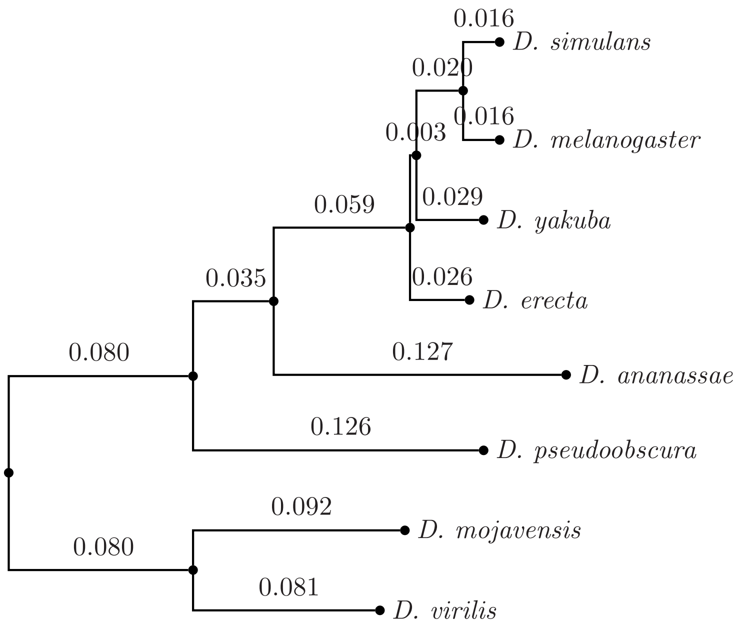

Fig. 22.2. Phylogenetic tree for whole genome alignment of 8 Drosophila species.

produces a multiple sequence alignment for each region based on these reshuffled sequences.

22.2 Ultra-Conserved Elements

A position in a multiple alignment is *ultra-conserved* if for all species the same nucleotide appears in this position. An *ultra-conserved element* of length ℓ is a sequence of consecutive ultra-conserved positions $(n, n+1, \ldots, n+\ell-1)$ such that positions $n-1$ and $n+\ell$ are not ultra-conserved.

Example 22.1 Consider $S = 3$ toy genomes in a multiple alignment of length $N = 24$:

```
G--ACCCAATAGCACCTGTTGCGG
CGCTCTCCA---CACCTGTTCCGG
CATTCT---------CTGTTTTGG
    *          *****  **
```

where ultra-conserved positions are marked by a star `*`. This alignment contains three ultra-conserved elements, one of length 1 in position 5, one of length 5 covering positions 16–20, and one of length 2 in positions 23–24.

22.2.1 Nine-vertebrate alignment

We scanned the entire nine-vertebrate alignment described in Section 22.1 and extracted 1,513,176 ultra-conserved elements, illustrated in Figure 22.3. The median and the mean length of an ultra-conserved element are equal to 2 and 1.918, respectively.

We will focus on the 237 ultra-conserved elements of length at least 20, covering 6,569 bp in sum. These 237 elements are clustered together; they are only found in 113 of the 4,368 bins containing all 9 species. The length distribution is heavily skewed toward shorter sequences as seen in Figure 22.3, with 75.5% of these regions shorter than 30 bp and only 10 regions longer than 50 bp.

The longest ultra-conserved element in the alignment is 125 base pairs long:

```
CTCAGCTTGT CTGATCATTT ATCCATAATT AGAAAATTAA TATTTTAGAT GGCGCTATGA
TGAACCCATT ATGGTGATGG GCCCCGATAT CAATTATAAC TTCAATTTCA ATTTCACTTA
CAGCC.
```

The next-longest ultra-conserved elements are two elements of length 85, followed by one element for each one of the lengths 81, 66, 62, 60, 59, 58, and 56. In particular, there is exactly one ultra-conserved element of length 42, which is the *"meaning of life"* element discussed in [Pachter and Sturmfels, 2004a].

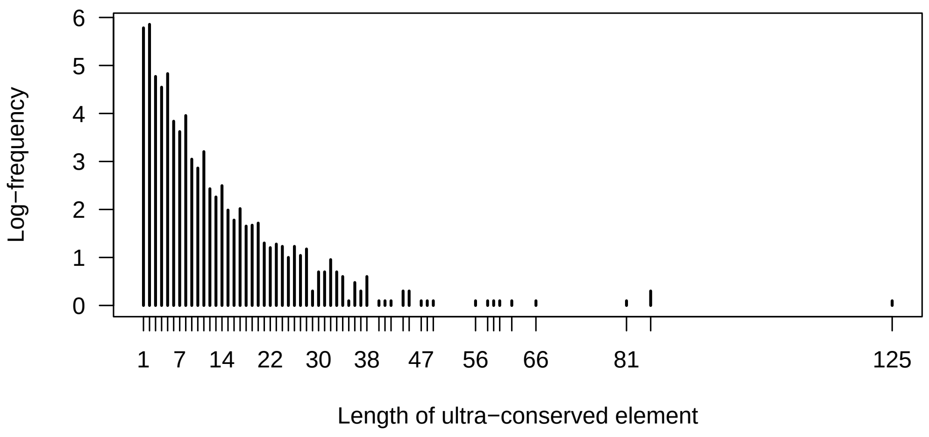

Fig. 22.3. Frequencies of vertebrate ultra-conserved elements ($\log_{10}$-scale).

There are 28 short, ungapped intervening sequences (at most 10 bp) between consecutive ultra-conserved elements, 18 of which are only a single nucleotide. These sequences typically represent changes between the fish species and the other vertebrates. Stringing together elements separated by less than 10 bases would reduce the number of ultra-conserved elements to 209, increase the base coverage to 6,636 bp, and bring the total number of regions greater than 50 bp in length to 26.

In the human genome, the `GC`-ratio (proportion of `G` and `C` among all nucleotides) is 41.0%. The ultra-conserved elements are slightly more `AT`-rich; for the 237 elements of length 20 or longer, the `GC`-ratio is 35.8%. Similar `AT`-richness is, however, also present in some parts of the alignment that do not contain ultra-conserved elements, which constitutes one of the reasons why our attempts at predicting ultra-conserved elements from single species data using a hidden Markov model were unsuccessful.

22.2.2 ENCODE alignment

The 44 ENCODE regions contain 139,043 ultra-conserved elements, 524 of which are longer than 20 base pairs. These long elements cover 17,823 bp. By base coverage, 73.5% of the long elements are found in the manually chosen regions. The longest one is in region `ENm012`, of length 169 and consists of the DNA sequence:

```
AAGTGCTTTG TGAGTTTGTC ACCAATGATA ATTTAGATAG AGGCTCATTA CTGAACATCA
CAACACTTTA AAAACCTTTC GCCTTCATAC AGGAGAATAA AGGACTATTT TAATGGCAAG
GTTCTTTTGT GTTCCACTGA AAAATTCAAT CAAGACAAAA CCTCATTGA.
```

It does not contain a subsequence of length 20 or longer that is ultra-conserved in the nine-vertebrate alignment, however, the 169 base pairs are also ultra-conserved in the nine-vertebrate alignment if one excludes the three fish from consideration. The only overlap between the nine-vertebrate and ENCODE ultra-conserved elements occurs in the regions `ENm012` and `ENm005`, where there are 3 elements that are extensions of ultra-conserved elements in the nine-vertebrate alignment.

Table 22.1 shows the number of species aligned in the 44 ENCODE alignments and the respective five longest ultra-conserved elements that are of length 20 or larger. Omitted randomly selected regions do not contain any ultra-conserved elements of length at least 20.

22.2.3 Eight-Drosophila alignment

There are 5,591,547 ultra-conserved elements in the *Drosophila* dataset, with 1,705 elements at least 50 bp long and the longest of length 209 bp. We focus on the 255 *Drosophila* ultra-conserved elements of length of at least 75 bp, covering 23,567 bp total. These regions are also found clustered together, occurring over 163 bins out of the 2,985 bins with all 8 species aligned together.

Manually selected			Randomly selected		
Region	Spec.	Ultra-lengths	Region	Spec.	Ultra-lengths
ENm001	11	$28, 27, 23, 20_2$	ENr122	9	22
ENm002	8	$39, 28, 27, 26_4$	ENr213	9	$30, 27, 26, 24, 23_2$
ENm003	9	$38, 28_2, 26, 25_2$	ENr221	10	$36_2, 32_2, 29$
ENm004	8	$35, 26_2, 25, 20$	ENr222	10	$29, 22$
ENm005	10	$114, 62, 38, 34, 32$	ENr231	8	$26, 23, 20$
ENm006	8	–	ENr232	8	$26, 25, 20$
ENm007	6	–	ENr233	9	$25, 24, 20$
ENm008	9	$23, 22$	ENr311	10	$42, 31, 25, 21$
ENm009	10	–	ENr312	9	$60, 31, 22, 20_4$
ENm010	8	$86, 68, 63, 61, 60_2$	ENr313	9	27
ENm011	7	–	ENr321	10	$68, 44, 38, 37, 35$
ENm012	9	$169, 159, 125_2, 123$	ENr322	9	$126, 80, 79, 61, 55$
ENm013	10	$30, 26, 23, 22$	ENr323	8	$53, 50, 45, 42, 29$
ENm014	10	$41_2, 39, 26_2$	ENr331	9	26
			ENr332	10	26
			ENr334	8	$79, 50, 44, 37, 32$

Table 22.1. *Number of species and lengths of ultra-conserved elements in ENCODE alignments. Subindices indicate multiple occurrences.*

The shortest distance between consecutive ultra-conserved elements is 130 bp, and therefore collapsing regions is not considered for this dataset. The mean and median length of ultra-conserved elements are 2.605 and 2, respectively. The length distribution of all ultra-conserved elements is shown in Figure 22.4. This set of ultra-conserved elements is also somewhat more AT-rich, with a GC-ratio of 38.8% versus a GC-ratio of 42.4% across the entire *D. melanogaster* genome.

22.3 Biology of Ultra-Conserved Elements

22.3.1 Nine-Vertebrate Alignment

Using the UCSC genome browser annotations of known genes for the July 2003 (hg16) release of the human genome to investigate which ultra-conserved elements overlap known functional regions, we found that among the 237 ultra-conserved elements of length at least 20, 151 are in intragenic regions of 96 genes. Using the set of collapsed ultra-conserved elements as described in Section 22.2.1, intragenic regions cover 62.6% of the bases of these elements (Figure 22.5(a)), while intragenic regions cover only 56.3% of those at least 30 bp long (Figure 22.5(b)). Shorter ultra-conserved elements tend to correspond to exons, while longer ones are generally associated with introns and unannotated regions.

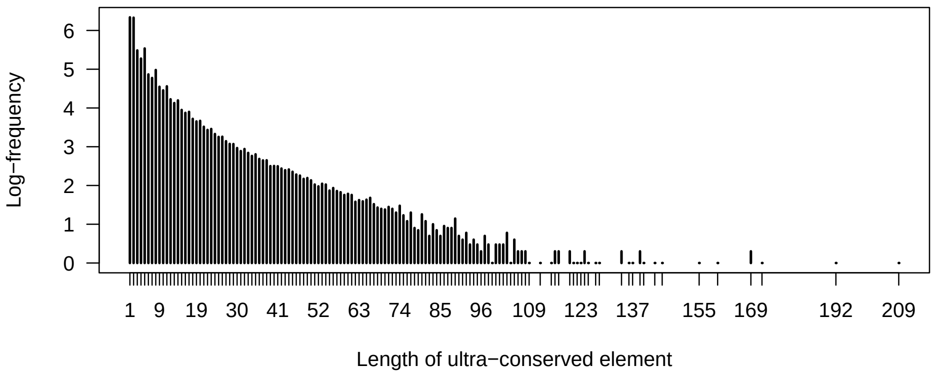

Fig. 22.4. Frequencies of *Drosophila* ultra-conserved elements ($\log_{10}$-scale).

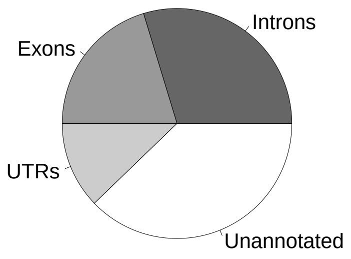

(a) 209 elements $\geq$ 20 bp

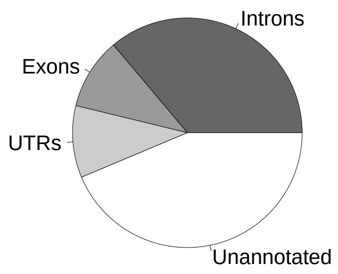

(b) 59 elements $\geq$ 30 bp

Fig. 22.5. Functional base coverage of collapsed vertebrate ultra-conserved elements based on annotations of known human genes.

On average, each gene is associated with 42.5 bp of ultra-conserved elements. Nine ultra-conserved elements cover a total of 306 bp in the intronic regions of *DPOA*, the alpha catalytic subunit of DNA polymerase. Six other genes are associated with more than 100 bp of ultra-conserved elements. Four of these genes are transcription factors involved in development (*SOX6*, *FOXP2*, *DACH1*, *TCF7L2*).

The remaining 86 elements of the original 237 did not overlap any annotated gene. However, by grouping together elements that have the same upstream and downstream flanking genes, there are only 27 super-regions to consider, with 51 unique flanking genes. Fifteen of these super-regions contain only one ultra-conserved element less than 30 bp in length, but there are 6 super-regions with at least 99 bp overlapping with ultra-conserved elements. At least one of the flanking genes for each of these 6 super-regions is a transcription factor located 1-314 kb away (*IRX3*, *IRX5*, *IRX6*, *HOXD13*, *DMRT1*, *DMRT3*, *FOXD3*, *TFEC*). The overall average distance to the closest flanking gene on either side is 138 kb and ranges from 312 bp to 1.2 Mbp.

We next study whether the genes near or overlapping with ultra-conserved elements tend to code for similar proteins. We divided the set of 96 genes with intragenic overlap into 3 groups based on where in the gene the overlap occurred: exon, intron or untranslated region (UTR). If ultra-conserved elements overlap more than one type of genic region, then the gene is assigned to each of the appropriate groups. The 51 genes flanking ultra-conserved elements in unannotated regions form a 4th group of genes. The Gene Ontology (GO) Consortium provides annotations for genes with respect to the molecular function of their gene products, the associated biological processes and their cellular localization [Ashburner *et al.*, 2000]. These GO annotations are available for 46 of the 54 genes with exonic overlap, for all of the 28 with intronic overlap, for 14 of the 20 with UTR overlap, and for 30 of the 51 genes flanking unannotated elements. Considering one GO annotation and one of the 4 gene groups at a time, we counted how many of the genes in the group are associated with the considered annotation. Using counts of how often this annotation occurs among all proteins found in the Uniprot database (release 4.1), we computed a p-value from Fisher's exact test for testing independence of association with the annotation and affiliation with the considered gene group. Annotations associated with at least 3 genes in a group and with a p-value smaller than 3.0×10^{-2} are reported in Table 22.2. DNA-dependent regulation of transcription and transcription factor activity are found to be enriched in non-exonic ultra-conserved elements, corresponding to previously reported findings [Bejerano *et al.*, 2004, Boffelli *et al.*, 2004a, Sandelin *et al.*, 2004, Woolfe *et al.*, 2005]. Conserved exonic elements tend to be involved in protein modification.

We scanned the human genome for repeated instances of these ultra-conserved elements and found that 14 of the original 237 elements have at least one other instance within the human genome. Each of these elements is at most 35 bp in length. Seven of them are found both between *IRX6* and *IRX5* and between *IRX5* and *IRX3* on chromosome 16. These genes belong to a cluster of Iroquois homeobox genes involved in embryonic pattern formation [Peters *et al.*, 2000]. These repeated elements include two 32 bp sequences that are perfect reverse complements of each other and two (of lengths 23 bp and 28 bp) that are truncated reverse complements of each other. Overall, there are 5 distinct sequences within 226 bp regions on either side of *IRX5* that are perfect reverse complements of each other and found in the same

GO Annotation	p-value
Exons	
protein serine/threonine kinase activity	4.545×10^{-3}
transferase activity	1.494×10^{-2}
neurogenesis	1.654×10^{-2}
protein amino acid phosphorylation	2.210×10^{-2}
Introns	
regulation of transcription, DNA-dependent	8.755×10^{-4}
transcription factor activity	2.110×10^{-3}
protein tyrosine kinase activity	4.785×10^{-3}
protein amino acid phosphorylation	1.584×10^{-2}
protein serine/threonine kinase activity	2.806×10^{-2}
UTRs	
regulation of transcription, DNA-dependent	1.403×10^{-4}
transcription factor activity	3.971×10^{-3}
Flanking	
transcription factor activity	3.255×10^{-11}
regulation of transcription, DNA-dependent	2.021×10^{-8}
development	5.566×10^{-3}

Table 22.2. *GO annotations of genes associated with vertebrate ultra-conserved elements.*

relative order (Figure 22.6). Furthermore, exact copies of the two outermost sequences are found both between *IRX4* and *IRX2* and between *IRX2* and *IRX1* on chromosome 5. Both of these regions are exactly 226 bp long. The repetition of these short regions and the conservation of their relative ordering and size suggests a highly specific coordinated regulatory signal with respect to these Iroquois homeobox genes, and strengthens similar findings reported by [Sandelin *et al.*, 2004].

The longest ultra-conserved element that is repeated in the human genome is of length 35 and is found in an exon of an actin gene, *ACTA1*. In the human genome, this sequence is also found in the exons of 3 other actin genes, the introns of 3 unrelated proteins, and 12 other unannotated regions. This sequence is found multiple times in the other vertebrate genomes as well: 13 times in chimp, 10 times in mouse, 5 times in both rat and dog, 4 times in tetraodon, 3 times in zebra fish, and twice in both fugu and chicken. However, the functional significance of the presence of multiple copies of this element in each of these vertebrate genomes is unclear.

```
54102348 TGTAATTACAATCTTACAGAAACCGGGCCGATCTGTATATAAATCTCACCATCCAATTAC
54102408 AAGATGTAATAATTTTGCACTCAAGCTGGTAATGAGGTCTAATACTCGTGCATGCGATAA
54102468 TCCCCTCTGGATGCTGGCTTGATCAGATGTTGGCTTTGTAATTAGACGGGCAGAAAATCA
54102528 TTATTTCATGTTCAAATAGAAAATGAGGTTGGTGGGAAGTTAATTT

55002049 AAATTAACTTCCCACCAACCTAATTTTTTCCTGAACATGAAATAATGATTTTCTGCCCGT
55002109 CTAATTACAAAGCCAACATCTGATCAAGCCAGCATCCAGAGGGGATTATCGCATGCACGA
55002169 GTATTAGACCTCATTACCAGCTTGAGTGCAAAATTATTACATCTTGTAATTGGATGGTGA
55002229 GATTTATATACAGATCGGCCCGGTTTCTGTAAGATTGTAATTACA
```

Fig. 22.6. Sequences found on either side of *IRX5*. Sequences underlined with a thick line are ultra-conserved with respect to the nine-vertebrate alignment. Sequences underlined with a thin line are not ultra-conserved but their reverse complement is. Indices are with respect to chromosome 16.

22.3.2 ENCODE Alignment

Based on the annotations of known human genes provided by the UCSC Genome Browser, 69.2% of the bases of the ultra-conserved elements of length at least 20 in the ENCODE alignment overlap intragenic regions (Figure 22.7(a)). However, longer sequences (at least 50 bp) are heavily biased towards intronic overlap, accounting for 67.7% of these sequences by base coverage (Figure 22.7(b)).

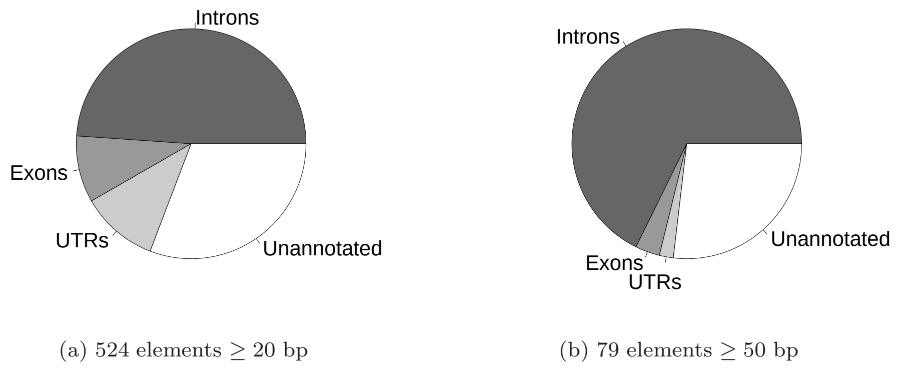

Fig. 22.7. Functional base coverage of ultra-conserved elements found in ENCODE regions based on annotations of known human genes.

Values for the gene density and non-exonic conservation level (human-mouse) are available for the randomly selected ENCODE regions (see Chapter 21 for a description). For these regions, the amount of base coverage by ultra-conserved elements is not correlated with gene density (Pearson correlation = -0.0589) and is moderately correlated with non-exonic conservation (Pearson correlation = 0.4350).

While we do not repeat the gene ontology analysis from the previous section, we note that the regions with the greatest amount of ultra-conserved elements by base coverage are regions with well-known genes involved in DNA-dependent transcriptional regulation (Table 22.3). The elements in these 5 regions account for 80.3% of the bases of the ultra-conserved elements found in this dataset. The 35 longest ultra-conserved elements, of length at least 69 bp, are also all found in these 5 regions.

	Ultra Coverage (bp)	Transcription Factor Genes	# Aligned Species
ENm012	9,086	*FOXP2*	9
ENr322	2,072	*BC11B*	9
ENm010	1,895	*HOXA1-7,9-11,13*; *EVX1*	8
ENm005	718	*GCFC*; *SON*	10
ENr334	549	*FOXP4*; *TFEB*	8

Table 22.3. *ENCODE regions with the greatest number of ultra-conserved elements by base coverage and their associated transcription factor genes.*

22.3.3 Eight-Drosophila Alignment

We analyzed the 255 ultra-conserved elements of length at least 75 bp using the Release 4.0 annotations of *D. melanogaster*. Approximately half of the conserved elements occur within 95 different genes (Figure 22.8(a)) and this proportion increases to 68.2% for the 59 sequences that are at least 100 bp (Figure 22.8(b)). Unlike the vertebrate dataset, longer regions are associated with exons, while shorter regions tend to correspond to unannotated elements.

On average, 125.7 bp of ultra-conserved sequences are associated with each gene by intragenic overlap. The three genes with the greatest amount of overlap with these conserved regions are *para* (765 bp), *nAcRα-34E* (426 bp) and *nAcRα-30D* (409 bp). All three of these genes are involved in cation channel activity, and the ultra-conserved elements correspond mostly with their exons. As with the nine-vertebrate dataset, the full set of 95 *D. melanogaster* genes is assessed for GO annotation enrichment, using all Release 4.0 *D. melanogaster* genes as the background set (Table 22.4). GO annotations exist for 78 of these 95 genes, which we did not differentiate further according to where in the gene overlap with an ultra-conserved element occurred. Genes involved in synaptic transmission are strongly overrepresented in genes that have an ultra-conserved element overlap with their exons, introns and UTRs. These genes include those with ion channel activity, signal transduction and receptor activity, with roles

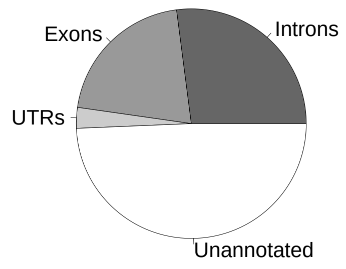

(a) 255 elements ≥ 75 bp

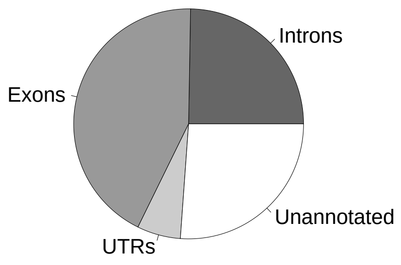

(b) 59 elements ≥ 100 bp

Fig. 22.8. Functional base coverage of ultra-conserved elements found in the *Drosophila* alignment based on annotations of known *D. melanogaster* genes.

in intracellular signaling cascades, muscle contraction, development and behavior. RNA binding proteins are also found to be overrepresented. Another group of overrepresented genes are those involved in RNA polymerase II transcription factor activity. These genes are strongly associated with development and morphogenesis.

The 130 ultra-conserved elements found in unannotated regions are grouped together into 109 regions by common flanking genes. These regions are flanked by 208 unique genes, 134 of which have available GO annotations. The distance from these ultra-conserved elements to their respective nearest gene ranges from 0.2-104 kb and is 16 kb on average. A number of transcription factors involved with development and morphogenesis are found within this set of genes. Five of the 10 flanking genes with ultra-conserved sequences both upstream and downstream are transcription factors (*SoxN*, *salr*, *toe*, *H15*, *sob*). In total, 44 unique transcription factors are found across the intragenic and flanking gene hits.

Ten of the original 255 ultra-conserved elements are repeated elsewhere in the *D. melanogaster* genome. However, all of these repeats correspond to annotated tRNA or snRNA, not homologous exons or regulatory regions. There are 10 ultra-conserved elements that overlap with tRNA (757 bp in sum), two that overlap with snRNA (191 bp in sum), and one that overlaps with ncRNA (81 bp). None of the ultra-conserved elements correspond to annotated rRNA, regulatory regions, transposable elements or pseudogenes.

GO Annotation	p-value
Exons, Introns, and UTRs	
synaptic transmission	3.290×10^{-9}
specification of organ identity	1.044×10^{-6}
ventral cord development	3.674×10^{-6}
RNA polymerase II transcription factor activity	4.720×10^{-6}
muscle contraction	8.714×10^{-6}
voltage-gated calcium channel activity	3.548×10^{-5}
RNA binding	7.650×10^{-5}
synaptic vesicle exocytosis	3.503×10^{-4}
leg morphogenesis	3.503×10^{-4}
calcium ion transport	6.401×10^{-4}
Flanking	
regulation of transcription	8.844×10^{-7}
neurogenesis	5.339×10^{-6}
ectoderm formation	8.285×10^{-6}
endoderm formation	2.125×10^{-5}
salivary gland morphogenesis	5.870×10^{-5}
Notch signaling pathway	1.591×10^{-4}
leg joint morphogenesis	1.788×10^{-4}
RNA polymerase II transcription factor activity	2.381×10^{-4}
salivary gland development	4.403×10^{-4}
signal transducer activity	5.308×10^{-4}
foregut morphogenesis	8.004×10^{-4}

Table 22.4. *GO annotations of genes associated with Drosophila ultra-conserved elements.*

22.3.4 Discussion

Previous studies have considered long stretches of perfectly conserved regions across shorter evolutionary distances [Bejerano *et al.*, 2004], or aligned regions above some relatively high threshold level of conservation [Boffelli *et al.*, 2004a, Sandelin *et al.*, 2004, Woolfe *et al.*, 2005]. We, however, focused on ultra-conserved elements across large evolutionary distances. This approach precludes our ability to capture all regions containing high levels of conservation, but allows us to identify regions that appear to be under the most stringent evolutionary constraints.

As found in previous studies of highly conserved sequences across vertebrate genomes, non-coding sequences near genes involved in transcriptional regulation are under exceptionally strong evolutionary constraints. Non-coding regions that are perfectly conserved across all 9 species, such as those found near the Iroquois homeobox genes on chromosome 16, are excellent candidates to be precise regulatory signals. Non-coding sequences near transcription factors are also found among the *Drosophila* conserved elements. However, in the fruit fly dataset, the exonic conservation is more more substantial. Although this conservation is due in part to a much shorter period of evolution, the exact conservation of exons whose gene products are involved in synaptic transmission may be fly-specific.

22.4 Probability of Ultra-Conservation

How long of an ultra-conserved element could occur simply by chance? In order to give an answer to this question, let us first assume that the nucleotides in the different positions in the alignment are mutually independent. Under this simplifying assumption, we compute the probability of observing an ultra-conserved element of a given length for the nine-vertebrate and Drosophila-alignments. While we assume that evolutionary changes to DNA at one position in the alignment occur independently from changes at all other, and in particular, neighboring positions, we allow for dependence of the occurrence of nucleotides in the genomes of different species (at any given position in the aligned genomes). More precisely, we use a phylogenetic tree model for our probability calculation.

Before being able to compute a probability, we must build a phylogenetic tree and estimate the parameters of the associated model. The tree for the nine-vertebrate alignment is shown in Figure 22.1. The topology of this tree is well-known, so we assume it fixed and use `paml` [Yang, 1997] to estimate model parameters by maximum likelihood. As input to `paml`, we choose the entire alignments with all columns containing a gap removed. The resulting alignment was 6,300,344 positions long for the vertebrates and 26,216,615 positions long for the Drosophila. Other authors (see Chapter 21 or [Pachter and Sturmfels, 2004a]) have chosen to focus only on synonymous substitutions in coding regions, since they are likely not selected for or against and thus give good estimates for neutral substitution rates. However, our independence model does not depend on the functional structure of the genome, that is, it sees the columns as i.i.d. samples. Thus, we believe that it is more appropriate to use all the data available to estimate parameters.

Many phylogenetic tree models exist (cf. Section 4.5) and we concentrate here on the Jukes-Cantor and HKY models. With the parameter estimates from `paml`, we can compute the probability p_{cons} of observing an ultra-conserved position in the alignment. Recall that the probability $p_{i_1 \ldots i_s}$ of seeing the nucleotide vector $(i_1, \ldots, i_s) \in \{\mathtt{A}, \mathtt{C}, \mathtt{G}, \mathtt{T}\}^s$ in a column of the alignment of s species is given by a polynomial in the entries of the transition matrices $P_e(t)$, which are obtained as $P_e(t) = \exp(Qt_e)$ where t_e is the length of the edge e

in the phylogenetic tree and Q is a rate matrix that depends on the model selected.

Under the Jukes-Cantor model for the nine-vertebrate alignment, the maximum likelihood (ML) branch lengths are shown in Figure 22.1 and give the probabilities

$$p_{\mathtt{AAAAAAAAA}} = \cdots = p_{\mathtt{TTTTTTTTT}} = 0.0455666...$$

Thus the probability of a conserved column under this model is $p_{\text{cons}} = 0.1823$. If we require that the nucleotides are identical not only across present-day species but also across ancestors, then the probability drops slightly to 0.1738.

Under the HKY model for the nine-vertebrate alignment, the ML branch lengths are very similar to those in Figure 22.1 and the additional parameter is estimated as $\kappa = 2.4066$ (in the notation of Figure 4.6, $\kappa = \alpha/\beta$). The root distribution was estimated to be almost uniform. These parameters give the probabilities

$$p_{\mathtt{AAAAAAAAA}} = \cdots = p_{\mathtt{TTTTTTTTT}} = 0.014706...,$$

which are much smaller than their counterpart in the Jukes-Cantor model. The HKY probability of a conserved column is $p_{\text{cons}} = 0.0588$. If we assume that nucleotides must also be identical in ancestors, this probability drops to 0.0494.

The binary indicators of ultra-conservation are independent and identically distributed according to a Bernoulli distribution with success probability p_{cons}. The probability of seeing an ultra-conserved element of length at least ℓ starting at a given position in the alignment therefore equals p_{cons}^{ℓ}. Moreover, the probability of seeing an ultra-conserved element of length at least ℓ anywhere in a genome of length N can be bounded above by Np_{cons}^{ℓ}. Recall that the length of the human genome equals roughly 2.8 Gbp and the length of *D. melanogaster* is approximately 120 Mbp. Table 22.5 evaluates the probability bound for different values of ℓ.

However, 46% of the ungapped columns in the nine-vertebrate alignment are actually ultra-conserved. This compares with the 18% we would expect with the JC model and the 5% under the HKY model. This suggests that the model of independent alignment positions is overly simplistic. If we collapse the alignment to a sequence of binary indicators of ultra-conserved positions, then a very simple non-independence model for this binary sequence is a Markov chain model (cf. Section 1.4 and Chapter 10).

In a Markov chain model, the length of ultra-conserved elements is geometrically distributed, i.e., the probability that an ultra-conserved element is of length ℓ equals $\theta^{\ell-1}(1-\theta)$, where θ is the probability of transitioning from one ultra-conserved position to another. The expected value of the length

	Nine-vertebrate (human)			Drosophila (*D. melanogaster*)	
	Jukes-Cantor	HKY		Jukes-Cantor	HKY
p_{cons}	0.1823	0.0588	p_{cons}	0.42865	0.23878
15	0.023	$9.72 \cdot 10^{-10}$	25	0.076	$3.38 \cdot 10^{-8}$
20	$4.60 \cdot 10^{-6}$	$6.83 \cdot 10^{-16}$	75	$3.07 \cdot 10^{-20}$	$2.69 \cdot 10^{-39}$
125	$1.11 \cdot 10^{-83}$	$4.16 \cdot 10^{-145}$	209	$1.54 \cdot 10^{-69}$	$1.20 \cdot 10^{-122}$

Table 22.5. *Probabilities of seeing ultra-conserved elements of certain lengths in an independence model with success probability p_{cons} derived from two phylogenetic tree models.*

of an ultra-conserved element is equal to $1/(1-\theta)$. The probability that an ultra-conserved element is of length ℓ or longer equals

$$\sum_{k=\ell}^{\infty} \theta^{k-1}(1-\theta) = \theta^{\ell-1}.$$

Therefore, the probability that at least one of U ultra-conserved elements found in a multiple alignment would be of length at least ℓ is equal to

$$1 - (1-\theta^{\ell-1})^U \approx U \cdot \theta^{\ell-1} \quad \text{for larger } \ell.$$

Restricting ourselves to the nine-vertebrate alignment (computations for the Drosophila alignment are qualitatively similar), we use the mean length of the ultra-conserved elements described in Section 22.3.1 to estimate the transition probability θ to 0.4785. Then the probability that at least one of the 1,513,176 ultra-conserved elements of the nine-vertebrate alignment is of length 25 or longer equals about 3%. The probability of seeing one of the U ultra-conserved elements being 30 or more bp long is just below 1/1000. However, the dependence structure in a Markov chain model cannot explain the longest ultra-conserved elements in the alignment. For example, the probability of one of the U elements being 125 or more bp long is astronomically small ($0.3 \cdot 10^{-33}$). This suggests that the Markov chain model does not capture the dependence structure in the binary sequence of ultra-conservation indicators. At a visual level, this already becomes clear in Figure 22.3. Were the Markov chain model true then due to the resulting geometric distribution for the length of an ultra-conserved element the frequencies on log-scale should fall on a straight line, which is not the case in Figure 22.3. Modeling the process of ultra-conservation statistically requires more sophisticated models, for which the phylogenetic hidden Markov models appearing, for example, in [Siepel and Haussler, 2004] provide a point of departure.

Bibliography

[Abril *et al.*, 2005] JF Abril, R Castelo, and R Guigó. Comparison of splice sites in mammals and chicken. *Genome Research*, 15:111–119, 2005. pages 152

[Adkins *et al.*, 2001] RM Adkins, EL Gelke, D Rowe, and RL Honeycutt. Molecular Phylogeny and Divergence Time Estimates for Major Rodent Groups: Evidence from Multiple Genes. *Mol Biol Evol*, 18(5):777–791, 2001. pages 397

[Agresti, 1990] A Agresti. *Categorical data analysis.* Wiley Series in Probability and Mathematical Statistics: Applied Probability and Statistics. John Wiley & Sons Inc., New York, 1990. A Wiley-Interscience Publication. pages 14

[Aji and McEliece, 2000] SM Aji and RJ McEliece. The generalized distributive law. *IEEE Trans. Inform. Theory*, 46(2):325–343, 2000. pages 44

[Alefeld and Herzberger, 1983] G Alefeld and J Herzberger. *An introduction to interval computations.* Academic press, New York, 1983. pages 377

[Alexandersson *et al.*, 2003] M Alexandersson, S Cawley, and L Pachter. Slam: cross-species gene finding and alignment with a generalized pair hidden markov model. *Genome Res*, 13(3):496–502, 2003. pages 154

[Allman and Rhodes, 2003] ES Allman and JA Rhodes. Phylogenetic invariants for the general Markov model of sequence mutation. *Math. Biosci.*, 186(2):113–144, 2003. pages 161, 361

[Allman and Rhodes, 2004a] ES Allman and JA Rhodes. Phylogenetic ideals and varieties for the general markov model, 2004. pages 313, 325, 328, 361, 364

[Allman and Rhodes, 2004b] ES Allman and JA Rhodes. Quartets and parameter recovery for the general Markov model of sequence mutation. *AMRX Appl. Math. Res. Express*, 2004(4):107–131, 2004. pages 108, 361, 364

[Altschul *et al.*, 1990] SF Altschul, W Gish, W Miller, EW Myers, and DJ Lipman. Basic local alignment search tool. *J Molecular Biology*, 215:403–410, 1990. pages 85

[Andrews, 1963] G Andrews. A lower bound on the volume of strictly convex bodies with many boundary points. *Trans. Amer. Math. Soc.*, 106:270–279, 1963. pages 181

[Apostol, 1976] TM Apostol. *Introduction to analytic number theory.* Springer-Verlag, New York, 1976. Undergraduate Texts in Mathematics. pages 228

[Ardila, 2004] F Ardila. A tropical morphism related to the hyperplane arrangement of the complete bipartite graph. *Discrete and Computational Geometry, to appear*, 2004. pages 123

[Aris-Brosou, 2003] S Aris-Brosou. How bayes tests of molecular phylogenies compare with frequentist approaches. *Bioinformatics*, 19:618–624, 2003. pages 388

[Ashburner *et al.*, 2000] M Ashburner, CA Ball, JA Blake, D Botstein, H Butler, JM Cherry, K Dolinski, SS Dwight, JT Eppig, MA Harris, DP Hill, L Issel-Tarver, A Kasarskis, S Lewis, JC Matese, JE Richardson, M Ringwald, GM Rubin, and G Sherlock. Gene ontology: tool for the unification of biology. the gene ontology consortium. *Nature Genetics*, 25:25–29, 2000. pages 410

[Bandelt and Dress, 1992] HJ Bandelt and AWM Dress. A canonical decomposition theory for metrics on a finite set. *Advances in Mathematics*, 92:47–105, 1992. pages 332, 336

[Bandelt *et al.*, 1995] HJ Bandelt, P Forster, BC Sykes, and MB Richards. Mitochondrial portraits of human population using median networks. *Genetics*, 141:743–753, 1995. pages 332

[Basu *et al.*, 2003] S Basu, R Pollack, and MF Roy. *Algorithms in real algebraic geometry*, volume 10 of *Algorithms and Computation in Mathematics.* Springer-Verlag, Berlin, 2003. pages 101

[Beerenwinkel *et al.*, 2004] N Beerenwinkel, J Rahnenführer, M Däumer, D Hoffmann, R Kaiser, J Selbig, and T Lengauer. Learning multiple evolutionary pathways from cross-sectional data. In *Proc. 8th Ann. Int. Conf. on Res. in Comput. Biol. (RECOMB '04), 27–31 March 2004, San Diego, CA*, pages 36–44, 2004. to appear in *J. Comp. Biol.* pages 284, 287, 295

[Beerenwinkel *et al.*, 2005a] N Beerenwinkel, M Däumer, T Sing, J Rahnenführer, T Lengauer, J Selbig, D Hoffmann, and R Kaiser. Estimating HIV evolutionary pathways and the genetic barrier to drug resistance. *J. Infect. Dis.*, 2005. to appear. pages 284

[Beerenwinkel *et al.*, 2005b] N Beerenwinkel, J Rahnenführer, R Kaiser, D Hoffmann, J Selbig, and T Lengauer. Mtreemix: a software package for learning and using mixture models of mutagenetic trees. *Bioinformatics*, 2005. to appear. pages 285

[Bejerano *et al.*, 2004] G Bejerano, M Pheasant, I Makunin, S Stephen, WJ Kent, JS Mattick, and D Haussler. Ultraconserved elements in the human genome. *Science*, 304:1321–1325, 2004. pages 410, 415

[Besag, 1986] J Besag. On the statistical analysis of dirty pictures. *Journal of the Royal Statistical Society*, B 48 No. 3:259–302, 1986. pages 280, 281

[Bickel, 1971] PJ Bickel. *Mathematical Statistics, Part I.* Holden-Day Inc., San Francisco, Calif., 1971. Basic ideas and selected topics, Holden-Day Series in Probability and Statistics. pages 6, 8

[Boffelli *et al.*, 2003] Dario Boffelli, Jon McAuliffe, Dmitriy Ovcharenko, Keith D Lewis, Ivan Ovcharenko, Lior Pachter, and Edward M Rubin. Phylogenetic shadowing of primate sequences to find functional regions of the human genome. *Science*, 299(5611):1391–4, 2003. pages 138, 164

[Boffelli *et al.*, 2004a] D. Boffelli, M.A. Nobrega, and E.M. Rubin. Comparative genomics at the vertebrate extremes. *Nature Reviews Genetics*, 5:456–465, 2004. pages 410, 415

[Boffelli *et al.*, 2004b] D Boffelli, CV Weer, L Weng, KD Lewis, MI Shoukry, L Pachter, DN Keys, and EM Rubin. Intraspecies sequence comparisons for annotating genomes. *Genome Research*, 14:2406–2411, 2004. pages 138

[Bosma *et al.*, 1997] Wieb Bosma, John Cannon, and Catherine Playoust. The MAGMA algebra system I: the user language. *J. Symb. Comput.*, 24(3-4):235–265, 1997. pages 81

[Bourque *et al.*, 2004] Guillaume Bourque, Pavel A Pevzner, and Glenn Tesler. Reconstructing the genomic architecture of ancestral mammals: lessons from human, mouse, and rat genomes. *Genome Res*, 14(4):507–16, 2004. pages 139

[Bray and Pachter, 2004] N Bray and L Pachter. Mavid: constrained ancestral alignment of multiple sequences. *Genome Res*, 14(4):693–9, 2004. pages 86, 393, 403

[Brown *et al.*, 1982] WM Brown, EM Prager, A Wang, and AC Wilson. Mitochondrial DNA sequences of primates, tempo and mode of evolution. *Journal of Molecular Evolution*, 18:225–239, 1982. pages 386

[Brown, 2002] TA Brown. *Genomes 2.* John Wiley & Son, Inc., 2002. pages 2, 138

[Brudno *et al.*, 2003] M. Brudno, S. Malde, A. Poliakov, C. Do, O. Courone, I. Dubchak, and S. Batzoglou. Global alignment: finding rearrangements during alignment. *Special issue on the Proceedings of the ISMB 2003, Bioinformatics*, 19:54i–64i, 2003. pages 393, 404

[Bryant and Moulton, 2004] D Bryant and V Moulton. Neighbornet: An agglomerative algorithm for the construction of planar phylogenetic networks. *Molecular Biology And Evolution*, 21:255–265, 2004. pages 332

[Buchberger, 1965] B Buchberger. *An algorithm for finding a basis for the residue* *class ring of a zero-dimensional polynomial ideal (in German).* PhD thesis, Univ. Innsbruck, Dept. of Math., Innsbruck, Austria, 1965. pages 98

[Bulmer, 1991] D Bulmer. Use of the method of generalized least squares in reconstructing phylogenies from sequence data. *Molecular Biology and Evolution*, 8(6):868–883, 1991. pages 335

[Burge and Karlin, 1997] C Burge and S Karlin. Prediction of complete gene structures in human genomic DNA. *Journal of Molecular Biology*, 268(1):78–94, 1997. pages 154

[Campbell *et al.*, 1999] A Campbell, J Mrazek, and S Karlin. Genome signature comparisons among prokaryote, plasmid and mitochondrial DNA. *Proceedings of the National Academy of Sciences USA*, 96(16):9184–9189, 1999. pages 136, 137

[Casanellas *et al.*, 2004] M. Casanellas, L.D. Garcia, and S. Sullivant. Small phylogenetic trees. http://www.math.tamu.edu/∼lgp/small-trees/small-trees.html, 2004. pages 308

[Catalisano *et al.*, 2002] M. V. Catalisano, A. V. Geramita, and A. Gimigliano. Ranks of tensors, secant varieties of Segre varieties and fat points. *Linear Algebra Appl.*, 355:263–285, 2002. pages 295

[Catanese *et al.*, 2004] Fabrizio Catanese, Serkan Hoşten, Amit Khetan, and Bernd Sturmfels. The maximum likelihood degree. to appear in the American Journal of Mathematics, 2004. pages 11, 112

[Cavalli-Sforza and Edwards, 1967] L. Cavalli-Sforza and A. Edwards. Phylogenetic analysis models and estimation procedures. *Evolution*, 32:550–570, 1967. pages 335

[Cavender and Felsenstein, 1987] J. Cavender and J. Felsenstein. Invariants of phylogenies in a simple case with discrete states. *Journal of Classification*, 4:57–71, 1987. pages 361

[Chargaff, 1950] E Chargaff. Chemical specificity of nucleic acids and mechanism for the enzymatic degradation. *Experientia*, 6:201–209, 1950. pages 135

[Chazelle, 1991] B Chazelle. An optimal convex hull algorithm and new results on cuttings. In *Proc. 32nd IEEE Symp. on Foundations of Computer Science*, pages 29–38, 1991. pages 183

[Chazelle, 1993] B Chazelle. An optimal convex hull algorithm in any fixed dimension. *Discrete Computational Geometry*, 10:377–409, 1993. pages 183

[Cohen and Rothblum, 1993] Joel E. Cohen and Uriel G. Rothblum. Nonnegative ranks, decompositions, and factorizations of nonnegative matrices. *Linear Algebra Appl.*, 190:149–168, 1993. pages 123

[Cohen, 2004] Joel E Cohen. Mathematics is biology's next microscope, only better; biology is mathematics' next physics, only better. *PLoS Biol*, 2(12):e439, 2004. pages 2

[Consortium, 2004] ENCODE Project Consortium. The encode (encyclopedia of dna elements) project. *Science*, 306(5696):636–40, 2004. pages 149, 393

[Cox *et al.*, 1997] David Cox, John Little, and Donal O'Shea. *Ideals, varieties, and algorithms.* Undergraduate Texts in Mathematics. Springer-Verlag, New York, second edition, 1997. An introduction to computational algebraic geometry and commutative algebra. pages 2, 93, 97, 101, 103, 244

[Craciun and Feinberg, 2004] G Craciun and M Feinberg. Multiple equilibria in complex chemical reaction networks: I. the injectivity property. *SIAM Journal of Applied Mathematics*, 2004. pages 100

[Cuyt *et al.*, 2001] A Cuyt, B Verdonk, S Becuwe, and P Kuterna. A remarkable example of catastrophic cancellation unraveled. *Computing*, 66:309–320, 2001. pages 374

[Darwin, 1859] C Darwin. *On the origin of species by means of natural selection, or* *the preservation of favoured races in the struggle for life.* John Murray, London, 1859. pages 71, 147

[De Concini *et al.*, 1982] Corrado De Concini, David Eisenbud, and Claudio Procesi. *Hodge algebras*, volume 91 of *Astérisque*. Société Mathématique de France, Paris, 1982. With a French summary. pages 107

[Demmel, 1997] James W. Demmel. *Applied numerical linear algebra.* Society for Industrial and Applied Mathematics (SIAM), Philadelphia, PA, 1997. pages 364

[Desper *et al.*, 1999] R. Desper, F. Jiang, O.-P. Kallioniemi, H. Moch, C.H. Papadimitriou, and A.A. Schäffer. Inferring tree models for oncogenesis from comparative genome hybridization data. *J. Comp. Biol.*, 6(1):37–51, 1999. pages 284

[Develin and Sturmfels, 2004] Mike Develin and Bernd Sturmfels. Tropical convexity. *Doc. Math.*, 9:1–27 (electronic), 2004. pages 121, 123

[Develin *et al.*, 2003] M Develin, F Santos, and B Sturmfels. On the tropical rank of a matrix. *MSRI Proceedings, to appear*, 2003. pages 121, 123

[Dewey *et al.*, 2004] Colin Dewey, Jia Qian Wu, Simon Cawley, Marina Alexandersson, Richard Gibbs, and Lior Pachter. Accurate identification of novel human genes through simultaneous gene prediction in human, mouse, and rat. *Genome Res*, 14(4):661–4, 2004. pages 137

[Dewey, 2005] Colin Dewey. Mercator: software for multiple whole-genome orthology map construction. Available at http://hanuman.math.berkeley.edu/ cdewey/mercator/, 2005. pages 393, 403

[Deza and Laurent, 1997] Michel Marie Deza and Monique Laurent. *Geometry of cuts and metrics*, volume 15 of *Algorithms and Combinatorics*. Springer-Verlag, Berlin, 1997. pages 71

[Douzery E. J. P. and D., 2003] Stanhope M. J. Douzery E. J. P., Delsuc F. and Huchon D. Local molecular clocks in three nuclear genes: divergence ages of rodents and other mammals, and incompatibility between fossil calibrations. *Molecular Biology and Evolution*, 57:201–213, 2003. pages 402

[Dress and Huson, 2004] A. Dress and Daniel Huson. Constructing splits graphs. *IEEE/ACM Transactions in Computational Biology and Bioinformatics*, 2004. pages 333

[Dress and Terhalle, 1998] Andreas Dress and Werner Terhalle. The tree of life and other affine buildings. In *Proceedings of the International Congress of Mathematicians*, number Extra Vol. III in Vol. III (Berlin, 1998), pages 565–574 (electronic), 1998. pages 125

[Dress *et al.*, 2002] A. Dress, J. H. Koolen, and V. Moulton. On line arrangements in the hyperbolic plane. *European J. Combin.*, 23(5):549–557, 2002. pages 107

[Durbin *et al.*, 1998] R Durbin, S Eddy, A Korgh, and G Mitchison. *Biological Sequence Analysis: Probabilistic Models of Proteins and Nucleic Acids.* Cambridge University Press, 1998. pages 2, 3, 4, 25, 28, 31, 150, 259

[Eichler and Sankoff, 2003] EE Eichler and D. Sankoff. Structural dynamics of eukaryotic chromosome evolution. *Science*, 301:793–797, 2003. pages 138

[Evans and Speed, 1993] S Evans and T Speed. Invariants of some probability models used in phylogenetic inference. *The Annals of Statistics*, 21:355–377, 1993. pages 161, 303, 312, 316

[Farris, 1972] J.S. Farris. Estimating phylogenetic trees from distance matrices. *American Naturalist*, 106:645–668, 1972. pages 335

[Felsenstein, 1978] J. Felsenstein. Cases in which parsimony or compatibility methods will be positively misleading. *Syst. Zool.*, 22:240–249, 1978. pages 400

[Felsenstein, 1981] J Felsenstein. Evolutionary trees from DNA sequences: a maximum likelihood approach. *Journal of Molecular Evolution*, 17:368–376, 1981. pages

335, 380

[Felsenstein, 2003] J Felsenstein. *Inferring Phylogenies*. Sinauer Associates, Inc., 2003. pages vii, 71, 156, 161, 336

[Felsenstein, 2004] J Felsenstein. PHYLIP (Phylogeny Inference Package) version 3.6. Distributed by the author, Department of Genome Sciences, University of Washington, Seattle, 2004. pages 88, 389, 390

[Fernández-Baca *et al.*, 2002] D Fernández-Baca, T Seppäläinen, and G Slutzki. Bounds for parametric sequence comparison. *Discrete Applied Mathematics*, 118:181–198, 2002. pages 214, 218, 219, 220

[Fitch and Smith, 1983] Walter M. Fitch and Temple F. Smith. Optimal Sequence Alignments. *PNAS*, 80(5):1382–1386, 1983. pages 213

[Fleischmann *et al.*, 1995] RD Fleischmann, MD Adams, O White, RA Clayton, EF Kirkness, AR Kerlavage, CJ Bult, JF Tomb, BA Dougherty, and JM Merrick et al. Whole-genome random sequencing and assembly of *haemophilus influenza* Rd. *Science*, 269(5223):496–512, 1995. pages 133

[Floyd, 1962] RW Floyd. Algorithm 97: shortest path. *Communications of ACM*, 5(6):345, 1962. pages 48

[Forney, 1973] G.D. Forney. The viterbi algorithm. *Proc. of the IEEE*, 61(3):268–278, 1973. pages 232

[Frieze *et al.*, 1998] A. Frieze, R. Kannan, and S. Vempala. Fast Monte Carlo algorithms for low rank approximation. In *39th Symposium on Foundations of Computing*, pages 370–378, 1998. pages 366

[Fukuda, 2004] Komei Fukuda. From the zonotope construction to the Minkowski addition of convex polytopes. *J. Symbolic Comput.*, 38(4):1261–1272, 2004. pages 194

[Galtier and Gouy, 1998] N. Galtier and M. Gouy. Inferring pattern and process: maximum likelihood implementation of a non-homogeneous model of dna sequence evolution for phylogenetic analysis. *Molecular Biology and Evolution*, 154(4):871–879, 1998. pages 400, 401

[Garcia *et al.*, 2004] L. D. Garcia, M. Stillman, and B. Sturmfels. Algebraic geometry of Bayesian networks. *J. Symbolic Comput.*, 2004. Special Issue Méthodes Effectives en Géometrie Algébrique (MEGA). pages 42, 108, 289, 364

[Garcia, 2004] L. D. Garcia. Algebraic statistics in model selection. In M. Chickering and J. Halpern, editors, *Proceedings of the* 20^{th} *Conference on Uncertainty in Artificial Intelligence*, pages 177–184. AUAI Press, Arlington, VA, 2004. pages 295

[Gatermann and Wolfrum, 2005] K Gatermann and M Wolfrum. Bernstein's second theorem and viro's method for sparse polynomial systems in chemistry. *Advances in Applied Mathematics*, 34(2):252–294, 2005. pages 100

[Gawrilow and Joswig, 2000] Ewgenij Gawrilow and Michael Joswig. polymake: a framework for analyzing convex polytopes. In Gil Kalai and Günter M. Ziegler, editors, *Polytopes — Combinatorics and Computation*, pages 43–74. Birkhäuser, 2000. pages 84

[Gawrilow and Joswig, 2001] Ewgenij Gawrilow and Michael Joswig. polymake: an approach to modular software design in computational geometry. In *Proceedings of the 17th Annual Symposium on Computational Geometry*, pages 222–231. ACM, 2001. June 3-5, 2001, Medford, MA. pages 84

[Geiger *et al.*, 2001] Dan Geiger, David Heckerman, Henry King, and Christopher Meek. Stratified exponential families: graphical models and model selection. *Ann. Statist.*, 29(2):505–529, 2001. pages 297

[Geiger *et al.*, 2002] D. Geiger, C. Meek, and B. Sturmfels. On the toric algebra of graphical models. *Annals of Statistics*, 2002. pages 272

[Geiger *et al.*, 2005] D. Geiger, C. Meek, and B. Sturmfels. On the toric algebra of graphical models. *Ann. Statist.*, to appear, 2005. pages 40, 289

[Geman and Geman, 1984] S. Geman and D. Geman. Stochastic relaxation, gibbs distributions and the bayesian restoration of images. *IEEE Transactions on Pattern Analysis and Machine Intelligence, PAMI-6*, pages 721–741, 1984. pages 280

[Gentleman *et al.*, 2004] Robert C Gentleman, Vincent J. Carey, Douglas M. Bates, Ben Bolstad, Marcel Dettling, Sandrine Dudoit, Byron Ellis, Laurent Gautier, Yongchao Ge, Jeff Gentry, Kurt Hornik, Torsten Hothorn, Wolfgang Huber, Stefano Iacus, Rafael Irizarry, Friedrich Leisch Cheng Li, Martin Maechler, Anthony J. Rossini, Gunther Sawitzki, Colin Smith, Gordon Smyth, Luke Tierney, Jean Y. H. Yang, and Jianhua Zhang. Bioconductor: Open software development for computational biology and bioinformatics. *Genome Biology*, 5:R80, 2004. pages 84

[Gentles and Karlin, 2001] AJ Gentles and S Karlin. Genome-scale compositional comparisons in eukaryotes. *Genome Research*, 4:540–546, 2001. pages 136

[Gibbs *et al.*, 2004] Richard A Gibbs, George M Weinstock, Michael L Metzker, Donna M Muzny, Erica J Sodergren, Steven Scherer, Graham Scott, David Steffen, Kim C Worley, Paula E Burch, Geoffrey Okwuonu, Sandra Hines, Lora Lewis, Christine DeRamo, Oliver Delgado, Shannon Dugan-Rocha, George Miner, Margaret Morgan, Alicia Hawes, Rachel Gill, Robert A Holt, Mark D Adams, Peter G Amanatides, Holly Baden-Tillson, Mary Barnstead, Soo Chin, Cheryl A Evans, Steve Ferriera, Carl Fosler, Anna Glodek, Zhiping Gu, Don Jennings, Cheryl L Kraft, Trixie Nguyen, Cynthia M Pfannkoch, Cynthia Sitter, Granger G Sutton, J Craig Venter, Trevor Woodage, Douglas Smith, Hong-Mei Lee, Erik Gustafson, Patrick Cahill, Arnold Kana, Lynn Doucette-Stamm, Keith Weinstock, Kim Fechtel, Robert B Weiss, Diane M Dunn, Eric D Green, Robert W Blakesley, Gerard G Bouffard, Pieter J De Jong, Kazutoyo Osoegawa, Baoli Zhu, Marco Marra, Jacqueline Schein, Ian Bosdet, Chris Fjell, Steven Jones, Martin Krzywinski, Carrie Mathewson, Asim Siddiqui, Natasja Wye, John McPherson, Shaying Zhao, Claire M Fraser, Jyoti Shetty, Sofiya Shatsman, Keita Geer, Yixin Chen, Sofyia Abramzon, William C Nierman, Paul H Havlak, Rui Chen, K James Durbin, Amy Egan, Yanru Ren, Xing-Zhi Song, Bingshan Li, Yue Liu, Xiang Qin, Simon Cawley, A J Cooney, Lisa M D'Souza, Kirt Martin, Jia Qian Wu, Manuel L Gonzalez-Garay, Andrew R Jackson, Kenneth J Kalafus, Michael P McLeod, Aleksandar Milosavljevic, Davinder Virk, Andrei Volkov, David A Wheeler, Zhengdong Zhang, Jeffrey A Bailey, Evan E Eichler, Eray Tuzun, Ewan Birney, Emmanuel Mongin, Abel Ureta-Vidal, Cara Woodwark, Evgeny Zdobnov, Peer Bork, Mikita Suyama, David Torrents, Marina Alexandersson, Barbara J Trask, Janet M Young, Hui Huang, Huajun Wang, Heming Xing, Sue Daniels, Darryl Gietzen, Jeanette Schmidt, Kristian Stevens, Ursula Vitt, Jim Wingrove, Francisco Camara, M Mar Alba, Josep F Abril, Roderic Guigó, Arian Smit, Inna Dubchak, Edward M Rubin, Olivier Couronne, Alexander Poliakov, Norbert Hubner, Detlev Ganten, Claudia Goesele, Oliver Hummel, Thomas Kreitler, Young-Ae Lee, Jan Monti, Herbert Schulz, Heike Zimdahl, Heinz Himmelbauer, Hans Lehrach, Howard J Jacob, Susan Bromberg, Jo Gullings-Handley, Michael I Jensen-Seaman, Anne E Kwitek, Jozef Lazar, Dean Pasko, Peter J Tonellato, Simon Twigger, Chris P Ponting, Jose M Duarte, Stephen Rice, Leo Goodstadt, Scott A Beatson, Richard D Emes, Eitan E Winter, Caleb Webber, Petra Brandt, Gerald Nyakatura, Margaret Adetobi, Francesca Chiaromonte, Laura Elnitski, Pallavi Eswara, Ross C Hardison, Minmei Hou, Diana Kolbe, Kateryna Makova, Webb Miller, Anton Nekrutenko, Cathy Riemer, Scott Schwartz, James Taylor, Shan Yang, Yi Zhang, Klaus Lindpaintner, T Dan Andrews, Mario Caccamo, Michele Clamp, Laura Clarke, Valerie Curwen, Richard Durbin, Eduardo Eyras, Stephen M Searle, Gregory M Cooper, Serafim Batzoglou, Michael Brudno, Arend Sidow, Eric A Stone, Bret A Payseur, Guillaume Bourque, Carlos Lopez-Otin, Xose S Puente, Kushal Chakrabarti, Sourav Chatterji, Colin Dewey, Lior Pachter, Nicolas Bray, Von Bing Yap, Anat Caspi, Glenn Tesler, Pavel A Pevzner, David Haussler, Krishna M Roskin, Robert Baertsch, Hiram Clawson, Terrence S Furey, Angie S Hinrichs, Donna Karolchik, William J Kent, Kate R Rosenbloom, Heather Trumbower, Matt Weirauch, David N Cooper, Peter D Stenson, Bin Ma, Michael Brent, Manimozhiyan Arumugam, David Shteynberg, Richard R Copley, Martin S Taylor, Harold Riethman, Uma Mudunuri, Jane Peterson, Mark Guyer, Adam Felsenfeld, Susan Old, Stephen Mockrin, and Francis Collins. Genome sequence of the brown norway rat yields insights into mammalian evolution. *Nature*, 428(6982):493–521, 2004. pages 138, 397

[Grayson and Stillman, 2002] Daniel R. Grayson and Michael E. Stillman. Macaulay 2, a software system for research in algebraic geometry. Available at http://www.math.uiuc.edu/Macaulay2/, 2002. pages 80, 244, 318, 321

[Greuel and Pfister, 2002] GM Greuel and G Pfister. *A Singular Introduction to Commutative Algebra*. Springer-Verlag, Berlin and Heidelberg, 2002. pages 84

[Greuel *et al.*, 2003] GM Greuel, G. Pfister, and H. Schoenemann. Singular, a computer algebra system for polynomial computations. Available at http://www.singular.uni-kl.de/, 2003. pages 244

[Griffiths and Marjoram, 1996] R. C. Griffiths and P. Marjoram. Ancestral inference from samples of dna sequences with recombination. *Journal of Computational Biology*, 3(4):479–502, 1996. pages 332

[Grötschel *et al.*, 1993] Martin Grötschel, László Lovász, and Alexander Schrijver. *Geometric Algorithms and Combinatorial Optimization*, volume 2 of *Algorithms and Combinatorics*. Springer-Verlag, 1993. pages 182, 192

[Grünbaum, 2003] Branko Grünbaum. *Convex polytopes*, volume 221 of *Graduate Texts in Mathematics*. Springer-Verlag, New York, second edition, 2003. Prepared and with a preface by Volker Kaibel, Victor Klee and Günter M. Ziegler. pages 63

[Guigó *et al.*, 2004] R Guigó, E Birbey, M Brent, E Dermitzakis, L Pachter, H Roest Crollius, V Solovyev, and MQ Zhang. Needed for completion of the human genome: hypothesis driven experiments and biologically realistic mathematical models. *arXiv q-bio.GN/0410008*, 2004. pages 138

[Gusfield *et al.*, 1994] D Gusfield, K Balasubramanian, and D Naor. Parametric optimization of sequence alignment. *Algorithmica*, 12:312–326, 1994. pages 58, 201, 216, 218

[Gusfield, 1997] D Gusfield. *Algorithms on Strings, Trees, and Sequences*. Cambridge University Press, 1997. pages 52, 58, 202, 213

[Hačijan, 1979] L. G. Hačijan. A polynomial algorithm in linear programming. *Dokl. Akad. Nauk SSSR*, 244(5):1093–1096, 1979. pages 192

[Hallgrimsdottir and Sturmfels, 2004] I Hallgrimsdottir and B Sturmfels. Resultants in genetic linkage analysis. *Journal of Symbolic Computation, to appear*, 2004. pages 134

[Hammer *et al.*, 1995] R Hammer, M Hocks, U Kulisch, and D Ratz. *C++ toolbox for verified computing: basic numerical problems*. Springer-Verlag, Berlin, 1995. pages 379, 380

[Hannenhalli and Pevzner, 1999] Sridhar Hannenhalli and Pavel A. Pevzner. Transforming cabbage into turnip: polynomial algorithm for sorting signed permutations by reversals. *Journal of the ACM*, 46(1):1—-27, 1999. pages 138

[Hansen and Sengupta, 1981] E Hansen and S Sengupta. Bounding solutions of systems of equations using interval analysis. *BIT*, 21:203–211, 1981. pages 379

[Hansen, 1980] E Hansen. Global optimization using interval analysis - the multidimensional case. *Numerische Mathematik*, 34:247–270, 1980. pages 374

[Hansen, 1992] E Hansen. *Global optimization using interval analysis*. Marcel Dekker, New York, 1992. pages 379, 384

[Hendy and Penny, 1989] M. Hendy and D. Penny. A framework for the quantitative study of evolutionary trees. *Systematic Zoology*, 38(4), 1989. pages 342, 345, 400

[Hendy and Penny, 1993] MD Hendy and D Penny. Spectral analysis of phylogenetic data. *Journal of Classification*, 10:5–24, 1993. pages 161

[Hibi, 1987] T. Hibi. Distributive lattices, affine semigroup rings and algebras with straightening laws. *Advanced Studies in Pure Mathematics*, 11:93–109, 1987. pages 293

[Hillier *et al.*, 2004] Ladeana W Hillier, Webb Miller, Ewan Birney, Wesley Warren, Ross C Hardison, Chris P Ponting, Peer Bork, David W Burt, Martien A M Groenen, Mary E Delany, Jerry B Dodgson, Asif T Chinwalla, Paul F Cliften, Sandra W Clifton, Kimberly D Delehaunty, Catrina Fronick, Robert S Fulton, Tina A Graves, Colin Kremitzki, Dan Layman, Vincent Magrini, John D McPherson, Tracie L Miner, Patrick Minx, William E Nash, Michael N Nhan, Joanne O Nelson, Lachlan G Oddy, Craig S Pohl, Jennifer Randall-Maher, Scott M Smith, John W Wallis, Shiaw-Pyng Yang, Michael N Romanov, Catherine M Rondelli, Bob Paton, Jacqueline Smith, David Morrice, Laura Daniels, Helen G Tempest, Lindsay Robertson, Julio S Masabanda, Darren K Griffin, Alain Vignal, Valerie Fillon, Lina Jacobbson, Susanne Kerje, Leif Andersson, Richard P M Crooijmans, Jan Aerts, Jan J van der Poel, Hans Ellegren, Randolph B Caldwell, Simon J Hubbard, Darren V Grafham, Andrzej M Kierzek, Stuart R McLaren, Ian M Overton, Hiroshi Arakawa, Kevin J Beattie, Yuri Bezzubov, Paul E Boardman, James K Bonfield, Michael D R Croning, Robert M Davies, Matthew D Francis, Sean J Humphray, Carol E Scott, Ruth G Taylor, Cheryll Tickle, William R A Brown, Jane Rogers, Jean-Marie Buerstedde, Stuart A Wilson, Lisa Stubbs, Ivan Ovcharenko, Laurie Gordon, Susan Lucas, Marcia M Miller, Hidetoshi Inoko, Takashi Shiina, Jim Kaufman, Jan Salomonsen, Karsten Skjoedt, Gane Ka-Shu Wong, Jun Wang, Bin Liu, Jian Wang, Jun Yu, Huanming Yang, Mikhail Nefedov, Maxim Koriabine, Pieter J Dejong, Leo Goodstadt, Caleb Webber, Nicholas J Dickens, Ivica Letunic, Mikita Suyama, David Torrents, Christian von Mering, Evgeny M Zdobnov, Kateryna Makova, Anton Nekrutenko, Laura Elnitski, Pallavi Eswara, David C King, Shan Yang, Svitlana Tyekucheva, Anusha Radakrishnan, Robert S Harris, Francesca Chiaromonte, James Taylor, Jianbin He, Monique Rijnkels, Sam Griffiths-Jones, Abel Ureta-Vidal, Michael M Hoffman, Jessica Severin, Stephen M J Searle, Andy S Law, David Speed, Dave Waddington, Ze Cheng, Eray Tuzun, Evan Eichler, Zhirong Bao, Paul Flicek, David D Shteynberg, Michael R Brent, Jacqueline M Bye, Elizabeth J Huckle, Sourav Chatterji, Colin Dewey, Lior Pachter, Andrei Kouranov, Zissimos Mourelatos, Artemis G Hatzigeorgiou, Andrew H Paterson, Robert Ivarie, Mikael Brandstrom, Erik Axelsson, Niclas Backstrom, Sofia Berlin, Matthew T Webster, Olivier Pourquie, Alexandre Reymond, Catherine Ucla, Stylianos E Antonarakis, Manyuan Long, J J Emerson, Esther Betran, Isabelle Dupanloup, Henrik Kaessmann, Angie S Hinrichs, Gill Bejerano, Terrence S Furey, Rachel A Harte, Brian Raney, Adam Siepel, W James Kent, David Haussler, Eduardo Eyras, Robert Castelo, Josep F Abril, Sergi Castellano, Francisco Camara, Genis Parra, Roderic Guigó, Guillaume Bourque, Glenn Tesler, Pavel A Pevzner, Arian Smit, Lucinda A Fulton, Elaine R Mardis, and Richard K Wilson. Sequence and comparative analysis of the chicken genome provide unique perspectives on vertebrate evolution. *Nature*, 432(7018):695–716, 2004. pages 138, 397

[Holland *et al.*, 2004] B. Holland, K.T. Huber, V. Moulton, and P. Lockhart. Using consensus networks to visualize contradictory evidence for species phylogeny. *Molecular Biology and Evolution*, 21(7):1459–1461, 2004. pages 333

[Hoşten *et al.*, 2004] Serkan Hoşten, Amit Khetan, and Bernd Sturmfels. Solving the likelihood equations. `math.ST/0408270`, 2004. pages 114, 347

[Huber *et al.*, 2002] K.T. Huber, M. Langton, V. Penny, D.and Moulton, and M. Hendy. Spectronet: A package for computing spectra and median networks. *Applied Bioinformatics*, 1(3):2041–2059, 2002. pages 332

[Huelsenbeck *et al.*, 2000] J. P. Huelsenbeck, B. Larget, and D. L. Swofford. A compound poisson process for relaxing the molecular clock. *Genetics*, 154(4):1879–1892, 2000. pages 400, 401

[Human Genome Sequencing Consortium, 2004] International Human Genome Sequencing Consortium. Finishing the euchromatic sequence of the human genome. *Nature*, 431(7011):931–945, 2004. pages 133, 134, 137, 143

[Huson and Bryant, 2005] Daniel Huson and D. Bryant. Estimating phylogenetic trees and networks using splitstree4. ???, 2005. pages 333

[Huson *et al.*, 2004] D Huson, T Dezulian, T Kloepper, and M Steel. Phylogenetic super-networks from partial trees. *IEEE Transactions on Computational Biology and Bioinformatics*, 1(4):151–158, 2004. pages 333

[Huson, 1998] D. Huson. Splitstree - a program for analyzing and visualizing evolutionary data. *Bioinformatics*, 14(1):68–73, 1998. pages 333

[IEEE Task P754, 1985] IEEE, New York. *ANSI/IEEE 754-1985, Standard for Binary Floating-Point Arithmetic*, 1985. A preliminary draft was published in the January 1980 issue of IEEE Computer, together with several companion articles. Available from the IEEE Service Center, Piscataway, NJ, USA. pages 373

[Ihaka and Gentleman, 1996] Ross Ihaka and Robert Gentleman. R: A language for data analysis and graphics. *Journal of Computational and Graphical Statistics*, 5(3):299–314, 1996. pages 84

[Imrich and Klavžar, 2000] Wilfried Imrich and Sandi Klavžar. *Product graphs*. Wiley-Interscience Series in Discrete Mathematics and Optimization. Wiley-Interscience, New York, 2000. Structure and recognition, With a foreword by Peter Winkler. pages 333

[International Human Genome Sequencing Consortium, 2001] International Human Genome Sequencing Consortium. Initial sequencing and analysis of the human genome. *Nature*, 409(6822):860–921, February 2001. pages 397

[John *et al.*, 2003] K. St. John, T. Warnow, B.Moret, and L. Vawter. Performance study of phylogenetic methods: (unweighted) quartet methods and neighbor joining. *Journal of Algorithms*, 48:174–193, 2003. pages 309

[Jukes and Cantor, 1969] TH Jukes and C Cantor. Evolution of protein molecules. In HN Munro, editor, *Mammalian Protein Metabolism*, pages 21–32. New York Academic Press, 1969. pages 161, 380

[Karlin and Altschul, 1990] S Karlin and SF Altschul. Methods for assessing the statistical significance of molecular sequence features by using general scoring schemes. *Proceedings of the National Academy of Sciences, USA*, 87:2264–2268, 1990. pages 85

[Kellis *et al.*, 2004] M. Kellis, B. Birren, and E. Lander. Proof and evolutionary analysis of ancient genome duplication in the yeast saccharomyces cerevisae. *Nature*, 8:617–624, 2004. pages 138

[Kent, 2002] James Kent. Blat- the blast like alignment tool. *Genome Biology*, 12(4):656–664, 2002. pages 86, 282

[Khachiyan, 1980] L.G. Khachiyan. Polynomial algorithms in linear programming. *USSR Computational Mathematics and Mathematical Physics*, 20:53–72, 1980.

pages 183

[Kimura, 1981] M. Kimura. Estimation of evolutionary sequences between homologous nucleotide sequences. *Proc. Nat. Acad. Sci. U.S.A.*, 78:454–458, 1981. pages 340

[Kolmogorov and Zabih, 2003] Vladimir Kolmogorov and Ramin Zabih. Multi-camera scene reconstruction via graph cuts. *European Conference on Computer Vision (ECCV)*, 2003. pages 280, 281

[Korf *et al.*, 2001] I. Korf, P. Flicek, D. Duan, and M. R. Brent. Integrating genomic homology into gene structure prediction. *Bioinformatics*, 17 Suppl 1:S140–8, 2001. pages 137

[Korf *et al.*, 2003] I Korf, M Yandell, and J Bedell. *BLAST*. O'Reilly & Associates, Sebastopol, CA, 2003. pages 86

[Körner, 1989] T. W. Körner. *Fourier analysis*. Cambridge University Press, Cambridge, second edition, 1989. pages 338

[Kuhn, 1955] HW Kuhn. The hungarian method for the assignment problem. *Naval Research Logistics Quarterly*, 2:83–97, 1955. pages 51

[Kulisch *et al.*, 2001] U Kulisch, R Lohner, and A Facius, editors. *Perspectives on encolsure methods*. Springer-Verlag, New York, 2001. pages 380

[Kulp *et al.*, 1996] David Kulp, David Haussler, Martin G. Reese, and Frank H. Eeckman. A generalized hidden markov model for the recognition of human genes in dna. In *Proceedings of the Fourth International Conference on Intelligent Systems for Molecular Biology*, pages 134–142. AAAI Press, 1996. pages 154

[Lake, 1987] J. A. Lake. A rate-independent technique for analysis of nucleaic acid sequences: evolutionary parsimony. *Molecular Biology and Evolution*, 4:167–191, 1987. pages 361

[Lander and Waterman, 1988] ES Lander and MS Waterman. Genomic mapping by fingerprinting random clones: a mathematical analysis. *Genomics*, 2:231–239, 1988. pages 142

[Landsberg and Manivel, 2004] J.M. Landsberg and L. Manivel. On the ideals of secant varieties of segre varieties. *Foundations of Computational Mathematics*, 4(4):397–422, 2004. pages 364

[Laubenbacher, 2003] R Laubenbacher. A computer algebra approach to biological systems. In *Proc. 2003 Intl. Symposium on Symbolic and Algebraic Computation*, 2003. pages 100

[Lauritzen, 1996] Steffen L. Lauritzen. *Graphical models*, volume 17 of *Oxford Statistical Science Series*. The Clarendon Press Oxford University Press, New York, 1996. Oxford Science Publications. pages 38, 40, 42, 288, 289

[Lenstra, 1983] H. W. Lenstra, Jr. Integer programming with a fixed number of variables. *Math. Oper. Res.*, 8(4):538–548, 1983. pages 50

[Levinson and Gutman, 1987] G Levinson and GA Gutman. Slipped-strand mispairing: a major mechanism for DNA sequence evolution. *Molecular Biology and Evolution*, 4:203–221, 1987. pages 165

[Levy *et al.*, 2004] D. Levy, R. Yoshida, and L. Pachter. Neighbor joining with subtree weights. *preprint*, 2004. pages 347, 356, 388

[Lin *et al.*, 2002] Y.-H. Lin, P.A McLenachan, A.R. Gore, M.J. Phillips, R. Ota, M.D. Hendy, and Penny D. Four new mitochondrial genomes and the increased stability of evolutionary trees of mammals from improved taxon sampling. *Molecular Phylogenetics and Evolution*, 19:2060–2070, 2002. pages 397

[Litvinov, 2005] G Litvinov. The maslov dequantization, idempotent and tropical mathematics: a very brief introduction. *arXiv.org:math/0501038*, 2005. pages 52

[Loh and Walster, 2002] E Loh and GW Walster. Rump's example revisited. *Reliable Computing*, 8:245–248, 2002. pages 374

[Madsen *et al.*, 2001] O Madsen, M Scally, CJ Douady, DJ Kao, RW Debry, R Adkins, HM Ambrine, MJ Stanhope, WW DeJong, and MS Springer. Parallel adaptive radiations in two major clades of placental mammals. *Nature*, 409:610–614, 2001. pages 397

[Marcotte *et al.*, 1999] E. M. Marcotte, M. Pellegrini, M. J. Thompson, T. Yeates, and D. Eisenberg. A combined algorithm for genome-wide prediction of protein function. *Nature*, 402:83–86, 1999. pages 271

[McAuliffe *et al.*, 2004] Jon D McAuliffe, Lior Pachter, and Michael I Jordan. Multiple-sequence functional annotation and the generalized hidden markov phylogeny. *Bioinformatics*, 20(12):1850–60, 2004. pages 164

[McMullen, 1971] P. McMullen. The maximum numbers of faces of a convex polytope. *J. Combinatorial Theory, Ser. B*, 10:179–184, 1971. pages 226

[Megiddo, 1984] Nimrod Megiddo. Linear programming in linear time when the dimension is fixed. *J. Assoc. Comput. Mach.*, 31(1):114–127, 1984. pages 192

[Mihaescu, 2004] Radu Mihaescu. The toric ideal of the unhidden markov model. ???, 2004. pages 243, 252

[Mindell and Honeycutt, 1990] D. P. Mindell and R. L. Honeycutt. Ribosomal rna in vertebrates: evolution and phylogenetic applications. *Ann. Rev. Ecol. Syst.*, 21:541–566, 1990. pages 401

[Mond *et al.*, 2003] DMQ Mond, JQ Smith, and D Van Straten. Stochastic factorisations, sandwiched simplices and the topology of the space of explanations. *Proc. R. Soc. London A*, 459:2821–2845, 2003. pages 25

[Moore, 1967] RE Moore. *Interval analysis.* Prentice-Hall, Englewood Cliffs, New Jersey, 1967. pages 374, 377

[Moore, 1979] RE Moore. *Methods and Applications of Interval analysis.* SIAM, Philadelphia, Pennsylvania, 1979. pages 376

[Mount, 1982] SM Mount. A catalogue of splice junction sequence. *Nucleic Acids Research*, 10(2):459–472, 1982. pages 152

[Murphy *et al.*, 2001] WJ Murphy, E Eizirik, WE Johnson, YP Zhang, OA Ryder, and SJ O'Brien. Molecular phylogenetics and the origins of placental mammals. *Nature*, 409:614–618, 2001. pages 397

[Myers, 1999] E Myers. Whole-genome dna sequencing. *IEEE Computational Engineering and Science*, 3(1):33–43, 1999. pages 135

[Nasrallah, 2002] JB Nasrallah. Recognition and rejection of self in plant reproduction. *Science*, 296:305–308, 2002. pages 388

[Neumaier, 1990] A Neumaier. *Interval methods for systems of equations.* Cambridge university press, 1990. pages 379

[Ota and Li, 2000] Satoshi Ota and Wen-Hsiung Li. Njml: A hybrid algorithm for the neighbor-joining and maximum likelihood methods. *Molecular Biology and Evolution*, 17(9):1401–1409, 2000. pages

[P. and G., 2003] Pevzner P. and Tesler G. Genome rearrangements in mammalian evolution: lessons from human and mouse genomes. *Genome Research*, 13(1):37–45, 2003. pages 271

[Pachter and Sturmfels, 2004a] L Pachter and B Sturmfels. The mathematics of phylogenomics. *submitted*, 2004. pages 171, 244, 357, 406, 416

[Pachter and Sturmfels, 2004b] Lior Pachter and Bernd Sturmfels. Parametric inference for biological sequence analysis. *Proc Natl Acad Sci U S A*, 101(46):16138–43, 2004. pages 201

[Pachter and Sturmfels, 2004c] Lior Pachter and Bernd Sturmfels. Tropical geometry of statistical models. *Proc Natl Acad Sci U S A*, 101(46):16132–7, 2004. pages 122

[Pachter *et al.*, 2002] Lior Pachter, Marina Alexandersson, and Simon Cawley. Applications of generalized pair hidden markov models to alignment and gene finding problems. *J Comput Biol*, 9(2):389–99, 2002. pages 154

[Peters *et al.*, 2000] T. Peters, R. Dildrop, K. Ausmeier, and U. Ruther. Organization of mouse iroquois homeobox genes in two clusters suggests a conserved regulation and function in vertebrate development. *Genome Research*, 10:1453–1462, 2000. pages 410

[Phillips and Penny, 2003] M.J. Phillips and D. Penny. The root of the mammalian tree inferred from whole mitochondrial genomes. *Molecular Phylogenetics and Evolution*, 28:171–185, 2003. pages 397

[Pin, 1998] Jean-Eric Pin. Tropical semirings. In *Idempotency (Bristol, 1994)*, volume 11 of *Publ. Newton Inst.*, pages 50–69. Cambridge Univ. Press, Cambridge, 1998. pages 52

[Pistone *et al.*, 2001] Giovanni Pistone, Eva Riccomagno, and Henry P. Wynn. Computational commutative algebra in discrete statistics. In *Algebraic methods in statistics and probability (Notre Dame, IN, 2000)*, volume 287 of *Contemp. Math.*, pages 267–282. Amer. Math. Soc., Providence, RI, 2001. pages 3

[R Development Core Team, 2004] R Development Core Team. *R: A language and environment for statistical computing*. R Foundation for Statistical Computing, Vienna, Austria, 2004. 3-900051-07-0. pages 309

[Radmacher *et al.*, 2001] M.D. Radmacher, R. Simon, R. Desper, R. Taetle, A.A. Schäffer, and M.A. Nelson. Graph models of oncogenesis with an application to melanoma. *J. Theor. Biol.*, 212:535–548, 2001. pages 284

[Rahnenführer *et al.*, 2005] J. Rahnenführer, N. Beerenwinkel, W.A. Schulz, C. Hartmann, A. von Deimling, B. Wullich, and T. Lengauer. Estimating cancer survival and clinical outcome based on genetic tumor progression scores. *Bioinformatics*, 2005. to appear. pages 284

[Rall, 1981] LB Rall. *Automatic differentiation, techniques and applications*, volume 120 of *Springer lecture notes in computer science*. Springer-Verlag, New York, 1981. pages 376

[Rambaut and Grassly, 1997] A. Rambaut and N. C. Grassly. Seq-Gen: An application for the Monte Carlo simulation of dna sequence evolution along phylogenetic trees. *Comput. Appl. Biosci.*, 13:235–238, 1997. pages 356, 368

[Raphael and Pevzner, 2004] B Raphael and P Pevzner. Reconstructing tumor amplisomes. *Bioinformatics*, 20 Suppl 1, Special ISMB/ECCB 2004 issue:I265–I273, 2004. pages 139

[Ratz, 1992] D Ratz. *Automatische ergebnisverifikation bei globalen optimierungsproblemen*. Ph.D. dissertation, Universitat Karlsruhe, Karlsruhe, Germany, 1992. pages 379, 384

[Richter-Gebert *et al.*, 2003] J Richter-Gebert, B Sturmfels, and T Theobald. First steps in tropical geometry. In GL Litvinov and VP Maslov, editors, *Proc. Conference on Idempotent Mathematics and Mathematical Physics*, 2003. pages 118

[Sainudiin *et al.*, 2005] R Sainudiin, SW Wong, K Yogeeswaran, J Nasrallah, Z Yang, and R Nielsen. Detecting site-specific physicochemical selective pressures: applications to the class-I HLA of the human major histocompatibility complex and the SRK of the plant sporophytic self-incompatibility system. *Journal of Molecular Evolution*, in press, 2005. pages 388

[Sainudiin, 2004] R Sainudiin. Enclosing the maximum likelihood of the simplest DNA model evolving on fixed topologies: towards a rigorous framework for phylogenetic inference. Technical Report BU1653-M, Department of Biol. Stats. and Comp. Bio., Cornell University, 2004. pages 386

[Saitou and Nei, 1987] N Saitou and M Nei. The neighbor joining method: a new method for reconstructing phylogenetic trees. *Molecular Biology and Evolution*, 4(4):406–425, 1987. pages 75, 347

[Salakhutdinov *et al.*, 2003] R. Salakhutdinov, S. Roweis, and Ghahramani Z. Optimization with em and expectation-conjugate-gradient. In *Proceedings of the Twentieth International Conference on Machine Learning (ICML-2003)*, 2003. pages 266

[Salakhutdinov *et al.*, 2004] R. Salakhutdinov, S. Roweis, and Ghahramani Z. Relationship between gradient and em steps in latent variable models. *in preparation*, 2004. pages 266, 267

[Sandelin *et al.*, 2004] A. Sandelin, P. Bailey, S. Bruce, P.G. Engström, J.M. Klos, W.W. Wasserman, J. Ericson, and B. Lenhard. Arrays of ultraconserved non-coding regions span the loci of key developmental genes in vertebrate genomes. *BMC Genomics*, 5:99, 2004. pages 410, 411, 415

[Sankoff and Blanchette, 2000] D Sankoff and M Blanchette. Comparative genomics via phylogenetic invariants for Jukes-Cantor semigroups. In *Stochastic models (Ottawa, ON, 1998)*, volume 26 of *CMS Conf. Proc.*, pages 399–418. Amer. Math. Soc., Providence, RI, 2000. pages 361

[Sankoff and Nadeau, 2003] D Sankoff and JH Nadeau. Chromosome rearrangements in evolution: from gene order to genome sequence and back. *Proceedings of the National Academy of Sciences, USA*, 100:11188–11189, 2003. pages 138

[Schmitz and Zischler, 2003] J. Schmitz and H. Zischler. A novel family of trna-derived sines in the colugo and two new retrotransposable markers separating dermopterans from primates. *Molecular Phylogenetics and Evolution*, 28:341–349, 2003. pages 397

[Schrijver, 1986] Alexander Schrijver. *Theory of linear and integer programming*. Wiley-Interscience Series in Discrete Mathematics. John Wiley & Sons Ltd., Chichester, 1986. A Wiley-Interscience Publication. pages 50

[Schwartz *et al.*, 2003] S Schwartz, WJ Kent, A Smit, Z Zhang, R Baertsch, RC Hardison, D Haussler, and W Miller. Human-mouse alignments with blastz. *Genome Research*, 13:103–107, 2003. pages 57, 86

[Seidel, 2004] Raimund Seidel. Convex hull computations. In Jacob E. Goodman and Joseph O'Rourke, editors, *Handbook of discrete and computational geometry*, Discrete Mathematics and its Applications (Boca Raton), chapter 22. Chapman & Hall/CRC, Boca Raton, FL, second edition, 2004. pages 192

[Semple and Steel, 2003] Charles Semple and Mike Steel. *Phylogenetics*, volume 24 of *Oxford Lecture Series in Mathematics and its Applications*. Oxford University Press, Oxford, 2003. pages vii, 71, 161, 312

[Shoup, 2004] Victor Shoup. NTL, A Library for doing Number Theory. Available at http://shoup.net/ntl/, 2004. pages 245

[Siepel and Haussler, 2004] A Siepel and D Haussler. Combining phylogenetic and hidden markov models in biosequence analysis. *Journal of Computational Biology*, 11:413–428, 2004. pages 164, 418

[Siepel, 2005] A. Siepel. personal communication, 2005. pages 400

[Simon *et al.*, 2000] R. Simon, R. Desper, C.H. Papadimitriou, A. Peng, D.S. Alberts, R. Taetle, J.M. Trent, and A.A. Schäffer. Chromosome abnormalities in ovarian adenocarcinoma: III. Using breakpoint data to infer and test mathematical models for oncogenesis. *Genes, Chromosomes & Cancer*, 28:106–120, 2000. pages 284

[Sneath and Sokal, 1973] Peter H.A. Sneath and Robert R. Sokal. *Numerical taxonomy: the principles and practice of numerical classification*. W.H. Freeman, San Francisco, 1973. pages 347

[Speyer and Sturmfels, 2004] David Speyer and Bernd Sturmfels. The tropical Grassmannian. *Adv. Geom.*, 4(3):389–411, 2004. pages 125, 129

[Speyer and Williams, 2004] D Speyer and L Williams. The tropical totally positive grassmanian. *Journal of Algebraic Combinatorics, in press*, 2004. pages 122

[Speyer, 2004] D Speyer. Tropical linear spaces. *submitted*, 2004. pages 128

[Stanley, 1999] Richard P. Stanley. *Enumerative combinatorics. Vol. 2*, volume 62 of *Cambridge Studies in Advanced Mathematics*. Cambridge University Press, Cambridge, 1999. With a foreword by Gian-Carlo Rota and appendix 1 by Sergey Fomin. pages 53, 285

[Steel *et al.*, 1992] M. A. Steel, M. D. Hendy, L. A. Székely, and P. L. Erdős. Spectral analysis and a closest tree method for genetic sequences. *Appl. Math. Lett.*, 5(6):63–67, 1992. pages 342, 345

[Strassen, 1983] V. Strassen. Rank and optimal computation of generic tensors. *Linear Algebra Appl.*, 52/53:645–685, 1983. pages 364

[Strimmer and Moulton, 2000] K. Strimmer and V. Moulton. Likelihood analysis of phylogenetic networks using directed graphical models. *Molecular Biology and Evolution*, 17:875–881, 2000. pages 337

[Strimmer *et al.*, 2001] K. Strimmer, C. Wiuf, and V. Moulton. Recombination analysis using directed graphical models. *Molecular Biology and Evolution*, 18:97–99, 2001. pages 337

[Studier and Keppler, 1988] JA Studier and KJ Keppler. A note on the neighbor-joining method of saitou and nei. *Molecular Biology and Evolution*, 5:729–731, 1988. pages 75

[Sturmfels and Sullivant, 2004] B Sturmfels and S Sullivant. Toric ideals of phylogenetic invariants. ???, 2004. pages 161, 303, 308, 313

[Sturmfels and Yu, 2004] B Sturmfels and J Yu. Classification of six-point metrics. *Electron. J. Combin.*, 11:Research Paper 44, 16 pp. (electronic), 2004. pages 312, 361

[Sturmfels, 1990] B Sturmfels. Gröbner bases and Stanley decompositions of determinantal rings. *Math. Z.*, 205(1):137–144, 1990. pages 98

[Sturmfels, 1993] B Sturmfels. *Algorithms in invariant theory*. Texts and Monographs in Symbolic Computation. Springer-Verlag, Vienna, 1993. pages 105

[Sturmfels, 2002] B Sturmfels. *Solving systems of polynomial equations*, volume 97 of *CBMS Regional Conference Series in Mathematics*. Published for the Conference Board of the Mathematical Sciences, Washington, DC, 2002. pages 93, 118

[Susko, 2003] E Susko. Confidence regions and hypothesis tests for topologies using generalized least squares. *Molecular Biology and Evolution*, 2003. pages 335, 336

[Swofford, 1998] DL Swofford. *PAUP*. Phylogenetic analysis using parsimony (* and other methods)*. Sunderland Mass., 1998. pages 390

[Swox, 2004] AB Swox. Gmp, the gnu multiple precision arithmetic library. Available at http://swox.com/gmp/, 2004. pages 245

[Szabo and Boucher, 2002] A Szabo and K Boucher. Estimating an oncogenetic tree when false negatives and positives are present. *Math. Biosci.*, 176:219–240, 2002. pages 296

[Székely *et al.*, 1993] LA Székely, MA Steel, and PL Erdős. Fourier calculus on evolutionary trees. *Adv. in Appl. Math.*, 14(2):200–210, 1993. pages 303, 312, 316, 332, 342, 345

[Tesler, 2002] G Tesler. Efficient algorithms for multichromosomal genome rearrangements. *Journal of Computer and System Sciences*, 65(3):587–609, 2002. pages 138, 139

[Thomas *et al.*, 2003] J W Thomas, J W Touchman, R W Blakesley, G G Bouffard, S M Beckstrom-Sternberg, E H Margulies, M Blanchette, A C Siepel, P J Thomas, J C McDowell, B Maskeri, N F Hansen, M S Schwartz, R J Weber, W J Kent, D Karolchik, T C Bruen, R Bevan, D J Cutler, S Schwartz, L Elnitski, J R Idol, A B Prasad, S-Q Lee-Lin, V V B Maduro, T J Summers, M E Portnoy, N L Dietrich, N Akhter, K Ayele, B Benjamin, K Cariaga, C P Brinkley, S Y Brooks, S Granite, X Guan, J Gupta, P Haghighi, S-L Ho, M C Huang, E Karlins, P L Laric, R Legaspi, M J Lim, Q L Maduro, C A Masiello, S D Mastrian, J C McCloskey, R Pearson, S Stantripop, E E Tiongson, J T Tran, C Tsurgeon, J L Vogt, M A Walker, K D Wetherby, L S Wiggins, A C Young, L-H Zhang, K Osoegawa, B Zhu, B Zhao, C L Shu, P J De Jong, C E Lawrence, A F Smit, A Chakravarti, D Haussler, P Green, W Miller, and E D Green. Comparative analyses of multi-species sequences from targeted genomic regions. *Nature*, 424(6950):788–93, 2003. pages 282, 397, 398, 400

[Valiant, 1979] L Valiant. The complexity of computing the permanent. *Theoretical Computer Science*, 8:189–201, 1979. pages 51

[Varchenko, 1995] A Varchenko. Critical points of the product of powers of linear functions and families of bases of singular vectors. *Compositio Math.*, 97(3):385–401, 1995. pages 11

[Venter *et al.*, 2001] J C Venter, M D Adams, E W Myers, P W Li, R J Mural, G G Sutton, H O Smith, M Yandell, C A Evans, R A Holt, J D Gocayne, P Amanatides, R M Ballew, D H Huson, J R Wortman, Q Zhang, C D Kodira, X H Zheng, L Chen, M Skupski, G Subramanian, P D Thomas, J Zhang, G L Gabor Miklos, C Nelson, S Broder, A G Clark, J Nadeau, V A McKusick, N Zinder, A J Levine, R J Roberts, M Simon, C Slayman, M Hunkapiller, R Bolanos, A Delcher, I Dew, D Fasulo, M Flanigan, L Florea, A Halpern, S Hannenhalli, S Kravitz, S Levy, C Mobarry, K Reinert, K Remington, J Abu-Threideh, E Beasley, K Biddick, V Bonazzi, R Brandon, M Cargill, I Chandramouliswaran, R Charlab, K Chaturvedi, Z Deng, V Di Francesco, P Dunn, K Eilbeck, C Evangelista, A E Gabrielian, W Gan, W Ge, F Gong, Z Gu, P Guan, T J Heiman, M E Higgins, R R Ji, Z Ke, K A Ketchum, Z Lai, Y Lei, Z Li, J Li, Y Liang, X Lin, F Lu, G V Merkulov, N Milshina, H M Moore, A K Naik, V A Narayan, B Neelam, D Nusskern, D B Rusch, S Salzberg, W Shao, B Shue, J Sun, Z Wang, A Wang, X Wang, J Wang, M Wei, R Wides, C Xiao, C Yan, A Yao, J Ye, M Zhan, W Zhang, H Zhang, Q Zhao, L Zheng, F Zhong, W Zhong, S Zhu, S Zhao, D Gilbert, S Baumhueter, G Spier, C Carter, A Cravchik, T Woodage, F Ali, H An, A Awe, D Baldwin, H Baden, M Barnstead, I Barrow, K Beeson, D Busam, A Carver, A Center, M L Cheng, L Curry, S Danaher, L Davenport, R Desilets, S Dietz, K Dodson, L Doup, S Ferriera, N Garg, A Gluecksmann, B Hart, J Haynes, C Haynes, C Heiner, S Hladun, D Hostin, J Houck, T Howland, C Ibegwam, J Johnson, F Kalush, L Kline, S Koduru, A Love, F Mann, D May, S McCawley, T McIntosh, I McMullen, M Moy, L Moy, B Murphy, K Nelson, C Pfannkoch, E Pratts, V Puri, H Qureshi, M Reardon, R Rodriguez, Y H Rogers, D Romblad, B Ruhfel, R Scott, C Sitter, M Smallwood, E Stewart, R Strong, E Suh, R Thomas, N N Tint, S Tse, C Vech, G Wang, J Wetter, S Williams, M Williams, S Windsor, E Winn-Deen, K Wolfe, J Zaveri, K Zaveri, J F Abril, R Guigó, M J Campbell, K V Sjolander, B Karlak, A Kejariwal, H Mi, B Lazareva, T Hatton, A Narechania, K Diemer, A Muruganujan, N Guo, S Sato, V Bafna, S Istrail, R Lippert, R Schwartz, B Walenz, S Yooseph, D Allen, A Basu, J Baxendale, L Blick, M Caminha, J Carnes-Stine, P Caulk, Y H Chiang, M Coyne, C Dahlke, A Mays, M Dombroski, M Donnelly, D Ely, S Esparham, C Fosler, H Gire, S Glanowski, K Glasser, A Glodek, M Gorokhov, K Graham, B Gropman, M Harris, J Heil, S Henderson, J Hoover, D Jennings, C Jordan, J Jordan, J Kasha, L Kagan, C Kraft, A Levitsky, M Lewis, X Liu, J Lopez, D Ma, W Majoros, J McDaniel, S Murphy, M Newman, T Nguyen, N Nguyen, M Nodell, S Pan, J Peck, M Peterson, W Rowe, R Sanders, J Scott, M Simpson, T Smith, A Sprague, T Stockwell, R Turner, E Venter, M Wang, M Wen, D Wu, M Wu, A Xia, A Zandieh, and X Zhu. The sequence of the human genome. *Science*, 291(5507):1304–51, 2001. pages 134

[Viterbi, 1967] AJ Viterbi. Error bounds for convolutional codes and an asymptotically optimum decoding algorithm. *IEEE Transactions on Information Theory*, 13:260–269, 1967. pages 232

[Vogelstein *et al.*, 1988] B Vogelstein, E Fearon, and S Hamilton. Genetic alterations during colorectal-tumor development. *N. Engl. J. Med.*, 319:525–532, 1988. pages 284

[von Heydebreck *et al.*, 2004] A. von Heydebreck, B. Gunawan, and L. Füzesi. Maximum likelihood estimation of oncogenetic tree models. *Biostatistics*, 5(4):545–556, 2004. pages 284

[Warshall, 1962] S Warshall. A theorem on boolean matrices. *Journal of the ACM*, 9(1):18, 1962. pages 48

[Waterston *et al.*, 2002] Robert H Waterston, Kerstin Lindblad-Toh, Ewan Birney, Jane Rogers, Josep F Abril, Pankaj Agarwal, Richa Agarwala, Rachel Ainscough, Marina Alexandersson, Peter An, Stylianos E Antonarakis, John Attwood, Robert Baertsch, Jonathon Bailey, Karen Barlow, Stephan Beck, Eric Berry, Bruce Birren, Toby Bloom, Peer Bork, Marc Botcherby, Nicolas Bray, Michael R Brent, Daniel G Brown, Stephen D Brown, Carol Bult, John Burton, Jonathan Butler, Robert D Campbell, Piero Carninci, Simon Cawley, Francesca Chiaromonte, Asif T Chinwalla, Deanna M Church, Michele Clamp, Christopher Clee, Francis S Collins, Lisa L Cook, Richard R Copley, Alan Coulson, Olivier Couronne, James Cuff, Val Curwen, Tim Cutts, Mark Daly, Robert David, Joy Davies, Kimberly D Delehaunty, Justin Deri, Emmanouil T Dermitzakis, Colin Dewey, Nicholas J Dickens, Mark Diekhans, Sheila Dodge, Inna Dubchak, Diane M Dunn, Sean R Eddy, Laura Elnitski, Richard D Emes, Pallavi Eswara, Eduardo Eyras, Adam Felsenfeld, Ginger A Fewell, Paul Flicek, Karen Foley, Wayne N Frankel, Lucinda A Fulton, Robert S Fulton, Terrence S Furey, Diane Gage, Richard A Gibbs, Gustavo Glusman, Sante Gnerre, Nick Goldman, Leo Goodstadt, Darren Grafham, Tina A Graves, Eric D Green, Simon Gregory, Roderic Guigó, Mark Guyer, Ross C Hardison, David Haussler, Yoshihide Hayashizaki, LaDeana W Hillier, Angela Hinrichs, Wratko Hlavina, Timothy Holzer, Fan Hsu, Axin Hua, Tim Hubbard, Adrienne Hunt, Ian Jackson, David B Jaffe, L Steven Johnson, Matthew Jones, Thomas A Jones, Ann Joy, Michael Kamal, Elinor K Karlsson, Donna Karolchik, Arkadiusz Kasprzyk, Jun Kawai, Evan Keibler, Cristyn Kells, W James Kent, Andrew Kirby, Diana L Kolbe, Ian Korf, Raju S Kucherlapati, Edward J Kulbokas, David Kulp, Tom Landers, J P Leger, Steven Leonard, Ivica Letunic, Rosie Levine, Jia Li, Ming Li, Christine Lloyd, Susan Lucas, Bin Ma, Donna R Maglott, Elaine R Mardis, Lucy Matthews, Evan Mauceli, John H Mayer, Megan McCarthy, W Richard McCombie, Stuart McLaren, Kirsten McLay, John D McPherson, Jim Meldrim, Beverley Meredith, Jill P Mesirov, Webb Miller, Tracie L Miner, Emmanuel Mongin, Kate T Montgomery, Michael Morgan, Richard Mott, James C Mullikin, Donna M Muzny, William E Nash, Joanne O Nelson, Michael N Nhan, Robert Nicol, Zemin Ning, Chad Nusbaum, Michael J O'Connor, Yasushi Okazaki, Karen Oliver, Emma Overton-Larty, Lior Pachter, Genis Parra, Kymberlie H Pepin, Jane Peterson, Pavel Pevzner, Robert Plumb, Craig S Pohl, Alex Poliakov, Tracy C Ponce, Chris P Ponting, Simon Potter, Michael Quail, Alexandre Reymond, Bruce A Roe, Krishna M Roskin, Edward M Rubin, Alistair G Rust, Ralph Santos, Victor Sapojnikov, Brian Schultz, Jorg Schultz, Matthias S Schwartz, Scott Schwartz, Carol Scott, Steven Seaman, Steve Searle, Ted Sharpe, Andrew Sheridan, Ratna Shownkeen, Sarah Sims, Jonathan B Singer, Guy Slater, Arian Smit, Douglas R Smith, Brian Spencer, Arne Stabenau, Nicole Stange-Thomann, Charles Sugnet, Mikita Suyama, Glenn Tesler, Johanna Thompson, David Torrents, Evanne Trevaskis, John Tromp, Catherine Ucla, Abel Ureta-Vidal, Jade P Vinson, Andrew C Von Niederhausern, Claire M Wade, Melanie Wall, Ryan J Weber, Robert B Weiss, Michael C Wendl, Anthony P West, Kris Wetterstrand, Raymond Wheeler, Simon Whelan, Jamey Wierzbowski, David Willey, Sophie Williams, Richard K Wilson, Eitan Winter, Kim C Worley, Dudley Wyman, Shan Yang, Shiaw-Pyng Yang, Evgeny M Zdobnov, Michael C Zody, and Eric S Lander. Initial sequencing and comparative analysis of the mouse genome. *Nature*, 420(6915):520–62, 2002. pages 397

[Watson and Crick, 1953] J Watson and F Crick. A structure for deoxyribose nucleic acid. *Nature*, 171:964–967, 1953. pages 134

[Wetzel, 1995] R Wetzel. Zur visualisierung abstrakter Ähnlichkeitsbeziehungen. Master's thesis, Fakultät Mathematik, Universität Bielefeld, 1995. pages 333, 334

[Winkler, 1984] P Winkler. Isometric embeddings in products of complete graphs. *Discrete Applied Mathematics*, 7:221–225, 1984. pages 333

[Wolf *et al.*, 2000] M. J. Wolf, S. Easteal, M. Kahn, B. D. McKay, and L. S. Jermiin. Trexml: A maximum likelihood program for extensive tree-space exploration. *Bioinformatics*, 16:383–394, 2000. pages 389

[Woolfe *et al.*, 2005] A. Woolfe, M. Goodson, D.K. Goode, P. Snell, G.K. McEwen, T. Vavouri, S.F. Smith, P. North, H. Callaway, K. Kelly, K. Walter, I. Abnizova, W. Gilks, Y.J.K. Edwards, J.E. Cooke, and G. Elgar. Highly conserved non-coding sequences are associated with vertebrate development. *PLoS Biology*, 3:7, 2005. pages 410, 415

[Wu and Jeff, 1983] C Wu and F Jeff. On the convergence properties of the EM algorithm. *Ann. Statist.*, 11(1):95–103, 1983. pages 21

[Wu and Li, 1985] CI Wu and WH Li. Evidence for Higher Rates of Nucleotide Substitution in Rodents Than in Man. *PNAS*, 82(6):1741–1745, 1985. pages 397

[Yang and Roberts, 1995] Z Yang and D Roberts. On the use of nucleic acid sequences to infer early branchings in the tree of life. *Molecular Biology and Evolution*, 12:451–458, 1995. pages 400, 401

[Yang, 1997] Z Yang. PAML: A program package for phylogenetic analysis by maximum likelihood. *CABIOS*, 15:555–556, 1997. pages 309, 390, 416

[Yap and Pachter, 2004] Von Bing Yap and Lior Pachter. Identification of evolutionary hotspots in the rodent genomes. *Genome Res*, 14(4):574–9, 2004. pages 162

[Yoder and Yang, 2000] AD Yoder and Z Yang. Estimation of primate speciation dates using local molecular clocks. *Molecular Biology and Evolution*, 17:1081–1090, 2000. pages 401

[Yu *et al.*, 2002] Jun Yu, Songnian Hu, Jun Wang, Gane Ka-Shu Wong, Songgang Li, Bin Liu, Yajun Deng, Li Dai, Yan Zhou, Xiuqing Zhang, Mengliang Cao, Jing Liu, Jiandong Sun, Jiabin Tang, Yanjiong Chen, Xiaobing Huang, Wei Lin, Chen Ye, Wei Tong, Lijuan Cong, Jianing Geng, Yujun Han, Lin Li, Wei Li, Guangqiang Hu, Xiangang Huang, Wenjie Li, Jian Li, Zhanwei Liu, Long Li, Jianping Liu, Qiuhui Qi, Jinsong Liu, Li Li, Tao Li, Xuegang Wang, Hong Lu, Tingting Wu, Miao Zhu, Peixiang Ni, Hua Han, Wei Dong, Xiaoyu Ren, Xiaoli Feng, Peng Cui, Xianran Li, Hao Wang, Xin Xu, Wenxue Zhai, Zhao Xu, Jinsong Zhang, Sijie He, Jianguo Zhang, Jichen Xu, Kunlin Zhang, Xianwu Zheng, Jianhai Dong, Wanyong Zeng, Lin Tao, Jia Ye, Jun Tan, Xide Ren, Xuewei Chen, Jun He, Daofeng Liu, Wei Tian, Chaoguang Tian, Hongai Xia, Qiyu Bao, Gang Li, Hui Gao, Ting Cao, Juan Wang, Wenming Zhao, Ping Li, Wei Chen, Xudong Wang, Yong Zhang, Jianfei Hu, Jing Wang, Song Liu, Jian Yang, Guangyu Zhang, Yuqing Xiong, Zhijie Li, Long Mao, Chengshu Zhou, Zhen Zhu, Runsheng Chen, Bailin Hao, Weimou Zheng, Shouyi Chen, Wei Guo, Guojie Li, Siqi Liu, Ming Tao, Jian Wang, Lihuang Zhu, Longping Yuan, and Huanming Yang. A draft sequence of the rice genome (oryza sativa l. ssp. indica). *Science*, 296(5565):79–92, 2002. pages 143

[Yu *et al.*, 2005] J Yu, J Wang, W Lin, S Li, H Li, J Zhou, P Ni, W Dong, S Hu, C Zeng, J Zhang, Y Zhang, R Li, Z Xu, X Li, H Zheng, L Cong, L Lin, J Yin, J Geng, G Li, J Shi, J Liu, H Lv, J Li, Y Deng, L Ran, X Shi, X Wang, Q Wu, C Li, X Ren, D Li, D Liu, X Zhang, Z Ji, W Zhao, Y Sun, Z Zhang, J Bao, Y Han, L Dong, J Ji, P Chen, S Wu, Y Xiao, D Bu, J Tan, L Yang, C Ye, J Xu, Y Zhou, Y Yu, B Zhang, S Zhuang, H Wei, B Liu, M Lei, H Yu, Y Li, H Xu, S Wei, X He, L Fang, X Huang, Z Su, W Tong, Z Tong, J Ye, L Wang, T Lei, C Chen, H Chen, H Huang, F Zhang, N Li, C Zhao, Y Huang, L Li, Y Xi, Q Qi, W Li, W Hu, X Tian, Y Jiao, X Liang, J Jin, L Gao, W Zheng, B Hao, S Liu, W Wang, L Yuan, M Cao, J McDermott, R Samudrala, GK Wong, and H Yang. The genomes of oryza sativa: A history of duplications., 2005. pages 143

[Zang, 2001] KD Zang. Meningioma: a cytogenetic model of a complex benign human tumor, including data on 394 karyotyped cases. *Cytogenet. Cell Genet.*, 93:207–220, 2001. pages 284

[Ziegler, 1995] GM Ziegler. *Lectures on polytopes*, volume 152 of *Graduate Texts in Mathematics*. Springer-Verlag, New York, 1995. pages 63, 226

Index